



Grant Agreement No.: 226479

# SafeLand

Living with landslide risk in Europe: Assessment,  
effects of global change, and risk management strategies

7<sup>th</sup> Framework Programme  
Cooperation Theme 6 Environment (including climate change)  
Sub-Activity 6.1.3 Natural Hazards

## Deliverable 1.1

Landslide triggering mechanisms in Europe – Overview and State of the Art

Work Package 1.1 – Identification of mechanisms and triggers

Deliverable/Work Package Leader: UNIMIB

Revision: 2 – Final

April 15<sup>th</sup>, 2012

Rev.	Deliverable Responsible	Controlled by	Date
0	UNIMIB	SGI-MI	30/1/2010
1	UNIMIB	SGI-MI	30/09/2010
2	UNIMIB	SGI-MI	15/04/2012

## SUMMARY

This Deliverable is aimed at providing a comprehensive overview of the physical processes responsible of the triggering of landslides, with special attention paid to the landslide types occurring in Europe. A general overview of the geotechnical aspects of landslide triggering, including classical and recent theoretical developments and examples, is first provided (Chapter 2); then possible triggering mechanisms are described which include: rainfalls and changes in slope hydrology (Chapter 3); changes in slope geometry (Chapter 4); earthquakes (Chapter 5); snowmelt and permafrost degradation (Chapter 6); deglaciation (Chapter 7); rock/soil weathering (Chapter 8); Volcanic processes (Chapter 9) and human activity (Chapter 10).

## Note about contributors

The following organisations contributed to the work described in this deliverable:

### **Lead partner responsible for the deliverable:**

[UNIMIB]

*Deliverable prepared by:*

Giovanni B. Crosta

Federico Agliardi

Paolo Frattini

Rosanna Sosio

### **Partner responsible for quality control:**

[SGI-MI]

*Deliverable reviewed by:*

Alberto Callerio

### **Other contributors:**

[SGI-MI]: Gianfrancesco Rocchi, Giovanni Vaciago, Alberto Callerio, M. Fontana, R. Previtali.

[CNRS]: Anke Spickermann, Jean-Philippe Malet.

[AMRA]: Luciano Picarelli, Antonio Santo, Giuseppe Di Crescenzo

[ETHZ]: Sarah Springman

[UPC]: Eduardo E. Alonso, Jubert Pineda, Nuria M. Pinyol, Enrique Romero.

[AUTH]: Kyriazis Pitolakis, Stavroula Fotopoulou, Kaliopi Kakderi, Evi Riga, Olga Ktenidou.

---

## CONTENTS

<b>1</b>	<b>INTRODUCTION (<i>UNIMIB</i>).....</b>	<b>7</b>
1.1	SCOPE AND RATIONALE OF THE DELIVERABLE .....	7
1.2	DEFINITION AND CLASSIFICATIONS.....	8
1.3	LANDSLIDE TRIGGERINGS .....	10
<b>2</b>	<b>GEOTECHNICAL ASPECTS OF LANDSLIDES TRIGGERING (<i>SGI-MI</i>) .....</b>	<b>12</b>
2.1	INTRODUCTION .....	12
2.2	CLASSIFICATION SYSTEMS .....	15
2.3	GEOTECHNICAL CLASSIFICATION AND MODELLING OF SATURATED GEOMATERIALS.....	18
2.3.1	“Fine grained materials” .....	19
2.3.2	“Coarse grained, uncemented materials” .....	39
2.3.3	“Rocks” .....	54
2.3.4	Geotechnical classification.....	58
2.4	NUMERICAL EXAMPLES.....	60
2.4.1	General .....	60
2.4.2	Example 1 – 1D stress relief in clayey materials .....	60
2.4.3	Example 2 – Slopes in CB1 clays and the effects of $K_0$ .....	65
2.4.4	Example 3 – Comparison between CA and CB1 clays.....	71
2.4.5	Example 4 – Comparison between SA and SB sands.....	76
<b>3</b>	<b>LANDSLIDE TRIGGERING BY RAINFALLS AND CHANGES IN SLOPE HYDROLOGY (<i>UNIMIB</i>) .....</b>	<b>84</b>
3.1	PHYSICAL PROCESS - RAINFALL INFILTRATION.....	84
3.1.1	Rainfall infiltration - shallow soils.....	85
3.1.2	Rainfall infiltration - deep soils.....	88
3.2	PHYSICAL PROCESS: CHANGES OF GROUNDWATER LEVELS.....	89
3.3	CURRENT ANALYSES APPROACHES AT DIFFERENT SCALES - RAINFALL INFILTRATION .....	91
3.3.1	Rainfall infiltration - shallow soils.....	91
3.3.2	Rainfall infiltration - deep soils.....	94
3.4	CURRENT ANALYSES APPROACHES AT DIFFERENT SCALES - CHANGES OF GROUNDWATER LEVELS .....	98
3.5	EXAMPLES .....	101
3.5.1	Overview of intense rainfall on volcanic soils–regional and local scale (AMRA).....	101
3.5.2	Overview of rainfall impacts on the dynamics of landslides developed in over-consolidated and weathered clays – Example of the Trièves Plateau and the Bacelonnette Basin landslides (French Alps) (CNRS) .....	122
3.5.3	Rainfall on complex large rockslides: Ruinon rockslide (Valfurva) (Crosta and Agliardi, 2002) .....	128

3.5.4	Campo Vallemaggia landslide (Bonzanigo et al., 2007).....	131
3.5.5	Spriana landslide (Agliardi et al., in press; Belloni and Gandolfo, 1997)	133
3.5.6	Ca' Lita landslide (Ronchetti et al., 2010).....	136
3.5.7	Vallcebre landslide ( <i>Corominas et al., 2005</i> ) .....	139
3.5.8	Vajont landslide (SGI-MI).....	141
<b>4</b>	<b>LANDSLIDE TRIGGERING BY CHANGES IN SLOPE GEOMETRY (<i>UNIMIB, SGI-MI</i>).....</b>	<b>144</b>
4.1	CHANGE INDUCED BY EROSION ( <i>UNIMIB</i> ) .....	145
4.1.1	Physical process .....	145
4.2	NUMERICAL MODELING [ <i>SGI-MI</i> ] .....	152
4.2.1	Key geotechnical characteristics of the clay considered in this study	153
4.2.2	Elasto-plastic constitutive model of the clay considered in this study	155
4.2.3	Model parameters of the clay considered in this study .....	159
4.2.4	Case A1 .....	164
4.2.5	Case A2 .....	176
4.2.6	Case A3 .....	178
4.2.7	Case B1 .....	181
4.2.8	Case B2 .....	188
4.2.9	Final remarks.....	192
<b>5</b>	<b>EARTHQUAKES (<i>AUTH</i>).....</b>	<b>194</b>
5.1	INTRODUCTION .....	194
5.2	GENERAL CLASSIFICATION OF EARTHQUAKE TRIGGERED LANDSLIDES .....	194
5.3	PARAMETERS AFFECTING SEISMIC SLOPE STABILITY .....	195
5.3.1	Ground Properties .....	195
5.3.2	Size of landslides.....	198
5.3.3	Shaking characteristics.....	198
5.4	METHODS TO ESTIMATE SEISMIC SLOPE DISPLACEMENTS.....	200
5.5	EXAMPLES .....	200
5.5.1	Las Colinas landslide caused by the 2001 El Salvador earthquake	200
5.5.2	Slope failures during the 2004 Niigata-Ken Chuetsu earthquake in Japan	205
5.5.3	Higashi-Takezawa slide (Type-A).....	209
5.5.4	Naranoki slide (Type-B) .....	213
5.5.5	Musikame slide (Type C).....	215
5.5.6	The 1980 Calitri landslide caused by the Irpinia earthquake, Italy	218
5.5.7	Corniglio landslide, Apennines region, Italy .....	220
5.5.8	The Tangjiashan landslide caused by the 2008 Sichuan (Wenchuan) earthquake, China .....	224
5.5.9	Synthesis of the selected cases histories .....	230

---

<b>6</b>	<b>LANDSLIDES TRIGGERING BY SNOWMELT AND PERMAFROST DEGRADATION (ETHZ).....</b>	<b>231</b>
6.1	LANDSLIDE DISTRIBUTION IN EUROPE ARISING FROM DEGRADING PERMAFROST AND SNOWMELT .....	233
6.2	PHYSICAL PROCESSES AND RELATED CONSTRAINTS TO THAWING AND FREEZING .....	234
6.3	CURRENT ANALYSIS APPROACHES AT DIFFERENT SCALES (DISTRIBUTION MODELS) .....	240
6.4	POTENTIAL CLIMATE CHANGE IMPACTS.....	242
6.5	EXAMPLES .....	245
6.5.1	Val Pola landslide, Italy .....	245
6.5.2	Ritigraben Torrent, Switzerland.....	247
6.5.3	Bèrard Rock Glacier (Southern French Alps).....	247
6.5.4	1987 Debris Flows in the Swiss Alps .....	248
<b>7</b>	<b>LANDSLIDE TRIGGERING BY DEGLACIATION (UNIMIB) .....</b>	<b>249</b>
7.1	PARAGLACIAL SLOPE MODIFICATION PROCESSES.....	249
7.1.1	Slope steepening.....	249
7.1.2	Slope debutting .....	252
7.2	PARAGLACIAL LANDSLIDES.....	253
7.2.1	Rock slope response to paraglacial modifications .....	253
7.2.2	Large-scale catastrophic rock slope failure.....	256
7.2.3	Progressive rock slope failure .....	260
7.2.4	Deep-Seated Gravitational Slope Deformations .....	264
7.2.5	Rockfalls .....	268
<b>8</b>	<b>LANDSLIDE TRIGGERING BY ROCK/SOIL WEATHERING (UPC).....</b>	<b>271</b>
8.1	GENERAL ASPECTS (UNIMIB) .....	271
8.1.1	Physical process .....	271
8.1.2	Previous studies.....	272
8.2	EXAMPLE: DEGRADATION OF A WEALD SILTSTONE.....	274
8.2.1	Geology .....	275
8.2.2	Profiles of index properties .....	277
8.2.3	Seismic tomography.....	280
8.2.4	Weathering profiles and strength tests .....	284
8.2.5	Rock matrix properties from laboratory tests .....	285
8.2.6	Conclusions .....	289
<b>9</b>	<b>VOLCANIC PROCESSES (UNIMIB).....</b>	<b>291</b>
9.1	TRIGGERING MECHANISMS: DEBRIS AVALANCHES .....	291
9.2	TRIGGERING MECHANISMS: LAHARS .....	297
9.3	APPROACHES.....	297
9.3.1	Numerical modeling.....	297
9.3.2	Analogical modeling .....	298
9.4	EXAMPLES .....	299

---

9.4.1	Tenerife (Canary Islands).....	299
9.4.2	Stromboli (Aeolian Islands).....	300
<b>10</b>	<b>LANDSLIDE TRIGGERING DUE TO HUMAN ACTIVITY (SGI-MI).....</b>	<b>302</b>
10.1	INTRODUCTION .....	302
10.2	TAILINGS .....	303
10.3	IMPOUNDING OF RESERVOIRS .....	309
10.4	SMALL SCALE EARTHWORKS.....	309
10.5	FARMING .....	311
<b>11</b>	<b>REFERENCES.....</b>	<b>313</b>

# 1 INTRODUCTION (UNIMIB)

## 1.1 SCOPE AND RATIONALE OF THE DELIVERABLE

The term “landslide” describes a wide variety of processes that result in the gravitational movement of slope-forming materials including rock, soil, artificial fill, or a combination of these. The geomaterials may move by falling, toppling, sliding, spreading, or flowing. Among landslides, different typologies are recognized, mainly by the class of material involved and by the prevalent movement mechanism.

Several comprehensive reviews and classifications of landslide types and mechanisms have been published in the scientific and technical literature, most often organised by landslide type based on kinematics, involved materials, and state of activity (e.g. (Varnes, 1978; Cruden and Varnes, 1996), or according to a geotechnical classification criteria (e.g. Skempton and Hutchinson, 1969; Hutchinson, 1988). A specific landslide type can be triggered by different combinations of actions (surcharge, unloading, saturation, strength degradation, cyclic loading, etc.); at the same time, similar actions may result in very different instability types, depending on scale, material, internal structure, geometry and evolution of the involved slopes. However, a comprehensive treatment of the landslide problem from the point of view or their triggering processes, as the one proposed here, has been rarely attempted in the past.

In order to fill this gap, and to provide a valuable support to researchers and practitioners, this Deliverable is aimed at giving a comprehensive overview of the physical processes responsible of landslides triggering, with special focus on the landslide types occurring in Europe and surrounding regions.

The document is composed of two main sections, namely:

- a general overview of the geotechnical aspects of landslide triggering (Chapter 2), including classical and recent developments (with examples). This part is aimed at setting up a theoretical framework of landslide mechanisms in different geomaterials (granular soils, clays, rock), under different landslide triggers;
- a detailed thematic description (with examples) of different landslide triggers including:
  - rainfall and changes in slope hydrology (Chapter 3);
  - changes in slope geometry due to excavation or erosion (Chapter 4);
  - earthquakes and related dynamic actions (Chapter 5);
  - snowmelt and permafrost degradation (Chapter 6);
  - deglaciation and related processes in the paraglacial environment (Chapter 7);
  - rock/soil weathering and related degradation (Chapter 8);
  - volcanic processes (Chapter 9);
  - human activity (Chapter 10).

## 1.2 DEFINITION AND CLASSIFICATIONS

Starting from the work of Varnes (1978), Cruden and Varnes (1996) proposed a taxonomic classification which considers, in addition to the movement mechanism at the initial stage of motion and the material, the state of activity and the rate of movement (Figure 1-1):

1) **SLIDES**: mass movements characterised by a distinct zone of weakness that separates the sliding portion from the more stable underlying material, leading to the definition of a so-called sliding boundary. The shape of the rupture surface permits one to classify slides in rotational and translational as following:

- Rotational slide where the surface of rupture is curved concavely upward and the slide movement is roughly rotational about an axis parallel to the ground surface and transverse across the slide.

- Translational slide in which the sliding mass moves along a roughly planar surface with little rotation or backward tilting.

A block slide is a translational slide in which the moving mass consists of a single unit, or a set of few closely related units, moving downslope as a relatively coherent mass.

2) **FALLS**: Falls are abrupt movements of rocks masses and boulders that become detached from steep slopes or cliffs. Separation occurs along discontinuities such as fractures, joints, and bedding planes, while the movement occurs by free-fall, bouncing, and rolling. Falls are strongly influenced by gravity, mechanical weathering, and the presence of interstitial water.

3) **TOPPLES** are distinguished by the forward rotation of a rock/soil unit or units about some pivotal point, below or low in the unit, under the actions of gravity and forces exerted by adjacent units or by fluids in cracks.

4) **FLOWS** are characterised by the presence of a gravity driven mass movement involving a significant internal distortion. The flow category includes several typologies differing one from the other in fundamental ways:

- a. Debris flow is a form of rapid mass movement in which a combination of loose soil, rock, organic matter, air, and water mobilize as a slurry that flows downslope. Debris flows are commonly caused by intense surface-water flow caused by heavy precipitation or fast snowmelt, leading to the erosion and mobilization of loose soil or rock on steep slopes. Debris flows can be ignited also by nearly-saturated shallow landslides that occur on steep slopes.

- b. Debris avalanche which consists of a very rapid to extremely rapid mass movement of non saturated material which remains laterally unconfined and unchannelled along most of its length.

- c. Earthflow as an intermittent flow-like movement of plastic clayey earth. The flow is elongated and usually runs on moderate slopes, under saturated conditions. Dry flows of granular material are also possible.

- d. Mudflow which consists of an earthflow of material, wet enough to flow rapidly, and containing at least 50 percent sand-, silt-, and clay-sized particles. In some reports of mudflow occurrences, generally found on newspaper or tv news, mudflows and debris flows are commonly referred as “mudslides.”

- e. Creep, as an imperceptibly slow, steady, downward movement of slope-forming soil or rock. Movement is caused by shear stress sufficient to produce permanent deformation, but too small to produce shear failure.

---

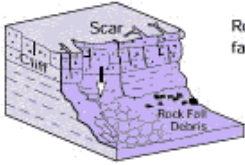
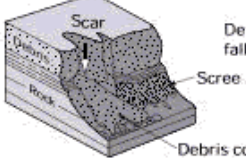
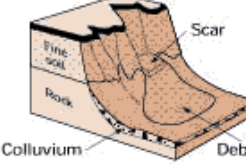
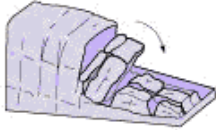
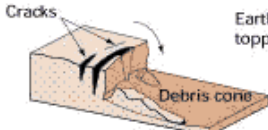
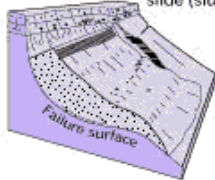
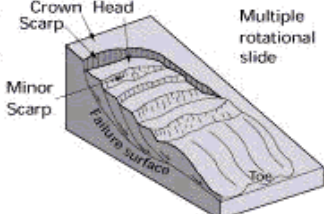
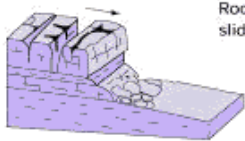
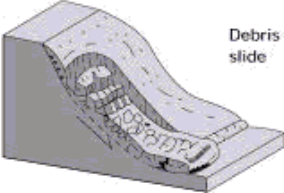
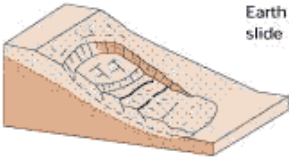
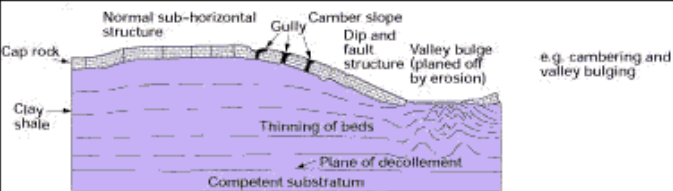
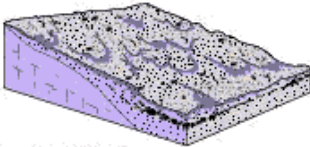
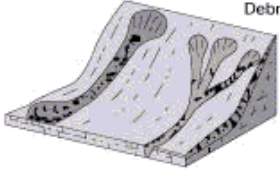
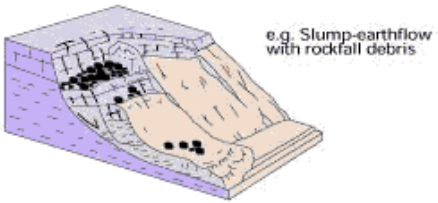
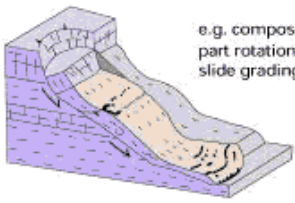
Material		ROCK	DEBRIS	EARTH
Movement type				
FALLS		 Rock fall	 Debris fall Scree Debris cone	 Earth fall Colluvium Debris cone
		 Rock topple	 Debris topple Debris cone	 Earth topple Debris cone
SLIDES	Rotational	 Single rotational slide (slump) Failure surface	 Multiple rotational slide Crown Scarp Head Scarp Minor Scarp Failure surface Toe	 Successive rotational slides
	Translational (Planar)	 Rock slide	 Debris slide	 Earth slide
SPREADS	 Earth spread Cap rock Normal sub-horizontal structure Gully Camber slope Dip and fault structure Valley bulge (planned off by erosion) Thinning of beds Plane of décollement Competent substratum e.g. cambering and valley bulging			
FLOWS	 Solifluction flows (Periglacial debris flows)	 Debris flow		 Earth flow (mud flow)
COMPLEX	 e.g. Slump-earthflow with rockfall debris		 e.g. composite, non-circular part rotational/part translational slide grading to earthflow at toe	

Figure 1-1 - Classification of type of landslides (Modified after Varnes, 1978).

5) LATERAL SPREADS consisting of a mass movement dominated by lateral extension and accompanied by shear or tensile fractures, as usually occur on very gentle slopes or flat terrains. The failure is caused by liquefaction of saturated, often loose and cohesionless sediments (usually sands and silts), generally triggered by a strong earthquake ground motions from high magnitude events. When coherent material, either rock or soil, rests on a potentially liquefiable stratum, the upper unit may undergo fracturing and extension and may then subside, translate, rotate, disintegrate, or flow. Lateral spreading in fine-grained materials on shallow slopes is usually a progressive phenomenon: the failure starts suddenly in a small area and spreads rapidly afterward. Often, the initial failure is a rotational landslide, but in some materials movement occurs for no apparent reason.

Combination of two or more of the above types is usually denoted as a **COMPLEX LANDSLIDE**.

### **1.3 LANDSLIDE TRIGGERINGS**

Landslides can be promoted by different factors (geological, morphological, physical and human among the others), while the term “trigger” commonly refers to an external stimulus that causes an immediate response in terms of landslide activity. Landslide triggering factors which will be treated in this Deliverable are:

1) RAINFALLS In most of the cases, the main trigger of landslides is heavy or prolonged rainfall. Generally, a landslide triggered by rainfall is usually related to an exceptional short lived event, such as the rainfall associated with a particularly intense thunderstorm, or in the opposite a long duration rainfall event with lower intensity, or a combination of both. Reduction of effective material strength by percolating water is generally considered as the primary cause of rainfall induced landslides.

2) EROSION Failures can be triggered by undercutting of the slope by a river, especially during a flood, or by bank and lateral erosion in coastal settings, especially within clay slopes and fissured material. Undercutting and excavation reduces stability by increasing the gradient of the slope and by removing toe weighting.

Landslides such as debris flows may initiate by mobilization of a channel bed due to surface erosion due to water flow

3) SNOWMELT Particularly in mountain areas, snowmelt can be a key mechanism in the landslide initiation by a sudden increase of temperature, leading to rapid melting of the snow pack. Then, the water infiltrate into the ground and, in the presence of underlying impervious layers of frozen soil or rock, leads to a rather rapid increase of soil pore pressure. Such an effect can be enhanced by precipitation, adding groundwater to the system and accelerating at the same time the rate of thawing.

4) WEATHERING Prolonged weathering of bedrock causes the reduction of material strength, leading to the creation of a regolith layer weaker than the parent rock, which may slide.

5) EARTHQUAKES Several area prone to landslides have experienced at least moderate ground motion intensities in recorded times. The occurrence of earthquakes in steep landslide-prone areas greatly increases the likelihood that landslides will occur, due to the ground shaking itself or caused by the induced dilation of soil materials, which allows rapid infiltration of water right afterwards. Strong earthquakes may cause widespread landsliding and other ground failure (i.e. liquefaction).

6) VOLCANIC PROCESSES Magmatic intrusions or phreatic explosions are among the most prominent factors at triggering the failure in volcanic edifices. Volcanic lava may induce high rates of thawing, causing volcanic debris flows (also known as lahars) constituted by a deluge of rock, soil, ash, and water that accelerate rapidly on the steep slopes of volcanoes.

## 2 GEOTECHNICAL ASPECTS OF LANDSLIDES TRIGGERING (SGI-MI)

### 2.1 INTRODUCTION

The identification and modelling of the processes that may trigger movements and, in extreme cases, uncontrolled failure of natural and artificial slopes form an essential part of landslide hazard and risk assessment studies.

This chapter provides a common framework for the characterization and evaluation, from a geotechnical viewpoint, of the different landslide types and mechanisms observed in practice in the wide variety of geosystems discussed in this Report.

As shown in Figure 2-1, in the simplest case of a slope of finite height and infinite lateral extent in homogeneous rigid-perfectly plastic material characterized by the Mohr-Coulomb failure criterion with effective cohesion  $c'$ , effective angle of shear resistance  $\phi'$ , movement along cylindrical surfaces and no external loads, with some well known simplifications static considerations lead to the following stability equation (Bishop, 1965):

$$F = \frac{\sum [c' \cdot l + (P - u \cdot l) \cdot \tan \phi']}{\sum W \cdot \sin \alpha} \quad [2-1]$$

where:

$F$  = ratio between the shear strength ( $\tau_r$ ) mobilized along the cylindrical surface considered in the analysis and the driving shear stress ( $\sum \tau_d$ )

$l$  = width of  $i^{th}$  slice

$u$  = pore pressure acting on the base of the  $i^{th}$  slice

$W$  = total weight of the  $i^{th}$  slice

$$P = W - \frac{1}{F \cdot m_\alpha} (c' \cdot l \cdot \sin \alpha - u \cdot l \cdot \tan \phi' \cdot \sin \alpha)$$

$$m_\alpha = \cos \alpha \left( 1 + \frac{\tan \alpha \cdot \tan \phi'}{F} \right)$$

$\alpha$  = as defined in Figure 2-1.

Similarly, in the case of a wedge of finite height and infinite lateral extent with a vertical back surface and basal shear plane inclined at a slope  $\alpha$  towards the free face, characterized by the same Mohr Coulomb failure criterion, static considerations lead to the stability equation defined in Figure 2- 2.

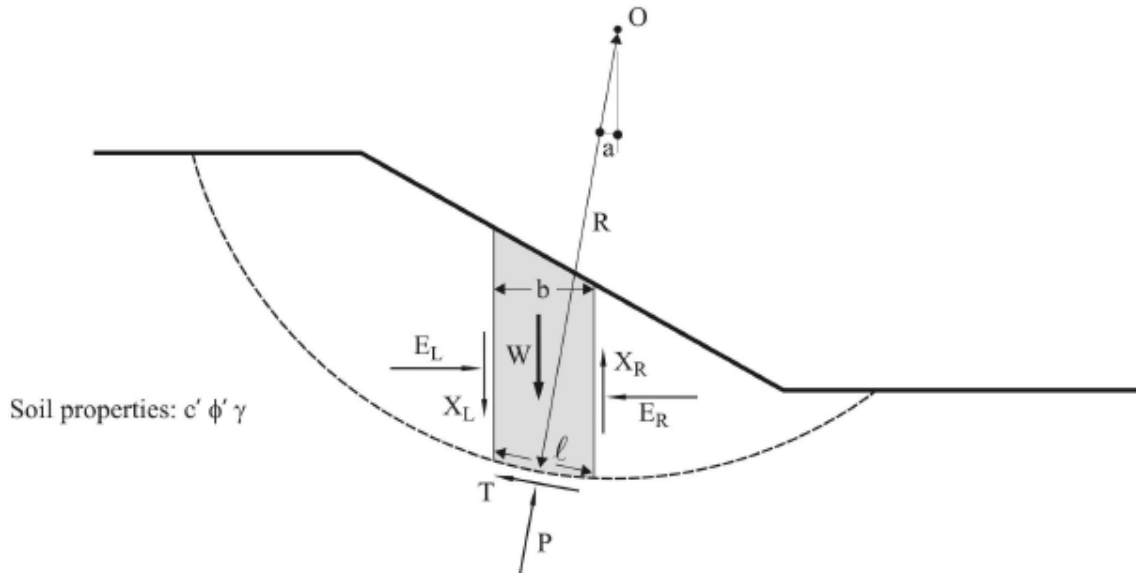
The factors which determine the triggering of movements can be clearly identified in Equation [2-1], independently of the causative processes and the complexity of the specific geosystem under consideration:

- a) increase in driving shear stress  $\sum \tau_d$
- b) decrease in shear strength  $\sum \tau_r$

The most common causative processes are listed in Table 2-1 (adapted from Leroueil, 2001). Combinations of (a) and (b) often act simultaneously as a direct result of external processes, as in the case of basal erosion or excavations, which can cause both an increase in  $\tau_d$ , through

**BISHOP'S SIMPLIFIED METHOD OF SLICES**

Failure is assumed to occur by rotation of a block of soil on a cylindrical slip surface centred in O. By examining overall moment equilibrium about O an expression for the factor of safety is obtained. It is assumed that the interslice forces are horizontal.



For slice shown: at base - normal stress  $\sigma$ , shear stress  $\tau$ , pore pressure  $u$

Mohr-Coulomb failure criterion:  $s = c' + (\sigma - u) \tan \phi'$   
Mobilized shear strength  $\tau = s/F$  where  $F$  is factor of safety

$$\text{Now } P = \sigma l, \quad T = \tau l, \quad \text{so } T = \frac{l}{F} (c' + (P - ul) \tan \phi') \quad (1)$$

$$\text{Resolve vertically: } P \cos \alpha + T \sin \alpha = W - (X_R - X_L)$$

Assuming  $X_R = X_L = 0$  (i.e interslice forces horizontal)

$$P = [W - \frac{l}{F} (c' \sin \alpha - u l \tan \phi' \sin \alpha)] / m_\alpha \quad (2)$$

$$\text{where } m_\alpha = \cos \alpha (1 + \tan \alpha \frac{\tan \phi'}{F})$$

$$\text{Overall MOMENT equilibrium (about O): } \Sigma WR \sin \alpha = \Sigma TR \quad (3)$$

Rearranging and substituting for  $T$  gives:

$$F_m = \frac{\Sigma (c' l + (P - ul) \tan \phi')}{\Sigma W \sin \alpha} \quad (4)$$

As this equation contains  $F$  on both sides it has to be solved iteratively. Convergence is usually quick and so the method is usable for hand calculation, although it is time consuming.

**Figure 2-1 - Bishop's simplified method of slices (Nash, 1987).**

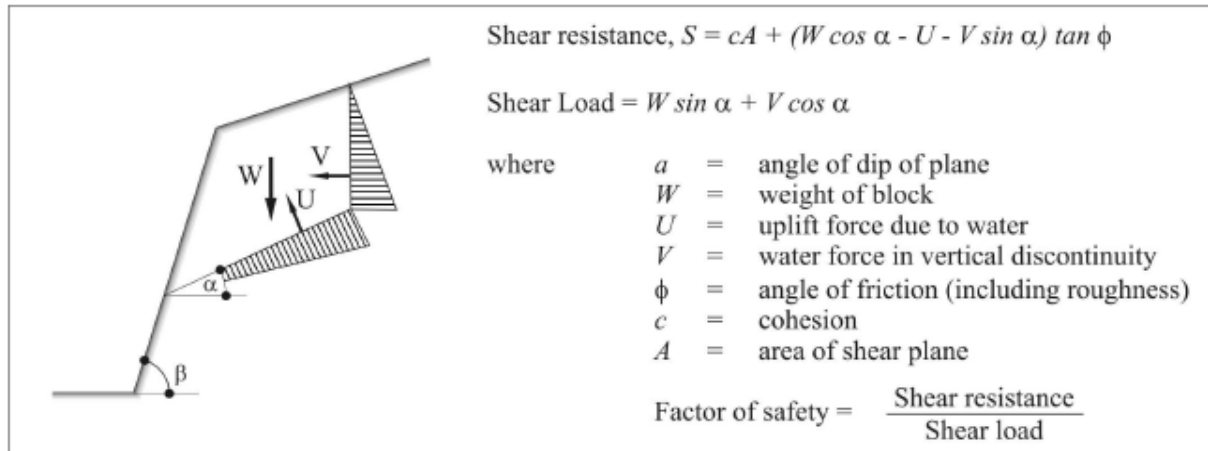


**Figure 2-2 - Analysis of sliding block in rock (Hencher, 1987).**

increased slope angle and/or height, or a decrease in  $\tau_r$ , through a reduction in total and effective stress.

More subtly, combinations of (a) and (b) may also occur simultaneously and interactively as a result of internal (destruction/damage) processes in the geomaterials, as will be discussed later.

Considering how triggering factors and processes operate in specific geosystems and how they determine the type and mechanism of movement, it is clear that the whole subject is highly complex, since the same triggering factor or process can result in significantly different outcomes in terms of landslides hazard and, consequently, risk. For example, similar basal erosion or excavation will cause completely different types of movement in “quick clays” and in “mechanically overconsolidated clays”, resulting in significant differences in terms of type, magnitude and rate of movement, and therefore in completely different risk profiles.

**Table 2-1 - Triggering factors with examples of common causative processes (adapted from Leroueil, 2001).**

Triggering factor	Common causative processes
Increase in driving shear stress $\tau_d$	<ul style="list-style-type: none"> <li>- Erosion or excavation at the toe</li> <li>- Surcharging at the top</li> <li>- Rapid drawdown</li> <li>- Fall of rock onto the slope and other impulsive loading</li> <li>- Earthquake</li> </ul>
Decrease in shear strength $\tau_r$	<ul style="list-style-type: none"> <li>- Infiltration due to rainfall, snowmelt, irrigation, leakage from utilities</li> <li>- Construction activities, e.g. pile driving</li> <li>- Weathering (rebound/swelling, physical, chemical)</li> <li>- Fatigue and excess pore pressure due to cyclic loading</li> </ul>
<p>Note: Many processes affect both <math>\tau_d</math> and <math>\tau_r</math>; association to one or the other in the table is indicative only</p>	

---

## 2.2 CLASSIFICATION SYSTEMS

The complexity of carrying out landslide hazard and risk assessments for real geosystems derives from the following main aspects:

- a) Wide variety of geosystems and geomaterials.
- b) Intrinsic difficulty in obtaining complete and reliable knowledge of the initial conditions of the slope in terms of the spatial variation of the type and characteristics of the different geomaterials in the system, geostatic stress and hydraulic and hydrogeological conditions (including groundwater chemistry) even when resorting to “state of the art” site investigation techniques.
- c) Complex behaviour of geomaterials, characterized by laws and parameters which may vary with the type of geomaterial and its initial conditions and the stage of movement (pre-failure; failure; post-failure and reactivation).
- d) Variations of stress state ( $\tau_d$ ) and strength ( $\tau_r$ ) over a wide variety of time scales, from minutes to centuries, as a result of the time dependent behaviour of geomaterials and of external variations in hydraulic and hydrogeological conditions (including groundwater chemistry).
- e) Wide variety of climatic conditions and possible evolution with time.

This complexity is reflected in the wide variety of type, magnitude and rates of movements observed in practice.

Several classifications have been proposed to classify the different types of slope movements in relation to the type of material in which they occur (Varnes, 1978; Hutchinson, 1988; Cruden & Varnes, 1996).

These classifications focus on geomorphological aspects, describing the types of movement in great detail, but typically relating them to broad and ill defined categories of geomaterials (“Rock”; “Debris”; “Earth”).

In so far as the type of movement is governed by the mechanical behaviour of the material involved and this in turn depends on complex combinations of factors as described above, attempts have been made to refine and supplement geomorphological classifications with additional details on the nature, state and geotechnical characteristics of the geomaterials and the stage of movement.

For example, Carson (1976) examined the control exerted by liquidity index (or water content) in determining whether instability in clays occurs by flow or by sliding. Generally speaking, the type of movement in these materials can be placed in an order compatible with increasing water content of the failed material: falls; deep rotational slips; shallow rotational slips; translational or slab slides; earth flows and mud flows. Extending on this, it is evident how quick flows in sensitive clays with high water content fit in this pattern.

Building on the work of Skempton and Hutchinson (1969), Hutchinson (1988) proposed a geotechnical classification, also applicable to slope movements in clays, which focuses on the “soil fabric conditions”, distinguishing between first time slides in previously unsheared ground and slides on pre-existing shears, and on pore water pressure conditions, distinguishing between ‘undrained’, ‘drained’ and ‘intermediate’ conditions.

Based on the work of Vaunat et al. (1992), Vaunat et al. (1994), Leroueil et al. (1996) and Locat (1999, as reported by Leroueil, 2001) a more comprehensive geotechnical classification has been proposed (Leroueil, 2001), relating in a 3D matrix (Figure 2-3):

- Slope movement, as described in geomorphological classifications;
- Movement stage, classified as pre-failure, failure, post-failure, reactivation;
- Materials, as described in Figure 2-4.

Each relevant combination is characterized by (terminology as used by Leroueil, 2001):

- (a) constitutive laws and parameters;
- (b) predisposition factors;
- (c) triggering (or aggravating) processes
- (d) revealing factors, if any; and
- (e) consequences of movement.

Although still relatively simplistic in certain respects and certainly amenable to improvement, the classification of material types shown in Figure 2-4 broadly reflects the current understanding of the behaviour of different geomaterials in relation to the issue of slope stability as seen from a geotechnical point of view.

Two issues are of particular interest both for the correct application and/or for further development of this classification and for their significant impacts on the qualitative and quantitative evaluation of triggering processes in the different types of geomaterials:

- structure; and
- stress history.

Both structure and stress history derive from the geological history of the geosystem; at the same time they have a significant impact on:

- the occurrence and rate of those processes of progressive degradation of the materials usually referred to as “weathering”;
- the mechanical response of the geosystem to “weathering” and to other processes which affect either  $\tau_d$  or  $\tau_r$ , altering the equilibrium of the slope.

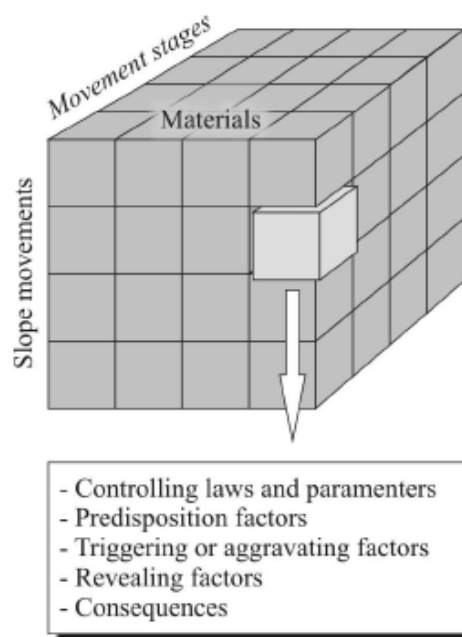


**Figure 2-3** - Schematic characterization of slope movements (Leroueil et al., 1996).

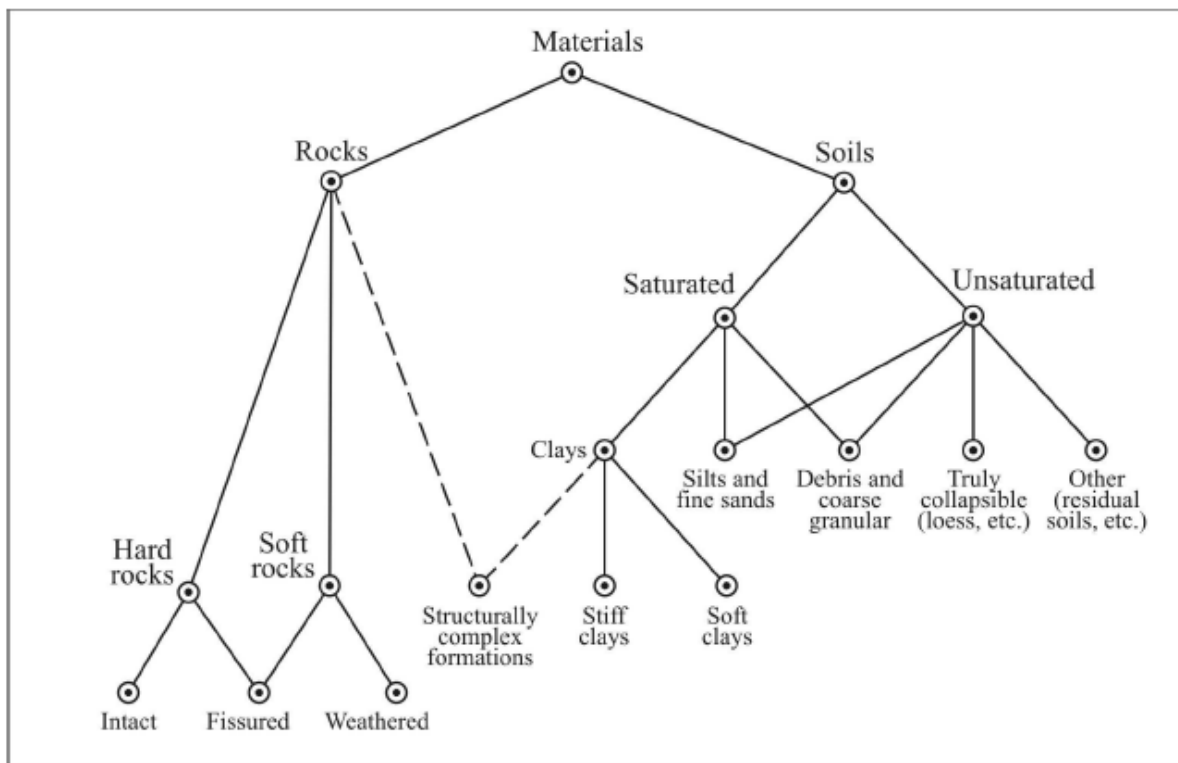


**Figure 2-4** - Material types considered in the geotechnical characterization of slope movements by Vaunat et al. (1994), modified by Locat (1999) (Leroueil, 2001).

As pointed out, for example, by Leroueil (2001), a good understanding of slope movements can be obtained only from a joint effort by geologists, geomorphologists and geotechnical engineers. As water is a major factor in slope behaviour, the contribution of hydrologists and hydrogeologists is also important. Slope movements must therefore be seen as a multidisciplinary domain.

### Structure

Picarelli (1991) and D'Elia et al. (1998) defined the following four types of structure at different scales:

- **mega structure** (tens of metres to kilometres), including faults, folds and other features, as induced for example by tectonic or deep gravitational movements, rebound etc.;
- **macro structure** (metres to tens of metres), including bedding planes, joints and major heterogeneities;
- **meso structure** (centimetres to decimetres), including fissures, pockets or laminae of soils of different grain size;
- **micro structure**, related to soil particles, their arrangement (fabric) and possible bonding between them (Mitchell, 1976).

At the scale of mega and macro structure, the presence of structural discontinuities can have a major impact on the behaviour of both soils and rocks compared to that of intact material,

both in terms of mechanical behaviour (strength, deformability) and in terms of mass permeability, hence the need to take this into account in any classification.

For given levels of triggering factors, these discontinuities can result in ‘first time’ slides or ‘reactivations’ in slopes which otherwise would be stable. Several examples exist of landslides which exploited pre-existing discontinuities not caused by previous sliding; for example, the Ancona (Italy) landslide exploited discontinuities of tectonic origin (Hegg, 1984, Santaloia et al., 2004).

Depending on the strength of the intact material and the nature and spacing of the discontinuities in relation to the scale of the problem, the behaviour of the slope may be governed by and needs to be modeled in terms of sliding on specific discontinuity or in terms of the strength of an ‘equivalent’ continuum (Hoek and Brown 1980a, b; Hoek and Bray, 1981).

It is important to identify whether these discontinuities are pre-sheared or not, since this may have significant effects on the shear resistance  $\tau$ , that can be mobilized along the discontinuity as will be highlighted later.

Meso and micro structure operate at a scale which is several times smaller than the slope. With the exception of localized effects on mega and macro discontinuities, meso and micro structure can be considered within the framework of an ‘equivalent’ continuum and will be treated in detail later.

#### Stress history and initial (natural) stress state

As a result of tectonic stresses and/or exhumation and rebound, in mudrock and in heavily mechanically overconsolidated clay, horizontal effective stresses are commonly equal to or even greater than vertical effective stress, as shown, for example, in Figure 2-5 (Taylor and Cripps, 1987). Similar or higher values have been quoted in rock by Hoek and Brown (1980a), irrespective of rock type.

While traditional limit equilibrium methods of slope stability analysis, as exemplified by Equation [2-1], do not consider the natural state of stress in their formulation, as highlighted for example by Duncan and Dunlop (1969), Vaughan (1994), Potts et al. (1997) and in the examples in Section 2.4 of this Report, numerical finite element analyses show that stress concentrations at the toe of a slope are significantly affected by the initial (natural) stress state. In materials prone to strain softening, the high stress concentrations associated with high values of earth pressure coefficient can initiate progressive failure, i.e. the progressive propagation of a discontinuity through the soil or rock mass where high localized shear strains have forced localized ‘failure’ whereas post failure conditions exist over part of the sliding surface even before any significant movement has taken place.

### **2.3 GEOTECHNICAL CLASSIFICATION AND MODELLING OF SATURATED GEOMATERIALS**

With reference to the geotechnical classification of geomaterials shown in Figure 2-4, this Section discusses the geotechnical behaviour of saturated soils and rock with a view to providing an insight into the underlying physical mechanisms, as a basis for a possible refinement and clarification of the classification and to provide a rational basis for defining appropriate constitutive modelling and parameters for advanced numerical analysis of landslide triggering.

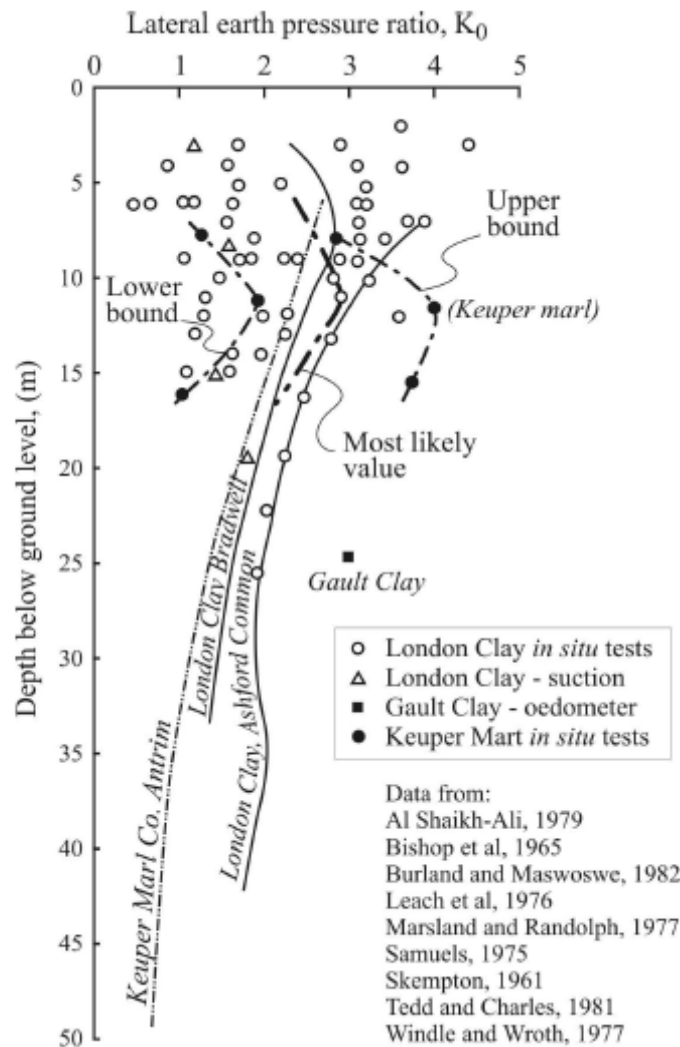


**Figure 2-5** - Distribution with depth of horizontal stresses (expressed as  $k_0$ ) in UK overconsolidated clays (Taylor and Cripps, 1987).

For a detailed discussion of unsaturated soils, reference shall be made to the reports from other work packages (WP 1.2 in particular), which are specifically devoted to this subject.

### 2.3.1 “Fine grained materials”

For the purposes of this Report, “fine grained materials” refers to those materials which, by virtue of their mineralogical composition and grain size, are characterized and influenced by significant interparticle “surface forces” (Lambe and Whitman, 1968; Mitchell, 1976), collectively referred to as “clays” for simplicity.

#### 2.3.1.1 Intact clayey material (importance of the microstructure)

The behaviour of homogeneous, continuous (not fissured) clay material depends both on the void ratio and the current stress state, as implied by the principles of Critical State Soil

Mechanics (Roscoe et al., 1958; Schofield and Wroth, 1968), and on the microstructure (fabric and bonding, Mitchell, 1976) of the material. The presence of microstructure has several implications (Burland, 1990; Leroueil and Vaughan, 1990; Leroueil, 1998) and determines the selection of the constitutive model to be used to replicate and predict the behaviour of the material (Nagaraj and Miura, 2001; Rocchi et al., 2003).

The most effective techniques to identify the presence of microstructure are:

- a) comparing the ‘initial’ state and the compression curve of the natural material (‘undisturbed’ specimens) as given by the voids ratio and by the mean or vertical geostatic effective stress with the isotropic or oedometric compression curve (intrinsic compression line – ICL) of material reconstituted in the laboratory at a moisture content not less than 1.5 times the Liquid Limit (Burland, 1990), taking care not to modify the porewater chemistry in the process;
- b) comparing the behaviour in drained and undrained triaxial tests of ‘undisturbed’ specimens of the natural material reconstituted to the geostatic effective stress conditions in situ according to the Bjerrum (1973) procedure with that of material reconstituted in the laboratory as described above, consolidated as necessary to replicate analogous  $k_o$  and void ratio conditions as the reconstituted ‘undisturbed’ specimen.
- c) comparing the shear wave velocity  $V_s$  determined in situ on natural material by means of cross-hole tests with that determined in the laboratory by means of bender elements on specimens reconstituted as described above (Shibuya et al., 1999). A similar comparison with the  $V_s$  of reconstituted ‘undisturbed’ specimens (Bjerrum, 1973 procedure) allows the sample disturbance to be evaluated, providing useful information on the validity of the comparisons described at points (a) and (b) above.

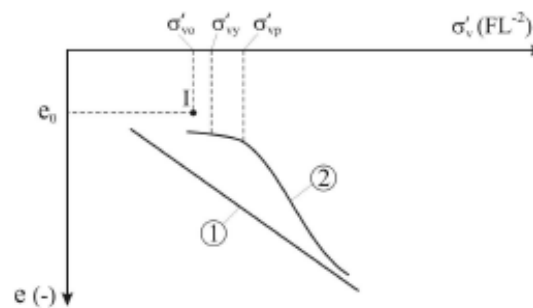
According also to Nagaraj and Miura (2001), the following cases can occur (in brackets the corresponding terminology used by them):

**CA Clays with initial states above the ICL (naturally cemented clays), Figure 2-6**

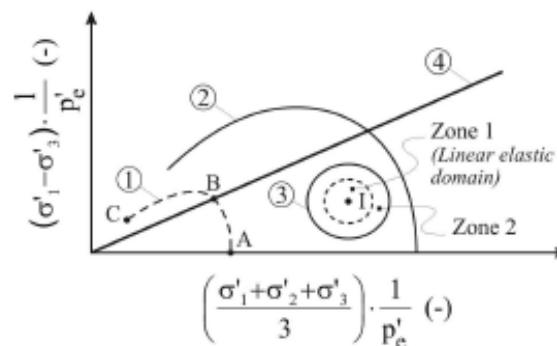
Initial states located above the intrinsic compression line are indicative of metastable microstructure. With reference to the framework proposed by Jardine et al. (1991) and Jardine (1992), in their natural state these materials have the following characteristics:

- Different Limit State Surfaces between natural and reconstituted materials. The Limit State Surface, representing the “gross yield” of the natural material is outside that of reconstituted material and is strain rate dependent.
- Conventional (or apparent) vertical preconsolidation pressure  $\sigma_{vp}$  greater than the geostatic vertical effective pressure.
- Zones around the point representing the initial effective stress state within which the behaviour is linear elastic (Zone 1) and non-linear elastic (Zone 2).
- Outside Zone 2, even within the Limit State Surface of the natural material, generation of destruction processes with associated irreversible visco-plastic strains and strain rate dependent behaviour; hence, the outer boundary of Zone 2 represents the “true yield” of the natural material. The volumetric component of the visco-plastic strains for states outside the Limit State Surface of the reconstituted material results in contractant behaviour, (i.e. reduction in void ratio or development of positive excess pore pressure in drained or undrained conditions respectively).

- As a consequence of the destruction process and of the associated visco-plastic strains taking place in the pre-failure stage up to failure and of the additional remoulding energy delivered to the material in the post-failure (propagation) stage, the Limit State Surface of the natural material shrinks, leading to conditions which may be governed by the behaviour of the reconstituted material where all the microstructure has been removed (Aversa et al., 1993; Cotecchia and Chandler, 1997; Loroueil, 1998; Rocchi et al., in preparation). In undrained conditions, the destruction processes may lead to development of high excess pore pressures and to a substantial reduction of undrained shear strengths from peak to remoulded conditions; in the extreme case represented by “quick clays” (Torrance, 1987), the remoulded material may behave as a fluid, making these clays particularly susceptible to landslide activity and dramatic geotechnical failures (Eden et al., 1971, Tavenas et al., 1971). Considering typical failure and post failure conditions and mechanisms, residual effective strength envelopes are of secondary significance in these materials.



- ① Oedometric curve of reconstituted material (ICL<sub>0e</sub>)
- ② Oedometric curve of natural material
- I Initial state of natural material



- ① Limit state surface of reconstituted material
  - { A-B Roscoe-Rendulic yield surface
  - { B-C Hvorslev failure surface
- ② Limit state surface of natural material (“gross yield”)
- ③ “True yield” surface of natural material
- ④ Critical state line
- I Initial stress state of natural material

**Figure 2-6 - Basic elements of clay behaviour – Material type CA.**

In these materials the preconsolidation pressure  $\sigma_{vp}'$  as (typically) determined conventionally from oedometer tests is due primarily, if not exclusively, to bonding, rather than mechanical preconsolidation, and as such it is better referred to as “apparent” preconsolidation pressure; it is strain rate dependent and does not reflect the “true yield” of the natural material; in oedometric conditions the “true yield” stress  $\sigma_{vy}$  is significantly lower than  $\sigma_{vp}'$  (see Bjerrum, 1967a; Larsson et al. 1997; Rocchi et al., 2003; Rocchi et al., 2006; Rocchi et al., 2007).

For the same reason, the earth pressure coefficient at rest  $k_0$  cannot be evaluated from empirical formulae based on the behaviour of the material under oedometric (1D) stress relief. The behaviour of these materials can be reproduced realistically only by means of elasto-viscoplastic constitutive models which simulate appropriately in the time domain the effects of progressive destruction of the microstructure (see for example Adachi et al., 1996; Kim and Leroueil, 2001; Rocchi et al., 2003; Kimoto and Oka, 2005; Hinchberger and Qu, 2009 and Rocchi et al., in preparation).

In relation to the overburden and degree of bonding, these clays may appear either as ‘soft clays’ or as ‘stiff/hard clays’ as defined by common classifications. The use of this terminology in the classification of Figure 2-4 does not convey sufficient information to distinguish this type of clays and their associated behaviour from the other types of clays described below.

For this reason these clays need to be classified also in terms of “sensitivity”. Commonly, sensitivity is defined as the ratio of the undisturbed to the remoulded undrained shear strength, as determined for example by in situ vane tests. On account of the long tradition of the Norwegians in investigating the properties of these materials, it seems appropriate to continue to measure sensitivity in terms of strength (“strength sensitivity”); however, it is useful to classify clays also in terms of “stress sensitivity”, as suggested by Cotecchia and Chandler (2000); for the sake of simplicity, in this Report “stress sensitivity” is defined as the ratio of the geostatic vertical effective stress ( $\sigma_{vo}'$ ) to the equivalent vertical effective stress on the ICL corresponding to the in situ void ratio ( $\sigma_{ve}'$ ); by definition,  $\sigma_{vo}'/\sigma_{ve}'$  is greater than 1 in material type CA and lower than 1 in material type CB as defined below.

Many examples are well documented in the technical literature of clays that fall into this category (Nagaraj and Miura, 2001). In Europe they are encountered, for example, in Norway (Drammen clay, Bjerrum, 1967a; etc.), Sweden (Väsby clay, Chang, 1981; etc.), the U.K. (Bothkennar clay, Burland, 1990, Hight et al., 1992; etc.) and Italy (Pisa upper clay, Berardi et al., 1991, Rampello et al., 1996, Mesri et al., 1997, Rocchi et al., in preparation; etc.). Further afield, they are encountered, for example, in Canada (Batiscan clay, Leroueil et al., 1985; Berthierville clay, Kabbaj et al., 1988, Leroueil et al., 1988, Kim and Leroueil, 2001; etc.) and in Japan (Ariake clay, Hanzawa et al., 1990, Tanaka et al., 1996; Osaka clay, Adachi et al., 1995, Rocchi et al., 2006; etc.). Indeed most mechanically normally consolidated or only slightly mechanically overconsolidated natural clays fall into this category (Burland, 1990).

The typical response of CA materials to excavation or basal erosion is illustrated in the examples in Section 2.4.

**CB** Clays with initial states *below* the ICL (mechanically overconsolidated clays with or without cementation), figures 7 and 8

Clays with initial states below the ICL can be either without (type CB1) or with (type CB2) bonding; their microstructure is stable at the initial stress state in situ irrespective of the presence of bonding.

With reference to the general framework presented here, in their natural state type CB1 materials have the following characteristics:

- Limit State Surface practically coincident with that characteristic of the reconstituted material.
- Conventional vertical preconsolidation pressure  $\sigma_{vp}'$  greater than the geostatic vertical effective pressure  $\sigma_{vo}'$ ;
- Zones around the point representing the initial effective stress state within which the behaviour is linear elastic (Zone 1) and non-linear elastic (Zone 2).
- Outside zone 2 up to the Limit State Surface and on the Limit State Surface, mainly plastic behaviour; for all practical purposes visco-plastic strains and strain rate dependency can be considered negligible; the volumetric component of the plastic strains result in a moderately contractive or dilatant behaviour depending on the

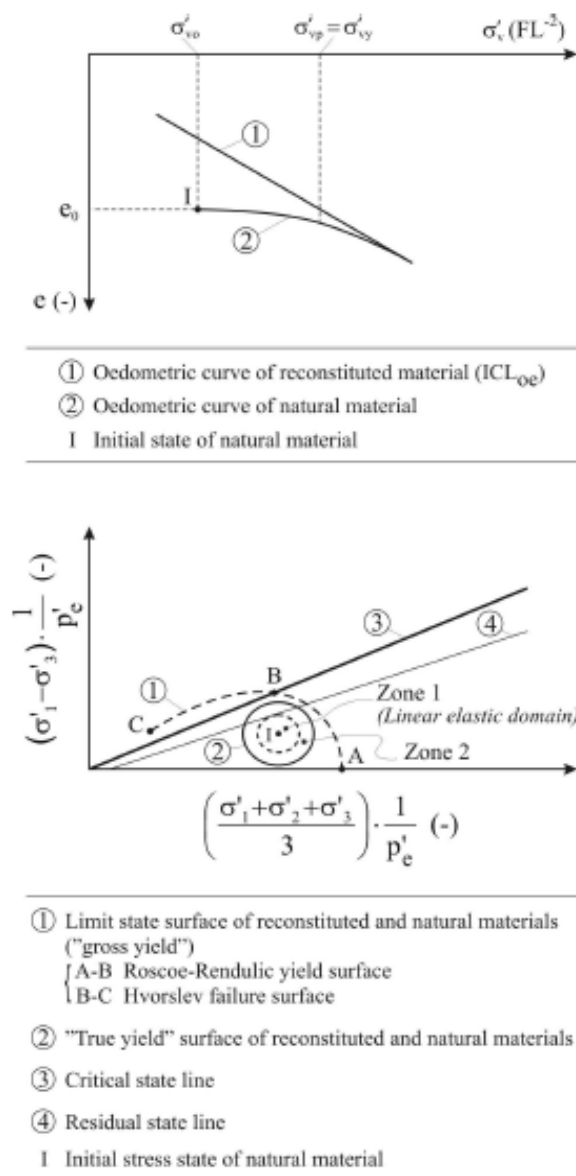
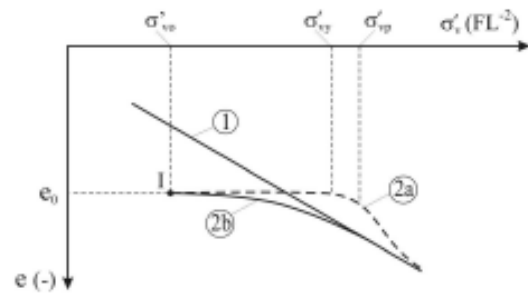


**Figure 2-7 - Basic elements of clay behaviour – Material type CB1.**

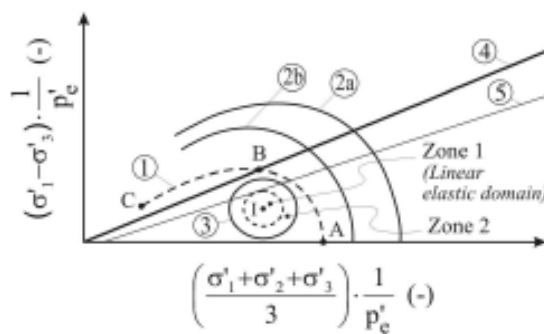
distance of the current state from the ICL, becoming progressively more dilatant as this distance increases, implying a greater drop in resistance from peak to critical state, according to the principles of Critical State Soil Mechanics; under certain circumstances governed essentially by clay contents and activity, water chemistry and effective confining pressure, in the more highly sheared zones significant lowering of the effective strength envelope may occur, from critical state to ‘residual’ (see for example Skempton, 1985).



- ① Oedometric curve of reconstituted material ( $ICL_{0e}$ )
- ②a Oedometric curve of natural material with strong bonds
- ②b Oedometric curve of natural material with weak bonds\*
- I Initial state of natural material

(\*) Bonds progressively lost during loading before reaching the  $ICL_{0e}$

For simplicity  $\sigma'_{vy}$  and  $\sigma'_{vp}$  are shown for the "strong bonds" case only.



- ① Limit state surface of reconstituted material
  - A-B Roscoe-Rendulic yield surface
  - B-C Hvorslev failure surface
- ②a Limit state surface of natural material with strong bonds ("gross yield")
- ②b Limit state surface of natural material with weak bonds ("gross yield")
- ③ "True yield" surface of natural material
- ④ Critical state line
- ⑤ Residual state line
- I Initial stress state of natural material

Figure 2-8 - Basic elements of clay behaviour – Material type CB2.

---

Conventional vertical preconsolidation pressure  $\sigma_{vp}'$  as typically determined from oedometer tests is practically linked only to mechanical pre-compression; in heavily mechanically overconsolidated clays,  $\sigma_{vp}'$  is not necessarily equal to the maximum vertical effective stress  $\sigma_{vmax}'$  experienced by the deposit; plastic strains during drained unloading may cause a partial loss of “memory” (Calabresi and Scapelli, 1985).

The earth pressure coefficient at rest  $k_o$  can be reasonably evaluated from empirical formulae based on the behaviour of the material under oedometric (1D) stress relief.

The behaviour of these materials can be reproduced by elasto-plastic constitutive models with volumetric and kinematic hardening capable of reproducing non-linearity also inside the Limit State Surface (see for example Al-Tabba and Wood, 1989; Stallebrass and Taylor, 1997).

Considering the geological history necessary to generate them, real materials whose initial states lies below the ICL tend to be also bonded to some extent, hence truly type CB1 materials are rare.

The presence of bonding between particles gives to type CB2 materials in their natural states the following characteristics:

- Different Limit State Surfaces between natural and reconstituted materials; the Limit State Surface, representing the “gross yield” of the natural material is outside that of reconstituted material and is strain rate dependent.
- Conventional or apparent vertical preconsolidation pressure  $\sigma_{vp}'$  greater than the geostatic vertical effective pressure  $\sigma_{vo}'$ .
- Zones around the point representing the initial effective stress state within which the behaviour is linear elastic (Zone 1) and non-linear elastic (Zone 2).
- Outside Zone 2, even within the Limit State Surface of the natural material, generation of destruction processes with associated irreversible visco-plastic strains and strain-rate dependent behaviour; hence the outer boundary of Zone 2 represents the “true yield” of the natural material. For current states below the ICL, the volumetric component of the plastic strains results in moderately contractive or dilatant behaviour depending on the distance of the current state from the ICL, becoming progressively more dilatant as this distance increases. For current states above the ICL, the behaviour is always contractive.
- As a consequence of the destruction processes and of the associated visco-plastic strains taking place in the pre-failure stage up to failure and of the additional remoulding energy delivered to the material in the post-failure (propagation) stage the Limit State Surface of the natural material shrinks, leading to the same conditions applicable to CB1 materials. For any specific set of conditions, a more significant drop from peak to post-peak resistance occurs compared to CB1 material due to loss of bonding, in addition to the effects of dilatancy (see for example Burland et al., 1996). As for CB1 materials, under certain circumstances governed essentially by clay contents and activity, water chemistry and effective confining pressure, in the more highly sheared zones significant lowering of the effective strength envelope may occur, from critical state to ‘residual’ (see for example Skempton, 1985).

In CB2 materials bonding results in the conventional vertical preconsolidation pressure  $\sigma_{vp}'$ , as typically determined from oedometer tests, being greater than would derive from mechanical preconsolidation alone. As such,  $\sigma_{vp}'$  is best referred to as the “apparent” preconsolidation pressure; it is strain rate dependent and does not reflect the “true yield” of the natural material.

---

The earth pressure coefficient at rest  $k_0$  depends both on the stress history and on the history of bonding in the deposit; the empirical formulae based on the behaviour of the material under oedometric 1D stress relief are rigorously applicable only when bonding formed after the current stress state has been achieved and the “true” (geological)  $\sigma_{vmax}'$  is known; where bonding developed before the end of stress changes,  $k_0$  cannot be evaluated on this basis.

The behaviour of these materials can be reproduced realistically only by constitutive models which simulate appropriately the effects of destruction processes; this can be done building on the models developed so far based on elasto-plasticity (see for example Gens and Nova, 1993; Rouiainia and Wood, 2000; Kavvadas and Amorosi, 2000; Amorosi and Kavvadas, 2000; Asaoka et al., 2000; Liu and Carter, 2002; Baudet and Stallebrass, 2004; Callisto and Rampello, 2004; Karstunen et al. 2005; Gens et al., 2005) or, better still, on elasto-viscoplasticity (see for example: Adachi et al., 1996; Kim and Leroueil, 2001; Rocchi et al., 2003; Kimoto and Oka, 2005; Hinchberger and Qu, 2009; Rocchi et al., in preparation, for soils and Nawrocki and Mroz, 1998; Adachi et al., 1998; Adachi et al., 1999; Adachi et al., 2005; Zhang et al., 2005 for rocks).

Many examples of these materials are well documented in the technical literature. In Europe they are encountered, for example, in the U.K. (London clay, Gasparre et al., 2007, Sorensen et al., 2007; etc.) and in Italy (Taranto clay, Cotecchia and Chandler, 1997; Plio-pleistocene clays along the Adriatic coastline at Ancona and Petacciato sites, Hegg, 1984; Lessloss, 2007; Todi, Vallericca and Pietrafitta clays, Central Italy, Burland et al., 1996; Georgiannou and Burland, 2001; etc.).

The typical response of CB1 and CB2 materials to stress relief and excavation or basal erosion is illustrated in the examples in Section 2.4.

**CO Clays with initial states on the ICL (normally consolidated clays with or without cementation), figures 9 and 10**

Clays with initial states on the ICL can be either without (type CO1) or with (type CO2) bonding; their microstructure is stable at the initial stress state in situ irrespective of the presence of bonding.

With reference to the general framework presented here, in their natural state type CO1 materials have the following characteristics:

- Limit State Surface practically coincident with that characteristic of the reconstituted material.
- Conventional vertical preconsolidation pressure  $\sigma_{vp}'$  equal to the geostatic vertical effective pressure  $\sigma_{vo}'$ .
- Zones within the Limite State Surface and with boundary surfaces passing through the point representing the initial effective stress state within which the behaviour is linear elastic (Zone 1) and non-linear elastic (Zone 2).
- Outside zone 2, within and on the Limit State Surface, mainly plastic behaviour; for all practical purposes visco-plastic strains and strain rate dependency can be considered negligible; the volumetric component of the plastic strains results in a moderately contractive or dilatant behaviour depending on the distance of the current state from the ICL, becoming progressively more dilatant as this distance increases, implying a greater drop in resistance from peak to critical state, according to the principles of Critical State Soil Mechanics; under certain circumstances governed essentially by clay contents and activity, water chemistry and effective confining pressure, in the

more highly sheared zones significant lowering of the effective strength envelope may occur, from critical state to ‘residual’ (see for example Skempton, 1985).

The earth pressure coefficient at rest  $k_0$  can be reasonably evaluated from empirical formulae based on the behaviour of the material under oedometric (1D) conditions.

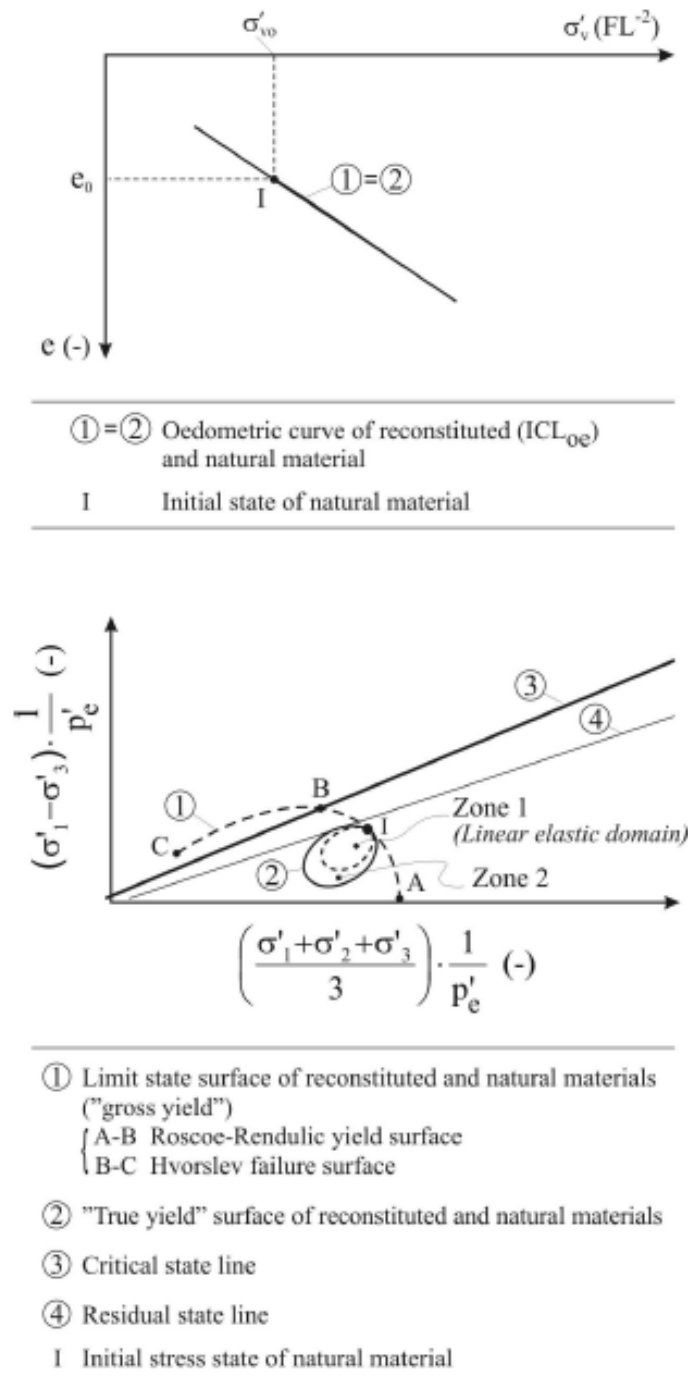


**Figure 2-9** - Basic elements of clay behaviour – Material type CO1.

The behaviour of these materials can be reproduced by elasto-plastic constitutive models with volumetric and kinematic hardening capable of reproducing non-linearity also inside the Limit State Surface (see for example Al-Tabba and Wood, 1989; Stallebrass and Taylor, 1997).

Considering the geological history necessary to generate them, real materials whose initial states lies on the ICL tend to be also bonded to some extent, hence truly type CO1 materials

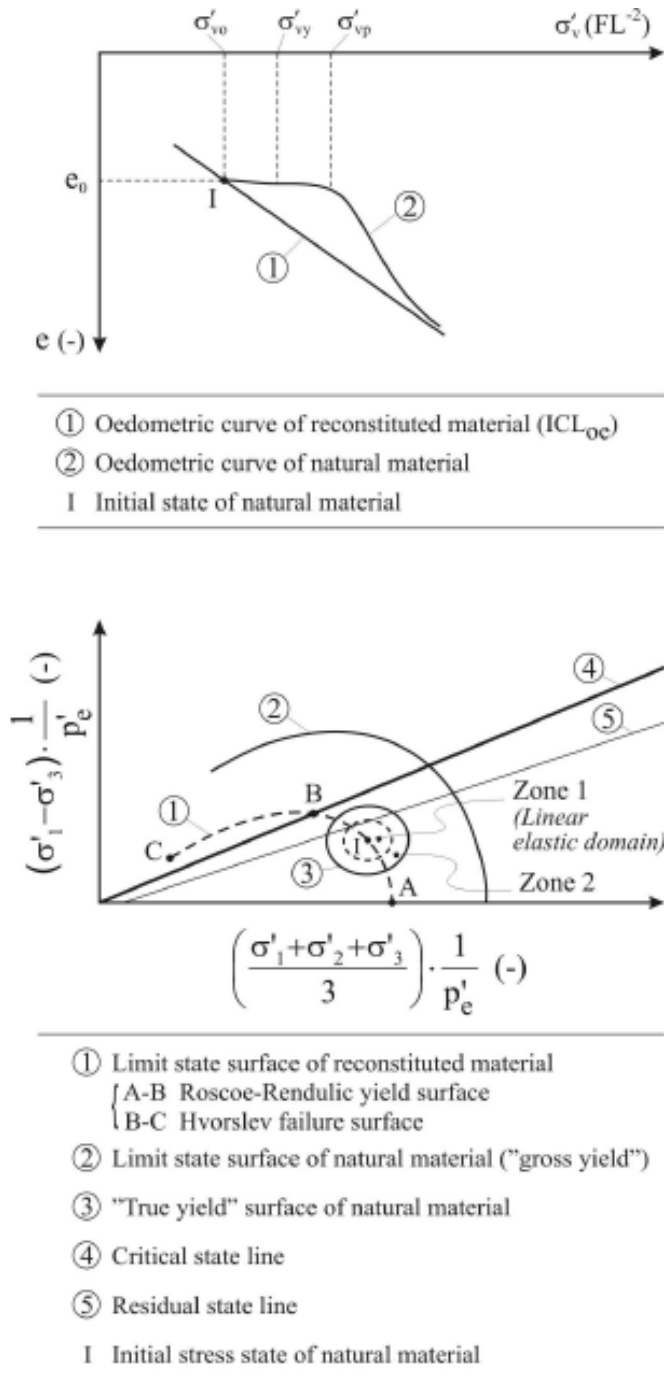


**Figure 2-10 - Basic elements of clay behaviour – Material type CO2.**

are rare; some example might be represented by Gosport clay (U.K.), recent deltaic Mississippi clay (U.S.A.), Troll field clay (North Sea, U.K. Sector) below 25 m depth (all these examples are taken from Burland, 1990) and Guasticce clay below 20 m depth (Rocchi et al., 1991). The presence of bonding between particles gives type CO2 materials in their natural states the following characteristic:

- Different Limit State Surfaces between natural and reconstituted materials; the Limit State Surface, representing the “gross yield” of the natural material is outside that of reconstituted material and is strain rate dependent.
- Conventional or apparent vertical preconsolidation pressure  $\sigma_{vp}'$  greater than the geostatic vertical effective pressure  $\sigma_{vo}'$ .
- Zones around the point representing the initial effective stress state within which the behaviour is linear elastic (Zone 1) and non-linear elastic (Zone 2).
- Outside Zone 2, even within the Limit State Surface of the natural material, generation of destruction processes with associated irreversible visco-plastic strains and strain-rate dependent behaviour; hence the outer boundary of Zone 2 represents the “true yield” of the natural material. For current states below the ICL, the volumetric component of the plastic strains results in moderately contractive or dilatant behaviour depending on the distance of the current state from the ICL, becoming progressively more dilatant as this distance increases. For current states above the ICL, the behaviour is always contractive.
- As a consequence of the destruction processes and of the associated visco-plastic strains taking place in the pre-failure stage up to failure and of the additional remoulding energy delivered to the material in the post-failure (propagation) stage the Limit State Surface of the natural material shrinks, leading to the same conditions applicable to CO1 materials. For any specific set of conditions, a more significant drop from peak to post-peak resistance occurs compared to CO1 material due to loss of bonding, in addition to the effects of dilatancy (see for example Burland et al., 1996). As for CO1 materials, under certain circumstances governed essentially by clay contents and activity, water chemistry and effective confining pressure, in the more highly sheared zones significant lowering of the effective strength envelope may occur, from critical state to ‘residual’ (see for example Skempton, 1985).

In CO2 materials bonding results in the conventional vertical preconsolidation pressure  $\sigma_{vp}'$ , as typically determined from oedometer tests, being greater than would derive from mechanical preconsolidation alone. As such,  $\sigma_{vp}'$  is best referred to as the “apparent” preconsolidation pressure; it is strain rate dependent and does not reflect the “true yield” of the natural material.

The earth pressure coefficient at rest  $k_0$  depends both on the stress history and on the history of bonding in the deposit; the empirical formulae based on the behaviour of the material under oedometric 1D stress conditions are rigorously applicable only when bonding formed after the current stress state has been achieved and the “true” (geological)  $\sigma_{vmax}'$  is known; where bonding developed before the end of stress changes,  $k_0$  cannot be evaluated on this basis.

As for the CB2 materials, the behaviour of CO2 materials can be reproduced realistically only by constitutive models which simulate appropriately the effects of destruction processes; this can be done building on the models which have been developed so far based on elasto-plasticity or, better still, on elasto-viscoplasticity.

**Table 2-2 - Time for dissipation of excess pore pressures in clay slopes**  
(Taylor and Cripps, 1987; Leroueil, 2001)

Clay/clay shale	Material type	Slope height H (m)	Time for excess pore pressure dissipation $t_{eq}$	Reference
La Bosse-Galin (France)	CA	4÷5	4 to 10 days	Blondeau and Queyroi, 1976
Mexico City (Mexico)	CA	4÷8	1 month	Alberro, 1979
Hede (Sweden)	CA	5.5	2 months	Rankka, 1994
Kimola (Finland)	CA	12	3 months	Kankare, 1969
Saint-Hilaire (Canada)	CA	8	6 months	Lafleur et al., 1988a; Lafleur et al., 1988b; Laflamme and Leroueil, 1999
Riviere Vachon (Canada)	CA	24	6 months	Laflamme and Leroueil, 1999
London (UK)	CB2	6÷12	50 years	Skempton, 1977; Chandler, 1984
Isle of Sheppey (UK)	CB2	44	2000 years	Bromhead and Dixon, 1984
Panama mudrocks	CB2	-	> 55 years	Banks et al. (1975)
Bisaccia (Italy)	CB2 <sup>(*)</sup>	100	>10 <sup>5</sup> years	Fenelli and Picarelli, 1990; Di Nocera et al. 1995
Pierre shale (USA)	CB2	-	>10 <sup>6</sup> years	Neuzil, 1993
Note: (* ) Heavily fissured				

### Final considerations on intact clays

The strain rate dependent behaviour and its engineering consequences (creep, stress relaxation, fatigue) are particularly significant in bonded materials where destruction processes (progressive breakdown of bonds) may be activated by changes of stress or strain in the deposit.

Creep, stress relaxation and fatigue phenomena have been observed in the laboratory, where fully controlled conditions can be determined, for a wide variety of type CA materials (Bishop and Lovenbury, 1969; Marchand, 1982; Leroueil and Marques, 1996; Larsson, 1977; Tavenas et al., 1978), type CB2 materials (Bishop and Lovenbury, 1969; D'Elia, 1991; D'Elia, 1994) and rocks (Attewell and Farmer, 1973; Yoshinaka and Osada, 1974; Tien et al, 1990; Adachi et al., 1998; Aydan and Nawrocki, 1998).

Experimental evidence in the field of creep, stress relaxation and fatigue phenomena due only to breakdown of bonds are instead rare; in saturated clayey slopes, movements happening in the time domain may be due both to progressive breakdown of bonds and to other phenomena linked essentially to change in effective stresses in the slope due, for example, to variation of the hydraulic boundary conditions, dissipation of excess pore pressures still present in the slope as a consequence of artificial cuts or natural basal erosion, stress redistribution in the slope as a consequence of decay of the effective strengths from peak to residual conditions, etc.. Example of pore pressure equilibration phenomena are given in Table 2-2. Each case reported in the table is defined by the name of the clay, the material type (according to the classification described in this Section), the slope height (H), the time for pore pressure equilibration ( $t_{eq}$ ) and the reference.

In the simpler case represented by rapid cuts or basal erosion the time necessary to reach pore pressure equilibrium is strictly related to:

- Deformability characteristics of the clay which govern both the amount and sign of the excess pore pressure and the overall behaviour in the pre-failure and possibly failure stages; as the behaviour of the material is strongly non linear, the deformability characteristics may vary with time and need to be determined by appropriate elasto-plastic or, preferably, elasto-viscoplastic constitutive models.
- Permeability characteristics of the clay which may vary with time as a consequence of variation (increase) of void ratio and of joint/fissure development.
- Geometry of the slope (height and inclination).

The very short time necessary to reach pore pressure equilibrium observed in material type CA compared to that necessary to reach similar conditions in material type CB2 can be well understood in the light of the general behaviour described above for the different materials and of the following relationship proposed by Henkel (1960) for determining initial excess pore pressure ( $\Delta u$ ) as a function of stress changes:

$$\Delta u = \beta \cdot \left( \frac{\Delta \sigma_1 + \Delta \sigma_2 + \Delta \sigma_3}{3} \right) + \alpha \cdot \sqrt{(\Delta \sigma_1 - \Delta \sigma_2)^2 + (\Delta \sigma_2 - \Delta \sigma_3)^2 + (\Delta \sigma_3 - \Delta \sigma_1)^2} \quad [2-2]$$

where:

$\Delta \sigma_i$  = changes of total principal stress

$\alpha, \beta$  = excess pore pressure parameters.

As highlighted by Leroueil (2001), in rapid excavation (artificial or natural) there is a decrease in pore pressure (development of negative excess pore pressure) associated with reduction in mean total stresses.

In heavily overconsolidated clays of the type CB, the parameter  $\alpha$  is negative and the shear stresses generate additional negative excess pore pressure in such a way that the difference in pore pressure between the end of excavation and the steady state condition is significant.

On the other hand, in clays of the type CA the parameter  $\alpha$  is positive and the shear stresses generate positive excess pore pressure, compensating to some extent the negative excess pore pressure due to the change in mean total stresses. In these conditions, the resulting overall changes in pore pressure due to excavation can be quite small and dissipate quickly.

Back analyses of the pore pressure variation with time such as those reported in Laflamme and Leroueil (1999), where the excavation at Saint Hilaire has been simulated by finite element analyses assuming linear elasticity ( $\alpha = 0$ ), result in the need to assign unnecessarily high values of stiffness to the soil to match the observed rapid equilibration of excess pore pressures.

The examples in Section 2.4 show how the use of appropriate constitutive models in numerical FEM analyses is sufficient to replicate realistic pore pressure responses as discussed above without the need to invoke unrealistic stiffness parameters for the clay.

Further insight in the overall stress-strain time dependent behaviour of geomaterials is provided by Tatsuoka et al. (1999) and Tatsuoka et al. (2000).

Destruction processes in bonded materials can be activated also by isotropic stress relief (swelling); as highlighted by Leroueil (2001), two different situations may occur:

- The bonds are strong and the soil remains microstructured even at zero effective confining stresses; the soil has tensile strength;
- At some stage (yield), the bonds start progressively to break and damage to the microstructure begins to take place (Bishop et al., 1965; Calabresi and Scarpelli, 1985; Calabresi and Rampello, 1987; Rampello, 1989; Leroueil and Vaughan, 1990; Rampello, 1991).

More destructive effects can be caused by stress relief in oedometric or in more general stresses conditions, such as occur in sloping ground.

Considering the case represented by horizontal ground level (oedometric conditions) and clayey deposits of the type CO or CB, during unloading the material will have a propensity to expand and to increase in water content as a consequence of both the decrease of mean effective stresses and the increase of the deviatoric stresses. In bonded clays type CO2 or CB2, the expansion will be restrained compared to that occurring in unbonded clays type CO1 or CB1 until stress conditions are reached where the breakdown of bonds (destruction processes) and the formation of joint/fissures both parallel to the ground surface (Hofmann, 1966; Ferguson, 1967; Nicholson and Hough, 1967; Nichols, 1980) and with inclination compatible with passive earth pressure conditions (Terzaghi, 1961) begin to take place (Figure 2-11).

In hard clays and soft mudrocks, weathering profiles characterized by a reduction of effective strength envelopes, reduction of undrained shear strength ( $s_u$ ), increase of water content ( $w_n$ ), increase of fissures frequency are the hallmark of past and, presumably, still ongoing breakdown of bonds (destruction processes) and loss of dilatancy induced by stress relief. Typical examples of weathered profiles are reported by Cripps and Taylor (1981) on the basis of data from Peterson (1958) in Bearpow shale (Canada), Skempton and La Rochelle (1965) and Chandler and Apted (1984) in London clay (UK), Chandler (1969) in Keuper marl (UK), Chandler (1972) in Lias clay (UK), Spears and Taylor (1972) in Coal Measures mudrocks (UK), Russel and Parker (1979) in Lower Oxford clay (UK).

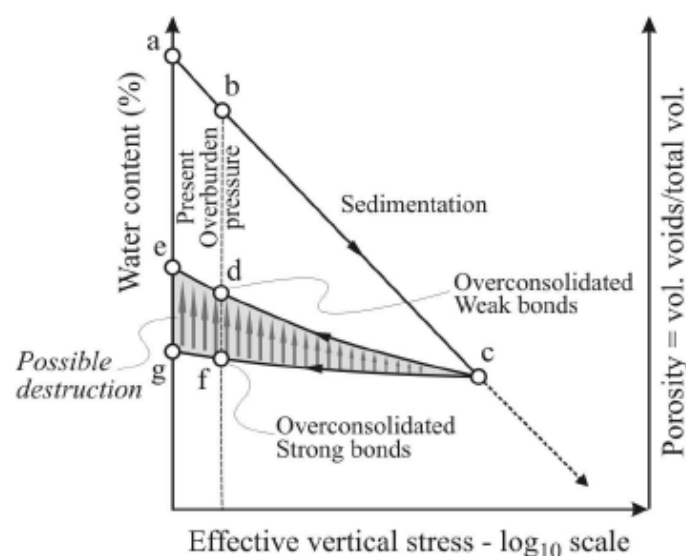


**Figure 2-11 - Schematic geological history of materials type CO and CB (modified from Bjerrum, 1967b and Fleming et al., 1970).**

The examples in Section 2.4 show how the use of appropriate constitutive model in numerical FEM analyses is sufficient to replicate realistic weathering profiles.

The depth and the degree of weathering caused by stress relief by erosion are governed essentially by the following factors:

- thickness of removed material;
- geometry of the slope (height and inclination);
- characteristics of the materials forming the slope;
- overlying recent deposits which slow down the weathering processes;
- rate of excess pore pressure dissipation.

Breakdown of bonds, loss of dilatancy and pore pressure equilibration are processes that happen in the time domain and govern the morphology and the style of slope failures. As reported by Taylor and Cripps (1987) “*mass instability can follow very soon after the formation of a steep slope; in the case of actively-eroding cliffs considered by Skempton and Hutchinson (1969) (see also Bromhead, 1978) slopes of about 30° can be produced by strong marine erosion. These rapidly become unstable so that successive stage of slope angle reduction takes place in increasing orders of time. In the case of steeper slopes instability occurs as deep-seated rotational sliding. Cliffs which have not been subjected to erosion for periods of between 30 and 150 years are found to rest at angles of between 13° and 20°. Hutchinson (1967) records that those cliffs are affected by shallow rotational slips. Freedom from basal erosion for periods of some hundreds of years, produces cliffs with inclinations of between 8° and 13° of which unstable ones are subjected to successive shallow rotational slips or minor surface processes. Unstable inland slopes which lie at angles of 8° to 12° are probably several thousand years old. For these slopes instability takes the form of markedly non-circular rotational slips or shallow translational slab slides*”.

Similar considerations have been reported by Richards and Lorriman (1987).

### **2.3.1.2 Jointed and fissured clayey material (importance of the mesostructure)**

Because of their brittle properties and the drop from peak to post-rupture strength, until reaching, at increasing strains, critical state and residual state strengths, most naturally, originally intact, clays can develop joints and fissures during geological unloading and/or tectonic activity.

Depending on the geological processes involved, the strength available along the discontinuities can be controlled by that mobilized at the post-rupture stage or at the residual state condition, leading to operational effective strength envelopes significantly lower than those characteristic of the intact material (Marsland and Butler, 1967; Marsland 1971; Marsland, 1974; Georgiannou and Burland, 2001).

Looking, for example, at the distribution of structurally complex clay formations and stiff jointed/fissured clays in Italy (Figure 2-12), two significant cases can be identified:

- The jointed/fissured, autochthonous Plio-Pleistocene clays of marine or lacustrine origin, outcropping along the Adriatic coast and in some internal areas (Esu, 1966; Manfredini et al., 1985; D’Elia et al., 1998); these clays belong to material type CB2, being, in their intact state, mechanically heavily overconsolidated and bonded;

- The intensely fissured, allochthonous clays of Cretaceous-Miocene age, sedimented in a marine environment, diffusely outcropping along the Appennine Chain (D'Elia, 1991; D'Elia et al., 1998); these clays too belong to material type CB2, but differ from the previous ones because they have been displaced by tectonics for great distances up to more than 100 km from their sediment basin in the Oligocene-Pliocene age (Dallan Nardi and Nardi, 1975; AGI, 1985).

In the case of jointed/fissured Plio-Pleistocene clays the discontinuities due to stress relief and mild tectonic activity may have characteristics similar to those of slip surfaces and shear bands commonly observed in triaxial tests on intact specimens. As reported by Burland et al. (1996) the formation in the laboratory of slip surfaces and shear bands at peak strength is followed by a rapid decay of strength until post-rupture strength is reached on the slip surface. The post-rupture effective strength envelope on discontinuities has been found to be close to the intrinsic critical state failure envelope of the reconstituted material. In particular:

- At low effective confining stresses the post-rupture strength, and hence the strength along the discontinuities of the deposits in the field, may be represented by an angle of

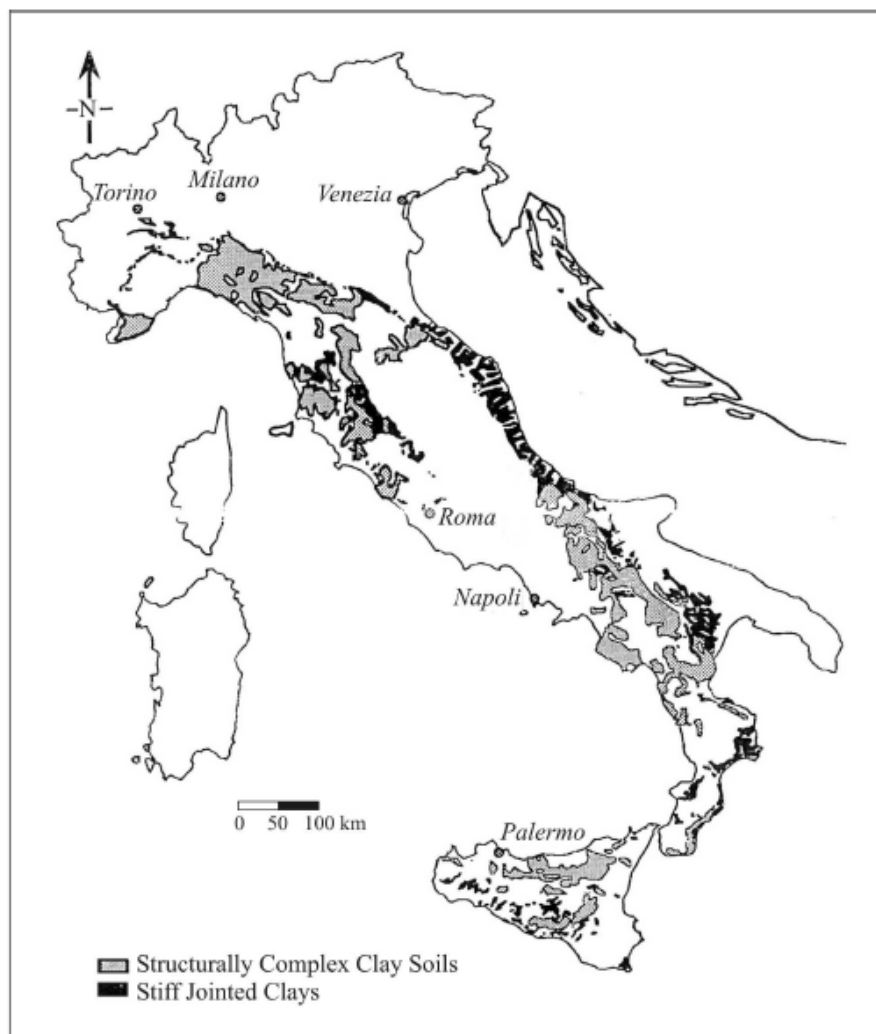


**Figure 2-12 - Distribution of structurally complex clay soils and stiff jointed clays in Italy (D'Elia et al., 1998).**

shearing resistance approximately equal to that characteristic of critical state condition ( $\phi_{cs}'$ ) and by a small apparent cohesion ( $c'$ ) whose value can lie between 0 kPa and perhaps 10 kPa;

- At low to moderate effective confining stresses the post-rupture strength may be represented only by  $\phi_{cs}'$ ;
- At higher effective confining stresses (the actual value depending on the type of clay), as a consequence of particle orientation which begins immediately after rupture, the post-rupture strength may be represented by angles of shearing resistance intermediate between  $\phi_{cs}'$  and that characteristic of the residual condition  $\phi_r'$ .

The assessment of the overall “operational” strength of jointed/fissured clays, which is influenced by the strengths of both the intact material and of the discontinuities, is a difficult matter. However there is increasing evidence that at low to moderate effective confining stresses the intrinsic critical state angle of shearing resistance  $\phi_{cs}'$  can be taken as a representative parameter; in many instances the inclusion of a small on apparent cohesion  $c'$  (let us say less than 10 kPa) is justified; it should be pointed out that this conclusion is mainly supported by back analyses of first-time slides (Skempton, 1977; Chandler, 1984) carried out with very simplified approaches and assumptions, i.e. limit equilibrium methods, linear effective strength envelopes, and, often, assumed (rather than measured) pore pressure distribution at the time of failure along the failure slip surfaces.

The rapid post-peak drop of strength experienced by materials CB2 results largely from changes in microstructure due mainly to breaking of bonds and from loss of dilation (Viggiani et al., 1993; Viggiani et al., 1994); in materials CB1 the loss of strength is less dramatic and essentially due to loss of dilation (Atkinson and Richardson, 1987); on balance, other things being equal, the operational strengths of jointed/fissured materials CB1 can be reasonably considered similar to those defined for materials CB2 because the benefit of bonding in CB2 materials is substantially reduced when dealing with jointed/fissured materials.

Numerous back analyses of first time failures in CA type materials carried out with very simplified approaches and assumptions, i.e. limit equilibrium method, linear effective strength envelopes and assumed pore pressure distribution along the slip surface (Kenney, 1967 and Janbu, 1977 for Norwegian clays, Eden and Mitchell, 1970, Eden and Mitchell, 1973, Lefebvre and La Rochelle, 1974, Lo and Lee, 1974 for Champlain clays, Canada) indicate that the conditions at the time of failure appear to correspond to “drained” conditions and operational effective strengths near to  $\phi_{cs}'$  with a small cohesion intercept, in a similar manner to CB materials (see also Tavenas and Leroueil, 1981). These results are in line with the general framework described here:

- apparent “drained” conditions are the result of undrained shearing generating significant positive excess pore pressures (positive value of  $\alpha$  in equation [2-2]) compensating the negative pore pressure generated by total mean stress in saturated materials ( $\beta = 1$  in equation [2-2]);
- as for CB materials, progressive failure and strain compatibility result in operational effective strengths at the time of failure typically corresponding to post-rupture strengths.

According to the classification adopted in Italy for Structurally Complex Formations shown in figures 13 and 14 (AGI, 1979), based on the data reported for example by Esu (1977), AGI (1979) and D’Elia et al. (1998), the intensely fissured clays of Cretaceous-Miocene age, also referred to as “scaly clays”, can be classified as materials A2, B1, B2 and B3 with arenaceous/pelitic (A/P) associations less or significantly less than unity. Their complexity is given by the presence of sheared, disarranged and chaotic mesostructures determined by the tectonic deformations which hugely displaced the soils/rocks from their original basins.

Materials A1 shown in Figure 2-13 may be considered to behave in similar manner to jointed/fissured Plio-Pleistocene clays.

As reported for example in D’Elia et al. (1998), in the cases represented by materials A2, B1, B2 and B3, the clay component results in an aggregate of hard fragments or shear lenses one millimetre to some centimetres in size; fragments and shear lenses have smooth and polished surfaces and are generally iso-oriented; however, their average orientation may vary from place to place within short distances (from few centimetres to several decimetres) and are therefore often described as “chaotic”. The single fragments are predominantly constituted by bonded clayey aggregates with possible inclusion of lithorelicts.

Similar materials are present in other areas of the world; typical examples are the Bearpaw, Cucaracha, Pepper and Pierre hard clays and clay shales in Central and North America (Ringheim, 1964; Been, 1967; Banks et al., 1975), Keuper marl, Lower Lias and Oxford clays outcropping in UK and Germany (Chandler, 1969; Chandler, 1972; Parry, 1972; Gudheus and Wichter, 1977; Marsland, 1977).

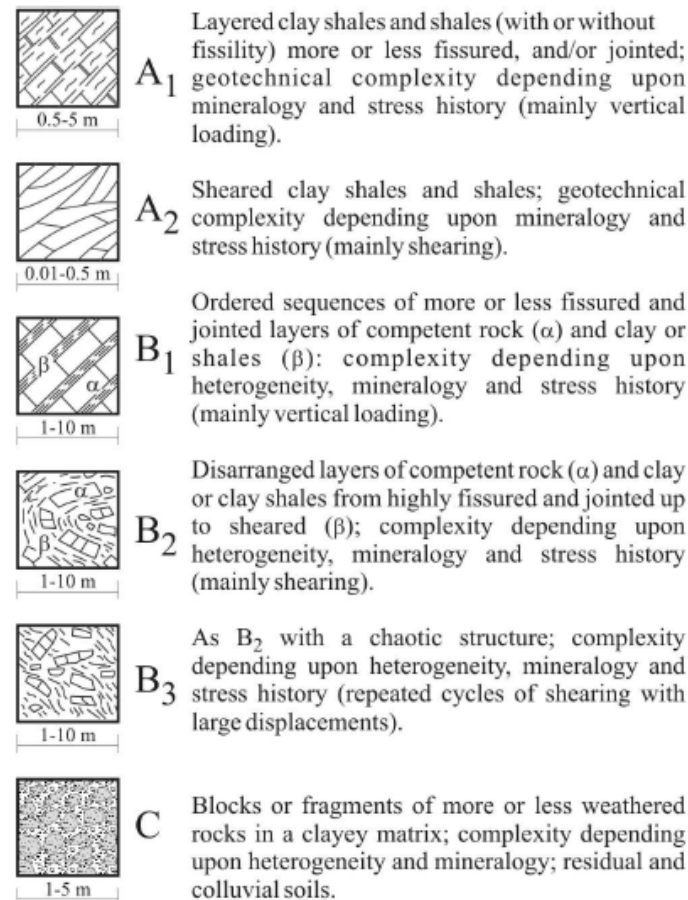


**Figure 2-13** - Types of elementary complexities (from A.G.I., 1979).

The main issues which characterize the behaviour of these difficult materials are well documented in AGI (1977), AGI (1979), AGI (1985) and in many papers published in the technical literature (see for example D'Elia, 1991; D'Elia et al., 1998); only some major remarks are summarized below:

- In comparison with jointed/fissured Plio-Pleistocene clays, stress relief in “scaly clays” causes a more pronounced effect in terms of mesostructure loosening (i.e. non uniform expansion and opening of fissures between fragments); at surfaces exposed to the atmosphere, cycles of wetting-drying (physical weathering) and chemical weathering may rapidly induce further changes to the mesostructure, favouring increase of water content and softening also of the fragments; the final result is a material constituted by hard lithorelicts surrounded by a softer clayey matrix (material C of Figure 2-13). A geotechnical assessment of this process is presented, for example, by Botts (1998).
- Undisturbed sampling of these materials is rather difficult, if not impossible; opening of fissure is easily achieved with consequent inability to maintain the mean effective pressure existing in situ through suction pressures. It is quite common in these materials to measure degrees of saturation significantly lower than 1 even in samples retrieved below the water level.
- Because of bonds in the fragments the grain size distribution obtained by usual methods does not reflect the real amount of clay minerals.

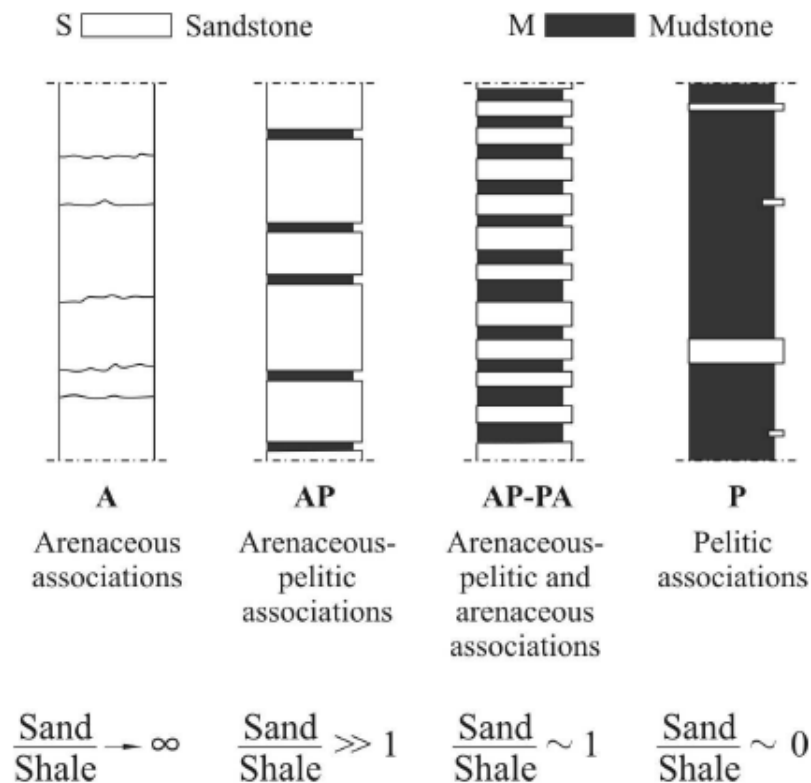


**Figure 2-14** - Classification of arenaceous-pelitic association from the engineering point of view (A.G.I., 1979).

- The compression indexes ( $C_r$  and  $C_c$ ) and the coefficients of primary consolidation ( $c_v$ ) determined in oedometer tests are significantly influenced by the strains necessary to close of the fissures, previously opened by sampling disturbance. Similar considerations apply to the response of triaxial drained tests in terms of volumetric strains, resulting in the material appearing as less dilatant than would be if tested in fully undisturbed conditions.
- The swelling index ( $C_s$ ) determined in oedometer tests, is strongly influenced by the degree of bonding in the fragments; high swelling strains are typical of weak bonding, while low swelling strains characterize strongly cemented fragments.
- The effective strength envelope is influenced by the shear strength of the fragments and the shear strength between the fragments; as a consequence, test results may depend more markedly than in joint/fissured Plio-Pleistocene clays on:
  - ✓ Dimensions of the specimens; specimens of diameter at least equal to 100 mm are mandatory for triaxial tests on these materials.
  - ✓ Type of tests. In direct shear tests failure surfaces are imposed; effective strength envelopes depend on the direction of imposed movements compared to the average orientation of the fragments. In triaxial drained tests the slip surface and the shear band formation are free to develop along paths characterized by minimum resistances (i.e. mainly through the fissures); as expected, experimental evidence shows that the effective strength envelope determined by

triaxial drained tests is close to that obtained by direct shear tests on specimens where the failure plane are parallel to the average orientation of the fragments.

On the basis of the above considerations, at low to moderate effective confining pressures, the operational strength commonly results significantly lower than the post-rupture strength of reconstituted specimens and may approach the residual value (Skempton, 1985; Picarelli and Olivares, 1998); typically the latter condition may be achieved when the fissures are planar, polished and well aligned. These considerations are reflected in the relatively high frequency and extent of landsliding where these materials occur at depths of interest in hilly or mountainous terrain.

## **2.3.2 “Coarse grained, uncemented materials”**

### **2.3.2.1 General**

In uncemented materials coarse enough that interparticle surface forces can be neglected (i.e. from silts to gravels), the most important problem for landslide hazard and risk assessment is certainly represented by the understanding and modelling of phenomena which, under saturated conditions, may lead to sudden undrained instability and to catastrophic liquefaction flow slides.

According to Hutchinson (1988), liquefaction flow slides are “*characterized by the sudden collapse and extensive, very to extremely rapid run-out of a mass of granular materials or debris, following some disturbance. An essential feature is that the material involved has a meta-stable, loose or high porosity structure. As a result of disturbance this collapses, transferring the overburden load wholly or partially onto the fluid, in which excess pore pressures are generated. The consequent loss of strength gives the failing material, briefly, a semi-fluid character and allows a flow slide to occur*”.

Under some circumstances, governed essentially by an unfavourable combination of loose fabric and sufficiently high mean effective and deviatoric stresses, liquefaction flow slides may be spontaneously triggered by small disturbances (such as vibrations, rising of the water table, limited changes in slope geometry, etc.) even in situations where the original slope inclination is less than necessary to ensure full stability in conventional drained limit equilibrium analyses.

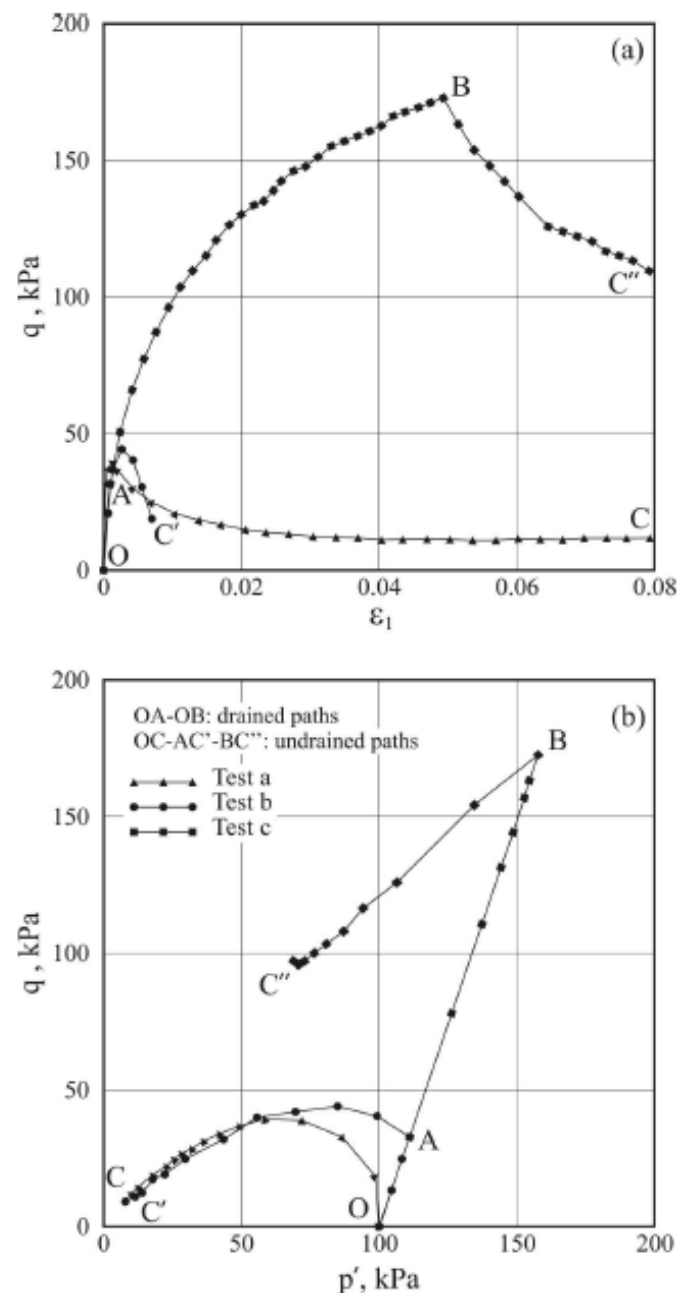


**Figure 2-15** - (a) Stress-strain relationship; (b) effective stress paths in undrained triaxial tests on loose specimens previously sheared in drained conditions (Di Prisco et al., 1995).

The experiment reported by Casagrande (1936) (see also Morgenstern, 2000-2001) consists of a tank filled with fine sand in a loose saturated state with free water standing on the surface. A Three illustrative examples, reported by Casagrande (1936), Sasitharan et al. (1993) and Di Prisco et al. (1995), are here described below to highlight the issue.

weight was placed on the surface of the sand; then a stick was thrust into the sand, some distance from the weight which suddenly sank. The slight but rapid deformation induced by the penetration of the stick caused a local collapse of the fabric associated with development of excess pore pressure which propagated progressively throughout the entire soil mass resulting in total loss of bearing capacity.

The experiment reported by Di Prisco et al. (1995) consists of a triaxial test carried out on a specimen of loose saturated sand. After isotropic consolidation to a mean effective pressure  $p_c' = 100$  kPa, the specimen was sheared in drained conditions up to a deviatoric stress  $q = 172$  kPa associated to a mean effective pressure  $p' = 150$  kPa; in this stress condition the stress ratio  $q/p'$  was equal to  $\cong 1.1$ , corresponding to a mobilized friction angle of  $27.7^\circ$  significantly lower than the angle of friction at critical state ( $\phi_{cs}' = 32^\circ$ ). Collapse occurred immediately after the drainage valve was closed, in undrained conditions (test -c- in Figure 2-15).

The experiment reported by Sasitharan et al. (1993) consists of two triaxial tests carried out on specimens of loose saturated sand (Figure 2-16). After isotropic consolidation to a mean effective pressure  $p_c' = 350$  kPa, the first specimen, with a void ratio of 0.804, was loaded in undrained compression; after reaching a peak deviatoric stress of approximately 130 kPa, the specimen experienced a dramatic drop of deviatoric stress to a minimum shear resistance of approximately 55 kPa. After anisotropic consolidation ( $p' = 300$  kPa and  $q = 100$  kPa) the second specimen, with similar void ratio, was subjected in drained conditions to a stress path

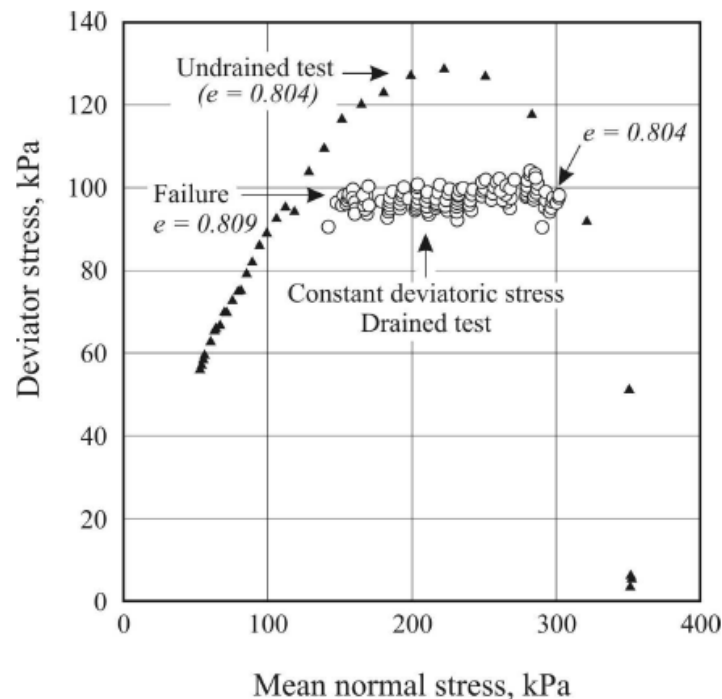


**Figure 2-16** - Effective stress paths of undrained and drained triaxial tests on loose specimens (Sasitharan et al., 1993).

characterized by a decrease in  $p'$  at constant  $q$ . As soon as the stress point reached the corresponding point on the stress path of the first specimen tested in undrained conditions, a dramatic failure occurred with generation of positive excess pore pressure, similar to that observed in the first specimen; the generation of positive excess pore pressure was caused by the inability of the sand to behave in fully drained conditions as a consequence of the development of large plastic volumetric strains.

The mechanisms, conditions and rules which determine the occurrence of liquefaction flow slides have been thoroughly investigated and debated in the last fifty to sixty years; research is still in continuous development leading to a formidable growth of very promising tools for

the assessment and analysis of the phenomena involved both during initiation of failures and subsequent downward propagation (run-out) of the unstable soil mass (see for example Gu et al., 1993; Pastor et al., 2002; Azizian, 2004; Pastor et al., 2005a, Pastor et al., 2005b). It is out of the scope of the Report to provide a comprehensive description of all the aspects which characterize the behaviour of saturated coarse grained materials; the attention is here focused only on the main issues which are considered helpful both for the characterization and classification of the material and for the choice of constitutive models to be used in analyses of slope behaviour up to initiation of instability phenomena.

As most theoretical and experimental efforts have been addressed on siliceous sands and silty sands, the discussion is here limited to these types of materials; however it is believed that the conceptual framework emerging for siliceous sands and silty sands may be helpful to guide, with appropriate adjustments, the studies of other types of materials such as gravels and gravelly sands/sandy gravels; the same applies for coarse materials of calcareous/carbonate nature (see for example Porcino and Marciandò, 2010).

### 2.3.2.2 *Clean sands*

Conventionally clean sands refer to materials with fine content (passing to the 200 ASTM sieve) less than 5%. The undrained behaviour of these materials is governed by the following main aspects.

#### 1. Steady State (SS).

At large strains in the final stage of conventional triaxial tests (isotropically consolidated, loading in undrained compression), specimens prepared at the same void ratio ( $e_c$ ) with different mean effective consolidation pressures ( $p_c'$ ) exhibit almost identical behaviour, deforming at constant volume, with equal constant deviatoric stress and equal constant mean effective stress; this condition, called the Steady State (Castro, 1975; Castro and Poulos, 1977) or the Critical State (Schofield and Wroth, 1968), is represented by the point C in the  $e$ - $q$ - $p'$  space or by the points C' and C'' in the  $q$ - $p'$  and  $e$ - $p'$  planes respectively (Figure 2-17). The state of stress at the Steady State ( $q_{SS}$ ;  $p_{SS}'$ ) depends on the void ratio alone. The line joining the Steady State points C'' for different void ratios represents the projection of the Steady State Line (SSL) on the  $e$ - $p'$  plane; for sand sheared in undrained conditions (i.e. at constant void ratio) the pore pressure increases or decreases depending on the initial mean effective consolidation pressure ( $p_c'$ ) so as to bring the mean effective stress to the value representative of the Steady State condition ( $p_{SS}'$ ).

At the Steady State condition the stress ratio ( $M = q_{SS}/p_{SS}'$ ) is a function of the “critical state” or “constant volume” angle of friction ( $\phi_{SS}'$  or  $\phi_{cs}'$ ) and of the Lode angle ( $\theta$ ); as known, in triaxial compression and triaxial extension the following values apply in compression ( $M_c$ ) and in extension ( $M_e$ ):

$$M_c = \frac{6 \cdot \sin \phi_{SS}'}{3 - \sin \phi_{SS}'} \quad [2-3]$$

$$M_e = \frac{6 \cdot \sin \phi_{SS}'}{3 + \sin \phi_{SS}'} \quad [2-4]$$

In plane strain conditions,  $M_{ps}$  is intermediate between  $M_c$  and  $M_e$ .

The Steady State Line is an intrinsic property of the material; for a given sand its position in the  $e$ - $q$ - $p'$  space or in the  $e$ - $p'$  plane is independent of the initial fabric, the stress path (Lode angle  $\theta$ ), the type of test (drained, undrained, etc.) (see for example Ishihara, 1993; Riemer and Seed, 1997) and is determined only by the mean grain size ( $D_{50}$ ) and the grain size distribution, together with the grain shape (angular, rounded, etc.);  $D_{50}$  and grain size distribution may be well represented by the range of void ratio given by the difference between the void ratio at the loosest ( $e_{max}$ ) and densest ( $e_{min}$ ) states of packing achieved in standard laboratory procedures (see for example Cubrinowski and Ishihara, 2000); for all sands the shape of SSL in the  $e$ - $\log(p')$  plane is not straight (see for example Ishihara, 1993; Verdugo and Ishihara, 1996; Riemer and Seed, 1997; Li and Wang, 1998).

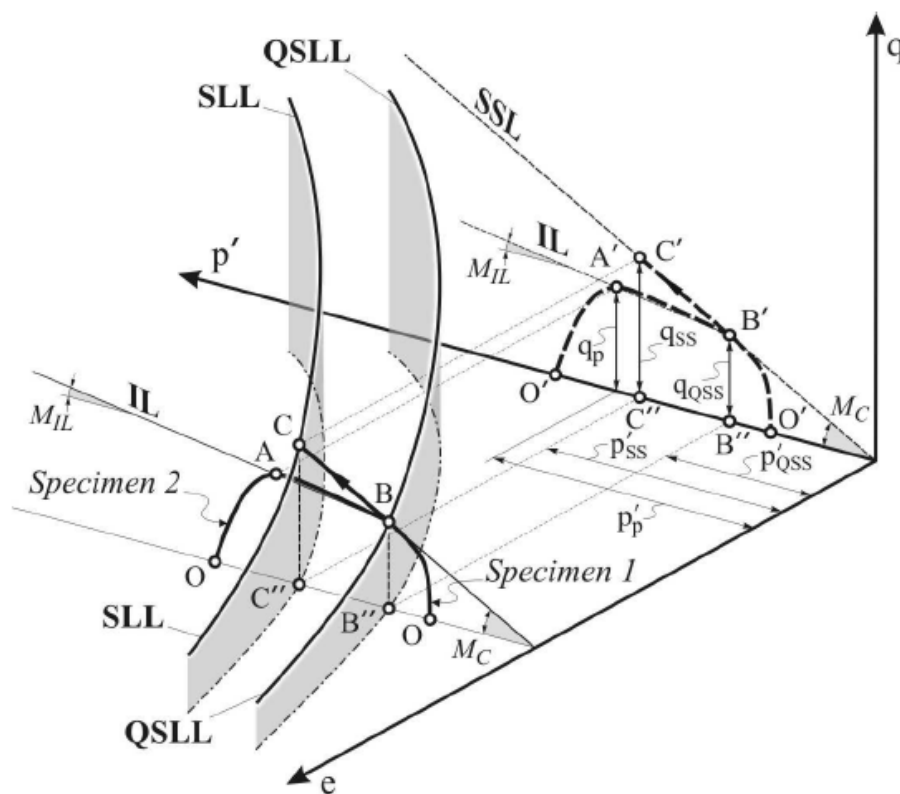


**Figure 2-17** - Basic elements of sand behaviour (modified from Ishihara, 1993)

In a sand profile, represented by known initial void ratios, the undrained shear strengths at the Steady State ( $s_{u,SS}$ ) may be easily evaluated by using the following equation (see for example Castro, 1987; De Alba et al., 1988; Marcuson et al., 1990):

$$s_{u,SS} = \frac{q_{SS}}{2} \cdot \cos \varphi_{SS}' = \frac{M}{2} \cdot \cos \varphi_{SS}' \cdot p_{SS}' \quad [2-5]$$

provided always that  $p_{SS}' - p_c' = \Delta u_{max} \leq u_o - u_c$  and  $u_c = -(70 \div 100)$  kPa = cavitation pressure.

In so far as it is linked to the strength parameter  $M$ ,  $s_{u,SS}$  also depends on the Lode angle ( $\theta$ ) and is therefore different in triaxial compression, triaxial extension and plane strain conditions.

## 2. Compression Lines (isotropic and oedometric)

The compression lines (isotropic and oedometric) of mechanically normally consolidated sands are not unique; they are significantly affected by the void ratio and fabric attained at the end of deposition. At high stresses, normally beyond values of practical interest for siliceous sands but potentially significant for some calcareous/carbonate or volcanic materials characterized also by intraparticle voids, both loose and dense sands may yield due to the onset of particle crushing and converge to a single compression line, usually referred to as “limiting compression curve” (Pestana and Whittle, 1995), which is “unique” for any given mineralogy when grain crushing becomes prevalent and which has been shown to be strain rate dependent (Pestana and Whittle, 1998) as is typical of all phenomena associated with damage and destruction processes (of intraparticle bonds, in this case).

## 3. Phase Transformation (PT), Quasi Steady State (QSS) and Initial Dividing Line (IDL)

Before reaching the Steady State, specimens prepared at the same void ratio ( $e_c$ ) with different mean effective consolidation pressures ( $p_c'$ ) and loaded in conventional undrained triaxial tests exhibit large differences in the stress-strain behaviour.

If the density is high or the mean effective consolidation pressure is sufficiently low, deviatoric stresses increase monotonically with increasing axial strains until the Steady State is finally reached (Figure 2-18 and specimen 1 in Figure 2-17); at the beginning of the test some contractive behaviour may be observed, followed by dilative behaviour. The state at which the behaviour changes from contractive to dilative has been called Phase Transformation (Ishihara et al., 1975); the points of Phase Transformation and those located along the stress path following the achievement of the Phase Transformation conditions may be characterized by stress ratio  $q/p'$  or mobilized angle of friction similar to that at the Steady State (Ishihara, 1993).

If the density is low or the mean effective consolidation pressure is sufficiently high, the sand exhibits a contractive strain softening behaviour resulting in a drop of deviatoric stresses associated with the development of significant strains; only at relatively high strain this behaviour may change from contractive to dilative, leading to an increase of deviatoric stresses until the Steady State is finally reached (Figure 2-19 and specimen 2 of Figure 2-17); this type of behaviour, observed by many researchers (see for example Castro, 1975; Hanzawa, 1980; Mohamed and Dobry, 1984; Konrad, 1990a; Konrad, 1990b; Vaid et al., 1990; Been et al., 1991; Georgiannou et al., 1990, etc.) may be commented as follows:

- The case where the change from contractive to dilative behaviour follows a temporary drop in deviatoric stresses over a significant range of strain may be considered a particular case of Phase Transformation; such case has been called the Quasi Steady State (Alarcon-Guzman et al., 1988; Been et al., 1991; Ishihara, 1993, etc.) as opposed to the Steady State which is reached at larger strains. Also in this case the points of Phase Transformation and those located along the stress path following the achievement of the Phase Transformation conditions may be characterized by stress ratio  $q/p'$  or mobilized angle of friction similar to that at the Steady State (Ishihara, 1993).

- The minimum deviatoric stress reached at Phase Transformation may be considerably lower than the undrained shear strength available at the Steady State; the former may be given by:

$$s_{u,QSS} = \frac{q_{QSS}}{2} \cdot \cos \varphi_{ss} = \frac{M}{2} \cdot \cos \varphi_{ss} \cdot p_{QSS} \quad [2-6]$$

with  $p_{QSS}' < p_{ss}'$  and  $q_{QSS} < q_{ss}$  (Figure 2-17).

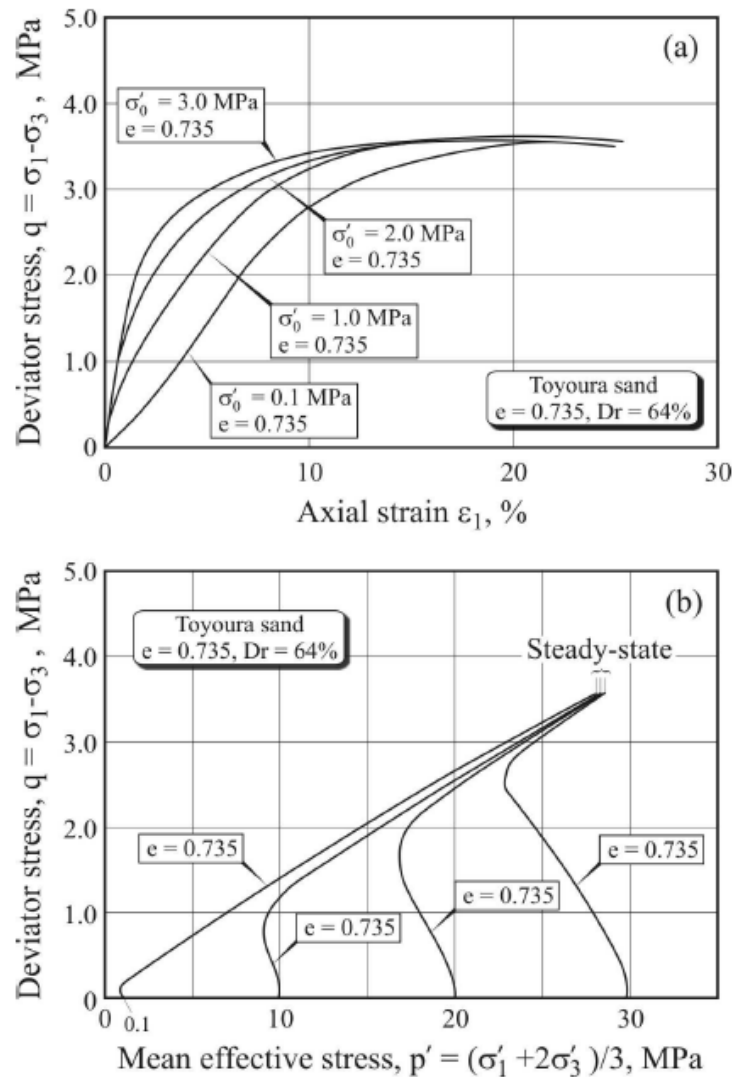


**Figure 2-18** - (a) Stress-strain relationship; (b) effective stress paths in undrained triaxial tests on moist-placed dense specimens of Toyoura sand (Ishihara, 1993).

As highlighted by Yoshimine et al. (1999), if undrained shearing results in Quasi Steady State and then Steady State occurs following hardening at large strains, a problem arises in the definition of which state should be considered appropriate to represent the undrained strength for slope stability evaluation. Where static driving shear stresses exceed the Quasi Steady State strength, triggering mechanisms which may bring the slope towards the Quasi Steady State condition result in large displacements or even gross failure and flow slides. The undrained Steady State strength achievable at large strains is unlikely to be appropriate for the analysis of the initiation of flow deformations; furthermore, in the field, once stability is

temporarily lost and significant movements take place, the overall behaviour of the sliding soil mass may become dynamic and turbulent, casting doubts on the possibility that it continues to behave as observed in the specimen in the laboratory.

As highlighted by Ishihara (1993), from the results of conventional undrained triaxial tests carried out on specimens prepared at different void ratios ( $e_c$ ), with different mean effective consolidation pressures ( $p_c'$ ) it is possible to distinguish between two classes of initial states

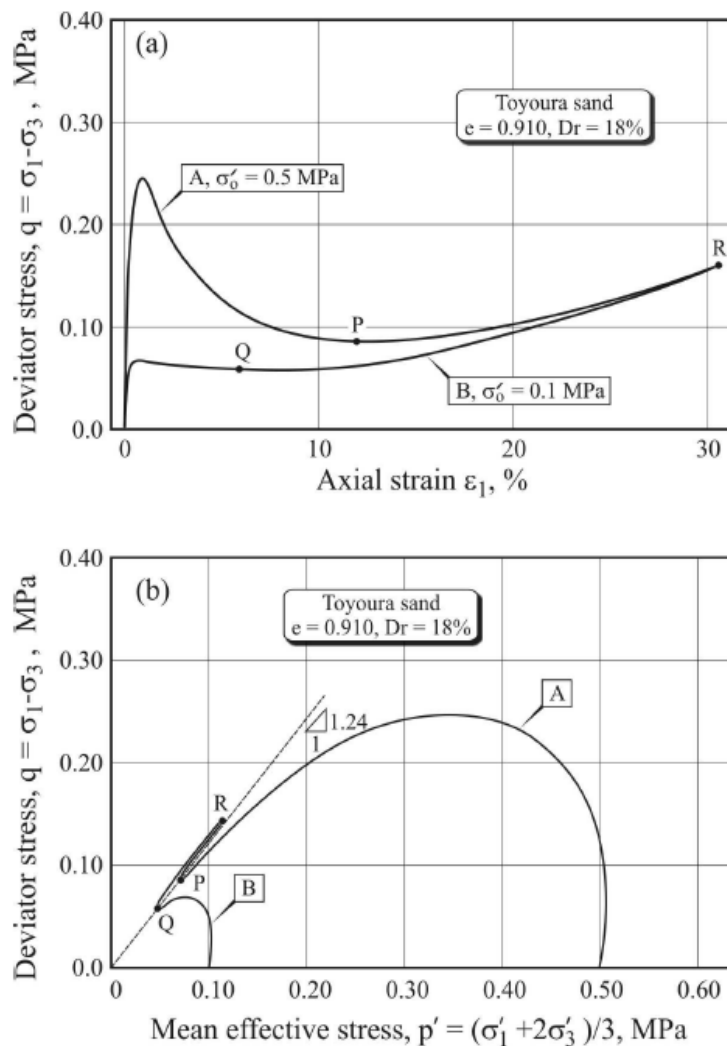


**Figure 2-19** –(a) Stress-strain relationship; (b) effective stress paths in undrained triaxial tests on moist-placed loose specimens of Toyoura sand (Ishihara, 1993).

( $e_c$ ;  $p_c'$ ) where a temporary drop in shear stresses can or cannot occur, as shown for example in Figure 2-20. A line of demarcation can be drawn through the data points separating the initial states with and without the occurrence of minimum strength; such a boundary line has been called the Initial Dividing Line (IDL). By definition, only the materials with initial states located above the IDL may be susceptible to initiation of flow instability phenomena. These materials are identified as type **SA**, while those whose initial states are located below the IDL and are thus found not to be susceptible to flow sliding are identified here as **SB**.

From the same tests it is possible to define the minimum deviatoric stresses representative of the minimum Quasi Steady State strengths, which may be safely used in slope stability evaluation in SA materials as discussed above. This may be achieved by considering the results of all tests carried out on specimens with initial states located above and on the IDL and by plotting in the  $e$ - $p'$  plane the states characterized by  $e_c$  and by mean effective pressure reached at Phase Transformation (minimum deviatoric stress); also in this case a line can be drawn representing a safe boundary through the experimental data as shown for example in Figure 2-21; this line has been called the Quasi Steady State line (QSSL).

Contrary to the SSL, both the IDL and the QSSL are influenced by the initial fabric and the stress path (Lode angle  $\theta$ ) (see for example Georgiannou et al., 1990; Ishihara, 1993; Yoshimine et al., 1998; Yoshimine et al., 1999); influences exerted by void ratio non-uniformity in the specimens or by mechanical preconsolidation and drained pre-shearing have been also highlighted by Thomson and Wong (2008) and Di Prisco et al. (1995), respectively. The pronounced influence of initial fabric on the position in the  $e$ - $p'$  plane of IDL and QSSL is shown for example in Figure 2-22 adapted from Ishihara (1993) where the two lines obtained from specimens of Toyoura sand prepared by moist-placement and dry deposition methods are compared; both the IDL and the QSSL of the specimens prepared by the dry

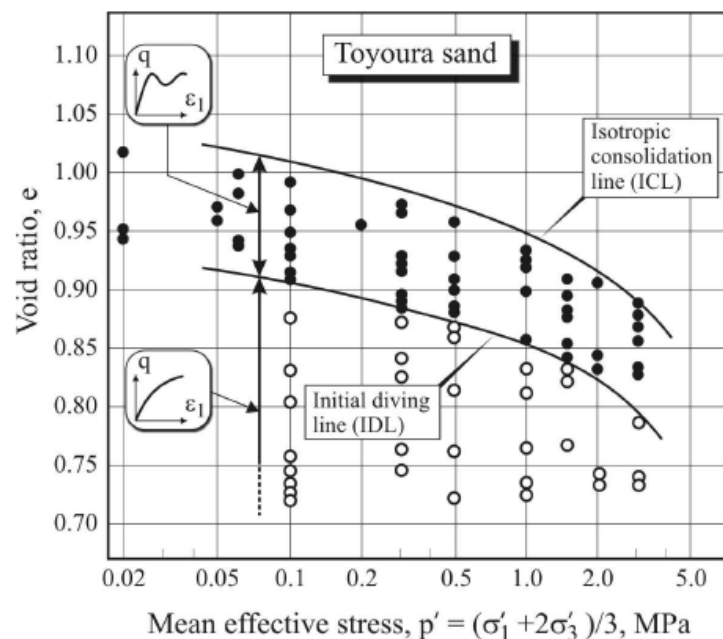


**Figure 2-20** - IDL from moist-placed specimens of Toyoura sand: solid circles indicate that the QSS was observed; open circles denote conditions of PT without decrease in shear stress (Ishihara, 1993).

deposition method are located well below the analogous lines of the specimens prepared by the moist placement method. However, in spite of the difference observed in the IDL and QSSL, specimens with different initial fabric (i.e. different initial void ratios), consolidated at the same mean effective pressure ( $p'_c$ ), may lead to minimum QSS strengths of the same order of magnitude, as in the example shown in Figure 2-22 where  $s_{u,QSS} = 0.27 \cdot p'_c$  and  $s_{u,QSS} = 0.24 \cdot p'_c$  have been obtained in compression tests on specimens prepared by dry deposition and moist placement respectively; the SS strength of specimens prepared by the dry

deposition method, which at equal mean effective consolidation pressures result in lower void ratios. will be significantly higher than for specimens prepared by moist placement.

For the reasons highlighted above, in order to gather appropriate information on the QSSL and IDL for slope stability analyses, it is always desirable:

- To carry out some special boreholes for the recovery of “undisturbed” samples by recurring, for example, to freezing techniques (see for example Adachi and Tokimatsu, 1994; Goto et al., 1994; Segoo et al., 1994; Yoshimi et al., 1994; Hofman, 1997; Segoo et al., 1998; Yoshimi, 2000; Lo Presti et al., 2006).
- To carry out laboratory tests on “undisturbed” samples, reconsolidated to the in situ stress conditions and sheared following the effective stress changes expected to occur in the field which may lead to initiation of instability phenomena. In general, triaxial compression tests exhibit the higher QSS strength, whereas triaxial extension tests result in the lower resistance; simple shear (plane strain) tests exhibit intermediate behaviour (see for example Yoshimine et al., 1998; Yoshimine and Ishihara, 1998). As expected, simplified analyses carried out by Yoshimine et al. (1999) to compare laboratory and field observations revealed that the undrained response in the field is more similar to that observed in simple shear tests; this conclusion is similar to the recommendation given by Bjerrum (1972) for clayey materials of type CA, which also are characterized by meta-stable microstructures.

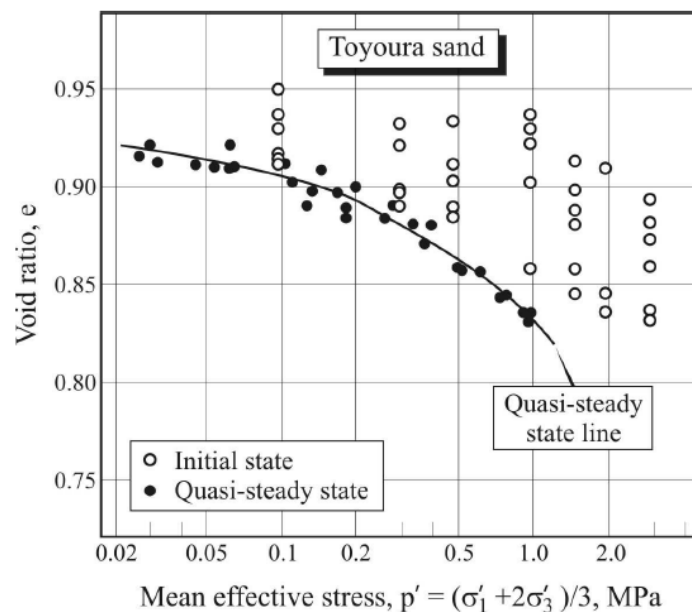


**Figure 2-21** - QSSL for moist-placed specimens of Toyoura sand (Ishihara, 1993).

Undisturbed sampling in special boreholes may be also helpful to determine in situ void ratio profiles which may be used as benchmarks for the calibration of results obtained by interpretation of conventional in situ tests, such as cone penetration tests, standard penetration tests, cross hole tests, etc., which may be more easily and extensively carried out.

The results from laboratory tests on “undisturbed” samples may be useful to select the more appropriate technique to prepare reconstituted specimens in the laboratory in order to reproduce, as far as possible, similar results.

#### 4. Collapse or Instability Surface (CS or IS).

By definition, when sheared in undrained conditions, type SA materials exhibit strain softening behaviour with a drop of deviatoric stress as soon as threshold peak stress conditions ( $q_p$ ;  $p_p'$ ) are attained. As shown for example by Sladen et al. (1985) and by Ishihara (1993), these threshold peak stress conditions form in the  $e$ - $q$ - $p'$  space a planar surface, with a unique slope  $M_{IL}$ , emerging from the QSSL (Figure 2-17). This surface has been called the Collapse Surface (Sladen et al., 1985) or the Instability Surface (Lade, 1993). If the threshold peak stress conditions are normalized to the corresponding mean effective stress at the QSS ( $p_{QSS}'$ ), the Collapse or Instability Surface converge in the  $q/q_{QSS}$ - $p'/p_{QSS}'$  plane to a single line called the Collapse Line (CL) or the Instability Line (IL) which may be represented by the following equation (Ishihara, 1993):

$$\frac{s_{u,p}}{p_c'} = \frac{q_p}{2 \cdot p_c'} = \frac{1}{2} \cdot \left[ M_{IL} \cdot \frac{p_p'}{p_c'} + (M - M_{IL}) \cdot \frac{p_{QSS}'}{p_c'} \right] \quad [2-7]$$

The zone bounded by the CL or IL and the SSL has been called the Instability Zone (Lade and Pradel, 1990; Leong et al., 2000).

In analogy to what has been discussed for the IDL and the QSSL, also the CL (or the IL) depends on initial fabric, stress path (Lode angle  $\theta$ ), etc.. However, also in this case, in spite of the difference which may be observed in the position of the CS (or IS), specimens with different initial fabric (i.e. different initial void ratios), consolidated at the same mean

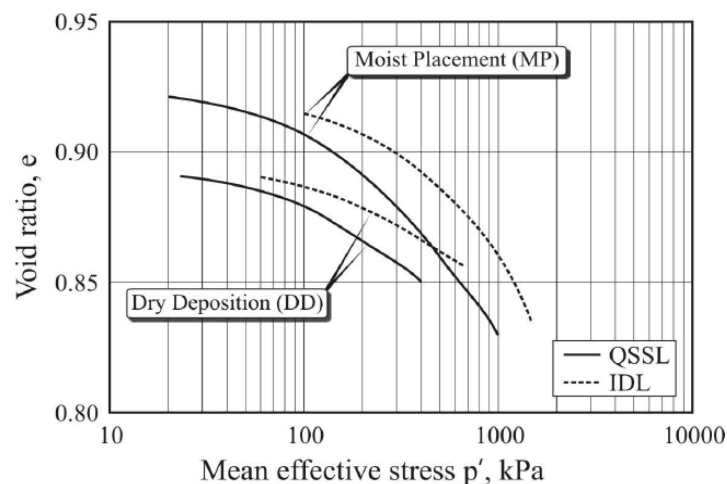


**Figure 2-22** - Comparison between IDL and QSSL for specimens of Toyoura sand prepared by moist-placement (MP) and dry deposition (DD) methods (Ishihara, 1993).

effective pressure ( $p_c'$ ), may lead to minimum peak strengths of the same order of magnitude, as reported by Ishihara (1993) for tests in compression on specimens of Toyoura sand prepared by dry deposition method ( $s_{u,p} = 0.30 \cdot p_c'$ ) and moist placement method ( $s_{u,p} = 0.33 \cdot p_c'$ ).

From a constitutive modelling point of view the CS (or IS) represents a yield locus beyond which large plastic contractive strains begin to take place (Lade, 1992; Chu et al., 1993); depending on the drainage conditions the propensity of the material to develop large plastic contractive strains when the stress points are located in the Instability Zone may be

accompanied by large excess pore pressure (undrained conditions prevailing) or large plastic volumetric strains (drained condition prevailing); as highlighted by Chu et al. (2003), from the point of view of hazard and risk assessment the occurrence of undrained or drained conditions has a profound influence on both the type and the consequences of the instability; very rapid flow like instability occurs only when undrained conditions prevail; drained “instability” is accompanied only by large progressive deformation.

When sheared in undrained conditions, specimens of type SB materials exhibit strain hardening behaviour, with continuous increase of deviatoric stress along the SSL or slightly above, until the SS strength is finally reached. The same specimens sheared in drained conditions are characterized by curvilinear failure envelopes located above the SSL; as a consequence of the development of plastic dilative strains, instability and strain softening behaviour may occur until the SS strength is finally reached; however this type of instability cannot produce flow like failures.

The typical response of slopes in SA and SB materials to rapid disturbance, for example by surcharging at the top of the slope, is illustrated in the example in Section 2.4.

### 2.3.2.3 Silty sands

Often in nature sand deposits contain some non-plastic (i.e. with negligible surface forces effects) fines consisting of particles with dimension of silt and clay. The deposition of sand with some fines may lead to materials with higher void ratios and lower permeability, the combination of these two factors possibly resulting in a higher potential for undrained (contractive) flow like instability.

Recent research on the influence of fines content on the overall behaviour of the material indicates that:

- Sands with fines content may have lower undrained strengths and be more liquefiable than clean sands (Lade and Yamamuro, 1997; Yamamuro and Lade, 1997; Zlatovic and Ishihara, 1997; Yamamuro and Lade, 1998; Lade et al., 2009); this is supported also by the experimental results reported in Ishihara (1993) related to the undrained strengths  $s_{u,QSS}$  and  $s_{u,p}$  of loose silty sands and of loose sandy silts compared to analogous results obtained for loose clean sands, as summarized in Table 2-3.
- These findings appear to conflict with the testing methods normally used to estimate liquefaction potential; simplified liquefaction evaluation techniques widely used in practice, which adopt standard and cone penetration testing, apparently consider silty content as a mitigating factor in the evaluation of liquefaction (Youd et al., 2001).
- At the same void ratio, as fine content increases, the undrained strength initially decreases, then increases as soon as a threshold fine content beyond about 30% is reached (Pitman et al., 1994; Zlatovic and Ishihara, 1995; Thevanayagam et al., 1996).

**Table 2-3** - Comparison between undrained strengths of loose clean sands, silty sands and sandy silts.

Material	FC (%)	$s_{u,QSS}$	$s_{u,p}$
Clean Toyoura sand	< 5	$(0.24 \div 0.27) \cdot p_c' ^{(1)}$	$(0.30 \div 0.33) \cdot p_c' ^{(1)}$
Tia Juana silty sand	10 ÷ 15	$(0.15 \div 0.17) \cdot p_c' ^{(2)}$	$0.21 \cdot p_c' ^{(1)}$
Lagunillas sandy silt	> 50	$(0.09 \div 0.14) \cdot p_c' ^{(2)}$	$0.19 \cdot p_c' ^{(2)}$

Note: all results refer to specimens isotropically consolidated and sheared in undrained compression

<sup>(1)</sup> Specimens prepared by moist placement and dry deposition methods

<sup>(2)</sup> Specimens prepared by dry deposition and water sedimentation methods

As reported and discussed by Thevanayagam et al. (1996), Thevanayagam (1998), Thevanayagam (1999), Thevanayagam and Liang (2001), Thevanayagam (2002), Thevanayagam et al. (2002), etc., the behaviour of mixed materials, such as silty sands, are entirely different from that of clean sands and “pure” silts.

With reference to the soil mix classification scheme proposed for example by Thevanayagam et al. (2002) (see Figure 2-23), as a consequence of particle size disparity and availability of pores larger than the finer particles, at low fine content (FC) some of the finer particles may remain inactive without significantly affecting or contributing to the force chain; yet they contribute to the global void ratio  $e_o$ .

Where the particle size disparity ratio  $R_d = D_{10}/d_{50}$  ( $D_{10}$  = diameter of the sandy particles at 10% finer;  $d_{50}$  = diameter of the silty particles at 50% finer) is higher than a threshold value and fine content is lower than a threshold value (TFC or  $FC_{th}$ ), the global void ratio  $e_o$  ceases to be an index appropriate to represent the nature of contact density of active particles. In these cases the soil behaviour is much better represented by the equivalent intergranular void ratio ( $e^*$ ) defined by the following equation (Thevanayagam and Liang, 2001, Rahman and Lo, 2008):

$$e^* = \frac{e_o + (1-b) \cdot FC}{1 - (1-b) \cdot FC} \quad [2-8]$$

valid for  $0 < b < 1$ , where the parameter  $-b-$  denotes the portion of the fine grains that contributes to the active intergrain contacts;  $b = 0$  means that none of the fine grains actively contribute to supporting the coarse grain skeleton; for  $b > 0$  some of the fine grains actively contribute to supporting the coarse grain skeleton; the parameter  $-b-$  depends on the  $D_{10}/d_{50}$  grain size disparity and on grain characteristics. The threshold values for  $D_{10}/d_{50}$  and TFC reported in the published literature are of the order of 6.5 and  $0.3 \div 0.40$ , respectively.

Where, instead, the ratio  $D_{10}/d_{50}$  is relatively low and there is a sufficient amount of finer grains ( $TFC > 0.3 \div 0.40$ ), the coarser grains become dispersed, contributing much less to the force chain, which is then governed mainly by the finer particles producing a behaviour in line with the global void ratio; this is the case of sandy silts.

In light of these considerations, it has been found that if the laboratory tests on silty sands with  $D_{10}/d_{50} \gg 6.5$  and  $TFC < 0.3$  were interpreted in terms of equivalent intergranular void ratio ( $e^*$ ), instead of the measured global void ratio, the results would be consistent with those observed in clean sands with global void ratio equal to  $e^*$  (see for example Thevanayagam et al., 2002, Thevanayagam and Martin, 2002; Chu and Leong, 2002 and Rahman and Lo, 2008; Chiu and Fu, 2008); provided this correction is carried out, the behavioural framework described for clean sands is applicable also to silty sands.

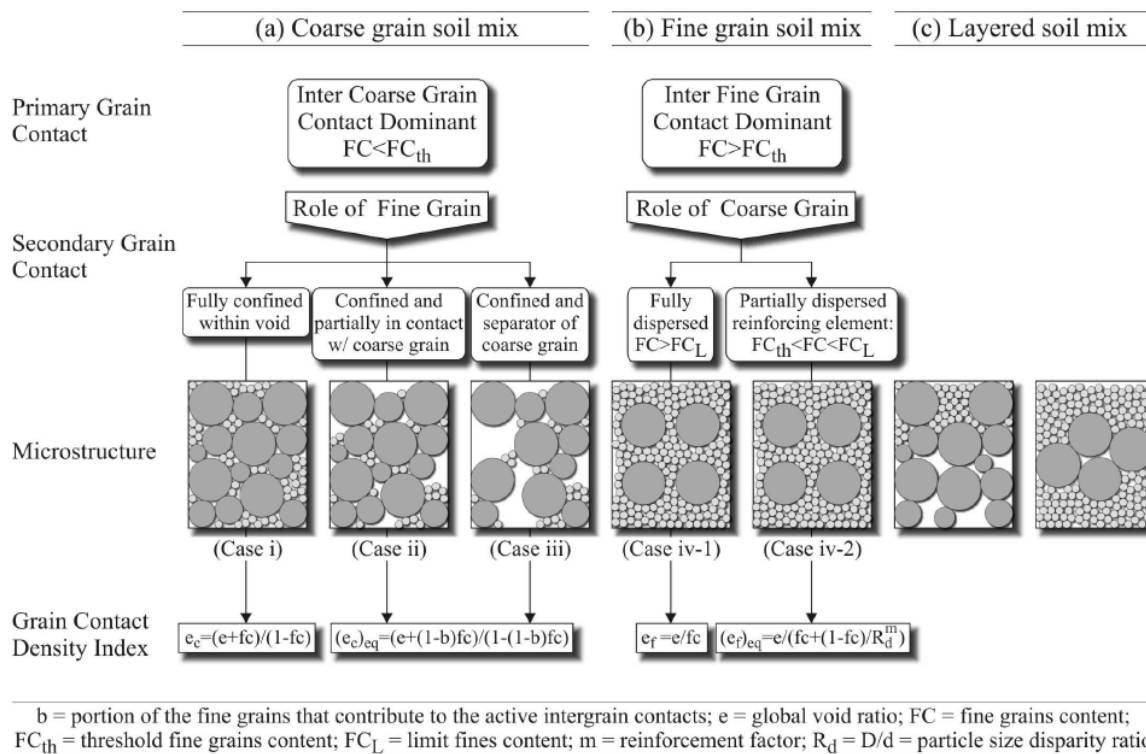


**Figure 2-23 - Intergranular soil mix classification (Thevanayagam et al., 2002).**

As discussed by Thevanayagam and Martin (2002), this conceptual framework and consideration of relative permeability between clean and silty sands may explain and resolve the apparent contradiction with empirical criteria for the evaluation of liquefaction resistance based on penetration testing.

Research is still in progress to further validate this promising approach, extending it also to materials with high silt content.

#### 2.3.2.4 Soils with transitional behaviour

In recent years attention has been devoted by several researchers to mixed materials where the coarse fraction is characterized by sand or silt and the fine fraction contains clay minerals (see for example Martins et al., 2002; Ferreira and Bica, 2006; Nocilla et al., 2006; Nocilla and Coop, 2008). These workers highlight that these materials are characterized by:

1. non-unicity of the “normal compression line” at low stress;
2. no apparent yield in the normal compression lines and therefore non-unicity at high stress, as opposed to what happen in clean sands;
3. non-unicity of the SSL.

The following observations may be made with respect to these findings:

1. non-unicity of the “normal compression line” at low stress presumably depends on fabric in the same manner as discussed above for clean sands;
2. yielding and convergence of the normal compression lines in sands are associated with particle crushing, which presumably is prevented at comparable stresses by what Martins et al. (2002) refer to as the “cushioning” effect of the fines or to the much larger number

---

of particle “contacts” which result in less stress concentrations in the skeleton for any given level of applied pressure;

3. the statement on the non-unicity of the SSL seems to be based on an interpretation of the results of undrained triaxial tests where points actually representative of the QSS have been attributed to SS. The non-unicity of the QSSL in sands has been thoroughly discussed above.

It seems that the framework described above for clean and silty sands can reasonably apply to transitional soils too; further study is necessary to validate this.

### ***2.3.2.5 Constitutive modelling of clean sands and silty sands***

Simulation of the main aspects of the behaviour of coarse grained materials as discussed above, including non linear behaviour, shear-induced plastic volumetric strains (dilation/contraction), strain softening/hardening, inherent and shear induced anisotropy and its evolution, etc., may be attempted only by adopting elasto-plastic constitutive models with the following basic characteristics:

- They shall be consistent with the framework of Critical State Soil Mechanics (Schofield and Wroth, 1968; Atkinson and Bransby, 1978; Wood, 1990).
- They shall include advanced plasticity modelling concepts such as mixed isotropic and kinematic hardening, i.e. multisurfaces plasticity, bounding surface plasticity, generalized plasticity, multimechanisms plasticity, etc. and non- associative flow rules (Dafalias and Popov, 1975; Mroz et al., 1978; Prevost, 1978; Dafalias and Herrmann, 1982; Aubry et al., 1982; Prevost, 1985; Lade and Kim, 1988; Pastor et al., 1990; Prevost, 1993; Di Prisco et al., 1993; Beaty and Byrne, 1998; Elgamal et al., 2002; Yang et al., 2003).
- They preferably should adopt, for each selected material, the same constitutive parameters at all densities by including state parameters as essential variables to describe the current state of the material compared to the SS or other characteristic states (Jefferies, 1993; Crouch and Wolf, 1994; Crouch et al., 1994; Wood et al., 1994; Manzari and Dafalias, 1997; Cubrinowski and Ishihara, 1998; Wan and Guo, 1998; Gajo and Wood, 1999; Li et al. 1999; Li and Dafalias 2000; Li, 2002; Wang et al., 2002).
- They shall assume the parameter M variable with the Lode angle ( $\theta$ ) (Grammatikopoulou et al., 2007).
- They shall consider the effects induced by fabric, including its evolution (Dafalias and Manzari, 2004).

### 2.3.3 “Rocks”

#### 2.3.3.1 *Intact material*

In dealing with rock, it is essential to make the distinction between intact rock and rock mass. The basic principles which govern the mechanical behaviour of intact rock are the same that have been described above for soil, with differences being only a matter of degree (Johnston, 1991; Haberfield, 1998). Mineralogical and petrographic factors, as commonly used for their conventional geological description and classification, do not control the strength and stiffness of rocks which depend instead primarily on the characteristics (hardness, size, grading, shape) of the constituent minerals or particles, the packing (porosity, dry density relative to particle density) and structure (bond between particles and across pores, anisotropy of mineral and grain orientation, microfractures and flaws) of the material and the presence of water (Selby, 1987).

The presence of significant bonding allows the material to exist at states of stress which may be incompatible with the packing of the material and the strength that would derive purely from inter-particle friction and dilatancy. Much as described for bonded clayey soils of the type CA, CB2 and CO2, this results in the deformability and strength of rock depending upon the stress rate or strain rate used in testing, as documented for example by Serdengecti and Boozer (1961), Bieniawski (1970), Houpert (1974), Aydan et al., (1994), Aydan and Nawrocki (1998).

Distinctions between “soft” and “hard” rock, typically based on the unconfined compressive strength of intact material, are of only marginal practical significance in relation to pre failure and post failure behaviour of rocks in the context of landsliding. At the low confining stress levels typical of most landsliding, even materials that in other contexts may be classified as “soft” rocks are characterized by intact rock strength well in excess of applied shear stresses. For example, falls in both “soft” rocks - chalk from Kent (Hutchinson, 1988) and “hard” rocks (Hsü, 1975) can generate a very large run-out when the energy involved exceeds a threshold value, although, clearly, the actual values involved in the two cases are significantly different.

#### 2.3.3.2 *Rock mass*

In these conditions the behaviour of slopes is typically governed by the presence and nature of discontinuities in the rock mass. Depending on the number, type, orientation and roughness of discontinuities, the nature and thickness of the filling material, if any, the geometry of the slope, the stability of the slope may be analyzed in terms of sliding along predetermined discontinuities or in terms of an equivalent continuum. Figure 2-24 shows the four main types of failure together with typical pole plots representative of the structural conditions likely to lead to such failures. In all cases, movement has to be kinematically admissible, and this depends also on the geometry (dip and direction) of the free face (natural or artificial slope).

Circular failures (case -a- in Figure 2-24) are similar in all respects to the type of failure that develops in soil; they can occur in heavily and randomly fractured rock, with no dominant set of discontinuities or where the persistent sets of discontinuities in the slope do not result in kinematically admissible mechanisms.

The mechanical characteristics of the rock mass could be determined directly from in situ or laboratory samples, if these were of sufficient size to be representative of the discontinuous rock mass (Hoek, 1983; Hencher, 1987). While this is possible, at least in theory, in special

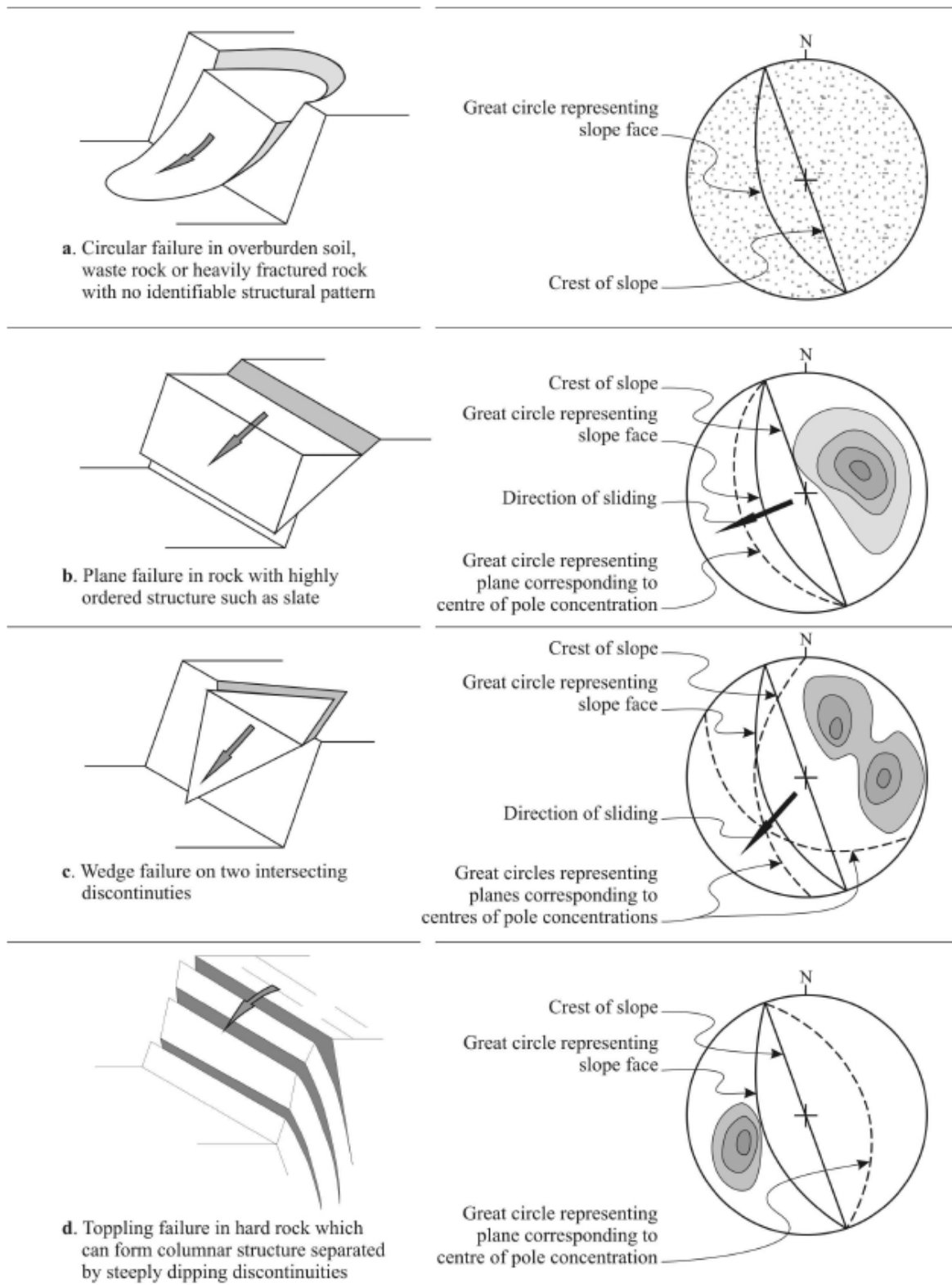


**Figure 2-24** -Main types of slope failure and stereo plots of structural conditions likely to give rise to these failures (Hoek and Bray, 1981).

cases such as the scaly clays of the Italian Appennines (Picarelli and Olivares, 1998), typically it is necessary to resort to indirect methods. Various empirical failure criteria have been proposed to take into account discontinuities in an “equivalent” continuum, for example by Patton (1966), Ladanyi and Archambault (1970) and Ladanyi and Archambault (1972). The most widely used criterion is that initially proposed by Hoek and Brown (1980a, b), who sought to link the empirical failure criterion, which defines curvilinear failure envelopes for all rock types, to geological observation by means of one of the rock mass classification schemes then available and for this purpose used the Rock Mass Rating (RMR) proposed by Bieniawski (1976). The criterion was subsequently progressively refined by Bray (reported by Hoek, 1983), Ucar (1986), Londe (1988), Hoek and Brown (1988), Hoek (1990), Hoek et al. (1992), Hoek (1994), Hoek and Brown (1997), Sjöberg (1997) and Sjöberg et al. (2001). To overcome limitations of the RMR classification, especially for very weak rock masses, the Geological Strength Index (GSI) was introduced and developed by Hoek et al. (1992), Hoek (1994), Hoek et al. (1995), Hoek et al. (1998), Hoek and Marinos (2000), Marinos and Hoek (2000a, b), and Marinos and Hoek (2001). Sjöberg et al. (2001), Pierce et al. (2001) and Hoek et al. (2002) introduced the concept of construction induced disturbance to account for the damage induced to the rock mass by blasting and stress release.

The companion approach for the empirical estimation of rock mass modulus is described by Hoek and Diederichs (2006).

Planar failures (case –b- in Figure 2-24) occur in rock masses with highly ordered structure such as many sedimentary or meta-sedimentary rocks, where failure often exploits bedding planes, especially where they have been presheared by even mild tectonic movements (see for example Skempton, 1985). Wedge failures (case –c- in Figure 2-24) occur in rock masses with two or more intersecting discontinuity sets. In both cases stability analyses must be carried out by adopting the “discontinuous model” and/or the “block theory” (Goodman, 1997), with appropriate shear strength of the individual joint. Recent advances in numerical analysis include the development of techniques for the explicit modelling of discontinuous masses and of fracture propagation, which can be of particular interest in relation of triggering.

The nature of friction between two rock surfaces is discussed in detail by Selby (1987), based on the work by Lama (1972). Based on the work of Newland and Allely (1957), Patton (1966) and Einstein et al. (1970), the failure envelope for shearing along a planar surface in rock can be expected to have the following characteristics:

- At low normal stress the apparent angle of friction will approximate the angle of residual shearing resistance of the material plus the angle that asperities make with the horizontal, with the asperities sliding over each other;
- At relatively high normal stress, after the asperities have suffered a certain amount of dilation and their effective area has reduced accordingly, their strength may be exceeded and they will shear through. This will result in an apparent cohesion intercept and a frictional angle equal to the angle of residual shearing resistance of the material. For very weak material and/or very high stress, the asperities may shear at their base, without dilatancy.

In actual fact, real failure envelopes deviate from and lie below the idealized bilinear envelope described above for pure material and totally interlocking surfaces because interlocking is lost before failure as a result of displacements and because of non uniform stress distributions on the surfaces of the asperities which may partially fracture before maximum strength is reached, resulting in curvilinear envelopes.

---

Of particular importance is the filling that may accumulate in the discontinuity. Whether such filling is the result of alteration in situ of the rock surfaces, washing-in, fault gouge or the product of degradation and fracturing of asperities during shearing, it will separate the asperities of the joint walls and, as it becomes thicker, it will progressively reduce the contact between the joint walls until the contact is wholly prevented and the strength of the joint is reduced to that of the infill. In constant normal stiffness (CNS) tests on toothed joints in “soft rock”, an infill thickness to asperity height ratio ( $t/a$ ) of 1.4 has been found to be “critical”, whereby the joint shear behaviour changes from dilative (governed by the asperities) to contractive (governed by the infill) when  $t/a$  exceeds the critical value (Indraratna et al., 1998).

Direct measurements of joint strength in the field are difficult and no wholly satisfactory techniques have been developed yet. Attempts have been made with large field shear boxes (very expensive), tilt tests and pull tests (cheaper, but with limitations on their representativeness and repeatability). In all cases, the results depend on the length of the sample, due to the mobilization of larger but less steeply inclined asperities in larger samples, to the extent that for very long joints, even at low normal stress, the frictional resistance is likely to be that of the residual angle of friction of the rock plus two or three degrees (Barton, 1981; Selby, 1987).

Indirect estimates of joint strength may be made by measuring joint roughness by means of profile gauges, a ruler or a plate of known dimensions, and comparing the results with published charts (Barton and Choubey, 1977), but this method too is subject to severe limitations and need a large number of determinations to provide representative results. Laboratory shear boxes may be used to determine joint strength under known stress conditions, but the limitations related to sample size mentioned above apply. In common practice this strength is assessed by using empirical criteria as suggested for example by Barton (1971), Barton (1973), Barton and Choubey (1977), Barton and Bandis (1980), Bandis et al. (1981), Davis and Salt (1986), Barton (1986) and Barton (1999).

### ***2.3.3.3 Structurally complex formations***

Common typical features of these formations are alternating layers of arenaceous (occasionally limestone) rock of good geotechnical characteristics and pelitic material. The pelitic component is often fissile and sheared and has poor geotechnical characteristics; depending on the degree of bonding and Unconfined Compressive Strength (UCS), the pelitic component may overlap with the intact, jointed/fissured or intensely fissured hard overconsolidated clays type CB1 and CB2.

A typical example is represented by flyschs, which are widespread particularly around the Mediterranean Sea and in Central Europe (Sovinc, 1977; Bober and Zabuski, 1993; Dounias and Marinos, 1993).

Classifications of these formations have been made by taking into account both the lithological features and the complexity of structural characteristics (see for example AGI, 1979). Simplifying, structural complexity is given by:

- Presence of two or more component with different geotechnical characteristics;
- More or less intricate geometrical relationships between the various components;
- Changes induced in the original structure by deformation processes;
- Alteration and weathering.

Possible associations between arenaceous (A) and pelitic (P) materials are based on the value of the A/P ratio (Figure 2-14).

No particular difficulty is encountered in sampling and testing the two basic components if they have a rock-like behaviour; however, significant difficulties may be encountered in sampling and testing the pelitic component where this is highly fissured and has poor characteristics, as already discussed in relation to scaly clays.

Besides the geotechnical complexity determined by the association in quick succession of very different materials, additional geotechnical complexity derives from the spatial variability of the different lithotypes. More or less intense tectonic deformations and gravitational displacements subsequent to the emplacement and the diagenesis of these sediments may modify their original structure by various degrees up to obliterating it completely (Figure 2-13).

Where the layers are still regularly arranged and are crossed by spaced joints (Class A in Figure 2-13), bedding planes and tectonic discontinuities subdivide the mass into blocks; with the necessary caution, geotechnical models (discontinuous or continuous) may be developed with reference to the considerations and criteria discussed for homogeneous rock masses. Where the “equivalent” continuous model is applied, reference can be made to a modified strength criterion specifically developed for flysch formations (see for example Hoek et al., 1998 and Marinis and Hoek, 2001).

In the case of significant tectonic deformations and gravitational displacements the complexity is given by the introduction of features which significantly modify the original structure of the formation, as schematized by Esu, 1977 and reported in AGI, 1979.

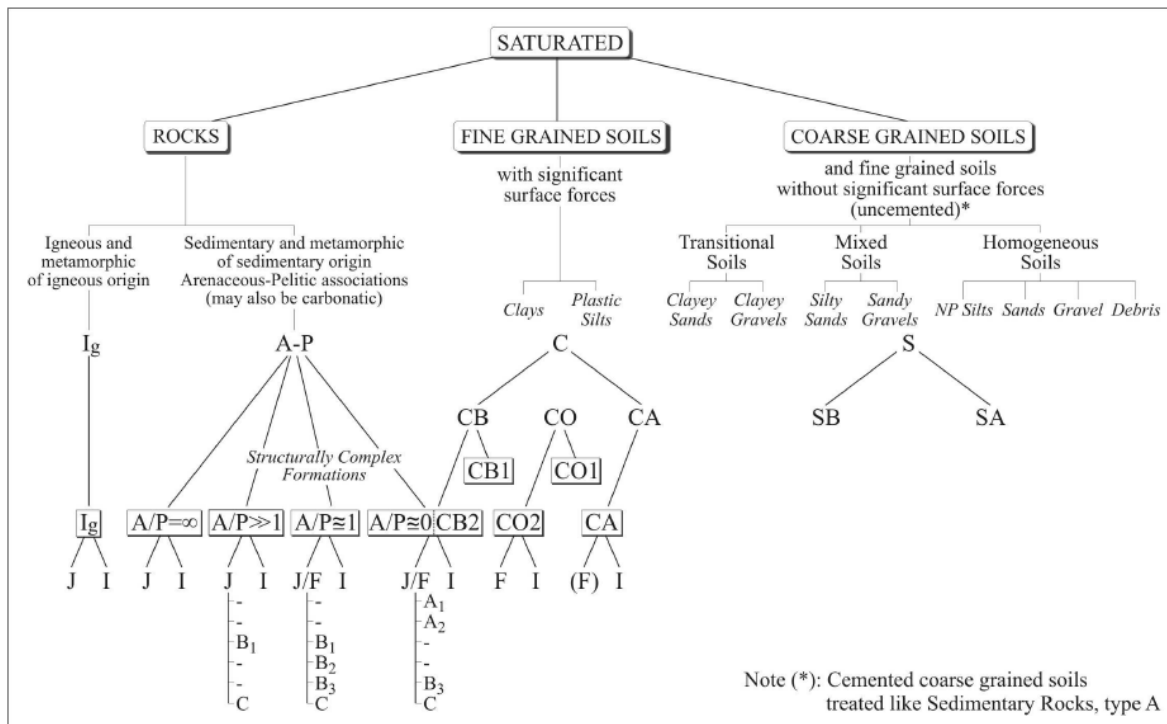
In this case and in presence of association of coarse and fine grained materials represented by A/P ratios lower than 20%, the geotechnical model may be developed with reference to the considerations and criteria applicable to intensely fissured CB1 and CB2 clays.

#### **2.3.4 Geotechnical classification**

As discussed in Section 2.2, the current trend is to extend traditional, mainly geomorphological, classifications of landslides to encompass geotechnical aspects; in particular, reference has been made in Section 2.2 to the geotechnical classification reported in Leroueil (2001) relating a 3D matrix (Figure 2-3):

- Slope movement, as described in geomorphological classifications;
- Movement stage, classified as pre-failure, failure, post failure, reactivation;
- Materials, as described in Figure 2-4.

Based on the discussion of the geotechnical behaviour of saturated soils and rocks presented above, a possible refinement of the classification of saturated materials is shown in Figure 2-25 in an attempt to provide a rational basis for defining appropriate constitutive modelling and parameters for advanced numerical analysis of landslide triggering in these materials, as discussed above and shown, for example, in the numerical examples in Section 2.4.



Note (\*): Cemented coarse grained soils treated like Sedimentary Rocks, type A

**Figure 2-25** - Revised classification of material types for the geotechnical characterization of slope movements (based on classification by Vaunat et al., 1994 and Locat, 1999).

---

## 2.4 NUMERICAL EXAMPLES

### 2.4.1 General

With reference to some of the issues discussed in the previous Sections related to soils classification and behaviour, some numerical examples are described below to highlight current capabilities offered by Geotechnical Engineering to analyse in deeper details problems related to slope behaviour in terms of both stability and movements until triggering of local or global failure. The numerical analyses of post failure conditions and run-out are beyond the scope of this work package.

The numerical examples have been carried out by means of finite element method (FEM) and appropriate constitutive models developed and implemented in various FEM and FDM codes by Studio Geotecnico Italiano srl and Autosoft sas. The examples deal with the following topics:

1. **Example 1** – Response of clayey materials CO1 (normally consolidated, unbonded) and CO2 (normally consolidated, bonded) to stress relief in 1D (oedometric) conditions due to erosion processes, including the occurrence of “mechanical weathering”.
2. **Example 2** – Response of clayey materials CB1 (mechanically overconsolidated, unbonded) to slope forming, asymmetric stress relief in 2D conditions due to basal erosion or excavation, including the effects of the initial  $K_0$  conditions on the overall delayed failure behaviour.
3. **Example 3** – Response of clayey materials CA (metastable microstructure, bonded) to slope forming, asymmetric stress relief in 2D conditions due to basal erosion or excavation. including comparisons with that observed in clayey materials CB1 (mechanically overconsolidated, unbonded).
4. **Example 4** – Response to drained (slow) and undrained (fast) surcharging of sandy materials SA and SB in underwater slopes formed by accretion (sedimentation or filling).

### 2.4.2 Example 1 – 1D stress relief in clayey materials

Let us consider geological deposits consisting of clay materials sedimented under water in 1D (oedometric) conditions and consolidated along the normal consolidation line which, for the sake of simplicity, is here considered coincident with the oedometric intrinsic compression line ( $ICL_{oe}$ ). At the end of the sedimentation phase the material may or may not be reinforced by diagenetic processes leading to some bonding between particles.

In the absence of bonding, at the end of the sedimentation phase the clayey material may be classified as CO1 (normally consolidated, unbonded); its behaviour is simulated by an elastoplastic constitutive model of the CAM-CLAY family, in which both generalized plasticity within the Intrinsic State Boundary Surface and variation of the strength parameter  $M$  with the Lode angle ( $\theta$ ) have been introduced, referred to below as CAM-CLAY-GEN.

In the presence of bonding, at the end of the diagenetic processes the material may be classified as CO2 (normally consolidated, bonded); its behaviour is simulated by an elastoplastic constitutive model similar to that of the unbonded material, with the addition of a Yield Surface, similar in shape, but with dimension larger than the Intrinsic State Boundary Surface; current stress states outside the Intrinsic State Boundary Surface are allowed, until the Yield Surface is reached; in which case destruction processes are activated leading to the development of additional plastic strains associated with a progressive shrinking of the Yield

**Table 2-4 - Intrinsic parameters of the CAM-CLAY-GEN and CAM-CLAY-DES constitutive models.**

LL (%)	PI (%)	$\lambda$ (-)	$v_\lambda$ (-)	OCR (-)	$v'$ (-)	$\kappa$ (-)	$\varphi_{cs}'$ (°)	$a_c$ (-)
70	40	0.175	2.89	1	0.2	0.035	20	0.002

LL = limit liquid  
 PI = plasticity index  
 $\lambda$  = slope of the intrinsic isotropic compression line ( $ICL_{iso}$ ) in the  $v$ - $\ln(p')$  plane  
 $v = 1 + e$  = specific volume  
 $e$  = void ratio  
 $p'$  = mean effective stress  
 $v_\lambda$  = specific volume on the  $ICL_{iso}$  at  $p' = 1$  kPa  
 OCR = mechanical overconsolidation ratio at the end of the sedimentation phase  
 $v'$  = Poisson ratio  
 $\kappa$  = slope of the elastic wall in the  $v$ - $\ln(p')$  plane  
 $\varphi_{cs}'$  = angle of friction at critical state  
 $a_c$  = parameter which govern the rate of plastic strains, excluding those induced by destruction processes

Surface until it overlaps the State Boundary Surface (fully loss of bonding); this constitutive model is referred to below as CAM-CLAY-DES.

Following sedimentation and diagenesis (if any), 1D (oedometric) erosion processes take place until the current ground level is reached; at the end of the erosion phase the materials may be classified as CB1 (mechanically overconsolidated, unbonded) or CB2 (mechanically overconsolidated, bonded).

The FEM analyses described below have been carried out in 1D conditions; they consider erosion processes occurring in drained conditions, with various thicknesses ( $H_e$ ) of material removed (60 m, 120 m and 180 m).

The intrinsic parameters of the constitutive models, which characterize both the CAM-CLAY-GEN and the CAM-CLAY-DES constitutive models, have been selected to be representative of clayey materials of relatively high plasticity, such as London clays (Table 2-4). In Table 2-4 the parameter  $a_c$  which governs the rate of plastic strain generation in the CLAM-CLAY-GEN is also given. Other parameters, such as those which define the initial dimension of the Yield Surface and govern both the rate of plastic strains generated by destruction processes and the rate of shrinking of the Yield Surface in the CAM-CLAY-DES model have been selected to be representative of relatively strong bonded materials.

The main results of the numerical simulations can be summarized as follows (all depths refer to final ground level after erosion):

- For the case represented by  $H_e = 180$  m, Figures 2-26-a, b show the states of materials CO1/CB1 (unbonded) and CO2/CB2 (bonded) in terms of void ratios ( $e$ ) and vertical effective stresses ( $\sigma_v'$ ) at the end of the sedimentation phase and during the erosion phase; Figure 2-26-a refers to materials at shallow depths ( $\cong 1$  m below the final ground level), while Figure 2-26-b refers to material at greater depths ( $\cong 30$  m below the final ground level).

At shallow depths, the numerical simulation replicates well the behaviour of materials CO1/CB1 (unbonded) and CO2/CB2 (bonded) discussed in Section 2.3.1 and shown qualitatively in Figure 2-11; for materials CO2/CB2 a more realistic swelling line would be obtained using elasto-viscoplastic constitutive models. It is highlighted that below a

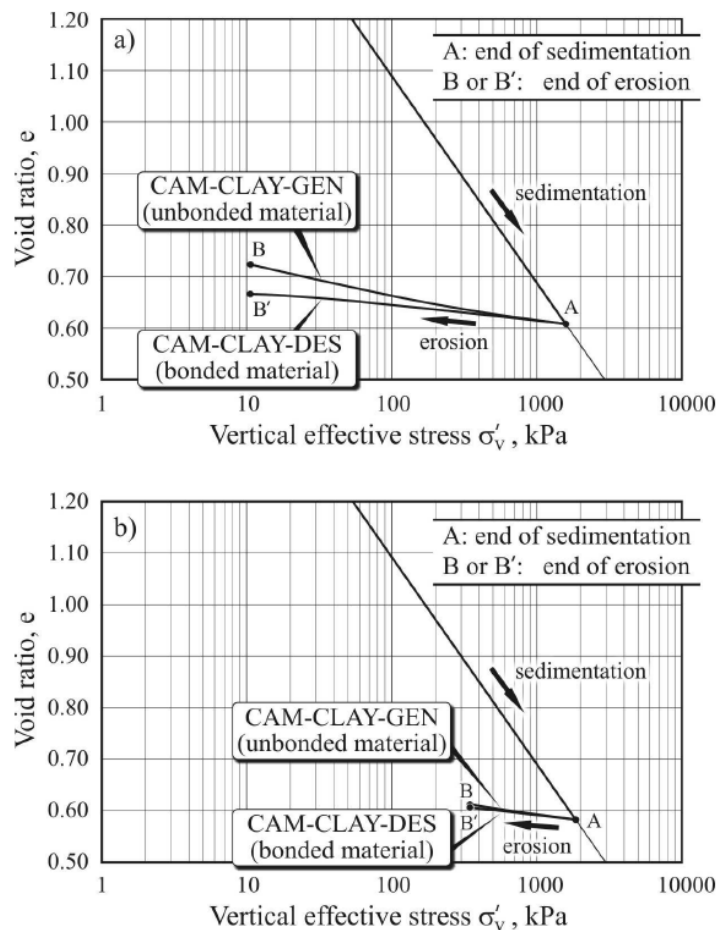


**Figure 2-26** - Numerically simulated geological history of type CO and CB clays. Final depth 1 m (a) and 30 m (b) following 180 m of erosion.

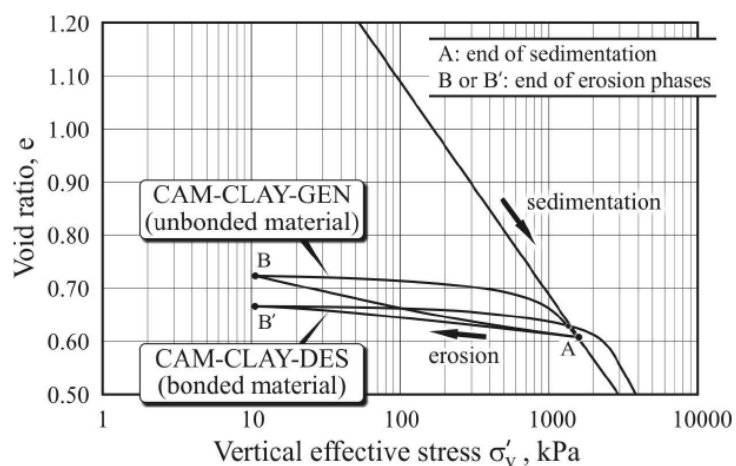


**Figure 2-27** - Numerically simulated reloading in oedometric conditions of type CB clays at 1 m depth following 180 m of erosion.

threshold vertical effective stress, both the materials CO1/CB1 (unbonded) and CO2/CB2 (bonded) exhibit significant increase of void ratios, as a result of the development of significant deviatoric and volumetric plastic strains due to deviatoric stresses which approach conditions of passive failure; as already discussed in Section 2.3.1, the occurrence of significant plastic strain can result (particularly in unbonded or weakly bonded materials) in a loss of memory of the maximum vertical effective stress  $\sigma_{vmax}'$  experienced by the deposit before erosion; this is shown (Figure 2-27) by the numerical simulation of the behaviour of shallow materials reloaded in oedometric conditions after the end of the erosion phase; in the case of unbonded materials CO1/CB1 the conventional interpretation of the numerically simulated oedometer test would lead to determining a preconsolidation pressure  $\sigma_{vp}'$  lower than  $\sigma_{vmax}'$ . The opposite would occur with strongly bonded materials CO2/CB2. Even though the material has experienced significant damage during unloading, on reloading conventional interpretation of the numerically simulated oedometric test would lead to determining a preconsolidation pressure  $\sigma_{vp}'$  greater than  $\sigma_{vmax}'$ .

At greater depths, both the materials CO1/CB1 and CO2/CB2 exhibit essentially elastic

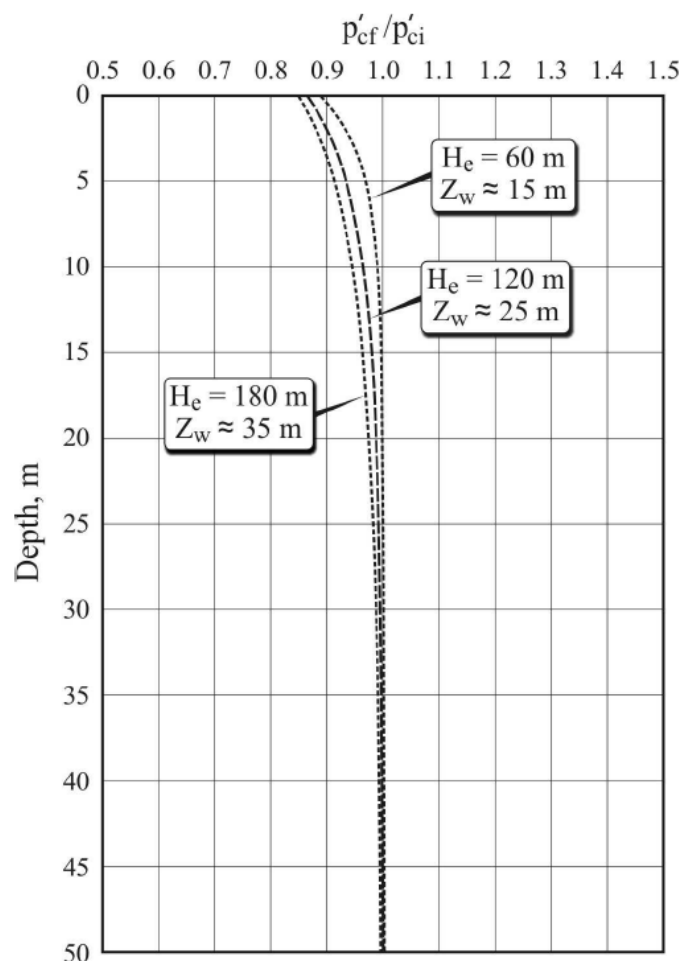


**Figure 2- 28** - Numerically simulated profiles of  $p'_{cf}/p'_{ci}$  ratios and thickness of damaged material CB2 for different thickness of erosion (60 m, 120 m, 180 m).

behaviour, both in oedometric unloading (Figure 2-26-b) and in oedometric reloading to  $\sigma_{vmax}'$ . Obviously, reloading of bonded materials CO2/CB2 would result in an apparent conventional preconsolidation pressure  $\sigma_{vp}'$  greater than both  $\sigma_{vmax}'$  and  $\sigma_{vp}'$  of the material unloaded to shallow depth.

- A critical depth ( $z_w$ ) may be defined above which significant plastic strains develop, leading to possible loss of memory of the maximum vertical effective stress previously experienced by the deposit, and below which predominately elastic behaviour occurs. From a constitutive modelling point of view,  $z_w$  may be inferred by plotting as a function of depth the ratio between the isotropic pressures which define the State Boundary Surface (for unbonded materials) or the Yield Surface (for bonded materials) at the end ( $p_{cf}'$ ) and at the beginning ( $p_{ci}'$ ) of the erosion phase. For the bonded materials CO2/CB2, Figure 2-28 shows the results of the numerical simulation for  $H_e$  equal to 60 m, 120 m and 180 m in terms of  $p_{cf}'/p_{ci}'$ ; as discussed in Section 2.3.1, the greater the thickness of material removed, the greater the thickness of the material where significant plastic strains occur. Similar results have been obtained for the unbonded material CO1/CB1.

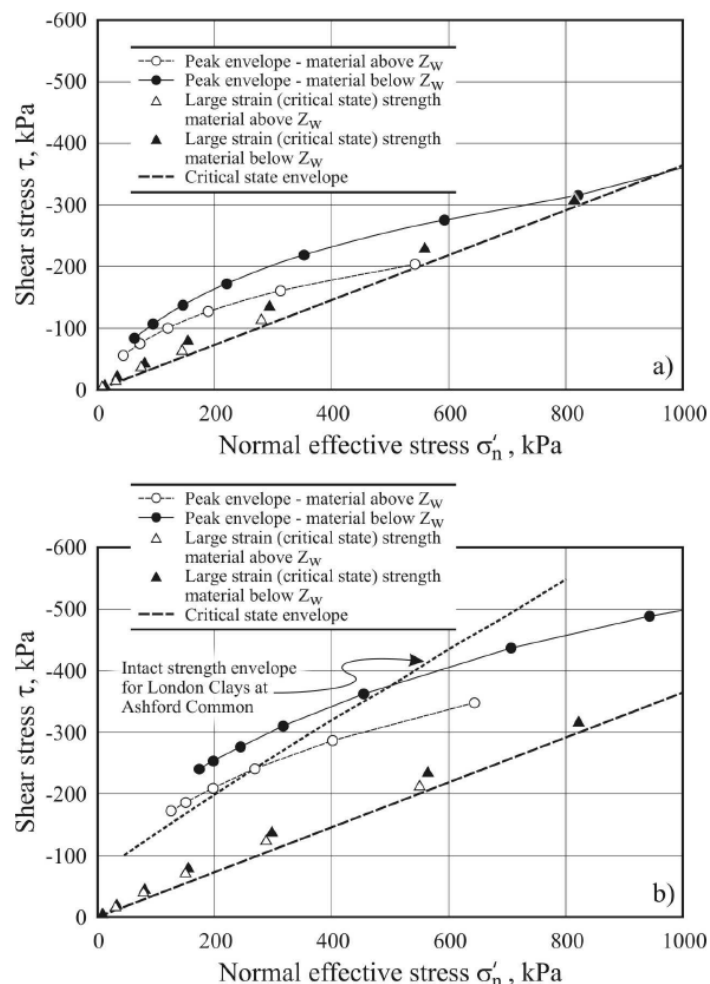


**Figure 2- 29** - Numerically simulated strength envelopes from triaxial tests in compression on (a) CO1/CB1 and (b) CO2/CB2 materials from depths above and below the critical depth following 180 m of erosion.

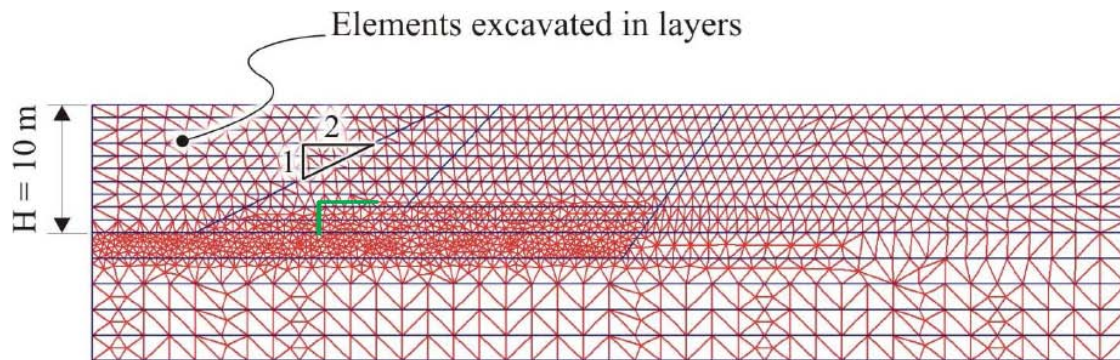


**Figure 2-30** - Finite element mesh for numerical simulation of erosion or excavation in CB1 clays.

- For  $H_e = 180$  m, Figure 2-29-a compares the effective strength envelopes at peak and at large strains (critical state conditions) obtained from numerically simulated triaxial tests on the unbonded materials CO1/CB1, “sampled” above and below the depth  $z_w$ . A similar comparison is reported in Figure 2-29-b for bonded materials CO2/CB2. In both cases, materials “sampled” above  $z_w$  exhibit lower peak effective strength envelopes, thus resulting, in conventional terms, “mechanically weathered”.  
Peak and large strains effective strength envelopes from numerical simulations on bonded materials CO2/CB2 compare well with those determined for intact London clays at Ashford Common (see Burland et al., 1996).

#### 2.4.3 Example 2 – Slopes in CB1 clays and the effects of $K_o$

Let us consider the 10 m high slope, inclined 1 (vertical): 2 (horizontal), shown in Figure 2-30, as examined by Potts et al. (1997) in their FEM 2D analyses of delayed failure in stiff overconsolidated clays. It has been re-analysed here by considering an elasto-plastic constitutive model, applicable to clayey materials CB1 (mechanically overconsolidated, unbonded), similar to that used in the example described in Section 2.4.2, extended to simulate the decay of the effective strength envelope from critical state to residual conditions; this constitutive model is referred to below as CAM-CLAY-GEN- $\phi_{cs}' \rightarrow \phi_r'$ .

The initial states of the materials CB1, represented by the void ratio ( $e$ ) and the vertical effective stress ( $\sigma_v'$ ), have been evaluated so that they are compatible with the selected values of  $K_o$  which in the analyses have been chosen to be equal to 1, 1.5 and 2 (Figure 2-31); as a first approximation, the following equation has been considered as compatibility relationship:

$$K_o = (1 - \sin \phi_{cs}') \cdot \sqrt{OCR} \quad [2-9]$$

where:

$OCR = \sigma_{vmax}' / \sigma_{vo}' =$  mechanical overconsolidation ratio.

With the exception of OCR, which varies depending on the selected  $K_o$ , the intrinsic parameters of the constitutive model are the same as those shown in Table 2-4; according to Potts et al. (1997), the decay of strengths from critical state to residual state has been linked to the cumulative deviatoric plastic strain ( $\epsilon_d^p$ ) as shown in Figure 2-32.

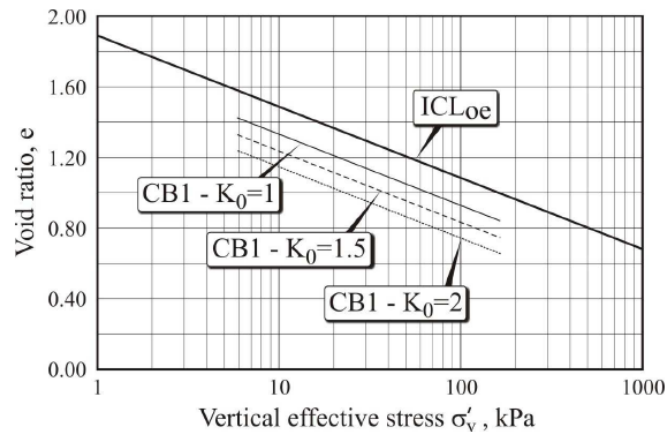


**Figure 2-31** - Initial states in  $e - \log(\sigma'_v)$  plane of CBI clays in Examples 2 and 3 for different values of  $K_o$ .

Arbitrary, constant values of  $K_o$  have been used in the analyses to allow easy comparison with the results published by Potts et al. (1997), although it is clear the constant values of  $K_o$  with depth are unrealistic in practice. In the analyses, the excavation down to 10 m depth below the original ground level has been carried out instantaneously in undrained conditions, while the response of the slope after excavation has been evaluated in coupled consolidation conditions, according to the Biot's theory for porous saturated materials.

The initial pore pressure regime has been assumed to be hydrostatic with the water table located at the original ground surface; after excavation, pore pressures have been set equal to 0 kPa on both the excavated surfaces and the remaining original ground surface.

The vertical and bottom boundaries of the mesh have been assumed to be impermeable; clay permeability has been assumed to be of the order of  $1 \times 10^{-9} \div 1 \times 10^{-10}$  m/s, linearly decreasing with depth. Only vertical displacements have been allowed on the vertical boundary of the mesh, while the bottom boundary has been fixed in both the vertical and the horizontal directions. The numerical method has been validated leading to results substantially in agreement with those published by Potts et al. (1997) when using similar constitutive models and parameters.

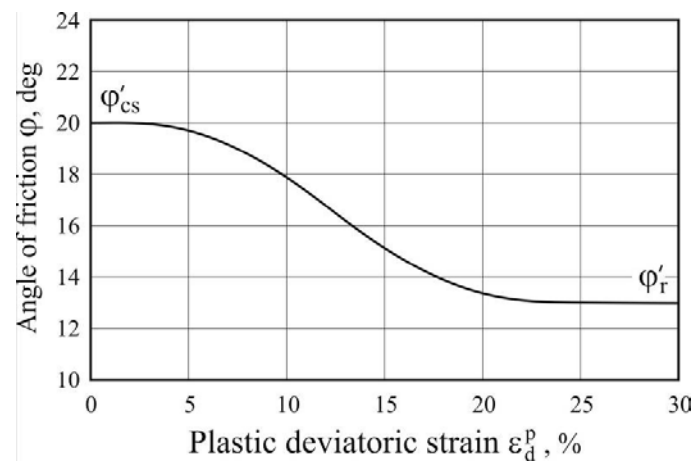


**Figure 2-32** - Variation of the angle of friction  $\phi'$  with the cumulative plastic deviatoric strain  $\varepsilon_d^p$  for CBI clays in Example 2.

The main results of the numerical analyses can be summarized as follows:

- Figure 2-33 shows the mid-slope horizontal displacements for different values of  $K_0$  as a function of time since excavation; Figure 2-34 shows the failure surfaces for different values of  $K_0$ , as inferred from the high cumulative deviatoric plastic strains which tend to localize in a relatively thin shear band. As discussed in Section 2.2, both the time to failure and the shape of the failure surfaces are significantly influenced by the initial  $K_0$  conditions.
- Progressive propagation of the localized deviatoric plastic strains is observed, starting from the toe and proceeding toward the middle and upper part of the slope (Figure 2-35). At failure, different effective strength envelopes apply in different portions of the failure surface; at the toe of the slope, where the cumulative deviatoric plastic strains are high, residual strength conditions prevail (compare Figure 2-32 with Figure 2-34), while in the upper part of the slope the current strength at the time of failure is near peak or critical state strength.

The overall response of the slope predicted by the FEM analyses described above is in line with predictions by others (see for example the FEM analyses described in more detail by Potts et al., 1997) and, more importantly, with actual behaviour observed in the field (see for example Burland et al., 1977; Cooper et al., 1998, Mesri and Shahien, 2003).

Figure 2-36 shows the excess pore pressures at failure (suction positive, as per definitions in the computer code) for the different values of  $K_0$  considered in the analyses. It is observed that some residual negative (stabilizing) excess pore pressures are still present in the slope near the failure surface. If the stability of the slope were analyzed by means of simplified limit equilibrium methods (LEM) assuming pore water pressures corresponding to the steady state condition (excess pore pressure equal to zero) and failure surfaces as predicted by the FEM analyses, the “operational” effective strength parameters at failure would correspond to the angle of shear resistance at critical state ( $\phi_{cs}'$ ) and an intercept of apparent cohesion in the range of 15÷20 kPa. This is in line with typical recommendations given in design practice for intact materials, which, however, fail to promote an adequate appreciation of the complexity of the phenomena involved, making the selection of “operational” parameters for LEM analyses often arbitrary.

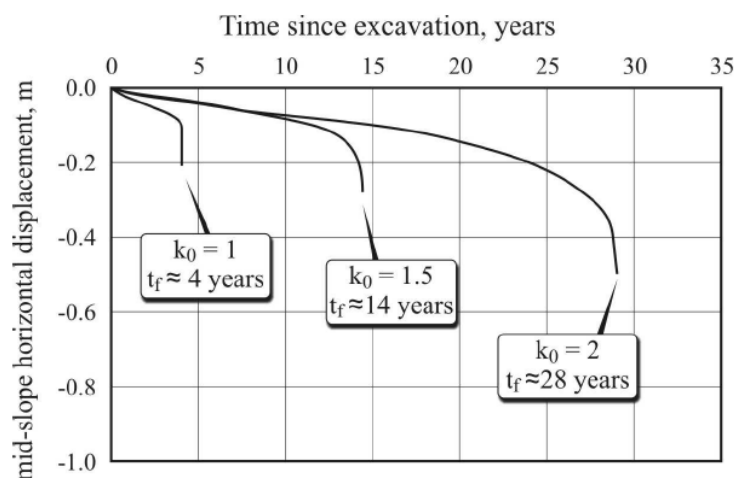


**Figure 2-33** - Numerically simulated mid-slope horizontal displacements as a function of time since excavation for a 1(v): 2(h), 10 m high slope in CB1 clays for different values of  $K_0$ .

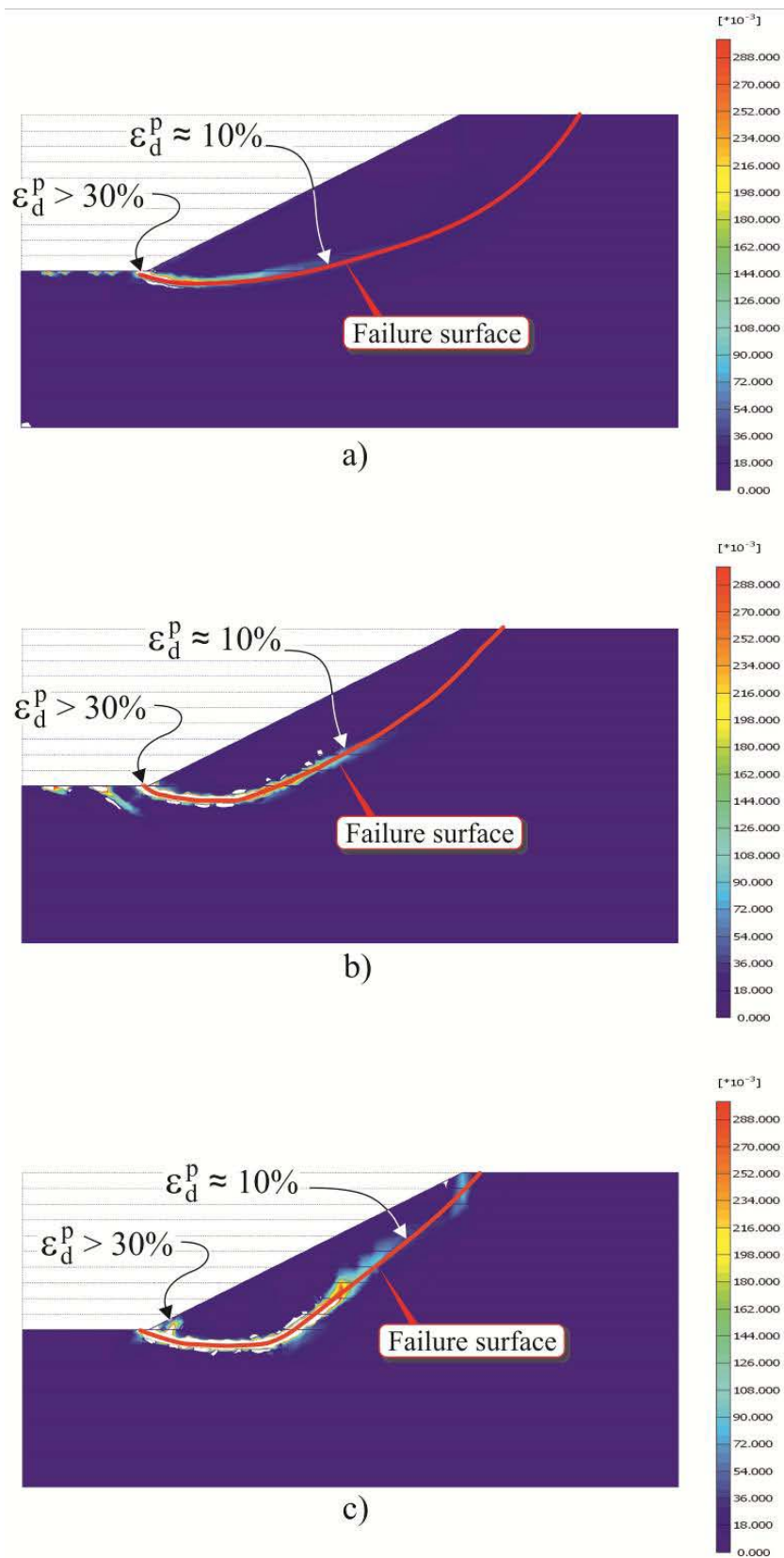


**Figure 2-34** - Numerically simulated distributions of cumulative deviatoric plastic strains at failure for a 1(v): 2(h), 10 m high slope in CB1 clays for (a)  $Ko = 1$ , (b)  $Ko = 1.5$ , (c)  $Ko = 2$ .

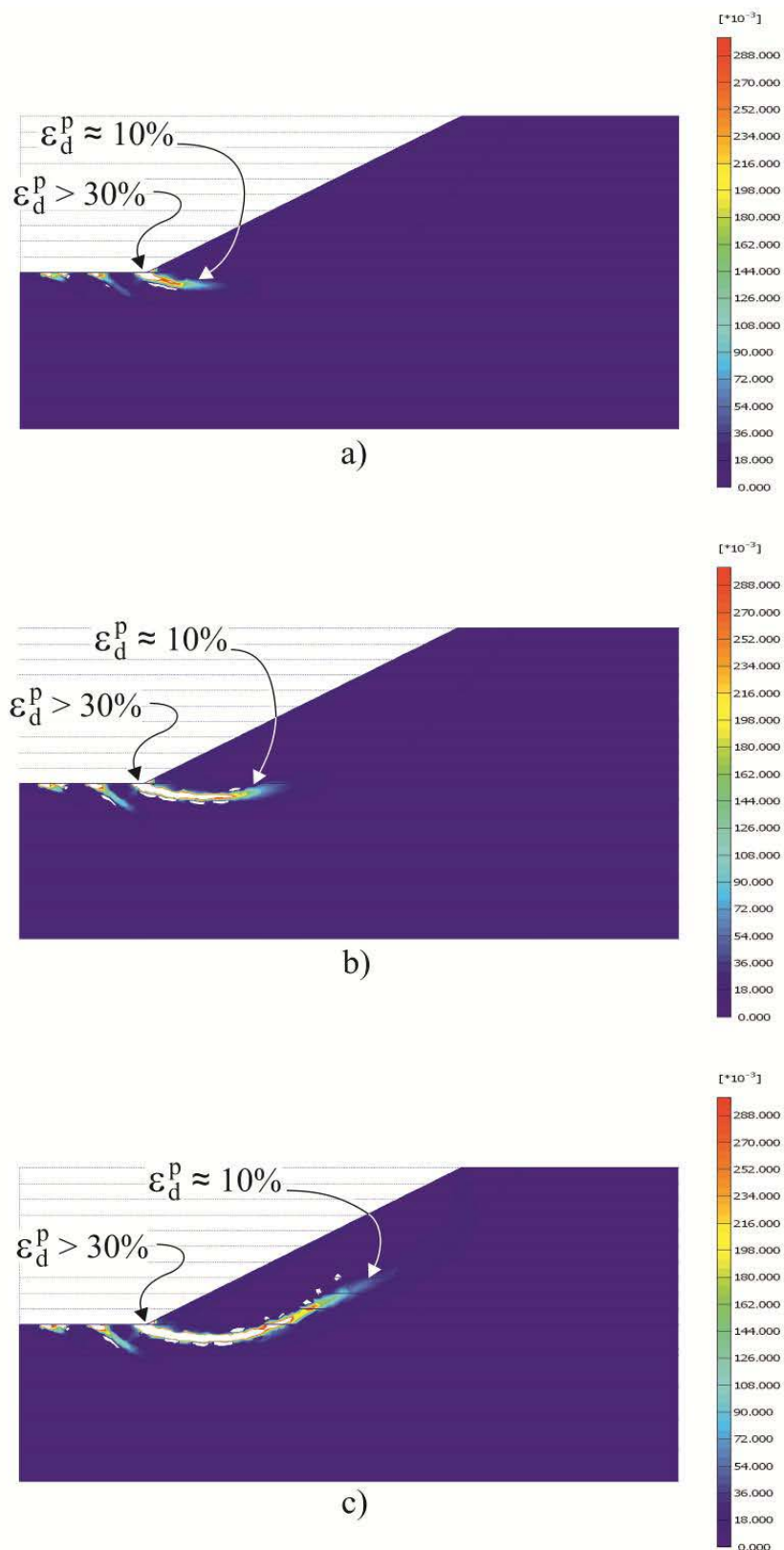


**Figure 2-35** -: Numerically simulated distributions of cumulative deviatoric plastic strains for a 1(v): 2(h), 10 m high slope in CB1 clays with  $K_o = 1.5$  at (a) 5 years, (b) 10 years, (c) 14 years (failure) since excavation.

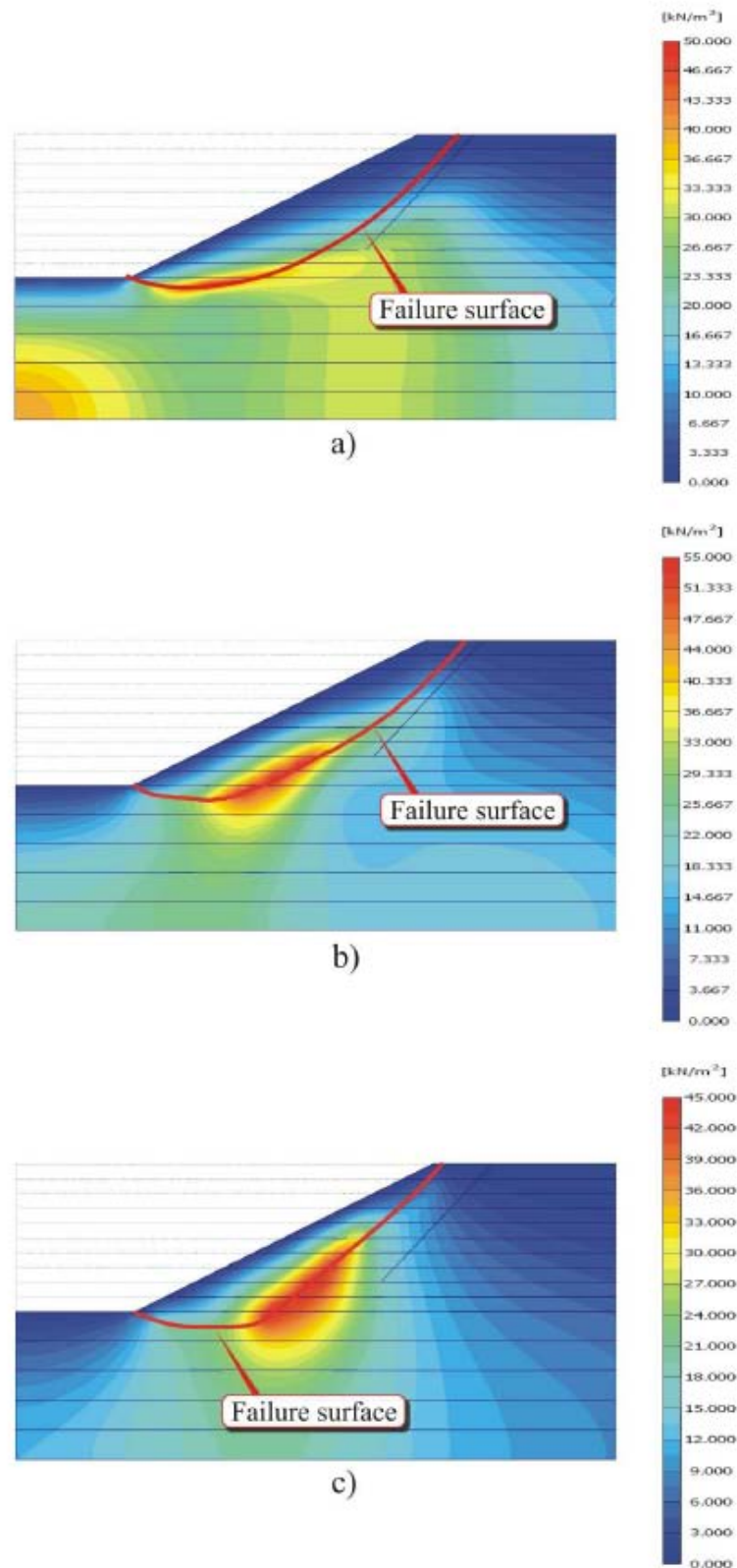


**Figure 2-36** - Numerically simulated distributions of excess pore pressures at failure for a  $1(v): 2(h)$ , 10 m high slope in CB1 clays for (a)  $K_o = 1$ , (b)  $K_o = 1.5$ , (c)  $K_o = 2$ .

#### 2.4.4 Example 3 – Comparison between CA and CB1 clays

Let us consider two 10 m high slopes inclined 1 (vertical): 3 (horizontal) (Figure 2-37), one excavated in clayey materials CB1 (mechanically overconsolidated, unbonded) and the other in clayey materials CA (metastable microstructure, bonded) with a 3 m “crust” of CB1 material.

The clay materials CB1 have been simulated by the elasto-plastic constitutive model CAM-CLAY-GEN used in the example described in Section 2.4.2. The initial states, represented by the void ratio ( $e$ ) and the vertical effective stress ( $\sigma_v'$ ), have been evaluated so that they are compatible with the selected values of  $K_o = 1$  (see Figure 2-31). With the exception of OCR, which depends on the selected  $K_o$ , the intrinsic parameters of the constitutive model are the same as those shown in Table 2-4.

The clay materials CA below the clayey “crust” have been simulated by the elasto-viscoplastic model developed by Rocchi et al. (2003), up-dated as described in Rocchi et al. (2006) and Rocchi et al. (2007); this constitutive model is referred to as QUICK-CLAY. The initial states, represented by the void ratio ( $e$ ) and the vertical effective stress ( $\sigma_v'$ ), considered in the analyses are shown in Figure 2-38; the initial stress conditions have been evaluated by assuming  $K_o = 0.6$ . The parameters of the model have been selected to represent typical CA materials, such as the Upper Pisa clays (see for example Rocchi et al, in preparation); they are shown in Table 2-5. The clayey “crust” overlying the clayey materials CA has been considered mechanically overconsolidated, unbonded, hence schematized by the CAM-CLAY-GEN constitutive model. The initial states, represented by the void ratio ( $e$ ) and the

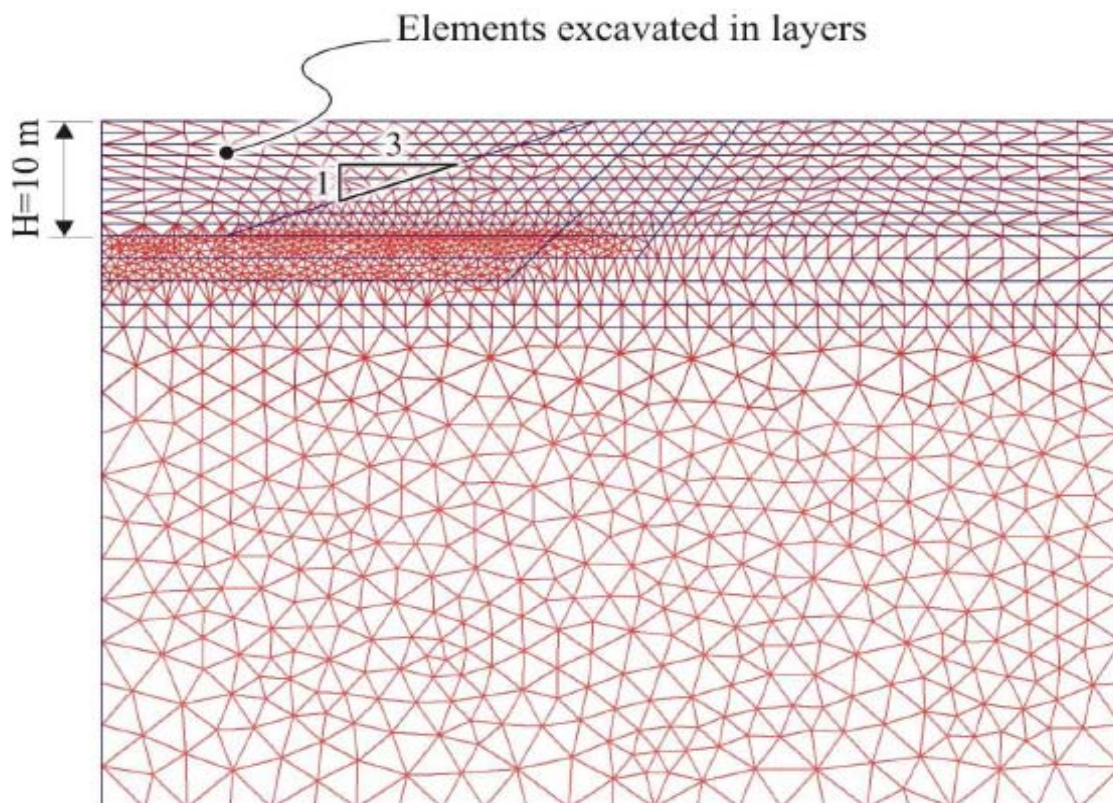


**Figure 2-37** - Finite element mesh for comparative numerical simulations of erosion or excavation in CBI and CA clays.

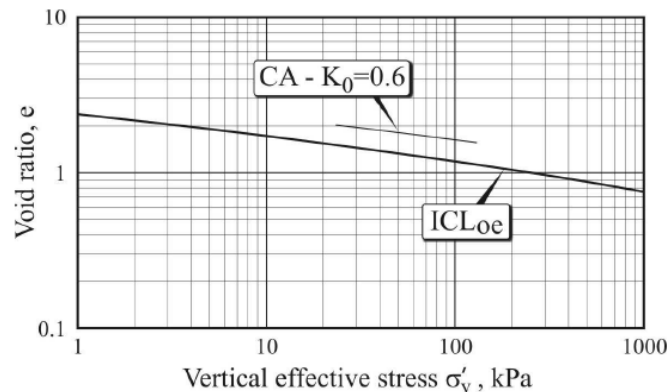


**Figure 2-38** - Initial states in  $\log(e) - \log(\sigma'_v)$  plane of CA clays in Example 3.

vertical effective stress ( $\sigma'_v$ ), have been evaluated so that they are compatible with the selected values of  $K_0$  which have been chosen to decrease with depth from 4 at ground level to 1.5 at 3 m depth. The intrinsic parameters of the constitutive model are shown in Table 2-6. The parameters adopted for the clay “crust” and the underlying clayey materials CA lead to the undrained shear strength profile shown in Figure 2-39.

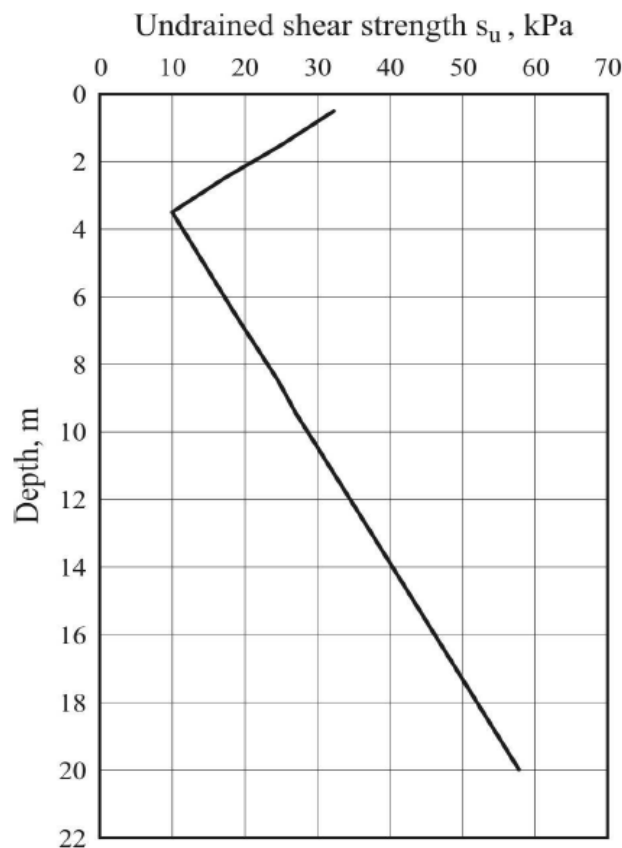


**Figure 2-39** - Numerically simulated profile of undrained shear strength vs depth for CA clays with 3 m thick “crust” of CBI clays.

**Table 2-5 - Parameters of the elasto-viscoplastic (QUICK-CLAY) constitutive model for the materials CA.**

LL (%)	PI (%)	$\lambda^*$ (-)	$v_{\lambda}$ (-)	$p_{cno}'/p_{cio}'$ (-)	$v'$ (-)	$\phi_{cs}'$ (°)	$\kappa^*$ (-)	$\mu_i$ (days)	$m$ (-)	$l$ (-)
70	40	0.095	3.44	15	0.25	24	0.018	$1.9 \times 10^{15}$	9	11

$z$  = depth below original ground level  
 LL = limit liquid  
 PI = plasticity index  
 $e_o$  = initial void ratio  
 $\lambda$  = slope of the intrinsic isotropic compression line ( $ICL_{iso}$ ) in the  $\ln(v)$ - $\ln(p')$  plane  
 $v = 1 + e$  = specific volume  
 $e$  = void ratio  
 $p'$  = mean effective stress  
 $v_{\lambda}$  = specific volume on the  $ICL_{iso}$  at  $p' = 1$  kPa  
 $p_{cno}'$  = initial mean effective stress linked to the INYL as defined by Rocchi et al., 2003, evaluated by considering  $\sigma_{vy}' = 1.4 \cdot \sigma_{vo}'$   
 $\sigma_{vy}'$  = “true” yield stress in oedometric conditions  
 $\sigma_{vo}'$  = vertical effective geostatic stress  
 $p_{cio}'$  = initial mean effective stress linked to the IRYL as defined by Rocchi et al., 2003  
 $v'$  = Poisson ratio  
 $\kappa$  = slope of the elastic wall in the  $\ln(v)$ - $\ln(p')$  plane  
 $\phi_{cs}'$  = angle of friction at critical state  
 $\mu_i, m, l$  = parameter related to the first mechanism of the elasto-viscoplastic constitutive model

In both cases the excavation phase down to 10 m depth below the original ground level has been carried out in two days in undrained conditions; the response of the cut slope after excavation has been evaluated in coupled consolidation conditions, according to the Biot’s theory for porous saturated materials.

**Table 2-6 - Intrinsic parameters of the CAM-CLAY-GEN constitutive model for the clayey “crust”.**

LL (%)	PI (%)	$\lambda^*$ (-)	$v_{\lambda}$ (-)	$K_o$ (-)	$v'$ (-)	$\kappa^*$ (-)	$\phi_{cs}'$ (°)	$a_c$ (-)
70	40	0.095	3.44	4→1.5	0.25	0.018	24	0

LL = limit liquid  
 PI = plasticity index  
 $\lambda$  = slope of the intrinsic isotropic compression line ( $ICL_{iso}$ ) in the  $\ln(v)$ - $\ln(p')$  plane  
 $v = 1 + e$  = specific volume  
 $e$  = void ratio  
 $p'$  = mean effective stress  
 $v_{\lambda}$  = specific volume on the  $ICL_{iso}$  at  $p' = 1$  kPa  
 $K_o$  = earth pressure coefficients at rest, decreasing with depth as indicated in the main text  
 $v'$  = Poisson ratio  
 $\kappa$  = slope of the elastic wall in the  $\ln(v)$ - $\ln(p')$  plane  
 $\phi_{cs}'$  = angle of friction at critical state  
 $a_c$  = parameter which govern the rate of plastic strains, excluding those induced by destruction processes

The initial pore pressure has been assumed to be hydrostatic with the water table at the original ground surface; after excavation, on both the excavated surfaces and on the original ground surface, pore pressures have been set equal to 0 kPa.

The vertical and bottom boundaries of the mesh have been assumed to be impermeable. The permeability of materials type CB1 has been assumed of the order of  $1 \times 10^{-9} \div 1 \times 10^{-10}$  m/s, linearly decreasing with depth.

The permeability of materials type CA and of the clayey “crust” has been assumed equal to  $1.5 \times 10^{-10}$  m/s.

Only vertical displacements have been allowed on the vertical boundary of the mesh, while the bottom boundary has been fixed in both the vertical and the horizontal directions.

The main results of the numerical analyses, can be summarized as follows:

- Figure 2-40 shows the mid-slope horizontal displacement for the two cases considered as a function of time. As discussed in Section 2.3.1, in the two cases, failure conditions are reached at considerably different times, i.e. 10 days for CA clays and approximately 70 years for CB1 clays. Figure 2-41 compares the failure surfaces for the two cases considered, as inferred from the high accumulated shear strains. While in CB1 materials shear plastic strains tend to localize in a unique, relatively narrow shear band, in CA materials multiple shear bands are observed which reach greater depths than in CB1 materials.
- Figure 2-42 compares the excess pore pressures (suction positive, as per definitions in the computer code) at 10 days after excavation, corresponding to failure conditions for materials type CA. The excess pore pressure distributions in the two cases are very different; while in CB materials they correspond essentially to the distribution of negative excess pore pressures induced by undrained unloading, in CA materials the excess pore pressures are generally low, appearing to correspond to complete dissipation to the steady state conditions. In fact, localized positive excess pore pressures near the multiple shear bands confirm that shear induced positive excess pore pressures have compensated and locally exceeded the negative excess pore pressures induced by reduction of mean total stress by undrained unloading, and that this mechanism prevails, rather than consolidation.

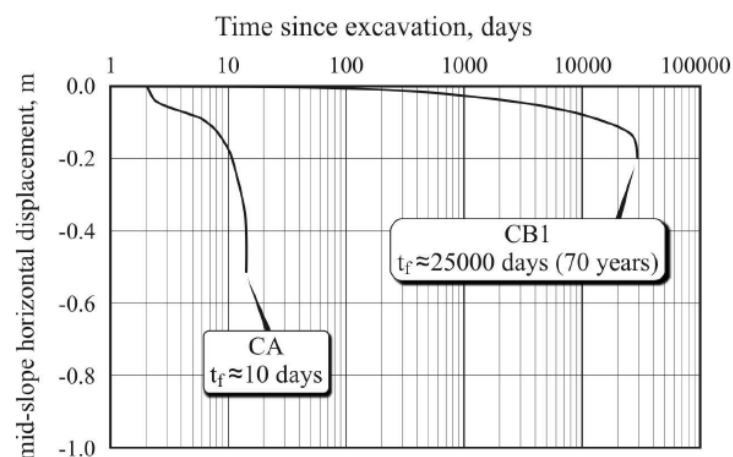


**Figure 2-40** - Numerically simulated mid-slope horizontal displacements as a function of time since excavation of a  $1(v): 3(h)$ , 10 m high slope for CA and CB1 clays.

- If stability of the slope in CA materials were analyzed by means of simplified limit equilibrium methods, assuming pore water pressures corresponding to the steady state condition (excess pore pressure equal to zero) and the failure surface predicted by the FEM analysis, the effective stress parameters at failure would correspond to the angle of shear resistance at critical state ( $\phi_{cs}'$ ) and an intercept of apparent cohesion in the range of 10÷12 kPa, depending on which failure surface is considered. This is in line with typical recommendations given in design practice, which, however, fail to promote an adequate appreciation of the complexity of the phenomena involved, making the selection of “operational” parameters for LEM analyses often arbitrary.

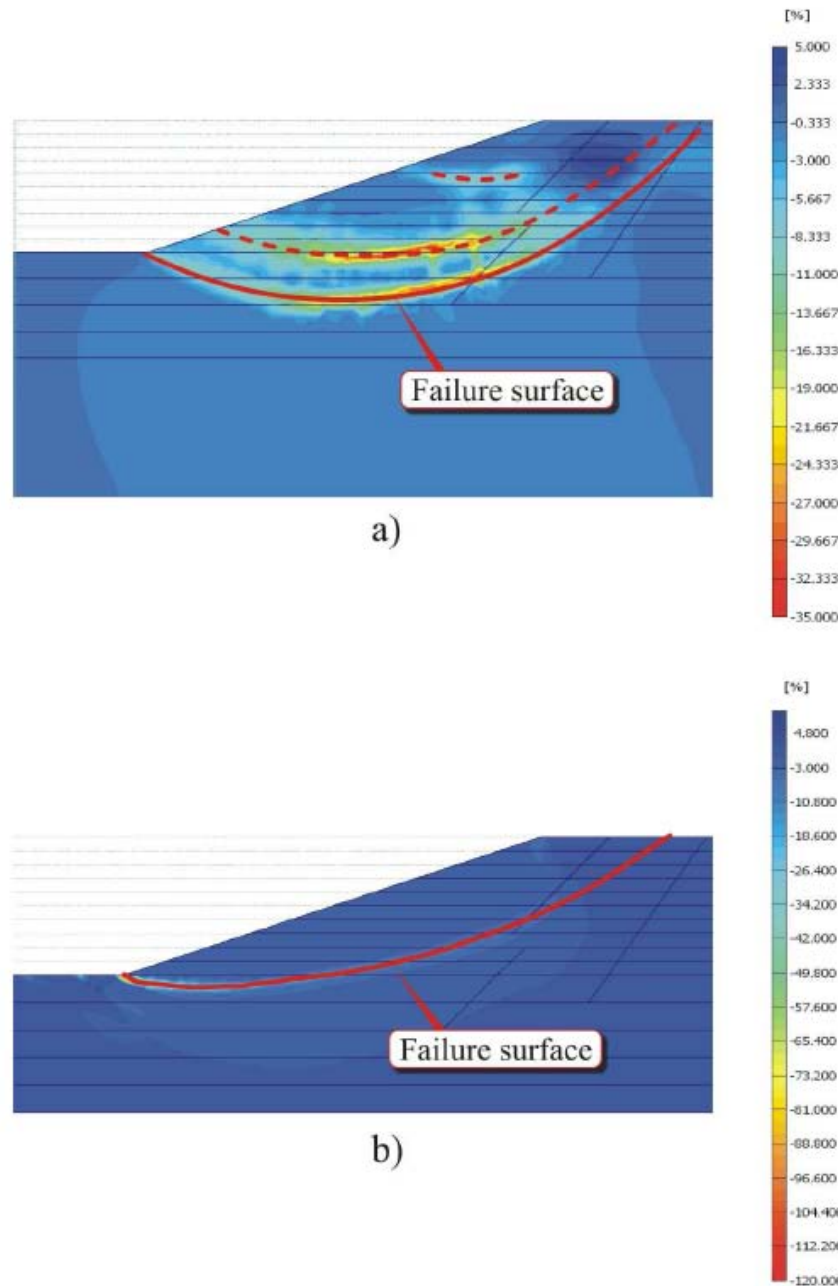


**Figure 2-41** - Numerically simulated distributions of cumulative shear strains at failure for a  $I(v): 3(h)$ , 10 m high slope in (a) CA clays ( $K_o = 0.6$ ) and (b) CB1 clays ( $K_o = 1$ ).

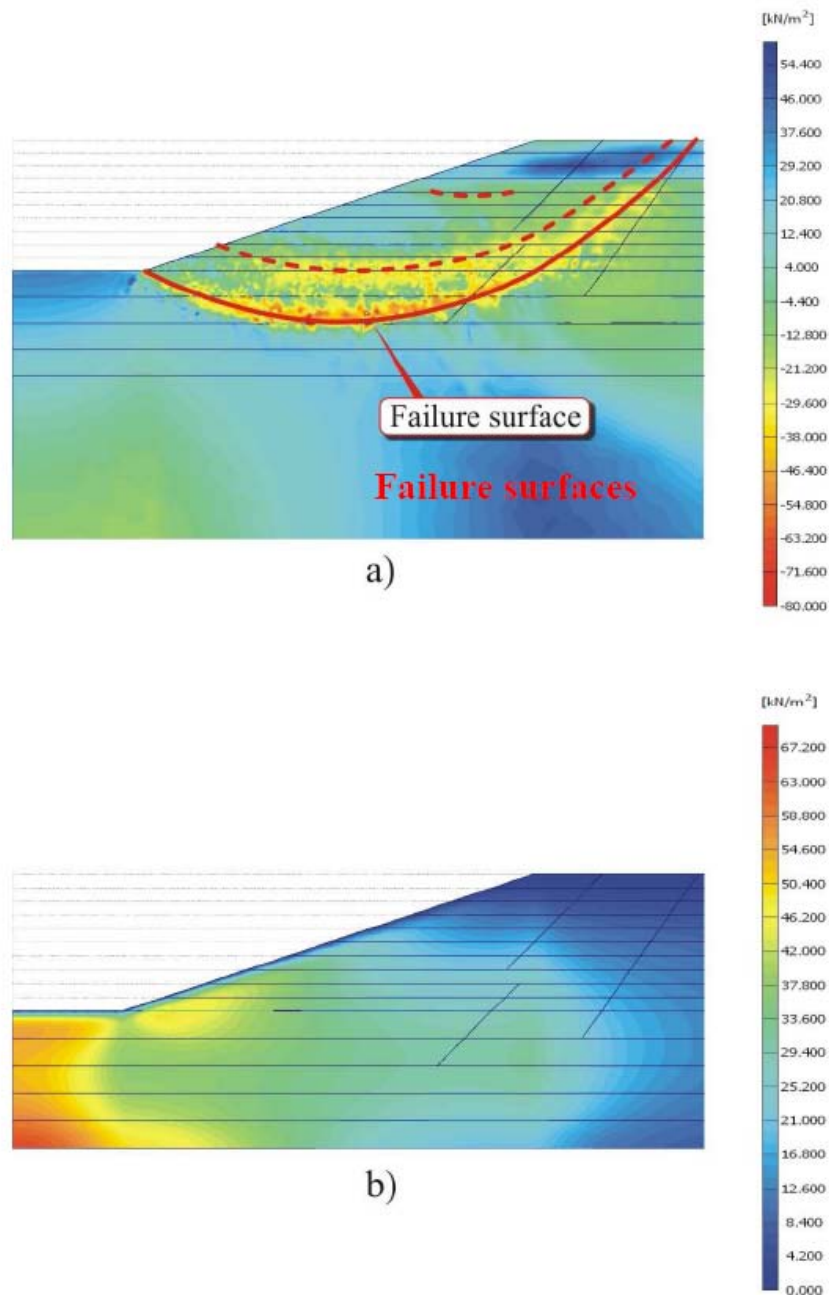


**Figure 2-42** - Numerically simulated distributions of excess pore pressures for a 1(v): 2(h), 10 m high slope at 10 days in (a) CA clays ( $K_o = 0.6$ ) and (b) CB1 clays ( $K_o = 1$ ).

#### 2.4.5 Example 4 – Comparison between SA and SB sands

Let us consider two 10 m high underwater slopes inclined 1 (vertical): 3 (horizontal) (Figure 2-43) which have been formed by accretion (sedimentation or filling) of sandy materials SA (initial states above the IDL) or SB (initial states below the IDL). Both slopes are subjected to both rapid and slow surcharge.

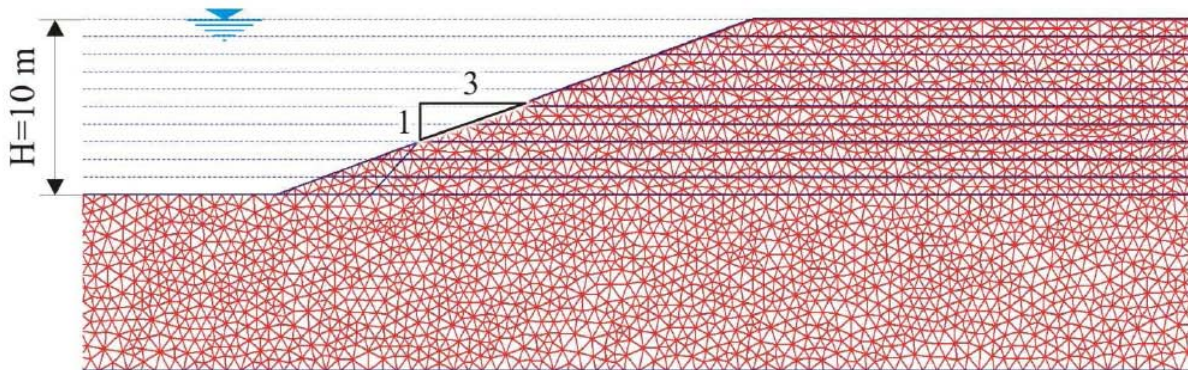


**Figure 2-43** - Finite element mesh for comparative numerical simulations of the response to slow and fast surcharging of sandy materials SA and SB in underwater slopes formed by accretion (sedimentation or filling).

The sandy materials have been simulated by the elasto-plastic constitutive model described in Li and Dafalias (2000), referred to below as SAND-GEN. The parameters of the model considered in the analyses (Table 2-7) have been selected to replicate typical characteristics and behaviour of fine sands as described in Section 2.3.2. The initial states, represented by the void ratio ( $e$ ) and the mean effective stress ( $p'$ ) considered in the analyses are shown in Figure 2-44 for both SA and SB materials; in the same figure the initial states are compared with the SSL and the IDL. The initial stress conditions in the slope have been derived using a procedure similar to that considered by Lade (1999) for determining the consolidation stress states in slopes based on the work of Lowe and Karafiath (1960); the initial stress conditions of SA materials fall within the “instability zone” between the SSL and the IL (Figure 2-45a); the initial stress conditions of SB materials fall outside the “instability zone”, lying well below the IL (Figure 2-45b).

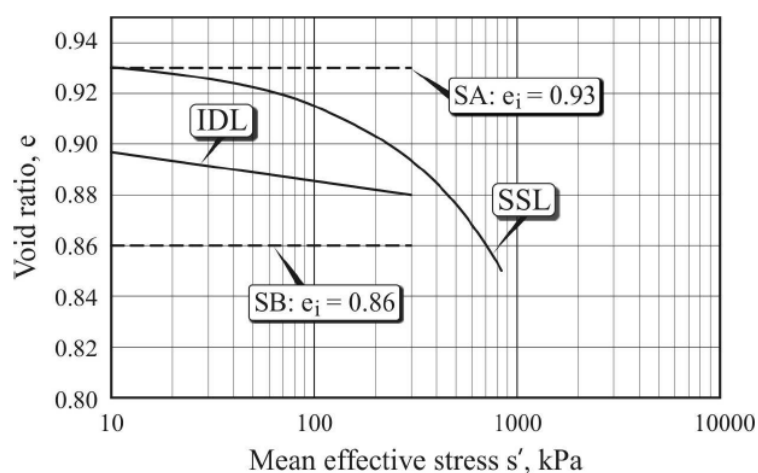


**Figure 2-44** - Initial states of SA and SB materials considered in the analyses, relative to the SSL and the IDL.

**Table 2-7 - Parameters of the SAND-GEN constitutive model for the materials SA and SB.**

$G_0$ (MPa)	$\nu'$ (-)	$M_c$ (-)	$M_c/M_e$ (-)	$e_{(p'=0)}$	$\lambda$ (-)	$\xi$ (-)	$d_0$ (-)	$m$ (-)	$h_1$ (-)	$h_2$ (-)	$n$ (-)
125	0.15	1.25	0.706	0.934	0.019	0.7	2	3.5	3.15	3.05	1.1

$G_0$  = parameter which define the shear modulus according to the empirical relationship by Richart et al. (1970)  
 $\nu'$  = Poisson's ratio  
 $M_c$  = strength parameter in triaxial compression  
 $M_e$  = strength parameter in triaxial extension  
 $e_{(p'=0)}$  = void ratio on the SSL at  $p' = 0$  kPa  
 $p'$  = mean effective stress  
 $\lambda, \xi$  = parameters which define the SSL  
 $d_0, m$  = parameters which govern the flow rule (dilatancy)  
 $h_1, h_2, n$  = parameters which govern the hardening rule

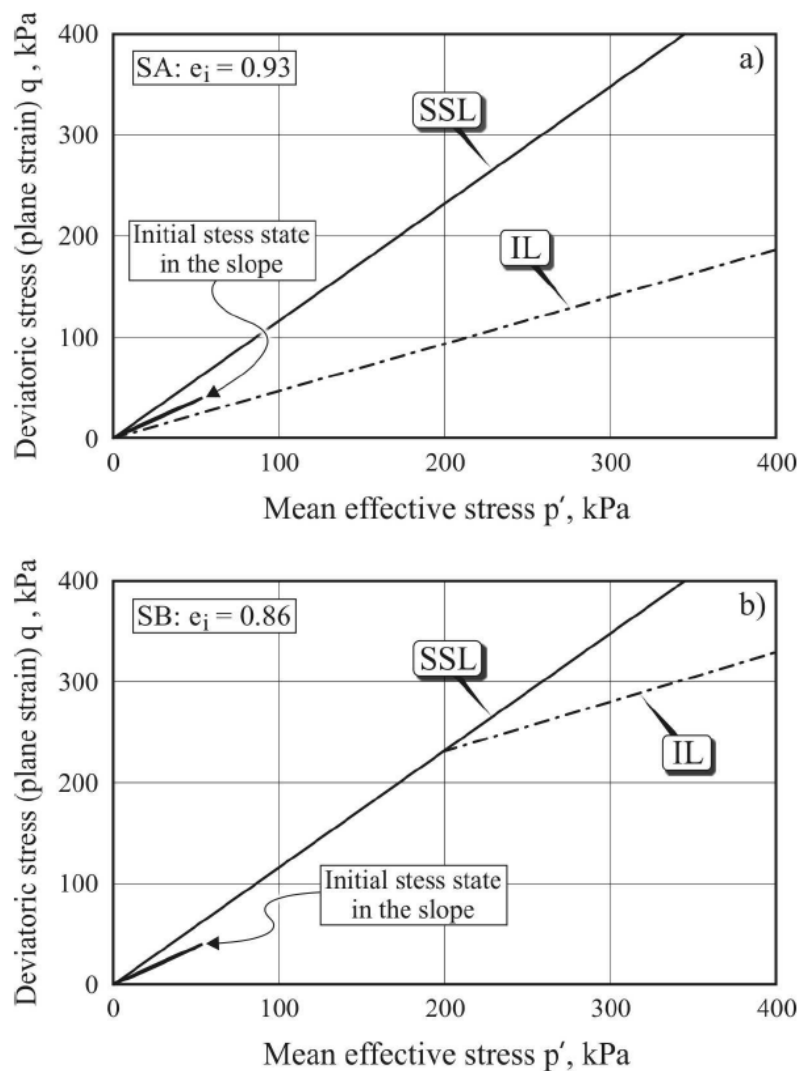


**Figure 2-45 - Initial stress conditions in the accretion slopes considered in the analyses, relative to the SSL and the IL: (a) SA material; (b) SB material.**

Figure 2-46 shows the results of simulated undrained triaxial tests in compression on specimens of SA materials isotropically consolidated at equal void ratios and at different mean effective consolidation stresses; they exhibit similar pattern of behaviour as determined in the experimental tests shown in Figure 2-19). Figure 2-47 shows the results of similar simulated tests on SB material, which compare qualitatively with the experimental results shown in Figure 2-18, albeit for denser material. Figure 2-48 shows the results of a numerically simulated drained-undrained triaxial carried out using the same procedure as used for the experimental test –c- described by Di Prisco et al. (1995), see Section 2.3.2 and Figure 2-15.

Only vertical displacements have been allowed on the vertical boundary of the mesh, while the bottom boundary has been fixed in both the vertical and the horizontal directions.

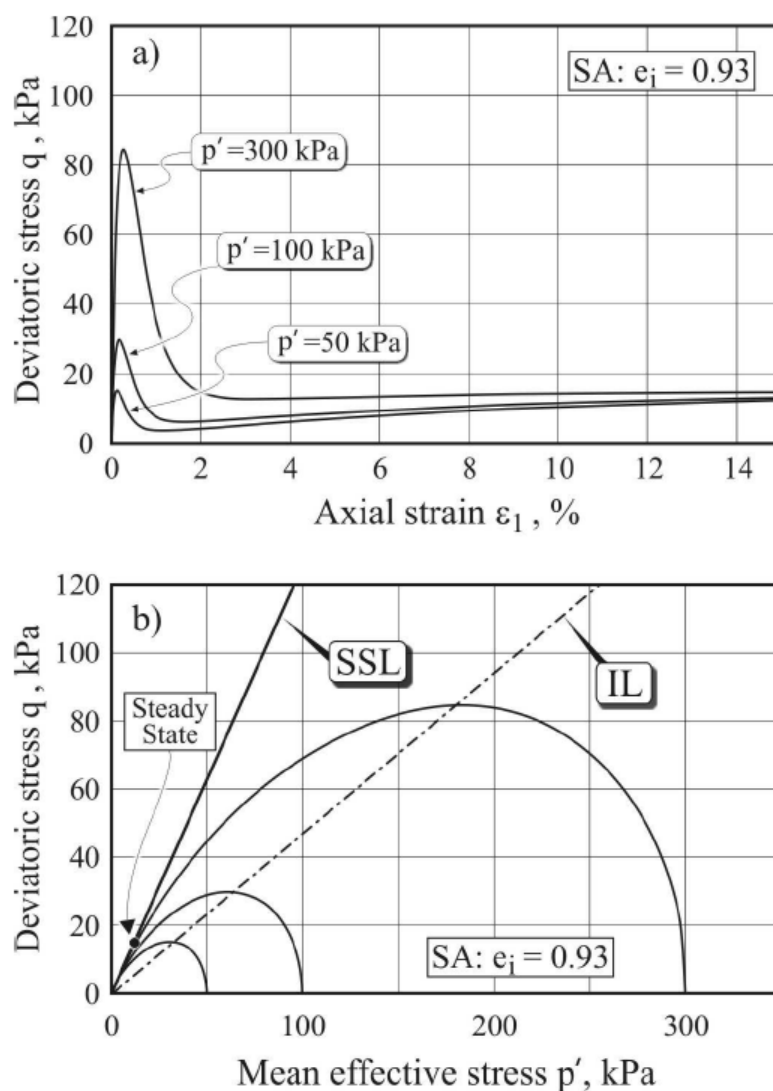


**Figure 2-46** - Numerically simulated undrained triaxial tests in compression on isotropically consolidated specimens of SA material: (a) Stress-strain relationship; (b) effective stress paths.

For both material types, the analyses have been carried out both in drained and undrained conditions by progressively applying a surcharge at the top of the slope to failure or to a maximum of 100 kPa.

The results are shown in Figure 2-49 and Figure 2-50 for SA and SB materials respectively, in terms of cumulative shear strains (undrained and drained conditions) and excess pore pressures (undrained conditions) (suction positive, as per definitions in the computer code).

As shown in the figures, while in SB material the slope is stable in both drained and undrained conditions, in SA material the slope, whose initial stress states lie in the instability zone, remains stable in drained conditions but fails in undrained conditions at very small applied loads.

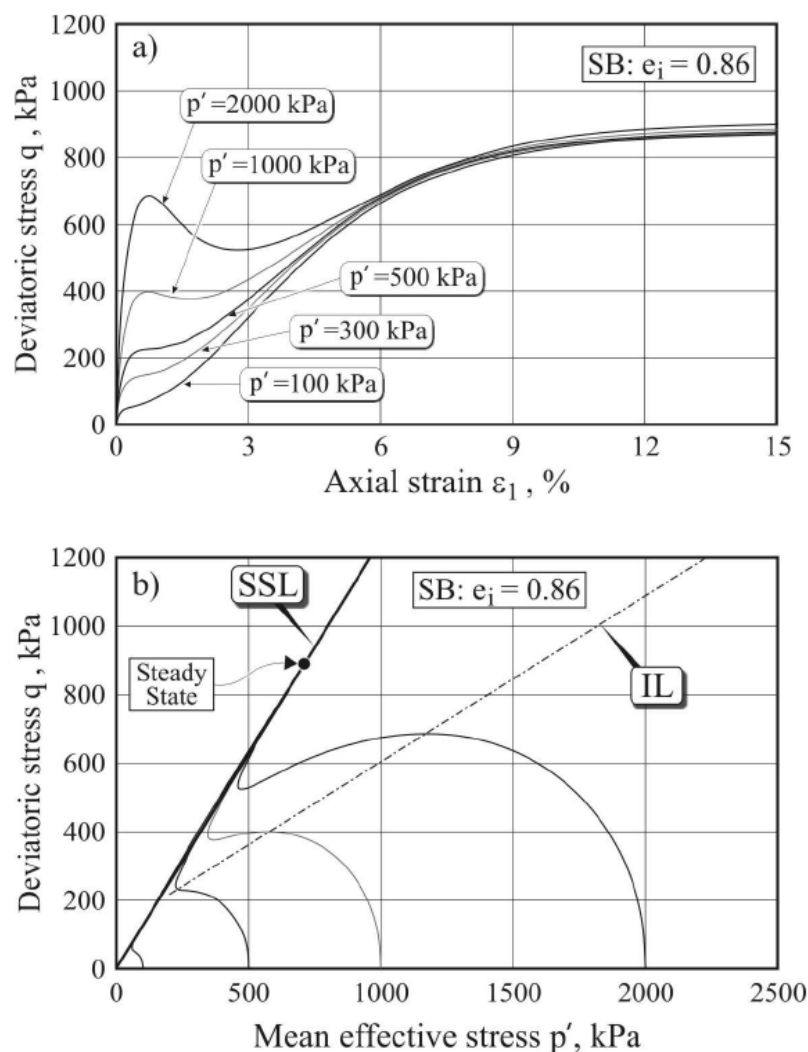


**Figure 2-47** - Numerically simulated undrained triaxial tests in compression on isotropically consolidated specimens of SB material: (a) Stress-strain relationship; (b) effective stress paths.

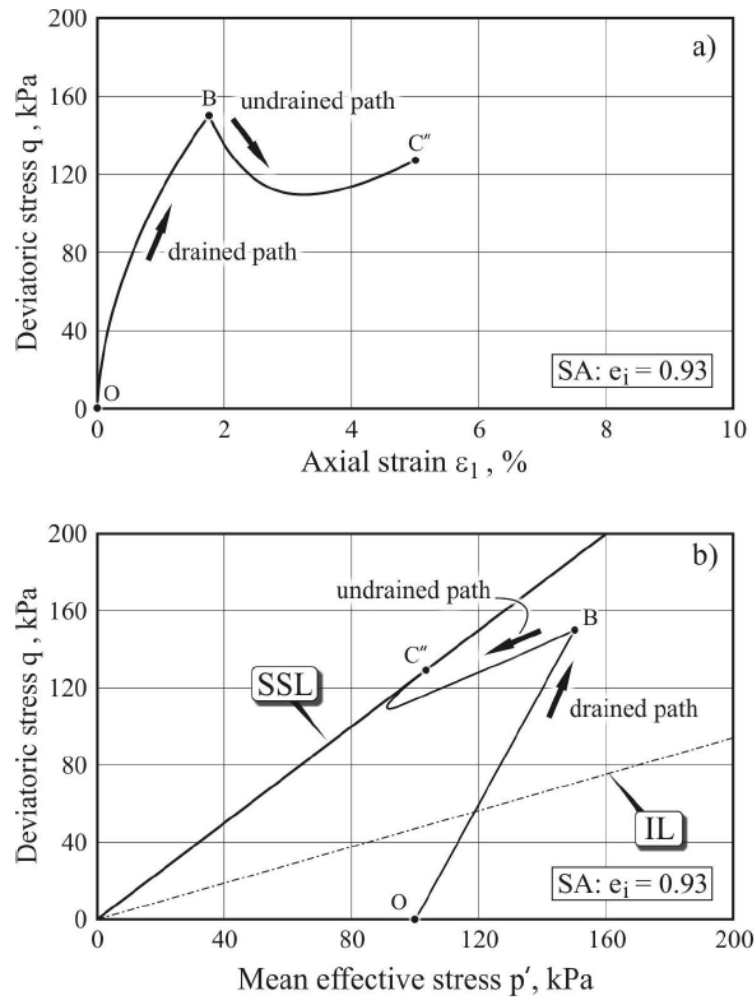


**Figure 2-48** - (a) Stress-strain relationship; (b) effective stress paths in numerically simulated undrained triaxial test on a specimens of SA material previously sheared in drained conditions previously sheared in drained conditions.

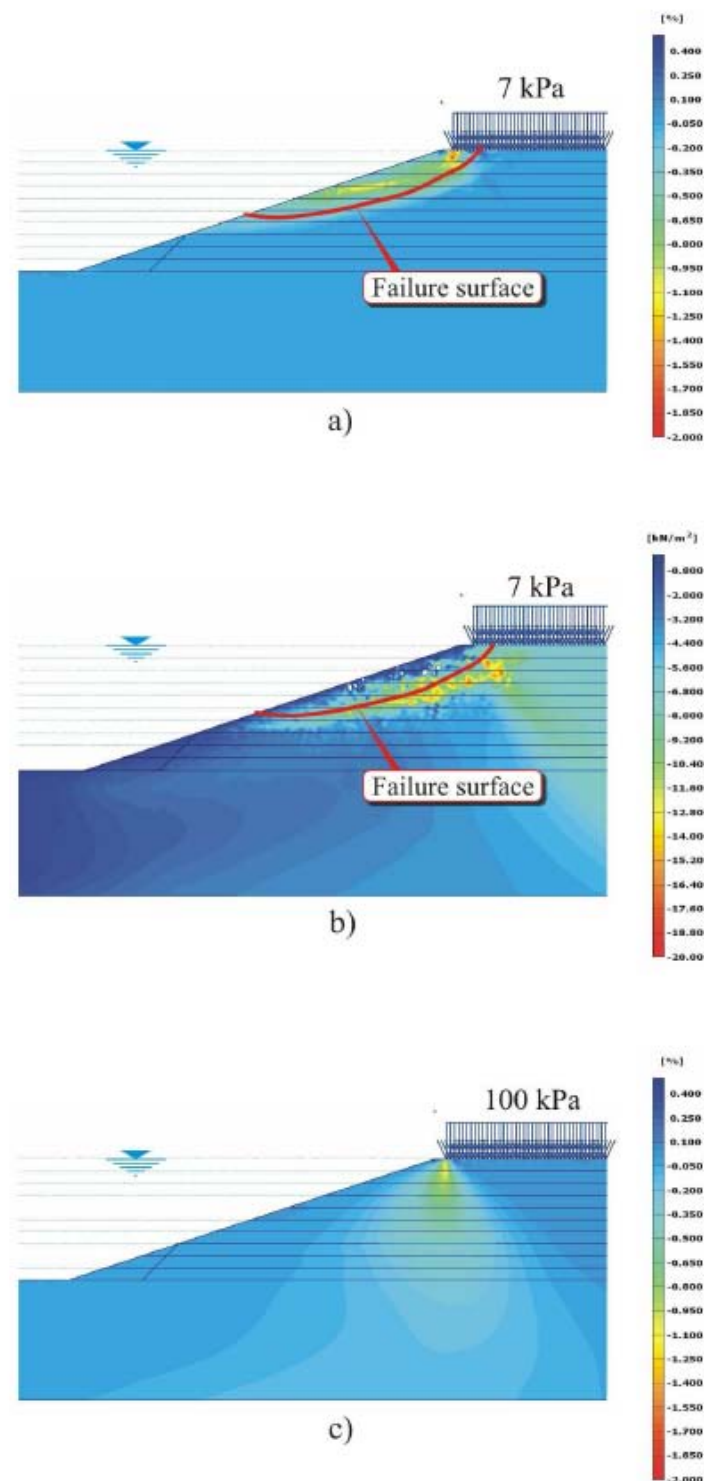


**Figure 2-49** - Response to surcharging of underwater slopes formed by accretion in SA materials: (a) undrained conditions, surcharge = 7 kPa (triggering of slope failure), cumulative shear strains; (b) undrained conditions, surcharge = 7 kPa (triggering of slope failure), excess pore pressures; (c) drained conditions, surcharge = 100 kPa (slope stable), cumulative shear strains.

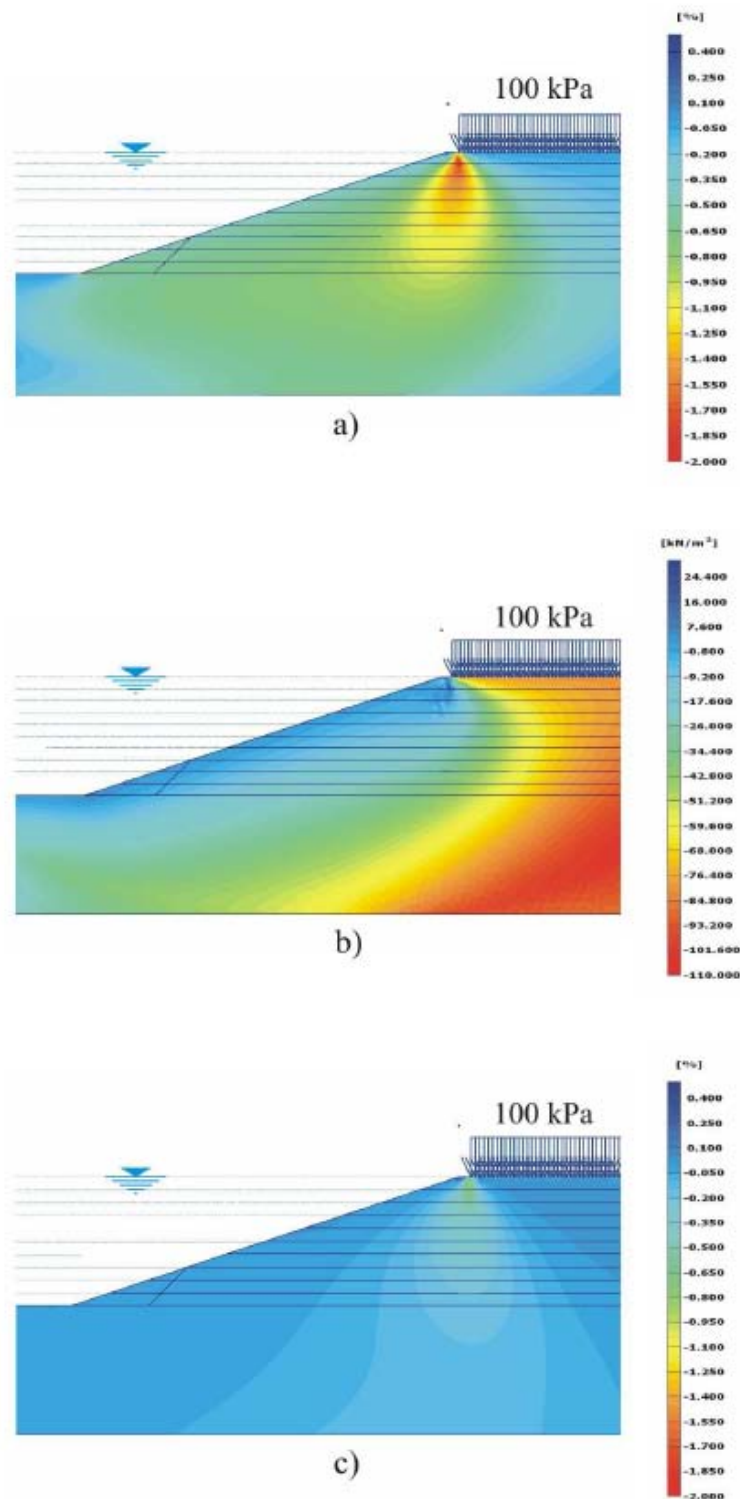


**Figure 2-50** - Response to surcharging of underwater slopes formed by accretion in SB materials: (a) undrained conditions, surcharge = 100 kPa (slope stable), cumulative shear strains; (b) undrained conditions, surcharge = 100 kPa (slope stable), excess pore pressures; (c) drained conditions, surcharge = 100 kPa (slope stable), cumulative shear strains.

### 3 LANDSLIDE TRIGGERING BY RAINFALLS AND CHANGES IN SLOPE HYDROLOGY (UNIMIB)

Hillslope hydrology is one of the most important factors in landslide triggering. Two processes mainly control changes in slope hydrology that may lead to failure: infiltration of water from the surface and rising of groundwater levels by impoundment of water in a reservoir. Infiltration can occur as a consequence of rainfall, snowmelt, irrigation, leakage from aqueducts, and is influenced by degree of saturation, evapotranspiration and interception; lateral flow into the soil, rock fracturing, etc.. The relative rates of these processes generate spatial and temporal changes in the amount of infiltration, the transient level of the groundwater and runoff.

#### 3.1 PHYSICAL PROCESS - RAINFALL INFILTRATION

Water movement into the soil is generally conceptualized in three stages: infiltration, redistribution, and drainage or deep percolation. At the initial stage (infiltration) capillary forces, or matric potentials, dominate. Redistribution occurs at the next stage by gravitational and capillary effects. Drainage and wetting may occur simultaneously. The deep percolation is the last stage of water movement which occurs as the wetting front reaches the water table. The physical properties of the soil (thickness, permeability, moisture content, porosity) and bedrock (fractures and interstices) control the water movement both at the micro and hillslope scale (Anderson and Burt, 1978; Montgomery et al., 1997; Sidle et al., 2000).

Water movement into the soil depends primarily on hydraulic conductivity ( $K$ ) at the matric-scale, and on the presence of preferential flow network and large macropores created by subsurface erosion at hillslope-scales. Hydraulic conductivity varies non-linearly with volumetric moisture content from dry conditions to maximum saturation ( $K_{SAT}$ ) (figure 3-1).

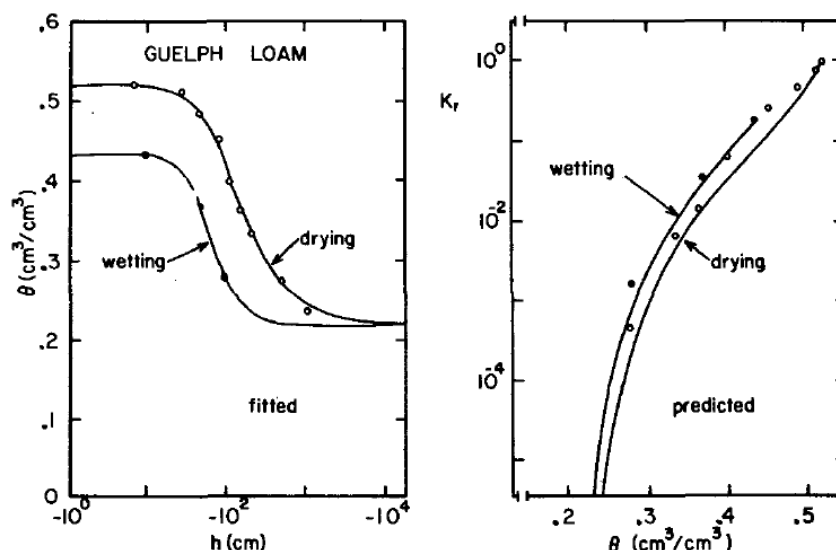


**Figure 3-1** - Soil hydraulic characteristic curves. Left: volumetric soil water content ( $\theta$ ) as a function of pressure ( $h$ ). Right: relative hydraulic conductivity ( $K_r$ , defined as the ratio of unsaturated conductivity on saturated conductivity) as a function of pressure head (from Van Genuchten, 1980).

Along the soil profile,  $K_{SAT}$  generally decreases with depth according to changes in soil physical properties (bulk density, pore-size and preferential flowpath distribution, Harr, 1977; Tsukamoto and Ohta, 1988; Montgomery and Dietrich, 1989). The incorporation of organic matter in the upper soil and the activity of roots also contribute at producing highly permeable surface soils horizons above less permeable layer. Matric suction controls the hydrologic conductivity and the available storage capacity. Relationships between degree of saturation, matric suction and hydrologic conductivity are not simple (Fredlund and Rahardjo 1993, Wang and Thomas 2000) and usually depend on soil characteristics (e.g. grain size, bulk density).

The presence of a preferential flow pattern is frequent, particularly in regolithic soils and, for subsurface flow conditions, it may be more relevant than matric flow. The effects of preferential flow patterns are very difficult to quantify, being spatially and temporally non-linear (Rogers and Selby, 1980; Harp et al., 1990; Woods and Rowe, 1996).

Landslide induced by rainfall events are highly influenced by the pattern of rainfall, and topographic and soil characteristics of the site (Jackson, 1966; Cannon and Ellen, 1985). A number of field studies monitored dynamic pore water pressures in response to rainfall in shallow (Wieczorek, 1987; Keefer and Johnson, 1983) and in deeper regoliths (Oyagi et al., 1977; Iverson and Major, 1987; Coe et al., 2003). However, few cases documented dynamic pore pressures during failure events either triggered by natural (Sidle and Swanston, 1982) or artificially-induced rainfall (Harp et al. 1990; Ochiai et al., 2004). Monitoring reports a consistent trend of behaviour. Pore-water pressure increase has been observed during the early stages of infiltration abruptly decrease just prior to failure (Harp et al., 1990; Harp et al., 2009). Piping effects and dilatation of the landslide mass (Iverson et al., 2000; Iverson, 2005) are possible causes of the observed decrease in pore pressure (Harp et al., 1990), which is particularly evident for rapidly evolving movements whereas a contractive behaviour can cause an increase in pore pressure (Harp et al., 2009).

The general mechanism by which rainfall triggers landslides is the reduction of the soil or rock effective strength (Terzaghi, 1936) due to the increase of water pressure developed by water infiltration (Campbell, 1975; Sidle and Swanston, 1982).

Although nearly saturated or artesian conditions are often required to reach instability (O'Loughlin and Pearce, 1976; Sidle and Swanston, 1982), landslides have been observed to occur also under unsaturated conditions (Anderson et al. 1980).

In unsaturated conditions, capillary forces contribute to the effective strength by a magnitude which depends on the soil properties (i.e. particle and pore size), matric suction ( $u_a - u_w$ ), degree of saturation  $\theta$  and fluid interface properties (Bishop, 1959; Lambe and Whitman, 1969; Mitchell, 1976; Lu and Likos, 2006). Capillary forces in unsaturated soils allow the soil to remain stable at angles much steeper than the friction angle. A minimum degree of saturation of 85% is considered to induce saturated soil mechanics principles (Fredlund and Rahardjo, 1987). Unsaturated conditions are typical of steep slopes and thin soils with the presence of vegetation roots.

### **3.1.1 Rainfall infiltration - shallow soils**

Different mechanisms and environmental factors control subsurface flow and slope instability in shallow soils. Among them, the following can be highlighted:

(1) **Rapid accretion of pore water pressure** due to infiltration from the surface (Iverson and La Husen, 1989; Reid et al., 1997; Okura et al., 2002) and development of a wetting front within the unsaturated soil deposit moving downward (figure 3-2). Rainwater infiltrates the soil as a water flux with zero pore water pressure behind the wetting front (Bear, 1972). The loss of strength occurs is induced by the decrease of the matric suction above the wetting front causing a drop in the apparent cohesion (Fredlund and Morgenstern, 1977; Fredlund and Rahardjo, 1993; Reid, 1994) eventually associated to the development of positive pore-water pressures at the sliding surface (Sidle and Swanston, 1982). For this hydrological condition, the sliding surface is located at the wetting front, within the soil profile.

The formation of a wetting front a short-duration high-intensity rainfall with relatively dry soils (Iverson, 2000).

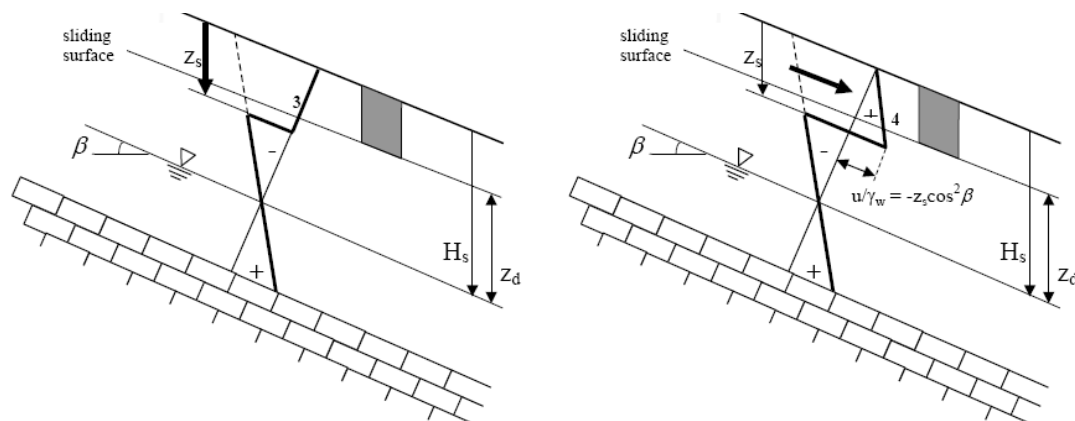


**Figure 3-2** - Schematic representation of the the wetting front model (left), with potentially the formation of a perched water-table (right) (Crosta, 1998, modified from Rahardjo et al., 1995).

(2) **Rising of the water table** (Wilson and Wieczorek, 1995), with a consequent rise of the pore water pressure. Failures are triggered by positive pore pressures on the slip plane which is located at the contact with bedrock (Iverson and Major, 1987; Coe et al., 2003; Simoni et al. 2004). In this case, a threshold for slope instability can be expressed as a critical increase in pore pressure ratio,  $r_u$ , (Bishop, 1954) as:

$$r_u = h_w / Z \quad [3-1]$$

with  $h_w$  = groundwater height and  $Z$  = soil depth.

Preferential flow paths as macropores (e.g. Mosley, 1979, 1982) or pipes within the soil (e.g. Uchida et al., 2001), bedrock fractures (e.g. Mathewson et al., 1990, Montgomery et al., 1997) facilitate rapid pore pressure response to rainfall.

High infiltration capacity, in conjunction with shallow soil above steep low permeable bedrock, creates the condition that eases the formation of a perched water table above the bedrock (Dunne, 1978; Pierson, 1980). The transient development of a perched water table usually happens within the regolith (Swanston, 1967; Gray and Megahan, 1981; Sidle and Swanston, 1982) and in zones of convergent subsurface flow, as geomorphic hollows (Anderson and Burt, 1978; Pierson, 1980). The development of a perched water table, which reduces the negative pore water pressure and starts seepage parallel to slope that contribute to

the initiation or acceleration of landslides, could be initiated by two processes: variations of unsaturated permeability of the soil with variations in matric suction (i.e., permeability function) and the decreasing saturated permeability with increasing depths (due to the decrease in the degree of weathering at greater depths).

(3) **Pulses** of rain can lead to rapid pore pressure rise much faster than expected by advection. This phenomenon was observed in the presence of high ground water content and pressure head field near-zero (Zimmermann et al., 1966. Humphrey, 1983; Torres et al., 1998). A pressure wave which travels through the unsaturated zone, governs the relatively quick dynamic response to incoming precipitation. The rapid displacement of pre-existing soil-water into the saturated zone can generate a rapid pore pressure rise.

(4) Iverson and Major (1986) underlined the role of **seepage forces** in slope stability. According to their analyses, the minimum slope stability occurs when the angle between seepage force vector and the normal to the slope is  $90^\circ - \phi$ , where  $\phi$  is the internal friction angle of the slope material. Horizontal seepage is thus more critical for steep slopes, where the slope angle is nearly or equal to  $\phi$ .

(5) Landslides in shallow soils can also be triggered by the **upwelling of pore pressures** from fractured bedrock underlying the more weathered regolith (Montgomery et al., 1997; van Asch and Buma, 1997). This process is very rapid and typically occurs as a response to peak inputs in wet soils during high intensity rainfalls. The rapid response is due to pressure-wave type propagation of pre-existing pore water (nearly saturated) into the upper unsaturated layer (Torres et al., 1998). The propagation of groundwater from bedrock into the unsaturated zone is another cause of perched water table formation (Torres et al., 1998).

(6) **Pipeflow** may significantly contribute to landslide initiation (e.g. Pierson, 1980; Jenkins et al., 1988; Sidle, 1994; Crosta and Di Prisco, 1999). Ohta et al. (1981) and Pierson (1983) reported that 50–90% of landslide scars had soil pipes in headscarps. The diameter of soil pipes observed in landslide scars ranges from 1 to 30 cm, and the both ephemeral and perennial pipeflows are observed (Uchida et al, 2001). Richards and Reddy (2007) describes several types of piping (Figure 3-3), which are relevant to landslides (Hencher, 2010) : suffosion (or eluviation), i.e. the washing out or dissolution of material en masse leaving a loose framework of granular material, prone to collapse; dispersion of clay soils by rainwater in the vadose zone; backwards erosion from a spring, the pipe forms (for some reason) and then material is gradually lost from that opening; erosion along some pre-existing opening such as a master joint or decayed roots.

Three main controls are exerted by pipeflow on the occurrence of landslides (Uchida et al, 2001): (1) the concentration of water into the soil pipe network (Pierson, 1983; Onda, 1994) (2) the rapid drainage of water to downslope (Mosely, 1982); (3) the erosion along pipeflow. Soil pipes can contribute to slope stability by increasing the rate of soil drainage and limiting the development of a perched water table. However, if the rate of water concentration (process 1) is in excess of the pipeflow transmission capacity (process 2), the pipe is filled with water during a rain event, increasing pore water pressure in the surrounding matrix. In this case, the soil pipe induced the slope instability. Instability can also result from piping erosion (Onda, 1994; Crosta and Di Prisco, 1999).

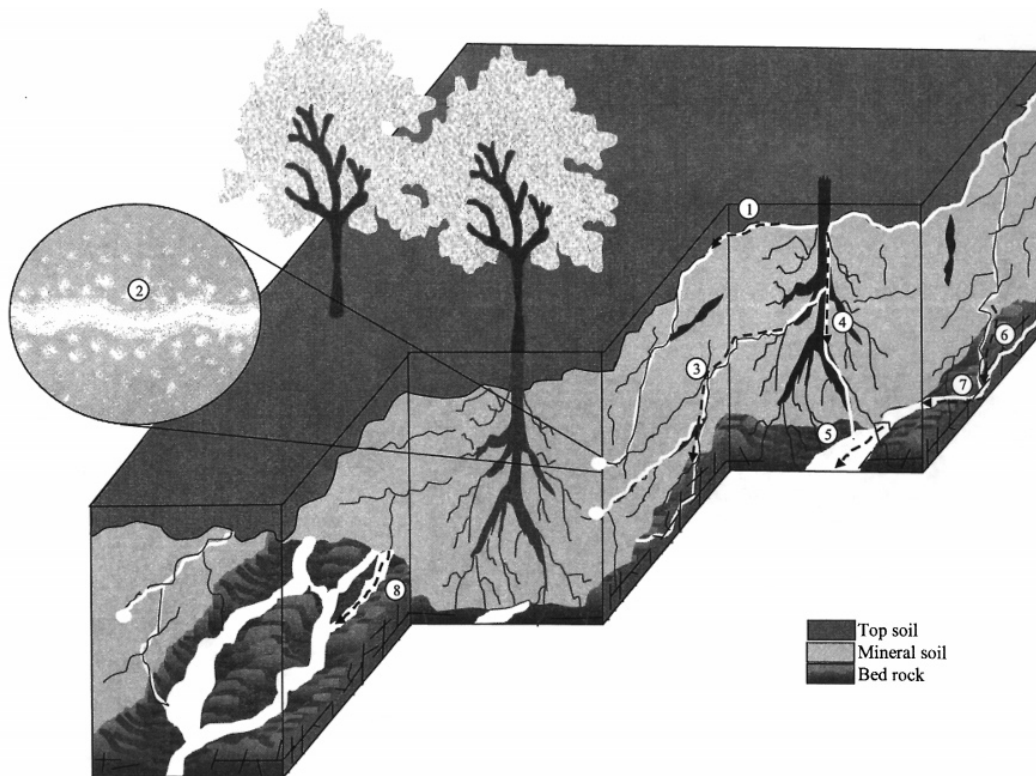


**Figure 3-3.** A conceptual model of preferential flow pathways in a hillslope. Pathways include (1) preferential flow in the organic-rich soil; (2) macropores interacting with mesopores to enlarge preferential flow during wet conditions; (3) connection of macropores by physical interaction; (4) connection through porous zones of buried organic matter (decayed roots); (5) contact with a perched groundwater at the bedrock; (6) preferential flow into and through shallow bedrock fractures; (7) exfiltration of water from shallow bedrock fractures; and (8) flow over microchannels on the surface of bedrock or other substrate (i.e., substrate topography control). (from Sidle et al, 2000).

(6) Landslides triggered by long rainfall periods can also experience fluidization at the time of failure (Iverson and La Husen, 1989). In this case, shearing causes **contraction** and consequent increase of pore pressure at the sliding surface (Iverson et al., 2000; Iverson, 2005). Contractive shear failure occurs in loose soils, as the initial soil porosities tend to approach the lower critical-state. Soil contraction increases the pore pressure and can reach levels nearly sufficient to balance total normal stresses, inducing rainfall triggered liquefaction (Iverson et al., 2000). On the contrary, dense soils are stabilized by dilatative behaviour.

### 3.1.2 Rainfall infiltration - deep soils

In deep soils, monitoring data indicate complex interaction among rainfall data and mass movement observation. While pore pressures within the landslide mass may respond to individual rainfall inputs, and the response is more or less rapid depending on hydraulic conductivity, some accumulation of precipitation is necessary to initiate the movement. Long duration less intense rainfall allow for the rise of the groundwater table and the occurrence of

deep failures by means of the reduction of shear strength. Longer antecedent precipitation periods have to be considered to establish a successful correlation among landslide events and precipitation.

Deep-seated mass movements experience seasonal episodes of accelerated movements, due to seasonal rainy periods, rapid snowmelt, and regional climate perturbations (Kalisser and Fleming, 1986; Bovis and Jones, 1992). The velocity of the landslide movement increases or decreases in response to the corresponding variation of pore pressures. The pore pressure responds to large rainfall input within several days at moderate depth (7-10 m, Reid, 1994), and within several weeks to several months at larger depth (12-20 m, Iverson and Major, 1987; Baum and Reid, 2000; Coe et al., 2003).

### **3.2 PHYSICAL PROCESS: CHANGES OF GROUNDWATER LEVELS**

The slopes adjacent to reservoirs and rivers often experience landsliding due to fluctuations in water levels (Morgenstern, 1963; Schuster, 1979). This fluctuations can be induced by: (1) seasonal or extraordinary operations in the reservoir (impoundment, drawdown); (2) river level changes during floods and drawdown when the river level drops; (3) breaching in a dyke; (4) sea level rise; (5) storm tide (Jia et al 2009).

Jones et al. (1961) found that about 30% of the landslides in the vicinity of Roosevelt Lake in United States from 1941 to 1953 occurred as a result of drawing down the water level in the reservoir. Nakamura (1990) reported that about 60% of the landslides around reservoirs in Japan occurred under drawdown conditions. In China, a reservoir-induced landslide near Zhaxi dam claimed over 70 workers in 1961 (Jin and Wang, 1988). In 1963 a catastrophic failure of the left bank slope occurred in Vajont Reservoir in Italy, with a formation of a flood wave that caused more than 2000 casualties (Müller, 1964).

Raising the water level can also trigger landslides. Numerous failures occurred, for example, during the initial filling of the Panama Canal (Lane, 1967). In Austria, several ancient landslides near the Capatsch dam slipped over 10 m during its initial reservoir inundation from 1965 through 1969 (Breth, 1967) Recently, numerous slope failures were associated with water level fluctuations during the operation of the Three Gorges Reservoir in China, resulting in deaths and great economic losses (Wang et al, 2004, Liao et al., 2005, Wang et al, 2008, Jiang et al 2010).

As seen from the examples, water table fluctuation of reservoir can led to instability both during impoundment and rapid drawdown.

Impoundment is especially critical when the reservoir banks consist of high permeability rocks. In that case, if the reservoir water level suddenly rises in a certain time, it rapidly seeps into the slope and produces very great uplift pressure at the slope base. The process reduces the effective stress of the rocks of the reservoir bank and easily causes the instability of the slope or a landslide (Wu, 2003).

Drawdown of reservoir water level can cause deformation of landslides. There are two main factors leading to deformation of landslides: on one hand, drawdown of the reservoir increases water gradient and seepage force of landslide mass. Seepage force pointing along the tangent of seepage surface increases sliding force and forms a deformation in the landslide mass. As a result, the stability of landslide decreases. Furthermore, if the phreatic surface declines, the effective stress of landslide mass rises and the slope can undergo a consolidation deformation.

A more detailed illustration of the nature of the drawdown is offered by Figure 3-4. The drawdown change in water level in the vicinity of slope implies (Pinyol et al, 2008):

1) A change in total stress conditions against the slope (see Figure 3-4). The slope is then subjected to a stress relaxation of constant intensity ( $\Delta\sigma = H_D\gamma_w$ ) in the lower part and a linearly varying stress distribution in its upper part. The bottom horizontal surface experiences a uniform decrease of stress of intensity,  $H_D\gamma_w$ .

2) A change in hydraulic boundary conditions. In its new state, water pressures against the slope are given by the hydrostatic distribution on the slope face and by the uniform water pressure value  $p_w = (H - H_D)\gamma_w$  on the horizontal lower surface.

The variation of the hydrostatic pressures induces a change in total stress inside the slope, producing a change in pore pressure. If dilatancy is present, due to shear effects, additional pore water not in equilibrium with the new boundary conditions will be generated, resulting in a transient flow regime. If soil permeability is high pore pressures will dissipate fast (drained reaction).

The processes leading to pore water pressures changes within an initially submerged slope, later subjected to drawdown, depend on several soil parameters and “external” conditions (Alonso and Pinyol, 2009): soil permeability (saturated and unsaturated), soil water retention properties, mechanical soil constitutive behaviour, rate of water level lowering and boundary conditions. In addition, landslides in Three Gorge Reservoir area indicate that water percolates through loose deposits to the incompetent beds along tectonic fissures. This often lead to the softening the slip zones, reducing landslide stability (Jian et al. 2009).

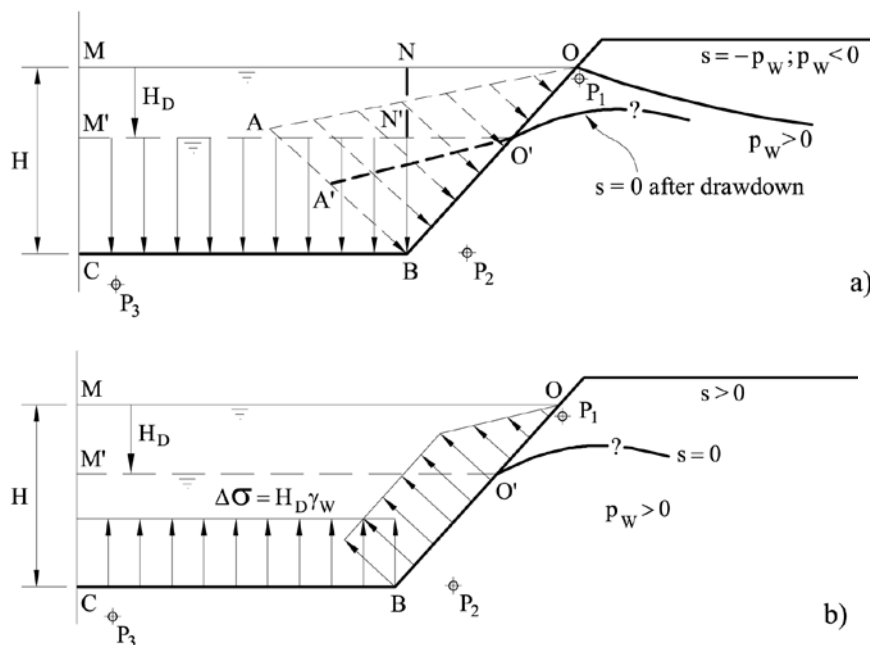


**Figure 3-4.** The drawdown scenario: (a) Hydrostatic stresses acting against the exposed slope surface. (b) Change in applied stresses on the exposed boundaries induced by a drawdown  $H_D$ . Symbols:  $p_w$  = pore pressure,  $s$  = suction,  $\sigma$  = stress;  $\gamma_w$  = water unit weight (from Pinyol et al., 2008).

### 3.3 CURRENT ANALYSES APPROACHES AT DIFFERENT SCALES - RAINFALL INFILTRATION

#### 3.3.1 Rainfall infiltration - shallow soils

The relationship between rainfall, water table fluctuations and landslide movement is often difficult to establish and the prediction of place and time of landslide occurrence is still a challenging issue, because the properties of earth materials and slope conditions may vary greatly over short distances, and the timing, location and intensity of triggering events are generally difficult to forecast.

In particular, for the case of shallow landslides, the relationship between landslide occurrence and meteorological events encouraged the investigation of the relationship between rainfall and geotechnical hazards by means of:

- Empirical approaches which relate rainstorm characteristics (storm mean and maximum hourly intensity, storm duration, rainfall amount, and antecedent rainfall) to landslide occurrence (Caine, 1980, Figure 3-5; Sidle and Swanston, 1982; Sidle 1984a, 1986; Wieczorek, 1987; Dhakal, 1995; Crosta and Frattini, 2001; Wieczorek and Glade, 2005). The definition of the most critical rainfall conditions depends on the soil characteristics and initial state (soil moisture content). In particular, shallow landslides and debris flows often occur during, or suddenly after, short intense rainfall.

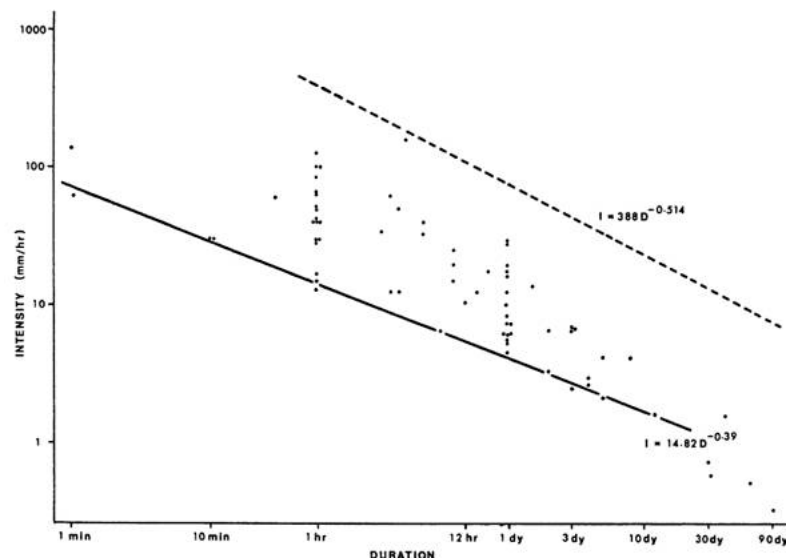


**Figure 3-5.** Example of intensity-duration landslide triggering thresholds (solid line). The dashed curve is the global maximum precipitation intensity (from Caine, 1980)

- Physically-based approaches, where spatially distributed landslide models integrate hydrological models for the description of the dynamics of infiltration and saturation phenomena, together with geotechnical approaches on the side of stability analysis. In particular, the slope stability is investigated as a function of hydrological conditions and rainfall characteristics, with the aim of quantifying (i) the conditions at which shallow landslides can be triggered in terms of intensity-duration rainfall thresholds

(IED curves, Frattini et al., 2009); (ii) the extent of shallow landslides occurrence (i.e., the number of events, the area involved by landsliding), as a function of rainfall return period (Crozier and Glade, 1999; Dhakal and Sidle, 2004); (iii) the time-dependent stability of sliding surfaces passing through the unsaturated zone by evaluating the apparent cohesion of the soil layer as a function of changing moisture content, (e.g. Frattini et al. 2004). Different models have been developed to model the landslide triggering as a function of dynamic variables as the hydrological conditions and land use changes (Montgomery and Dietrich, 1994; Wu and Sidle, 1995; Borga et al., 1998; Pack et al., 1998).

Area-based models of slope hydrology usually attempt to account for infiltration and vertical movement of water into the ground surface in some simplified way (infiltration through unsaturated zone and into the saturated zone, below the rising phreatic surface), modelling the longitudinal movement of groundwater by downslope seepage (seepage flow within the phreatic zone).

#### Richards equation model

There are numerous techniques for the estimation of infiltration rates, which broadly refer to three categories: a) empirical models (e.g. Kostikov, 1932; Horton, 1940; Philip, 1957), b) Green Ampt models, c) Richards equation models.

The unsteady, variably saturated, percolating flow in response to rainfall can be described by the Richards equation (Richards, 1931). Saturated and unsaturated conditions are considered by allowing the hydraulic conductivity to vary with water content as follows:

$$\frac{\partial \psi}{\partial t} \frac{\partial \theta}{\partial \psi} = \frac{\partial}{\partial x} \left[ K_L(\psi) \left( \frac{\partial \psi}{\partial x} - \sin \alpha \right) \right] + \frac{\partial}{\partial y} \left[ K_L(\psi) \left( \frac{\partial \psi}{\partial y} \right) \right] + \frac{\partial}{\partial z} \left[ K_z(\psi) \left( \frac{\partial \psi}{\partial z} - \cos \alpha \right) \right] \quad [3.2]$$

in which  $x$ ,  $y$ , and  $z$  are the axes of a reference coordinate system with  $z$  normal to the slope,  $\psi$  is groundwater pressure head,  $\theta$  the soil volumetric water content,  $t$  is time,  $\alpha$  the slope angle, and  $K_L$ ,  $K_z$  are the hydraulic conductivity in lateral and normal direction, respectively. The equation serves as the basis for various numerical approximations (Terlien, 1996; Iverson, 2000).

For shallow soils, it is possible to simplify the Richards equation [3.2] treating the problem as one-dimensional (Iverson, 2000). According to rainfall intensity, duration and initial soil moisture, the simplified Richards equation leads to three further simplified hydrological models, namely: a wetting-front model, a steady state model, and a pressure head diffusive model, as described in the following.

#### Wetting-front model

For initially dry soils ( $K_z \ll K_{SAT}$ ), the diffusion term can be neglected, and Richards equation can be reduced to a simple form that describes the short time responses of a flux of water within the soil, by the sole gravity effect (Iverson, 2000).

The model assumes the formation of a wetting front (Green and Ampt, 1911): the soil is saturated at a volumetric water content of  $\theta_s$  (with the exception of the entrapped air) down to the wetting front, where the water content drops abruptly to the previous value  $\theta_0$ , which represents the initial water content:

$$\frac{\partial \psi^*}{\partial t^*} + \frac{\partial \psi^*}{\partial z^*} \left[ \cos^2 \alpha \frac{I_z}{K_z} \frac{C_0}{C(\psi)} \frac{dK_z^*}{d\psi^*} \right] = 0 \quad [3-3]$$

where  $\psi^*$  is the groundwater pressure head normalized by the depth of failure surface,  $z^*$  is the vertical coordinate  $z$ , normalised by the depth of failure surface,  $H$ ,  $\alpha$  is the surface slope,  $I_z$  is the infiltration rate along  $z$ ,  $K_z$  and  $K_z^*$  are respectively, the hydraulic conductivity and the conductivity normalized by the saturated conductivity  $K_{SAT}$ .  $t^*$  is a dimensionless time, equal to  $tD_0/H^2$  (where  $D_0 = K_{SAT}/C_0$ , and  $C_0$  is the minimum value of  $C(y) = d\theta/d\psi$ ). The change in volumetric water content per unit change in pressure head, close to storage coefficient  $D_0$  represents the maximum diffusivity governing transmission of pressure head, and it is reached in proximity of saturation. This equation corresponds to the piston-flow model described by Green and Ampt (1911) for infiltration (Figure 3-6).

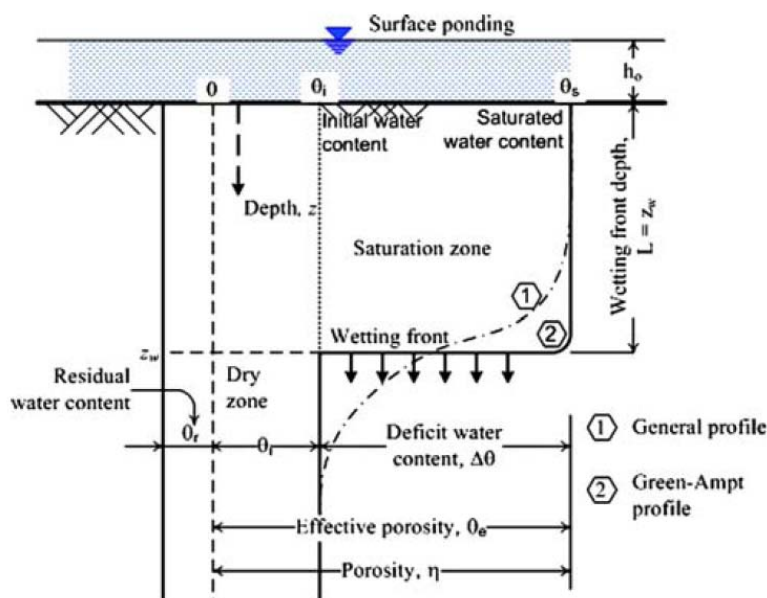


**Figure 3-6** - Infiltration profile for Green-Ampt model (after Muntohar, Liao, 2009).

The mechanical process that leads to failure is that of an increase of transient pore water pressure and progressive reduction of shear strength in the upper part of the soil profile during rainfall percolation. The failure surface develops within the soil profile, and it is usually controlled by vertical changes in hydrological and geotechnical soil properties throughout depth (Van Asch and Sukmantalya 1993, Terlien 1996; Rahardjo et al., 2001) the underlying impermeable bedrock. Shallow failure can be triggered with a maximum depth of a  $w$  meters.

#### Pressure head diffusion equation (PHDE)

In the case of quasi-saturated conditions the flux term can be neglected, and the Richards equation describe the short-term responses to intense rainfall events, which lead to a water content in soil close to saturation. The PHDE model reduces to a pressure head diffusive equation in which hydraulic conductivity,  $K_z$ , and water capacity,  $C(\psi)$ , are assumed to approximate constant values of  $K_{sat}$  and  $C_0$ , respectively. The assumption of a constant value for both  $K_z$  and  $C(\psi)$  is reasonable only for small variation in soil saturation (Hillel, 1998):

$$\frac{\partial \psi^*}{\partial t^*} = \frac{C_0 K_z^* \cos^2 \alpha}{C(\psi)} \frac{\partial^2 \psi^*}{\partial z^{*2}} \quad [3-4]$$

The pressure head response to complex rainfall sequences, with varying intensities and irregular durations, is obtained by summing a series of responses to rainfall of fixed intensity and duration.

Steady-state model,

Steady near-surface groundwater flow develops as long –term pressure head responses. In the case of saturated conditions, a model is developed to describe quasi-steady state pressure. The model assumes that rainfall influences groundwater only by modulating steady or quasi-steady water table heights and groundwater flows parallel to hillslope. These conditions can be encountered in response to low-intensity rainfall, over periods ranging from days to months. Eq. [3.2] reduces to (Hurley and Pantelis, 1985):

$$\frac{\partial}{\partial z^*} \left[ K_z^* \left( \frac{\partial \psi^*}{\partial z^*} - \cos \alpha \right) \right] = 0 \quad [3-5]$$

A further approximation can reduce the model to the steady flow condition proposed by Montgomery and Dietrich (1994). The model describes the groundwater flux above a reference depth  $\delta$  by Darcy’s law for slope-parallel flow. Thus, the relevant solution for the Richards equation is:

$$\psi = (z - \delta) \cos \alpha + \frac{I_z}{K_L} \frac{A}{b} \cot \alpha \quad [3-6]$$

where A is the drainage area and b is the width of the slope element over which the flux is measured. Montgomery and Dietrich (1994) adopted the steady-state contour-based hydrological model of subsurface flow developed by O’Loughlin (1986) to identify potential failure zones. They assume that the feature that governs the location of landslides is the local surface topography which defines local slope gradients and shallow subsurface flow convergence. Differences in size and timing of landslides are attributed to spatial variations in soil properties and thickness (Montgomery and Dietrich 1994). Another complicating factor in predicting the timing of landslides (similar to establishing rainfall triggering thresholds) is the modeling of vertical percolation, which is assumed as immediate for thin soils (1–1.5 m) and low spatial variation.

**3.3.2 Rainfall infiltration - deep soils**

For deep seated landslides, the relationship between landslide occurrence and meteorological events is even more complicated. The displacement rate of active slides essentially depends on the rate of pore pressure changes along the slip surface. However, measurement of water pressure is difficult for deep-seated landslides because of: heterogeneity of rock masses, concentration of water in a small volume occupied by fractures, high velocity that can damage measuring devices and destroy boreholes (Cappa and Guglielmi, 2004).

For these reasons, water infiltration is derived from measurements of precipitation, and the effect of water pressures are indirectly obtained from a correlation between rainfall events and landslide velocity variations.

The transient response of soil pressure to rainfall is delayed in time, and controlled by many other factors that are less relevant for shallow soils, such as: subsurface later flow, regional groundwater flow, distribution and activity of springs, strong variability of vertical stratigraphy passing from soil cover to bedrock, presence and activity of geological structures (faults, folds, overthrusts). To understand the behaviour of large landslides a number of different approaches have been used in the Literature.

(1) Analysis of monitoring data to identify the empirical relationship between landslide activity and precipitation (Ibsen and Casagli, 2004; Hong et al, 2005; Bonzanigo et al, 2007; MacFarlane, 2009) or landslide activity and water table fluctuations due to infiltration (Corominas et al 2005, Figure 3-7; Van Asch et al, 2009; Ronchetti et al, 2010). Differently from shallow landslides, the analysis is normally focused on single phenomena at a local scale, and the effects of water pressures are thus indirectly obtained from a correlation between rainfall events and landslide velocity variations (Follacci, 1999; Cappa and Guglielmi, 2004)

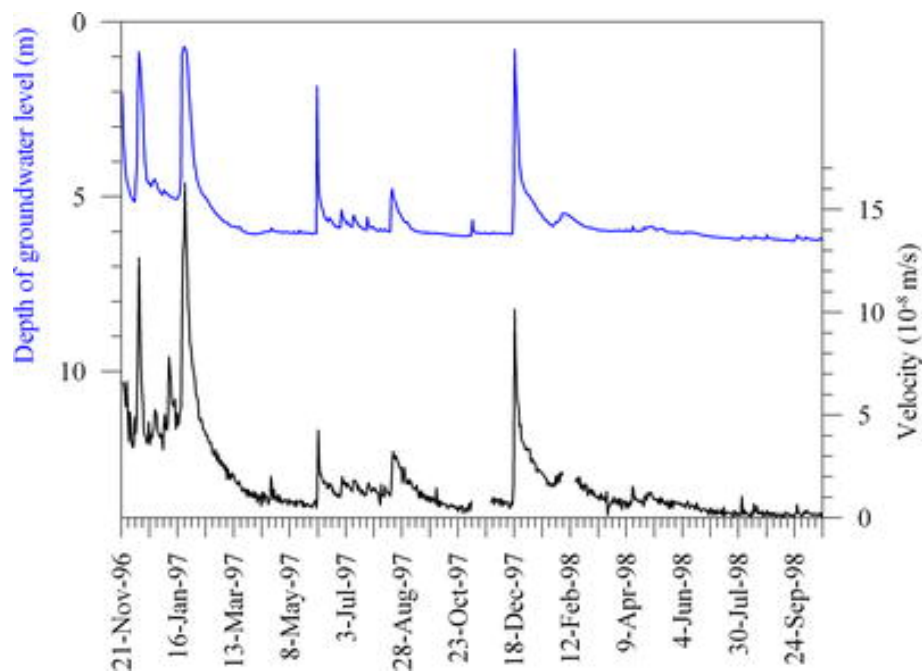


**Figure 3-7** - Piezometric record (blue line) and landslide velocity (black line) at a borehole in the Vallcebre landslide, Eastern Pyrenees, Spain (from Corominas et al, 2005).

(2) Indirect methods based on the study of natural hydrogeochemistry rock-water (Compagnon et al., 1997; Guglielmi et al., 2000, Guglielmi et al., 2002, De Montety et al, 2007, Figure 3-8; Madritsch and Millen, 2007; Martins-Campina et al, 2008) and on artificial tracing experiments (Bonnard et al., 1987) were developed in order to locate water flow paths through the rock mass and to estimate pore pressures at the scale of the landslide. These

methods confirm that it is possible to define water infiltration areas, to determine groundwater flow paths, and to estimate water transit and renewal times (Guglielmi et al., 2002).

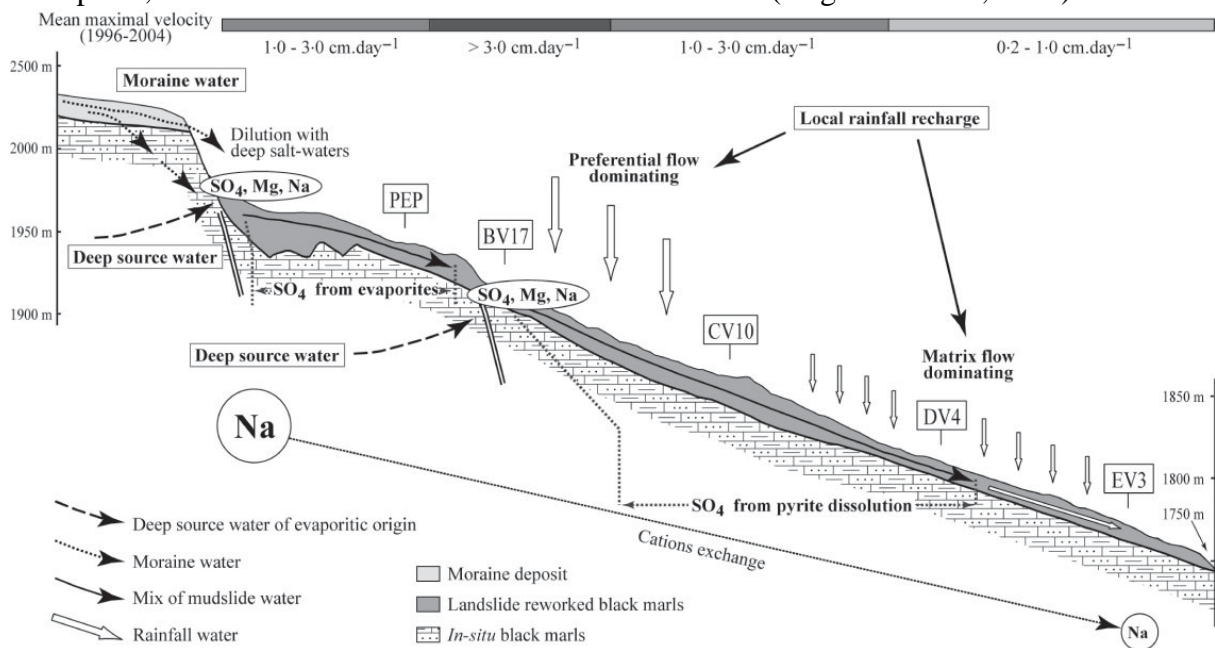


**Figure 3-8** – Synthetic scheme representing the hydrological concept of the Super-Sauze mudslide as interpreted from hydrochemical analyses, with indication of the mudslide velocities (from De Montety et al, 2007).

(3) Modelling of landslide hydrology using simple analytical methods (e.g., tank model, Hong et al., 2005) or transient hydrogeological 2D or 3D finite element or difference models (Miller and Sias, 1998; Tacher et al., 2005, Figure 3-9; Malet et al, 2005; Shrestha et al., 2008). Difficulties in hydrogeological modelling of deep-seated landslides lies in the heterogeneity of the rock masses and in the difficulty to model the effect of fractures and failure surface on the drainage system.

(4) For landslides in rock slopes, the analysis of different factors driving the failure of the slope needs numerical hydromechanical modelling (Cappa and Guglielmi, 2004). This implies calculations with models that account for drainage in a stable fractured medium, and hydromechanical laws for discontinuities (Vengeon, 1998, Bonzanigo et al., 2001, Guglielmi et al, 2005, Figure 3-10).

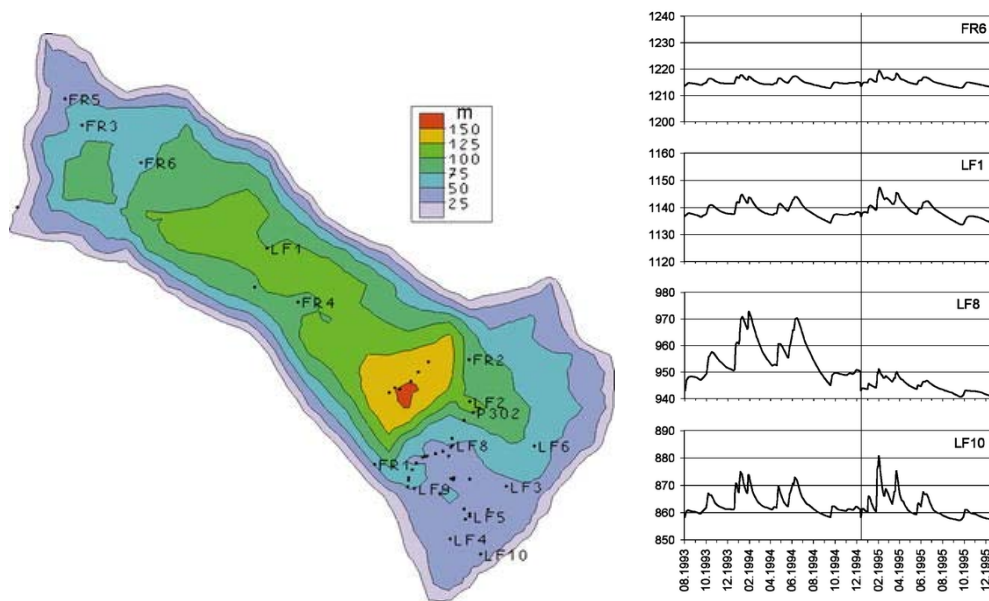


**Figure 3-9** – Right: computed hydraulic head (m a.s.l) in some piezometers at the main slip surface level. Left: piezometer location and total thickness of La Frasse landslide, Switzerland (from Tacher et al, 2005).

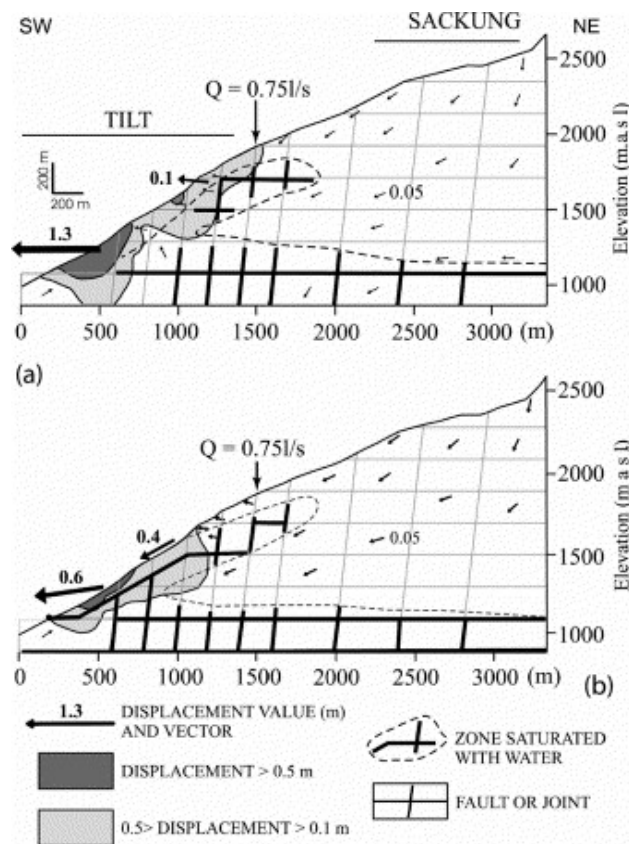


**Figure 3-10** – Results of coupled hydromechanical modelling: (a) Model ‘A’, only with pre-existing faults; (b) Model ‘B’, with pre-existing faults and a 28°-dipping failure surface (from Guglielmi et al, 2005).

### 3.4 CURRENT ANALYSES APPROACHES AT DIFFERENT SCALES - CHANGES OF GROUNDWATER LEVELS

There are numerous approaches proposed to study the effect of groundwater fluctuation on slope stability.

(1) Analysis of monitoring data to study the relationship between water fluctuation within a reservoir and landsliding (MacFarlane, 2009, Figure 3-12; Walker and Santi, 2004; Liao et al, 2005, Wang et al, 2008) for both drawdown (Figure 3-11) and water table rising (Figure 3-12).

(2) Numerical modelling (finite element or difference methods) has been used to study complex problem such as changing water levels. Most studies focused on the calculation of the flow regime under rapid drawdown conditions (Griffiths and Lane, 1999, Pauls et al, 1999; Lane and Griffiths, 2000, Rinaldi et al., 2004; Berilgen, 2007; Jiang et al, 2010) Numerical studies have investigated the influence of slope geometry, soil properties, the rate of water level rise and water level drawdown. One limitation of most of these studies is that they are pure flow models, uncoupled from soil mechanics. However, a coupled flow – mechanical analysis is needed for a proper interpretation and consistency of results (Alonso and Pinyol, 2009, Figure 3-13). In particular, the initial changes in pore pressure associated with stress unloading are not accounted in flow models. These changes are controlled by the soil mechanical constitutive equation. Without this coupling, the initial pore pressures do not change.

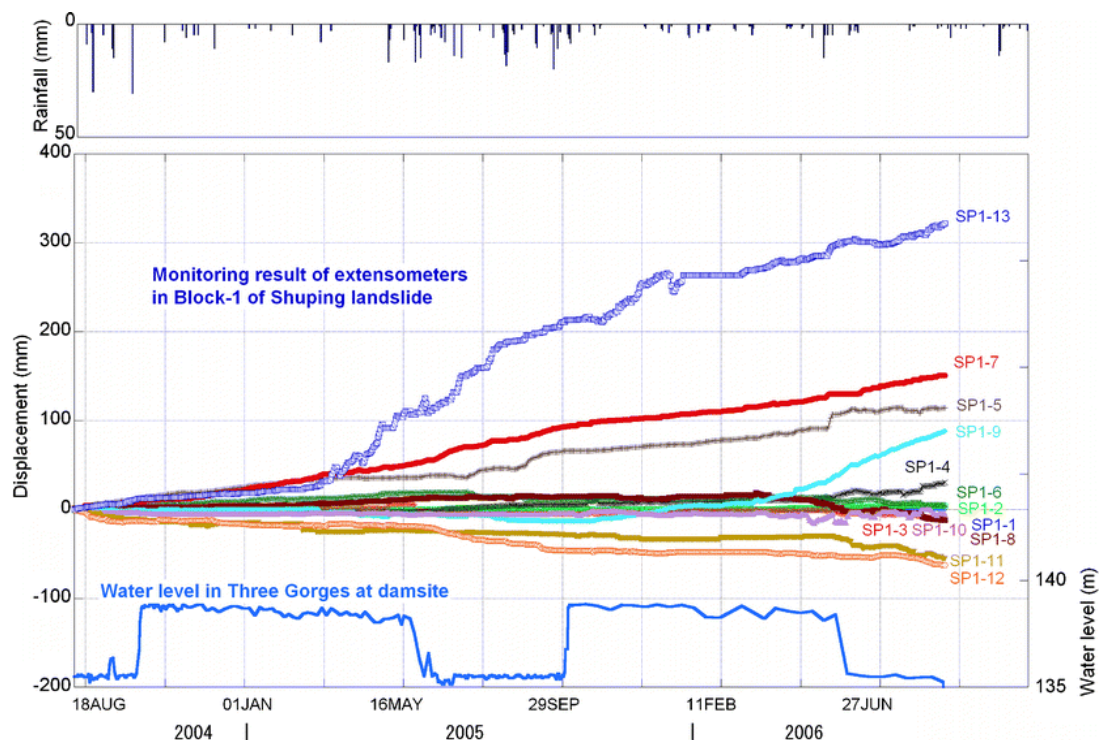


**Figure 3-11** – Example of reaction to water level fluctuations: monitoring results with the drum extensometers for the period from August 2004 to August 2006 in Block-1 of the Shuping landslide, Three Gorges Reservoir, China. (from Wang et al, 2008).

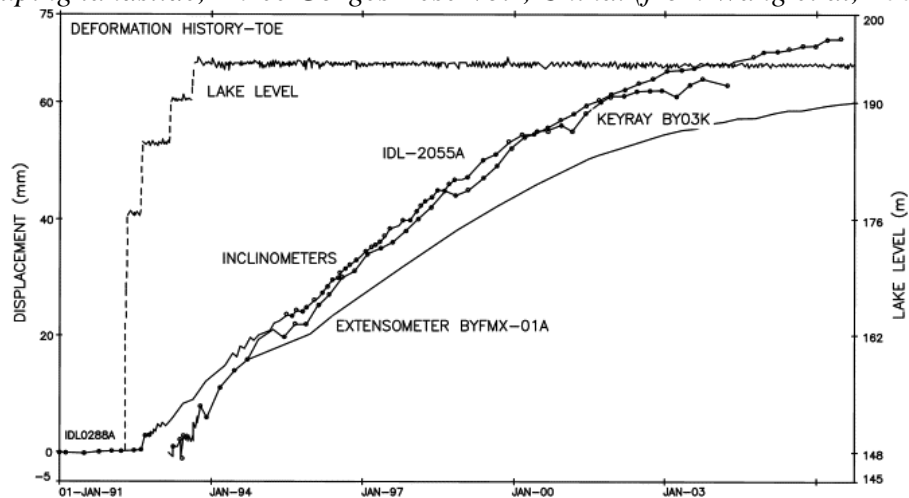


**Figure 3-12** – Example of reaction to lake filling with a long term creep movement recorded at Byford Creek slide, New Zealand. (from MacFarlane, 2009).

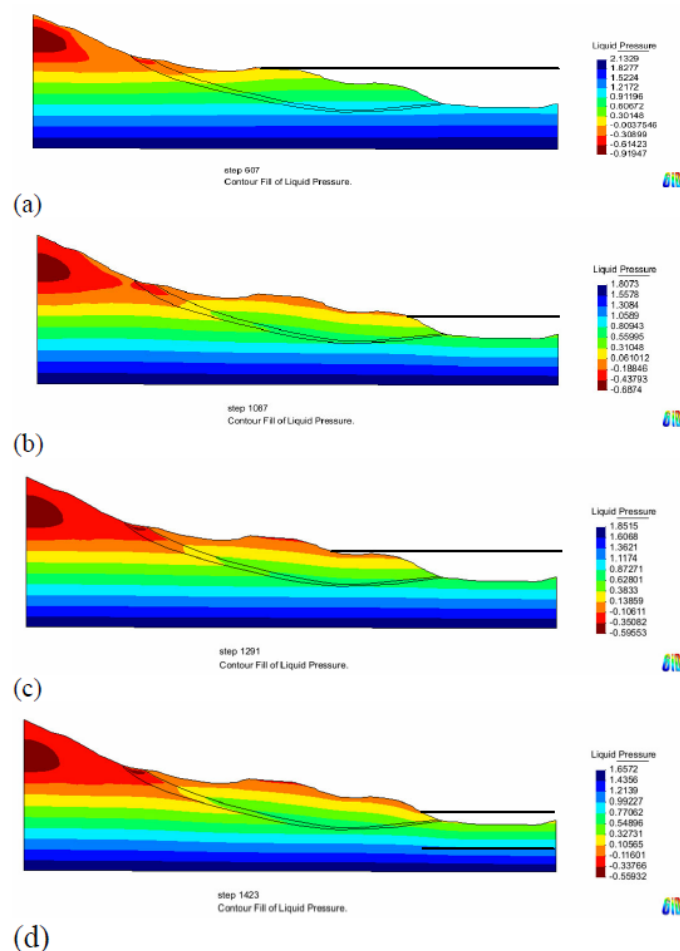


**Figure 3-13** – *Finite element hydro-mechanical coupled analysis for Canelles reservoir landslide (Huesca, Aragón, Spain): calculated pore water pressure distribution at (a) April 2004; (b) September 2005; (c) April 2006; and (d) August 2006, when crack was first observed (from Alonso and Pinyol, 2009).*

(3) Physical model experiments have been recently developed to deepen the understanding of failure modes and mechanisms associated with changes in water level adjacent to a slope (Jia et al 2009). Small-scale 1 g tests have been presented (Zhang et al., 2004, Hu et al., 2005), providing a general indication of slope behaviour related to water level lowering adjacent to a slope. Due to the reduced scale, the installation of instrumentation is difficult, and the stress levels are far from real cases. For this last reason, a number of centrifuge model tests have been conducted (Xu et al., 2005; Naoki et al., 2004). These models have a deficiency related to grain size effects and side boundary effects (Jia et al 2009). A few full-scale studies have also been reported in the literature (Rinaldi et al., 2004; Luo et al., 2005; Jia et al 2009, Figure 3-14) revealing the physical behavior and failure mode of saturated–unsaturated soil slope subjected to water level fluctuations.

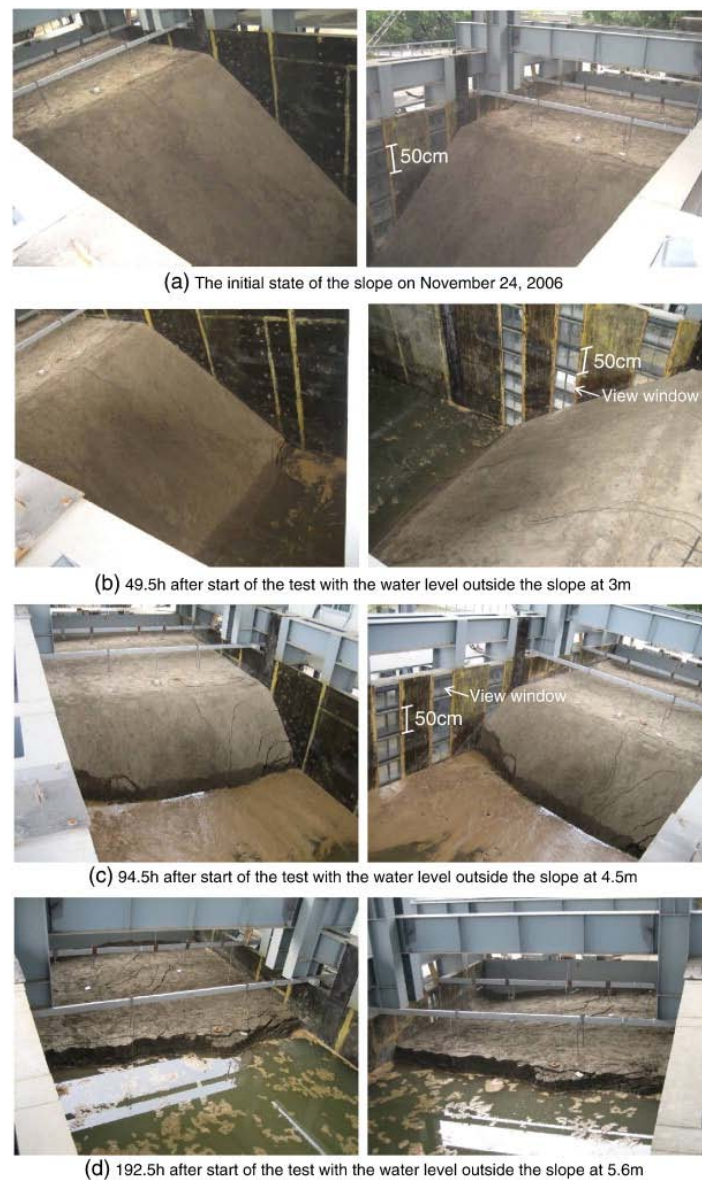


**Figure 3-14** - Appearance of the large-scale physical model slope when raising the water level (from Jia et al 2009).

### 3.5 EXAMPLES

#### 3.5.1 Overview of intense rainfall on volcanic soils–regional and local scale (AMRA)

Shallow landslides are probably the most frequent mass movements involving pyroclastic deposits in Campania region (Southern Italy) and, as shown by the large number of victims and the huge economic damage caused in the last years (Table 3.1), it represents one of the most severe natural hazards (Calcaterra et al. 1997; Celico and Guadagno, 1998; Del Prete et al. 1998; Di Crescenzo and Santo, 1999; de Riso et al. 1999; Cascini et al., 2000; de Riso et al., 2004).

Particularly, three recent events caused tragic consequences and reaffirmed this trend: on April 30, 2006, a severe storm in the Ischia Island (Vezzi mountain) triggered four mass movements, causing 4 victims (Figure 3-15a); on March 4, 2005 a great subtriangular

landslide on the Lattari Mountains (at Nocera, a small town in the Salerno province) killed 3 persons (Figure 3-15b); on March 3, 2005, a complex landslide occurred in the fine-grained loose pyroclastic deposits of flysch on the slope at Avellino (Figure 3-15c).

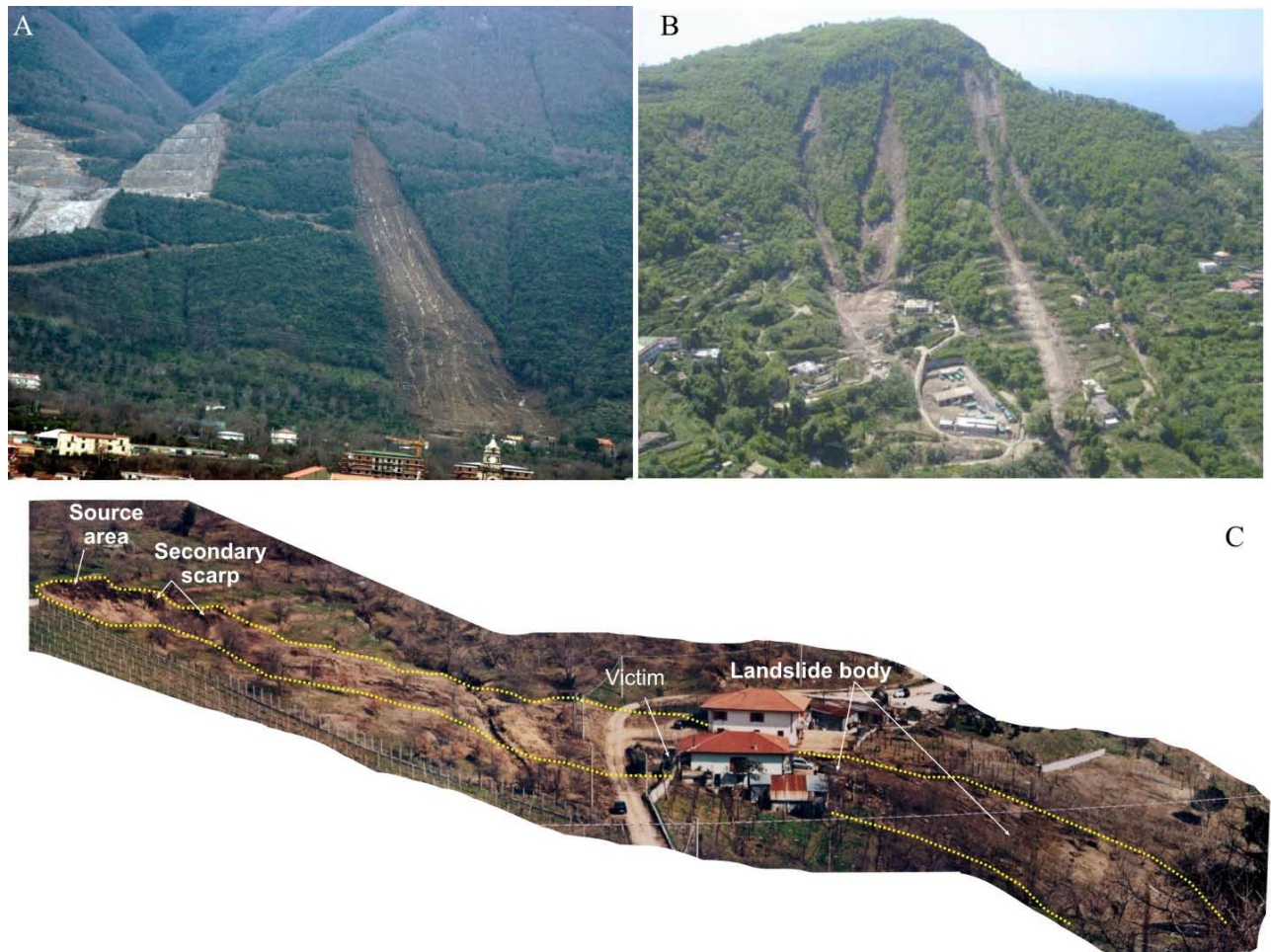


**Figure 3-15** – (a) The area of Lattari Mountains (Nocera village), (b) Vezzi mountain (Ischia island) and (c) Bosco de' Preti involved in flow-type landslides.

**Table 3.1** - List of the most important rainfall-induced flow-type landslides in Campania region (the numbers in brackets are the number of consecutive rainy days before the event).

Site	Date	Events	Rainfall (mm)	Damage	Victims
Amalfi, Atrani, Maiori, Gragnano	07.10.1540	Multiple	N.A.	-	Many
Strani	31.08.1588	Multiple	N.A.	-	Some
Quindici	1640	Multiple	N.A.	-	40
Cetara	09.11.1735	-	N.A.	Damage at Cetara	Some
Vietri sul mare	25.01.1736	-	N.A.	Considerable damage at Vietri sul mare	-
Gragnano	1741	-	N.A.	-	1

Cava de' Tirreni	03.09.1750	-	N.A.	Some damage at Cava dei Tirreni	Many
Cetara	35.05.1762	-	N.A.	Bridges, roads and building	50
Gragnano	1764	-	N.A.	-	43
Salerno district	11.09.1773	-	N.A.	Considerable damage at Cava dei Tirreni e Vietri sul mare properties	362
Cetara	1823	Multiple	N.A.		8
Gragnano	22.01.1841	Multiple	122.6 (4)		
Maiori	1846	Single	N.A.	-	1
Salerno district	7- 8.10.1899	-	N.A.	Considerable damage at Cava dei Tirreni and Vietri sul mare	4
Cervinara	1903	-	-	-	?
Amalfitana Coast (Cetara, Amalfi, Maiori) Ischia (Casamicciola), Vico Equense, Torre del Greco	23- 24.10.1910	Multiple	N.A.	Major damage occurred in Cetara	240
Amalfitana Coast	26.03.1924	Multiple	102.4 (1)	Major damage at Veticca minore, Praiano and Positano	100
Gragnano	28.05.1930	Single	N.A.	-	-
Castellammare	31.08.1931	Multiple	N.A.	-	2
Gragnano–Castellammare	20.08.1935	Single	91,7 (1)		4
Nocera–Sarno–Vietri	02.10.1949	Multiple	198 (1)		5
Pozzano	25.12.1950	Single	N.A.		
Pozzano–Bagni	09.03.1951	Single	N.A.		
Salerno–Minori–Tramonti–Cava–Vietri–Nocera	25- 26.10.1954	Multiple	504 (2)	Considerable damage: 350 injured and 10000 homeless. Destruction of buildings, industries, roads, railways and aqueducts	318
Nocera Inferiore	10.03.1958	Single	N.A.		
San Felice a Cancellò	15.10.1960	Single	N.A.		

**Table 3.1(Continue).** - List of the most important rainfall-induced flow-type landslides in Campania region (the numbers in brackets are the number of consecutive rainy days before the event).

Site	Date	Events	Rainfall (mm)	Damage	Victims
Nocera (S. Pantaleone)	08.12.1960	Single	148.8 (2)		
Nocera (S. Pantaleone)	04.11.1961	Single	111,2 (1)		
Plama Campania	24.05.1962	Single	N.A.		
Gragnano–Pimonte–Castellammare	17.02.1963	Multiple	249.2 (3)	Many damages in Gragnano village.	4

Sarno	21.02.1963	Single	219 (7)		
Pellezzano	25.09.1963	Single	152,2 (1)	-	-
Salerno– Amalfi–Cava de’Tirreni	27.02.1963	Multiple	182.2 (5)		2
Vico Equense (Scrajo); Arola– Ticciano	23-24.11.1966	Single	81,8 (1)		
Castellammare (Pozzano)	14.04.1967	Single	N.A.		
Sarno	09.01.1968	Single	25,0 (5)		
Cava de’Tirreni– Agerola–Scraio– Seiano	24.03.1969	Multiple	91,6 (1)		
Nocera (S. Pantaleone)	14.08.1970	Single	N.A.		
Gragnano	02.01.1971	Single	159.6 (3)		6
Gragnano	21.01.1971	Single	196 (1)		
Nocera-Pagani (S. Pantaleone)	06.03.1972	Single	115 (2)		1
Massalubrense (Mitigliano)	16.02.1973	Single	57 (3)	Building	10
Capri	21.02.1974	single	N.A.		2
Vico Equense (Scrajo)	04.11.1980	Single	N.A.		
Pozzano	14.11.1982	Single	N.A.		
Palma Campania– Catellammare Vico Equenze	22.02.1986	Multiple	99,4 (5)		8
Gragnano, Castellammare	23.02.1987	Single	182,0 (1)		
Tramonti	07.01.1988	Single	N.A.		
Pozzano	23.11.1991	Single	N.A.		
Bracigliano	03.10.1992	Single	80 (2)		
Sarno	26.05.1994	Single	N.A.		

**Table 3.1(Continue).** - List of the most important rainfall-induced flow-type landslides in Campania region (the numbers in brackets are the number of consecutive rainy days before the event).

Site	Date	Events	Rainfall (mm)	Damage	Victims
Castellammare, Nocera, Pagani, Amalfitana coast	10.01.1997	Multiple	56 (3)	Roads and buildingFlood of Sarno river. Shallow landslides in Naples area. Many landslides and damages in the Sorrento Peninsula.	5
Lauro	13.11.1997	Single	61,4 (2)	Many damages in Sannio area.	1
Sarno– Quindici–San Felice a	05.05.1998	Multiple	92.4 (2)	Sarno, Siano, Bracigliano, Quindici and S. Felice a Canello villages were hit by landslides.	144

Cancello					
Cervinara, San Martino V.C.	16.12.1999	Multiple	321,2 (2)	Cervinara village was destroyed. Many damages in S. Martino V.C.	5
Nocera (Salerno)	04.03.2005	Single		Some buildings destroyed	4
Avellino, Contrada,, Aiello sul Sabato	4-5.03.2005	Multiple	101 (2)	Roads and buildings	1
Ischia (Viezzi M.)	30.04.2006	Multiple		Some buildings destroyed	4
Ischia (Casamicciola)		Multiple		Many damages in the Casamicciola village	1

Historical data regarding the events occurrence show that the most frequent instabilities on a widespread sector of the Campania slopes are flow-type landslides which involve thin cohesionless, unsaturated pyroclastic soils, widely diffused over an area of about 2000 km<sup>2</sup> where more than 100 towns are located.

In all listed cases (tab. 1), landslides are triggered by significant rainfall occurring after a more or less long-lasting wet period.

The triggering and propagation mechanisms are strongly influenced by a generalised proneness of the slopes and, in particular, by the geotechnical soil properties, as well as by the topography, geology, geomorphology and hydrogeology characteristics of the source and propagation areas. In the presence of a state generally prone to instability, local factors of different types (rockfall or slide from natural subvertical rocky cliffs or anthropogenic scarps, water flow coming from fissured bedrock or pomiceous layers, etc.) are those which cause a given single slope to fail or not.

Post-failure movement and propagation is often catastrophic, due to the the high velocity (several kilometres per hour), large involved soil mass (up to about 150000 m<sup>3</sup>), and long runout (up to some kilometers).

According to Cruden and Varnes (1996) classification scheme the types of movements are complex, resulting from the rapid evolution of initial slides (rarely falls) into flows. However, the category of flows includes a wide spectrum of phenomena with reference to the pattern of movement, velocity and runout (Hutchinson 1998; Hungr et al., 2001).

Within the Italian scientific community the characteristics of the initial instability and, consequently, the classification of the flow-like landslides involving the pyroclastic deposits, are not clearly defined and commonly accepted.

In particular, some Authors (like Revellino et al, 2004; Guadagno and Revellino, 2005) hypothesized that the initial slides developed into extremely rapid flows, growing substantially in volume by incorporating materials and surface water. These landslides are called *debris avalanches* if involved unchannelled hillslope sectors (open slopes) or *debris flows* if the landslides becomes confined in gullies (channelled hillslope sectors) at least in their initial stages. In the case of the Campania, many debris flows becomes confined in gullies in the middle or lower sectors of the slope, trasforming them into debris flows.

Picarelli and Olivares (2001), Cairo and Dente (2003) and Picarelli et al. (2008), following Hungr et al. (2001) and Hutchinson (2004), hypothesized that static liquefaction was the triggering mechanism for a large volume of the landslides. In this case the Authors classified the landslides as a flowslide because of the style of the landslides consisting of a liquefied soil body, very similar to the flow of viscous fluid (Olivares and Picarelli, 2001; Musso e

Olivares, 2004). If a drainage channel is present along the movement path, the flowslide turns into a liquefied debris flow (Picarelli et al., 2008).

Despite differing opinions among various research groups and technicians, the complexity and frequency of the phenomenon, together with the severe destruction and loss associated, attracted great attention from the scientific community and national authorities.

In the following the geological setting, the macrozoning of the Campania area susceptible to flow-like landslides, the stratigraphic characteristics of the source areas and an overview of the relationships between rainfall and instabilities are described.

### Geological framework

During the Quaternary, the area today known as Campania (Figure 3-16) experienced extensive tectonic phenomena which caused the rising of the Apennines chain and the formation of a wide depressed graben area (Campanian Plain). Those events were accompanied by intense explosive volcanic activity. Aside from the marine environment, different volcanoes were active in the continental area, covering a significant part of the region with pyroclastic deposits.

According to the mode of transport and deposition, the pyroclastic deposits can be classified as falls, flows and surges (Picarelli et al., 2006). The gravity induced fallout of ejects from an eruptive column generated pyroclastic fall deposits which mantle topography, consisting of clasts formed by scoriae (> 10 cm), pumiceous (1-10 cm), and fine lapilli and ash (< 1cm). Fall deposits are often graded and characterized by parallel bedding, tending to be very well sorted at any given horizon.

Pyroclastic flow and surge deposits represent the movement of large volumes of pyroclastic material with the general behavior of lava flows. Pyroclastic flow deposits are often graded, commonly poorly sorted and massive. Surge deposits are better sorted, fine-grained, thinner and bedded than pyroclastic flow deposits.

Figure 16a illustrates a simplified geological map of Campania with the location of such deposits. The thickness of these depends on (1) the distance from the vent and (2) the slope of the depositional surface; thus, the thickness is higher in the vicinity of the volcanic centres and on plains, and is lower in the distal areas and on steep slopes.

Moving from North to South, the first volcanic centre is Roccamonfina, whose activity can be divided into two phases: the first one started about one million years ago, ending 400 ky ago; the second one developed between 250 ky and 170 ky ago. The volcano is now definitely inactive.

The volcanic centres located to South are younger and still active. The Phlegrean Fields district consists of several volcanic edifices located in the middle of the Campanian Plain graben (Figure 3-17). The activity of Phlegrean Fields started in the upper Pleistocene; about 45 ky ago (Di Girolamo et al., 1984). The main product is the so called Ignimbrite Campana (about 39 ky) which covers 150 km<sup>3</sup>, and was essentially deposited by pyroclastic flows; the eruption which produced the Ignimbrite Campana led to formation of the phlegrean caldera, a collapse structure having a diameter of 14 km. Another important product of Phlegrean Fields is the well known Yellow Neapolitan Tuff. These deposits present significant differences in terms of degree and type of alteration and, in particular, the following two facies can be distinguished: altered lithified deposits named Yellow tuff and unaltered unlithified pyroclastic products named Pozzolana. The transition between Yellow Tuff and Pozzolana corresponds to the vanishing of alteration, far from the eruptive vent inside the caldera (figure. 3.17). Finally, the Neapolitan Yellow Tuff deposits consists of two members: the

---

basal one is made up of at least six fall units, while the upper one consists of several flow depositional units.

Starting from about 12 ky ago until 1538 AD, the Phlegrean district produced non lithified pyroclastic deposits (pyroclastic fall and flow deposits) through several cones and rings which originated within the caldera: these deposits were essentially spread towards the East (Figure 3-16a). Pyroclastic fall deposits are represented by the Pomici Principali (10 kyr BP) and Agnano Monte Spina (4 ky BP) which reached some sector of the Campanian Appenines and interbedded with Somma-Vesuvius fall products.

The Mt. Somma-Vesuvius system consists of an older volcano, the Mt. Somma, whose activity was characterised by explosive plinian phases (Rolandi et al., 2000), and of the Vesuvius volcano which formed during the Middle Age within the Mt. Somma caldera. The main historic eruptions of Vesuvius occurred from 79 AD to 1944 (Lirer et al, 1993; Rosi et al., 1993; Rolandi et al, 2000).

In the distal area of Somma-Vesuvius region only fall deposits are well represented since pyroclastic flow and surge do not travel to great distance from the volcano but are present in the proximal area.

The air-borne products consisting of pumice, scorias and ash have been mainly directed by the stratospheric wind mostly along N-NE dispersion, where they mostly mantled the Appennine sedimentary relief (Figure 3-16a). Only the products of the 79 AD eruption (Figure 3-16a) were pushed in the S-SE direction towards the Lattari Mountains (Surrentine Peninsula).

Pyroclastic fall layers of each eruptive event are well preserved and sorted in the distal areas and are covered by fall deposits of next eruptions, whose repose periods are testified by humified pyroclastic ash layers interbedded between fall layers.

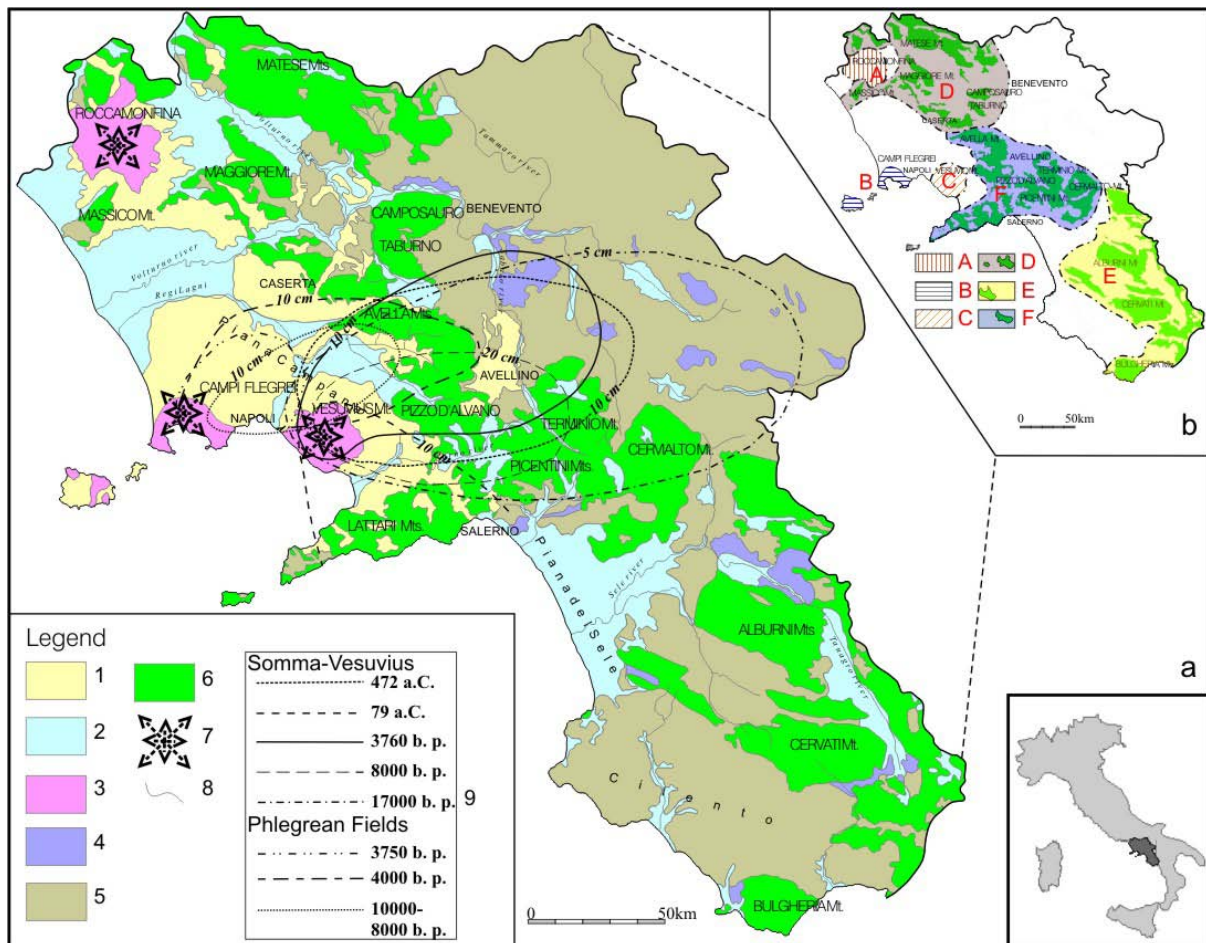


**Figure 3-16** – (a) Geological map of the Campania Region; (b) pyroclastic macro-areas. 1. Pyroclastic air-borne deposits (Quaternary). 2. Alluvial deposits (Quaternary). 3. Lavas, pyroclastic flows and tuffs (Quaternary). 4. Arenaceous conglomerates (Pliocene). 5. Marly arenaceous terrigenous deposits with clay interbeds (Tertiary). 6. Carbonate rocks (Mesozoic). 7. Volcanic centres. 8. Rivers. 9. Pyroclastic air-fall deposits of Phlegrean Fields and Somma-Vesuvius.

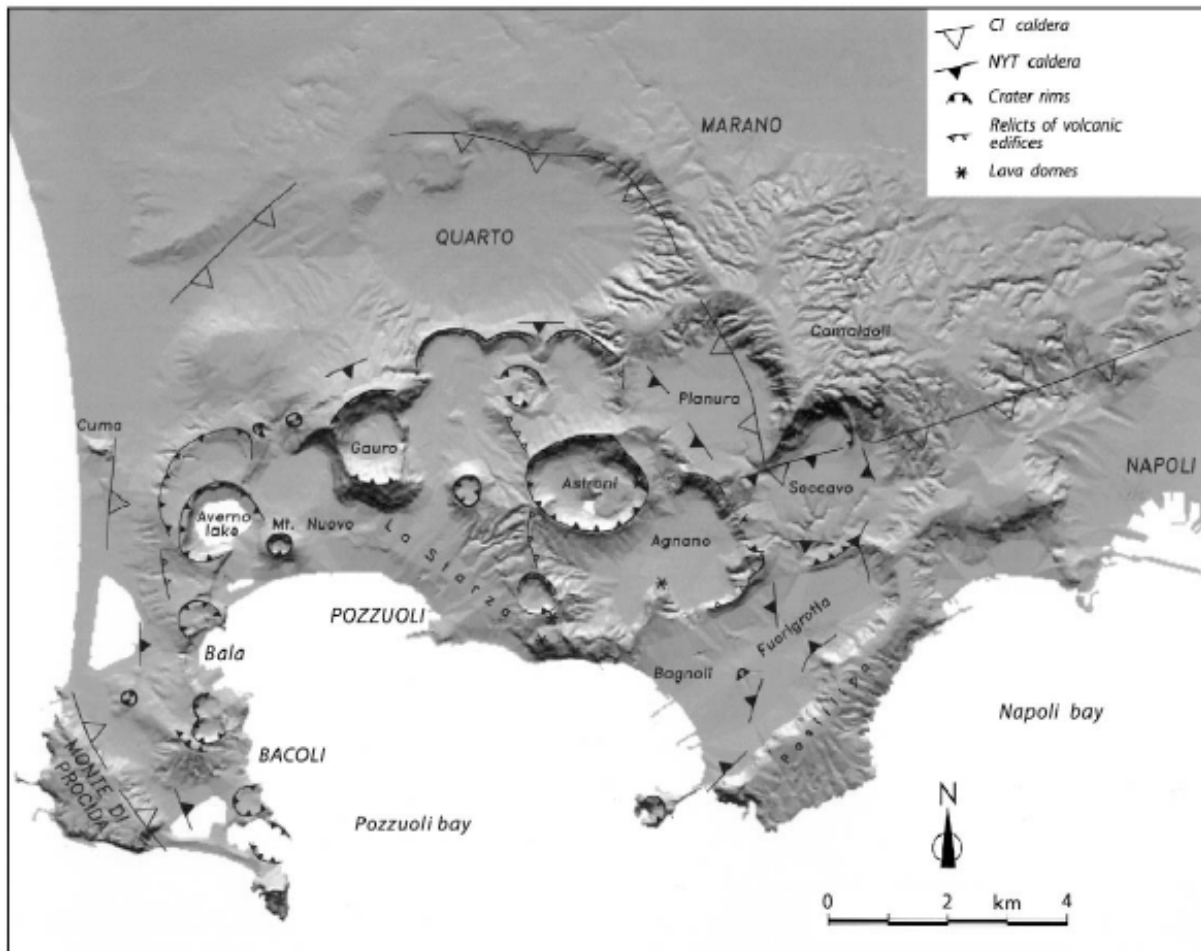


**Figure 3-17** - Structural sketch map of the Campi Flegrei region.

#### Macro-zoning of areas susceptible to flow-type landslides

In the territory of the Campania Region the pyroclastic deposits can be differentiated according to age, deposition mechanism, grain size and nature of the bedrock. Moreover, owing to the complexity of its geological-structural setting the characteristics and the distribution of the flow-type landslides in these deposits are different.

In Campania the six following macro-areas are present (Figure 3-16b):

- *Roccamonfina volcano area (A)*. In this macro-area the bedrock is constituted by lava. The pyroclastic products are very old (more than 150 ky) and consist of fine-grained or humified ash. Flow-type landslides are practically absent;
- *Phlegrean Fields and phlegrean inlands (B)*. The pyroclastic soils were deposited on tuff through flow, surge or fall. The average slope angles are quite high (30°-45°) and tuffaceous cliffs are frequent. This area is subjected to small to medium-size flow-type landslides;
- *Northern side of the Mt. Somma-Vesuvius system (C)*. Coarse pyroclastic materials (pumice and scoria) are spread (proximal deposits). The slope angles are quite gentle: values higher than 35° can be found only along main drainage channels around the volcano. Only small flow-types can be recognized;

- *Matese Mt., Maggiore Mt., Massico and Tifatini Mts. (D)*. The calcareous slopes are mantled by airborne products erupted from Roccamonfina and Phlegrean Fields. On the southern slopes, where the smallest amount of vegetation favours run-off, the largest part of the oldest deposits (about 100 kys) has been almost completely eroded. The northern slopes present some tens of centimetres of weathered ash. No flow-type landslides can be recognized;
- *Marzano Mt., Cilento and Vallo di Diano (E)*. Because of the large distance from vents, only thin deposits of pyroclastic soil (a few decimetres) are present, mostly on the northern slopes. Pumice is almost absent, while ash is generally weathered. No flow-type landslides can be recognized;
- *Lattari Mts., Sorrentina Peninsula, Picentini Mts., Pizzo d'Alvano Mt., Avella Mts. (F)*. These mountains are the closest ones to the Somma- Vesuvius system. In the last 15 ky they have been mantled by the products of several eruptions, thus the maximum theoretical thickness of primary deposits should range between 4 and 7 m (De Vita and Celico, 2006). Steep slopes have been repeatedly subjected to flow-type landslides.

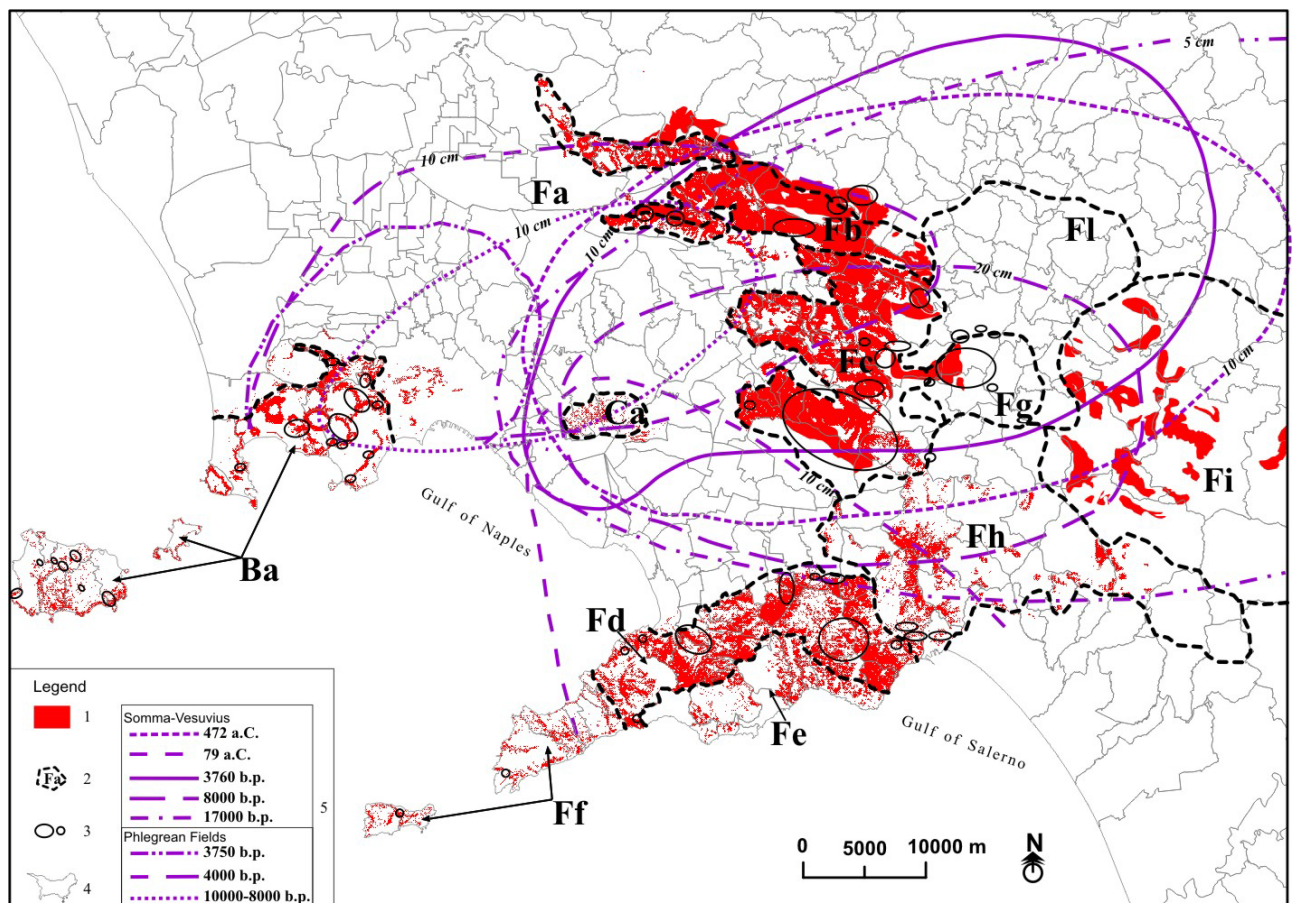


**Figure 3-18** - Zoning of the macro-areas B and F. 1. Potential sources of flow-type landslides in pyroclastic materials. 2. Sector; 3. Landslide or group of landslides. 4. Boundary of municipality. 5. Pyroclastic airborne deposits of Somma-Vesuvius and of Phlegrean Fields.

The macro-area B and, in particular, the macroarea F in the western side of the Campanian Apennine (Figure 3-18) are characterized by a unique geological setting with a great convergence of geological/morphological factors and of volcanic activity. Therefore, some important factors could be considered:

- 1) the slope morphology characterized by elevated steepness ( $>30^\circ$ ), mostly shaped by tectonics and karst processes;
- 2) the stratigraphy (§ 3) and the main features of the volcanic component: thickness of sequence on the top of the slope between 0,5 and 2 m; a grain size falling in the range of silty sands with gravel (mostly primary airborne deposits); absence of plasticity (unweathered ash); absence of true cohesion (non altered ash); low density (primary deposits of airborne ash); very high in situ porosity (even exceeding 70%); an usual unsaturated state and a saturated permeability around  $10^{-6}$  m/s;
- 3) the presence of road cuts and rocky cliffs.

These factors, in particular the second, can explain why the macro-areas A, C, D and E (Figure 3-16b) are only marginally affected by flow-type landslides. In contrast, these are widespread in the macro-areas B and F, very often interested by catastrophic slope failures, characterized by high energy and generally to be considered as unpredictable. (tab. 3.2).

In the sectors B and F, macro-zoning can be further developed accounting for the slope angle and excluding those covers which have a thickness less than 50cm. By means of a GIS application, a selection of all those slopes with impervious bedrock which have an angle comprised between  $13^\circ$  and  $45^\circ$ , and those with pervious bedrock which have an angle comprised between  $30^\circ$  and  $45^\circ$  was performed. Thus, on the basis of the nature of the pyroclastic cover and bedrock, further sub-areas have been identified (Figure 3-18):

- *Phlegrean area (Ba)*. Pyroclastic deposits (mostly consisting of ash) covers a bedrock of volcanic tuffs and lavas and generally do not exceed 2-3m. In this area also small flow-type landslides can occur: the largest ones (tab. 2) reach tens of thousands of cubic metres.
- *Caserta Mts. and southern slope of the Avella Mts. (Fa)*. These calcareous mountains are located at the boundary of the dispersion area of the Somma-Vesuvius deposits (Figure 3-15a, 3.17). Pyroclastic covers, mainly made up by weathered ash and pumice, reach thicknesses in the range of 1m. Only small flow-type landslides have been identified.
- *Avella, Roccarainola and Cervinara Mts. (Fb)*. This sector is located in the distal axial area of the airborne deposits of the Somma-Vesuvius and Phlegrean Fields systems. The pyroclastic cover overlies fractured limestone and consists of the products of several eruptions reaching a maximum total thickness of 4m. This zone experienced several large flow-type landslides as the Cervinara one (Tab. 3.1).
- *Pizzo d'Alvano, Monteforte and Mugnano Mts. (Fc)*. This zone is located in the distal axial zone of the dispersion products of the Somma-Vesuvius system. The thickness of the pyroclastic cover which rests on fractured carbonate rock, range from 4 to 7 m. In 1998 this area was subjected to a lot of large flow-type landslides (Tab. 3.1).
- *Northern sector of Lattari Mts. (Fd)*. The sector is located in the axial and proximal areas of the airborne products of the 79 AD Vesuvius eruption, thus the pyroclastic cover (maximum thickness 2m), is the result of only one eruption. In the past this sector, whose bedrock is constituted by fractured limestone, experienced large flow-type landslides.

- *Southern sector of Lattari Mts. (Fe)*. This zone is located in the distal axial area of the airborne products of the 79 AD eruption. The thickness of the pyroclastic cover, which overlies fractured limestone, is only 1m thick, thus only small flow-type landslides (tens thousands of cubic metres) can take place.
- *Sorrentina peninsula and Capri island (Ff)*. Also this sector is located in the marginal area of the airborne deposits of the 79 AD eruption. The pyroclastic cover on the carbonatic bedrock is intermittent with a thickness of less than 1m. Only small local flow-type landslides can develop.
- *Irpinia hills (Fg)*. The bedrock consists of flysch or clay. The slopes, which are quite gentle (15-25°), are located in the axial zone of the airborne products of Somma-Vesuvius and Phlegrean Fields systems. The cover is generally thicker than 2 m. In this context, flow-type landslides can occur having a moderate size (less than 10,000 m<sup>3</sup>) but a long run-out.
- *Salerno Mts. (Fh)*. This sector is located in the marginal dispersion area of the airborne deposits of Somma-Vesuvius system. Discontinuous pyroclastic covers up to 1m thick rest on fractured carbonate rocks. Isolated small flow-type landslides can take place.
- *Picentini Mts. (Sector Fi)*. The zone is located in the very distal dispersion area of the airborne deposits of Somma-Vesuvius and Phlegrean Fields. The pyroclastic covers have a high clay content and include ancient paleosoils reaching a total thickness of about 2 m. Flow-type landslides are not usual and can reach a volume of a few tens of thousands of cubic metres.
- *North-eastern sector of the Irpinia hills (Fl)*. It is located in the distal area of the dispersion zone of the airborne deposits of Somma-Vesuvius system and includes slopes with a flysch and terrigenous bedrock too. A thin pyroclastic layer (max 0.5m) crops out. Flow-type landslides are small (a few hundreds of cubic metres).

**Table 3.2 - Features of the main flow-type landslides in the 19<sup>th</sup> century**

Sector	Site	Date	Length (m)	Volume (m <sup>3</sup> )
Ba	Ischia	2006	450	3*10 <sup>4</sup>
Fb	Cervinara	1999	2*10 <sup>3</sup>	4*10 <sup>4</sup>
Fb	Avella	1998	15*10 <sup>2</sup>	2*10 <sup>4</sup>
Fb	Cancello	1998	8*10 <sup>2</sup>	3*10 <sup>4</sup>
Fc	Sarno	1998	2-4*10 <sup>3</sup>	5*10 <sup>5</sup>
Fc	Bracigliano	1998	1-2*10 <sup>3</sup>	15*10 <sup>4</sup>
Fc	Siano	1998	14*10 <sup>2</sup>	4*10 <sup>4</sup>
Fc	Quindici	1998	1-4*10 <sup>3</sup>	5*10 <sup>5</sup>
Fd	Gragnano	1764-1997	2-10*10 <sup>2</sup>	1-6*10 <sup>4</sup>
Fe	Maiori	1954	10 <sup>3</sup>	5*10 <sup>4</sup>
Ff	Massalubrense	1973	3*10 <sup>2</sup>	7*10 <sup>3</sup>
Fg	Avellino	2005	4*10 <sup>2</sup>	2*10 <sup>4</sup>
Fh	Montoro Inf.	1997	2*10 <sup>3</sup>	3*10 <sup>4</sup>
Fi	Salza	1970	4*10 <sup>2</sup>	20*10 <sup>3</sup>

Stratigraphic characteristics of the landslide areas

Historical and bibliographic analyses of flow-type instabilities occurred in Campania show that the first report on the stratigraphic characteristics is that of Lazzari (1954) describing landslides occurred during the storm in October, 1954, on the Amalfi-Salerno coast and the Sorrento Peninsula. Stratigraphy of single landslides was also analyzed by Civita and Lucini (1968) and Civita et al. (1975) on the Scrajo (1966) and Mitigliano (1973) landslides respectively. In these reports the Authors first pointed out the pyroclastic nature of the materials involved and the notable presence of pumice layers in the landslide area.

On January, 1997, several hundreds mass movements occurred in the Sorrento Peninsula and the Napoli area, causing 5 victims (Calcaterra et al., 1997, Calcaterra and Guarino, 1999). Di Crescenzo e Santo (1999) analyzed twelve selected landslides the stratigraphy of the source areas and the failure surfaces as observed from field surveys (Figure 3-19). With regard to Avella and Partenio Mountains, two debris flows occurred on 5<sup>th</sup> may 1998 on the northern slope of the E-W ridge between Mt. S. Angelo Palomba and the castle of Canello (Caserta) and numerous landslides triggered in the Valle Caudina area during the night of 15 December 1999. In the simplified stratigraphic column exposed on the eastern sector of the detachment zone of one of the Canello landslides the failure surface is located by Chiessi et al.(2003) and Esposito et al. (2003) at the joining point between the undifferentiated colluvium (soil with dispersed pumice and limestone fragments) and underlying bedrock.

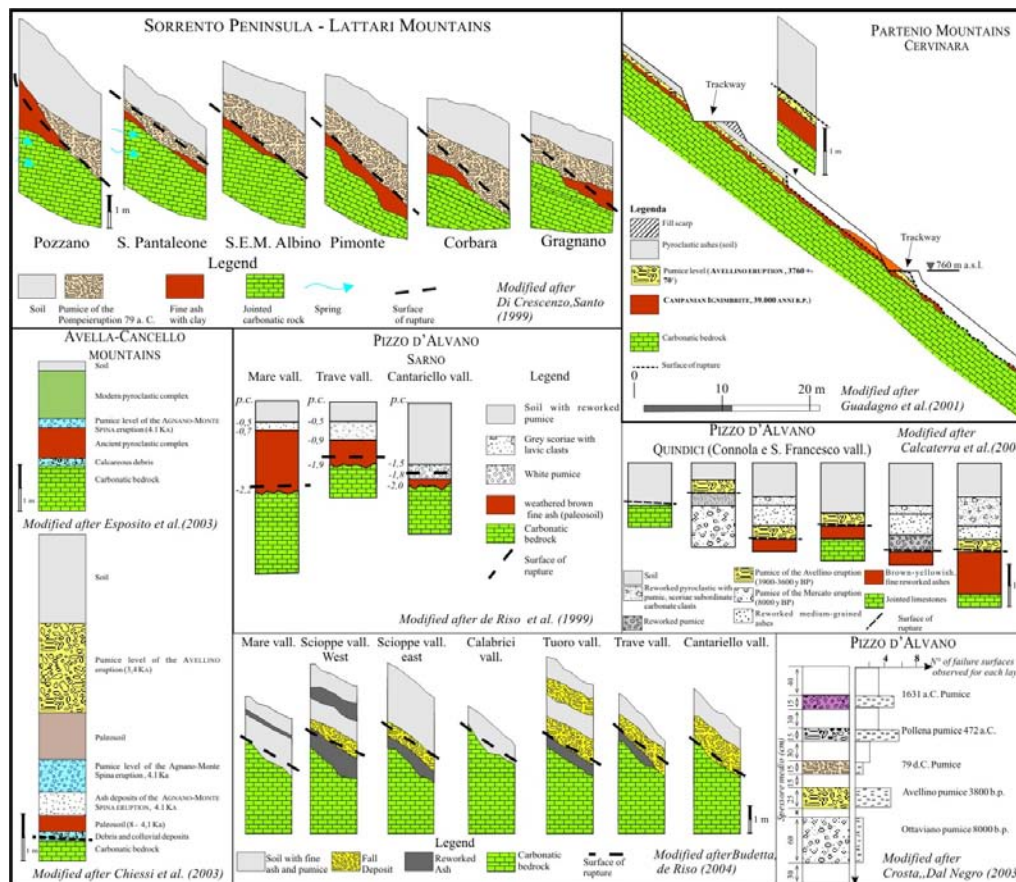


**Figure 3-19 - Stratigraphic columns of some flow-type landslides in the macroarea F.**

One of the numerous landslides which occurred on the northern slope of the Partenio Mountains reached the town of Cervinara causing the death of five people and considerable damage. More specifically, the surveys have shown the presence of a layer of falling pumice dating back to the so-called Avellino eruption of 3760 years b. p. This pumice layer lies on a characteristically silty-clay yellowish soil attributed to the Campanian Ignimbrite (35.000 years b.p., Rosi and Sbrana, 1987). On a schematic reconstruction of the source area stratigraphic sequence, the ruptured surface is located at the bottom of the pumice layer, above the Campanian Ignimbrite (Fiorillo et al., 2001).

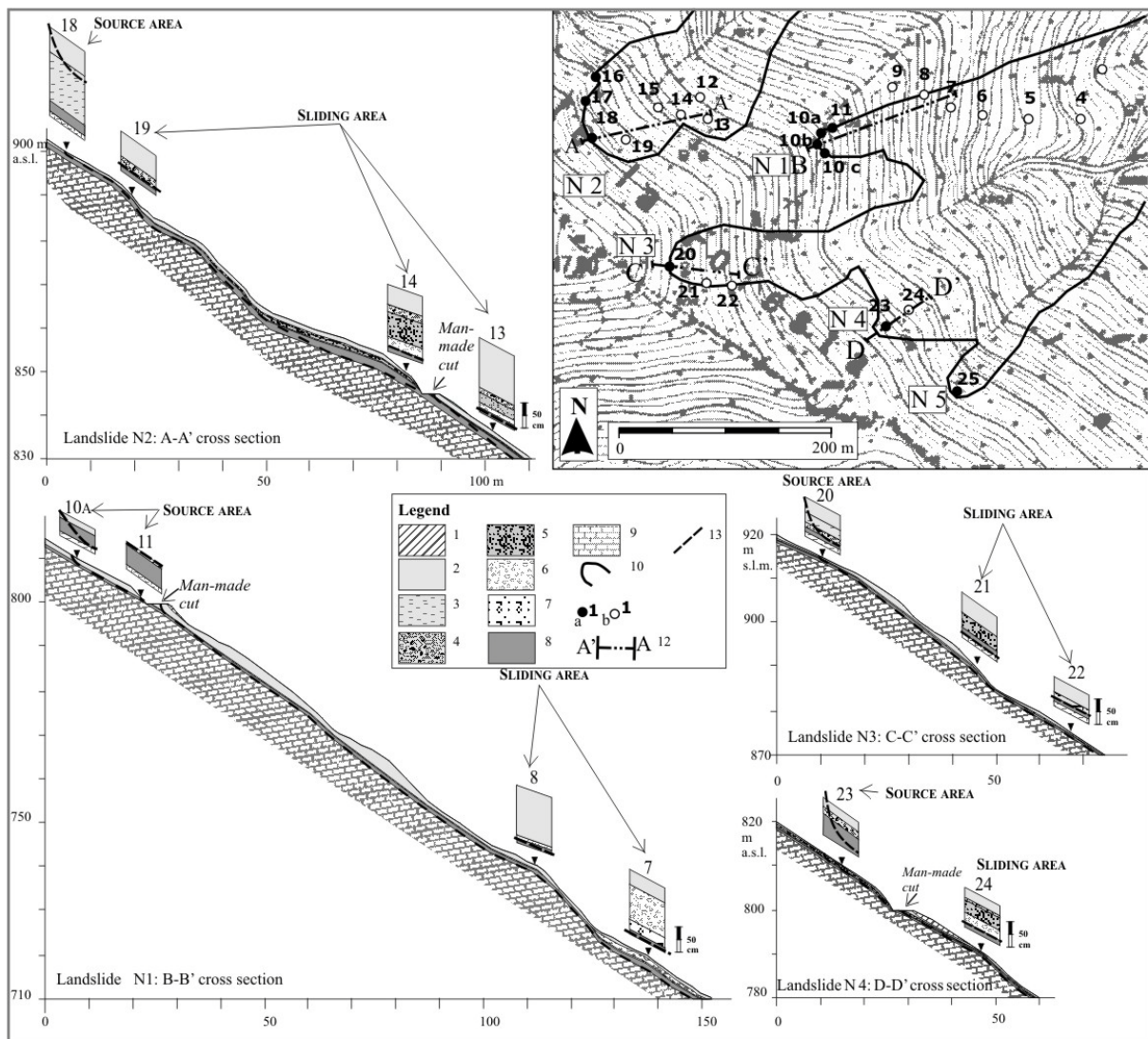


**Figure 3-20 - Landslide distribution and geologic cross section of the La Foresta Mountain (Bracigliano). Key: 1) man-made deposit; 2) soil; 3) weathered pyroclastic deposit (paleosoil); 4) pumice of the Pollena eruption (AD 472); 5) weathered and brown fine ash (paleosoil); 6) pumice of the Mercato Eruption ( 8010 ±35a); 7) volcanic sand of the Mercato eruption (8010 ±35a); 8) weathered brown fine ash with clay lower; 9) jointed limestone; 10) landslide limit; 11) location and number of stratigraphic column in the**

*source area (a) and in the sliding area (b) ; 12) trace of cross section; 13) surface of rupture (modified from Di Crescenzo and Santo, 2005).*

**Table 3.3** - Summary of the fallout deposits recognized in the detachment areas of the landslides of carbonatic contexts.

Context	Pomice layers
Sorrento peninsula – Lattari Mountains	Pompei AD 79
Pizzo d’Alvano-Quindici	Pollena (AD 472), Avellino (4000 b.p.) and Mercato (8000 b.p.)
Pizzo d’Alvano-Sarno	Pollena (AD 472) and Mercato (8000 b.p.)
Avella e Partendo Muntains	Agnano-M. Spina(4000 b.p.) and Avellino (4000 b.p.)

On 5-6 May, 1998, after intense and prolonged rainfall hundreds of slope failures (moistly channelled and mixed flows) affected the Pizzo d’Alvano impacting the towns of Sarno, Quindici, Siano and Bracigliano. These landslides displaced several million cubic metres of slope materials over a wide area causing 159 deaths. In this case, several stratigraphic columns and models for the triggering of the flow-type landslides were analyzed both in the source areas (Rolandi et al, 2000; Celico et al., 2000; Calcaterra et al., 2000b) and in the context affected by phenomenon (Del Prete et al., 1998; Cascini et al, 2000; de Riso et al., 1999, Pareschi et al, 2002). The slide surfaces are always located within the pyroclastic cover and, in particular, at the base of a pumice layer (Calcaterra et al., 2000b, Crosta and Dal Negro, 2003) or, only rarely, in the fine reworked ash.

Finally, Di Crescenzo and Santo (2005) analyzed the detailed stratigraphy of the most important landslides of the carbonatic contexts and the positions of the rupture surfaces in the volcanoclastic sequences recognized in the detachment areas. In Figure 3-20 the stratigraphic columns of the La Foresta mountain (Pizzo d’Alvano- Bracigliano) is showed.

Briefly, the eruptions from Mount Vesuvius and Phlegrean Fields recognized in landslide areas of all analyzed campanian contexts are indicated in table 3.3.

#### Rainfall and flow-type landslides in volcanic soils - An overview

The complexity of the landslide phenomena, and in particular the role of rainfall infiltration and run-off, often requires a hazard analysis at a regional scale (1:25000 and smaller) and at an urban or local scale (1:5000 or higher).

An example, on a regional scale refers to a back-analysis directed at testing the meteorological and hydrological maps as possible indicators of imminent instability phenomena inside the sectors F and B of the Campania Region (Cascini and Ferlisi, 2003; Cascini, 2008; Picarelli et alii, 2008;). In this area, rainfall triggers such phenomena although different intensity and duration are necessary passing from autumn to spring; in any case a minimum duration of many hours is necessary to trigger instability of significant magnitude (Cascini et alii, 2005).

Taking into account some meteorological and hydrological maps furnished in Figure 3-16 of the event which occurred at Cervinara (15<sup>th</sup>-16<sup>th</sup> December 1999; table1, Fb sector of Figure 3-18) as a consequence of rainfall which had started about 40 hours beforehand, it is possible to notice two different zones affected by heavy cumulated rainfall: one inside the pyroclastic cover (zone 1), where rapid movement originated, and the second one outside (zone 2).

Moreover, it is interesting to note that in zone 1 the accumulated rainfall over 24 hours reached values dating back to a period of 10-20 years earlier which rapidly increased in the following hours (Figure 3-19d). The results of this approach encourage due the availability of the meteorological and hydrological maps for some other portions of zone 1 (Rossi et al. 2004), where hazard maps and rainfall threshold value are present, should have activated the emergency plan some hours before the event occurrence.

On a large or local scale and referring to recurrent rainfall-induced flow-type landslides in Campania Region several studies have been carried out to define the hydrological thresholds. The definition of rainfall threshold for the triggering of mass movements in pyroclastic deposits can have an important role in helping the risk mitigation.

Rainfall thresholds can be defined on an empirical or a physical basis. Empirical thresholds are obtained by studying rainfall conditions which resulted in slope failures. Most commonly, the intensity, duration and cumulative precipitation during an event are to be considered.

Generally, empirical thresholds are presented as lower limit curves separating areas with specific combinations of values of plotted variables (Guadagno, 1991; Calcaterra et al., 2000). Physically based thresholds attempt to link regional or local rainfall measurements hydrological model (Cascini and Sorbino, 2003; Calcaterra et al., 2004; Sorbino et alii, 2007; Andriola et alii, 2010).

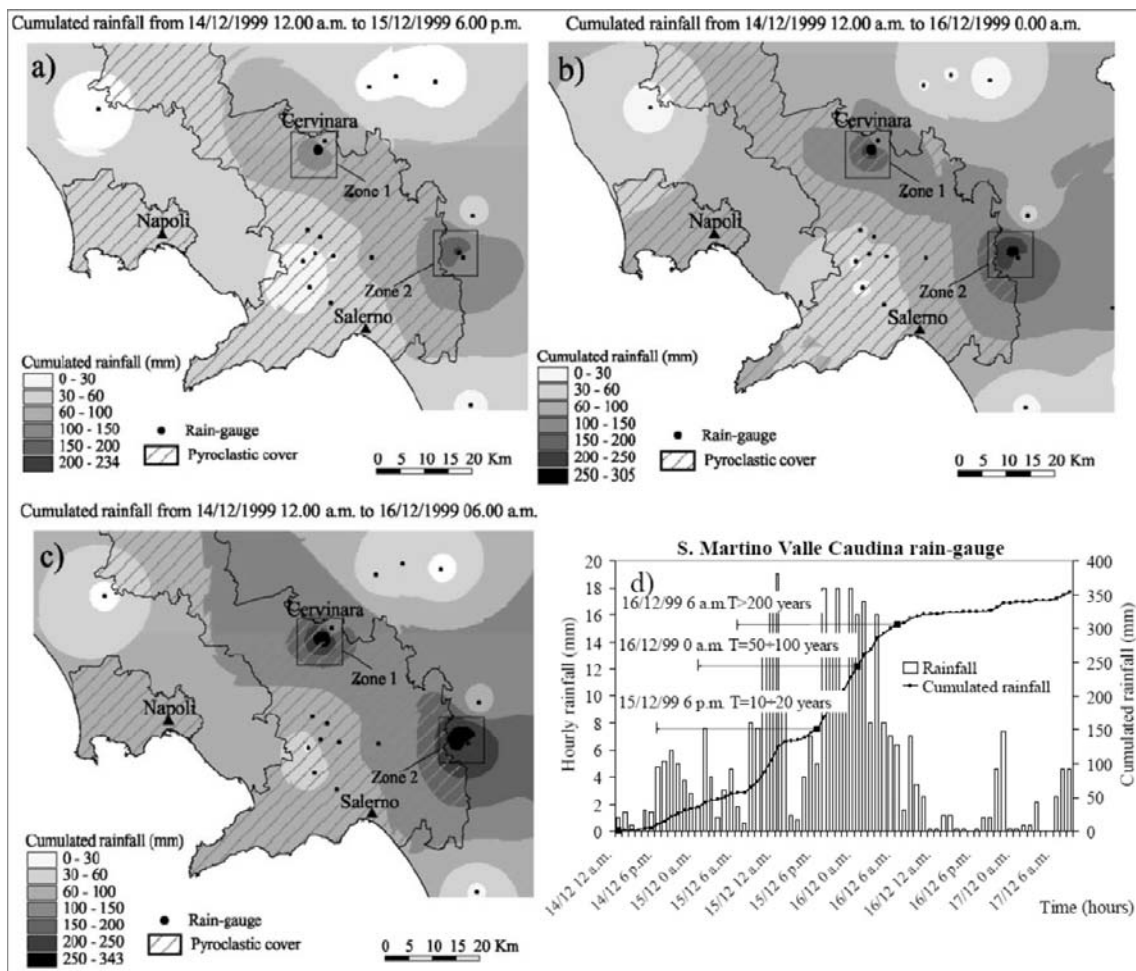


Figure 3-21 - An example of interpolation at regional scale of the meteorological maps

(Cervinara events) and a geological and geomorphological unit defined as at high risk. Aerial distribution of cumulative rainfall at different times (a, b, c). Cumulative and hourly rainfall recorded at a rain-gauge inside zone 1, and return period (T) of the backwards cumulative rainfall over 24 h period (d) (Cascini et alii, 2005).

Physically based threshold calculations are calibrated by using rainfall events for which rainfall measurements and the location and time of slope failures are known. Physical thresholds are not widely developed and, generally, they require detailed knowledge of the boundary conditions, which are seldom available outside specially equipped test fields (rain gauges, piezometers, tensiometers) (Cascini et alii, 2005; Cascini et al., 2008; Picarelli et al., 2008).

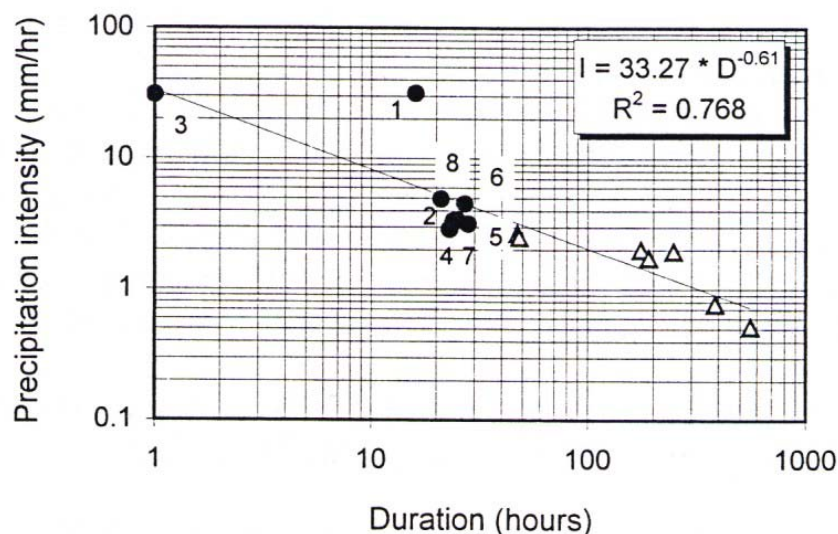
Various combinations of the rainfall parameters (total –cumulative– rainfall; antecedent rainfall; rainfall intensity and rainfall duration) have been attempted.

The empirical relationship between rainfall intensity, rainfall duration and slope instability has been thoroughly documented.

Guadagno (1991) found an intensity-duration threshold very similar to those by Moser and Hohensinn (1983) for an area in the Alps ( $I = 176.40 \cdot D^{-0.90}$ ;  $0.1 \text{ hr} < D < 1000 \text{ hr}$ ). This threshold has been reviewed by Calcaterra et al. (2000) (Figure 3-22). In addition to the regression line proposed (see Figure 3-22), a lower boundary for the case histories has also been calculated, which resulted in the following:

$$I = 28.10 \cdot D^{-0.74} \quad 1 \text{ hr} < D < 600 \text{ hr} \quad [1]$$

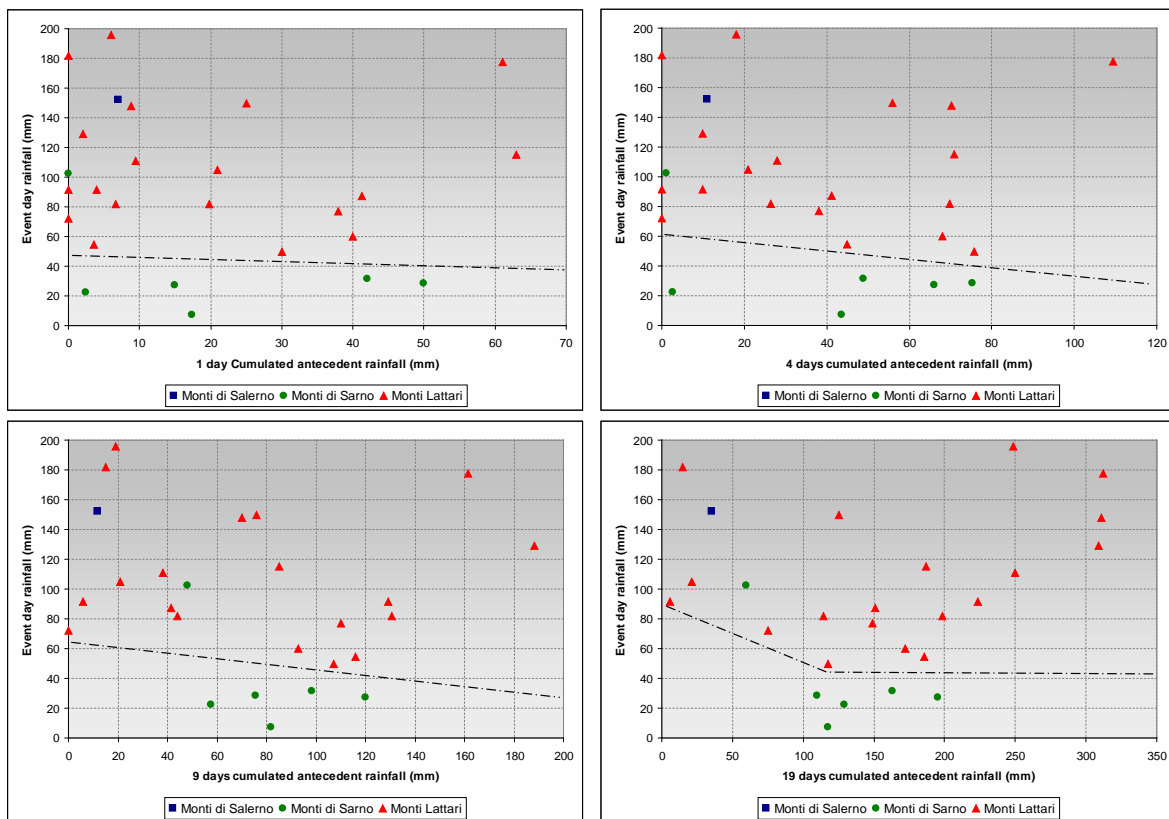
The relationship between duration and intensity for the January 9-12, 1997, events (tab. 1, Fd, Fe and Ff sectors) (De Falco et alii, 1997, Onorati and Pagliara, 1998, Calcaterra and Santo, 2004) is quite similar to those by Calcaterra et al. (2000) and Guadagno (1991). The landslides in this case occurred after 40 rainy hours and are characterized by medium intensity of 4mm/h.



**Figure 3-22** - Antecedent rainfall duration and intensity for landslides in the Campanian

pyroclastic. 1) Salerno (26.10.1954); 2) Quindici (07.04.1978); 3) Moschiano (27.08.1990); 4) Napoli (10.01.1997); 5) San Pantaleone (Nocera-Pagani) (10.01.1997); 6) Pozzano (10.01.1997); 7) Sarno (05.05.1998); 8) Quindici (05.05.1998). Triangles indicate data from Guadagno (1991) (Calcaterra et al. 2000).

It is known that antecedent total – cumulative - rainfall (expressed in mm) can be an important predisposing factor in the activation of slope failures (Wieczorek, 1987). In fact, De Vita (2000) and De Vita and Piscopo (2002) investigated instability processes on pyroclastic deposits of Lattari (Fd and Fe sectors), Sarno (Fc sector) and the Salerno Mountains (Fb sector). The study aimed to identify the rainfall conditions resulting in landslides, and to characterize the antecedent hydrologic conditions. Various antecedent rainfall intervals (1-, 4-, 9-, 19-, 39-, and 59-day) were considered to calculate the cumulative antecedent rainfall. In Figure 3-23 several thresholds for the Lattari, Sarno and Salerno mountains in the Campania Region are shown. In the graphs the dash dot lines represent lower-bound thresholds.



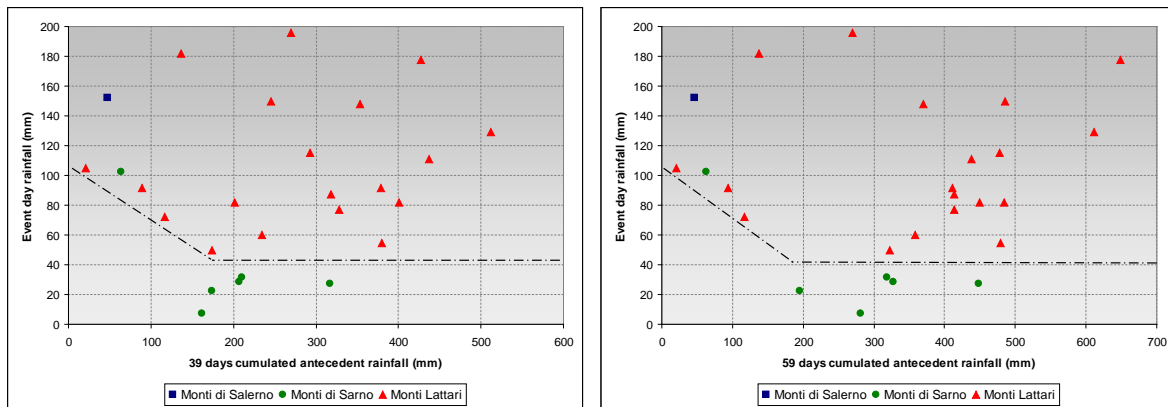


**Figure 3-23** - Lower-bound thresholds for the Lattari, Sarno and Salerno Mountains in the Campania Region considering various antecedent rainfall intervals. (De Vita, 2000).

The results seem to differentiate the Lattari-Salerno Mountains from the Sarno Mountains. The first case is characterised by rainfall on the day of the debris flow occurrence  $>50\text{mm}$  and significant cumulated rainfall in the antecedent periods. Otherwise, in the second case, rainfall on the day of the flow-type landslide occurrence was  $<32\text{mm}$  and cumulated rainfall in the antecedent periods appeared relevant and was characterised by a very homogeneous distribution in a long series of rainy days. In both cases, the threshold conditions appear as rare occurrences from rainfall historical series. In particular, estimating the ratio between cases with landslides and cases without landslides, a high frequency of landslide occurrences correspond to the mentioned threshold conditions (De Vita, 2000).

After the May 1998 disaster, rainfall thresholds were defined to protect the settlements at the top of the Pizzo d'Alvano ridge (Fb) from the residual risk (Rossi and Chirico, 1998). These thresholds have been defined by analyzing the relationships between daily rainfall and some flow-like landslides of the Campania Region. In the diagram of Figure 3-24 Chirico et al. (2000) plotted 2-day cumulative rainfall ( $P_e$ ) versus antecedent cumulative rainfall from the start of the rainy season ( $P_a$ ) and the related lower envelope curve. In the same diagram, two-day rainfall events that failed to trigger flow-type landslides are plotted with the related upper envelope. The distance between the envelopes indicates the uncertainty with respect to the use of the lower envelope as a hydrological threshold (Chirico et al., 2000).

Versace et al. (2000) and Sirangelo and Braca (2002) developed an hydrological model called Flair (Forecasting of Landslides Induced by Rainfall) to predict flow-like landslides incidences on the basis of the correlation of the rainfall amount and landslide occurrences.

The Flair model needs a preliminary calibration, based on the historical data, and uses a back-analysis procedure in order to verify the reliability of the proposed scheme prior to its use in a warning system.

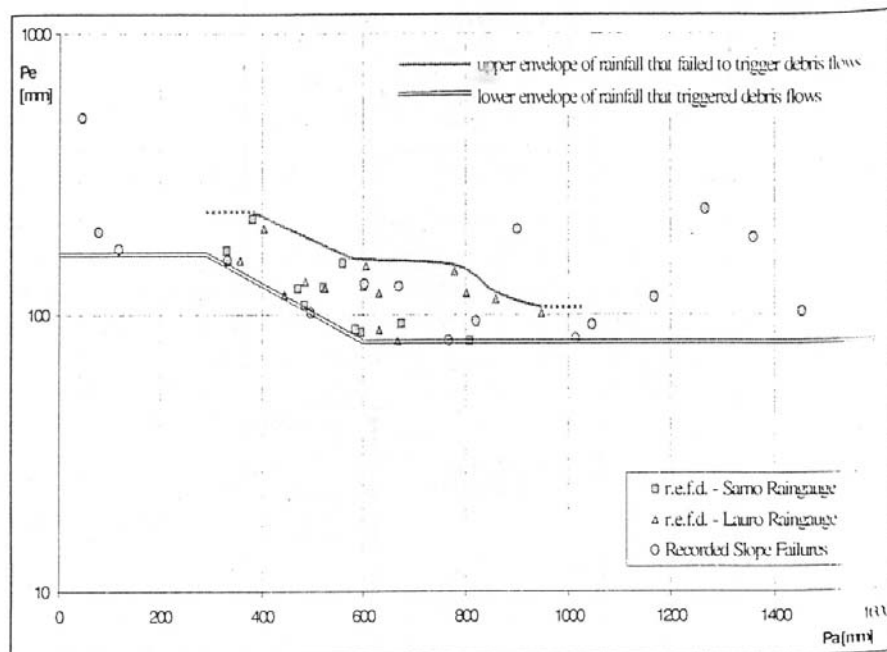


**Figure 3-24** - Two-day rainfall ( $P_e$ ) plotted versus seasonal antecedent rainfall ( $P_a$ ). Comparison between rainfall events that triggered debris flow and rainfall events that failed to trigger debris flow (r.e.f.d.) (Chirico et al., 2000).

A combination of empirical and physically based hydrological models was used by Fiorillo and Wilson (2004) to analyze historical data on rainfall and debris-flow occurrence in western Campania. Rainfall data from major storms recorded in recent decades in this area were compiled (Figure 3-25), including the daily series from several rain gauges located inside landslide areas, supplemented by hourly rainfall data from some of the principal storms.

In Figure 3-26, a threshold for each rain gauge has been plotted, employing the simple formula by Wilson (1989). Thresholds are correlated with storms that occur when soil moisture is close to field capacity. Rainfall needed to reach field capacity has been estimated in the range between 350 and 450 mm since the beginning of the rainy season. When soil moisture reaches field capacity, storms which fall below the thresholds can induce single debris flows, because of singular lithostratigraphic and hydraulic conditions (Fiorillo and Wilson, 2004).

Finally, as regard the flow-type landslides that take place along flysch slopes covered by pyroclastic deposits (sector Fl in Figure 3-18), antecedent seasonal rainfall is also thought to be important over a period as 90-120 days (Di Crescenzo et al., 2008) for March, 2005, and January, 1997, events (Tab. 3.1; Figure 3-27). The hypothesis of considering longer antecedent rainfalls are similar to those proposed by De Falco et al. (1997) and Onorati and Pagliara (1999).

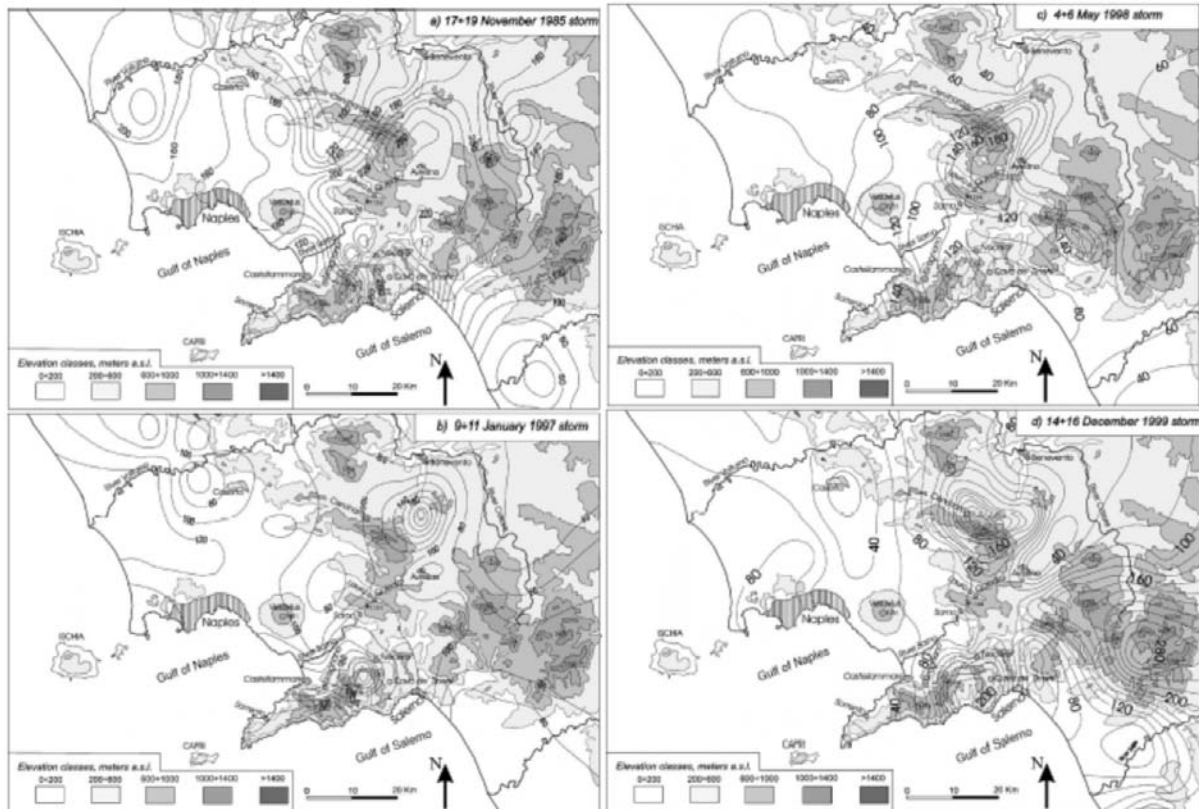


**Figure 3-25** - Isohyets of the main storms occurred in the last two decades in Western Campania: (a) November 1985; (b) January 1997; (c) May 1998; (d) December 1999 (Fiorillo and Wilson, 2004).

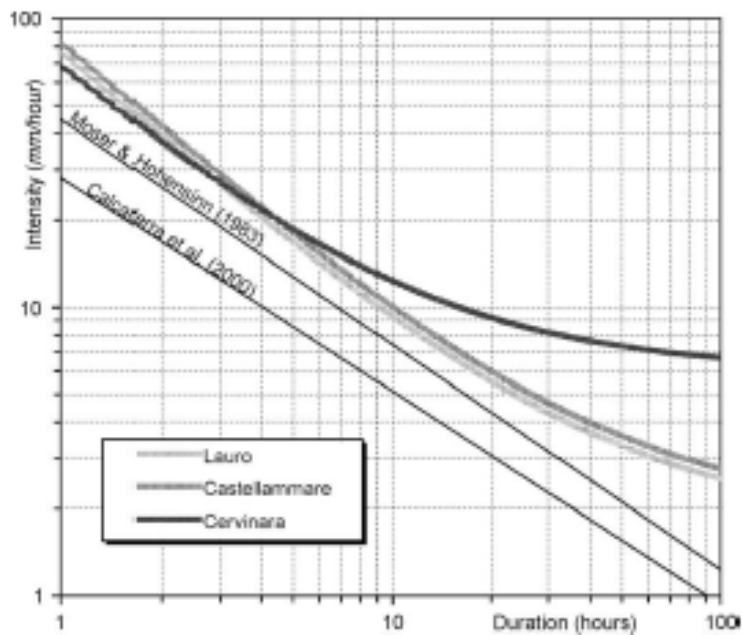


**Figure 3-26** - Hydrological thresholds for debris-flows initiation in the pyroclastic deposits of Campania (Fiorillo and Wilson, 2004).

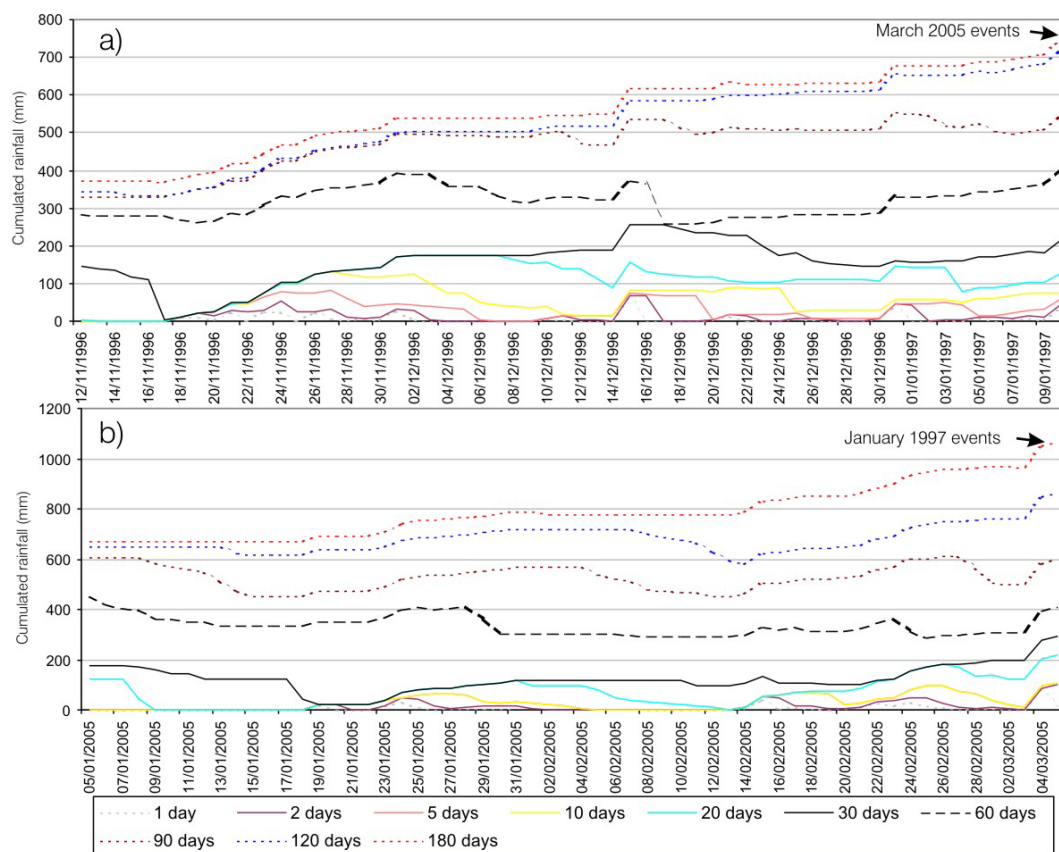


**Figure 3-27** - Cumulative rainfall for 1, 2, 5, 10, 20, 30, 60, 90, 120 and 180 days referred to two months before the March 2005 (a) and the January 1997 landslides (b).

### 3.5.2 Overview of rainfall impacts on the dynamics of landslides developed in over-consolidated and weathered clays – Example of the Trièves Plateau and the Barcelonnette Basin landslides (French Alps) (CNRS)

In the French Alps, hundreds of landslides have occurred in the overconsolidated varved clays of the Trièves Plateau, around 50 km south of Grenoble.

In Van Asch et al., 2009 the effect of groundwater fluctuations on the velocity pattern of slow-moving landslides is analysed on the example of two deep-seated landslides of the Trièves Plateau, namely the Monestier-du-Percy landslide (Giraud et al., 1980), and the Saint-Guillaume landslide (Azimi et al., 1994; Méric et al., 2007). The meteorological triggering conditions associate heavy rains in the two months preceding the onset of the failure (203 mm in February 1978 and 197 mm in March 1978, whilst the average rainfall is 155 mm per month for this period of the year), and a rapid melt of snow cover in the case of Monestier-du-Percy.

The Barcelonnette area that is part of the Ubaye-Valley in the South French Alps (Alpes-de-Haute-Provence) is another example that is highly affected by rainfall-controlled landslides consisting of reworked clays. Three large mudslides have occurred in the black marl facies of the Barcelonnette Basin, about 100 km North of Nice. The three mudslides, very active since decades, are in an intermediate stage of evolution, and their volume is respectively estimated at  $3.5 \times 10^6 \text{ m}^3$  for La Valette,  $1.5 \times 10^6 \text{ m}^3$  for Poche and  $0.9 \times 10^6 \text{ m}^3$  for Super-Sauze.

A basic requirement in landslide forecasting, quantitative risk assessment and management (e.g. design of early warning systems) is the identification of triggering mechanisms. The preparatory work towards failure is related to slope evolution in terms of related changes in stress field (Brunsden (1999)), of hydro-chemical and mechanical deterioration (e.g. damage), and of the development of crack systems (Boukharov et al. (1995), Kilburn and Petley (2003), Amitrano (2003)). The mechanisms leading to failure are dependent on the material. This section focus on mechanisms related to rainfall that might trigger landslides or local accelerations (debris flows) within already active landslides on over-consolidated and weathered clays.

If the stress state of a soil at equilibrium is less than that to which it was once consolidated (loaded), then the soil is denoted as overconsolidated. Gentle slopes consisting of clay that are affected by slow moving landslides may be divided into three zones: (a) the upper zone where there is a high degree of weathering and removal of material, (b) the intermediate zone where there is some weathering at the top part of the zone and (c) the partially weathered zone where the transition from the weathered material to the unweathered parent rock can be recognized. Factors influencing the rate of weathering are among others climate (temperature and rainfall), time and type of source rock (Lambe and Whitman (1969)). Garga et al. (2006) conducted a significant number of stress-path triaxial tests in order to study the stress-path dependent behavior of an overconsolidated weathered crust of Champlain clay in Eastern Ontario. These clay crusts are described as usually desiccated, fissured, anisotropic, lightly to highly overconsolidated, often oxidized, and may be unsaturated in situ (Albrecht and Benson (2001)). The overconsolidation developed in a crust is due to one or more of natural processes such as erosion, delayed consolidation, ground water fluctuation, desiccation or cementation. Generally, the weathered crusts have higher undrained shear strengths and preconsolidation pressures with corresponding lower water content and compressibility when compared with the underlying intact clay. The significantly less water content in this layer, often results in a liquidity index much less than unity, in contrast to the lower intact clay.

In the following a general view of potential triggering mechanisms observed in OC and reworked clays is given; examples where these mechanisms were investigated are also given.

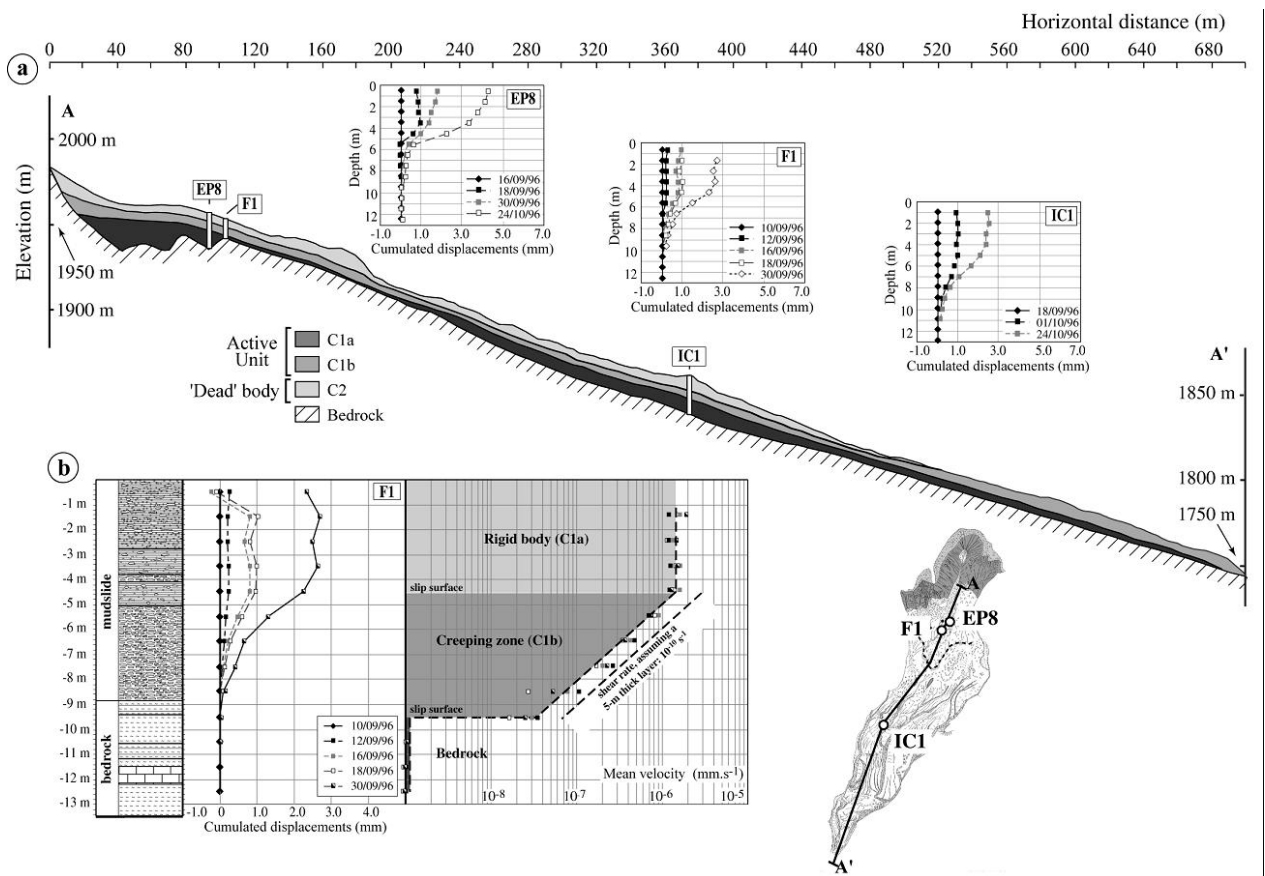
#### Shear strength of unsaturated soils

Rainfall can lead to the rising of the main groundwater level or to the development of perched water table, resulting in an increase in pore water pressure or a reduction in soil matric suction. Shear strength of unsaturated soils is dependent on the pore water pressure (Fredlund et al. (1978), Gan et al. (1988), Fredlund et al. (1996), Schanz (2007)). In a recent study Cokca and Tilgen (2009) have investigated the relationship between shear strength and soil suction of compacted Ankara clay. They have analysed the effects of compaction moisture content and soaking on the unsaturated shear strength and suction of Ankara clay using direct shear tests on samples compacted at optimum moisture content ( $w=20.8\%$ ), drier than optimum ( $w=14.8\%$ ,  $16.8\%$ ,  $18.8\%$ ) and wetter than optimum ( $w=22.8\%$ ,  $24.8\%$ ,  $26.8\%$ ). The soil suction versus moisture content curve was developed and the shear strength variation with respect to soil suction obtained for different stress states. It is shown that the soil suction versus moisture content curves bear a close relationship to the unsaturated shear strength of the soil. An increase in soil suction increases the shear strength. The increase of pore water pressure due to the rising of water table results in a decrease in shear strength on the potential failure surface to a point where equilibrium can no longer be sustained in the slope and then failure occurs as for example described in Ng and Shi (1998).

---

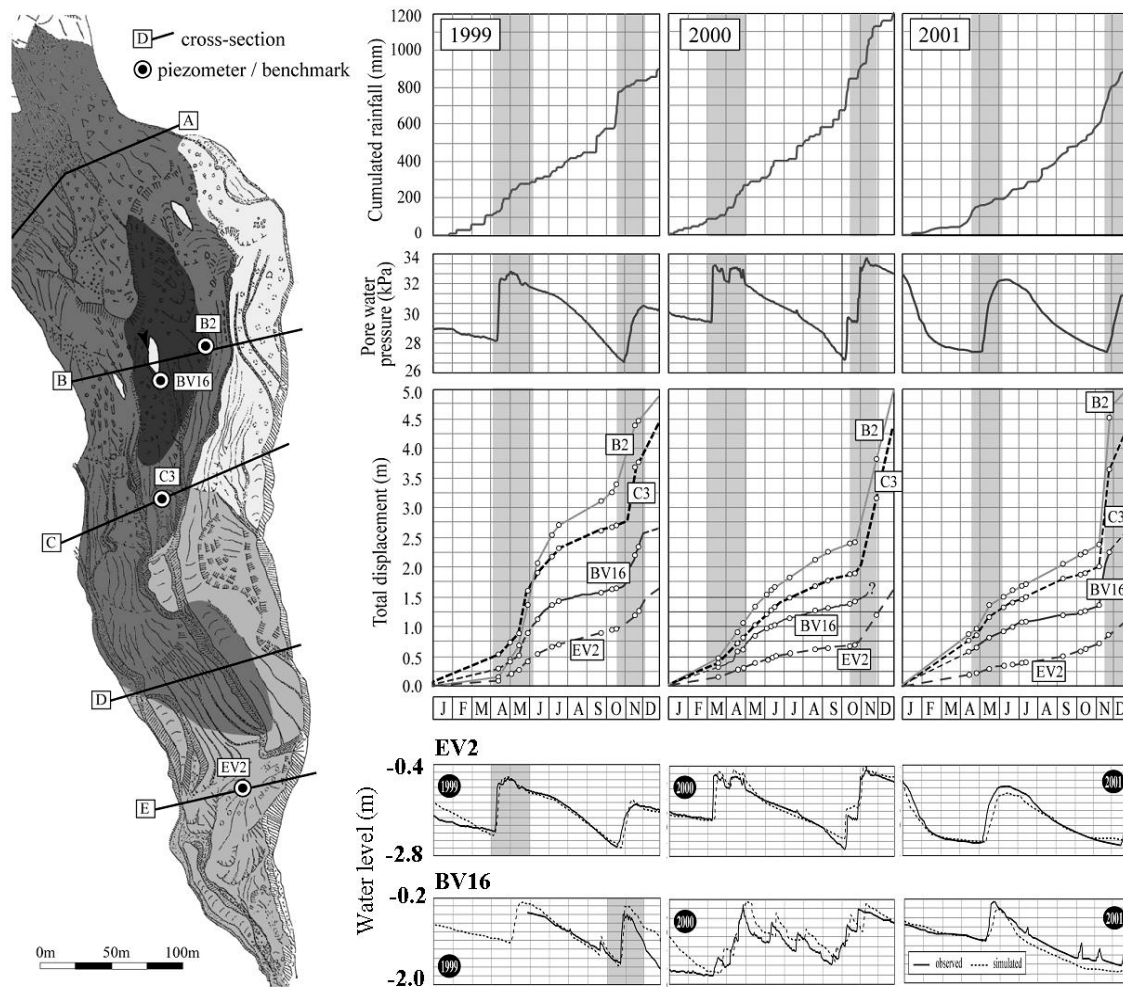
Ring shear tests performed on remoulded specimens of reworked black marls taken from the Super-Sauze landslide for several combinations of initial water content (3% to 30%) indicated an increase in the residual strength parameters up to a critical water content of 27-28% (Maquaire et al., 2003). After reaching the critical water content level, the cohesion suddenly decreases. The tested material originates from C1b unit as shown in Figure 3-28. The mesofabric of the resulting tectonized black marls is a fine-grained matrix crossed by several networks of fissures, spaced from a few millimeters to a few centimeters, subdividing the soil into very small clasts. The macrofabric is characterized by complex bedding surfaces (e.g. schistosity), calcareous joints and principal shears. Consequently, the black marls can be categorized as intensively fissured sediments.

Figure 3-29 gives the rainfall, pore water pressure, displacement and groundwater level pattern of several locations from 1999 to 2001. The displacement pattern exhibits a marked seasonal trend with two acceleration periods (Spring and Autumn) and two deceleration periods (Summer and Winter) (Fig. 2). The maximum daily displacements of each year are systematically observed in the snow melting periods with peaks from Mid-April to Mid-June, and in the heavy rainfall periods with peaks from Mid-October to Mid-November. Groundwater fluctuations exhibit the same trend throughout the mudslide however the relative position of the water level is dependent on local conditions; the highest pore water pressures being observed in the upper part (cross-section B) and decreasing down-slope.



**Figure 3-28** - *Geomechanical behaviour of the mudslide. a) Longitudinal geotechnical profile of the mudslide interpreted from borehole data, inclinometer measurements (EP8, F1 and IC1) and geophysical tomographies; b) Example of in-clinometric measurements at F1 borehole. The vertical distribution of velocity materializes respectively the potential solid-state (rigid body, active unit) and plastic-state behaviours of the mudslide (Malet, 2003).*

Consequently, displacement rates are also variable and decrease from the upper to the lower part of the mudslide. The depth of the average position of the groundwater table slowly decreases from the B cross-section (-0.50 m) to the E cross-section (-1.20 m). The rate of movement seems to be controlled by thresholds in pore water pressures which values are constant in time (Fig. 3). Observations over the period 1999-2005 at plot BV16 indicate that the ‘Spring acceleration’ is initiated at a threshold value of ca. 30 kPa while the ‘Autumn acceleration’ is triggered by a higher threshold value of ca. 32 kPa. Above these thresholds, the velocity increases with a non-linear fashion. The higher threshold value for the ‘Autumn acceleration’ may be explained by shear strength recovery due to an increase in undrained cohesion in summer (Salt (1988)) or by the development of excess pore water pressures (van Asch, 2005).



**Figure 3-29** - Cumulative rainfall, pore water pressure, displacement and groundwater levels of several locations from 1999 till 2001 (Malet, 2003).

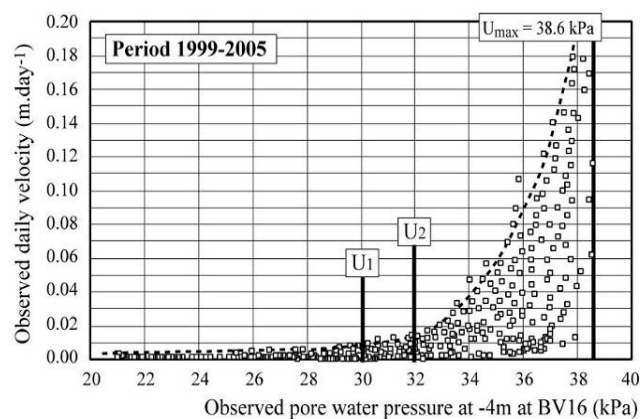


**Figure 3-30** – Super-Sauze landslide: Threshold in pore water pressures to trigger a surface velocity  $> 0.01 \text{ m.day}^{-1}$  for different observed rising and falling limbs at BV16 location.  $U_1$  is the ‘Spring’ threshold;  $U_2$  is the ‘Autumn’ threshold (Malet, 2003).

An increase of pore water pressure can be interpreted as the result of a rise in the groundwater table, or can occur due to wetting that starts at the slope surface. Berardi et al. (2005) argument that the evidence that shallow landslides developing in the subsurface strata of a slope occur during rainfall allows to consider as triggering mechanism the rapid variation and evolution of pore pressures (or the changes in soil matric suction) in the upper portion of the slope, not directly connected to the evolution and rise of groundwater surface (but due to wetting band movement). As a consequence, shear strength decreases in the unsaturated soil portion subjected to infiltration.

#### Damage mechanics

Petley (2005) has proposed a conceptual model for the development of progressive failure in cohesive landslides. It is assumed that the critical factor of safety at which the development of a shear surface is initiated by microcracking is reached through pore pressure fluctuations. Once microcrack formation has started the slope undergoes a small amount of creep-type displacement and the factor of safety drops slightly. In this stage the slope is still stable and a subsequent fall in pore pressure will lead to a rise in the factor of safety. After point interaction and coalescence of microcracks is achieved, further shear surface development leads to stress concentration and acceleration of sliding movements. Again the increase of pore water pressure results in a decrease of shear strength. But in this case the decrease is explained exclusively by damage mechanics. The concept is based on experiments on Gault clay that represents the Selbourne cutting slope experiment, in which an instrumented slope was led to failure as the result of pore-pressure elevation (Cooper et al. (1998)) and on samples from the Tessina landslide, located in northern Italy.

Taking into account the shear strength pore water pressure relation given above, this model might explain the phenomena of an apparent non-response of landslides to changes in pore pressure conditions. Most of the debris-flows occur during or after heavy and sustained rainfalls. In some cases snowmelt can be sufficient to form debris-flows, but for the remobilisation of overconsolidated landslide deposits a combination of thawing soils, rainfall and snowmelt is often invoked. This is particularly true for impermeable clayey material. An unclear point is that not all mudflow produce debris flow. In most cases, the mudflow experiences a significant creep behaviour (Picarelli (2001)), then decelerates and finally stop flowing after achieving a new hydro-mechanical equilibrium.

#### Seepage

Instability can also occur solely due to flow. As water flows through the soil there is a transfer of energy to the soil skeleton that causes a seepage force to act on the soil skeleton (Lee et al., 1983; Craig, 1987). In other words, the flow of groundwater through the pore space is accompanied by a friction force between the flowing fluid and the soil skeleton, named seepage force (Verruijt, 2001). Lambe and Whitman (1969) describe how seepage reduces the maximum slope angle compared to a slope without flow given the case of seepage parallel to the slope. Seepage can reduce effective stresses (provided upward flow) and can lead to erosion of the soil. In Ng (2009) reference is made to a test where failure (liquefaction) of a loose sand slope is believed to be initially triggered by seepage forces.

#### Confined groundwater flow

Instability can be caused by confined groundwater flow due to soil layering, or a localized buildup of pore water pressure as investigated in Lee et al. (2008). It is demonstrated that a

hydraulic heterogeneity affects the water flow pattern in the slope and may impede groundwater flow, causing the development of excess water pressure, finally leading to failure. But it is commented that, if the failure mechanism takes a few hours to develop, it may be possible that the excess pore pressures were dissipated in other preferential drainage paths. It is also mentioned that hydraulic conductivity, stratification, the existence of fissures and heterogeneities play an important role in the presented mechanisms. It determines for example the infiltration rate, the rate of groundwater rise or the magnitude of the seepage force. Due to the presence of small-scale anisotropy and large-scale heterogeneity in the permeability of intact and fissured material (Corominas et al., 1999; Malet et al., 2005b), large landslides have shown an erratic and complex response to rainfall (Noverraz et al., 1998, Corominas, 2000; Malet et al., 2005b).

### **3.5.3 Rainfall on complex large rockslides: Ruinon rockslide (Valfurva) (Crosta and Agliardi, 2002)**

The Ruinon rock slide is located on the right-hand side (NE) of the Valfurva, a NW–SE trending glacial valley deeply cut by the Frodolfo River, left-hand tributary of the Adda River in the Upper Valtellina, Central Italian Alps (Figure 3-31). The Ruinon rock slide occurs in phyllites, which are the dominant lithotype. The bedrock is cut by four main sets of alpine and recent fractures strongly controlling the geometry of slope instabilities in rock (Crosta and Agliardi, 2002). The whole slope has been affected by a large deep-seated slope deformation, recognized and analysed by Agliardi et al. (2001). The phenomenon is controlled by pre-existing structural features and is believed to have been triggered by postglacial debuttrressing. The Ruinon rock slide consists of a compound movement (combined translational and rotational sliding) of 13 Mm<sup>3</sup> of phyllite along a sliding surface up to 70 m deep. The rock slide extends between 1700 and 2120 m a.s.l., but the distribution of scarps and trenches suggests a possible upslope expansion up to 2200 m a.s.l. (Figure 3-32) involving more than 20 Mm<sup>3</sup> of rock.

Nowadays, the slope toe as the most active and hazardous sector within the deep-seated gravitational slope deformation, as demonstrated by measurements performed through side-aperture radar (SAR) interferometry, adopting the Permanent Scatterers techniques.

From the monitoring data, the authors recognize three main evolutionary patterns of displacements, namely: brittle, chaotic, and seasonal.

Brittle and chaotic patterns (Figure 3-33 a and b) were attributed to small-scale movements of single blocks or clusters of blocks showing spatially and temporally complex movements. It is possible that monitored fractures are alternatively subjected to opening or closure because of differential movements of adjoining blocks.

The third pattern of displacements could be defined as a seasonal slope creep (Figure 3-33 c). This consists of acceleration phases, according to a power law, during the rainy season (summer and late autumn), and of a decelerating phase or lack of movement during winter and early spring. This trend can be adopted to describe the evolution towards failure of large sectors of the landslide or, at least, the surficial response to the bulk rock slide evolution. The displacements due to seasonal creep are strongly related to the trend of cumulative rainfall, suggesting a primary role of rainfall and snow melting as triggering or activating factors of the rock slide. A further contribution to the seasonal activation of the slide is probably due to the snowmelt during late spring and summer. It can be noted that movements follow a power law trend, with increased cumulative displacement and displacement rate, both on a yearly

and a multi-yearly scale. The authors (CNRS) applied the “accelerating creep” theory by Fukuzono (1985) and Voight (1988, 1989) to the series of seasonal displacement data. The method based on Voight’s semi-empirical time-dependent failure criterion has been developed that is able to provide an efficient tool to forecast the failure of large deep-seated, creeping- type rock slides using surface-based monitoring data. The method consists of an application of Voight’s model to find “velocity curves” characterizing the nonlinear time-dependent behaviour of the rock mass towards failure. This is done by means of time series of displacement data, chosen on the basis of the landslide kinematics and morphoclimatic settings.

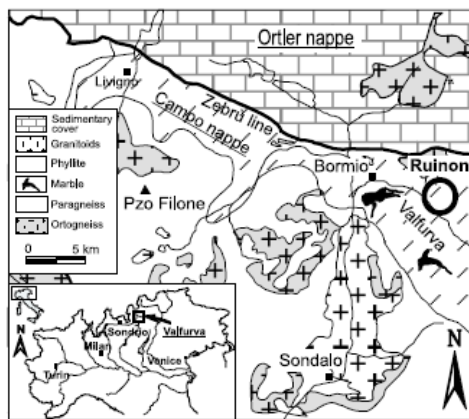


**Figure 3-31** – Geological sketch of the Upper Valtellina valley, location of the Ruinon rock slide is circled (Crosta and Agliardi, 2002).

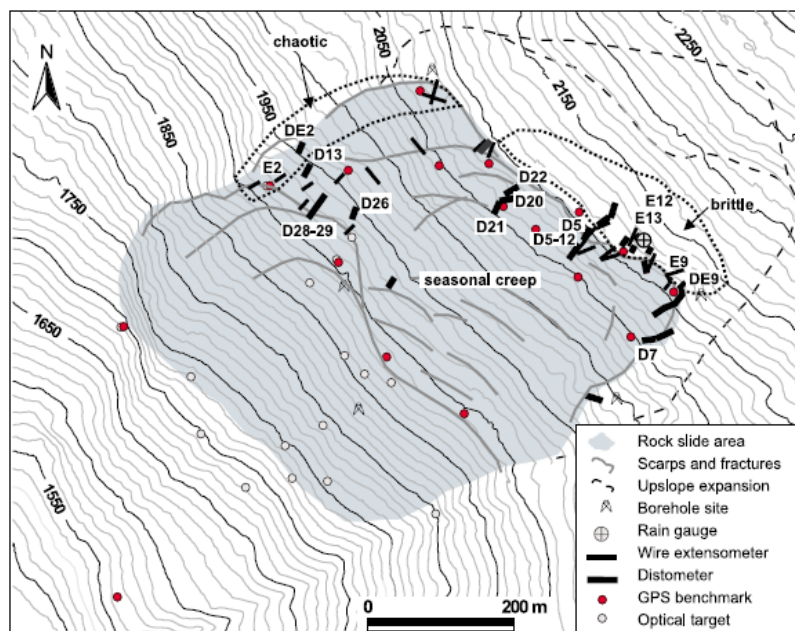


**Figure 3-32** – Map of the monitoring network. Dashed lines roughly limit landslide sectors with different displacement behaviors. Instruments showing a seasonal pattern of displacements are located within the grey area.

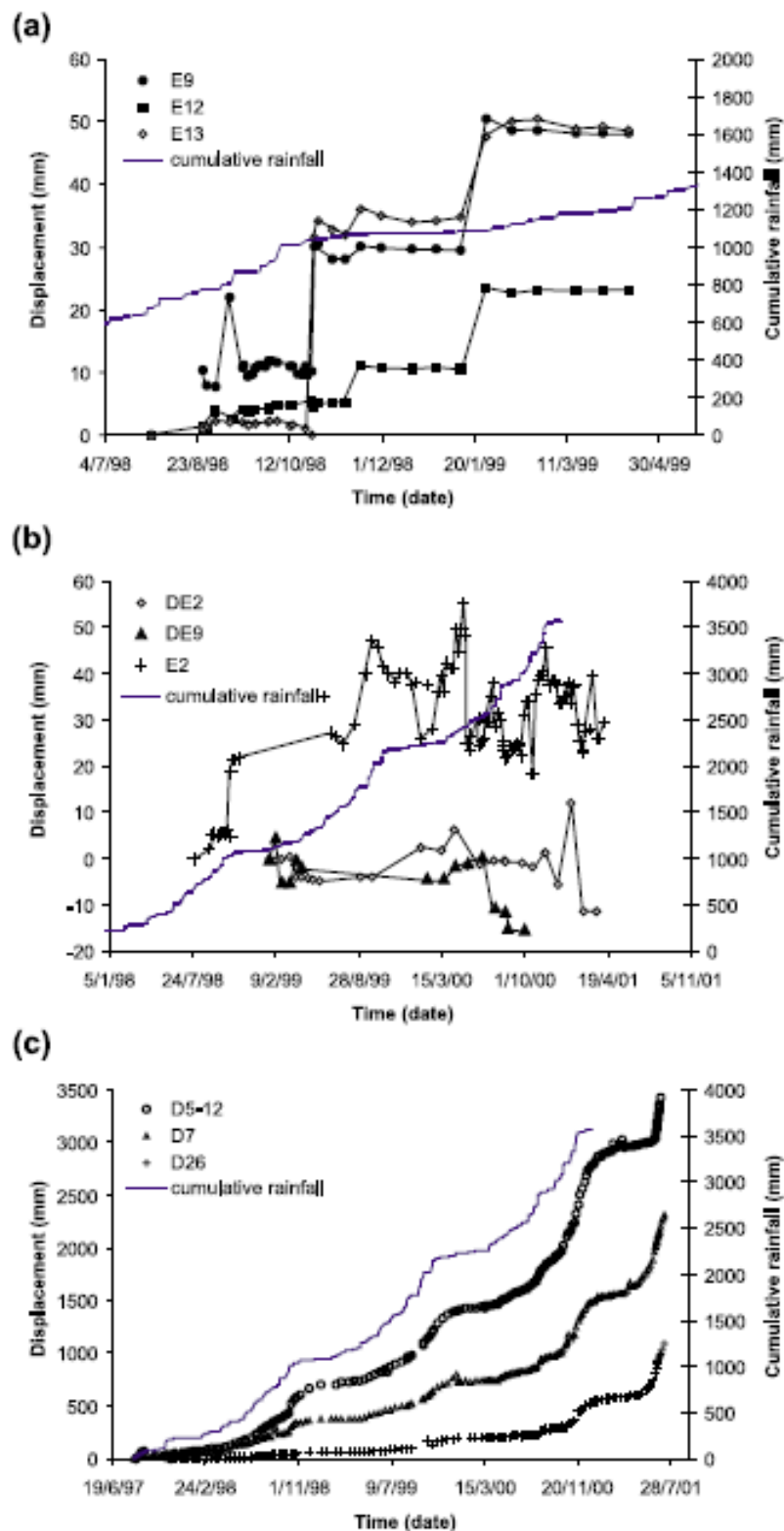


*Figure 3-33 – Different displacement patterns, obtained from the analysis of monitoring data. Time scales are different depending on the available set of measurements.*

### 3.5.4 Campo Vallemaggia landslide (Bonzanigo et al., 2007)

The Campo Vallemaggia landslide is a large deep seated, creeping landslide located in Canton Ticino (Swiss Alps), near the Italian border (Bonzanigo et al., 2007). The landslide involves about 800 M m<sup>3</sup> of crystalline rock up to 300 m deep. Surface displacements have been geodetically measured for over 100 years recording a cumulate displacement of approximately 30 m.

The displacement records show alternate periods characterised by acceleration and deceleration of movement, attesting the slide's characteristic pulsing nature. Accelerated movements are usually associated with periods of intense precipitations (Mondada, 1977; Bonzanigo et al., 2007).

Bonzanigo et al (2007) analysed the monitoring data. The movement trend is difficult to predict because of the complexity of the slide mass, which is divided into several blocks by sub vertical fault zones varying in thickness from several metres to tens of metres, with sub horizontal shear-slip surfaces developed along lithological boundaries or zones of varying alteration. Displacement records indicate differential movement between the different sectors of the landslide (i.e. Cimalmotto and Campo blocks, see Figure 3-34) and along the profile where they concentrate along internal shear zones of several m of thickness.

The movement was associated to different causes:

- accelerated erosion at the toe of the slide body induced by the floodwater of the Rovana river resulting in a exposed toe with a vertical height of 150 m. Historically, the erosion at the slope's toe has been primarily considered to explain the slope movement at Campo Vallemaggia. Bonzanigo et al (2007) estimated the eroded volume in the Campo block. By comparison of topographic maps from 1888 to 1994 the erosion rate varies from 56000 to 100000 m<sup>3</sup> per year.
- particular hydrogeological conditions (i.e. the presence of artesian overpressures which induced through saturation of the slide mass resulting in slide movements; Heim, 1897). Downward infiltration is favoured by subvertical open tension fractures, which are present in the undisturbed crystalline rock acting as pathways for precipitation to infiltrate into the substrate. Internally in the slide body, multiple subhorizontal zone of large shear deformation and mineralogical degradation results in a strong hydraulic anisotropy and the observed artesian conditions (Bonzanigo, 1999). The pore pressure response at depth (i.e. 200-300 m) to precipitations is observed with a time lag of approximately 1 to 3 months. The lagging effect can be only partly attributed to snow melt. Intense precipitation can provoke an almost immediate reaction, but the magnitude of the response depends more on the duration of the precipitation event than on its intensity (Bonzanigo et al., 2007). The authors recognized a threshold in hydraulic head that coincide with sudden accelerations of the slide mass. Velocities then return to background levels as pore pressures dissipate and drop below the threshold. Figure 3-35 show the landslide behaviour in response to intense and prolonged precipitation.
- Rock mass creep deformation. Elements of viscous creep deformation are evident in the inclinometer records, especially in the Cimalmotto block. Bonzanigo et al (2007) suggest a brittle elastic behaviour in the upper part of the landslide, which is mostly composed by unweathered gneiss. A transition to ductile strength can be observed as confinement and stress increase with depth, and it occur together with the lithology change to deeper schists. Here localized shear deformation is concentrated, thus posing the basal yield zone separating the moving landslide from the stable, undisturbed bedrock (Figure 3-36).

The heterogeneity and complexity of the landslide mass introduces different form of reaction delay between surface precipitation and its influence at depth along internal sliding surface. Furthermore, different patterns in the landslide reaction can be recognized based on intensity and duration of the precipitation events.

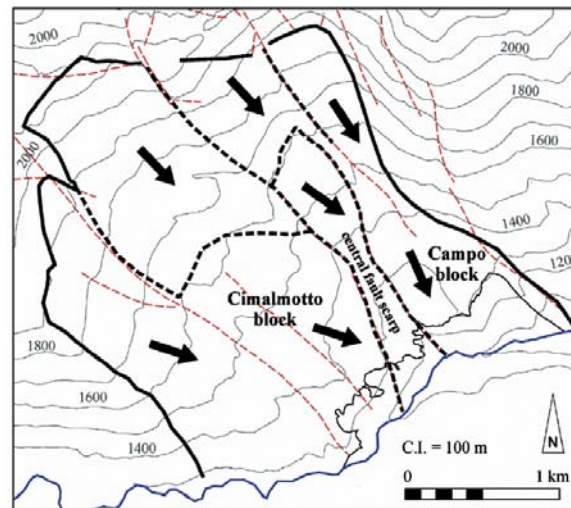


**Figure 3-34** - Schematic subdivision of the Campo Vallemaggia slide mass into distinct blocks (i.e. Cimalmotto and Campo blocks), based on their kinematic state and mechanical behaviour (from Bonzanigo et al., 2007).

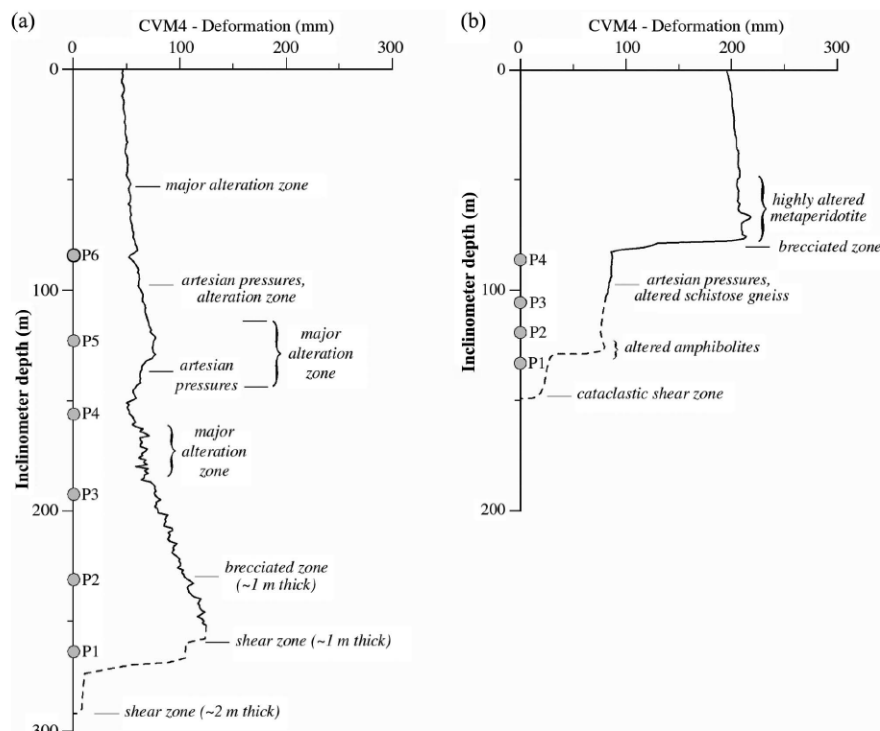


**Figure 3-35** - Cumulative deformation plots for inclinometers located in the Cimalmotto (a) and Campo (b) blocks. The shaded circles indicate piezometer locations (from Bonzanigo et al., 2007).

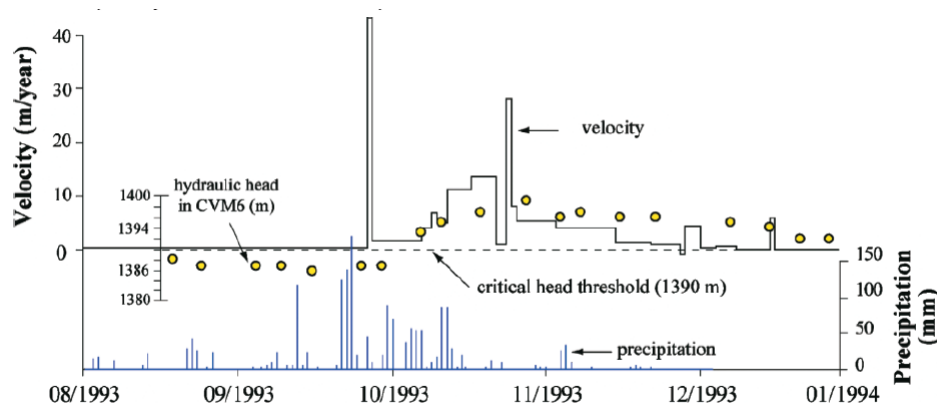


**Figure 3-36** - Relationship between precipitations, pore pressure response at depth and slide block velocity (measured at the geodetic station). 3 days period of intense precipitation, averaging 150 mm/day, was followed, 4 days later, by the largest slope movement (43 mm in one day) observed in the previous 5 years. The rainfall then subsides and the movement abruptly stopped. A moderate (<50 mm/day) 2 week period of precipitation started several days later: the pore pressure response and the slope movement was recorded two weeks after and continued for the next 3 months (from Bonzanigo et al., 2007).

### 3.5.5 Spriana landslide (Agliardi et al., in press; Belloni and Gandolfo, 1997)

The Spriana rockslide (Figure 3-37) affects a steep rock slope on the left-hand flank of the Val Malenco (Valtellina, Italian Central Alps), few kilometres north of Sondrio (Agliardi et al., in press).

The slope was carved by glacial activity in strongly deformed gneisses and schists.

The Spriana rockslide is a compound slide (i.e. mixed translational-rotational) involving up to 50 Mm<sup>3</sup> of slope debris and fractured rock with a basal failure zone 60 to 90 m deep, potentially daylighting at about 700 m a.s.l. (i.e. 150 m above the valley floor). The landslide is characterized by two main scarps, at 1150 and 1400 m a.s.l. (Belloni and Gandolfo, 1997, Agliardi et al., in press).

Although slope instability of the lower slope sector had already been mentioned in 1878, the landslide was firstly documented in 1912, when a shallow hydroelectric derivation tunnel came into operation. Evidences of landslide activity were the opening of several fractures, the appearing of springs, and the occurrence of shallow landslides in concomitance of large rainfall events (1927, 1960, 1961, 1963, 1966, with a major acceleration phase in 1977). The development of scarps in upper sectors of the slope (1150 m and at 1400 m) following subsequent stages of movement (during 1960-1961 and 1977), suggest a progressive failure of the involved rock slope.

Multiple factors could have triggered the landslide, including post-glacial debuttrressing and associated rock mass strength degradation, toe erosion, rainfall or snowmelt and related groundwater changes, reservoir level fluctuation, and the onset of progressive failure processes. Geotechnical site investigation and slope monitoring were carried out in 1978 (Cancelli, 1980, 1986) and 1989 (Belloni and Gandolfo, 1997). These consisted of 20 boreholes with complete core logging, a 150 m long horizontal exploration near Case Piazzo

(Figure 3-38), and 5 refraction seismic lines. A monitoring network was also progressively installed and automated, including piezometers (both standpipe and multipoint cells), borehole inclinometers, surface wire extensometers, a topographic network made of optical reflectors, and hydro-meteorological stations. Displacement measurements carried out since 1978 (topographic surveys only) and since 1990 (geotechnical monitoring network) revealed a seasonal pattern with the reactivation at the end of the snow season and a correlation with snowmelt occurrence (Belloni and Gandolfo, 1997). The above mentioned monitoring data, together with PS-InSAR satellite interferometry surveys (TeleRilevamentoEuropa s.r.l.-Regione Lombardia) were reviewed by Agliardi et al. (in press). The authors revealed that rockslide activity is characterised by slow movements (the velocity ranges between 0.3 – 4 cm/ys) with sudden acceleration phases (i.e. 1977, up to 300 cm/ys in; 1993, 9.7 cm/ys; 1996, 20 cm/yr; 2000, 7.6 cm/yr; 2002, 25 cm/yr, see Figure 3-39). Acceleration events generally show weak or no correlation with short intense rainfall, but seem related to prolonged rainfall causing the water table to rise up to 2.5-4 m. The analysis of rainfall time series since 1987, not accounting for snowmelt, suggests that sharp, impulsive acceleration events (e.g. 1996) occur when 7-day cumulative rainfall exceeds 150 mm, whereas major, long lasting acceleration phases (e.g. 2000, 2020) take place when 30-day cumulative rainfall exceeds 300 mm, leading to significant recharge of the perched water table cited above.

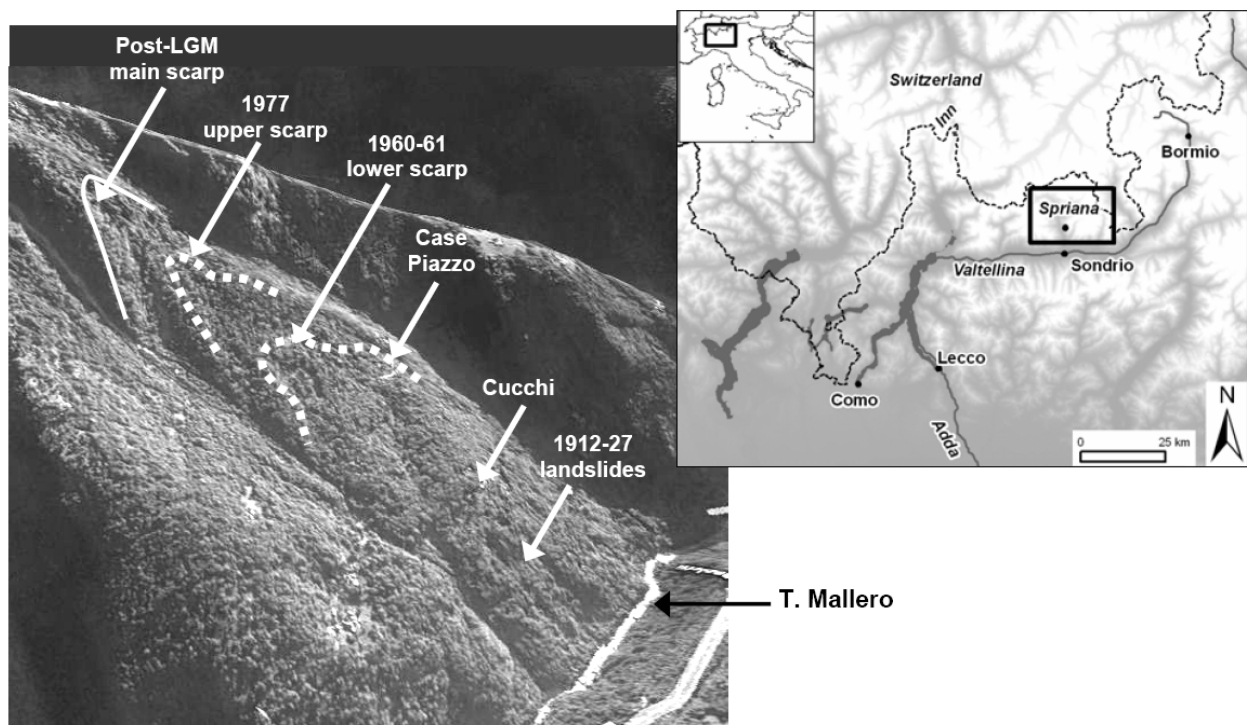


**Figure 3-37** -. Location map and NW view of the slope affected by the Spriana rockslide, showing the main features of the rockslide and related time of activation (from Agliardi et al., in press).

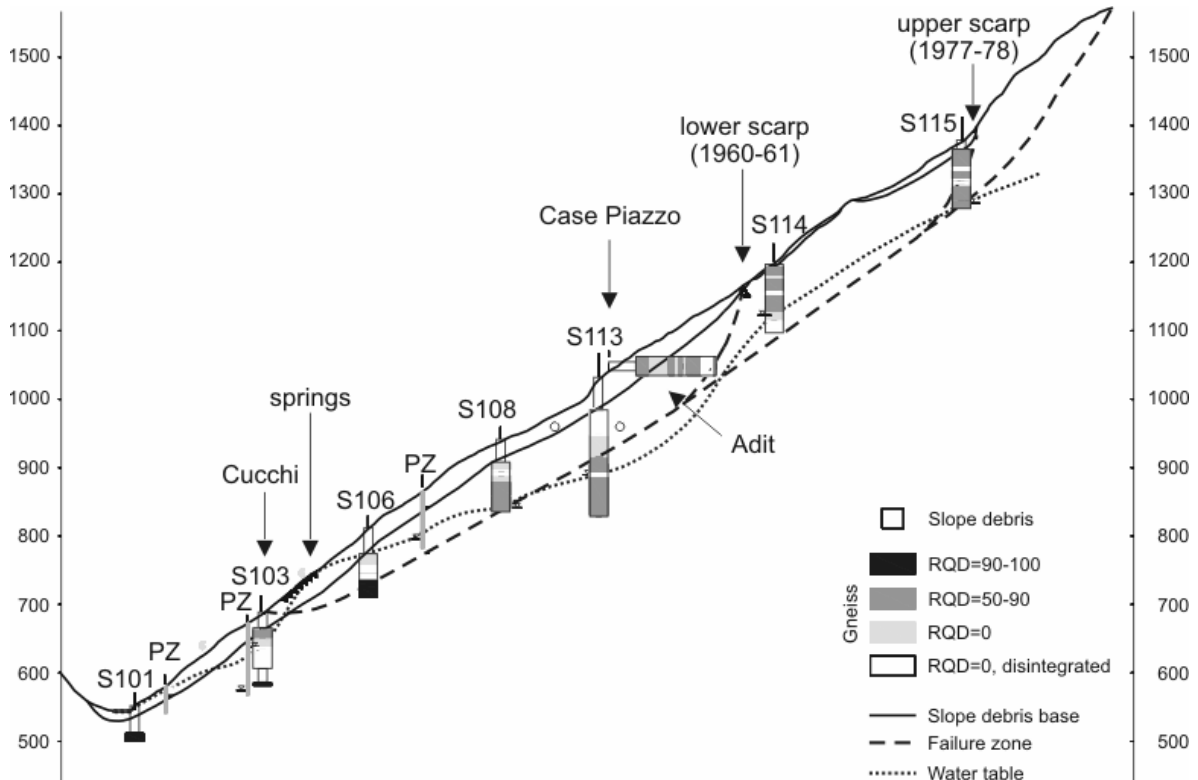


**Figure 3-38** - Geological model of the Spriana rock slide reconstructed according to borehole records (from Agliardi et al. in press). Below the lower scarp, slope instability involves both surface deposits up to 30-40 m thick and rock, whereas in the upper part, disintegrated rock is mainly affected. Heavily fractured gneissic rock masses were found well below the inferred rockslide up to depths exceeding 120 m, suggesting that weak/disturbed rock masses have existed before rockslide onset. Groundwater data derived from bore-hole records and piezometers suggest that a perched water table, characterised by average annual fluctuations in the range 1-1.5 m, is hosted by this near-surface fractured zone.

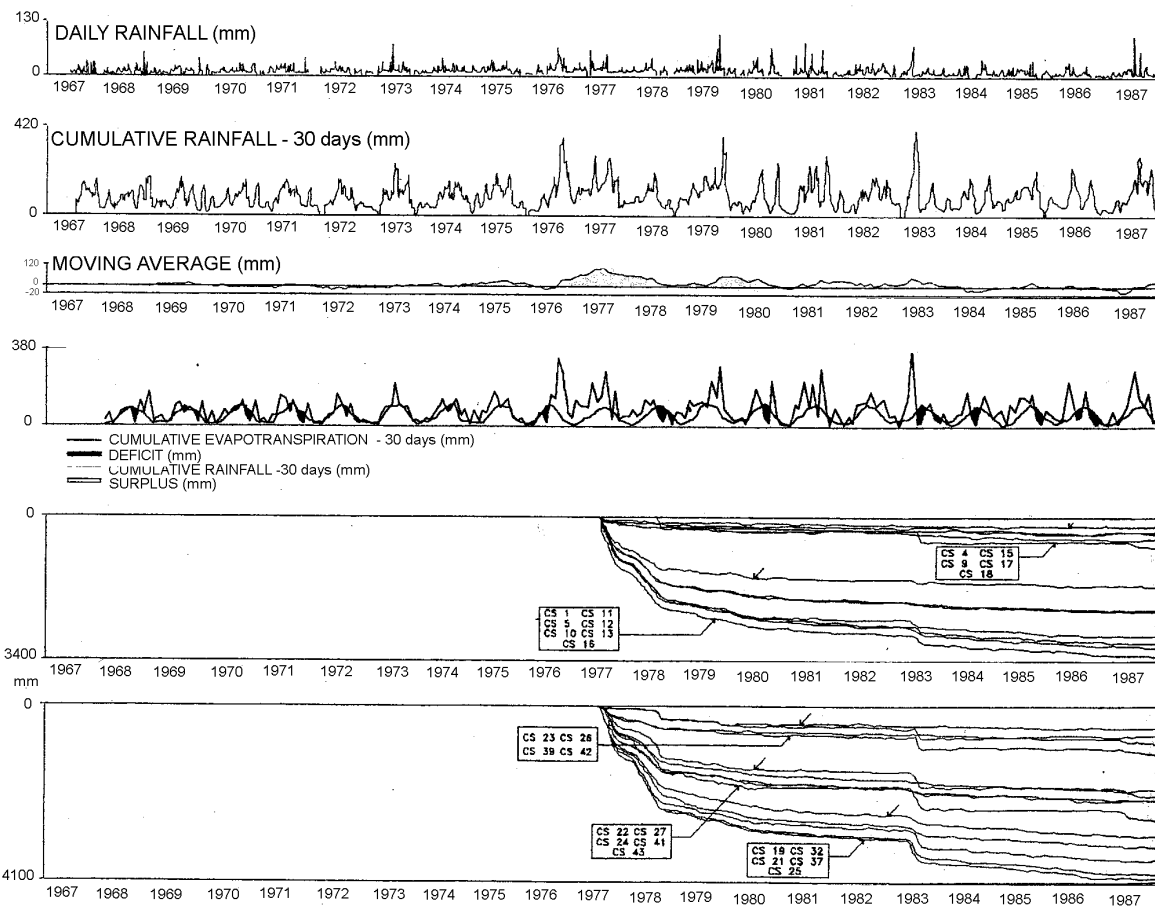


**Figure 3-39** - Rainfall and displacement monitoring data. The precipitations of long duration are the most critical for the landslide. Long precipitations allow the groundwater to recharge. Following rainfall periods movement can occur in restricted areas of the whole slide body, where they are not contemporaneous. The inclinometers indicate that the movement occurs primarily at 40-100 m of depth, whereas the surficial body is only translated (FROM Belloni and Gandolfo, 1997).

### 3.5.6 Ca' Lita landslide (Ronchetti et al., 2010)

The Ca' Lita landslide is a large and deep-seated mass movement located in the Secchia River Valley, in the sector of the Northern Apennines, about 70 km west of Bologna, Northern Italy (Figure 3-40). The Ca' Lita landslide is a complex and composite rototranslational rock slide - earth slide/flow that affects Cretaceous to Eocene flysch rock masses and clayey complexes, that can be classified as overconsolidated weak rocks.

The landslide extends from an elevation of 650m at the crown to 230m at the tip. Its total track length is approximately 3 km and its maximum width is about 1.4 km in the rear scarp area, with a maximum depth of about 50m in the upper part (Figure 3-41). The area displays numerous small springs lying in correspondence with permeability boundaries between the flysch slab and the clayey substratum, which by now is covered by thick debris deposits. The

depletion zone of the landslide unit acts as a basin that keeps the debris in a saturated state, promoting significant movements directly connected with severe meteo-climatic events.

The Ca' Lita landslide underwent several reactivations between 2002 and 2006 (Borgatti et al. 2006, 2008; Corsini et al. 2006). Corsini et al. (2006) analysed the style of movement in the period 2002–2004. Although, movements were prevalently taking place at rates of centimetres to metres per day, the authors describe peak velocities of about 10 m per day at the toe, while in the source area, rotational rock slides and traslational earth slides evolved at velocities of cm-dm per day. Locally, quite superficial mudflows, or collapses of the rockslide front, moved as fast as metres per hour. During 2002–2004 period the toe of the landslide has advanced for more than 400 m over a slope angle of about 10°, causing the filling of the local valley with a 30m thick deposit (Corsini et al., 2006).

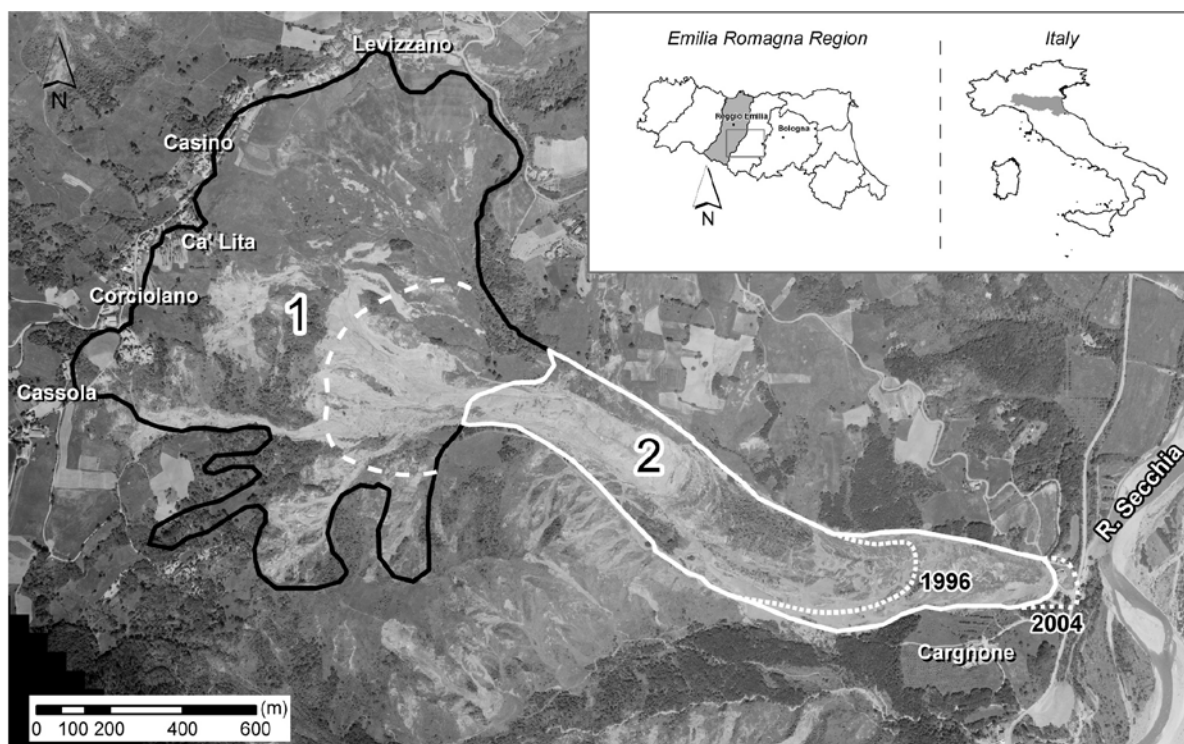


**Figure 3-40** - Location map the slope affected by the Ca' Lita landslide. In the sketch the two distinct phenomena that make up the Ca' Lita landslide are evidenced. 1: Rotational and – translational rock slides – earth slides. 2: Earth slides-earth flows. Broken white line: main scarp of the earth slide-earth flow. Dotted white lines: tip of the landslide deposits in 1996 and during the emergency phase of 2004.

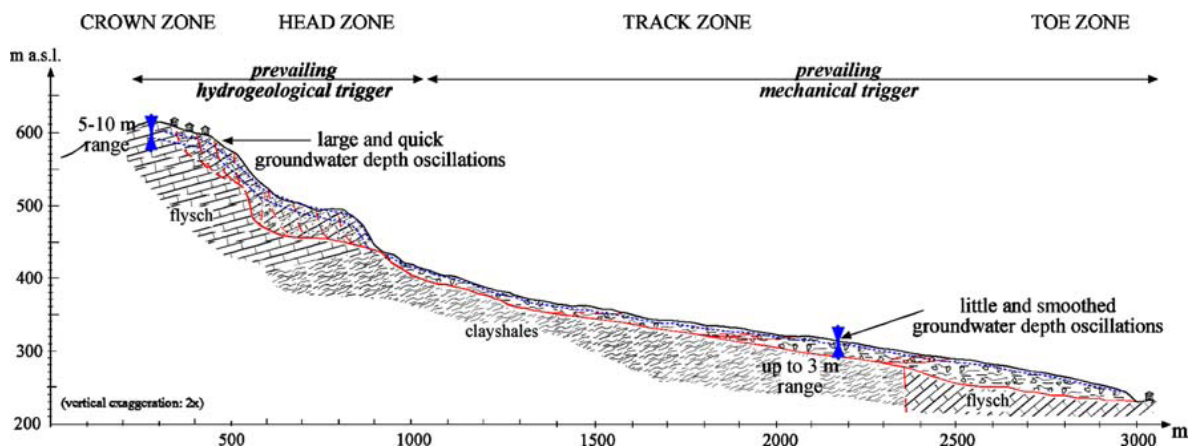


**Figure 3-41** - General cross section of Ca' Lita landslide with hydrological features and triggering mechanism of the different sectors (from Ronchetti et al., 2010).

Groundwater depth (GWD) was monitored in the four landslides for a period of about 2 years with piezometers equipped with electric transducers (Figure 3-42). Variable trends of GWD were observed in different sectors of the landslides. Wire extensometers recorded the landslide movement. Ronchetti et al. (2010), describe an approximately 2–3 months delay in the movement rate response to a prolonged period of rainfall (and of groundwater recharge). The delay period is characterized by trench widening with a slowly rising rate (up to 2 mm/day). This period is followed by an acceleration phase of 1 month that took the velocity to about 7 mm/day. The authors relate the acceleration phase to the prolonged high standing groundwater in the slope. As GWD increased, the velocity rapidly decreased to about 1 mm/day.

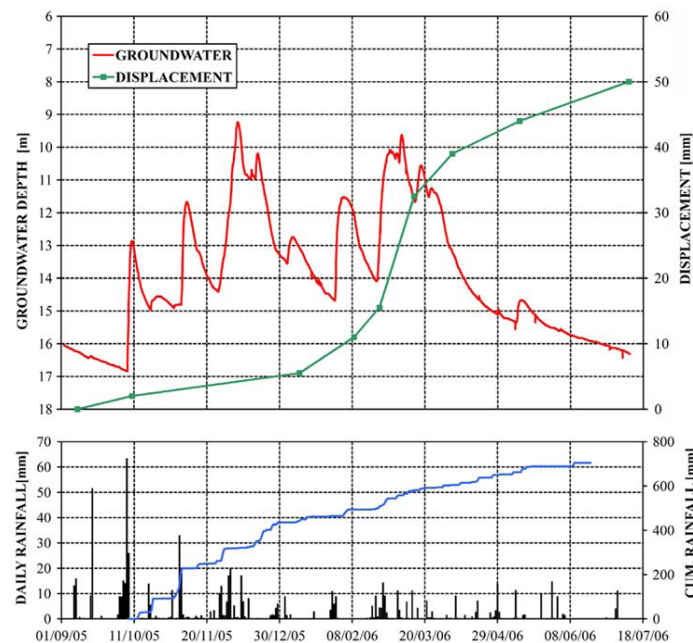


**Figure 3-42** - Piezometric data and displacement rate recorded in the crown zone. At the bottom, daily and cumulated rainfall.

### 3.5.7 Vallcebre landslide (Corominas et al., 2005)

The Vallcebre landslide is a large, active slope failure located in the upper Llobregat river basin, in the Eastern Pyrenees, 140 km north of Barcelona, Spain (Figure 3-43). The mobilised material consists of a set of shale, gypsum and claystone layers of continental origin gliding over a thick limestone bed, all of which are of Upper Cretaceous – Lower Palaeocene age. The dimensions of the slide mass are 1200 m long and 600m wide. The entire landslide involves an area of 0.8 km<sup>2</sup> that shows superficial cracking and distinct ground displacements. The age of the landslide is not known but it is known to have been active for several centuries at least.

Most of the evidence of surface deformation is situated at the boundaries of the slide units in the form of distinct shear surfaces and tension cracks. The lower unit of the Vallcebre landslide has been monitored since 1996 using conventional surveying and photogrammetry (Gili and Corominas 1992), differentialGPS (Corominas et al., 2005), boreholes equipped with inclinometers, wire extensometers and piezometers (Corominas et al., 1999, 2000).

The wire extensometer measure continuous displacements, with velocities reducing near to zero only during dry periods (Figure 3-44 a). The landslide mass move synchronically but with a different rate of displacement. Infiltration takes place along fissures, which are present in the gypsum lenses at shallow depth (up to 3 m) and by soil porosity. Changes in groundwater levels due to rainfall inputs are almost immediate at shallow depth. In this case, two basic types of responses have been observed, depending on the location of the piezometers. These located in tension zones, such as S5, show a smaller variation in groundwater level (ranging between 0.5 and 2 m) and a faster drainage compared to the piezometers located elsewhere (for example S2, S4 and S11). The latter piezometers experience changes of 2 to 5 m and a slower rate of groundwater level decrease. A close relationship between the groundwater level changes and landslide activity was measured using a wire displacement meter (Figure 3-44 b).

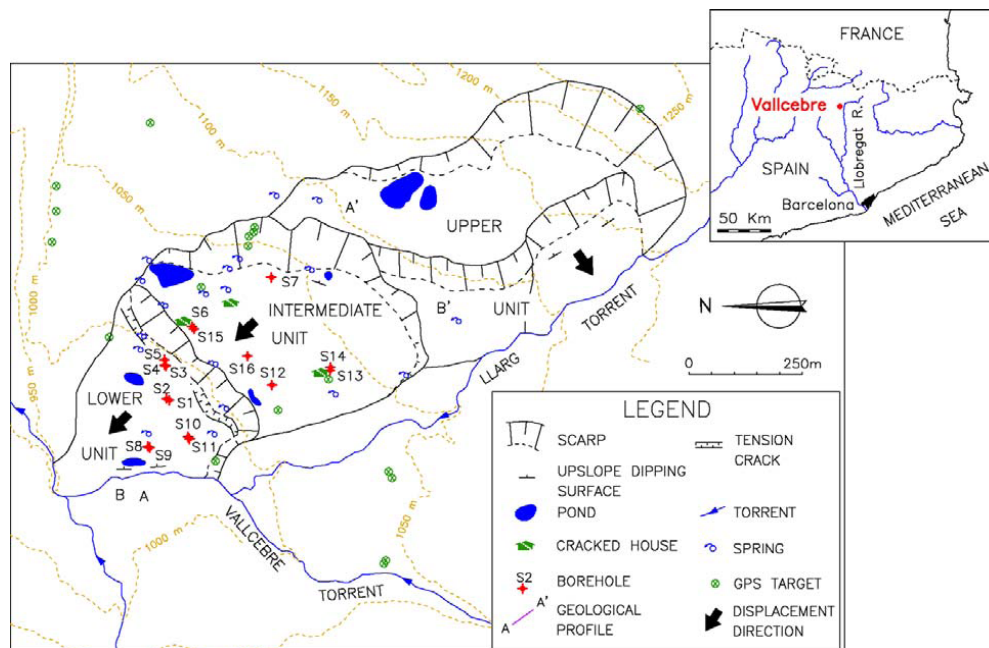


**Figure 3-43** - A longitudinal profile shows a stairshape with three main slide units of decreasing thickness towards the landslide toe.

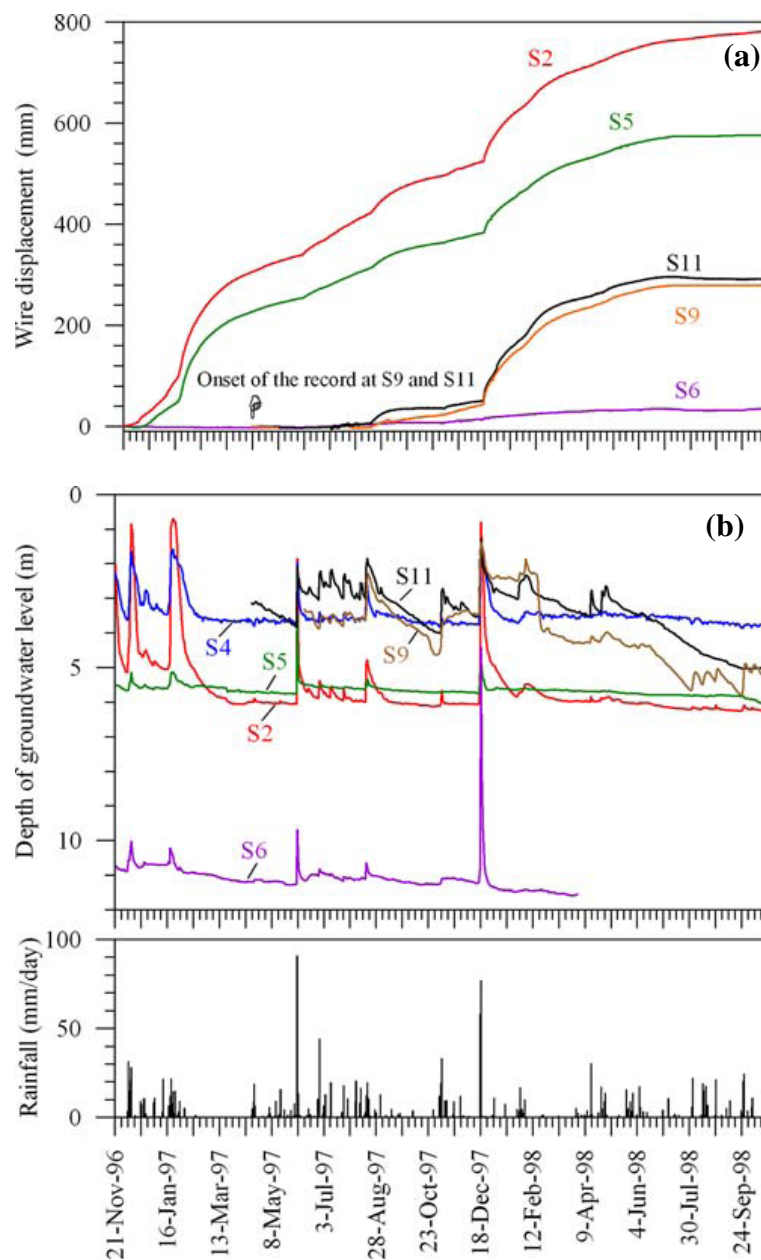


**Figure 3-44** – (a) Wire displacements at boreholes S-2, S-5, S6, S9 and S-11. (b) Piezometric records of boreholes S2, S4, S5, S6, S9 and S11 (Corominas et al., 2005).

### 3.5.8 Vajont landslide (SGI-MI)

Since October 9, 1963, the large volume and high velocity of the Vajont slide in Northern Italy, combined with the great destruction and loss of life that occurred, make it a key precedent landslide, particularly for slides caused, wholly or in part, by reservoirs filling (Hendron Jr. & Patton, 1985).

The Vajont disaster marked a turning point in the relative emphasis given in hydro projects to the reservoir slopes as compared to the dam site itself. Gruner (1969) noted that between 1964 and 1967 new regulations concerning reservoirs were introduced in France, Germany, Italy, Japan and the United States and new regulations were published by UNESCO.

The technical literature on Vajont slide is abundant, with an uninterrupted stream of studies and publications on the disaster as a whole or specific aspects continuing today, over 50 years after the event. It is likely that more information has been published and more analyses have been made of the Vajont slide than for any other slide in the world.

As noted by Hendron Jr. & Patton (1985), whose report provides one of the most detailed and extensive geotechnical review of the slide published in English and which is the basis for the considerations presented below, there are many contradictory statements and conclusions in the literature concerning the Vajont slide, especially those published in the immediate aftermath of the disaster (when criminal proceedings were still pending).

On October 9, 1963 approximately 270 million m<sup>3</sup> of rock slid from the side of Mt. Toc into the Vajont reservoir. The Vajont slide is located east of Longarone town, which is situated on the Piave river some 100 Km north of Venice, Italy (see Figure 3-45). The slide developed along the north slopes of Mt. Toc where the Vajont river had cut a canyon more than 300 m deep just above its junction with the Piave river. As a result of the slide, the topography underwent enormous changes along the foot of Mt. Toc as shown in Figures 3-46 and 3-47.

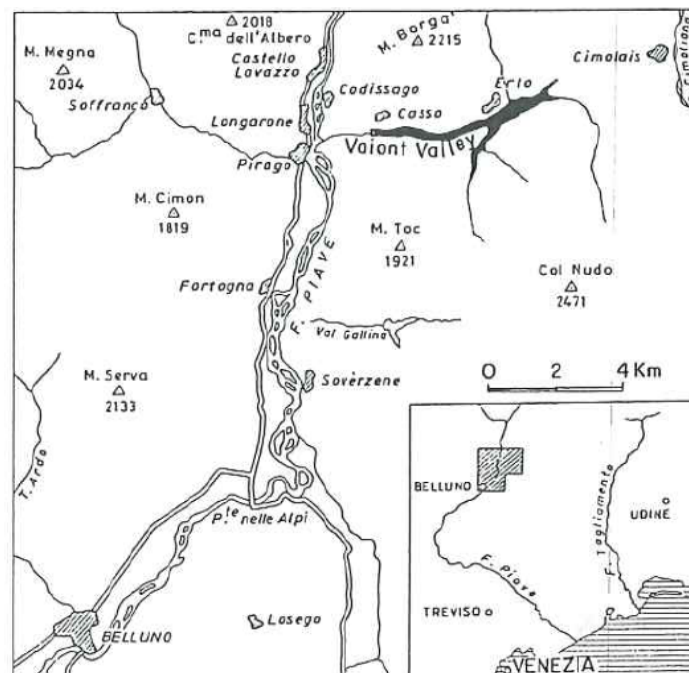


*Figure 3-45 - Location maps of the Vajont region, Italy (after Selli and Trevisan, 1964 as reported by Hendron and Patton, 1985)*

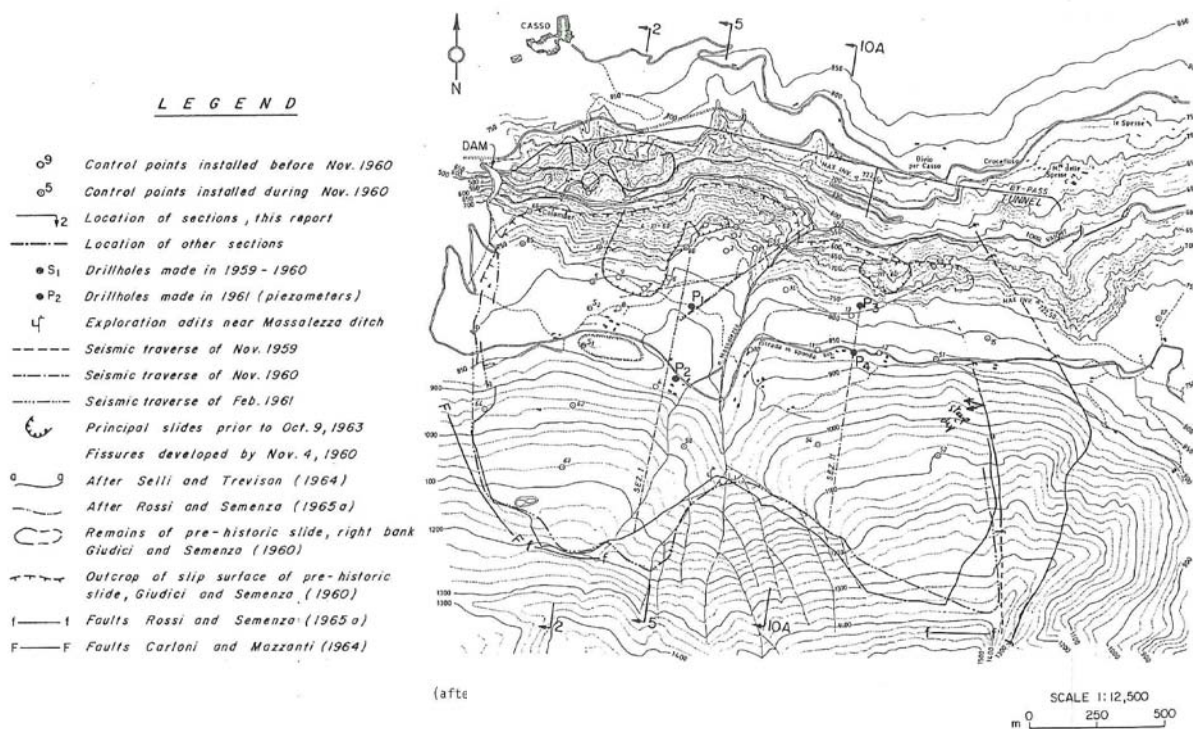


**Figure 3-46** - Plan view prior to the slide of 9 October 1963 (after Selli and Trevisan, 1964 as reported by Hendron and Patton, 1985)

The slide moved a 250 m thick mass of rock some 300 to 400 m horizontally and is estimated to have reached a velocity of 20 to 30 m/s before running up and stopping against the opposite side of the Vajont valley wall (Semenza, 1965). The slide filled the lower half of the Vajont reservoir (which had been drawn down to elevation 700 m from a level of 710 m just prior to the slide) in a matter of few tens of seconds.

The wave resulting from the displaced water propagated both upstream and downstream. The wave eroded trees and soil on the north side of the Vajont valley up to a maximum elevation of 935 m or 235 m above the reservoir level. The wave swept across the dam reaching over 100 m above its crest (435 m above the downstream base of the dam) and down to the Vajont gorge to the Piave river, where it had a height of some 70 m at the confluence with the Piave valley, destroying most of the town of Longarone and parts of other towns in the Piave valley (see Figure 3-48). Some 2043 persons died and many others were injured, almost all from the effects of the wave.

Hendron Jr. & Patton (1985) examined in detail the correlations between reservoir level, precipitation and rate of movement, pointing out also the erroneous opinion predominant before the October 1963 disaster that “a gradual stabilization of the moving mass would be brought about by raising the water level in individual steps”. Misinterpretation of previous empirical observations of the rate of movement of the slide depended on the assumption that all other factors were remaining constant and the reservoir level was the main variable controlling the stability of the slide. While the analysis by Hendron Jr. & Patton (1985) clearly indicated that preceding precipitation had a significant effect on the stability of the slide, their analysis confirmed the role of the reservoir level as a main variable affecting the

stability of the slide and that the slide would have failed even with no rainfall or snowmelt when the reservoir level approached the design level of 722.5 m. clearly indicated that preceding precipitation had a significant effect on the stability of the slide, their analysis confirmed the role of the reservoir level as a main variable affecting the stability of the slide and that the slide would have failed even with no rainfall or snowmelt when the reservoir level approached the design level of 722.5 m.



**Figure 3-47** - View of the slide of October, 9 1963 from the NE (Photograph by Prof. E. Bromhead, University of Kingston, UK).

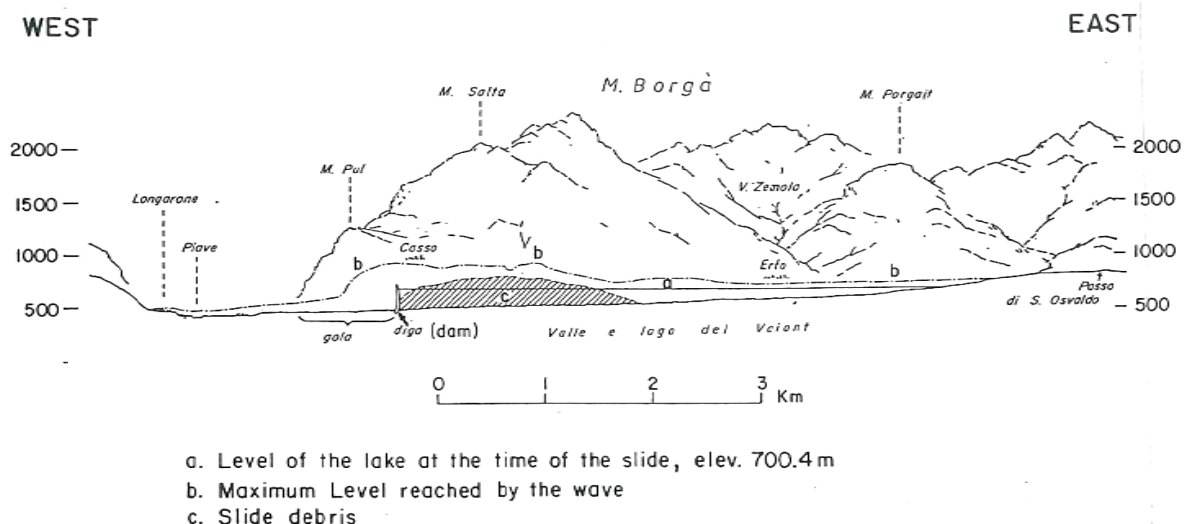


**Figure 3-48** - Longitudinal profile along the Vaiont Valley, looking North (after Selli and Trevisan, 1964 as reported by Hendron and Patton, 1985).

## **4 LANDSLIDE TRIGGERING BY CHANGES IN SLOPE GEOMETRY (UNIMIB, SGI-MI)**

The wide variety of geosystems and geomaterials and their spatial variability, geostatic stresses, hydraulic, hydrogeological and climatic conditions encountered in nature result in a wide variety of the type, magnitude and rate of slope movements observed in practice.

The wide range of possible triggering mechanisms and their relevance to different types of slope movement are amply discussed in Section 2, both from a phenomenological and a geotechnical perspective.

It is self evident that triggering of landslides by changes of slope geometry is associated with the resulting changes in driving stresses and resistances beyond a critical threshold.

In many instances, this is immediately apparent. However, in certain conditions there can be a significant delay between the causative change in slope geometry and the resulting landsliding, due to the mechanical and hydraulic behaviour of the materials involved, to the extent that the role of the changes in slope geometry are not recognized as a contributory process.

Attention is here focused on slope movements in mechanically overconsolidated, saturated clays, such as are encountered extensively in Italy and in many other areas in Europe.

In particular, attention is focussed here on triggering due to long term processes, such as swelling and mechanical weathering induced by dissipation of the negative excess pore pressures induced by erosion or excavation, while the processes and effects caused by relatively short term processes such as meteo-climatic conditions are dealt with in other Project deliverables.

Landslide activity in these formations occurs both as relatively shallow and as relatively deep seated phenomena, depending on a wide variety of factors such as, for example, pre-failure geometry and stress history, the characteristics (plasticity, bonding, fissuring) of the clay, macrostructural features of the deposit, the rate of previous and current erosion. While slope movements in these types of soils are typically relatively slow and seldom pose a direct threat to life (except as consequential damage where they impinge on sensitive infrastructures), they can have significant economic consequences as they may blight broad areas.

The root cause of these slope movements is invariably a change in slope geometry, either as a result of natural processes (erosion, deglaciation) which can vary in speed from very slow to relatively fast, and/or by anthropogenic processes.

Whatever the cause, changes in slope geometry due to erosion or excavation always involve the following effects, which are intrinsically interdependent:

- stress relief;
- changes of physical and mechanical characteristics, including degradation of stiffness and strength (mechanical weathering).

Chemical weathering may also occur in the material, but its occurrence is not strictly necessary to determine the conditions leading to triggering of slope movements, as will be shown later, and will not be dealt with here.

In saturated materials of low permeability, such as are considered here, the dissipation of the (negative) excess pore pressures induced by erosion or excavation can be significantly delayed before pore pressures come into equilibrium with the new hydraulic boundary conditions.

## 4.1 CHANGE INDUCED BY EROSION (UNIMIB)

Among the causes of possible changes of slope geometry, erosion is a major landslide triggering process, occurring as two primary agents, stream and coastal erosion. In both cases, erosion reduces slope stability by oversteepening. Bank and lateral erosion is a primary cause of landsliding in coastal settings, especially within clay slopes and fissured material.

### 4.1.1 Physical process

Stream erosion triggers landslides by different ways:

(1) **Streambanks erosion** as a combination of: (1) lateral erosion of the bank toe by fluvial entrainment of in situ bank materials, often termed hydraulic erosion; and (2) mass failure of the upper part of the bank due to gravity (figure 4-1). Non-cohesive sediment is eroded through discrete particle entrainment that can be quantified by using the magnitude of shear stress and particle size (Shields, 1936; Buffington and Montgomery, 1997). Cohesive sediment is eroded through entrainment of aggregates (ASCE, 1968; Thorne, 1982) in a more complex manner: cohesive riverbanks are usually poorly drained due to their silt and clay composition and thus may experience excess pore water pressures, one of the main agents of subaerial erosion (Thorne, 1982; Casagli et al., 1999). Clayey banks are also susceptible to desiccation cracking and slaking from wetting–drying cycles (Thorne, 1982), as well as freeze and thaw (Walker and Arnborg, 1966; Lawler, 1986, 1993; Gatto, 1995).

Slides due to bank erosion (Zezere et al., 1999) include falls, topples occurring in the banks of fluvial channels, chiefly during flash flood episodes. Although very frequent, they are usually small and can be easily obliterated by stream removal. In some cases, the initial slope movement is triggered by bank erosion evolving into a retrogressive failure controlled by the slope's morphostructural setting. Lateral erosion rate of a stream is related to the depth of the stream, the erodibility of the geologic material, and on the velocity of stream flow (Odgaard, 1989 a, b).

The fundamental mechanics of planar bank failure include basal erosion occurring at the underwater portion of the bank surface thus destabilizing the upper part of the bank (figure 4-1). The critical condition of planar bank failure occurs when the driving force of bank failure equals the bank resistance force (Thorne 1982). However, because the cohesive resistances of bank materials are different below and above the water surface, the overall bank resistance varies with the height of the water surface and thus changes with flow discharge.

The force-resistance relationships founded through flume experiments are controversial (Arulanandan et al., 1980). Fluctuating water tables (Casagli et al., 1999), seasonal vegetation (Thorne, 1990), active floodplain processes (Babaeyan-Koopaei et al., 2002), the effects of previous flow events (Hooke, 1979) and the presence of subaerial erosion all complicate the identification of controls on hydraulic erosion of cohesive riverbanks in natural channels. However, field studies have found other flow properties to be more strongly correlated to hydraulic erosion. Although Wolman (1959) and Knighton (1973) acknowledged the occurrence of subaerial processes, including freeze–thaw, their research introduced the possibility that discharge duration and variability affect hydraulic erosion rates. Later, Hooke (1979) showed that at sites where hydraulic processes were dominant over subaerial processes, the variable with the strongest correlation to bank erosion was event peak

discharge. Four possible flow properties emerged as controls on hydraulic erosion rates of cohesive riverbanks: magnitude (Arulanandan et al., 1980), duration (Wolman, 1959; Knighton, 1973), event peak (Hooke, 1979), and variability (Knighton, 1973).

The bank erosion rate was first linearly related to the excess near-bank velocity, (Ikeda et al.; 1981) which is the difference between depth averaged velocity and cross-sectional mean velocity. Therefore, the bank retreats if the excess near-bank velocity is greater than zero; otherwise, the bank advances. An erosion coefficient is included to account for variations in bend geometry and properties of bank material. This approach was adopted by Parker (1976), Johannesson (1985), Odgaard (1989 a,b), Crosato (1990), and Larsen (1995).

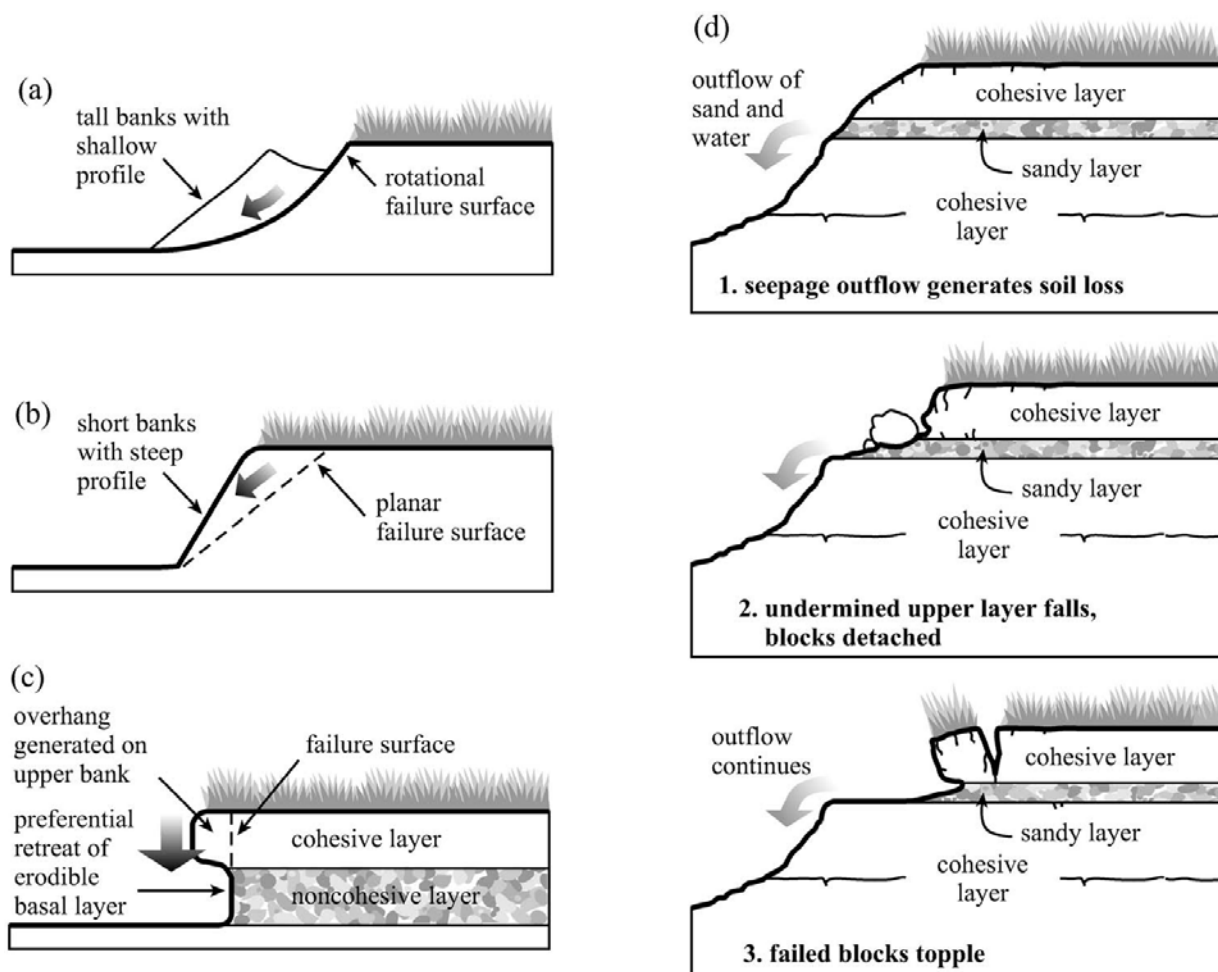


**Figure 4-1** - Bank failure mechanisms: (a) rotational; (b) planar; (c) cantilever; and (d) piping or sapping (FISRWG, 1998).

Odgaard (1989 a, b) suggested that the bank erosion rate could also be correlated to the near-bank flow depth rather than the excess near-bank velocity. Bank erosion rate is modeled as a function of excess bank height and bank stability conditions change resulting from deformation of the bank profile caused by direct fluvial shear erosion of the bank materials and nearbank bed degradation (Mosselman, 1991, 1992, 1998). Generalizations and

assumptions (e.g. use of an idealized bank geometry and simplified heterogeneity of the streambank material) have limited the capabilities of the above-mentioned models.

Since the late 1990s, the range of physical processes affecting streambank stability simulated by the previous models has increased. For example, Simon and Curini (1998), Rinaldi and Casagli (1999), and Simon et al. (2000) showed the importance of negative pore-water pressures on streambank stability, even simplifying the effects of the heterogeneity of the streambank material. Amiri-Tokaldany et al. (2003) averaged the shear-strength parameters of the various soil layers composing the streambank. Simon et al. (2000) appropriately accounted for the shear strength due to the cohesion of each soil layer, but neglected interlayer forces.

Recently developed hydrodynamic and sediment transport models (Nagata et al. 2000; Duan 1998; Duan 2001; Darby et al. 2002; Olsen 2003) have the capability of predicting not only bed degradation or aggradation but also channel width adjustments. The Osman and Thorne (1988) model linked basal bank erosion to bank failure processes and derived an analysis of bank stability for planar bank failure. Darby and Thorne (1996) extended the applicability of this model by considering pore-water pressure and hydrostatic confining pressure terms, and allowing the failure plane to pass through more than the toe of the bank.

Darby et al. (2002) replaced the bank erosion submodel within the two-dimensional depth-averaged numerical model, RIPA, with a new physically based bank erosion model. Basal erosion of cohesive bank material and subsequent bank failure as well as the transport and deposition of eroded bank material were simulated in their model to predict the evolution of meandering channels. However, the analysis of bank failure as a probabilistic phenomenon associated with hydrologic events, such as flooding, was not included.

Duan (2005) describes basal erosion as the result of fluvial entrainment of bank material by flow-induced forces, including drag force, resistance force, and lift force that act on the bank surface. The rate of basal erosion is the rate of bank material entrainment to the water body per unit channel length per unit time. Because bank failure frequently occurs in the recessing limb of a storm hydrograph, the frequency of bank failure was correlated to the frequency of flooding. The author treats bank failure as a probabilistic process, and the frequency of bank failure was derived from flood frequency.

Langendoen and Simon (2008) developed a stability analysis for heterogeneous streambanks that accounts for the dynamic effects of surface water (confining pressures) and porewater pressures on the factor of safety, and automatically searches for the slip surface that produces the smallest factor of safety. The authors (2008) showed the strong sensitivity of the computed factor of safety on the input parameters, especially pore-water pressures and effective cohesion.

(2) Surface water flow trigger coarse-grained landslides, such as debris flows may initiate by **mobilization of a channel bed** (figure 4-2, Takahashi 1991; Griffiths et al. 1997). In this case, the shear force of water mobilizes individual particles and the solid concentration increases until it reaches an equilibrium dependant on slope angle and water supply (e.g.

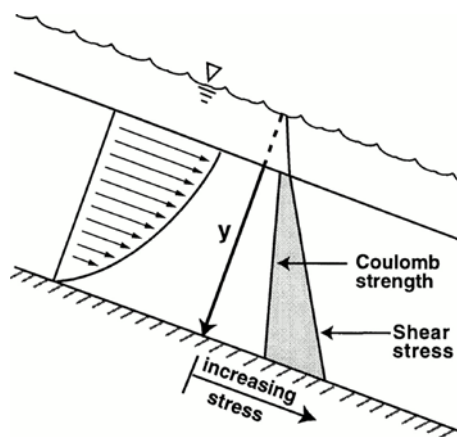


**Figure 4-2** - Schematic profile illustrating mobilization of an inertial grain flow on an infinite slope, as in the Takahashi model. The shear stress must exceed the Coulomb strength through at least part of the soil thickness (shaded region, Iverson, 1997).

Takahashi 1978, 1981, 2000). Debris flows thus initiate when a critical surface discharge is reached. This phenomenon is best described in terms of equilibrium of single particles to the hydrodynamic drag force rather than using the classical, limit-equilibrium analysis of a Mohr-Coulomb material employed for shallow slope stability (Chiew and Parker 1994; Buffington and Montgomery 1997; Armanini and Gregoretti 2000). Destabilization of bed material is the result of drag forces acting at the base of the flow, but may be aided by strength loss due to rapid undrained loading (Hutchinson and Bhandari, 1971), impact loading and liquefaction of the saturated channel fill (Sassa, 1985). Bed destabilization during a debris flow may affect not only bedload, but any erodible bed substrate. As shown in flume experiments, once the slope of the channel increases beyond approximately  $10^\circ$ , the bed itself may become unstable under the combination of gravity and drag forces imposed by the over-riding water flow (Bagnold, 1966).

Failure of bed material can be caused by turbulence and lift (Selby 1985) and by the transmission of basal shear stress to the bed. Sediments supplied to bed gullies are easily eroded when a water film of a certain thickness,  $h_0$ , appears at the surface of saturated debris (Takahashi 1978, 1981). This channel bed erosion and occasionally landslides induced by channel bank erosion cause the production of very highly sediment laden flow, i.e. debris flows. Eventually, a homogeneous bed subjected to drained loading at the base of a uniform debris flow is subjected to erosion by isolated grain-bed interactions (i.e., impact and scour) and generation of excess pore water pressures due to rapid undrained loading, with possible liquefaction (Hutchinson and Bhandari 1971; Sassa 1985).

The process of bed destabilization can be represented by a simple extension of the infinite slope stability theory (e.g. Morgenstern and Sangrey, 1978). The solution depends on the assumptions made concerning pore water pressure in the bed materials. Takahashi (1978, 1980, 1981) identified the critical conditions for the transformation of an accumulation of debris on a gully floor into a debris flow by comparing the shear stress at a given depth with the shear resistance of the material. In a first attempt, Takahashi (1978) assumed slope-parallel seepage and flow, combined with instant drainage, so that the pore fluid is hydrostatically

pressurized and flowing in a steady-state regime, with no excess pore-pressure. The tractive force of a sheet of water,  $h_0$  thick, on a bed of cohesionless material, inclined at an angle  $\beta$ , produces a shear stress  $\tau$  at depth  $y$  which is:

$$\tau = (c(\rho_s - \rho_f)y + \rho_f(y + h_0))g \sin \beta \quad [4-1]$$

while, the maximum shear resistance,  $\tau_f$ , is given by:

$$\tau_f = c(\rho_s - \rho_f)gy \cos \beta \tan \varphi'_s \quad [4-2]$$

where:  $c$  is the volumetric concentration of solids;  $\rho_s$  is the solid density,  $\rho_f$  is the fluid density,  $\varphi'_s$  is the friction angle of the bed material.

While these results are conceptually interesting, they are of little interest for practical application. One reason is that little is known about the shear strength of materials comprising the bed of a debris flow stream and its variation with depth. Often, there will be a layer of cohesionless, coarse material, underlain by a substrate possessing either true or apparent cohesion, such as glacial till or residual soil. Pore-pressures are also unlikely to be easily predictable, due to possible discharge gradients at the base of a steep-sided path segment or excess gradients generated by rapid loading and vibration due to the debris flow. Three-dimensional effects, i.e. the strength of lateral surfaces at the channel edge, are also likely to be important. Although the equations may help predict when erosion will begin to occur, the rate at which material is entrained into the flow requires further analysis and further difficult assumptions. Thus, the above equations can be regarded merely as conceptual guidelines.

Alternatively, the threshold for bed mobilization starting can be defined posing a critical runoff discharge (Panday and Huyakorn 2004, Berti and Simoni, 2005). Berti and Simoni (2005) describe the hydrologic response to rainfall by a kinematic wave model that computes the steady, fully-saturated, slope-parallel overland flow hydrograph at the outlet of the headwater basin and routes inflow along the debris-incised channel. The authors found that channel runoff along the debris-incised channel can be adequately estimated by subtracting from the inflow hydrograph at the basin outlet a channel outflow component which include soil storage and steady, slope-parallel subsurface flow within the channel bed.

The potential outflow discharge is computed by summing the component due to slope-parallel flow through the upper layer:

$$QS = -BHnKU \sin \alpha \quad [4-3]$$

and the component due to long-term leakage into the lower layer:

$$QL = -BKLdx \quad [4-4]$$

where  $K_U$  and  $K_L$  are saturated hydraulic conductivities of the upper and lower debris and  $Hn = H \cos \alpha$ . Moreover, the steady-state approximation adopted in (7) and (8) implies that the time required to reach steady-state flow is short enough that the transient component can be neglected. Field observations, real-time data and extensive analyses demonstrated that, in the present case, both conditions are satisfied.

Alternative to a theoretical definition of discharge threshold for debris flow initiation, Gregoretti (2000) and Tognacca et al. (2000) proposed an empirical threshold criterion. Both methods follow the approach of Bathurst et al. (1987) and include the representative grain-size as fundamental input parameter beside the channel slope. Such parameter corresponds, as proposed by both authors, to  $d_{50}$  (the diameter through which 50% of the total soil mass is passing).

(3) **Surface runoff** becomes an important process in recently burned watersheds (figure 4-3), where the removal of plant canopy and the duff layer covering forest soils, and the generation of water-repellent soils, can result in significant reduction of infiltration (Martin and Moody 2001; Conedera et al. 2003). Surface runoff is also an important process in high mountainous areas due to concentration of overland flow on steep rocky watersheds upstream the source areas (Berti et al. 1999; D’agostino and Marchi 2003). The latter condition is quite common in the European Alps, where most debris flows are initiated by concentrated surface flow at the bottom of channels filled by coarse loose debris (Tognacca et al. 2000). Although poorly-sorted, such debris contains a low fine fraction (less than 10–20% silt and clay) compared to soils involved in landslide-induced debris flows, and much higher hydraulic conductivity. Because of their ability to drain the rain water infiltrating from the surface, the moisture content of these materials is always far from saturation, therefore failure is very unlikely unless it occurs as a result of surface flow.

Berti and Simoni (2005) found that a limited surface water runoff (few centimetres) is enough to start the mobilization of the channel bed (as observed in the video recordings) and corroborates the validity of the empirical threshold. It also indicates that the computed “channel runoff threshold” and the empirical “debris flow triggering threshold” are very close each other. A fundamental condition for the occurrence of near-surface, slope-parallel flow is that the flow domain is bounded by a impermeable bed at the bottom.

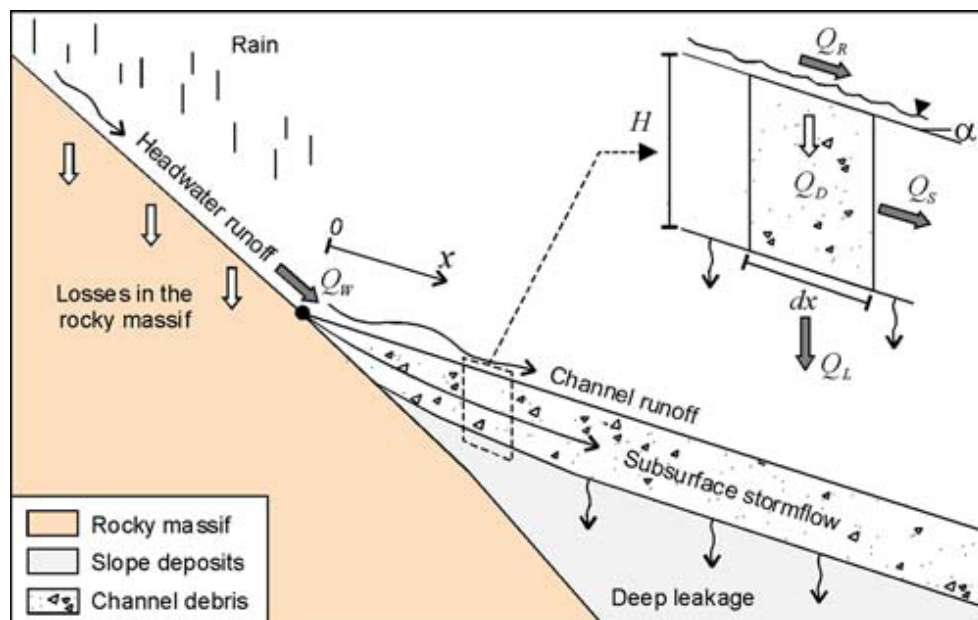


**Figure 4-3** - Conceptual scheme of the hydrologic response to rainfall in the debris flow initiation area used to model the process of channel runoff generation (Berti and Simoni, 2005).

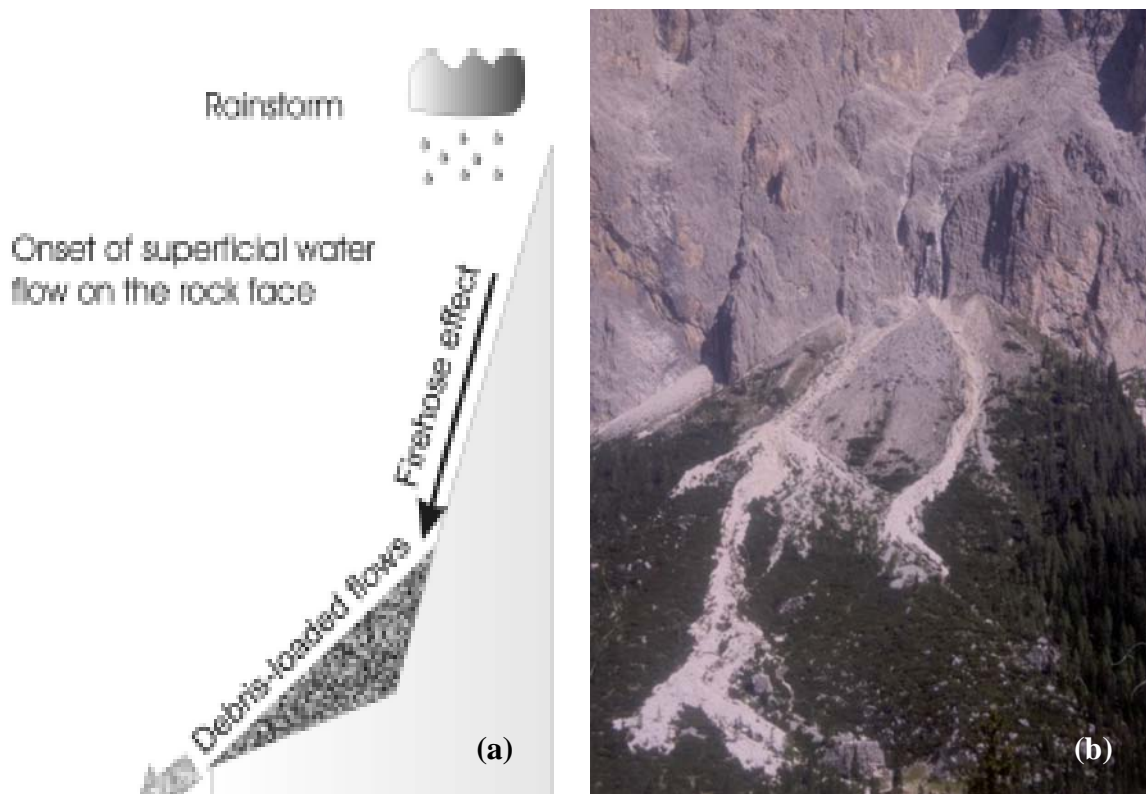


**Figure 4-4** – (a) Scheme of debris mobilisation due to high-speed water flow (firehose effect). (b) Example of firehose effect (Sasso Pordoio, Italy).

(4) A particular case of erosion triggering mechanism is the **firehose effect** (figure 4-4) caused by the impact of a high-speed stream of water on unstable sediment causing debris flow initiation (Johnson and Rodine, 1984).

In the coastal setting, landslides are primarily caused by erosion and the consequent unloading associated with removal of lateral support (Hutchinson 1975). In clay slopes, unloading produces expansion and softening of the exposed material, particularly if it is overconsolidated and dilatant. In jointed and fissured material, an expansion of discontinuities produces non-uniform shear strains and enhances the opportunity for the action of joint processes. Hutchinson (1975) distinguished among slope movement types which take place: moderate toe erosion causes shallow mudslide with the erosion confined almost entirely to the mudslide tongues; strong toe erosion allows in situ clay to be affected by removal of lateral support and causes deep-seated landslides.

---

## 4.2 NUMERICAL MODELING [SGI-MI]

Starting from the basic framework and the concepts discussed in Section 2, the numerical models presented below show how it is possible, using appropriate constitutive models, to replicate with good approximation the conditions that pertain in slopes in mechanically overconsolidated, unbonded, saturated clays as a result of the geological slope forming processes and to predict qualitatively and quantitatively their subsequent development and their response to anthropogenic changes.

In particular the numerical models presented below refer to the following typical cases, frequently encountered in Italy and elsewhere in Europe:

- A. Slow (geotechnically “drained”) formation of gentle slopes by erosion in hydraulic and mechanical equilibrium with the current boundary conditions with no previous slope movement and subsequent fast formation (typically by antropogenic processes) of a relatively steep erosion or excavation scarp at the toe of the slope; delayed failure is often observed in these conditions in engineering works, for example in railway and in motorway cuttings in the SE of England (Vaughan &Walbancke, 1973; Chandler & Skempton, 1974; Skempton, 1977; Chandler, 1984; Skempton, 1995; Potts et al., 1997; Vaughan et al., 2004; Bromhead & Ibsen, 2007) and in cuttings on the main motorways (A1, A14, A16) in central and southern Italy (SGI-MI project files).
- B. Relatively “fast” formation by geological processes of moderately steep slopes in mechanically overconsolidated, unbonded, saturated clays where the resulting pore pressure regime is not in equilibrium with the current boundary conditions (residual negative excess pore pressures), overlain by thick slabs of cemented coarse grained materials, representative, for example, of stratigraphic conditions frequent in central and southern Italy. These conditions are typically characterized by complex deformations, possibly involving valley bulging, squeezing and lateral spreading.

In both cases different models have been implemented and are presented below to explore also the effects induced by the possible presence within the clayey formation of layers of different permeability and/or stiffness, such as a layer of sand or of cemented marls. All cases considered are summarized in Table 4-1.

In line with the criteria outlined in Section 2, the numerical analyses have been carried out using for the clayey formation an elasto-plastic constitutive model with volumetric and kinematic hardening capable of reproducing non linearity also inside the State Boundary Surface (of the type described by Al Tabbaa & Muir Wood, 1989; Atkinson & Stallebrass, 1991; Stallebrass and Taylor, 1997); the model used, which is described in detail at point 4.2.2, has variable  $M$  (as a function of the Lode angle) and includes degradation of the angle of shearing resistance from the value at critical state ( $\varphi_{cs}'$ ) to the residual value ( $\varphi_{res}'$ ).

While no attempt has been made to replicate or to back-analyze any specific case history, realistic parameters and geometries have been used in the analyses; the results are in line with the behaviour of many case histories described in detail in the technical literature.

*Table 4-1 - Summary of cases considered*

<b>A</b>	<b>Fast basal erosion/excavation at the toe of a gentle slope previously in equilibrium</b>
A1	Homogeneous profile of mechanically overconsolidated, unbonded, saturated clay
A2	As A1, with a layer of “sand” at mid height of the excavation ( $k_s \gg k_c$ ; $E_s \approx E_c$ )
A3	As A1, with a layer of “cemented marls” at mid height of the excavation ( $k_m \approx k_c$ ; $E_m > E_c$ )
<b>B</b>	<b>Long term behaviour of moderately steep slope formed by geologically fast erosion, overlain by slab of cemented coarse grained material</b>
B1	Homogeneous profile of mechanically overconsolidated, unbonded, saturated clay below top slab
B2	As B1, with a layer of “sand” below the toe of the slope ( $k_s \gg k_c$ ; $E_s \approx E_c$ )
$K_c$ ; $k_s$ ; $k_m$ = current permeability of clay, sand and marl $E_c$ ; $E_s$ ; $E_m$ = current stiffness of clay, sand and marl	

*Table 4-2 - Typical plasticity characteristics of Italian Pliocene/Pleistocene clays*

Clays	Limit Liquid	Plastic Limit	References
Attigliano - Fabro	45÷55%	20÷25%	SGI-MI project files
Todi	67% 50%	39% 28%	Burland et al. (1996) AGI, 1985
Vallericca	60%	27%	Burland et al. (1996)
Petacciato	50÷60%	30÷40%	SGI-MI project files
Porto Empedocle	50÷60%	30÷40%	SGI-MI project files

#### 4.2.1 Key geotechnical characteristics of the clay considered in this study

The clay considered in this study has plasticity characteristics typical of Pliocene/Pleistocene clays outcropping extensively in Italy along the Tyrrhenian, Adriatic and Ionic coasts and the South coast of Sicily (see Table 4-2).

As shown In Figure 4-5 (Attigliano – Fabro; Todi; Vallericca clays), Figure 4-6 (Petacciato clay) and Figure 4-7 (Porto Empedocle clay), the initial states of these clays, as defined by their current normalized void ratio (void index,  $I_{vo}$ ) and vertical effective geostatic stress ( $\sigma_{vo}'$ ), are located well below the oedometric intrinsic compression line ( $ICL_{oed}$ ) evaluated according to the empirical relationships proposed by Burland (1990) and/or to specific eodometric tests carried out on reconstituted specimens; the  $ICL_{oed}$  represents the oedometric normal consolidation curve of clays with negligible sensitivity (Skempton, 1970; Burland, 1990; Cotecchia & Chandler, 1997).

The current initial states shown in Figures, 4-5, 4-6 and 4-7 reflect the significant erosion of these deposits which occurred in the geological timescale; indicatively, the maximum thickness ( $H_c$ ) of the materials removed by erosion, as inferred from geological considerations, are reported in Table 4-3.

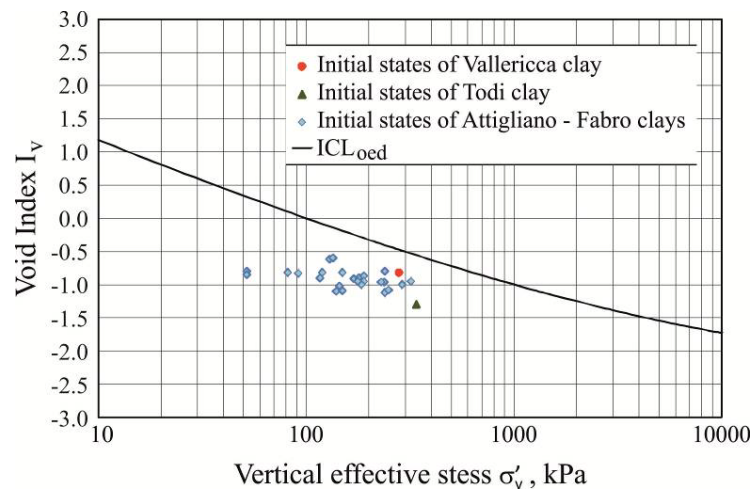


**Figure 4-5** - Initial states relative to the  $ICL_{oed}$  of Attigliano-Fabro, Todi and Vallericca clays (adapted from SGI-MI project files and Burland et al., 1997)

**Table 4-3** - Thickness of material removed by erosion ( $H_e$ )

Clays	$H_e$	References
Todi	430 ÷ 450 m	Burland et al. (1996)
Vallericca	220 m	Burland et al. (1996)
Petacciato	>180÷200 m	Cancelli et al. (1984) Santaloia et al. (2004)
Porto Empedocle	>> 70 m	SGI-MI project files

Clays with initial states below the  $ICL_{oed}$  are characterized by mechanical overconsolidation and by stable microstructures under present effective stresses in situ, irrespective of the presence of bonding.

As reported for example by Cotecchia & Chandler (1997), these natural clays may be characterized also by the presence of bonding, largely due to a film of amorphous calcite.

Even if natural clays may be characterized also by the presence of relatively weak bonding, for the sake of simplicity this has been disregarded in this study. With reference to the general framework presented in Section 2, only clays type CO1 (during sedimentation) which become type CB1 (after erosion) have been considered.

The very low permeability of these clays results in undisturbed sampling by push or rotary samplers being very effective; the mean effective geostatic pressures are typically preserved during good quality sampling thanks to the development of high negative pore pressures. Suctions as high as 650 to 900 kPa have been measured by various techniques in Pappadai clay (Cotecchia & Chandler, 1997) and in Porto Empedocle clay on undisturbed samples obtained at depths of 20 to 50 m (SGI-MI project files); high swelling pressures (250÷350 kPa) have been measured in oedometer tests on undisturbed specimens of Petacciato clay taken from depths of 5 to 15 m (SGI-MI project files).

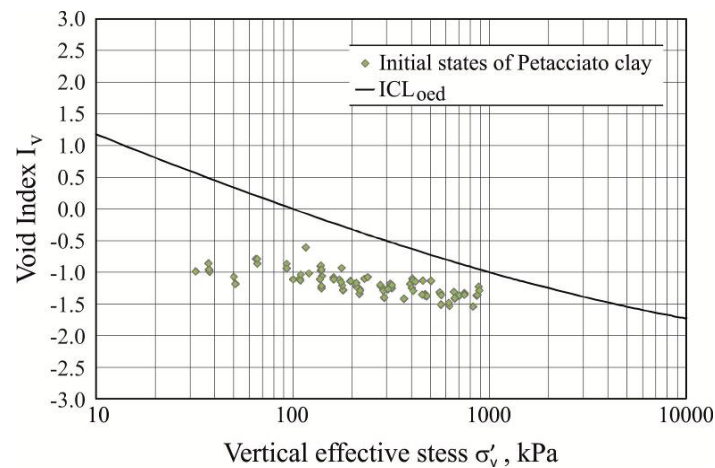


**Figure 4-6** - Initial states relative to the  $ICL_{oed}$  of Petacciato clay (adapted from SGI-MI project files)

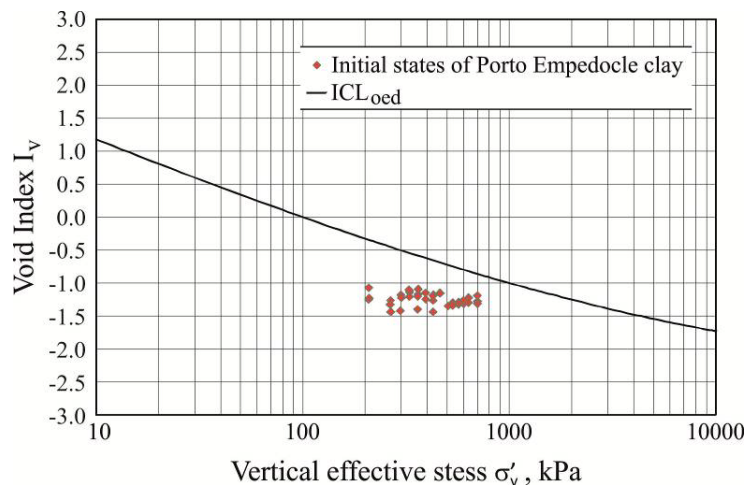


**Figure 4-7** - Initial states relative to the  $ICL_{oed}$  of Porto Empedocle clay (adapted from SGI-MI project files)

#### 4.2.2 Elasto-plastic constitutive model of the clay considered in this study

The adopted constitutive model considers both volumetric and kinematic hardening, generally as proposed by Al Tabbaa & Muir Wood (1989), Atkinson & Stallebrass (1991), Stallebrass & Taylor (1997); in particular it allows elasto-plastic deformations to be controlled by a single kinematic hardening yield surface located inside the conventional Modified Cam Clay state boundary surface.

The constitutive model has the following main characteristics:

1. The inner yield surface and the state boundary surface have the same shape and are described by the following equations:

Inner yield surface

$$f_i = \left( \frac{q - q_o}{M} \right)^2 + (p' - p_o')^2 - \left( r_e \cdot \frac{p_c'}{2} \right)^2 \quad [4-5]$$

$$q = \sigma_1' - \sigma_3' \quad [4-6]$$

$$p' = \frac{\sigma_1' + \sigma_2' + \sigma_3'}{3} \quad [4-7]$$

$\sigma_1'$  = maximum principal effective stress

$\sigma_3'$  = minimum principal effective stress

$\sigma_2'$  = intermediate principal effective stress

$p_c'$  = mean effective preconsolidation stress which defines the dimension of the state boundary surface, continuously updated

M = strength parameter variable with the Lode angle (see point 4 hereafter)

$q_o$ ;  $p_o'$  = coordinates of the centre of the inner yield surface, continuously updated

$r_e$  = parameter of the model which defines the dimension of the inner yield surface

State boundary surface

$$f_o = \left( \frac{q}{M} \right)^2 + p' \cdot (p' - p_c') \quad [4-8]$$

The dimensions of the inner yield surface and of the state boundary surface, which evolve according to the hardening rule, are linked by the parameter  $r_e$ .

2. The inner yield surface moves when the two conditions below are satisfied simultaneously:
  - the current stress state lies on the inner yield surface; and
  - the load increment is directed outwards,  $\pm 90^\circ$  relative to the normal to the inner yield surface.

The magnitude and direction of the movement of the inner yield surface is controlled by the mapping rule: the centre of the inner yield surface always moves along a vector joining the current stress state to its conjugate point on the state boundary surface; this ensures that, as the inner yield surface is dragged by the current stress state, it never intersects the state boundary surface.

3. When the stress state is within the inner yield surface, strains are governed by constitutive equations of isotropic elasticity; in all other cases the stress-strain behaviour is elasto-plastic; the deviatoric and volumetric plastic strains are evaluated by means of associated flow rules; the expansion or contraction of the inner yield surface and of the state boundary surface are evaluated by means of the volumetric hardening rule.

According to the theory of isotropic elasticity, the following relationships apply:

$$G = \frac{3 \cdot B \cdot (1 - 2 \cdot \nu')}{2 \cdot (1 + \nu')} = \text{shear modulus} \quad [4-9]$$

$\nu'$  = Poisson's ratio

$$B = \frac{v \cdot p'}{\kappa} = \text{bulk modulus}$$

$v = 1 + e =$  current specific volume

$p' =$  current mean effective stress.

According to the Modified Cam Clay model the hardening rule, which governs the dimension of the inner yield surface and of the state boundary surface, is given by the following equation:

$$\delta p'_c = -\frac{v \cdot p'_c}{\lambda - \kappa} \cdot \delta \varepsilon_v^p \quad [4-10]$$

The hardening rule derives from the following equations which related to the state boundary surface and the “elastic wall” of the Modified Cam Clay model:

$$v = v_\lambda - \lambda \cdot \ln \frac{p'}{p'_1} \quad [4-11]$$

$$v = v_\kappa - k \cdot \ln \frac{p'}{p'_1} \quad [4-12]$$

where:

$\lambda =$  slope of the normal consolidation line in the  $v$ - $\ln p'$  plane

$\kappa =$  slope of the “elastic wall” in the  $v$ - $\ln p'$  plane

$v_\lambda =$  specific volume on the normal compression line at a reference mean effective pressure  $p'_1$

$p'_1 =$  reference mean effective pressure, taken equal to 1 kPa.

$v_\kappa =$  specific volume on the “elastic wall” at a reference mean effective pressure  $p'_1$ .

The mapping rule and the kinematic hardening rule related to the inner yield surface are respectively given by the following expressions:

$$\begin{Bmatrix} \delta \varepsilon_v^p \\ \delta \varepsilon_\delta^p \end{Bmatrix} = \lambda_s \cdot \begin{Bmatrix} \frac{p' - p'_o - p' + \frac{p'_c}{2}}{r_e} \\ \frac{q - q_o - q}{r_e} \end{Bmatrix} \quad [4-13]$$

$$\begin{Bmatrix} \delta p'_o \\ \delta q_o \end{Bmatrix} = \begin{bmatrix} \frac{p' \cdot v}{a_c} \\ \frac{p' \cdot v}{a_c} \end{bmatrix} \cdot \begin{Bmatrix} \delta \varepsilon_v^p \\ \delta \varepsilon_\delta^p \end{Bmatrix} + \begin{Bmatrix} p'_o \\ q_o \end{Bmatrix} \cdot \frac{\delta p'_c}{p'_c} \quad [4-14]$$

where:

$\delta \varepsilon_v^p, \delta \varepsilon_\delta^p =$  increment of volumetric and deviatoric plastic strains

$\lambda_s$  = internal parameter of the model evaluated according to the consistency rule

$a_c$  = parameter of the model.

The expressions reduce to those of the Modified Cam Clay model when the inner yield surface and the state boundary surface are in contact.

4. According to experimental results published by Parry (1960),  $\varphi_{cs}'$  has been assumed to be stress-path independent; this implies a Mohr-Coulomb hexagon shape of the critical state failure surface with the strength parameter  $M$  variable with the Lode angle  $\theta$  or the parameter  $b = (\sigma_2' - \sigma_3')/(\sigma_1' - \sigma_3')$  (Ladd, 1991; Grammatikopoulou et al., 2007) according to the following relationship proposed by Li & Dafalias (2000):

$$M = M_c \cdot \frac{\sqrt{(1+c^2)^2 \cdot 4 \cdot c \cdot (1-c^2) \cdot \sin(3 \cdot \theta) - (1+c^2)}}{2 \cdot (1-c) \cdot \sin(3 \cdot \theta)} \quad [4-15]$$

where:

$$c = \frac{M_e}{M_c}$$

$M_e, M_c$  = strength parameters in extension and in compression respectively.

To account for the decay of the effective strength envelope caused by progressive realignment of platy particles in plastic clays (see for example Lupini et al., 1981), the parameter  $M$  has been also linked to the cumulative deviatoric plastic strain ( $\varepsilon_d^p$ ) according to the following equation:

$$M = M_r + (M_{cs} - M_r) \cdot \exp^{-0.5 \left( \frac{\varepsilon_d^p}{\varepsilon_\sigma} \right)^m} \quad [4-16]$$

where:

$M_r$  = strength parameter evaluated taking into account the angle of friction at residual conditions  $\varphi_r'$

$M_{cs}$  = strength parameter evaluated taking into account the angle of friction at critical state  $\varphi_{cs}'$

$\varepsilon_\sigma$  = parameter of the model

$m$  = parameter of the model.

Together with the initial stress state  $q_i$  and  $p_i'$ , the initial specific volume  $v = 1+e_i$  (where  $e_i$  = initial void ratio) and the initial position of the inner yield surface, the constitutive model is characterised by 11 parameters and 3 state variables.

Five parameters are those of the Modified Cam Clay model, i.e.  $\lambda, v_\lambda, \varphi_{cs}', \kappa$  and  $v'$ ; the parameters  $r_e$  and  $a_c$  govern respectively the dimension of the inner yield surface and the amount of the plastic strain inside the boundary state surface; the parameter  $\varphi_r', \varepsilon_\sigma$  and  $m$  govern the decay of the angle of friction from critical state to residual conditions; the parameter  $c$  represents the ratio between the strength parameter  $M$  in extension and in compression.

Two state variables are similar to those of the Modified Cam Clay model, i.e.  $v$  and  $p_c'$ ; the third state variable is the tensor which represent the centre of the inner yield surface.

For consolidation analyses the permeability coefficient of the soil ( $k$ ) and the bulk modulus of the water ( $B_w$ ) are also necessary.

The permeability coefficient may be given by (Taylor, 1948; Tavenas et al., 1983):

$$\log_{10} k = \log_{10} k_o - \frac{v_o - v}{C_k} \quad [4-17]$$

where:

$k_o$  = permeability coefficient at a reference value of the specific volume

$v$  = current specific volume

$v_o$  = reference value of the specific volume

$$C_k \approx 0.5 \cdot (v_o - 1).$$

The bulk modulus of the water  $B_w$  may be taken as  $2 \times 10^6$  kPa, as well documented in the literature.

### 4.2.3 Model parameters of the clay considered in this study

The parameters used in the analyses to model the clays described at point 4.2.1 have been evaluated as detailed below, assuming a representative value of the Liquid Limit equal to about 60%.

- The parameters  $\lambda$  and  $v_\lambda$  have been defined with the assumption that normal consolidation of the clay during the sedimentation phase took place following the oedometric intrinsic compression line ( $ICL_{oed}$ ) evaluated according to the empirical relationships given by Burland (1990).

Considering the shape of the state boundary surface, the intrinsic isotropic compression line ( $ICL_{iso}$ ), which is parallel to the  $ICL_{oed}$ , can be represented in the  $\log v - \log p'$  plane by the following values:  $\lambda^* = 0.0805$  and  $v_\lambda = 2.91$  (see Figure 4-8).

- The angles of friction at critical state ( $\phi_{cs}'$ ) and at residual state ( $\phi_r'$ ) have been assumed equal to  $25^\circ$  and  $13^\circ$ , respectively.
- The Poisson's ratio has been assumed equal to 0.15.
- The slope  $\kappa^*$  of the "elastic wall" in the  $\log v - \log p'$  plane has been assumed equal to  $\lambda^*/20$ ; this corresponds to an elastic shear modulus profile comparable to that evaluated by applying the empirical relationship proposed by Viggiani & Atkinson (1995) for unbonded normally consolidated materials (see Figure 4-9).

For high plasticity clays with  $LL = 60\%$ , this empirical relationship is given by the following equation:

$$G_o = p_r \cdot A \cdot \left( \frac{p'}{p_r} \right)^n \quad [4-18]$$

where:

$G_o$  = shear modulus at small strains

$p_r = 1 \text{ kPa}$   
 $A = 920$   
 $n = 0.8.$

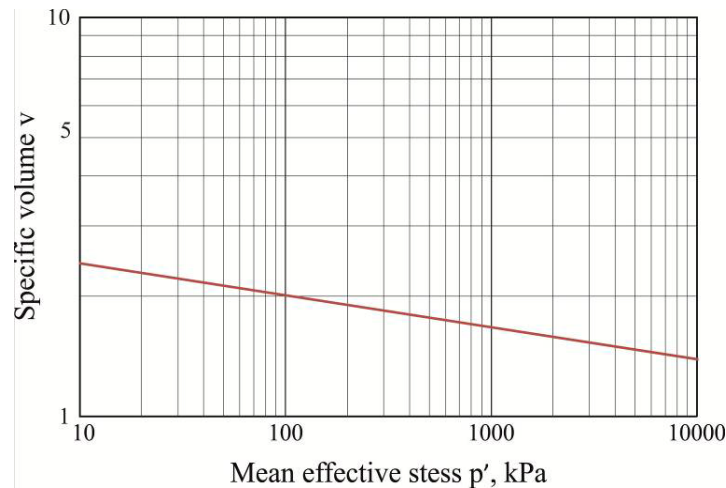


**Figure 4-8** - Isotropic intrinsic compression line ( $ICL_{iso}$ ) assumed for the CBI clay  
**Table 4-4** - Initial conditions and stress paths of the triaxial tests used for calibration of model parameters (source: SGI-MI project files)

Specimen	Test n°	$\sigma_{vc}'^{(1)}$ (kPa)	$\sigma_{rc}'^{(1)}$ (kPa)	$K_o^{(4)}$ (-)	$e_c^{(5)}$ (-)	Stress path
CI7-4	1.1	284	649	2.28	0.563	$p' = \text{const}; q \uparrow^{(2)}$
CI7-3	1.2	283	650	2.29	0.540	$p' = \text{const}; q \downarrow^{(3)}$
CI16-4	2.1	517	790	1.52	0.598	$p' = \text{const}; q \uparrow^{(2)}$
CI16-3	2.2	553	840	1.52	0.583	$p' = \text{const}; q \downarrow^{(3)}$

(1)  $\sigma_{vc}'$ ,  $\sigma_{rc}'$  = vertical and radial effective stresses at the end of the consolidation phase, respectively  
(2) failure in compression, i.e.  $\sigma_v' > \sigma_r'$   
(3) failure in extension, i.e.  $\sigma_v' < \sigma_r'$   
(4)  $K_o = \sigma_{rc}' / \sigma_{vc}'$   
(5)  $e_c$  = void ratio at the end of the consolidation phase

- The parameters  $a_c$  and  $r_e$  have been calibrated by means of back analyses of special triaxial tests, taken from the SGI-MI project files. The specimens have been consolidated anisotropically ( $K_o$  condition) as shown in Table 4-4; at the end of the consolidation phase, the initial states of the tested specimens are shown in the  $I_v - \log p'$  plane in Figure 4-10; the loading phase has been carried out by changing the deviatoric stress at constant mean effective stress; failure conditions have been reached both in compression (specimens CI7-4 and CI16-4) and in extension (specimens CI7-3 and CI16-3). A satisfactory agreement has been reached between the experimental results and the results of the numerical simulations where  $a_c = 0.17$  and  $r_e = 0.13$ , as shown in Figure 4-11 and in Figure 4-12, where the deviatoric stress  $q$  is plotted as a function of the

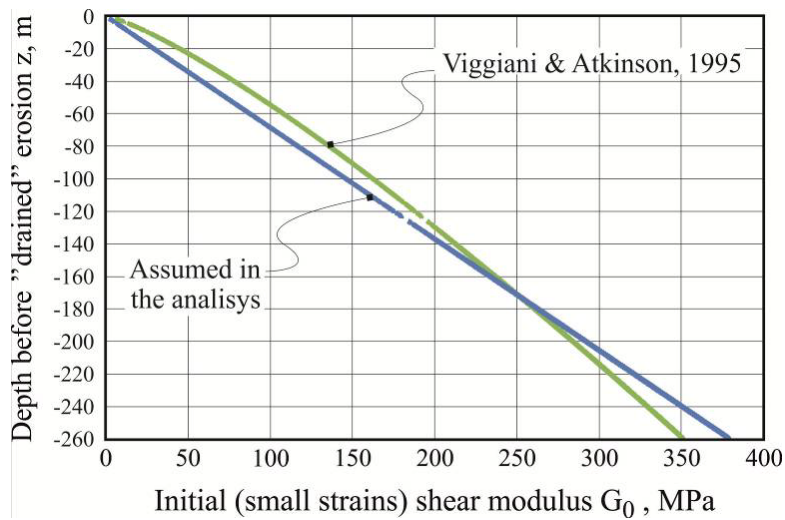


**Figure 4-9** - Profile of the initial (small strains) shear modulus assumed for the CB1 clay.

deviatoric strain  $\epsilon_s$  given by the following equation:

$$\epsilon_s = \frac{2}{3} \cdot (\epsilon_v - \epsilon_r) \tag{4-19}$$

where  $\epsilon_v$  and  $\epsilon_r$  are the vertical and radial strains, respectively.

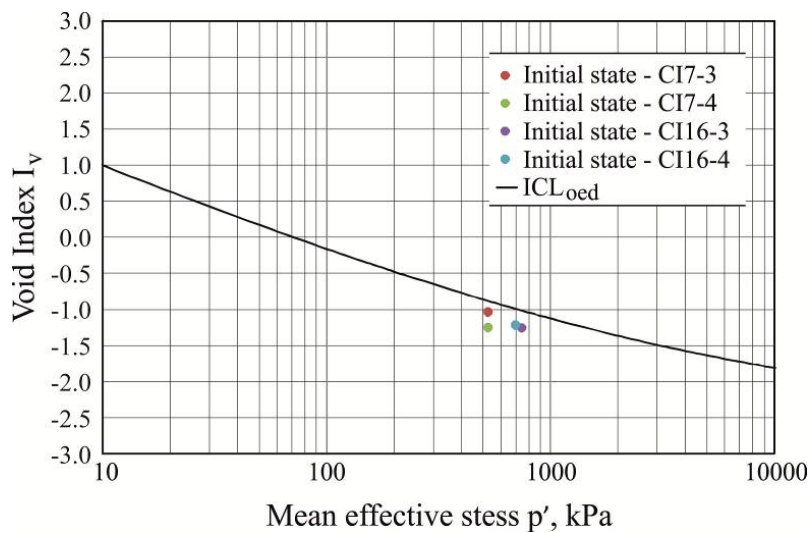


**Figure 4-10** - Initial states relative to the  $ICL_{iso}$  of representative specimens of CB1 clays selected for calibration of the parameters of the constitutive model (SGI-MI projects files)

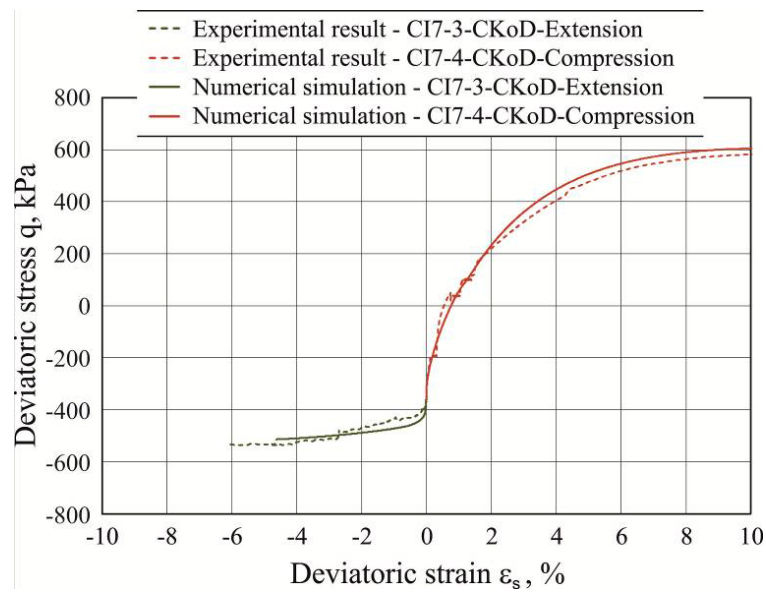


**Figure 4-11** - Experimental results versus numerical simulations of TX-CK<sub>o</sub>D tests carried out at  $p' = \text{constant}$  on specimens CI7-3 and CI7-4 of CB1 clay (SGI-MI projects files)

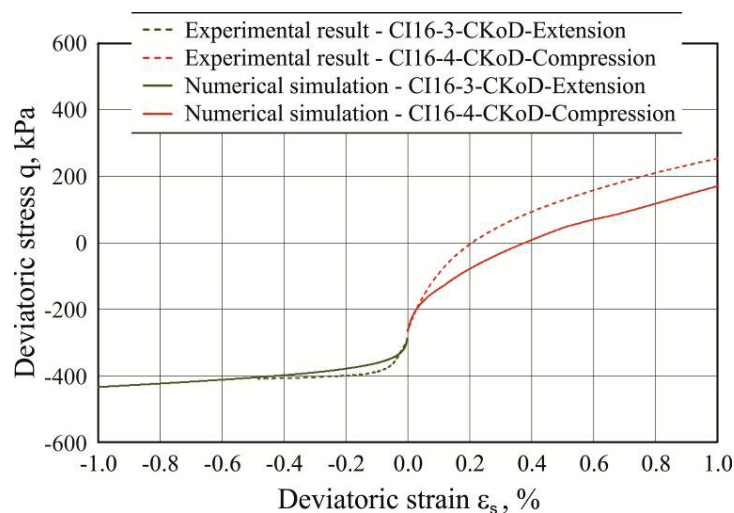


**Figure 4-12** - Experimental results versus numerical simulations of TX-CK<sub>o</sub>D tests carried out at  $p' = \text{constant}$  on specimens CI16-3 and CI16-4 of CB1 clay (SGI-MI projects files)

- The parameters  $\epsilon_{\sigma}$  and  $m$  have been selected in order to obtain degradation curves for the strength parameter  $M$  or the angle of friction comparable to those assumed by Potts et al. (1997) and Kovacevic et al. (2004) for London clay; values of  $\epsilon_{\sigma}$  and  $m$  equal to 11% and 3 have been obtained, respectively (Figure 4-13).
- The parameter  $c$  has been evaluated by assuming the following relationships for the strength parameters  $M_e$  and  $M_c$  (Atkinson & Bransby, 1978):

$$M_e = \frac{6 \cdot \sin \varphi'_{cs}}{3 + \sin \varphi'_{cs}} \quad [4-20]$$

$$M_c = \frac{6 \cdot \sin \varphi'_{cs}}{3 - \sin \varphi'_{cs}} \quad [4-21]$$

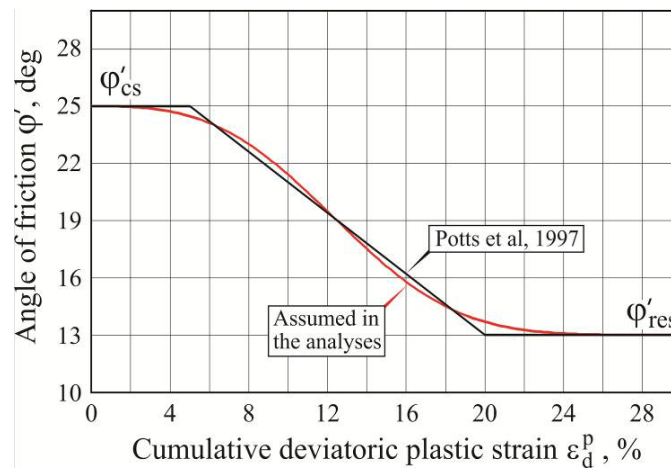


**Figure 4-13** - Variation of the angle of friction  $\varphi'$  with the cumulative plastic deviatoric strain  $\varepsilon_d^p$  assumed for the CBI clay

- The coefficient of permeability has been considered variable with the specific volume  $v$  according to the equation specified at point 4.2.2; at the reference specific volume  $v_0$  equal to 1.55, the coefficient of permeability  $k_0$  has been assumed equal to  $1 \times 10^{-11}$  m/s (Figure 4-14).

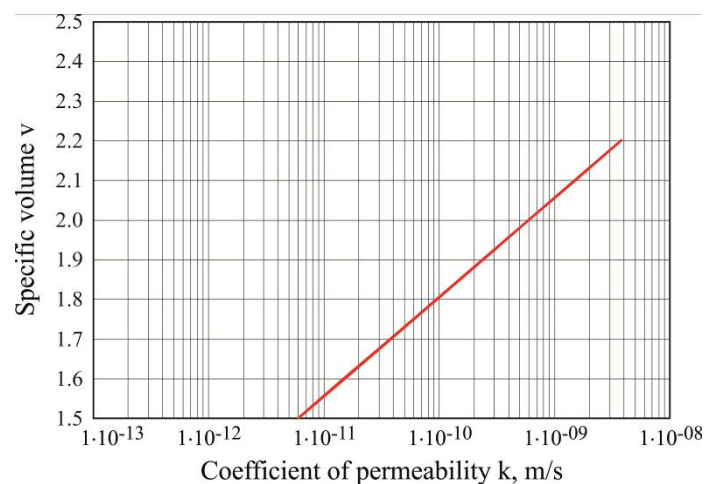


**Figure 4-14** - Coefficients of permeability assumed for the CBI clay

#### 4.2.4 Case A1

The model extends the issues addressed in examples 1 and 2 illustrated in Section 2. The objectives of the model are to simulate the following processes:

1. Starting from the end of the sedimentation of a saturated, unbonded, normally consolidated clayey deposit, slow (geotechnically “drained”) formation by erosion of a gentle slope in hydraulic and mechanical equilibrium with the current boundary conditions. The erosion is sufficiently slow not to generate any excess pore pressures relative to the piezometric regime in hydrostatic equilibrium with a groundwater level everywhere at a depth of 1 m below ground level (part 1).

The geometry of the slope in its current configuration at the end of this process is shown in Figure 4-15; steeper slopes such as those of cases B1 and B2 would not be stable in drained conditions.

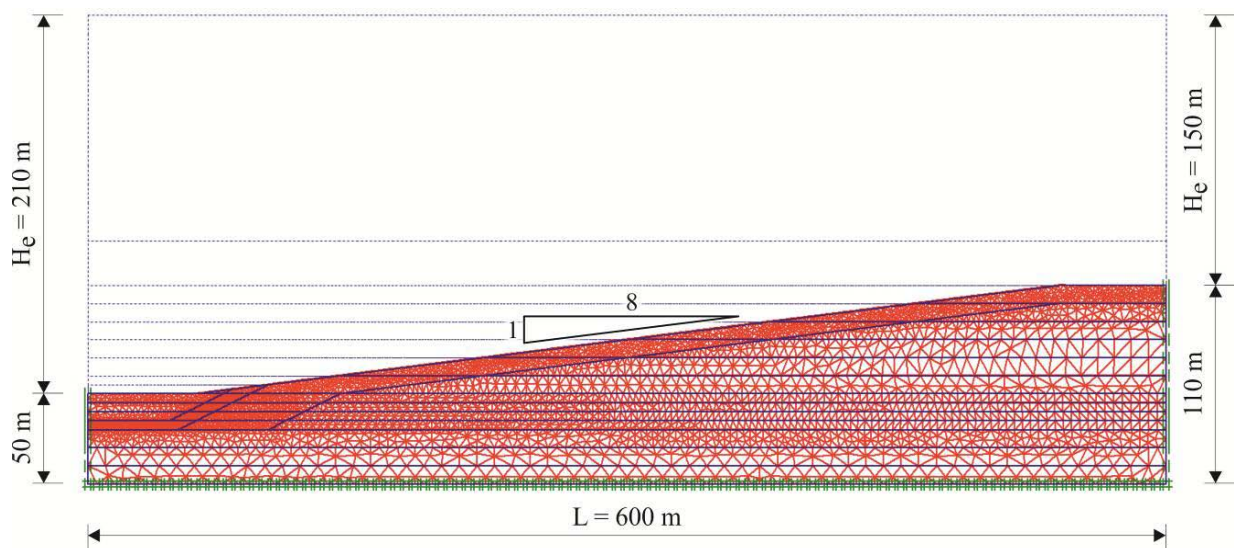


**Figure 4-15** - Case A – Finite element mesh for numerical simulation of gentle slope formation by “drained” erosion over geological timescales in CBI clay

2. Starting from the current configuration, the formation of a locally steeper scarp at the toe of the main slope as a result of relatively rapid basal erosion and/or anthropogenic excavation. In this phase the rate of erosion or excavation is sufficiently rapid to generate negative excess pore pressures and a different piezometric regime from the long term condition of hydrostatic equilibrium with a ground water level everywhere at a depth of 1 m below ground level (part 2).

The geometry of the slope following basal erosion/excavation at the toe is shown in Figure 4-16.

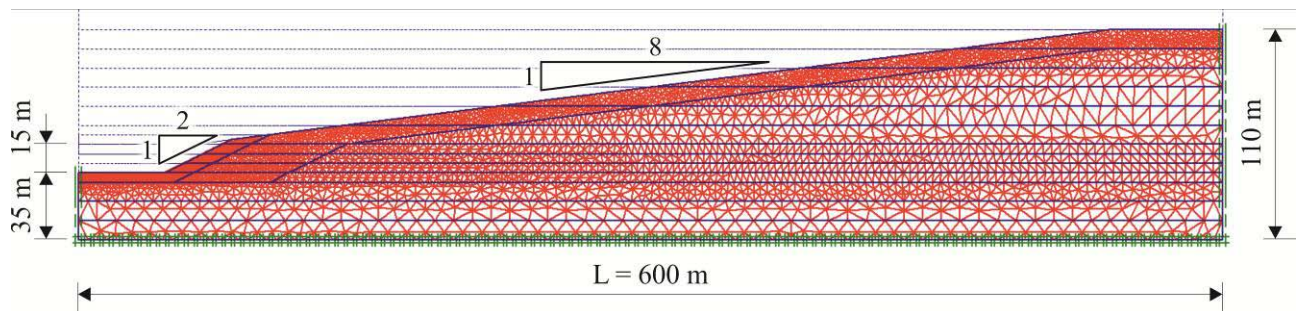


**Figure 4-16** - Case A – Finite element mesh for numerical simulation of rapid basal erosion or excavation at the toe of the gentle slope in CB1 clay

Compared to the one dimensional example (n° 1) described in Section 2, the process of mechanical weathering is investigated in part 1 of the case A1 model in two dimensions, producing different outcomes at different locations (uphill, midslope, downhill), with the thickness removed by erosion varying between 150 m (uphill) and 210 m (downhill).

Considering the mechanical boundary conditions (no horizontal movements on the vertical boundaries, implying symmetry), the geometry of the model is representative of a symmetrical valley with what is effectively an “infinite slope”, at least with respect to the area of influence of the basal erosion/excavation at the toe. No horizontal and vertical displacements are allowed at the base of the model, 50 m below the toe of the main slope before basal erosion/excavation.

The main results at the end of part 1 of the analysis may be summarized as follows:

- Whilst the rebound results in a generalized increase of the void ratio compared to the pre-erosion values, the increase is particularly significant in the top 25 to 35 m of the post-erosion profile, corresponding to the depth of the main “mechanical weathering” ( $z_w$ ) where it is clearly the result of significant volumetric and deviatoric plastic strains induced by stress conditions which approach passive failure (Figure 4-17 a, b, c for sections downslope, midslope and upslope respectively). It should be noted, however, that even at depths greater than  $z_w$  the behaviour of the soil may be not purely elastic; in the specific case under consideration, plastic strains occur as a result of erosion to the full depth investigated, as may be seen in Figure 4-18, which shows, as a function of depth after erosion, the ratio between the isotropic effective pressures which define the state boundary surface at the end ( $p'_{cf}$ ) and at the beginning ( $p'_{ci}$ ) of the erosion phase.

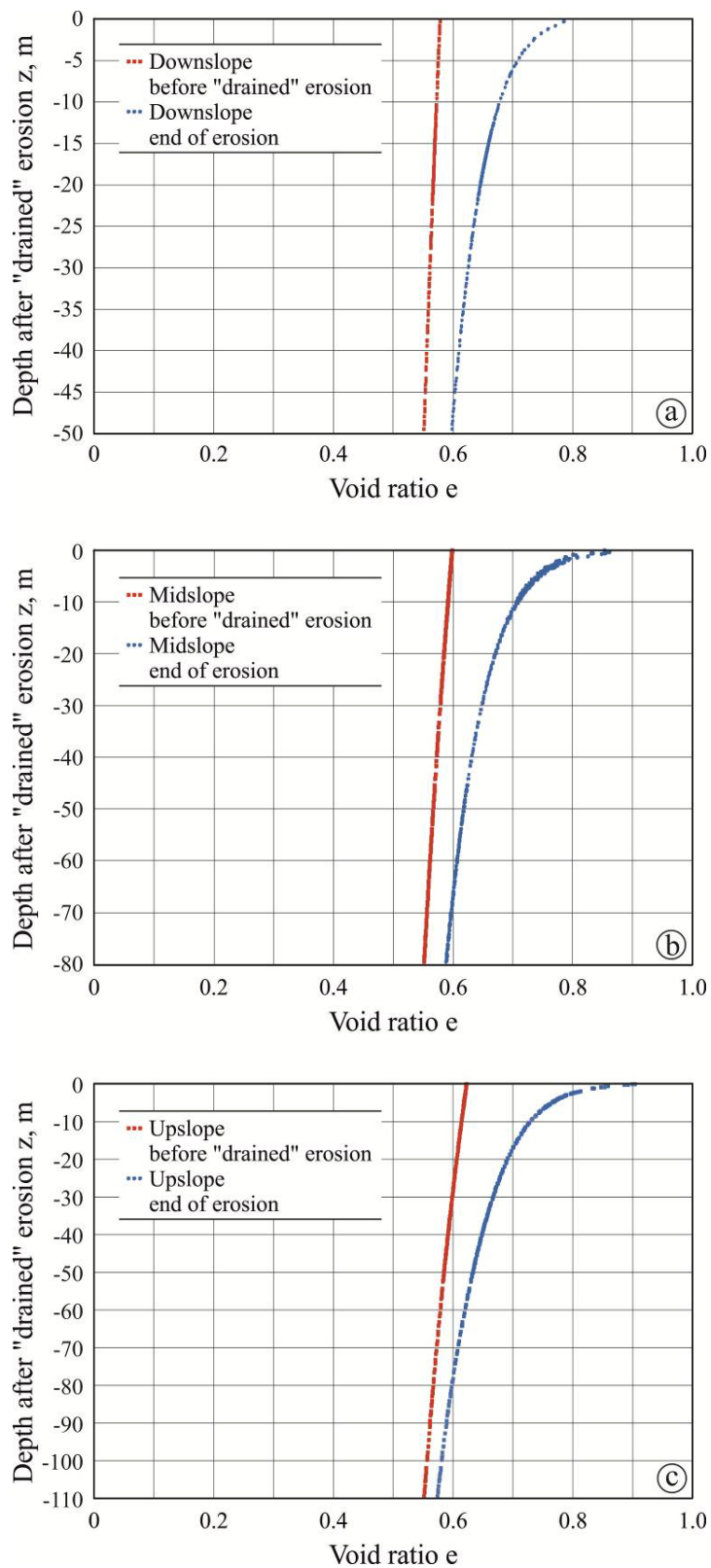


**Figure 4-17** - Case A1 – Numerically simulated void ratio profiles before and after “drained” erosion over geological timescales in CBI clay: a) downslope; b) midslope; c) upslope

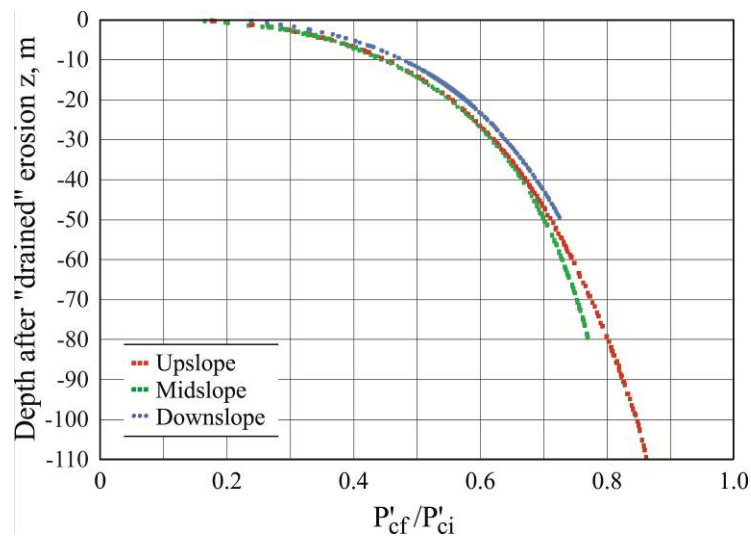


**Figure 4-18** - Case A1 – Numerically simulated profiles of  $\frac{P'_{cf}}{P'_{ci}}$  ratios after “drained” erosion over geological timescales in CBI clay

- The profiles of normalized void ratio ( $I_v$ ) as a function of post-erosion vertical effective stress ( $\sigma'_v$ ) shown in Figure 4-19 compare well with the typical profiles shown in Figures 4-5 to 4-7 for various Italian mechanically overconsolidated clays.

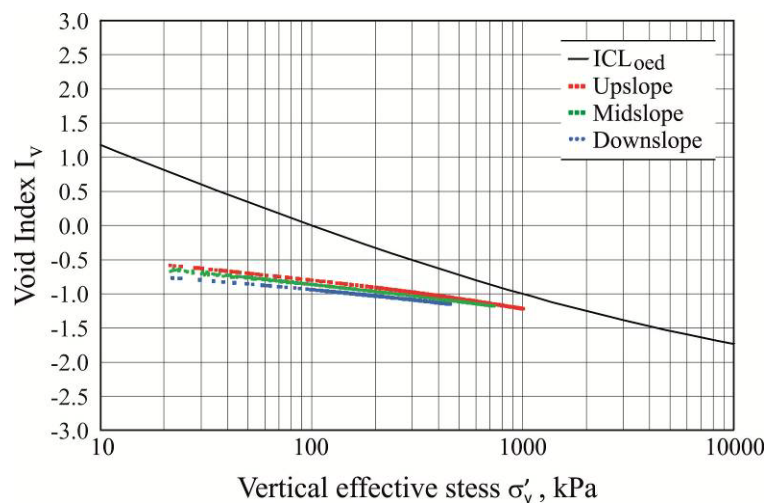


**Figure 4-19** - Case A1 – Numerically simulated initial states relative to the  $ICL_{oed}$  after “drained” erosion over geological timescales in CBI clay

- For the downslope and upslope sections, the coefficient of earth pressure at rest  $K_0$ , defined as the ratio between the horizontal and the vertical effective stresses after the end of the erosion, decreases with depth, with very high values approaching passive failure at shallow depth (Figures 4-20 a, b).

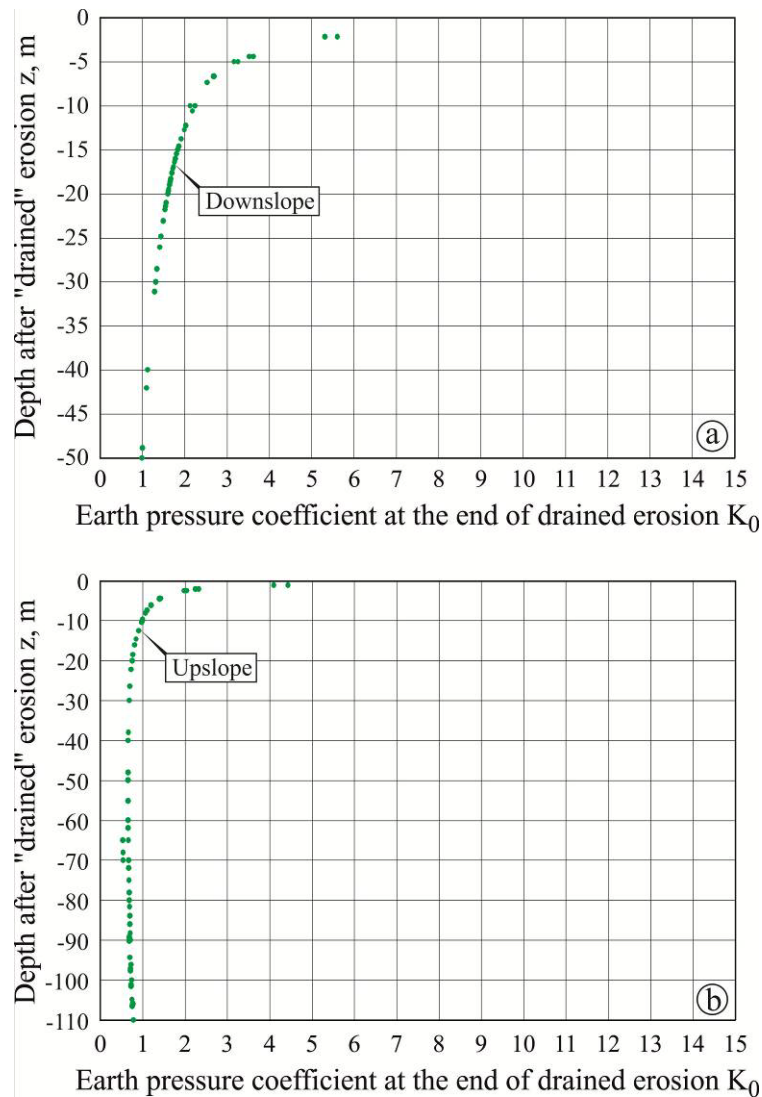


**Figure 4-20** - Case A1 – Numerically simulated  $K_0$  profiles after “drained” erosion over geological timescales in CBI clay: a) downslope; b) upslope

- For the downslope section, Figure 4-21 compares the effective stress envelopes at peak and at large strains obtained from numerically simulated drained triaxial tests in compression on materials “sampled” at 5 m and 35 m below ground level after erosion, isotropically consolidated at different mean effective stresses including those representative of conditions at the end of erosion. In both cases, both peak and large strain effective strength envelopes compare well with typical results for high plasticity clays (see for example Vaughan et al. 2004). The material sampled at 5 m exhibits lower peak effective strength envelopes, thus resulting, in conventional terms, more weathered.

It should be noted that, other things being equal, the degree and depth of “mechanical weathering” and of the corresponding decay of the peak strength envelope depend mainly on the flow rule (and its parameters which govern the development of plastic strains and the associated shrinking of the state boundary surface) and on the “brittleness” of the materials, i.e. the rate of strength reduction from  $\varphi_{cs}'$  to  $\varphi_{res}'$  as a function of deviatoric plastic strains. Differences in the flow rule and/or in the parameters and/or in the brittleness of the materials lead to different outcomes, as shown for example by comparing Figure 4-21 here with Figure 2-29a. This is particularly relevant, especially in unbonded materials, and results in the need for accurate calibration of the model parameters based on careful back-analysis of well targeted high quality laboratory tests, since it can affect the mechanism of failure predicted by the analysis, as described below.

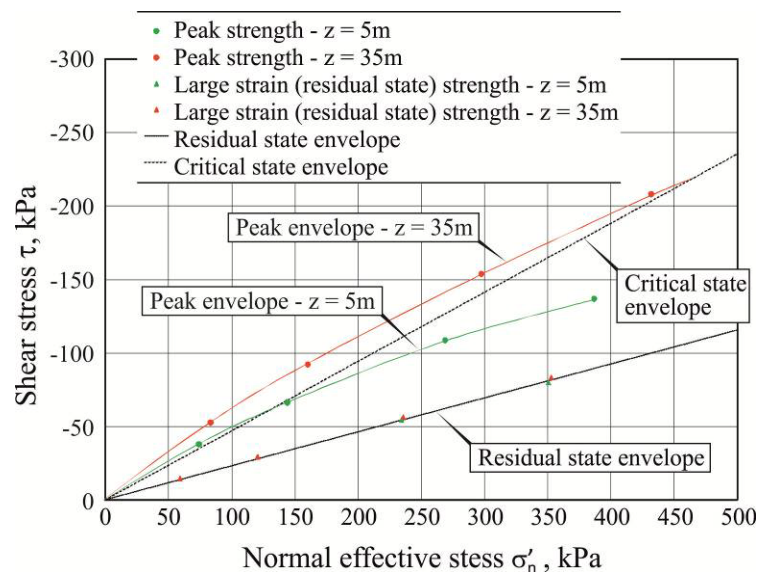


**Figure 4-21** - Case A1 – Numerically simulated effective stress envelopes from triaxial tests in compression on samples of CBI clay at different depths following “drained” erosion over geological timescales

The processes of delayed and progressive failure in unbonded materials are investigated in part 2 of the case A1 model under conditions characterized by sloping ground and initial states (void ratios, effective geostatic stresses, mechanical properties and coefficients of permeability) which vary spatially in the model as a result of the morphological changes induced by differential erosion at the geological timescale. These conditions are more realistic than considered in Section 2.

The analysis is carried out in the time domain under conditions of coupled consolidation. The mechanical boundary conditions are the same as used for the first part of the analysis; the model simulates the deepening and broadening of the valley. The vertical and the bottom boundaries of the model have been assumed to be impermeable.

The main results of part 2 of the analysis may be summarized as follows:

- Figures 4-22 a, b, c show the distribution of cumulative deviatoric plastic strains in the slope at  $t = 0$  years,  $t = 165$  years and  $t = 420$  years (failure) after basal erosion/excavation.

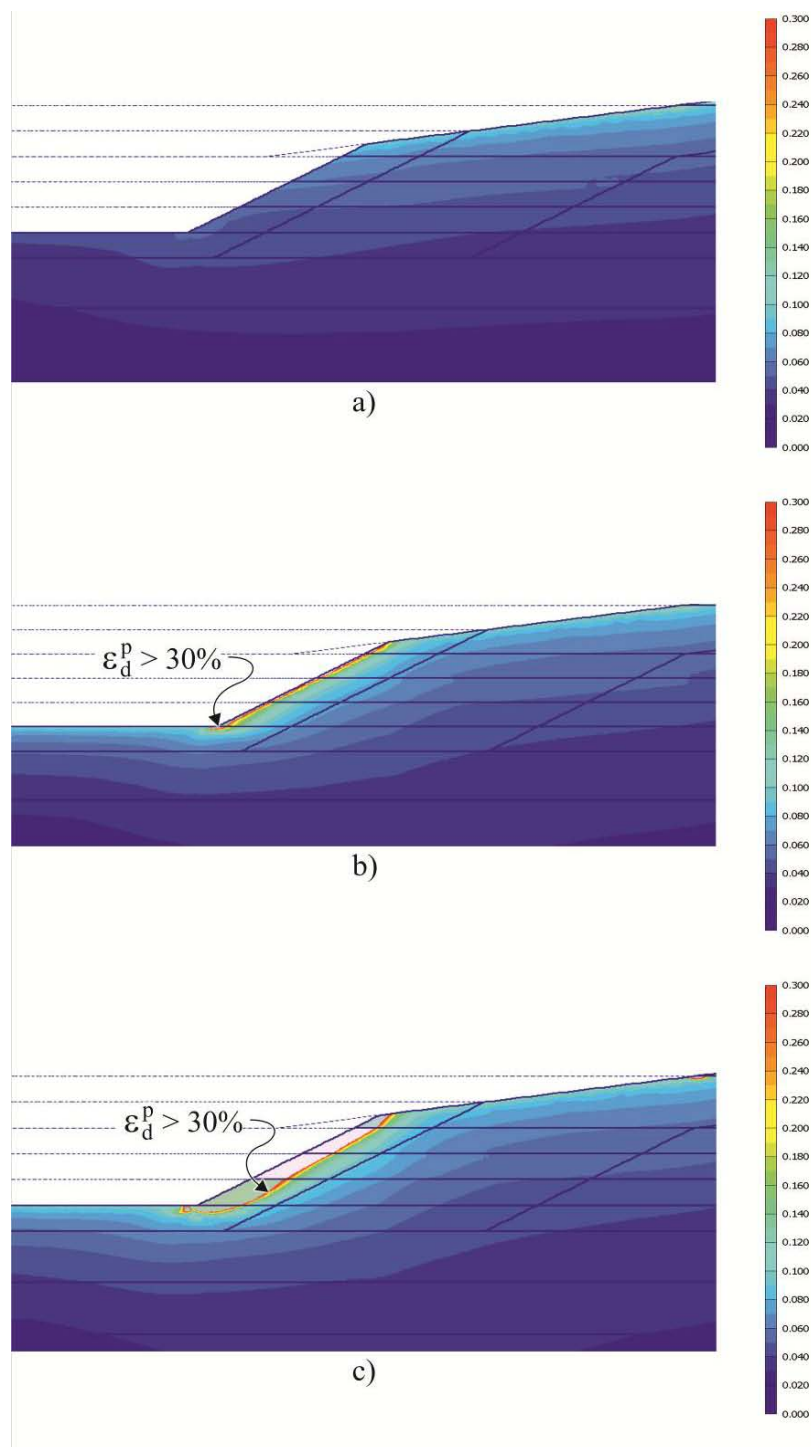


**Figure 4-22** - Case A1 – Numerically simulated distributions of cumulative deviatoric plastic strains at different times since rapid basal erosion or excavation in CB1 clay: a) at the end of rapid basal erosion or excavation; b) after 165 years; c) after 420 years

As a result of the absence of permeable layers in the profile, the negative excess pore pressures generated by the excavation are progressively dissipated and a “wetting front” penetrates into the slope from the ground surface, facilitated by the increase in permeability associated with the greater swelling at shallow depth. (Figures 4-23 a, b, c).

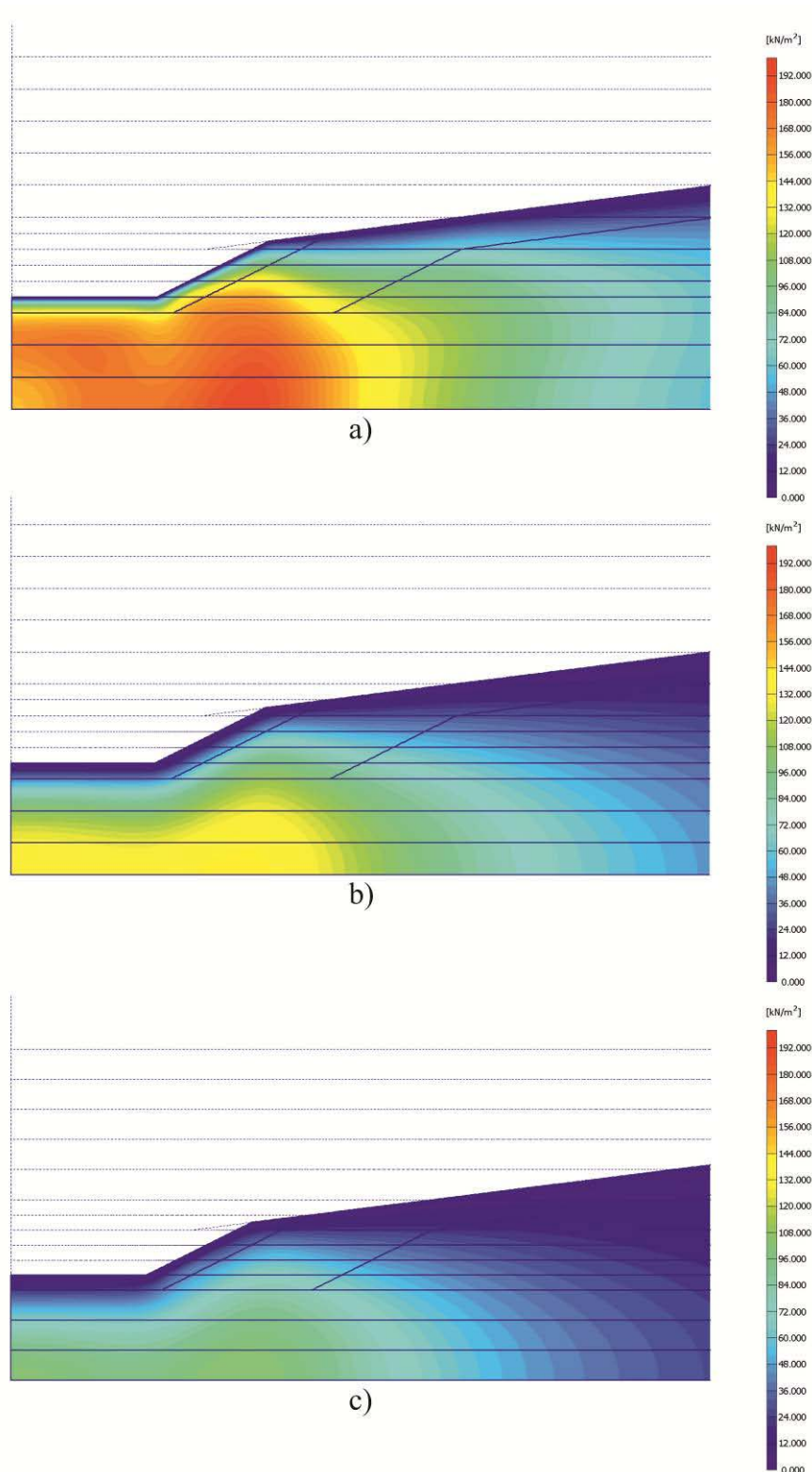


**Figure 4-23** - Case A1 – Numerically simulated distributions of excess pore pressures at different times since rapid basal erosion or excavation in CBI clay (positive values represent suctions): a) 10 years after rapid basal erosion or excavation; b) 165 years after rapid basal erosion or excavation ; c) 400 years after rapid basal erosion or excavation

As shown in Figure 4-24, the maximum suction in the clay deposit immediately after basal erosion or excavation is 250 kPa which is well within the maximum suction that can be sustained by the material, as discussed at point 4.2.1.

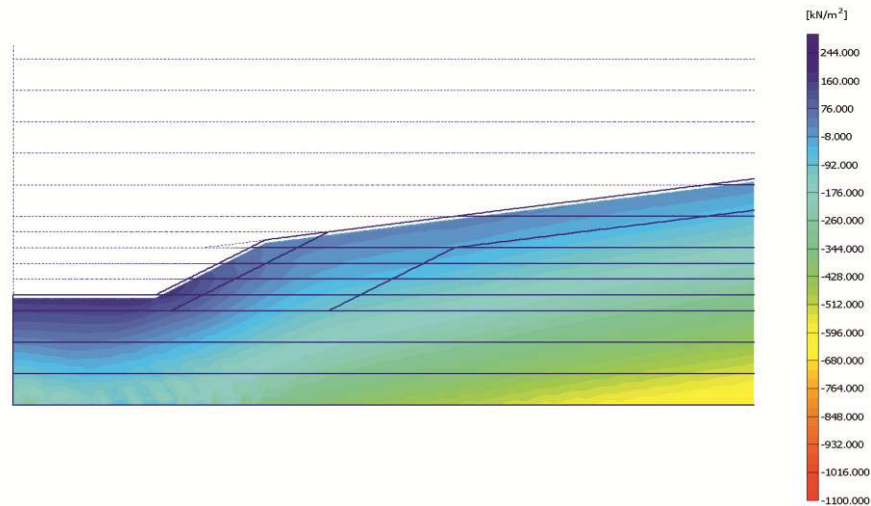


**Figure 4-24** - Case A1 – Numerically simulated distribution of pore pressures at the end of rapid basal erosion or excavation in CB1 clay (positive values represent suctions)

The high values of  $K_0$  at shallow depth and the relatively low peak strength envelope which is close to the angle of the toe scarp result in the development of a shallow but progressively thickening band of fully “softened” material at the scarp face. This type of development of the slope may be representative of the progressive exfoliation of denudated clay slopes where the material is directly exposed to prolonged wetting by weather without the benefit of the suction induced by vegetation and capillarity. Where wasting of material from the slope is not prevented, this process is continuously rejuvenated and results in a typical badland morphology (cárcavas in Spanish, calanchi in Italian) which is widespread in many areas in central and southern Italy (Figure 4-25).



**Figure 4-25** - Typical badland morphology in mechanically overconsolidated clays (cárcavas in Spanish, calanchi in Italian)

If the process is allowed to develop without rejuvenation by mass wasting, say by some form of surface facing, the “wetting front” will penetrate sufficiently into the slope to allow a “conventional” gross failure mechanism to form.

In the case considered here, “failure” occurs at  $t = 420$  years and involves a soil mass approximately 3 m thick.

The difference between the processes and mechanisms described above and those highlighted by example 2 of Section 2 are significant and worthy of close examination.

A deep seated failure was observed in that case, where even at shallow depth the clay had an effective strength envelope at small confining effective stresses well above the critical state line (Figure 2-29), much higher than here (Figure 4-21).

For a homogeneous soil profile, which of the two possible mechanisms will develop in a specific case will depend on the actual mechanical and mesostructural (fissuring) characteristics of the clay, the macrostructural (jointing) conditions of the deposit and the hydraulic boundary conditions.

- Figure 4-26 shows the horizontal displacements at 1/4, 1/2 and 3/4 height of the toe scarp, from basal erosion/excavation to failure. Figure 4-27 similarly shows the horizontal displacements at different distances (0, 2, 4, 6, 8 m) behind the exposed surface at mid-height of the toe scarp, from basal erosion/excavation to failure. Large pre-failure displacements are predicted by the analysis; however, only small relative displacements could be measured pre-failure over a timeframe of engineering interest, compared to typical system precision of most monitoring systems. The average rate of pre-failure horizontal displacement is approximately 3 mm/year.

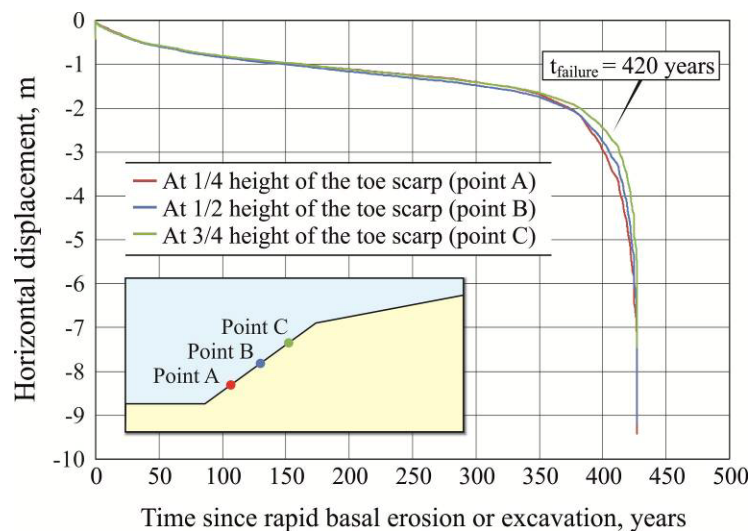


**Figure 4-26** - Case A1 – Numerically simulated horizontal displacements as a function of time since rapid basal erosion or excavation in CBI clay at different points on the “steep” scarp

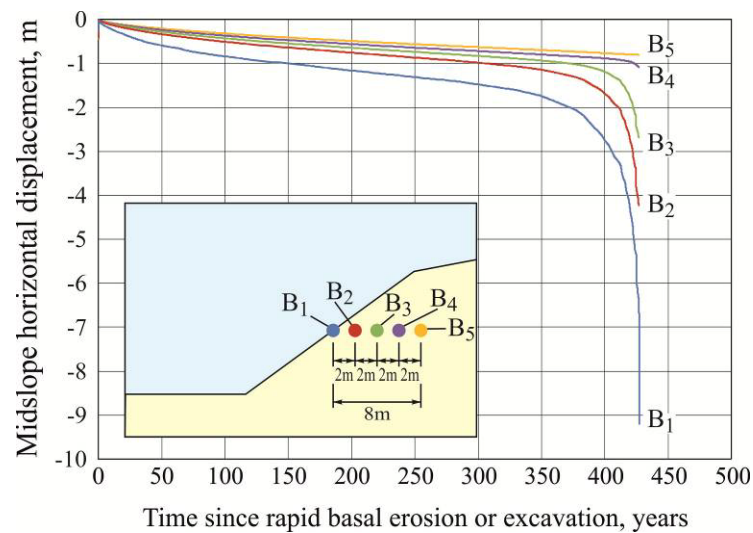


**Figure 4-27** - Case A1 – Numerically simulated horizontal displacements as a function of time since rapid basal erosion or excavation in CBI clay at different points along a section at midheight of the “steep” scarp

- Figures 4-28 a, b show the stress path of a clay element located near the failure surface at the toe of the scarp; the figures also shows the state boundary surface (S.B.S.) at different times, showing how it evolves as a result of the development of volumetric plastic strains, which govern  $p_c'$ , and of the change of the strength parameter  $M$  from critical state to residual values at high cumulative deviatoric plastic strains. Segment A-B represents the stress path during “drained” erosion over a geological timescale; segment B-C represents the stress path during rapid basal erosion/excavation; segment C-D represents the stress path during subsequent dissipation of excess pore pressures induced by basal erosion/excavation to failure; from C’-D the stress path is on and follows the current state boundary surface, approaching the critical state and the residual state from the “dry” side, which implies dilatant behaviour up to failure, as also evident in Figure 4-29 which shows locally generated negative excess pore pressures in the shear zone at the time of failure.



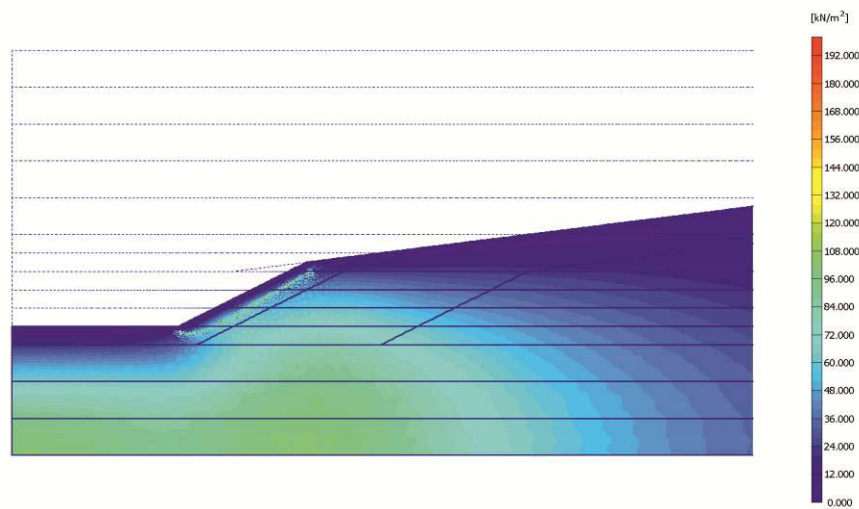


**Figure 4-29** - Case A1 – Numerically simulated distribution of excess pore pressures at  $t = 420$  years (failure) since rapid basal erosion or excavation in CBI clay (positive values represent suctions)

#### 4.2.5 Case A2

The model is similar to case A1 in all respects except for the presence of a 5 m thick dense sand layer mid-height in the steep scarp cut by basal erosion or excavation.

The sand layer is modelled using the widely used Hardening Soil Model (Schanz et al., 1999) and the parameters summarized in Table 4-5. As for the clay, the sand layer is assumed to be in a normally consolidated condition before the start of the “drained” erosion over a geological timescale.

**Table 4-5** - Parameters of the Hardening Soil Model for the sand layer

$\gamma_t$ ( $\text{kN/m}^3$ )	$\varphi'$ ( $^\circ$ )	$c'$ (kPa)	$\sigma_t$ (kPa)	$\psi$ ( $^\circ$ )	$E_{50}^{\text{Ref}}$ (MPa)	$E_{\text{oed}}^{\text{Ref}}$ (MPa)	$E_{\text{ur}}^{\text{Ref}}$ (MPa)	m (-)	$\nu'$ (-)	k (m/s)
20	40	20	0	3	50	50	150	0.55	0.2	$5 \times 10^{-5}$

$\gamma_t$  = natural unit weight  
 $\varphi'$  = angle of friction  
 $c'$  = apparent cohesion to account for non linearity of the effective strength envelope  
 $\sigma_t$  = tensile strength  
 $\psi$  = angle of dilatancy  
 $E_{50}^{\text{Ref}}$ ,  $E_{\text{oed}}^{\text{Ref}}$  = reference number of the Young's modulus in primary loading conditions  
 $E_{\text{ur}}^{\text{Ref}}$  = reference number of the Young's modulus in unloading-reloading conditions  
m = exponent of the Young's modulus  
 $\nu'$  = Poisson's ratio  
k = coefficient of permeability

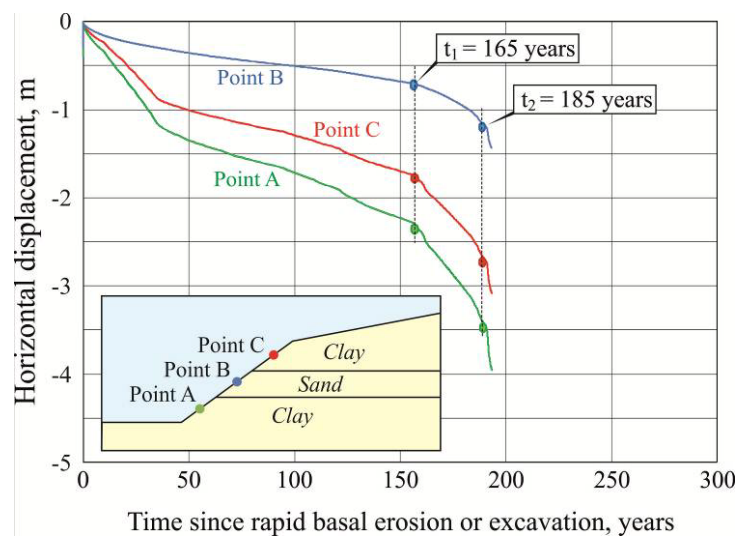
The main effect of the sand layer is to modify the hydraulic boundary conditions of the slope, since this layer is assumed to be fully drained at all times, both during initial erosion (like the clay) and during subsequent fast basal erosion or excavation. The piezometric levels in the

sand layer are in equilibrium with groundwater levels everywhere 1 m below the finished surface.

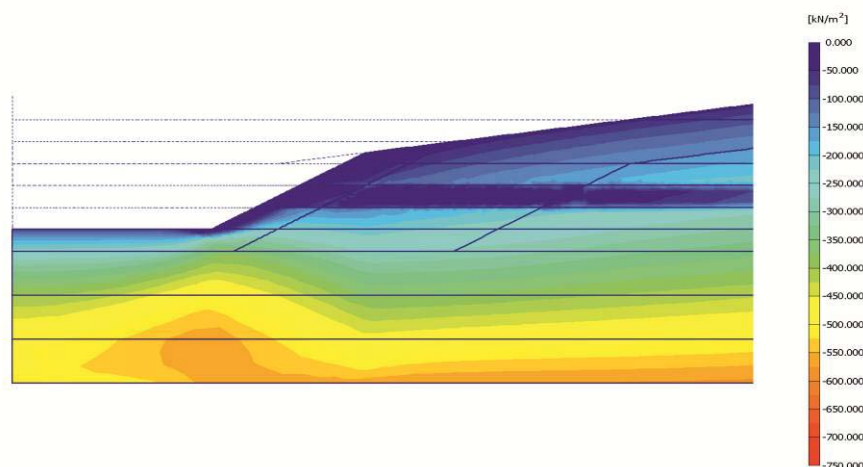
The presence of the sand layer allows a much more rapid neutralization of the negative excess pore pressures induced by basal erosion or excavation and introduces additional “wetting fronts”. This results in much faster failure of the slope and a significant modification of the mechanism of failure compared to case A1 with a homogeneous clay profile.

Figure 4-30 shows the horizontal displacements at 1/4 (in clay), 1/2 (in sand) and 3/4 (in clay) height of the toe scarp, from basal erosion/excavation to failure.

From the early stages of dissipation of the negative excess pore pressure, the horizontal displacements in the clay layers are much greater than in the sand, which consequently suffers a significant reduction in horizontal stresses at shallow depth, approaching total loss of confinement (see Figure 4-31).



**Figure 4-30** - Case A2 – Numerically simulated horizontal displacements as a function of time since rapid basal erosion or excavation at different points on the “steep” scarp including a sand layer at mid-height



**Figure 4-31** - Case A2 – Numerically simulated distributions of horizontal effective stresses at  $t = 165$  years since rapid basal erosion or excavation

Two critical points can be identified in the curves in Figure 4-30; at  $t_1 = 165$  years local failure mechanisms evolve in the clay layers above and below the sand, as may be seen in Figure 4-32, which shows the incremental shear strains in the slope at  $t_1 = 165$  years. At this stage the two mechanisms extend 3 to 4 m into the slope. Additionally, the presence of a ready source of water and the differential displacements between clay and sand result in high deviatoric plastic strains developing at the interface between the base of the upper clay layer and the sand, well beyond the failure surface.

Due to the low confining stresses and therefore the low strength in the sand, this is forced to adapt to the progressive deformation of the slope. As they develop, at  $t_2 = 185$  years the two mechanisms coalesce to form a single mechanism for the full height of the scarp. Global failure is thus reached much faster than for the homogeneous clay profile of case A1 (compare Figure 4-30 with Figure 4-26).

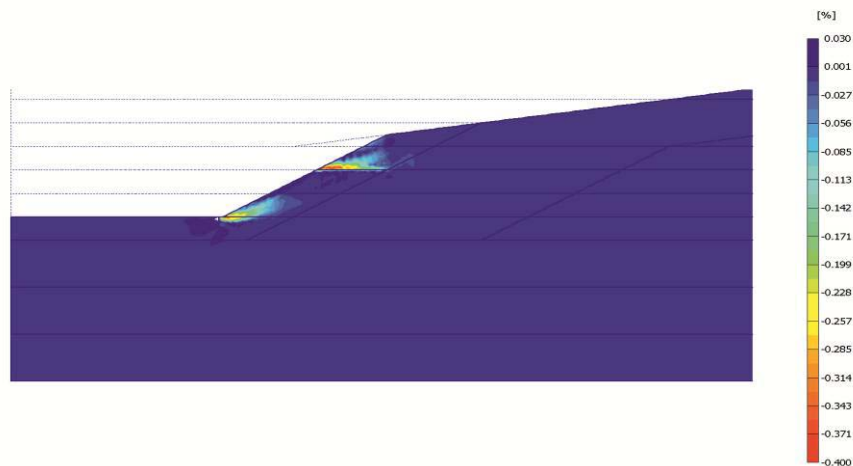


**Figure 4-32** - Case A2 – Numerically simulated distribution of incremental shear strains at  $t = 165$  years since rapid basal erosion or excavation

#### 4.2.6 Case A3

This model is similar to case A1 in all respects except for the presence of a 5 m thick marl layer mid-height in the steep slope cut by basal erosion or excavation. The marl layer is modelled using the Hardening Soil Model with parameters summarized in Table 4-6. As for the clay, the marl layer is assumed to be in a normally consolidated condition before the start of “drained” erosion over a geological timescale, the higher strength and stiffness being due to bonding developed between sedimentation and erosion.

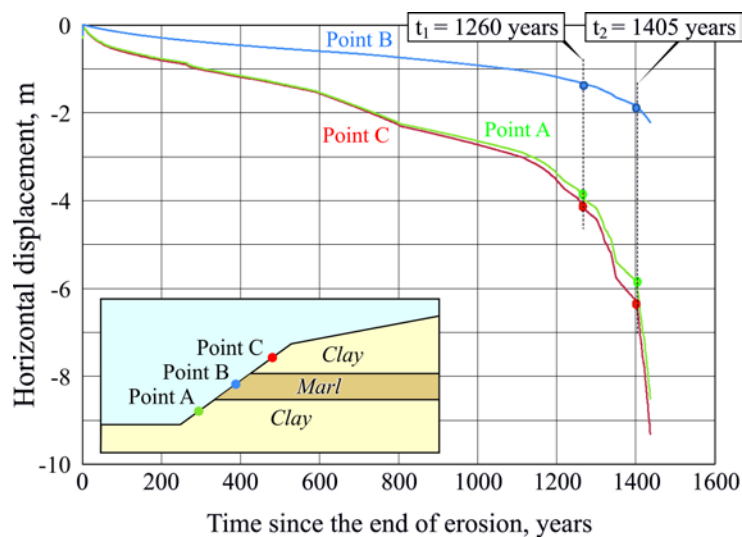
**Table 4-6 - Parameters of the Hardening Soil Model for the marl layer**

$\gamma_t$ (kN/m <sup>3</sup> )	$\phi'$ (°)	$c'$ (kPa)	$\sigma_t$ (kPa)	$\psi$ (°)	$E_{50}^{Ref}$ (MPa)	$E_{oed}^{Ref}$ (MPa)	$E_{ur}^{Ref}$ (MPa)	m	$\nu'$ (-)	k (m/s)
20	30	100	10	3	150	150	450	0.55	0.2	$1.5 \times 10^{-11}$

$\gamma_t$  = natural unit weight  
 $\phi'$  = angle of friction  
 $c'$  = cohesion  
 $\sigma_t$  = tensile strength  
 $\psi$  = angle of dilatancy  
 $E_{50}^{Ref}$ ;  $E_{50}^{Ref}$  = reference number of the Young's modulus in primary loading conditions  
 $E_{ur}^{Ref}$  = reference number of the Young's modulus in unloading-reloading conditions  
m = exponent of the Young's modulus  
 $\nu'$  = Poisson's ratio  
k = coefficient of permeability

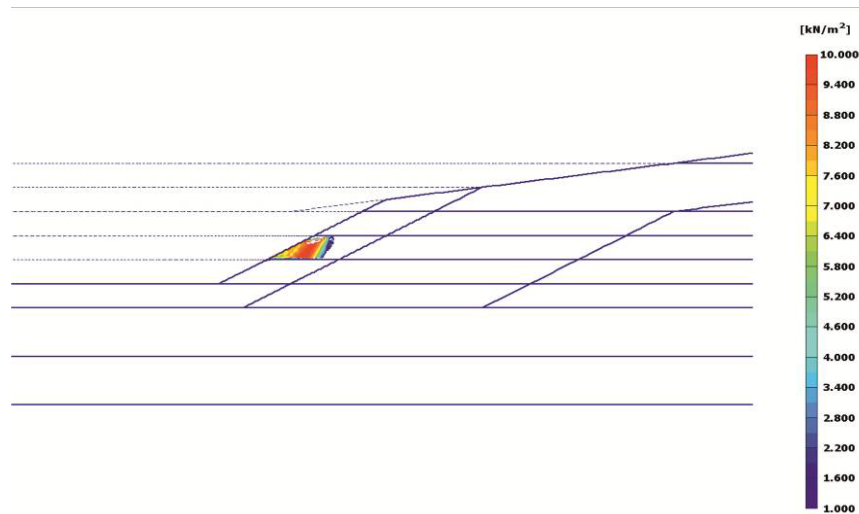
The main effect of the marl layer is to introduce a layer of similar permeability to the clay but with much higher stiffness. The marl layer acts as a reinforcement element in the slope, confining and retarding both swelling and subsequent failure compared to the case of homogeneous clay.

Figure 4-33 shows the horizontal displacements at 1/4 (in clay), 1/2 (in marl), 3/4 (in clay) height of the toe scarp, from basal erosion/excavation to failure.



**Figure 4-33 - Case A3 – Numerically simulated horizontal displacements as a function of time since rapid basal erosion or excavation at different points on the “steep” scarp**

From the early stages of dissipation of the negative excess pore pressures, the horizontal displacements in the clay layers are much greater than in the marl, which consequently suffers a significant reduction in horizontal stresses which become tensile at shallow depth (Figure 4-34).



**Figure 4-34** - Case A3 – Numerically simulated distribution of horizontal effective stresses at  $t = 1405$  years (failure) since rapid basal erosion or excavation (positive values represent tension)

As for case A2, two critical points can be identified in the curves in Figure 4-33. At  $t_1 = 1260$  years local failure mechanisms evolve in the clay layers above and below the marl as may be seen in Figure 4-35 which shows the incremental shear strains in the slope at  $t_1 = 1260$  years. At this stage the two mechanisms extend 3 to 4 m into the slope, as in case A2. However, notwithstanding the differential displacements between the upper clay and the marl, no localization is observed at the interface beyond the failure surface, presumably due to the lack of a ready source of water to neutralize the locally generated negative excess pore pressures resulting from the dilatant behaviour of the clay.

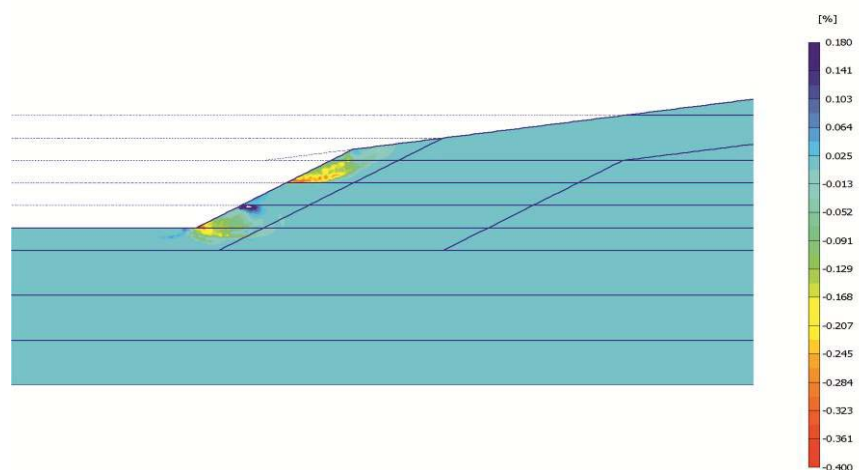


**Figure 4-35** - Case A3 – Numerically simulated distribution of incremental shear strains at  $t = 1260$  years since rapid basal erosion or excavation

Once the tensile strength of the marl is exceeded, at  $t_2 = 1400$  years the two local mechanisms coalesce into a single mechanism for the full height of the slope. Global failure is thus reached much slower than for the homogeneous clay profile of case A1 (compare Figure 4-33

with Figure 4-26), due to the reinforcing effect of the marl layer. In practice, additional phenomena, not modelled here, such as microstructural (debonding) and mesostructural/macrostructural (fissuring, jointing) effects in the marl, could be expected to reduce the tensile strength of this layer, with global failure occurring at some time intermediate between that indicated by the model for case A3 and that for the homogeneous soil profile of case A1.

The general pattern of behaviour and the failure mechanisms highlighted by the examples in Cases A2 and A3 are in line with observations of structural and bedding control on the failure mechanisms discussed, for example, by Bromhead and Ibsen (2007).

#### 4.2.7 Case B1

The objectives of the model are to simulate the following processes:

1. Starting from the end of the sedimentation of a saturated, unbonded, normally consolidated clayey deposit incorporating a 30 m thick layer of cemented coarse grained material, hereafter referred to as “conglomerate”, relatively fast formation by erosion of a complex morphology consisting of the complete removal of the top 150 m of clay material and the formation of a relatively steep (1V:1H) slope in the conglomerate and a gentler (1V:4H) 30 m high slope in the underlying clay deposit, for a maximum overall depth of erosion of 210 m (Figure 4-36).

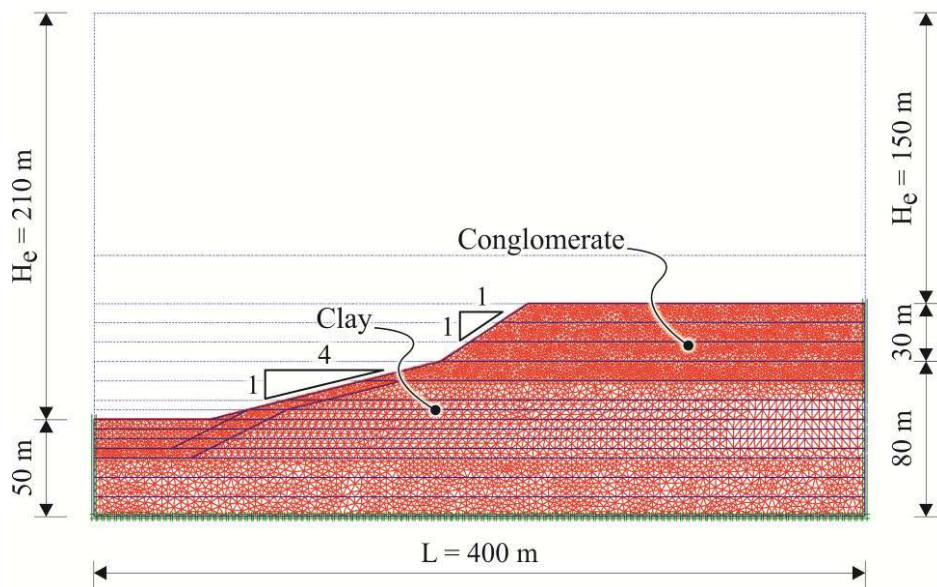


**Figure 4-36** - Case B – Finite element mesh for numerical simulation of complex slope formed by relatively fast erosion in CBI clay capped by conglomerate layer

The erosion is assumed to occur at a sufficiently fast rate to generate negative excess pore pressures in the clay deposit relative to the long term piezometric regime in hydrostatic equilibrium with a groundwater level everywhere at a depth of 1 m below the exposed surface of the clay or at the base of the conglomerate; in the specific case the rate of erosion has been set at 0.05 m/year such that the current configuration is reached in 4200 years.

2. After the erosion is terminated, evolution of the displacements and stability conditions of the slope in response to the progressive dissipation of excess pore pressures and to the associated "mechanical weathering", including the degradation of the strength envelope from peak to the critical and residual states as a result of the development of volumetric and deviatoric plastic strains.

The analysis has been carried out under coupled consolidation conditions in the time domain. The vertical and bottom boundaries of the model have been assumed to be impermeable. Considering the mechanical boundary conditions (no horizontal movements on the vertical boundaries, implying symmetry), the geometry of the model is representative of a symmetrical valley. No horizontal and vertical displacements are allowed at the base of the model, 50 m below the bottom of the valley.

The conglomerate has been modelled with an elasto-plastic constitutive model with a Mohr-Coulomb failure criterion and the parameters summarized in Table 4-7.

**Table 4-7 - Parameters of the elasto-plastic (Mohr-Coulomb) model for the conglomerate layer**

$\gamma_t$ (kN/m <sup>3</sup> )	$\phi'$ (°)	$c'$ (kPa)	$\sigma_t$ (kPa)	$\psi$ (°)	$E'$ (MPa)	$\nu'$ (-)	$k$ (m/s)
20	38	50	10	3	3400	0.2	$1 \times 10^{-5}$
$\gamma_t$ = natural unit weight $\phi'$ = angle of friction $c'$ = cohesion $\sigma_t$ = tensile strength $\psi$ = angle of dilatancy $E'$ = Young's modulus $\nu'$ = Poisson's ratio $k$ = coefficient of permeability							

The main results of the analysis at the end of the erosion phase may be summarized as follows:

- The distribution of negative excess pore pressures in the clay deposit at the end of the erosion phase is shown in Figure 4-37. Figures 4-38 a, b show the resulting profiles of pore pressures as would be measured at the two locations A and B shown in Figure 4-37.

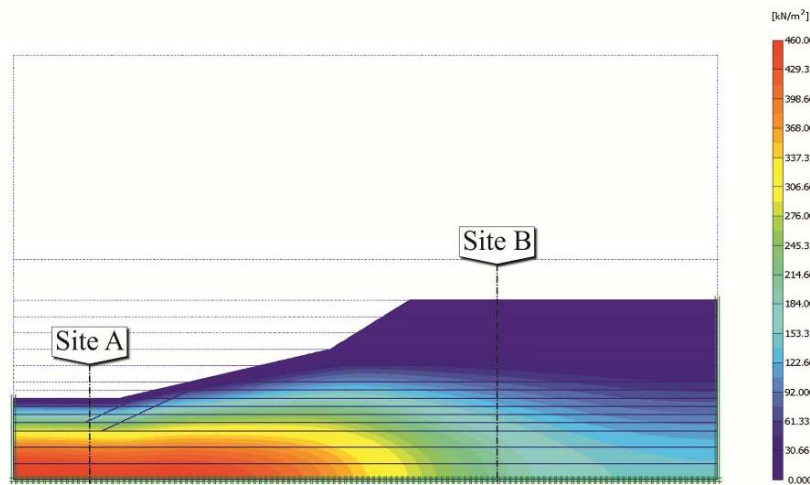


**Figure 4-37 - Case B1 – Numerically simulated distribution of excess pore pressures at the end of erosion**

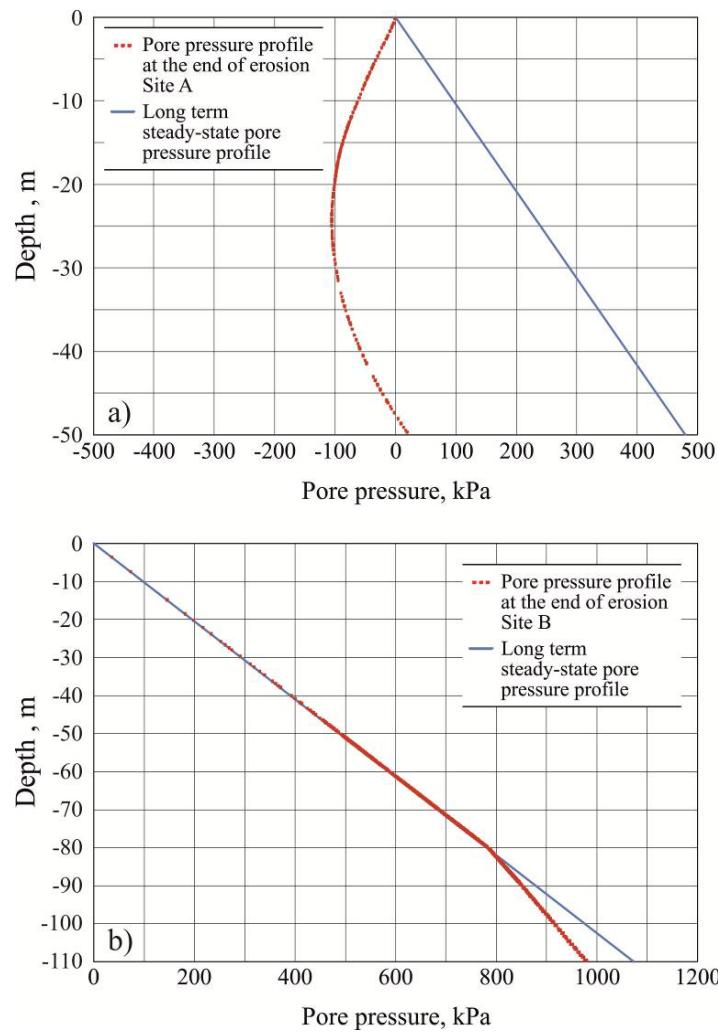


**Figure 4-38 - Case B1 – Numerically simulated pore pressure profiles at the end of erosion: a) Site A and b) Site B of Figure 4-37.**

- The slope angle in the clay is too steep to be sustained in the long term in drained conditions. Nevertheless, there is no sign of actual or incipient instability at the end of the erosion phase, thanks to the negative excess pore pressures in the clay deposit.
- The whole deposit undergoes significant vertical and horizontal displacements during erosion. Both the maximum vertical (Figure 4-39) and horizontal (Figure 4-40) displacements occur in the clay slope.

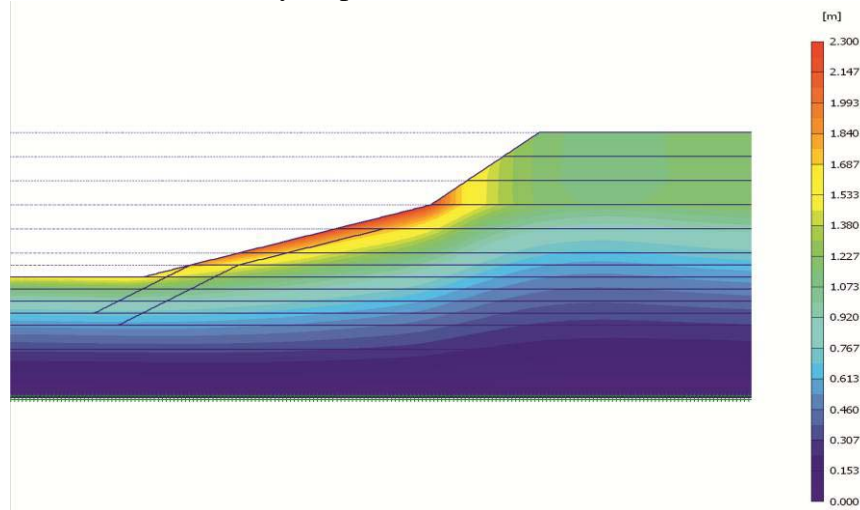


**Figure 4-39** - Case B1 – Numerically simulated distribution of vertical displacements at the end of erosion

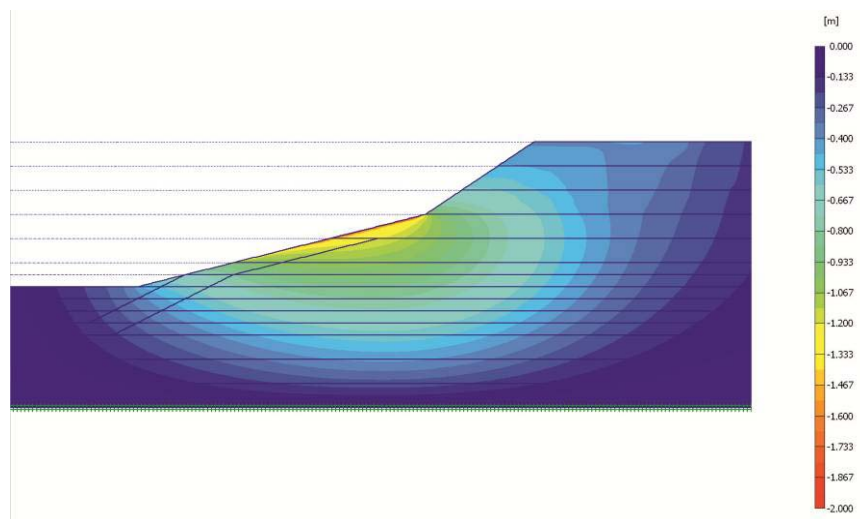


**Figure 4-40** - Case B1 – Numerically simulated distribution of horizontal displacements at the end of erosion

It is particularly interesting to note that the horizontal displacements of the conglomerate are much less than those of the clay just below, which appears to “squeeze” out of the slope (see Figures 4-41 and 4-42) and, in so doing it, subjects the conglomerate to significant extension, which results in tensile stresses in the model and the formation of joints parallel to the crest of the slope in practice.

The interaction of vertical and horizontal displacements at the valley side results in the conglomerate deforming with a localized depression forming behind a raised lip on the edge of the valley, as shown in Figure 4-43.

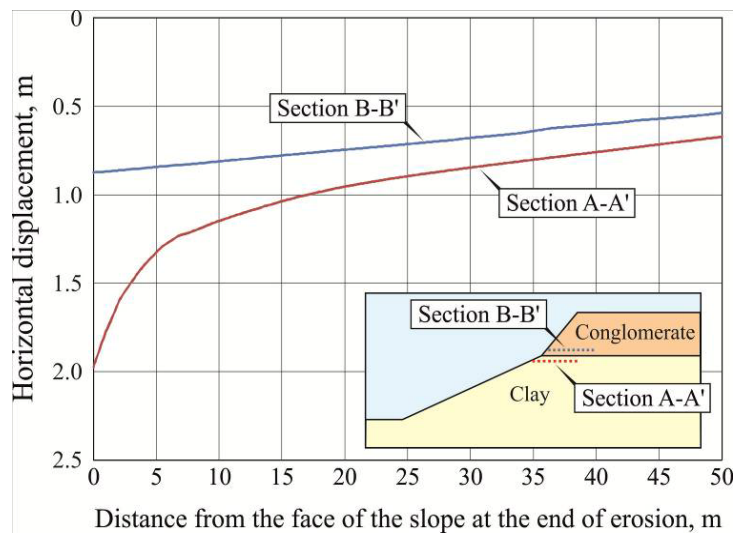


**Figure 4-41** - Case B1 – Numerically simulated horizontal displacements just above and just below the conglomerate/clay interface at the end of erosion

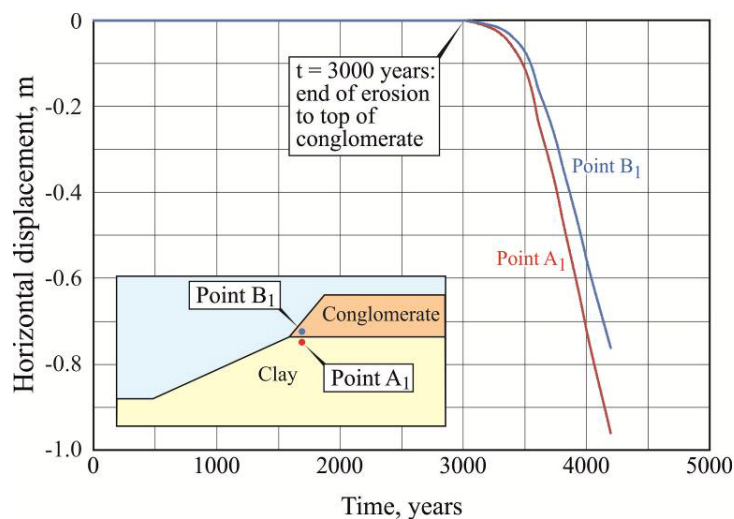


**Figure 4-42** - Case B1 – Numerically simulated horizontal displacements as a function of time during erosion at two points just above and just below the conglomerate/clay interface

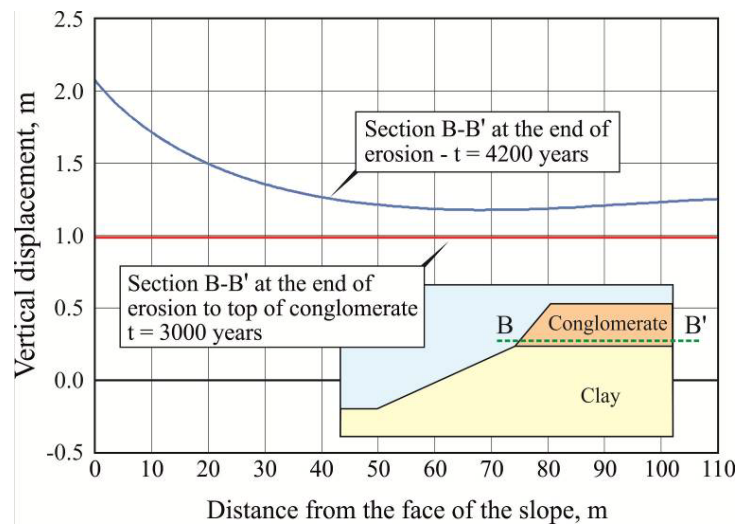


**Figure 4-43** - Case B1 – Numerically simulated vertical displacements just above the conglomerate/clay interface during and at the end of erosion

The main results of the analysis after the erosion phase may be summarized as follows:

- The negative excess pore pressures generated by the erosion are progressively dissipated, with a “wetting front” propagating into the slope from the ground surface, as for case A1.
- Failure occurs in the clay 2200 years after the end of erosion. The failure mechanism involves the entire portion of the slope in clay, nucleating and propagating from the toe, as may be seen in Figure 4-44 which shows a concentration of incremental shear strains in this area at failure.

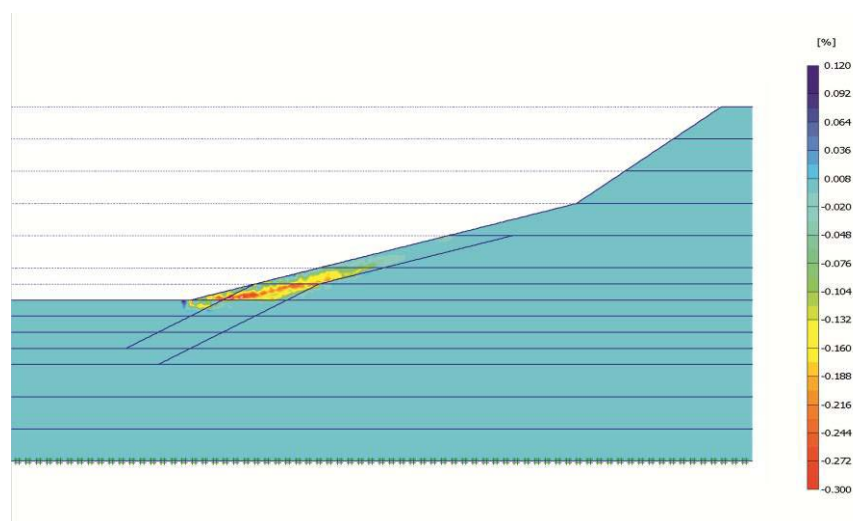


**Figure 4-44** - Case B1 – Numerically simulated distribution of incremental shear strains at  $t = 2200$  years (failure) after the end of erosion

- Figure 4-45 shows the horizontal displacements at the toe and midheight of the clay slope, from the end of the erosion to failure; larger displacements are observed at the toe, both prefailure and at failure, providing further confirmation that this is where failure nucleates.

The average rate of prefailure horizontal displacements is 1 mm/year at the toe and approximately 0.4 to 0.5 mm/year at midheight.

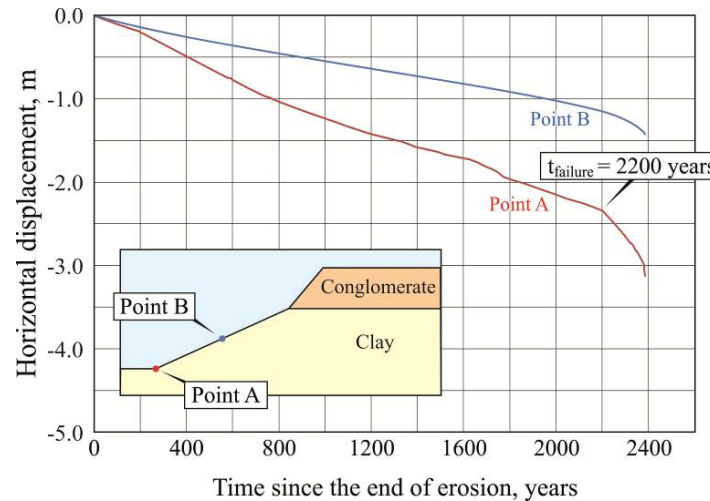


**Figure 4-45** - Case B1 – Numerically simulated horizontal displacements as a function of time since the end of erosion at the toe and mid-height of the slope in CBI clay

- Figure 4-46 shows the horizontal displacements of two points located just above and just below the interface between the conglomerate and the clay, from the end of the erosion to failure. The clay is shown to continue to squeeze out from under the conglomerate, following the same trend already observed before the end of the erosion (Figure 4-42).

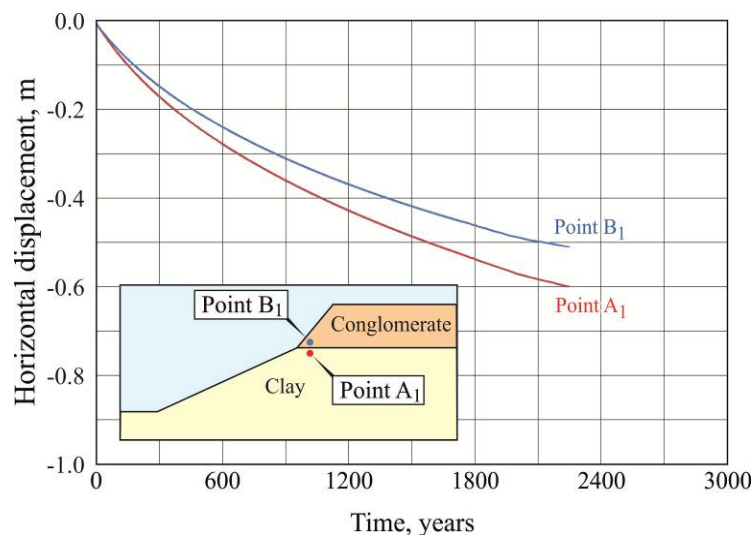


**Figure 4-46** - Case B1 – Numerically simulated horizontal displacements as a function of time since the end of erosion at two points just above and just below the conglomerate/clay interface

- Figure 4-47 shows the vertical displacements of the conglomerate at the time of failure in the clay slope below. The same pattern of displacement occurs as noted at the end of erosion, with the outer lip continuing to rise at an approximate rate of 0.1 mm/year, while the depression behind deepens slightly. If similar movements were reflected at the top of the conglomerate, they could be interpreted erroneously as backward rigid rotation due to deep seated sliding, while in reality the conglomerate is not yet directly involved in the failure mechanisms, at this stage.

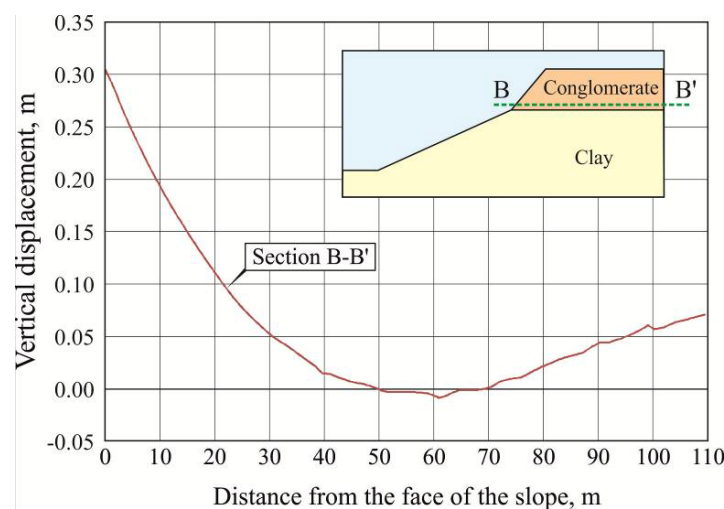


**Figure 4-47** - Case B1 – Numerically simulated vertical displacements just above the conglomerate/clay interface at the time of failure in the clay slope below

The general pattern of behaviour described above in terms of pore pressure profiles and horizontal and vertical displacements compares with the behaviour actually measured or predicted under similar stratigraphic and hydraulic conditions for other, albeit different, heavily overconsolidated scaly clay deposit at Bisaccia, as reported by Fenelli & Picarelli (1990), Picarelli & Urcioli (1993), Di Nocera et al. (1995), Picarelli (2007), Picarelli (2009).

#### 4.2.8 Case B2

Case B2 is in every respect similar to case B1, except for the presence of a 5 m thick layer of dense sand, 5 to 10 m below the base of the valley formed at the end of the erosion. The characteristics of the sand are the same as already described for case A2. This layer is considered fully “drained” at all times with piezometric levels in hydraulic equilibrium with groundwater levels everywhere at a depth of 1 m below the exposed surface of the clay or at the base of the conglomerate.

The presence of the sand layer results in lower negative excess pore pressures at the end of the erosion (Figure 4-48) compared to case B1 with homogeneous clay profile (Figure 4-37).

The failure mechanism (Figure 4-49) is the same as for case B1, but failure is reached much faster, 850 years after the end of erosion, due to the faster dissipation of negative excess pore pressures, both during erosion and thereafter, as shown by comparing Figure 4-50 with Figure 4-45.

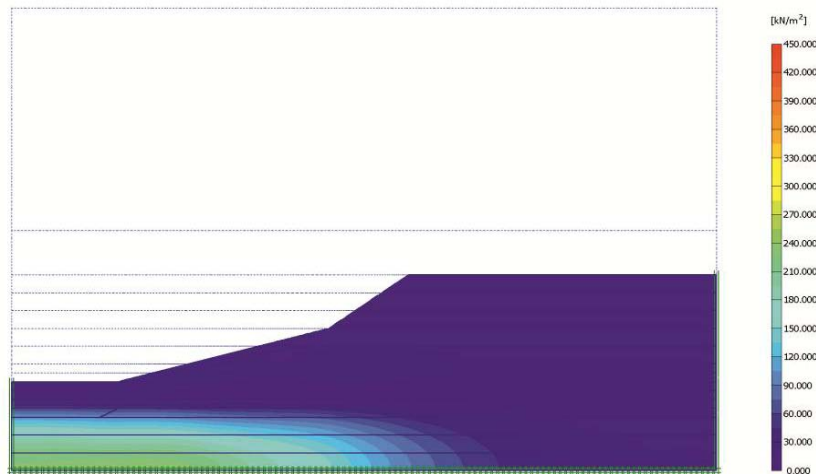


**Figure 4-49** - Case B2 - Numerically simulated distribution of excess pore pressures at the end of erosion

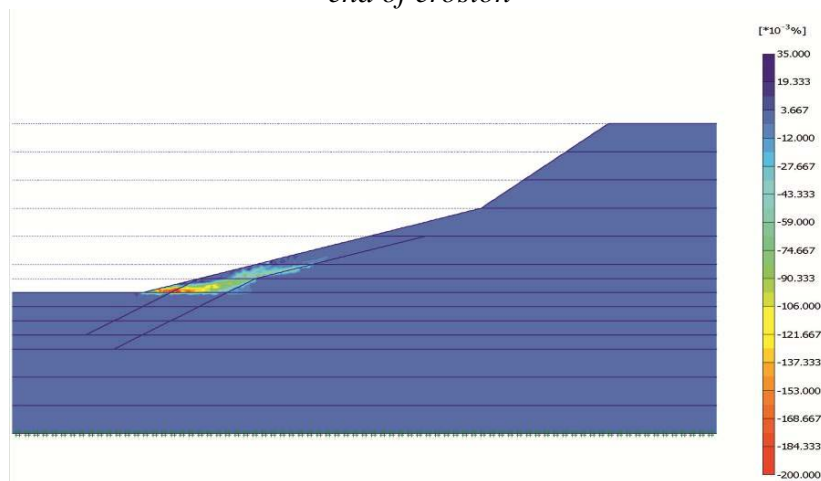


**Figure 4-49** - Case B2 – Numerically simulated distribution of incremental shear strains at  $t = 850$  years (failure) after the end of erosion

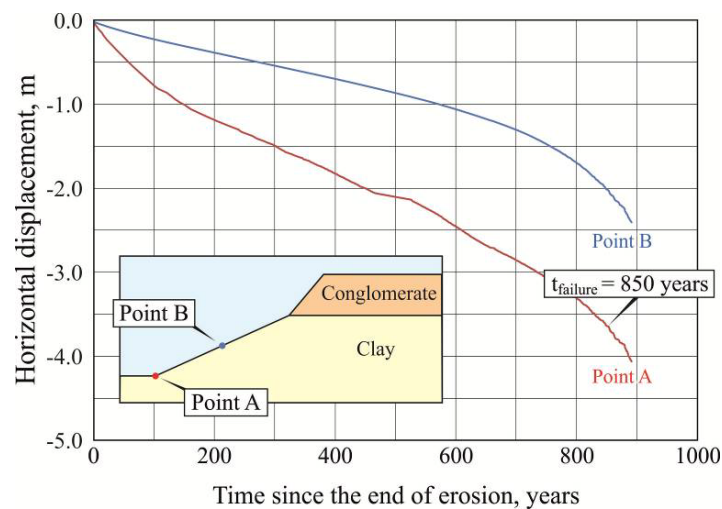


**Figure 4-50** - Case B2 – Numerically simulated horizontal displacements as a function of time since the end of erosion at the toe and mid-height of the slope in CB1 clay

The type of failure mechanisms shown for the Cases B1 and B2 indicates the likely further evolution of the slope. The failed mass of clay will slide along the basal surface as a quasi-rigid body, accumulating at the toe of the slope and exposing a steep rear scarp just below and possibly undermining the top slab of conglomerate.

The top scarp and the overlying slab, which has been jointed and broken up by the previous extension will then fail and collapse onto the clay slope below.

Riverine or marine erosion and removal of the slide debris from the toe area will rejuvenate the process which will tend to propagate backwards, progressively demolishing the top slab until equilibrium is reached, often in geological timescales; the final equilibrium will depend, inter alia, on the rate of erosion at the toe.

Even where equilibrium is reached, reactivation may be induced by transient changes in hydrogeological conditions, particularly where the clay deposits are interbedded with coarse grained, more permeable layers where artesian conditions may occur, and/or by slight local modification to the profile, for example by engineering works.

A dramatic example of the potential significance and impact of these mechanisms is provided by the case of Civita di Bagnoregio, between Viterbo and Orvieto (Central Italy), which has been studied in detail within Subproject no. 23 on “Guidelines for the Safeguard of Cultural Heritage against Natural Risk” of the IUGS-UNESCO Project no. 425 on “Landslide Hazard Assessment and Mitigation for Cultural Heritage Sites and Other Locations of High Societal Value”. This medieval town (Figure 4-51) is located atop a hill capped by approximately 70 m of soft tuff rocks overlying a layer of overconsolidated, saturated blue clay of plio-pleistocene of the type considered above, approximately 300 m thick (Figure 4-52).



*Figure 4-51 - Civita di Bagnoregio (VT, Italy). General view*

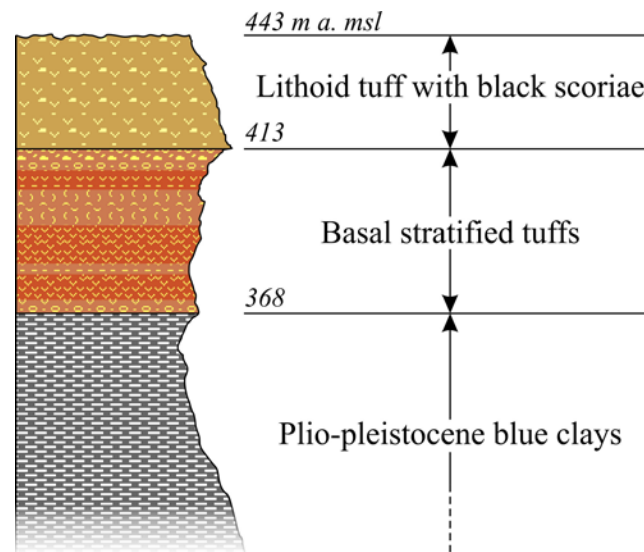


**Figure 4-52** - Civita di Bagnoregio (VT, Italy). Soil profile (after Delmonaco et al., 2003).

Erosion of the tuff cover has exposed the underlying clay to weathering which has resulted in the formation of typical badland morphology, dominated by denudated clay slopes, small gullies and ravines (calanchi) continuously rejuvenated by erosion as discussed above, flows and to a lesser extent small rotational slides, while the cliffs in the relict tuff cover are affected by falls. Landsliding has resulted in a slow but incessant reduction of the hilltop, finally causing the town to be abandoned in favour of a new town built in modern times on a nearby hill.

In line with the mechanisms predicted by the models presented above for cases B1 and B2, the causes of instability in the area have been attributed phenomenologically to a number of causes, originated by the erosion operated by the main water courses and propagating to the valley sides and finally to the overlying tuff cover, as summarized below and in Figure 4-53 (Delmonaco et al., 2003):

1. continued erosion of the stream beds;
2. decay of the geotechnical characteristics of the clays exposed to weathering, for a maximum thickness of 5 to 10 m, with a marked decay in the top 0.5 to 1m;
3. formation of mud flows in the top 0.5 to 1 m of the clay following intense rainfall; the removal of the surficial material results in the weathering of new portions of clay;
4. intense surface erosion due to meteorological agents;
5. deformation of the basal clays following weathering, which induces deformations in the overlying pyroclastic formation
6. ignition of fracturing in the pyroclastic formation due to lack of lateral restraint;
7. opening of existing joints and fractures in the compact pyroclastic formation due to (transient) hydrostatic pressure in the joints and initiation of falls;

The infiltration of rainwater into the fractured pyroclastic cover determines the formation of a perched watertable at the contact with the underlying clayey formation, with several localized

springs which favour the swelling and the mechanical degradation of the surficial layers of clay and consequently the undermining of the pyroclastic cover, initiating falls.

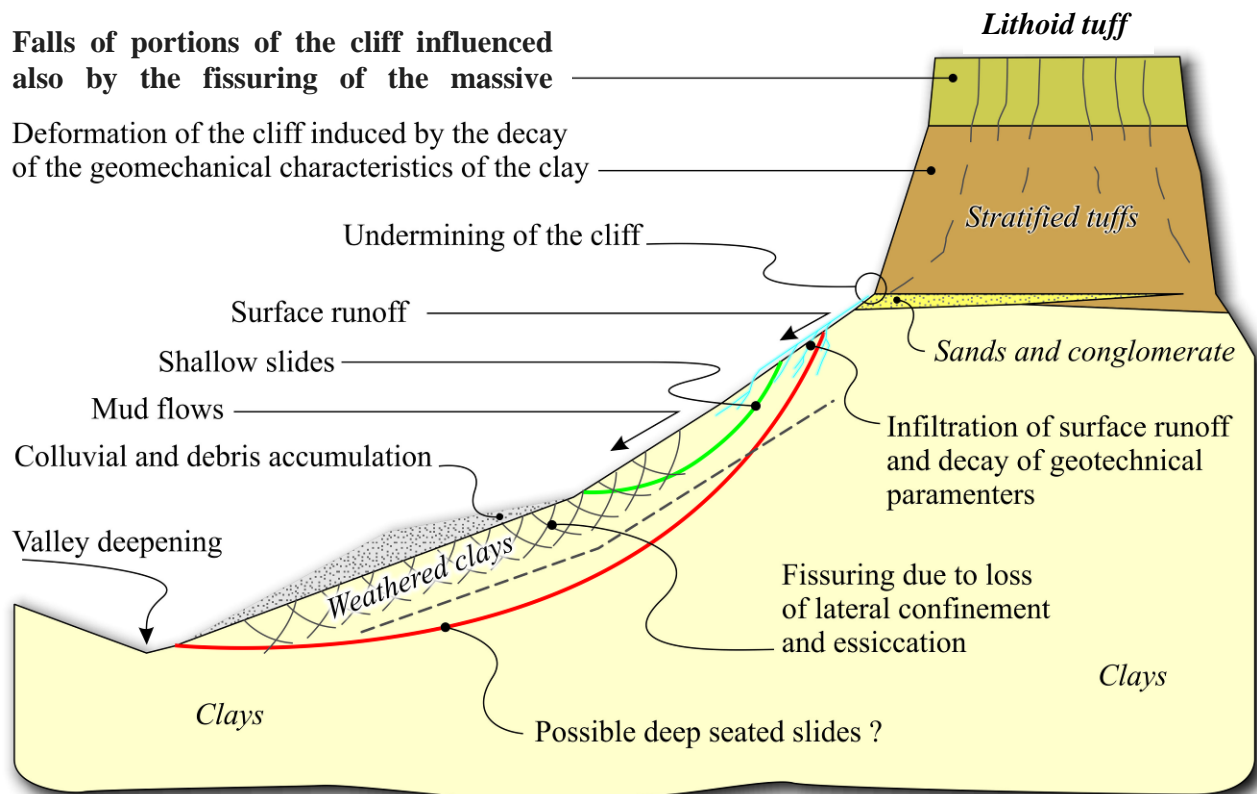


**Figure 4-53** - Civita di Bagnoregio (VT, Italy). Typical section and observed landslide mechanisms (after Delmonaco et al., 2003).

#### 4.2.9 Final remarks

The results presented above confirm the strong dependence of the slope behaviour on local details such as variations in permeability and/or stiffness within an otherwise homogeneous profile. Local details can have a strong impact on the pattern of pre-failure deformations, the time to failure, the type, shape and brittleness of the failure, all of which have a significant effect on the quantification of the hazard.

While reactivations of previous movements occur along relatively well defined pre-existing failure surfaces and at relatively well controlled and predictable mechanical parameters, first time movements involve much more complex processes, which can be modelled with some degree of realism only by the type of analysis presented above (Vaughan et al., 2004).

The depth and scale of sliding depend on several factors. In mechanically overconsolidated, unbonded, saturated plastic clays, where “weathering” progresses from the surface as a result of progressive dissipation of negative pore pressures, shallow mechanisms may prevail. The greater resilience to mechanical weathering of bonded clays prevents the formation of relatively shallow mechanisms, allowing the dissipation of the negative pore pressures to

proceed further before failure occurs at greater depth. Other significant factors include the rate and geometry of erosion, the “brittleness” of the materials (i.e. the rate of strength reduction from critical state to residual state conditions) and the presence and nature of structural “anomalies” (fissuring, jointing) in the deposit.

The models and results presented above refer to specific assumptions and parameters, without any pretence of generality; different results would have been obtained if the models had considered different assumptions.

The insight provided by this type of analyses corroborates the need for a multidisciplinary approach to the study of slope movements, involving expertise in geology, hydrogeology, geomorphology and geotechnical engineering.

This type of analysis may be used also as part of an iterative process to design and evaluate detailed investigation and monitoring of slopes; on one hand, it provides a guideline for the type of information that is necessary to define the geological/geotechnical model and to characterize in detail the geotechnical behaviour of the soils involved; on the other hand, and to even greater potential advantage, it can provide useful guidance on the optimal type and location of monitoring equipment and a framework for the rational evaluation of the results, also with regard to the accuracy and precision which are necessary in relation to the anticipated behaviour.

## 5 EARTHQUAKES (AUTH)

### 5.1 INTRODUCTION

The destructive impact of earthquakes can be greatly enhanced by the induced triggering of landslides during or after the shaking. Strong earthquakes can potentially trigger landslides that can induce catastrophic losses in terms of human lives and infrastructure damage. According to Wen et al., 2004, around 20% of the registered landslides are triggered by earthquakes. IN particular, China is the country characterized by significant casualties associated to slides triggered by earthquakes (Leroueil, 2001) and many seismic active countries around the world present records of slope failures causing tremendous damages and casualties. Seven case histories of earthquake induced landslides in different lithological and geomorphological settings and scales are described in the following, describing some of the most prominent seismically induced landslides in terms of direct and indirect losses: Las Colinas landslide from El Salvador, the Higashi-Takezawa, Naranoki, Musikame slides, the Tangjiashan landslide from Wenchuan, China. Two additional case histories from Italy have been included (the Calitri and Corniglio landslides), which although not so devastating as the previous ones, present particular interest for the European context. An overview of the selected case histories is presented in Table 5-1.

### 5.2 GENERAL CLASSIFICATION OF EARTHQUAKE TRIGGERED LANDSLIDES

Keefer (Keefer 1984; Keefer 2002), on the basis of the principles and terminology by Varnes (1978), classified the earthquake triggered landslides into three main categories on the basis of type of material, landslide movement, degree of internal disruption of the landslide mass and geologic environment (see Table 5-2):

**Category I:** Disrupted Landslides, which occur fast and at high inclinations ( $>35^\circ$ ) in discontinuous rock masses or weakly cemented materials.

**Category II:** Coherent Landslides either in rock or soil with deep slip weakened surfaces or with a relatively broad distributed shear zone, reported for inclinations  $>15^\circ$

**Category III:** Lateral Spreads and flows slides, associated to liquefaction in granular materials; if residual strengths are lower than static shear stresses, flow slides can develop at very low inclinations.

Three types of disrupted landslides – i.e. rock falls, disrupted soil slides, and rock slides - were found to be the most abundant, comprising about 80 percent of the earthquake induced landslides reported in Keefer (2002). Rodriguez and co-workers (Rodriguez et al, 1999) summarize the typical geometric characteristics of some of the most common slide categories.

**Table 5-1 – Selected landslide case histories**

ID	Site	Country	Location	Landslide Category	Triggering mechanism
1	Las Colinas landslide	El Salvador	Santa Tecla	flow (Cat. III)	earthquake
2	Higashi-Takezawa slide	Japan	Niigata-ken Chuetsu	flow (Cat. III)	earthquake
3	Naranoki slide	Japan	Niigata-ken Chuetsu	debris slide (Cat. I)	earthquake
4	Musikame slide	Japan	Niigata-ken Chuetsu	flow (Cat. III)	earthquake
5	Calitri landslide	Italy	Irpinia	flow (Cat. III)	earthquake
6	Corniglio Landslide	Italy	Apennines	earthslide (Cat. II)	earthquake+ intense rainfall
7	Tangjiashan landslide	China	Wenchuan	rockslide (Cat. I)	earthquake

(Table 5-3) including ranges of depth to the slip surface and the geometry of the slide in terms of the aspect ratio and the shape of the slip surface.

According to Keefer’s classification of earthquake-induced landslides, which are still the most comprehensive one, the selected case studies covering the three main Categories are: Las Colinas, Higashi-Takezawa, Musikame and Calitri slides belong to Cat. III, Naranoki and Tangjiashan landslides belong to Cat. I, while Corniglio belongs to Cat. II (see Table 5-1).

### 5.3 PARAMETERS AFFECTING SEISMIC SLOPE STABILITY

The most important parameters affecting seismic slope stability are:

1. physical, mechanical and dynamic properties of the ground;
2. geometry of the slope;
3. characteristics of shaking primarily related to Mw, R, local ground conditions and topographic effects.

#### 5.3.1 Ground Properties

There is a possibility of delayed initiation or reactivation of landslide movement subject to ground shaking, especially in coherent materials, associated with the potential reduction of the in situ shear strength (residual strength) and the variation of groundwater conditions (seismically induced pore pressures build-up). As an example, this was the case of the Irpinia earthquake occurred in Italy (M= 6.9), where several large earth flows and other coherent slides began their movement after from few hours to few days after the main shock. The post-earthquake movement of these landslides was inferred to be caused by the increased spring flow and pore-water pressures regime, associated with the tectonic deformation of the interested area (Keefer, 2002). Shear strain softening of soil materials, which can be related in its effectiveness to the number of (equivalent uniform) excitation cycles N, result to the degradation of the stiffness and strength properties of the soils: it may be considered as one of the major causes of most of the slides induced by earthquakes (Ishihara 1996).

**Table 5-2 - Characteristics of earthquake-induced landslides (Keefer, 2002).**

Name	Type of movement	Internal disruption	Water content D U P S S	Typical depths	Minimum slope (°)	Typical velocities	Typical volumes	Typical displacements
<b>Disrupted landslides</b>								
Rock falls	Bouncing, rolling, free fall	High or very high	× × × × ×	Shallow	40	Extremely rapid	Most less than $1 \times 10^4 \text{ m}^3$ ; maximum reported $2 \times 10^7 \text{ m}^3$	May fall to base of steep source slope and move as far as several tens or hundreds of meters farther, on relatively gentle slopes
Disrupted rock slides	Translational sliding	High	× × × × ×	Shallow	35	Rapid to very rapid	Most less than $1 \times 10^4 \text{ m}^3$ ; maximum reported $2 \times 10^9 \text{ m}^3$	May slide to base of steep source slope and several tens or hundreds of meters farther, on relatively gentle slopes
Rock avalanches	Complex, involving sliding, flow, and occasionally free fall	Very high	× × × × ×	Deep	25	Very rapid to extremely rapid	$5 \times 10^5$ – $2 \times 10^8 \text{ m}^3$ or more	Several kilometers
Soil falls	Bouncing, rolling, free fall	High or very high	× × × × ×	Shallow	40	Extremely rapid	Most less than $1,000 \text{ m}^3$ ; maximum volumes not well documented	Most come to rest at or near bases of steep source slopes
Disrupted soil slides	Translational sliding	High	× × × × ×	Shallow	15	Moderate to rapid	Most less than $1 \times 10^4 \text{ m}^3$ ; maximum reported $4.8 \times 10^7 \text{ m}^3$	May slide to base of steep source slope and several tens or hundreds of meters farther, on relatively gentle slopes
Soil avalanches	Complex, involving sliding, flow, and occasionally free fall	Very high	× × × × ×	Shallow	25	Very rapid to extremely rapid	Volumes not well documented; maximum reported $1.5 \times 10^8 \text{ m}^3$	Several tens of meters to several kilometers beyond steep source slopes
<b>Coherent landslides</b>								
Rock slumps	Rotational sliding	Slight or moderate	? × × × ×	Deep	15	Slow to rapid	Most between 100 and a few million $\text{m}^3$ ; maximum at least tens of millions of $\text{m}^3$	Typically less than 10 m; occasionally 100 m or more
Rock block slides	Translational sliding	Slight or moderate	? × × × ×	Deep	15	Slow to rapid	Most between 100 and a few million $\text{m}^3$ ; maximum at least tens of millions of $\text{m}^3$	Typically less than 100 m; maximum displacements not well documented
Soil slumps	Rotational sliding	Slight or moderate	? × × × ×	Deep	7	Slow to rapid	Most between 100 and $1 \times 10^5 \text{ m}^3$ ; occasionally $1 \times 10^5$ to several million $\text{m}^3$	Typically less than 10 m; occasionally 100 m or more
Soil block slides	Translational sliding	Slight or moderate	? × × × ×	Deep	5	Slow to very rapid	Most between 100 and $1 \times 10^5 \text{ m}^3$ ; maximum reported $1.12 \times 10^8 \text{ m}^3$	Typically less than 100 m; maximum displacements not well documented
Slow earth flows	Translational sliding and internal flow	Slight	× × × × ×	Generally shallow; occasionally deep	10	Very slow to moderate; occasionally, with very rapid surges	Most between 100 and $1 \times 10^6 \text{ m}^3$ ; maximum reported between $3 \times 10^7$ and $6 \times 10^7 \text{ m}^3$	Typically less than 100 m; maximum displacements not well documented

**Table 5-2 (Continued) - Characteristics of earthquake-induced landslides (Keefer, 2002).**

Continued									
Name	Type of movement	Internal disruption	Water content D U PS S	Typical depths	Minimum slope (°)	Typical velocities	Typical volumes	Typical displacements	
Lateral spreads and flows									
Soil lateral spreads	Translation on fluid basal zone	Generally moderate; occasionally slight or high	× ×	Variable	0.3	Very rapid	Most between 100 and 1 × 10 <sup>5</sup> m <sup>3</sup> ; largest reported 9.6 × 10 <sup>6</sup> m <sup>3</sup> .	Typically less than 10 m; maximum reported 600 m	
Rapid soil flows	Flow	Very high	? ? ? ×	Shallow	2.3	Very rapid to extremely rapid	Volumes not well documented; largest are at least several million m <sup>3</sup> .	A few m to several km	
Subaqueous landslides	Generally lateral spreading or flow; occasionally sliding	Generally high or very high; occasionally moderate or slight	× ×	Variable	0.5	Generally rapid to extremely rapid; occasionally slow to moderate	Volumes not well documented; largest are at least tens of millions of m <sup>3</sup> .	Not well documented, but some move more than 1 km	

\* Notes: Names: "rock" signifies bedrock that is relatively firm and intact prior to landslide initiation, and "soil" signifies loose, unconsolidated or poorly cemented aggregates of particles that may or may not contain organic materials. Internal disruption: "slight" signifies landslide consists of one or a few coherent blocks; "moderate" signifies several coherent blocks; "high" signifies numerous small blocks and individual soil grains and rock fragments; "very high" signifies nearly complete disaggregation into individual soil grains or small rock fragments. Depth: shallow signifies generally < 3 m deep; deep signifies generally > 3 m deep. Water content: D = dry; U = moist but unsaturated; PS = partly saturated; S = saturated. Velocity: very slow = 1 × 10<sup>-6</sup>-3 × 10<sup>-6</sup> m/min; slow = 3 × 10<sup>-6</sup>-3 × 10<sup>-5</sup> m/min; moderate = 3 × 10<sup>-5</sup>-0.001 m/min; rapid = 0.001-0.3 m/min; very rapid = 0.3-180 m/min; extremely rapid = >180 m/min. (Terminology after Varnes, 1978).

**Table 5-3 - Geometry of earthquake-induced landslides (Rodríguez et al, 1999).**

Slide type	Slide depth (m)	Slide shape factor ( $d/L$ ) <sup>a</sup>	Slip surface shape
Rock falls	3–5, depending on discontinuities spacing	= 0.15, only one data reported	Planar on outward dipping discontinuities
Disrupted rock slides	(No representative data)	(No representative data)	Predominantly planar, but other shapes were also reported
Coherent rock slides	20–50, given by geological features, such as weakness zones	0.08–0.10, apparent relationship with ground shaking	Circular or planar on outward dipping discontinuities
Disrupted soil slides	3–100, depending on geological setting	0.005–0.3, apparently dependent on ground shaking	Predominantly complex mechanism (rotational–translational), single mechanisms commonly planar
Coherent soil slides	6–50, apparently dependent on ground shaking	0.04–0.3, apparently dependent on ground shaking	Circular
Soil spreads and flows	6–40, depending on the ground shaking	0.007–0.20, depending on geological setting	Predominantly planar, some circular cases also reported

<sup>a</sup> ( $d/L$  = depth/length ratio)

A comprehensive overview of the dynamic strength characteristics of granular and cohesive soils playing a role in the slope seismic stability and relate induced displacements, may be found in Ishihara (1996), and Pitilakis (2010, in Greek).

### 5.3.2 Size of landslides

The size of landslides induced by an earthquake can be related not only to the earthquake magnitude and intensity, but also to the relation between slope aspect and ground shaking intensity during the strong motion phase (Li, 1978 in Wen et al, 2004). In terms of size, there seems to be no difference between earthquake and rainfall triggered landslides. However, in terms of lithology earthquake-induced landslides are recognized to be prevalent in stratified competent rocks in which slip surfaces generally occur along cross-bedding joints (Wen et al, 2004).

### 5.3.3 Shaking characteristics

#### Magnitude

According to Keefer (Keefer 1984; Keefer, 2002), approximate magnitudes of the smallest earthquakes likely to cause landslides of various types are:

- ~4.0 for rock falls, rock slides, soil falls and disrupted soil slides
- ~4.5 for soil slumps and soil block slides;
- ~5.0 for soil lateral spreads, rapid soil flows, subaqueous landslides, rock slumps, rock block slides, and slow earth flows;
- ~6.0 for rock avalanches; and
- ~6.5 for soil avalanches.

Smaller earthquake events can occasionally trigger landslides in correlation with non seismic causes. Hence, if a slope is in a marginally stable state, even a weak earthquake ( $M < 4$ ) can trigger the landslide mass movement.

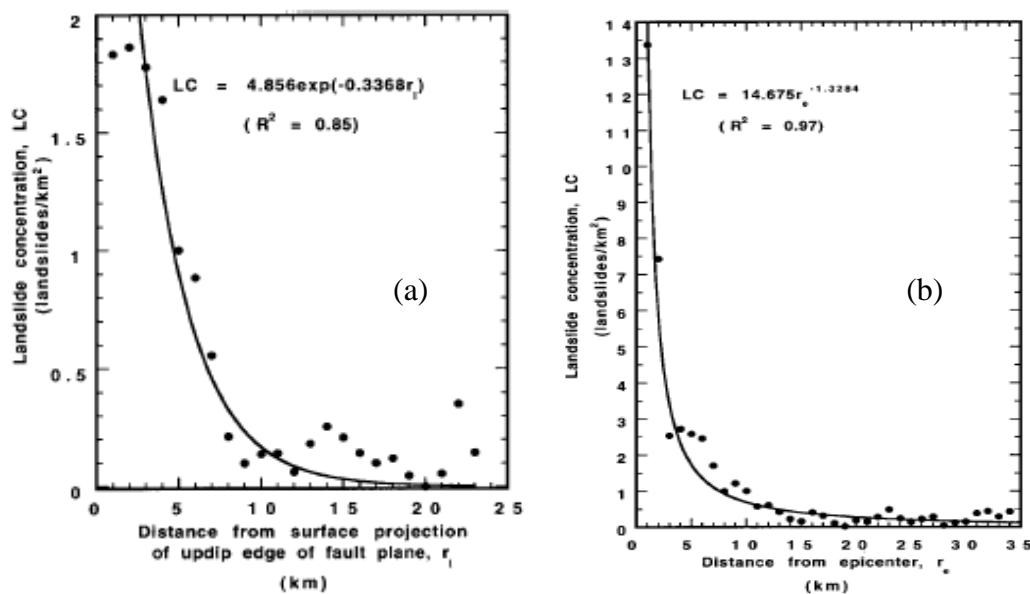


**Figure 5-1** - Relation of landslide concentration to the distance from the surface projection of the updip edge of the fault plane (a) and to the epicentral distance (b) for landslides in the southern Santa Cruz Mountains triggered by the 1989 Loma Prieta, California, earthquake (Keefer, 2002)

#### Epicentral Distance

Statistical analysis of the landslide distribution showed a strong correlation between landslide concentration, on the one hand, and distance from the epicenter, distance from the fault rupture, and slope inclination, on the other (Keefer, 2000). Landslide abundance showed an exponential decrease with increasing distance from the fault-rupture zone (Figure 5-1-a) but not with increasing epicentral distance (Figure 5-1-b) (Keefer, 2002).

#### Topographic amplification

The specific properties and geometrical features of the soil deposits can modify the characteristics (amplitude, frequency content and duration) of the travelling wave field, generating extra amplification (aggravation factor in the seismic input characteristics), attenuation or tensional effects in the ground influencing the deformation and, eventually, ground failure. Material damping, the impedance contrast between sediments and the underlying bedrock, and the characteristics of incident wavefield are considered to represent the governing factors for site amplification (Kramer and Stewart, 2004; Pitilakis, 2004). A fundamental period of the earthquake close to the natural period of the site can lead to resonance phenomena and, consequently, to an amplified energy content of the ground motion. Combining a low-frequency seismic input motion together with a resonance phenomenon in the low-frequency range, the slope failure potential assumes its highest values (Bourdeau et al., 2004).

Topographic irregularities can considerably affect the amplitude and frequency content of ground motions. In the case of hills or slopes this can be related to the triggering forces acting upon them, since amplified surface accelerations behind the crest may present larger destabilizing forces, potentially causing higher landslide risk. Amplification of both horizontal and vertical ground motion components normally takes place over a narrow zone

near the crest of the slope. This is due, among other factors, to the diffraction at the surface irregularities and surface wave generation: it can be observed both in the time domain (as an increase in the maximum observed amplitude near the crest, with respect to the maximum observed amplitude of the free-field) as well as in the frequency domain (as a spectral amplification over a narrow band of frequencies corresponding to wavelengths similar to the horizontal dimension of the slope) (Ktenidou, 2010).

While landslides triggered by precipitation are generally distributed uniformly along the slopes, landslides triggered by earthquakes tend to be clustered near ridge crests and hill slope toes. Densmore and Hovius (2000) in Wen-Fei Peng and co-workers (2009) attributed this ridge-crest clustering to topographic effects (as described above), and the clustering at hill slope toes to dynamic pore-pressure changes in the water-saturated material of lower hill slopes.

## **5.4 METHODS TO ESTIMATE SEISMIC SLOPE DISPLACEMENTS**

The stability of slopes subjected to earthquake loading can be evaluated by using several methods. Traditionally, in the common practice, the seismic slope stability is estimated by means of pseudo-static approaches, using linear or equivalent linear methods, or by using displacement based methods originated by the landmark works of Newmark (1965) and Makdisi and Seed (1978). The former methods express the stability of the slope in terms of an overall safety factor (SF) or safety margin (SM), while the calculated co-seismic displacement from the latter procedures, whether the procedure is simplified or advanced, shall be viewed more appropriately as an index of the seismic performance of the slope. The most recent approaches to calculate analytically the seismically induced slope deformation may be found in Bray and Travarsarou (2007) and Bray (2007). An overview of the different methods is given in Argyroudis and co-workers (2006).

Advanced stress-deformation analyses using appropriate numerical tools (continuum or discontinuum mechanics numerical approach) are becoming more and more attractive, as they can provide approximate solutions to problems which otherwise cannot be solved by conventional methods e.g. the complex geometry, material anisotropy, non-linear behavior, in situ stresses. However, apart from the complexity of such analyses, their main disadvantage is that they can only be used for specific case studies and not for parametric analyses aiming to evaluate the landslide risk at regional and even local scale.

## **5.5 EXAMPLES**

### **5.5.1 Las Colinas landslide caused by the 2001 El Salvador earthquake**

On 13 January 2001, an earthquake occurred off the coast of El Salvador (Central America), about 110 km S-SE of the capital San Salvador. The source parameters for this earthquake, as obtained by different agencies (Konagai et al, 2009), are given in Table 5-4.

The earthquake caused widespread damage to buildings and infrastructure due to ground shaking and earthquake-induced ground failures, including several large-scale landslides. The most tragic among them (and one of the most destructive landslides ever recorded so far) was the Las Colinas one, occurred on the steep northern flank of the Bálsamo Ridge, involving a total volume 183,500 m<sup>3</sup> of stratified volcanic deposits (Crosta et al., 2004c). Once triggered, the landslide developed into a flowslide, traveling northward an abnormally long distance of about 700 m into the Las Colinas neighborhood of Santa Tecla. It covered hundreds of residential houses, resulting in about 500 casualties.

The 13 January 2001 earthquake was well recorded by three accelerograph networks operating in El Salvador. For the Las Colinas landslide, the recording site of interest is named Santa Tecla, which was located about 83 km from the epicenter and about 1 km away from the landslide site. The time histories of the recorded motions along NS, EW and UD directions are shown in Figure 5-2-a, while the acceleration response spectra for 5% damping are illustrated in Figure 5-2-b (Konagai et al, 2009). The recorded PHGA exceeded 700 gals, an extremely high acceleration (corresponding to about 0.7g).

The failure mode of the Las Colinas landslide (Figure 5-3) was recognized as generally rotational in the upper part of the slope, and translational in the middle and lower portions. Extensive cracking was observed on the ridge crest in areas that did not slide, causing additional concern to the inhabitants and authorities.

The section involved in the slide is about 80m wide, with a depth of about 20m at the rotational part. As shown in Figures 3 and 4, the failure surface can be roughly divided into three zones.

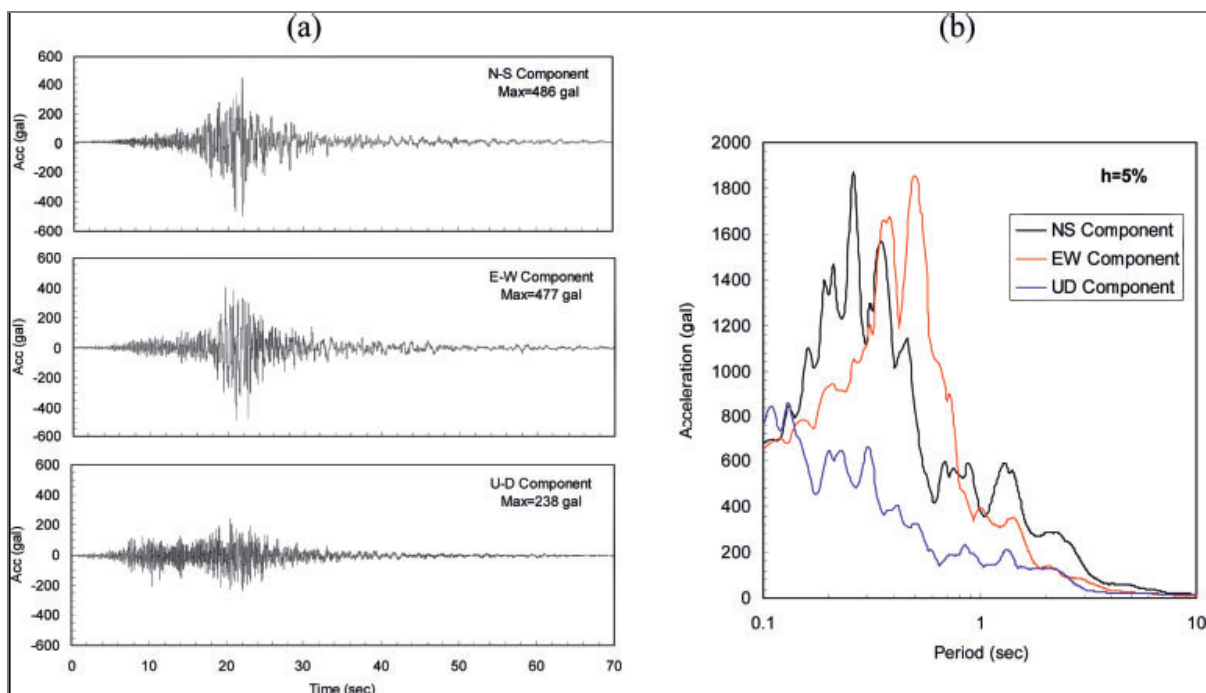


**Figure 5- 2** - (a) Acceleration records at Santa Tecla (original record from UCA, 2001; (b) Acceleration response spectra for 5% damping. Note: 1g =980 gal (Konagai et al, 2009).

**Table 5-4** - Source parameters of the 13 January 2001 El Salvador earthquake (Konagai et al, 2009).

Time (UTC)	Epicenter		Depth (km)	Magnitudes	Agency
	N°	W°			
17:33:32	13.049	88.660	60	$M_w = 7.7, M_s = 7.8, m_b = 6.4$	NEIC
17:33:46	12.97	89.13	56	$M_w = 7.7, M_s = 7.8, m_b = 6.4$	HRV
17:33:30	12.868	88.767	60	$M_w = 7.7$	CASC
17:33:31	12.8	88.8	60	$M_w = 7.6$	ERI

The uppermost zone (Zone 1) is a hollow of about 100 m in diameter, which was caved in some 10–20m from the original ground surface. North beyond the hollow, there appears a steepest zone (Zone 2) which becomes gradually gentle as it comes close to the toe (Zone 3). The inclination of the slope is about 26 degrees above the elevation of 960 m in Zone 2, and is about 9 degrees below the level in Zone 3.

The cross-section of the slope is shown in Figure 5-5. Four main geological strata in the slope section can be recognized: (1) pyroclasts, consisting of the ash layers known as Tierra Blanca, consolidated lapili and pumice layers; (2) brown ashes, consisting of basaltic fall and epiclastic deposits; (3) Paleo-soils, with 1.0–1.5m thickness; and (4) consolidated tuffs and ignimbrites. The geotechnical properties obtained for each unit are summarized in Table 5-3. An interesting feature of the Las Colinas landslide is the long runout distance relative to the small volume involved. Despite the low water content and relatively low potential energy, the sliding soil mass developed into a flow slide and traveled along 700 m, burying hundreds of houses and completely demolishing several cars along the way. Based on laboratory tests and field observation, the long runout distance can be related to the presence of weakly bonded materials, easy to be reduced in grain size during motion by fragmentation, grain crushing and fast shearing, allowing for a rapid and progressive decrease of the available strength both within the mass and along the topographic surface.

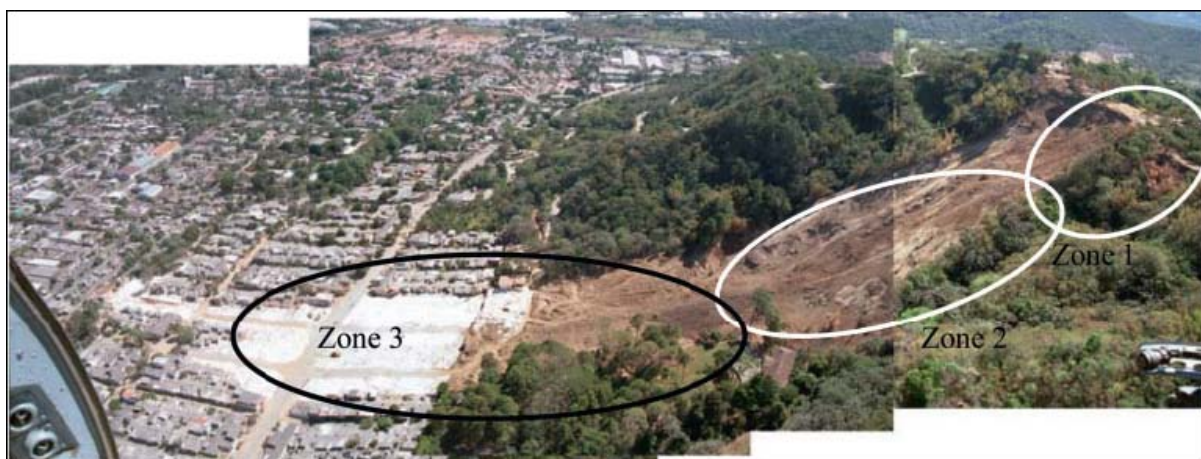


**Figure 5-3** - Overview of Las Colinas landslide in El Salvador (Konagai et al, 2009).

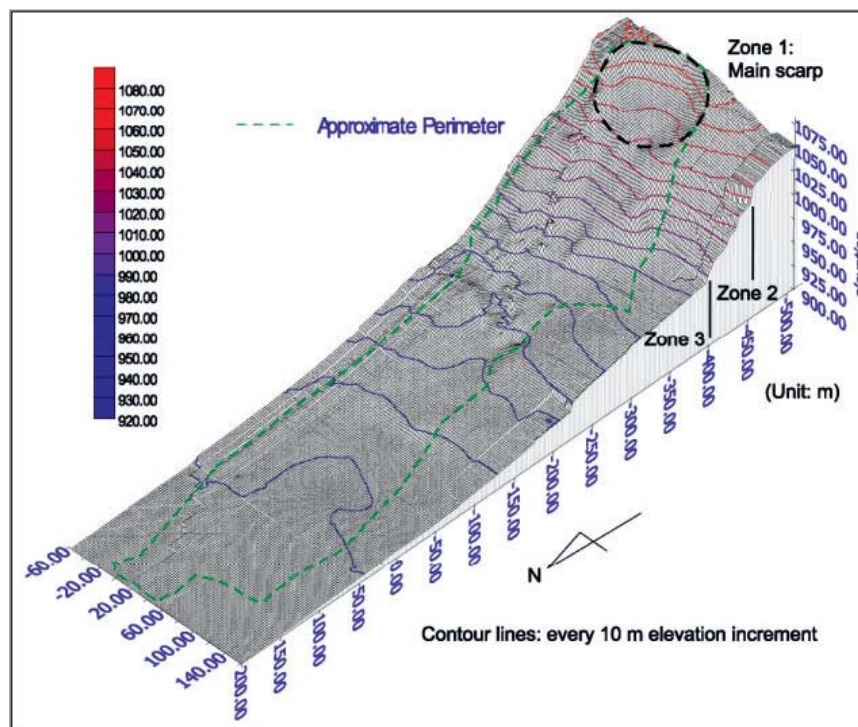


**Figure 5-4** - Details of the Las Colinas slope as measured in the field. The green marker delineates the location of the failed slope (JSCE, 2001).

The dipping direction of the weak soils towards the slope and the flat zone at the bottom of the ridge, with buildings and roads aligned in the flow direction, also contributed to the long travel distance (Crosta et al, 2005; K. Konagai et al, 2009).

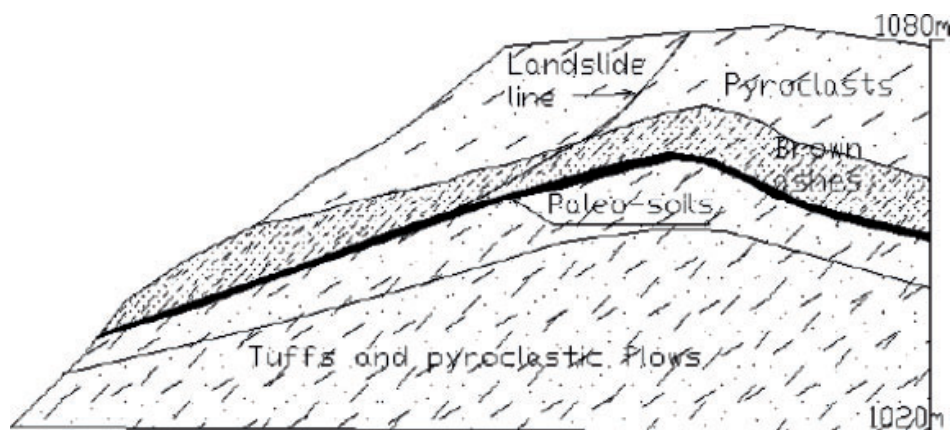


**Figure 5-5** - Cross-section of the Las Colinas slope showing the geological profile (Lotti and Associati, 2001).

**Table 5-3 - Properties of generalized geotechnical units in Las Colinas area (Lotti and Associati-Enel.Hydro, 2001).**

	Pyroclasts	Brown ashes	Paleosoils	Tuffs
Average thickness (m)	15–25	20–80	1.5	–
SPT ( $N$ )	10–40	10–40	8–10	Refusal
Density, $\rho$ (kg/m <sup>3</sup> )	1.50 E+03	1.53 E+03	1.76 E+03	1.90 E+03
Dry Unit Weight, $\gamma$ (kN/m <sup>3</sup> )	11	11	18	
Shear wave velocity, $V_s$ (m/s)	90–145	390–750	660–1100	
Poisson ratio, $\nu$	0.425	0.327	0.262	
Young's modulus, $E$ (MPa)	60	360	3,780	
Shear Modulus, $G$ (MPa)	20	150	1,670	
Max. Shear modulus, $G_{max}$ (MPa)	12–32	233–860	268–990	828–2,300
Cohesion, $c$ (kPa)	60–80	30–40	5–10	200
Angle of internal friction, $\phi$ (°)	30–40	26–34	20–24	35–38

Based on the field survey, three factors can be investigated as the possible triggering mechanism for the Las Colinas landslide: site amplification due to topographic effect, occurrence of liquefaction and residential development on the slope (Orense et al., 2002). Microtremor measurements and ground response analyses suggest that earthquake shaking was amplified due to strong impedance with the rock basement and steep ridge topography. Indications of potential liquefaction of the pumiceous sandy layer were also observed, which may be responsible for triggering the flow-like failure of the slope. Moreover continuous leveling and excavation for residential development may have also contributed to increased landslide hazard and risk.

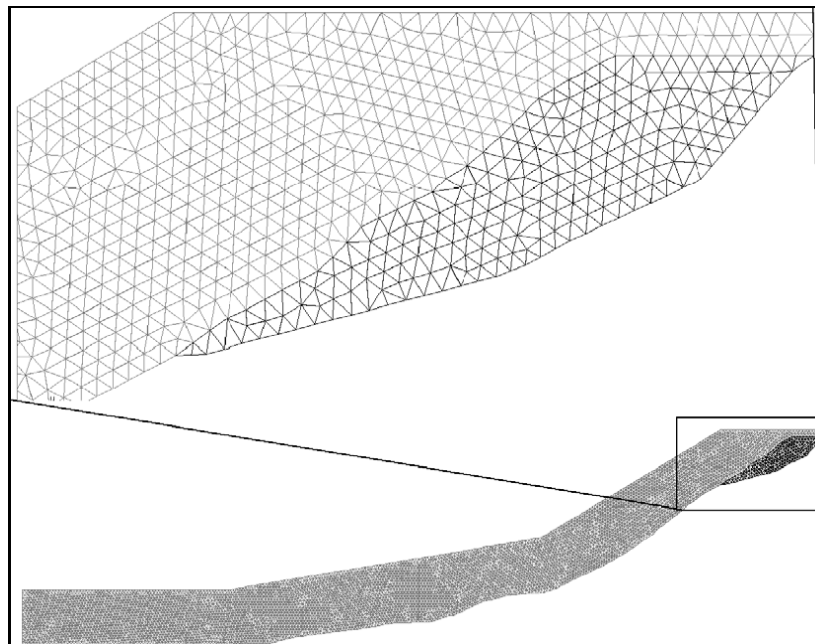


**Figure 5-6 - Space and slope domains discretized by the FE mesh for the landslide runout modeling (Crosta et al, 2005).**

**Table 5-5 - Summary of the main types of runout FE models (Crosta et al, 2005).**

Model #	Slide material					Surface material
	$\phi_{\text{initial}}$ (°)	$\phi_{\text{final}}$ (°)	$C_{\text{initial}}$ (kPa)	$C_{\text{final}}$ (kPa)	Softening	Reduction factor
1	20	20	1	1	No	0.5
2	25	10	1	0.1	Yes	0.5
3	25	20	1	0	Yes	0.5
4	25	10	1	0.1	Yes	No

Slope stability analyses have been performed for the case both under static and dynamic conditions, through limit equilibrium and finite element methods (Luo et al, 2004; Crosta et al, 2005). A series of limit equilibrium analyses was performed in order to evaluate slope stability conditions before and during the major January 2001 eqk. The factor of safety computed for static conditions ranges between 1.4 and 1.8 by using lower and higher values respectively for the strength parameters. For pseudo-static analyses, the critical seismic coefficient has been evaluated between 0.2 and 0.45 as a function of the strength parameters. These values are much lower than the peak ground acceleration as measured at the Santa Tecla station ( $> 0.4$  g) (Crosta et al, 2005). Considering the potential further aggravation of the ground motion due to topographic effects, this is by itself a causing factor for the landslide triggering.

Crosta et al., 2003, 2004a, b, c, adopted a finite element approach that allows for the simulation of the runout process, modeling the drop in resistance due to large deformations and localization of strain at the base of the mass (Figure 5-6). The finite element dynamic analyses shown large slope displacements to occur along the slope in phase with the peak accelerations occurrence, controlled mainly by the horizontal component. The landslide material has been modeled in different ways with the properties reported in Table 5-5. The model with the best performance allowed for strain softening and strength reduction along the failure and topographic surface (Crosta et al, 2005).

### 5.5.2 Slope failures during the 2004 Niigata-Ken Chuetsu earthquake in Japan

The 23 October 2004 Niigata–Ken Chuetsu earthquake ( $M_w=6.8$ ) in Japan caused more than 4000 slope failures within the area about 200 km N of the city of Tokyo. Among the great number of slope failures during the 2004 earthquake, 282 ground failures exceeded  $10^4$  m<sup>3</sup> and 10 exceeded  $10^5$  m<sup>3</sup> in terms of the affected areas. The failed soil mass flowed along several tens or hundreds of meters, causing serious consequences to human lives, houses, roads, agricultural facilities and lifelines. It also blocked streams, causing the generation of many water basins (Kokusho and Ishizawa, 2009).

The geological map of the area where most of the slope failures occurred during the earthquake is shown in Figure 5-7. The geology within the area of interest mainly consists of Neogene sedimented rocks, sand stones and mudstones. Synclines and anticlines are running parallel along the north-south direction as indicated in Figure 5-7; rivers flow almost in the same direction from N to S. Mountains are about 500m at the highest, while the slopes are mainly composed of weak sedimented rock, alternating layers of strongly weathered sandstones and mudstones. Bedding planes and dip planes have a strong effect on the natural slopes here, causing non-symmetric slope angles on the two sides of the mountain ridges; namely, slopes are gentle in dipping directions while obviously much steeper on infacing directions (Kokusho and Ishizawa, 2009).

In most of the slope failures, sandstones were highly responsible mainly because of their small strength due to diffused strong weathering. The strengths of sandstones are much smaller than those of interbedded mudstones. It should also be noted that the sandstones are characterised by permeability values of the order of  $10^{-3}$  cm/s greater than mudstones ( $10^{-4}$ - $10^{-6}$  as per JSCE Report 2005). It served as aquifer and may have applied excess pore-pressure

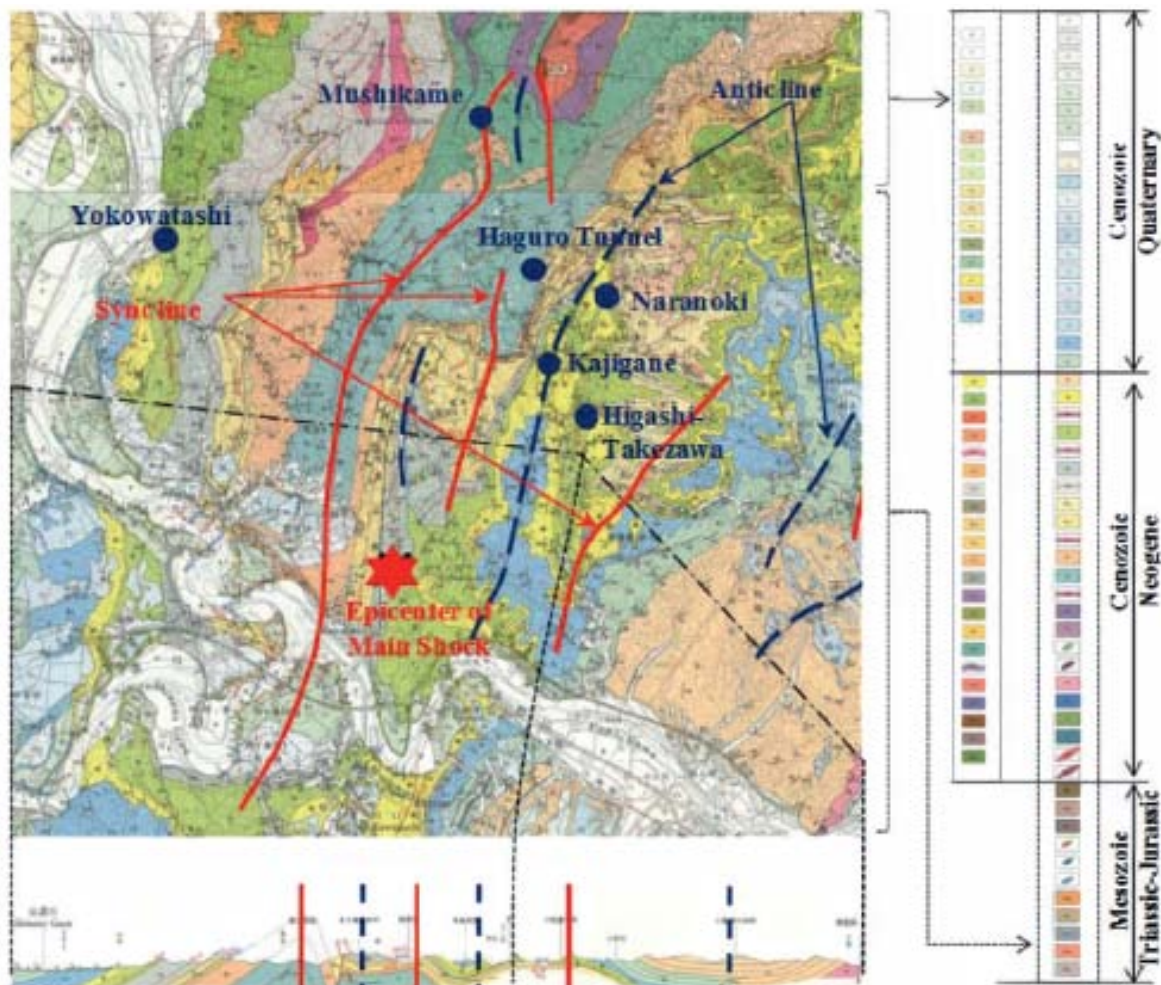


**Figure 5-7 - Geological map in the area of slope failures (Japan Geological Survey).**

leading to the reduction of slope stability during the earthquake. According to the precipitation records of Nagaoka (a city about 16km northwest of the epicenter), intense rainfalls during the last three days prior to the earthquake may have had some influence on the seismic instabilities during the earthquake (Sassa et al, 2005, Kokusho and Ishizawa, 2009). Figure 5-8 shows a map of the damaged area in which a great number of failed slopes are indicated with red spots. In the same map, the epicenters of the main shock (No.1) and the aftershocks (No.2-5) with the magnitudes larger than  $M_f=6.0$  are shown.

There were several earthquake recording stations near the damaged area deployed by JMA (Japan Meteorological Agency) and NIED (National Research Institute for Earth Science and Disaster Prevention). The locations of the JMA and K-net stations are indicated in Figure 5-8, and their longitudes, latitudes and elevations are listed in Table 5-6. The recorded values of the maximum horizontal ground accelerations are considerably high (700 -1600  $\text{cm}/\text{sec}^2$ ), with epicentral distances generally less than 10km.

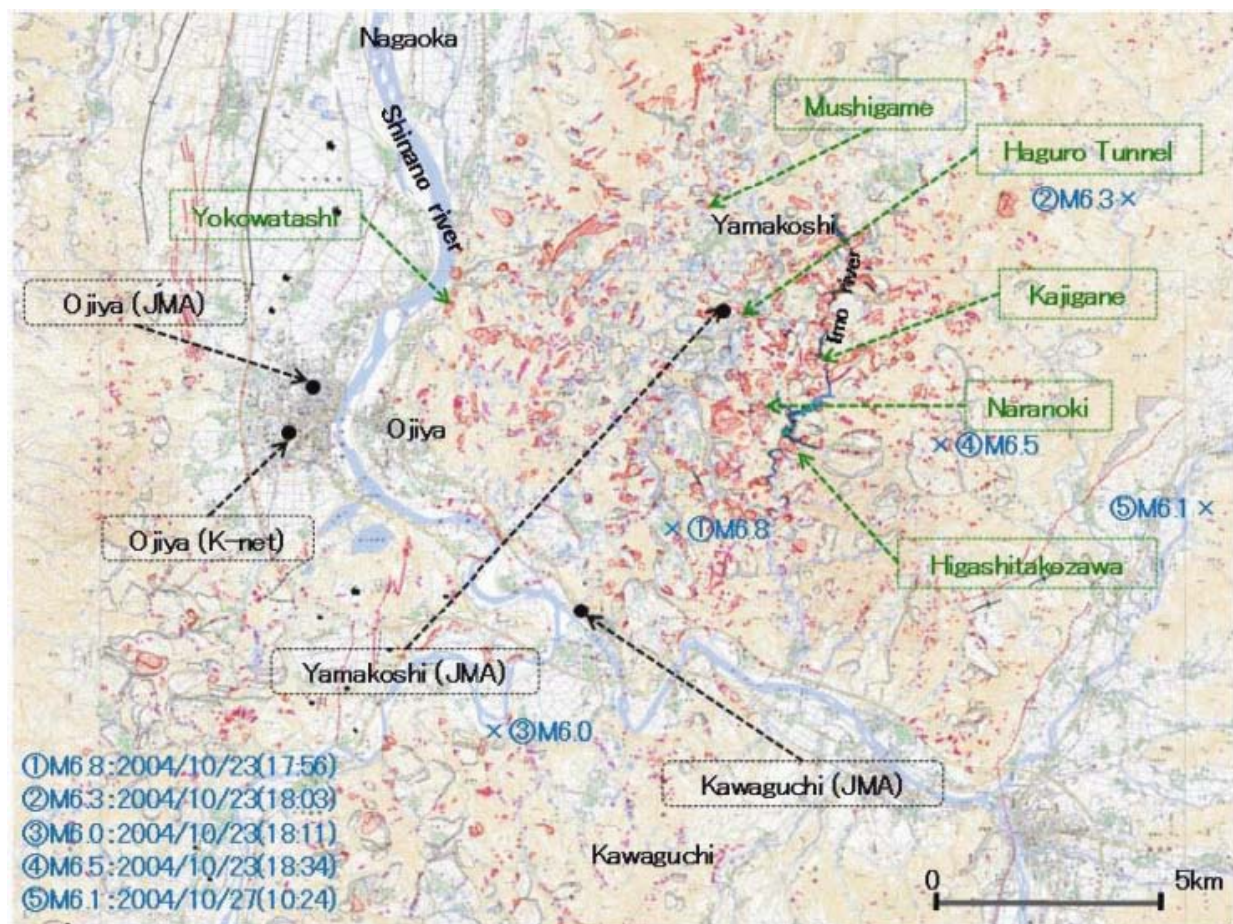


**Figure 5-8** - Epicenters of the main shock and major aftershocks during the 2004 Niigata-ken Chuetsu earthquake (Geographical Survey Institute).

**Table 5-6 - Strong motion recording stations during 2004 Niigata-ken Chuetsu earthquake.**

System	Site (Code)	Latitude (deg)	Longitude (deg)	MS Epicenter distance (km)	Max. Acc (EW) gal
JMA	Yamakoshi	37.327	138.890	4.3	723
JMA	Ojiya	37.310	138.795	7.0	898
JMA	Kawaguchi	37.268	138.861	2.5	1676
K-net	Ojiya (NIG 019)	37.306	138.790	7.4	1308

The slope failures due to the earthquake can be classified into 3 types (A, B and C) (Kokusho and Ishizawa, 2009) as schematically illustrated in Figure 5-9-a:

- A Deep slips parallel to sedimentation planes (parallel dip slip or daylight dip slip) in the case of gentle slopes of around 20 degrees.
- B Shallow slips not parallel to sedimentation planes (infacing dip slip) for steep slopes (>30 degrees).
- C Slips in strongly weathered colluvial soils originated from sandstones and mudstones in places, where koi-ponds and terraced paddy fields developed.

In Figure 5-9-b the horizontal displacements ( $\delta_{rn}$  and  $\delta_{rt}$  of the centroid and the slope toe, respectively) of six representative slope failures of failure modes A, B, C are plotted versus the initial slope inclinations  $\beta_0 = \tan \theta$  ( $\theta$  = slope angle). While the slope inclination increases in the order of Types-A, C, B, the slope displacements in Type-C obviously dominate, presumably due to the potential soil liquefaction or cyclic softening of highly saturated colluvial soils of Type C.

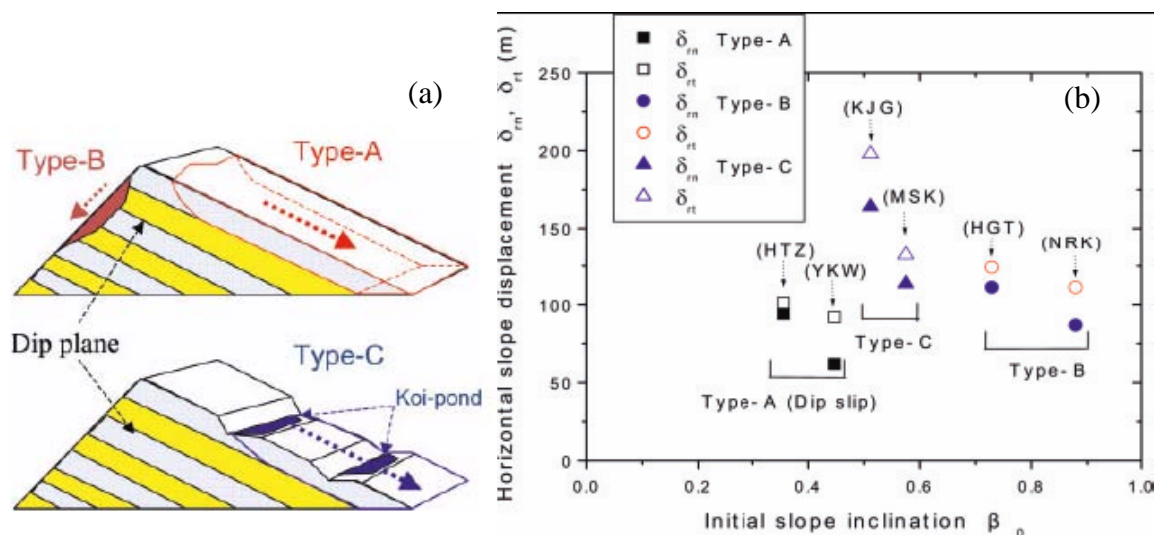


**Figure 5-9 – (a) Schematic image of 3 types of slope failures, A, B, and C, (b) Horizontal slope displacements versus slope inclination for 3 types of slope failures, A, B, and C, occurred during 2004 Niigata-ken Chuetsu Earthquake (Kokusho and Ishizawa, 2009).**

In the following, three cases representative of the different types of failure modes A, B and C are described, namely the Higashi-Takezawa (HTZ) for Type-A, Naranoki (NRK) for Type-B and Mushikame (MSK) for Type-C (Kokusho and Ishizawa, 2009). The location of the slopes is illustrated in figures 7 and 8.

### 5.5.3 Higashi-Takezawa slide (Type-A)

One of the typical Type-A failures during the 2004 Niigata-ken Chuetsu earthquake was the Higashi-Takezawa slide. The landslide mass filled up a valley, interrupting the river flow, causing the formation of a large water basin (Fig. 10). The landslide involved a soil volume of about 1,200,000 m<sup>3</sup> (Kokusho and Ishizawa, 2005), while the maximum dimensions in plan were about 300 m width and 250 m length, with a thickness of about 40 m (Kokusho and Ishizawa, 2005; Sassa et al., 2005). The landslide mass moved rapidly of about 100 m, hitting the opposite bank of the Imokawa river. One part of the sliding mass spread across the road and hit a school. From the head scarp of the landslide, consisting of a rather impermeable stiff siltstone, the inclination angle of the sliding surface was estimated by the aforementioned authors to be approximately 20°. The surprisingly large and rapid runoff of the soil mass motivated several researchers (among them Kokusho and Ishizawa, 2005; Tsukamoto and Ishihara, 2005; Sassa et al., 2005; Kokusho and Ishizawa, 2009) to study the Higashi–Takezawa landslide, providing different interpretations of the sliding process.

In the upper side of the slide, older scarps could be recognized, indicating that previous landslide events occurred in the past.

The geology consists of interbedded sandstone and mudstone of the Shiroya Formation of Pliocene and late Neogene. Field observation indicated that a huge block of sandstone with horizontal dimension of about 300 by 250m slid on a smooth slip plane constituted by mudstone (the material were so weathered to be considered as similar to a medium-dense sand with slight cementation).

Figure 5-11-a depicts a contour map of Higashi-Takezawa slope before the slide, while Figure 5-11-b shows the corresponding air image (the elevation step of each contour is equal to 2 m). Figure 5-12(a) depicts the contour map of the same slope after the failure of 28 October, 2004, and Figure 5-12-b is the corresponding photograph. In figures 11(a) and 12(a), the area affected by the slope failure is indicated by a thick curve.

The boundary of the affected area was determined from the two DEM data, in the presence of an elevation variation exceeding 1 m. The cross-sectional changes in the affected area developed are illustrated in Figure 5-13-a as obtained from DEM data before and after the earthquake (again Figures 5-11-a and 5-12-a). The slip surface shown by the dotted curve in Figure 5-13-a was determined from the exposed slip plane observed at the top of the slope, from the original location of the valley and by analysing the global changes of slope configuration (Kokusho and Ishizawa, 2009). Figure 5-13-b depicts an idealization of the displaced soil mass by a rectangular block in Higashi-Takezawa slope.



**Figure 5-10** - General view of the Higashi Takezawa landslide and the head scarp of past landslide (Sassa, 2005).

Figure 5-14 illustrates the cross-section of the slope along the line of the boreholes, as the simplification of the detailed chart provided by Yuzawa Sabo. At the bottom of Figure 5-13, soil logging results at the 4 boreholes obtained before the major restoration works are shown, in which soil types, water tables, estimated depths of the slip plane are indicated.

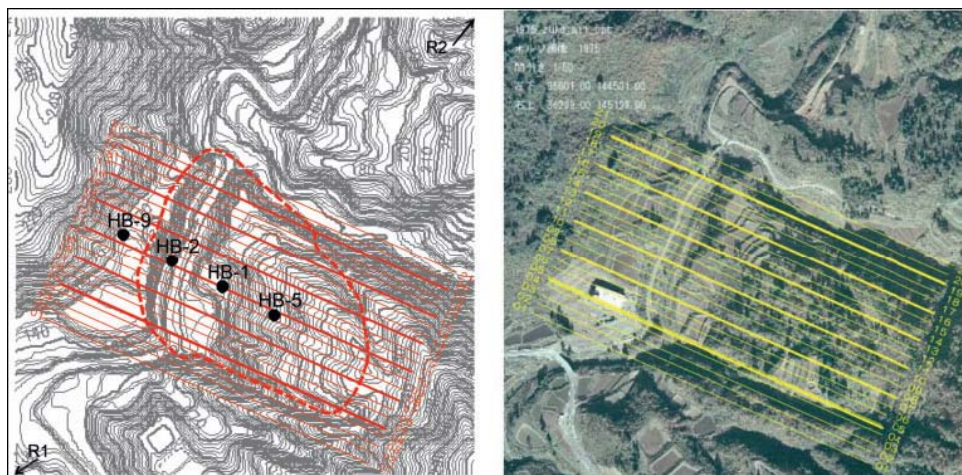


**Figure 5-11** - Contour map (a) and aerial image (b) of Higashi-Takezawa slide before the earthquake (based on photographs taken in 1975 and 1976) (JSCE 2007).

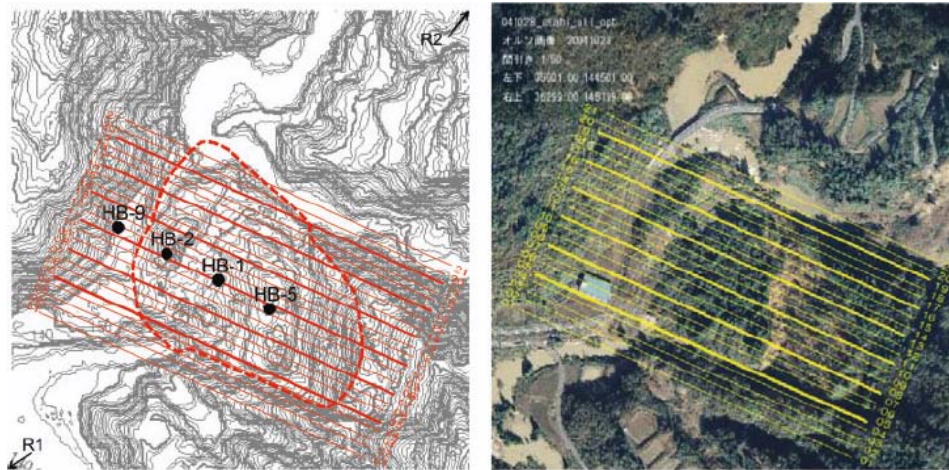


**Figure 5-12** - Contour map (a) and aerial image (b) of Higashi-Takezawa slide after the earthquake (based on photographs taken in 28, Oct. 2004) (JSCE 2007).

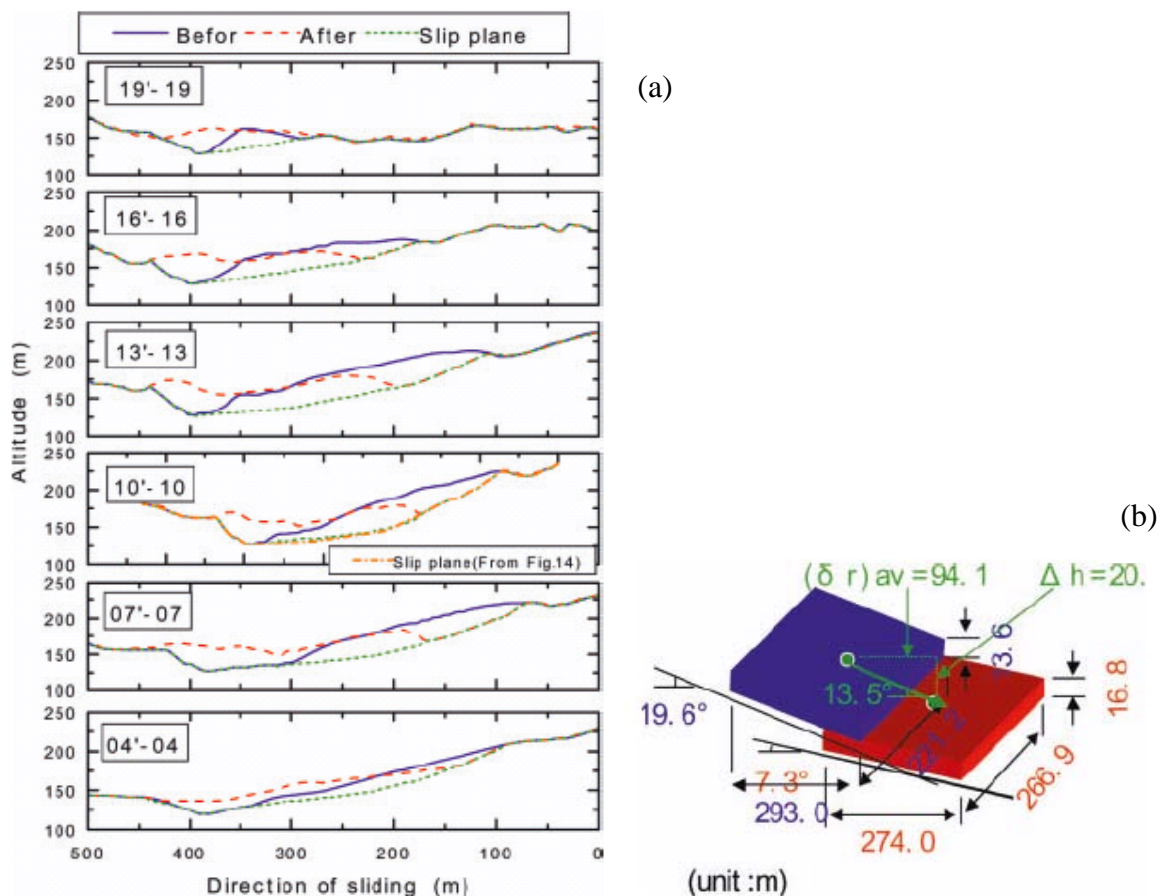


**Figure 5-13** - (a) Cross-sectional change of Higashi-Takezawa slope before and after the earthquake. (b) An Idealization of the sliding soil mass by means of a rectangular block in Higashi-Takezawa slope (Type A) (Kokusho and Ishizawa, 2009).

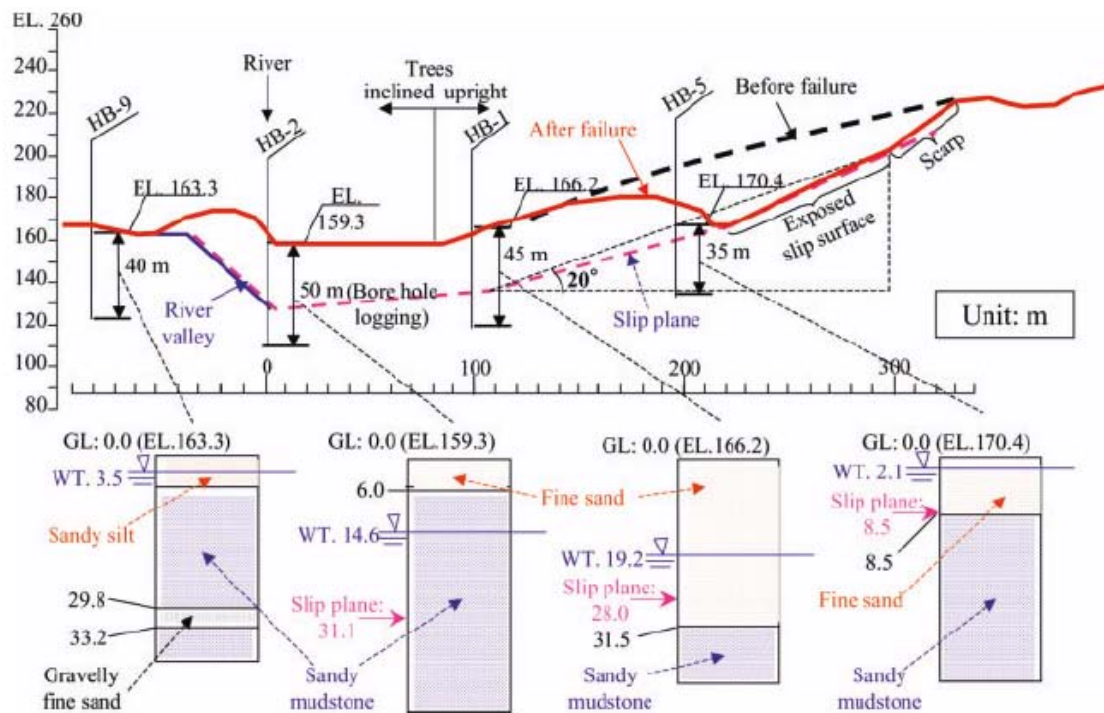


**Figure 5-14** - Cross section of the Higashi Takezawa slope (simplified after Yuzawa-Sabo, Ministry of Land, Infrastructure and Transport).

A numerical model was developed (Gerolymos and Gazetas, 2007) in order to simulate the seismic triggering, evolution and deposition of the Higashi Takezawa landslide by considering two mechanically coupled substructures: (a) the accelerating deformable body of the slide, and (b) the rapidly deforming shear band at the base of the slide. The constitutive model employed combines features of an extended Savage–Hutter approach for the sliding soil body, with (i) a Mohr–Coulomb failure criterion, (ii) Bouc–Wen hysteretic stress–strain relationship, and (iii) the Voellmy’s rheology for the deformation of the material within the shear band, exploiting the concept of grain crushing–induced instability. Three scenarios were analyzed by the Authors with reference to the location of the sliding surface and the susceptibility of sand to grain crushing: (1) shear band within the sand layer, with “stable” sand, (2) shear band within an assumed thin silt layer atop the siltstone with “stable” sand, and (3) shear band within the sand layer but sand susceptible to grain crushing. The residual displacement was calculated to be 0.65 m and 3.4 m for the first and second scenario, respectively. The observed displacement of approximately 100 m cannot be easily explained, with the above modeling: an extensive soil transformation and softening due to grain crushing shall be introduced as hypothesis (Gerolymos, 2009).

#### 5.5.4 Naranoki slide (Type-B)

Naranoki slide occurred at the steep slope of the right bank of the Imo river. The geology is mainly constituted by the Kawaguchi Formation of Pliocene which is composed by sandy mudstone layers interbedded with sandstone. Figure 5-15-a shows a global view of the collapsed slope: the run-out debris interrupted the river flow and local roads. Figure 5-15-b depicts a close-up view of the slide from the steep scarp on which sedimentation planes of mudstone and sandstone can be clearly observed. Thin surface layer slid down along the steep slip plane of infacing dip, tearing into pieces (Kokusho and Ishizawa, 2009).

The fines content of the interbedded sandstone was about 10–14%, the mean grain size was 0.1–0.12 mm, and undrained shear strength  $C_u = 11$  MPa. Soil particle density of sampled debris was  $2.62 \text{ g/cm}^3$ , fines content  $F_c = 40\%$ , natural water content  $W_n = 38\%$ , liquid limit  $LL = 29\%$  while the plastic limit  $PL$  was non-measurable (Kokusho and Ishizawa, 2009).

Figure 5-16-a shows the contour map before the slide, while Figure 5-16-b represents the corresponding aerial imagery (the elevation step of the contours is 2 m). Figure 5-17-a depicts the contour map of the same slope after the failure (28 October, 2004), while Figure 5-17-b is the corresponding aerial image. The thick curve in figures 16(a) and 17(a) indicates the boundaries of the affected area as determined from the two DEM data analysis, identifying the area characterised by an elevation difference greater than 1 m. The cross-sectional changes in the affected area before and after the earthquake as well as an idealization of displaced soil mass by a rectangular block are illustrated in Figure 5-18. The dotted line in Figure 5-18 locates the slip surface as estimated from the global changes of slope configuration and also from field observation (Kokusho and Ishizawa, 2009).



**Figure 5-15** - (a) Global view of Naranoki slide of Type-B. (b) Zoom-up of the steep scarp of sedimentation planes of mudstone and sandstone (Kokusho and Ishizawa, 2009).

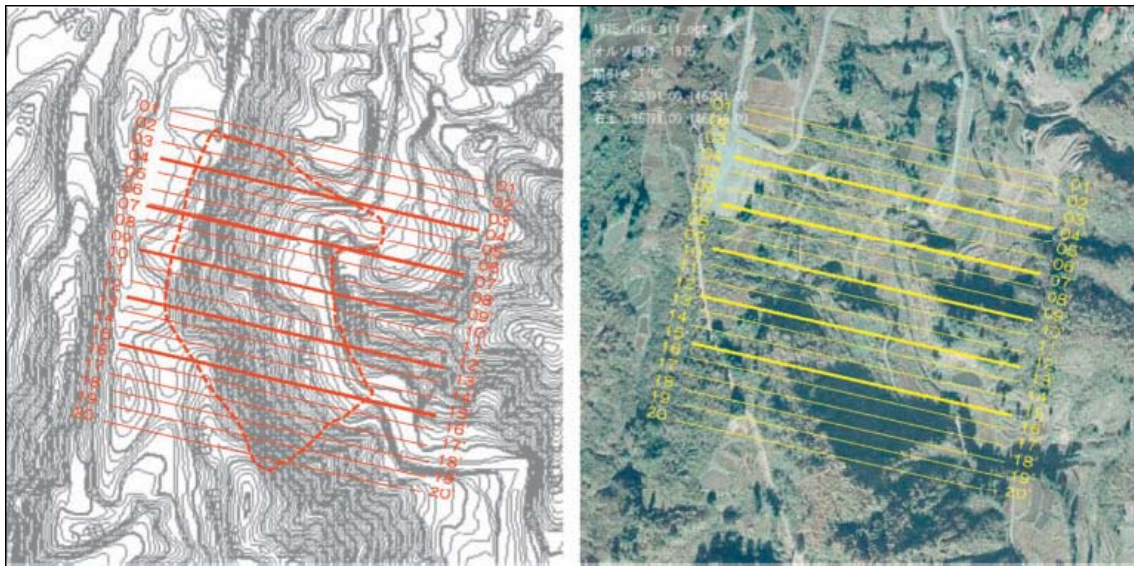


**Figure 5-16** - Contour map (a) and air-photograph (b) of Naranoki slide before the earthquake (based on photographs taken in 1975 and 1976) (JSCE 2007).

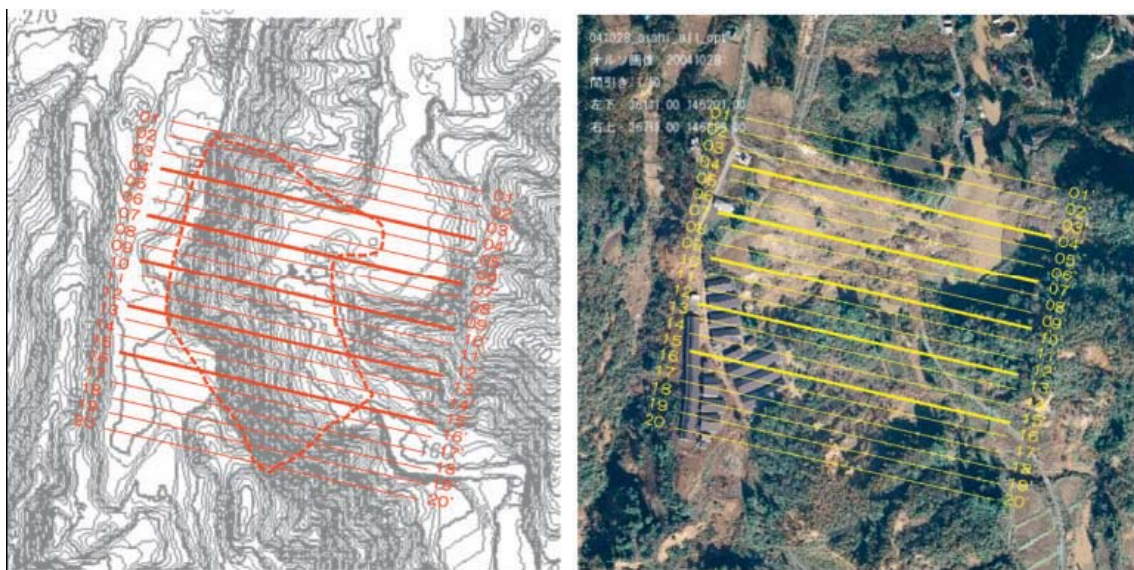


**Figure 5-17** - Contour map (a) and air-photograph (b) of Naranoki slide after the earthquake (based on photographs taken in 28, Oct. 2004) (JSCE 2007).

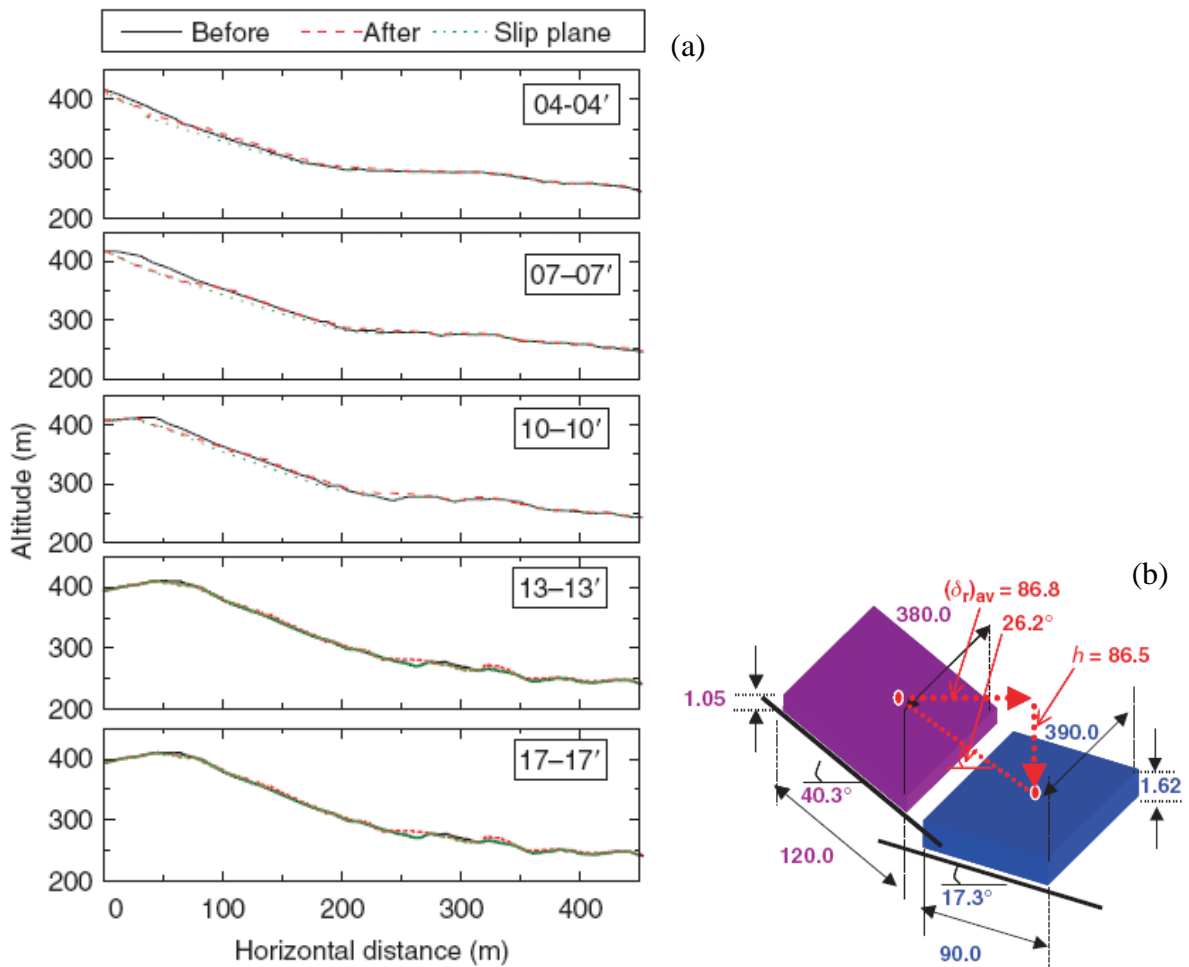


**Figure 5-18** - (a) Cross-sectional change of Naranoki slope before and after the earthquake. (b) An Idealization of sliding soil mass by a rectangular block in Naranoki slope (Type B) (Kokusho and Ishizawa, 2009).

### 5.5.5 Musikame slide (Type C)

Musikame slide occurred W of the Higashiyama anticline, where geology is constituted by the Araya formation of Miocene, characterised by dark gray massive mudstone interbedded with fine-grained sandstone. Figure 5-19-a shows the air image of the slide just after the failure. Figure 5-19-b shows a view of the slide from the top indicating that the muddy debris flowed within a long distance, crossing over a road, and reaching finally a stream. The crushed muddy soil mass slid down along a parallel dip plane, presumably constituted by mudstone (Kokusho and Ishizawa, 2009). The debris consisted of a very fine soil with  $D_{50} = 0.03\text{mm}$  and the fines content of more than 90%. Soil particle density of sampled debris was  $2.72\text{ g/cm}^3$ , natural water content  $W = 39\%$ , liquid limit  $LL = 47\%$ , plastic limit  $PL = 35\%$  and plasticity index  $PI = 12$  (Kokusho and Ishizawa, 2009).



**Figure 5-19** - (a) Aerial images of Mushikame slide (b) View from the top of the slide (Kokusho and Ishizawa, 2009).

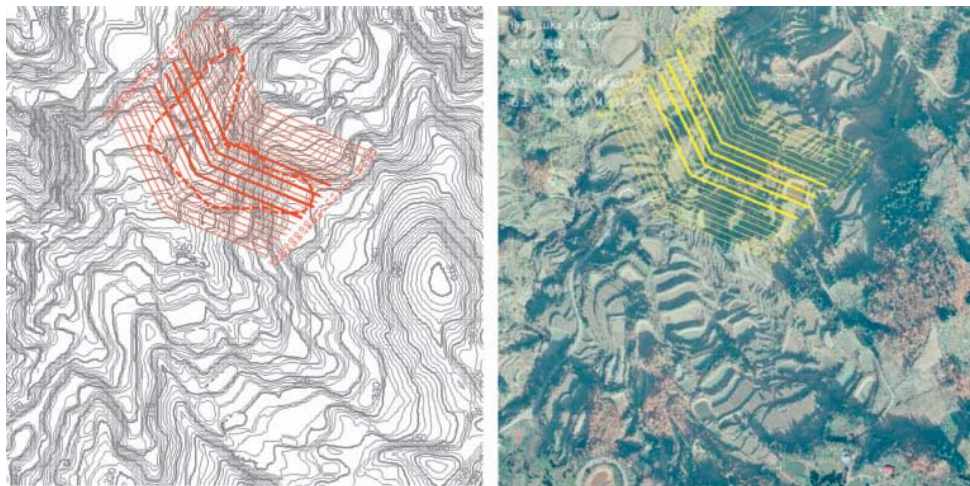


**Figure 5-20** - Contour map (a) and aerial image (b) of Mushikame slide before the earthquake (based on photographs taken in 1975 and 1976) (JSCE 2007).

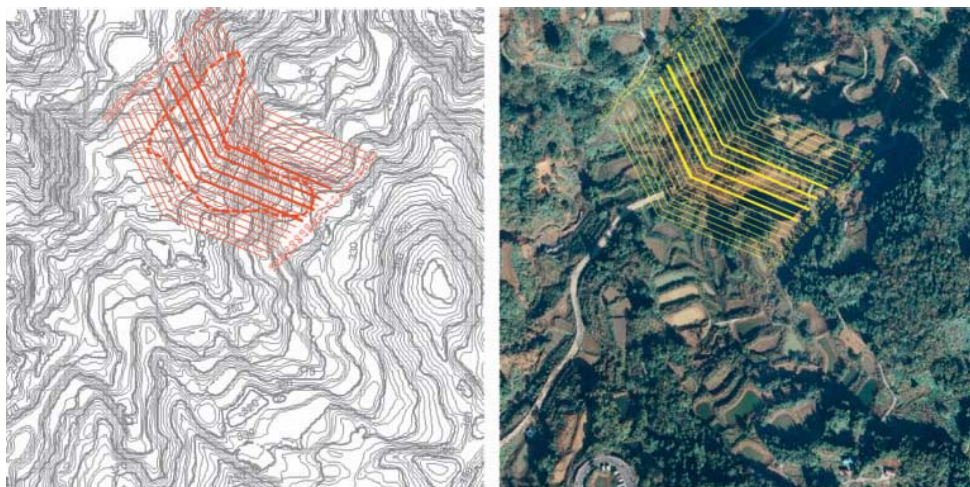


**Figure 5-21** - Contour map (a) and aerial image (b) of Mushikame slide after the earthquake (based on photographs taken in 28, Oct. 2004) (JSCE 2007).

Figure 5-20-a depicts a contour map of Mushikame slope before the slide and Figure 5-20-b shows the corresponding aerial imagery (the elevation step of the contours is 2 m). Figure 5-21-a depicts the contour map of the same slope after the failure (28 October, 2004), while Figure 5-21-b is the corresponding aerial image. The thick curve in figures 5-20 -a and 5-21-a indicates the boundary of affected area, recognised on the basis of the comparison of the DEM previous and after the sliding (displacement  $> 1\text{m}$ ) (Kokusho and Ishizawa, 2009).

The cross-sectional changes within the affected area before and after the earthquake, as well as an idealization of displaced soil mass by a rectangular block, are illustrated in Figure 5-22. The dotted line in Figure 5-22-a represents the slip surface as estimated from the global changes of slope configuration and field observation. The cross-sections traced outside the failed slope almost coincide before and after the earthquake, indicating that the tectonic effect is almost negligible in this case.

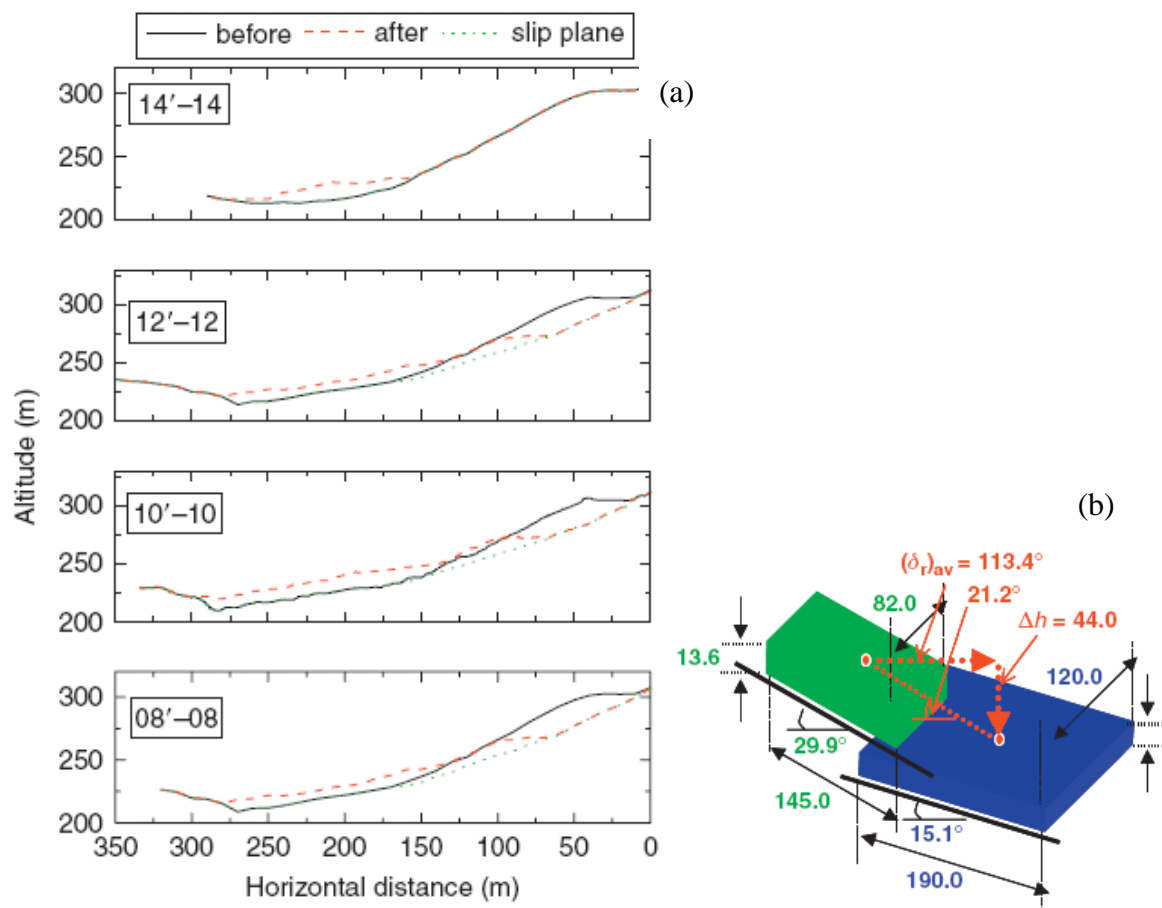


**Figure 5-22** - (a) Cross-sectional change of Mushikame slope before and after the earthquake. (b) An Idealization of sliding soil mass by a rectangular block in Mushikame slope (Type C) (Kokusho and Ishizawa, 2009).

---

### 5.5.6 The 1980 Calitri landslide caused by the Irpinia earthquake, Italy

The 23 November 1980  $M_s = 6.9$  Irpinia earthquake in Southern Italy triggered several mass movements (already active in the past, or not). Among them, one of the most pronounced in terms of effects produced was the reactivation of the Calitri landslide, repeatedly activated by past earthquakes, as reported in the literature since 1694. The town of Calitri in Irpinia (Southern Italy), which is located on the top of an approximately EW-trending hilly relief at the left bank of the Ofanto river, was severely damaged by the landslide. The Calitri area is known for the sequence of frequent mass movement reactivations due to major climatic and seismic events in history. Parise and co-workers (1997) argued that moderate and high magnitude earthquakes are probably capable of generating more pronounced and long lasting effects on slope stability at the site, in comparison with those induced by other triggering factors (Parise et al., 1997).

The earthquake event was characterised by a strike dip focal mechanism and ( $M_s=6.9$ ); the maximum horizontal acceleration, recorded at Sturno town during the 23/11/1980 mainshock, was 0.328 g (Nostro et al, 1997). From the records of the Calitri accelerometer station during the main shock of 23/11/1980 the maximum acceleration components were 0.145 g (NS), 0.125 g (WE), 0.162 g (UP).

The built-up area of Calitri is partially founded on the geological unit of the Ofanto river, which developed in the lower Pliocene as a piggy-back basin in the southern Apennines (Patacca et al, 1990; Martino et al, 2005). During Plio-Pleistocene, the Ofanto river basin hosted the sedimentation of transitional and marine deposits. So far, these deposits have been distinguished into two main sedimentary sequences: the Ciclo di Ariano (lower-middle Pliocene) and the Ciclo di Atessa (upper Pliocene-lower Pleistocene p.p.) (Patacca et al, 1990; Martino et al, 2005). In the Calitri area, the Cahotic Complex of the Argille Varicolori is interposed between the two sedimentary cycles of Ariano and Atessa, the thickness of these deposits is very variable, depending on the morphology of the Ofanto basin at the time of their emplacement. Figure 5-23 depicts the engineering geological cross section of the Calitri landslide along the dip direction trace.

Figure 5-24 shows the ground cracking pattern resulting from the activation of the landslide after the 1980 earthquake. The highest measured vertical displacement was greater than 4 m and caused the sinking of a house located at 100 m S of Repubblica square; at the end of the sinking, the roof of the building lay at the same elevation as the road. The entire mass mobilized was estimated to be about 23 Mm<sup>3</sup>.

Calitri landslide may be characterized as an earthflow and divided into three main areas: (i) a source zone, where tension cracks have downslope concavities; (ii) an accumulation zone, where compressional cracks have marked upslope concavities and (iii) an ablation zone, where longitudinal cracks are continuous for about 100 m. The earthflow reached and partially dammed the actual course of the Ofanto river. Measurements made 10 weeks after the earthquake of 23 November 1980 shown a rate of displacement along the earthflow channel of about 20 cm/h.

The analysis of the ground cracking pattern and landslide induced damage made possible to: (i) determine the boundaries of the portion of the slope (ii) recognise the 400–600 m-wide complex crown, totally included in the built-up area and (iii) identify the downslope earthflow and its supply zone (Martino et al, 2005). The complex configuration of the crown (activated by the 1980 earthquake) seems to reflect the coalescence of multiple landslide movements with individual time/space characters, in any case subjected to a more deep-seated, roto-translational and substantial overall movement. Hence, taking into account the landslide's complex origin and morphological evolution, the major triggering mechanisms of the Calitri landslide appear to be the shallow and deep-seated, multiple and successive gravity-induced destabilisation processes, the action of surface waters, weathering and primarily the strong ground shaking.

Various authors (Hutchinson, 1994; Gaudio et al, 2004) furtherly investigated the Calitri landslide after its reactivation by the Irpinia earthquake in 1980, demonstrating its deep-seated origin and assessing slope stability through conventional methods, e.g. the global limit equilibrium analysis (Hutchinson et al, 1985), displacement based approaches, such as the Newmark type methods (Gaudio et al, 2004) or numerical simulation under both static and dynamic conditions (Martino et al, 2005).

In particular, the numerical analyses performed (Martino et al, 2005) confirm the likelihood of seismically-induced reactivations of the Calitri landslide, according to a roto-translational slide mechanism with high translational components, and of a sliding surface located at a depth not exceeding 100 m from ground level. Moreover, the dynamic numerical simulation indicated a diversification of the effects induced by different seismic input frequencies, in

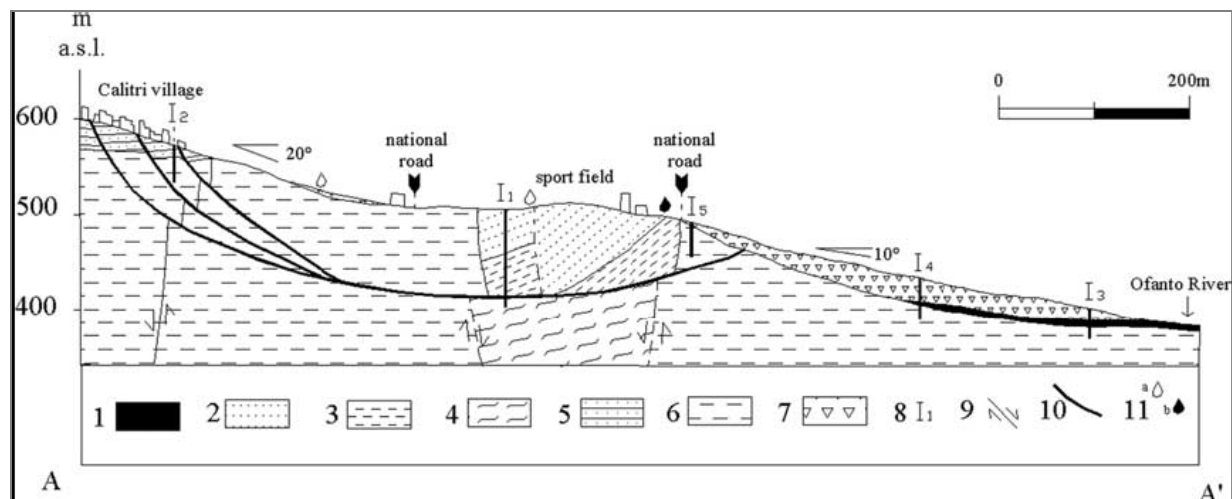


**Figure 5-23** - Engineering-geological section of the Calitri landslide along the dip direction of the slide: (1) Ofanto river alluvia, (2) Sabbie di Atessa sands; (3) Argille Azzurre di Atessa silty and marly clays; (4) Complesso Caotico di Argille Varicolori scaly clays; (5) Arenarie di Ariano sandstones; (6) Argille Azzurre di Ariano silty and marly clays; (7) landslide debris and talus deposits; (8) boreholes; (9) fault; (10) existing rupture surface; (11) spring: (a) seasonal, (b) permanent (Martino et al, 2005).

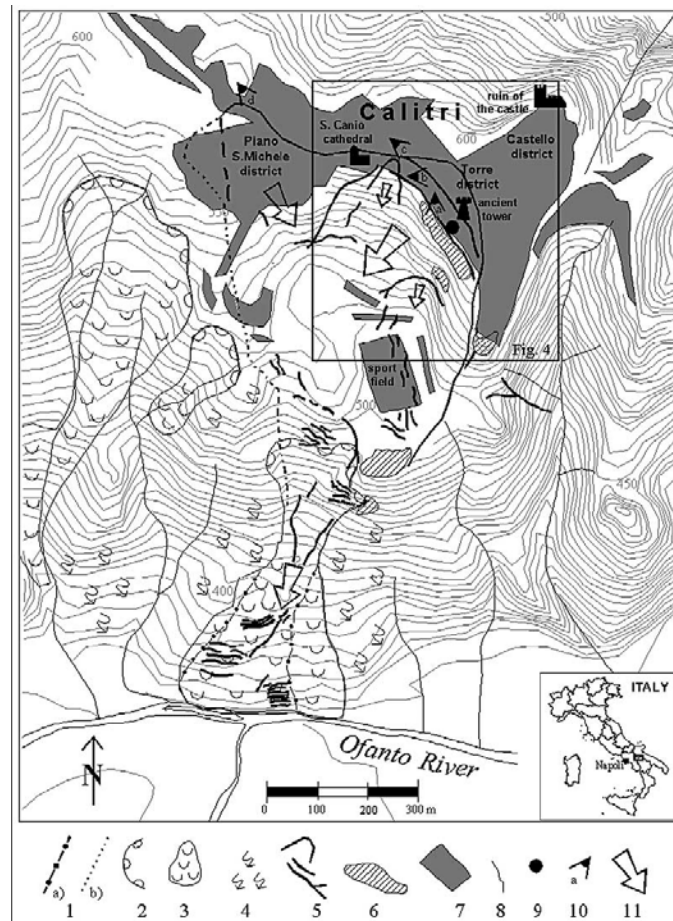


**Figure 5-24** - Geomorphological sketch showing ground cracking resulting from the activation of the Calitri landslide after the 1980 earthquake: (1a) boundary of the mobilised earthflow deposit, (1b) area involved by the landslide; (2) earthflow scarp; (3) earthflow deposit; (4) solifluxion; (5) ground cracks; (6) ground areas intensely cracked after the earthquake; (7) built-up area; (8) main watersheds; (9) location of ENEL accelerometric station; (10) point of photo coverage; (11) main directions of movement inside the landslide mass (Martino et al, 2005).

terms of propagation and deepening of slope instability, as well as of extent of the displacements. In particular, lower frequencies (0.75 Hz) are recognized to be more effective in re-trigger large volumes of highly-deformed soil, whereas higher frequencies only induce localized and shallow instabilities with less significant deformations.

### 5.5.7 Corniglio landslide, Apennines region, Italy

In European LessLoss Research Project (FP6), devoted to the estimation of losses from earthquakes and landslides, Callerio and co-workers (Callerio et al., 2007) apply their methodology of scenario-based probabilistic estimation (First Order Second Moment, or FOSM) of the direct loss caused by a landslide to a set of buildings lying within the area affected by the ground displacements of the Corniglio landslide (Figs. 25 and 26). The

Corniglio urban area (about 2300 inhabitants) is located in the mountainous Apennines region of NW Italy.

The time period of interest spans from September 1994 to December 1999, and was characterized by nearly continuous landslide activity. During this period, the major re-activations of the landslide (the so-called “Lama”, i.e. “blade”), and nearby portions, see Figures 25 and 26, were recognized to depend on two combined triggering factors:

- Intense rainfalls, particularly before the activation of Dec. 1995 and during all November 1996;
- Weak and moderate earthquake ground motion, particularly on occasion of the Correggio Earthquake of October 1996, of magnitude  $M=5.4$ , with an epicentral distance of about 70 Km from the site.

Through the entire time span, the observed displacements reached tens of m on the main slide body, the so-called “Lama”, while in the adjacent Corniglio Village the surface ground movements measured by the inclinometers reached typically 20 to 25 cm. All the sparse buildings present within the Lama area suffered heavy damage, while those located in the old centre of Corniglio suffered moderate to significant damage, such as cracks in masonry vaults, opening of structural joints, cracking of retaining walls and in linings.

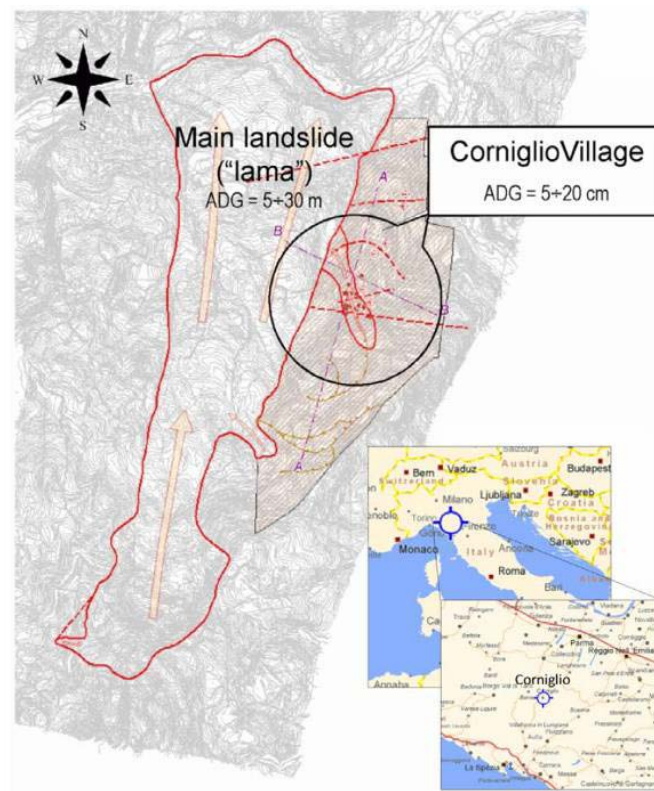


**Figure 5-25** - General plan of the area of Corniglio affected by the landslide phenomena during the years 1995-2000 (ADG = Absolute Ground Displacement) (LessLoss Deliverable No. 121).

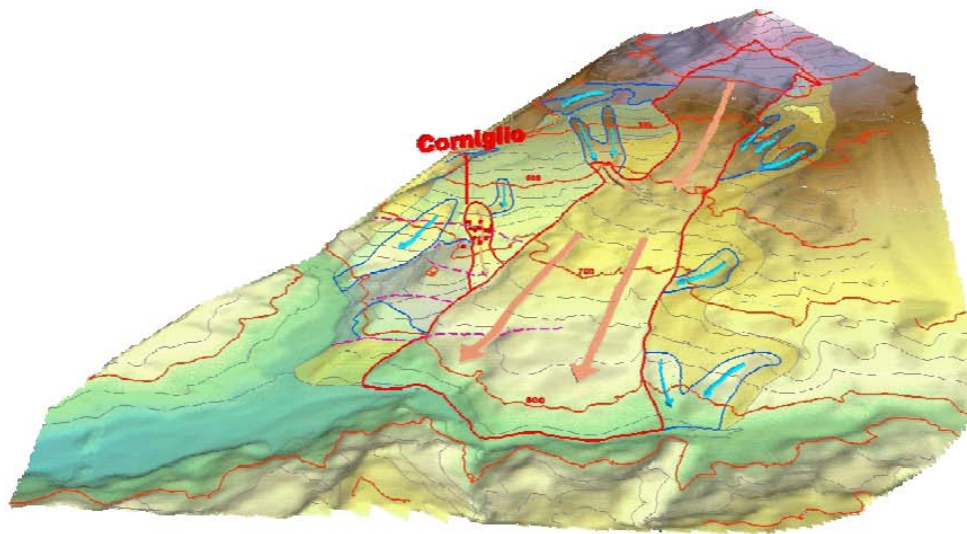


Figure 5-26 - 3D representation of the area of interest on the base of the DEM of the ground. The movement main direction of the Lama area is indicated by the arrows (LessLoss Deliverable No. 121).

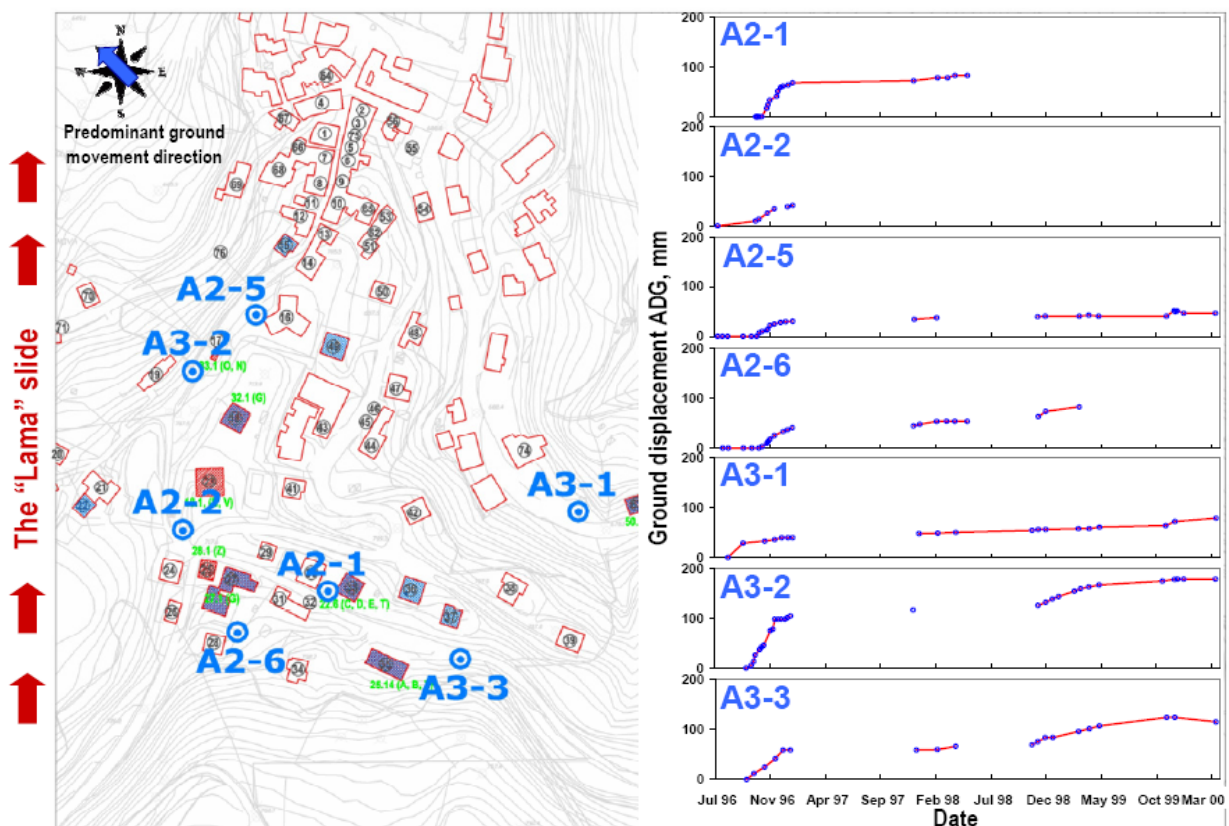
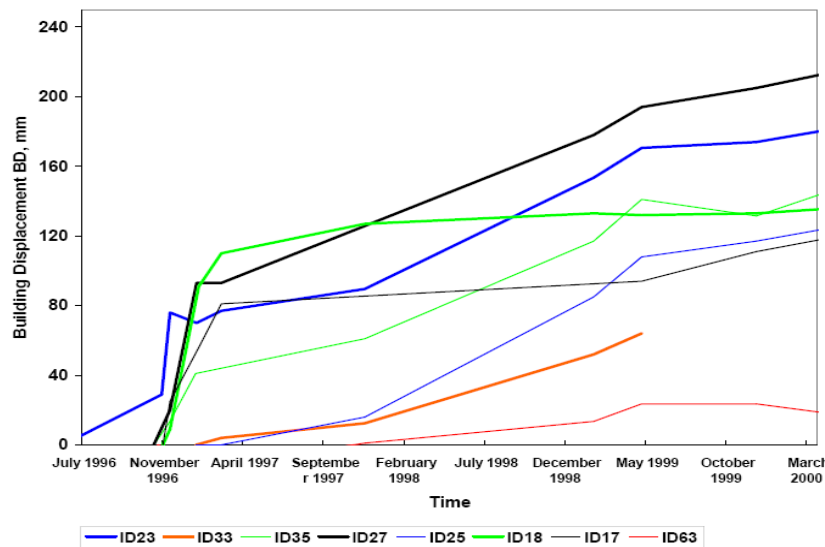


Figure 5-27 - Inclinometer readings (Callerio et al, 2007).



**Figure 5-28** - Building displacements from geodetic leveling (Callerio et al, 2007).

A substantial set of instrumental observations was collected during the progress of Lessloss activities, mainly from the Regional Authority in charge of the monitoring, consisting of:

- Inclinator data (Figure 5-27);
- Geodetic levelling data collected on several buildings within the village area for the entire period of interest (Figure 5-28).
- Crack aperture measurements in some buildings where damage particularly occurred.

The gaps in inclinometer readings were filled by the Authors on the basis of the nearly uninterrupted geodetic levellings of nearby buildings, under the hypothesis the building and the surrounding soil underwent no relative displacement within the time interval of interest.

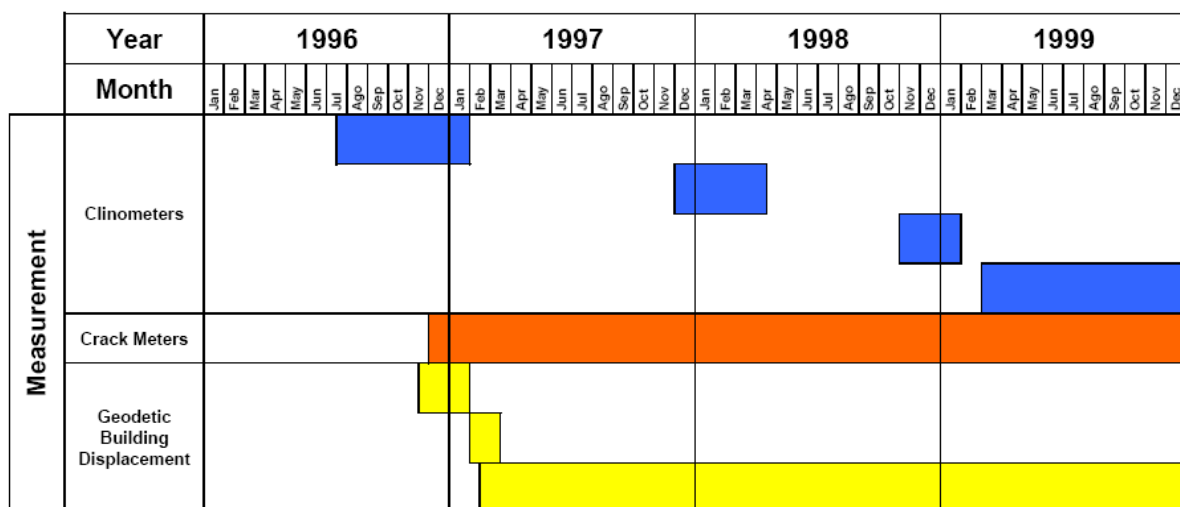


**Figure 5-29** - Data coverage during the period at study (Callerio et al, 2007).

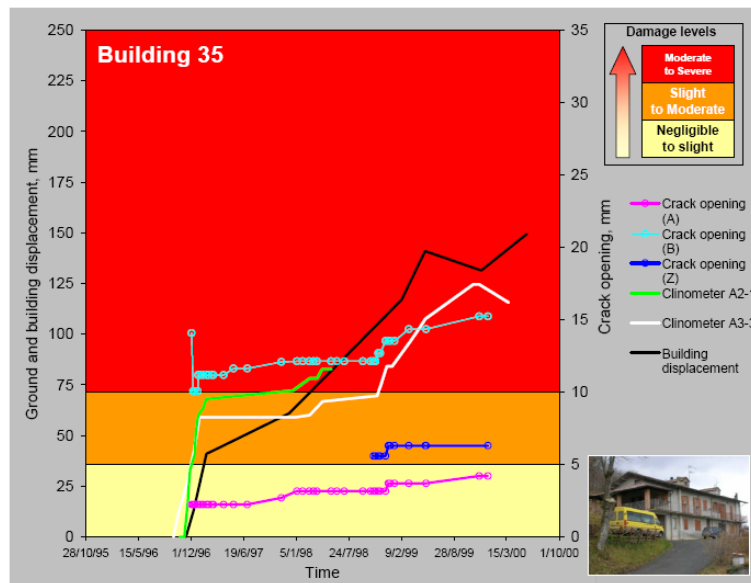


**Figure 5-30** - Correlation between absolute ground displacement (ADG, from nearby inclinometer observations), building displacement (DB, from geodetic levelling) and crack opening compared to the defined damage levels) (Callerio et al, 2007).

Inclinometer data were also in some cases extrapolated, again on the base of the nearby building displacements. Figure 5-30 depicts a correlation among absolute ground displacements ADG and nearby inclinometer observations, building displacement DB, from geodetic levelling and crack opening compared to the damage levels defined by Callerio and co-workers (Callerio et al, 2007) for one of the damaged buildings.

### 5.5.8 The Tangjiashan landslide caused by the 2008 Sichuan (Wenchuan) earthquake, China

On May 12<sup>th</sup>, 2008, the catastrophic Ms 8.0 Wenchuan earthquake occurred W of the Sichuan basin, China, causing more than 69000 casualties and an extensive structural damage to buildings and infrastructures. It also caused the failure of natural as well as engineered slopes in mountainous regions. It was the strongest earthquake recognized to be occurred in China and the most costly natural disaster in the past 100 years.

The focal mechanism of the earthquake was a successive massive fracture along the Longmenshan fault at 15 km depth, a thrust structure in Yingxiu. The seismic analysis of data confirmed that the major shock occurred on the Beichuan–Yingxiu Fault (Figure 5-31) with peak acceleration event greater than 600 gal (cm/sec<sup>2</sup>) at several sites. The largest PGA recorded during the main shock was 958 gal recorded at Wolong station in Wenchuan County, Sichuan. Figure 5-32 depicts the shake map of the earthquake where the earthquake intensity is related to the PGA and PGV values and to the expected damage state. Figure 5-33 shows the PGA contour as defined on the base of the attenuation relation proposed by Aydan and Ohta (2006) for interplate earthquakes. According to such a relation, the PGA value in the area of interest (Beichuan County) lies between 890 and 1050 gals.

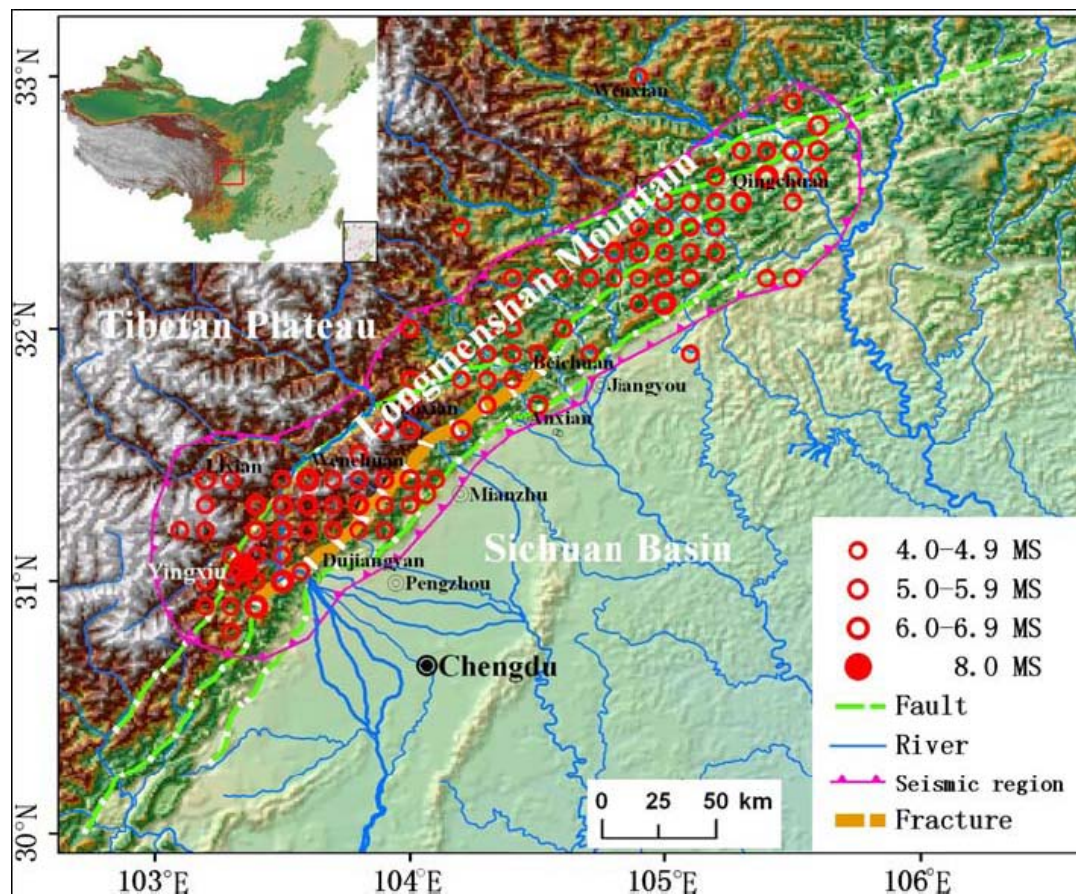


**Figure 5-31** - Location of the Wenchuan earthquake and the aftershocks (Cui et al, 2009).

The Longmenshan Mountains are prone to numerous landslides just due to their topography and steepness, also under normal conditions. The earthquake is reported to have caused almost 10,000 geohazards, including rock avalanches, rock flows, landslides, and debris flows. 26 of them are believed to have interested volumes of material exceeding 10 million cubic meters. Landslides and rockslides buried villages and towns resulted in numerous casualties, with two landslides killing about 2,500 persons in the Beichuan area. Debris flowed into rivers, creating approximately 33 major natural dams impounding earthquake lakes (Figure 5-34). The resulting lakes not only inundated inhabited areas, roads, and farmlands upstream but also pose a threat to large downstream cities in the event of blockage failures, particularly if failures occur sequentially. Water basins generated from earthquake landslides are regarded as the most dangerous geohazard occurred; mitigation efforts to lower or drain the water, or stabilize the blockages were considered as a priority (Cui et al, 2009). Hence, two progressive strategies have been proposed for the process of earthquake geohazards control in terms of different situations: (1) Disaster Emergency Response and Relief, and (2) Reconstruction Assistance for the succeeding period (Cui et al, 2009). The largest landslide-dammed lake was generated by the Tangjiashan landslide which blocked the upper portion of the Jianjiang River, 5 km from the Beichuan County Town. The rapid landslide rushed to the left bank of the river and buried the Yuanheba Village, causing 84

fatalities. The dam crest extended approximately 600 m across and 800 m along the valley (figures 35 and 36). The height of the dam varied from 82 to 124 m; from a rough calculation using the profiles its volume was estimated to be in the range of  $2.04 \times 10^7 \text{ m}^3$  (Xu et al, 2009). The Tangjiashan landslide generated dam was caused by a rock slide occurred in the interbedded soft rock and hard rock strata, which were formed from grayish black siltstone of the Qingping Formation of Cambrian age.

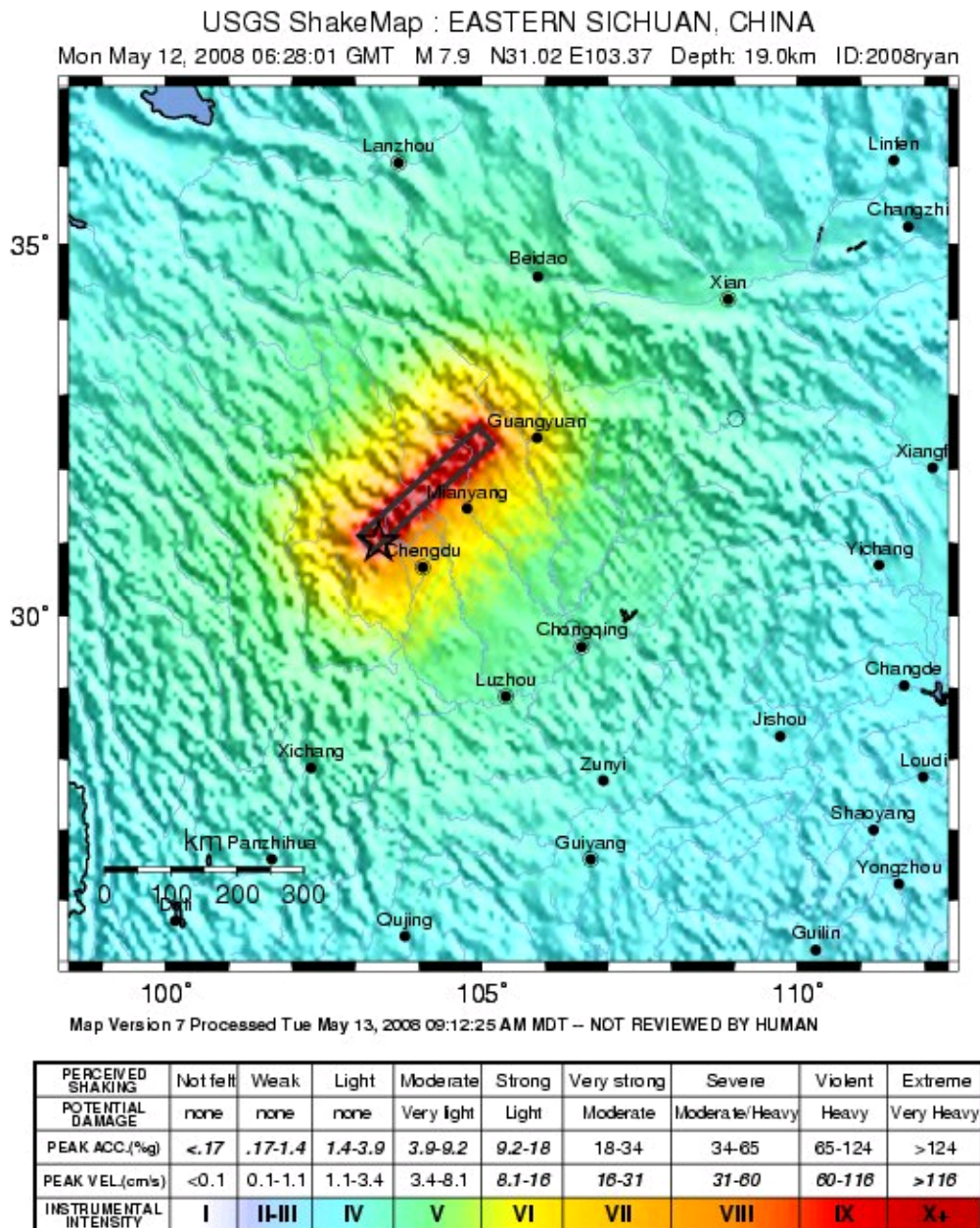
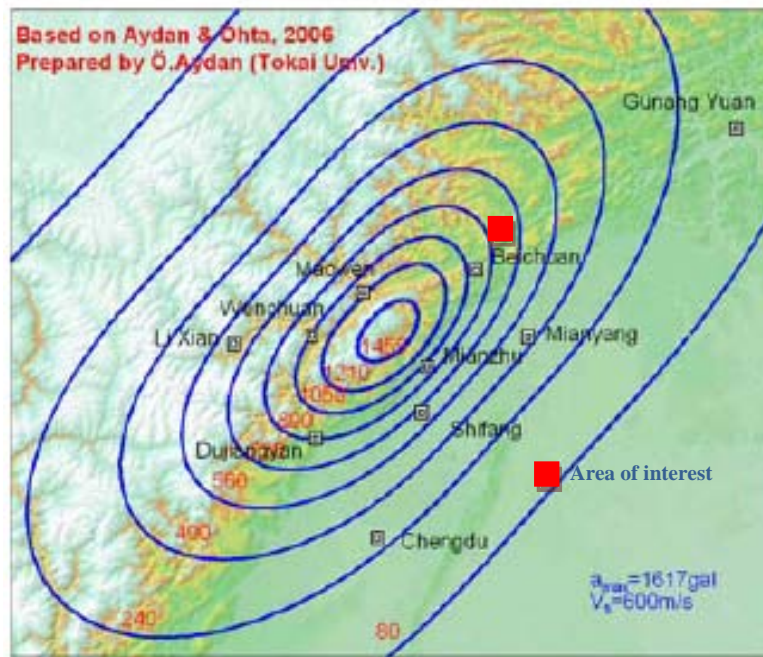
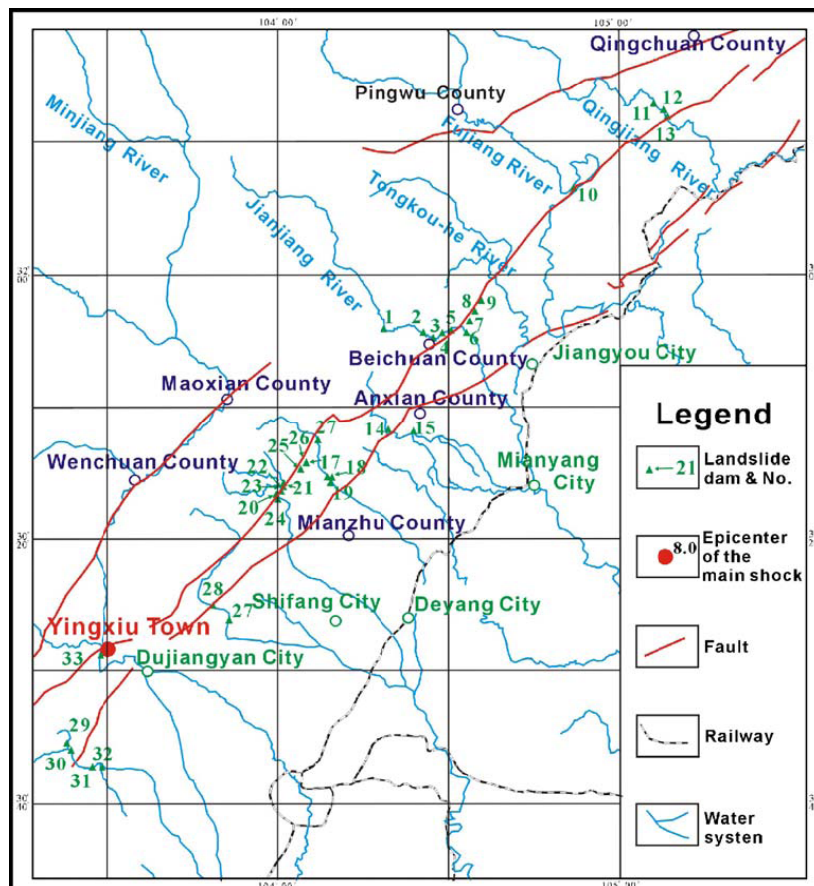


Figure 5-32 - Shake map of the Wenchuan earthquake (USGS).



**Figure 5-33** - Estimated maximum acceleration contours (Aydan et al, 2009). The location of the area of interest is shown with a red spot (PGA approximately 890 to 1050 gals).



**Figure 5-34** - Location of landslide dammed lakes (Yin et al, 2009).

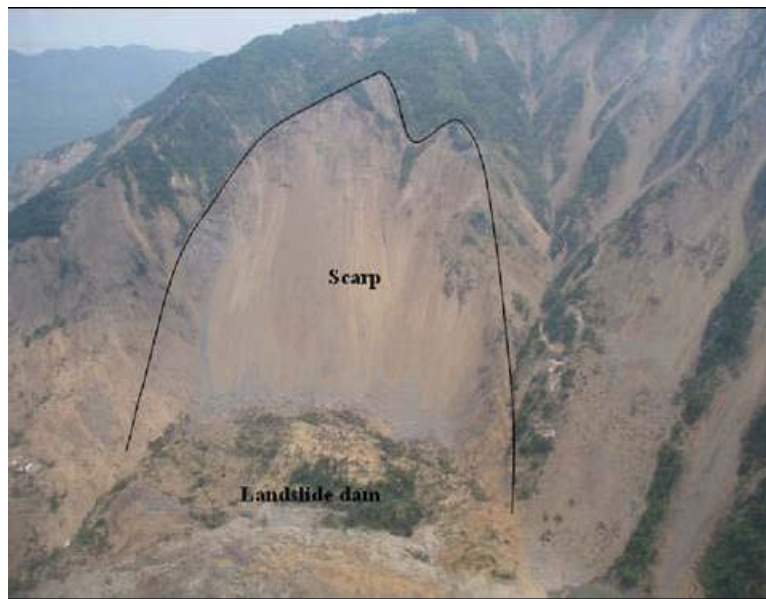


**Figure 5-35** - Overview of the Tangjiashan landslide dam.

According to the eye witness's description, the landslide occurred almost at the same time as the earthquake and traveled for a vertical distance of 540 m within 1 min, i.e. with an estimated speed of 10 m/s. The very large, steep scarp can be observed in figures 35 and 37.

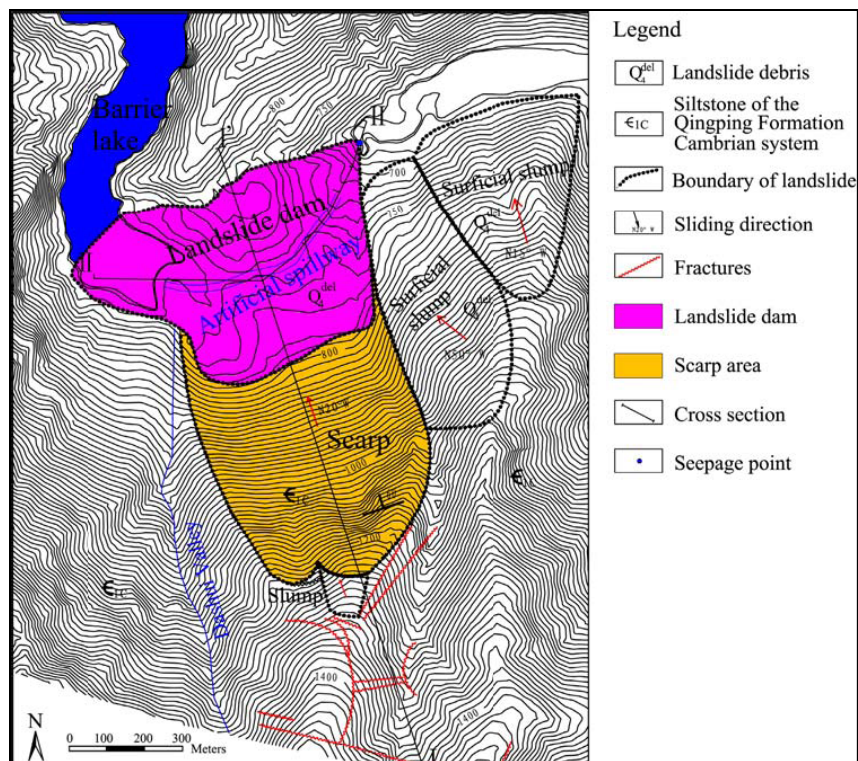


**Figure 5-36** - Engineering geological map of the Tangjiashan landslide (Xu et al, 2009, modified from Hu 2008).

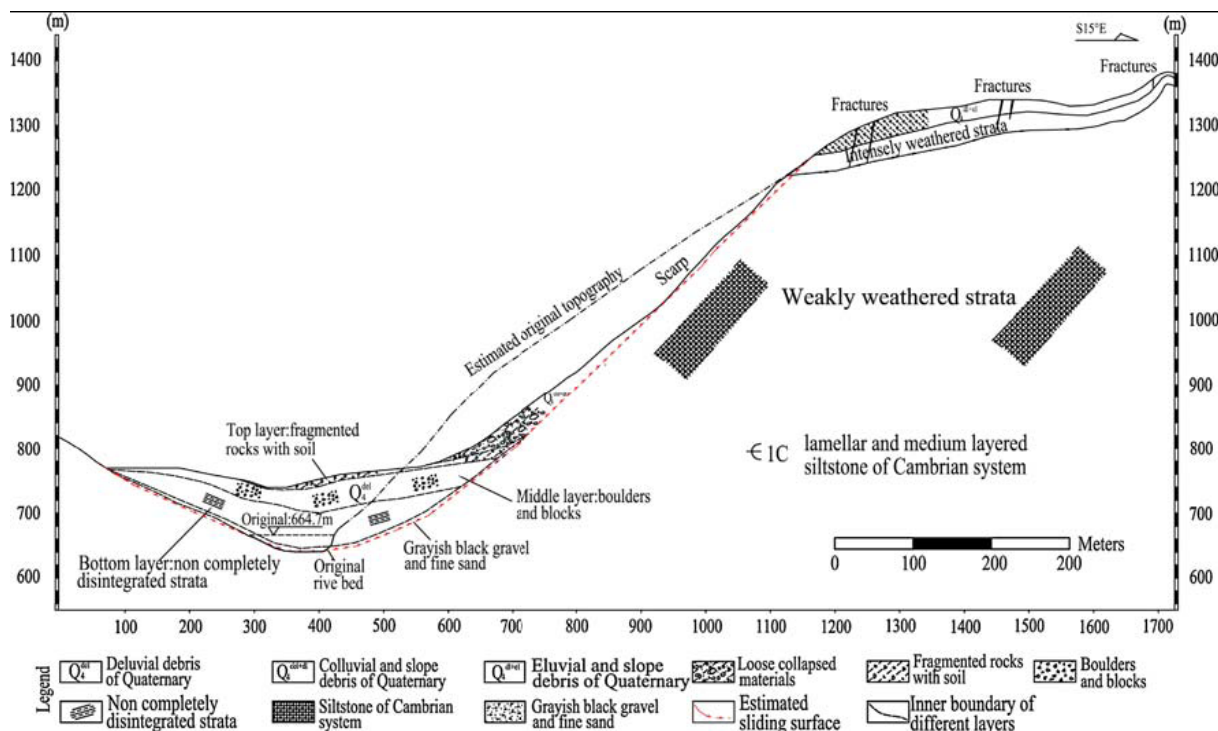


**Figure 5-37 - Geological profile I-10 through the Tangjiashan landslide and landslide dam (Xu et al, 2009).**

bottom layer consists of very weathered strata which retain their original structure. The average size of the boulders is 2 to 3 m with a maximum of 5 m. The blocks vary from 0.2 to 1.5 m. The top layer and middle layers comprise approximately 10% boulders, 60% blocks, 20% fragmented rocks, and 10% soil. Consequently, the bottom layer is relatively more consolidated and has a lower permeability than the middle and top layers.

Due to the collision of the landslide with the north river bank, the debris reached a thickness of 30–50 m at the north margin of the landslide dam. This is an area where the landslide debris ran up the opposite slope and then receded part of the distance of the initial run-up. The maximum capacity of the landslide lake was  $2.4 \times 10^8 \text{ m}^3$ , with a lake length of 20 km.

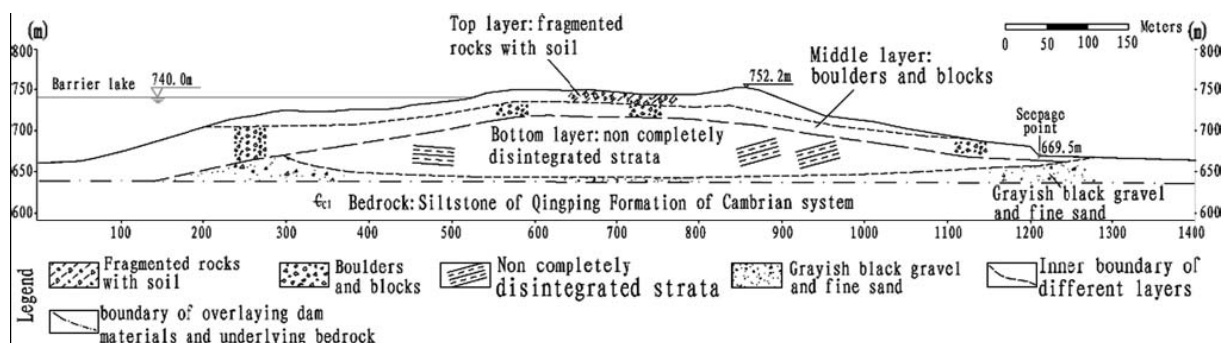


**Figure 5-38 - Cross-section II-II0 of the Tangjiashan landslide dam: note three-layered structure (Xu et al, 2009, modified from Hu 2008).**

### 5.5.9 Synthesis of the selected cases histories

Table 5-7 presents a synthesis of the main characteristics and data availability of the selected case histories that may be useful to the Safeland working activities.

*Table 5-7. Synthesis of the available data of the selected case studies*

		Landslide Case Hystories						
		Las Colinas landslide, El Salvador	Higashi-Takezawa slide, Niigata-ken Chuetsu, Japan	Naranoki slide, Niigata-ken Chuetsu, Japan	Musikame slide, Niigata-ken Chuetsu, Japan	Calitri landslide, Irpinia, Italy	Corniglio Landslide, Apennines region, Italy	Tangjiashan landslide, Wenchuan, China
<b>Scale</b>		site specific	site specific	site specific	site spacific	site specific	local	site specific
<b>Triggering mechanism</b>		earthquake	earthquake	earthquake	earthquake	earthquake	earthquake+ intense rainfall	earthquake
<b>Landslide Category</b>		flow (Cat. III)	flow (Cat. III)	debris slide (Cat. I)	flow (Cat.III)	flow (Cat. III)	earthslide (Cat. II)	rockslide (Cat. I)
<b>Data availability</b>	<b>Geology</b>	●●●	●●●	●●●	●●●	●●●		●●●
	<b>Topography</b>	●●●	●●●	●●●	●●●	●●●	●●●	●●●
	<b>Geotechnical characteristics</b>	●●●	●●●	●●●	●●●			●
	<b>Time history records/PGA,PGV values</b>	●●●	●●	●●	●●	●●●	●	●●
	<b>Numerical analysis</b>	●●●	●●●			●●●	●●●	
	<b>Damage observation/risk analysis</b>	<b>buildings</b>	●●	●			●	●●●
<b>infrastructure</b>		●●		●	●	●		●

● few data ●●sufficient data ●●●many data

## 6 LANDSLIDES TRIGGERING BY SNOWMELT AND PERMAFROST DEGRADATION (ETHZ)

Permafrost was defined by the Permafrost Subcommittee NC (North Central) Canada in 1988 as the ground which remains below 0°C for more than 2 years; the required climate conditions are representative of several high latitude and high altitude area in Europe (Figure 6-3 shows the location of permafrost in Europe). Current estimates indicate that 24% of the land surface of the Northern Hemisphere is covered by permafrost (Zhang et al., 2003). As the definition of permafrost does not define whether ice or snow must be present, an area of permafrost may not contain snow or ice, thus presenting a diverse set of engineering properties.

Studies have shown (Brown et al., 1981) that areas experiencing permafrost are denoted by a characteristic temperature-depth profile, as the one shown in Figure 6-1. The layer at the top of the profile is known as the *active* one, showing cyclical behaviour between frozen and unfrozen state depending upon local temperature conditions. The active layer is interesting from a geotechnical point of view as it heavily influences the behaviour of the underlying permafrost, acting as a buffer between the air (with its daily temperature changes) and the thermally stable ground below. The active layer is strongly exposed to instability as a result of the seasonal thawing (Duan and Naterer, 2009); it cause probably the greatest concern in the medium term (e.g., Rist, 2007) being extremely sensitive to thermal conditions driven by climate variability (Figure 6-2). Seasonal fluctuation of the energy balance components, modified through factors such as input radiation, snow cover, vegetation, water content, and groundwater flow can be seen in the changing thickness of the active layer year after year. This potentially increases hazard, especially with active-layer deepening due to global warming.

Along with permafrost, snow and specifically snowmelt need to be considered when predicting landslide behaviour in a rapidly changing climate. Figure 6-6 shows the winter distribution of snow in Europe in Feb 2003: it shows that, outside Russia, winter snow in Europe is concentrated in Scandinavia, Finland, northern areas of the UK (high latitude), high altitude mountain ranges (notably the Alps, Pyrenees, Apennines and Carpathians) with widespread snow cover in central Europe, including Poland, Belarus, Hungary and Romania. Summer snowcover in Europe is limited to the very high latitude (The Northern extremes of Norway and Finland).

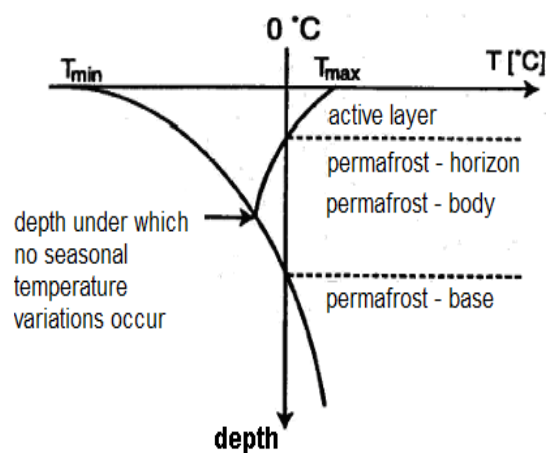


Figure 6-1 - Definition of Permafrost (Brown et al., 1981).

The effect of the snow melting on soil conditions is complex, requiring for an in-deep understanding of all the processes involved. Snow has a high surface albedo (i.e. is highly reflective of radiation from the sun) and a low thermal conductivity (i.e. is a good insulator for heat). As a result, snow of heights over 60-80cm acts as a thermal insulator, protecting the ground from the thermal effects of daily temperature and sunlight fluctuations, thus preventing or delaying melting of permafrost in regions where the climate is tending towards warmer temperatures.

When considering the effect of snowmelt on the underlying soil and the susceptibility of the latter to sliding, two aspects are of concern, namely the Snow Water Equivalent (SWE) of the snowpack and the melt rate. The SWE is the height of the water column that is obtained by melting the snowpack and is usually measured in millimetres; it is relevant because it determines the degree of saturation of the soil due to snowmelt. The melt rate is the volume of snow that melts per unit area and unit time, usually measured in millimetres per day. It is decisive for the same reasons as the precipitation rate in the case of landslide triggering due to rainfall. In fact, it leads to an excess pore pressure in the soil if it infiltrates the ground, or it can lead to erosion and debris flows if the discharge in a steep stream or river exceeds a certain threshold. Strictly speaking, the melt rate is not exactly the same as the infiltration rate because melt-water generated near the surface of the snowpack first has to percolate through it, filling all pores up to saturation. At the beginning of the melting period, it may take from hours to days until the wetting front reaches the ground. After a while, preferential flow channels form, and meltwater reaches the ground in a matter of seconds to minutes. If the snowpack contains buried ice crusts that are impermeable to water, the spatial distribution of the melt and the infiltration rate may show strong local variation at the scale of few metres. Melting of the snowpack requires a considerable supply of heat energy, as the latent heat of ice is approximately 334 kJ/kg. Heat sources that can contribute to snowmelt are short-wave (solar) radiation, long-wave radiation, (turbulent) heat exchange with the atmospheric boundary layer, infiltrating warm rain water and heat flux coming from the ground. The vapour content in the air influences the efficiency of the wind in delivering heat to the snowpack. Radiation and wind vary strongly over scales larger than a few metres in mountainous terrain: these heat sources as well as rain water vary strongly over time as well. Peak hourly melting rates may exceed the daily average by an order of magnitude.

Because of the importance of snow melt water in agriculture, water management and power generation, a large body of research has been devoted to the understanding in details of the relevant physical processes and to develop computational tools at various levels of detail and sophistication. A summary of this research and development with a list of relevant research papers, reports and books can be found in Section 4.2 of SafeLand Deliverable D1.2.

In order to understand the importance of snowmelt for the triggering of landslides, snowmelt can be treated in a similar way as rainfall. Measurements and model calculations indicate that the melt rate can easily reach 30–50 mm/day under rather normal circumstances. In somewhat less frequent situations, e.g., with windspeeds above 10 m/s and air temperature above 6°C in vapour-saturated air, the melt rate may exceed 100 mm/day. With even stronger wind and warmer air, melt rates above 250 mm/day can be attained. Depending on the local climate and soil conditions, such values may be near or above the threshold for triggering of debris flows. The return period of the corresponding weather situations varies strongly from one region to another, but is expected to lie in a range that is highly relevant for risk management in many areas in Europe.

---

In consideration of the nature of the possible triggers to slope instability, it is clear that problem is truly interdisciplinary in requiring a combination of knowledge of hydrological, glaciological, geophysical and mechanical disciplines in order to address the complexity of the processes and their consequences. The scientific and social interest in permafrost and rock glacier degradation in lower latitude mountain (Alpine) systems stems from the direct impact on infrastructure and population present at densities higher than those found in circumpolar regions. The steep gradients in slopes, geology and terrain, and precipitation patterns may enhance some processes, adding complexity.

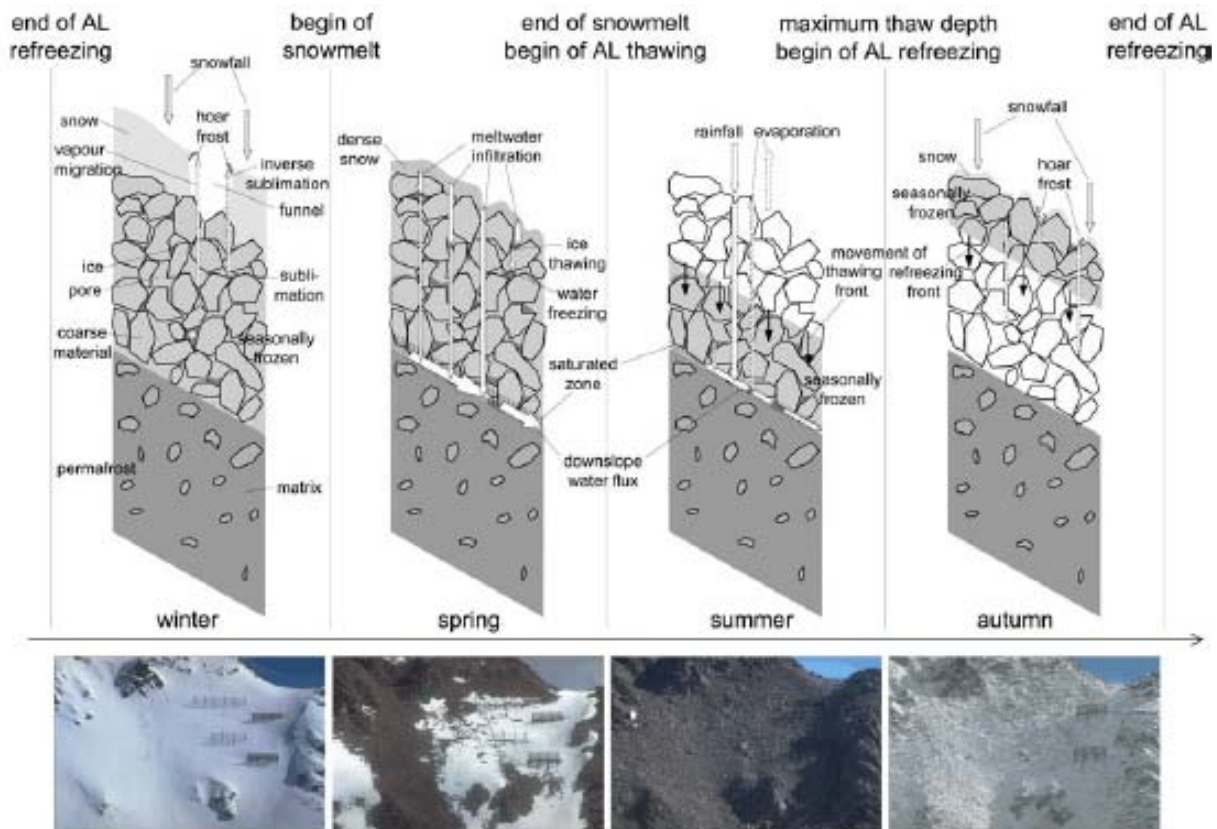


**Figure 6-2** - Hypothetical temporal distribution of hydrothermal processes in the active layer (AL) above alpine permafrost on steep scree slopes. The photos were taken by an automatic camera looking at the study site above Pontresina (CH) (Example from Rist, 2007, after Boike and Overduin, 1999; Photographs: Phillips, 2003).

## 6.1 LANDSLIDE DISTRIBUTION IN EUROPE ARISING FROM DEGRADING PERMAFROST AND SNOWMELT

As will be discussed in section 6.3.4, Permafrost in Europe is showing a trend of decreasing in abundance, while snow cover and duration is becoming less extensive. As a result, landslides in the Alps have been observed to be more common in the recent 20 years than previously (Soldati et al., 2004). Figure 6-4 depicts a global estimation of landslide hazard, indicating that landslide events in Europe are expected in the Alps, Apennines and the

Balkans (an extension of the Alps arch), coinciding with the tallest mountain ranges, and with areas of permafrost, snowmelt and glaciation.

## 6.2 PHYSICAL PROCESSES AND RELATED CONSTRAINTS TO THAWING AND FREEZING

As stated in the introduction of this section, Permafrost can be defined as soil at or below the freezing point of water (0°C) for a period of two or more years, with ice not necessarily present in the soil matrix. Permafrost extension varies together with the climate changes over a period of years, being mostly located at high latitudes. Above the permafrost, the active layer cycles through periods of above- and below-freezing temperatures depending on the season.

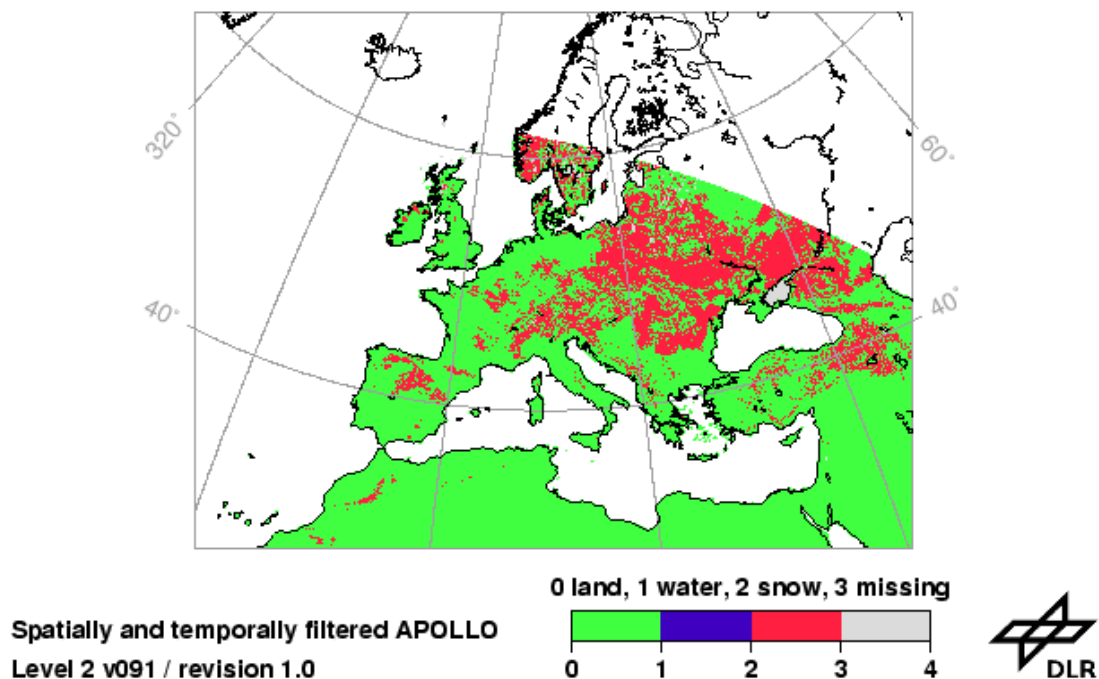


*Figure 6-3 - Distribution of snow in Europe on 01/03/06. Image taken from World Data Center website at [http://wdc.dlr.de/data\\_products/SURFACE/seviri\\_snow/20060301\\_snow\\_eu\\_lv2\\_cumulative.gif](http://wdc.dlr.de/data_products/SURFACE/seviri_snow/20060301_snow_eu_lv2_cumulative.gif).*

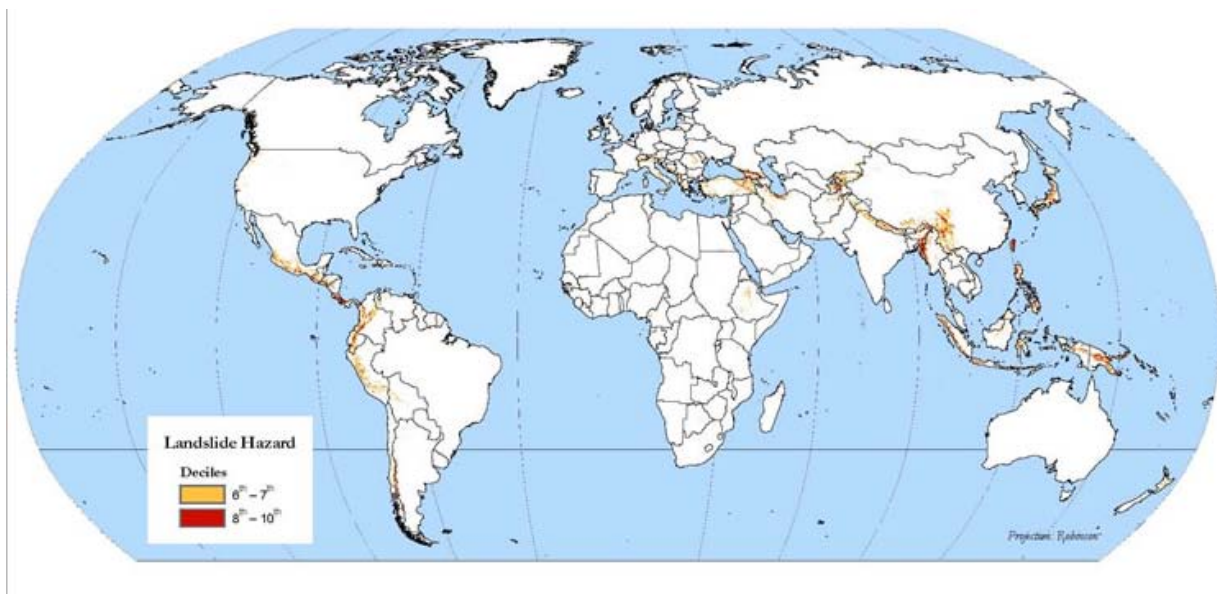


**Figure 6-4** - The worldwide distribution of landslide hazard (Dilley et al., 2005).

The depth of the active layer is particularly sensitive to variations of surface temperature. Alpine permafrost may exist at high altitudes in lower latitude regions, with rock glaciers being one of its most spectacular geomorphologic expressions. Rock glaciers occur in many mountainous regions and are complex inhomogeneous mixtures of ice with varying proportions of rock fragments (Giardino et al., 1987; Martin and Whalley, 1987; Barsch, 1996). They have been described in literature as a “lobate or tongue-shaped body of perennially frozen material supersaturated with interstitial ice and ice lenses that move downslope or downvalley by creep as a consequence of the deformation of ice contained in them and which are, features of cohesive flow” (Barsch, 1992). Haeberli (1985) refers to rock glaciers as a “visible expression of (steady state) creep of ice-supersaturated mountain permafrost bodies”, features of which are clearly seen in Figure 6-2. The glaciers are common in the Alps where as much as 20% of the downslope transport of debris may occur through rock glaciers (Haeberli, 1985).

Because the rock glaciers can flow downslope below the local limit of permafrost occurrence, they are sensitive indicators of climate variability (Haeberli et al., 2006).

The generation of rock glaciers is a subject of controversy (see Clark et al., 1998) but contenders now agree on the fact that rock glacier origin spans the spectrum from glacial (a glacier made of ice) to periglacial (frozen slope). This debate only confirms that rock glaciers are recognized to be complex geomorphic features: descriptions solely based on surface observations are not sufficient to characterize them or to understand physical processes responsible for their dynamical response to changes in climate.

Limited published data on the internal structure of rock glaciers are available (e.g., Whalley et al., 1994; Elconin and La Chapelle, 1997; Berthling et al., 1998; Arenson et al., 2002) from geophysical investigations and the few boreholes drilled into Alpine permafrost. The active layer provides probably the greatest concern to stability in the medium term (e.g., Rist, 2007) as it is extremely sensitive to thermal conditions driven by climate variability (Figure 6-5). Seasonal fluctuation of the energy balance components modified through factors such as input radiation, snow cover, vegetation, water content, and groundwater flow can be denoted in the changing thickness of the active layer year after year. This potentially increases hazard,

especially in the presence of active-layer deepening due to global warming (for example, the zone of continuous dark green in Fig. 4 showing the effect of degradation on the flanks of a rock glacier during a very warm year).

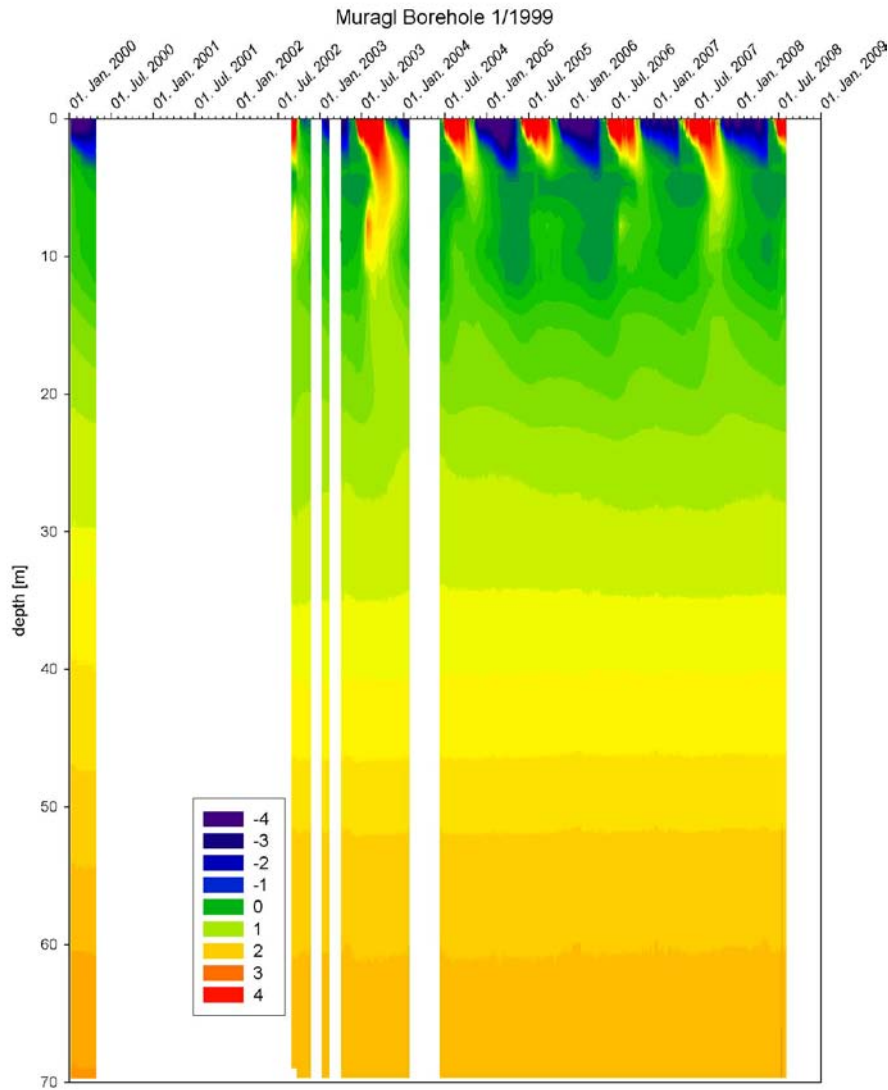


**Figure 6-5** - Temperature data from monitoring in boreholes on the Muragl rock glacier showing significant penetration of temperatures  $>2^{\circ}\text{C}$  to depth  $>10$  m in the flank of the rock glacier during the summer of 2003 (Source IGT boreholes, data by Arenson and Bleiker).

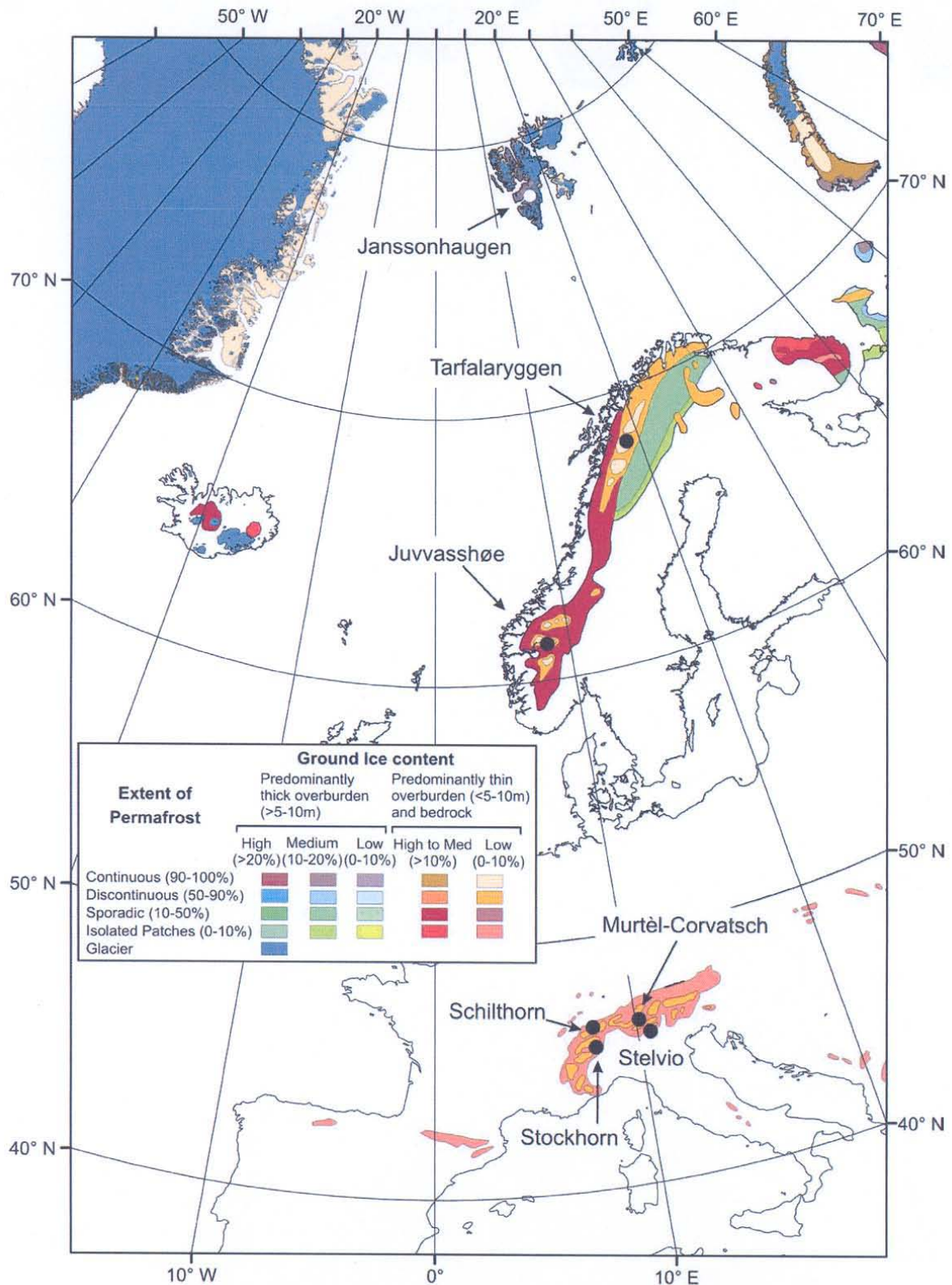


**Figure 6-6** - The location of PACE boreholes overlain on a map of permafrost distribution (Harris et al., 2009).

The underlying, perennially frozen, creeping mass sometimes contains ice alone or an ice-water-air-solids matrix. Well below the melting temperature of ice, any interstitial water present is accompanied by significant suctions contributing to an appearing of cemented behaviour. The material tends to be cohesive and relatively strong (Ting et al., 1983), although time-dependent deformation (creep) can be observed. It is rare to observe a failure within the body of a frozen rock glacier (Arenson, 2003), although the creep process can reduce substantially its strength. Along with temperature inching towards the melting point, increasingly amounts of ‘unfrozen’ water form around soil particles (so called premelting) owing to intermolecular forces (Williams, 1967; Stadler, 1997). The suctions within this interstitial water layer reduce with increasing volumes of unfrozen water, which, in turns, reduces the strength of the ice-soil mixtures. For mixtures with low solid content, the extent of such strength reduction was documented in laboratory experiments performed in the context of studying debris in both glacial or artificial granular ice (e.g., Ting et al., 1983; Arenson, 2003).

With higher solid content, granular friction and interlocking (dilation) becomes significant but precise quantification of the effect of interstitial meltwater on strength requires further laboratory testing, demanding for the combination of geophysical and geotechnical measurements on laboratory specimens. The reduction in strength effectively means that these layers can act as intense shear zones along which most of the deformation may occur. Because rock glacier motion is governed by motion and shear along these ‘weaker’ layers, the thermal state of rock glaciers plays a fundamental role in rock glacier dynamics (e.g., Haeblerli, 2006).

The thermal effects on rock glacier and alpine permafrost are central in the description of permafrost hydromechanical response. Mechanisms causing rapid heat flow into warm discontinuous permafrost, however, are not well understood (Nelson et al., 1999). Although the primary mechanism for heat transport in permafrost is by conduction, higher surface temperatures may also increase flow of interstitial water by accelerated thawing giving rise to significant internal advective heat transfer. Quantifying the magnitude and dynamics of this internal advective process remains a significant challenge for alpine permafrost researchers. Water dynamics in frozen soils are strongly influenced by phase change where unfrozen water content strongly depends on soil temperature (e.g. Williams, 1967). The relationships between frozen water and temperature is known as the soil freezing characteristic (SFC; Black and Tice, 1989), and is related to the soil water characteristic curve (SWCC; Fredlund and Xing, 1994) or water retention curve (WRC; Haverkamp and Parlange, 1986), which describes the relationship between water content and capillary pressure.

Snow inputs water into the soil as it melts, increasing the pore pressure ( $u$ ) in any water saturated zones and, therefore, reducing the effective stress. This may be coupled with the effect of reducing the overburden and also reducing the insulating effect that snow cover has on soil: this is a commonly acknowledged triggering event of landslides.

Due to the highly sensitive nature of the active zone, monitoring of the thickness of this layer can assist with understanding its reactions to local climatic changes and therefore help to predict future landslide events. The PACE (Permafrost and Climate in Europe) project takes geothermal profiles from drilled boreholes in high elevation mountain permafrost in Europe. Harris et al. (2003 and 2009) summarise the results of six/seven of the main boreholes drilled for the project. Figure 6-6 gives the locations of the seven boreholes discussed in the next section. All boreholes are 100m or greater in length.

---

**Table 6-1 - Minimum and maximum active layer depths recorded at European PACE boreholes (after Harris et al., 2009).**

Site	Minimum thickness (m)	Year with minimum thickness	Maximum thickness (m)	Year with maximum thickness
Janssonhaugen, Svalbard	1.42	1999	1.80	2006
Tarfalaryggen, Sweden	1.45	2000	1.63	2003
Juvvasshøe, Norway	1.95	2000	2.45	2003
Schilthorn, Switzerland	4.43	1999	8.55	2003
Stockhorn, Switzerland	2.88	2002	4.27	2003
Murtèl-Corvatsch, Switzerland	3.12	1999	3.5	2003, 2004, 2005

Table 6-1 shows the minimum and maximum active layer depths recorded by the PACE boreholes. The Scandinavian and Svalbard boreholes are characterised by a lower thickness of the active layer than the Alpine boreholes due to the summer surface temperatures being significantly lower in these areas (Harris et al., 2003).

On Svalbard, the mean air temperature from Dec-May 2005-2006 was 8.2oC above the 1961-1990 average at -4.8oC, and in Southern Norway the summers of 2002 and 2003 were warmer than average, with summer of 2003 providing exceptionally warm temperatures in the Alps (Harris et al., 2009). In Janssonhaugen (Svalbard), the 2005-06 above average winter temperature combined with a warm summer in 2006 gave the earliest thawing of all the 8 years recorded by the PACE project (Harris et al., 2009) the active layer recorded there was 0.18m thicker than in previous years in late summer 2006 (Isaksen et al., 2007). At Janssonhaugen and Juvvasshøe (Southern Norway) the ground conditions tend to be ice-poor bedrock with a thin or absent snow cover and a very low water content. This means that active layer thickness tends to be well correlated with the local summer air temperatures, and, thus, the active layer at Juvvasshøe was 20% deeper in the summers of 2003, 2004 and 2006 than in previous years.

The borehole at Murtèl-Corvatsch (Ch) shows active layer thicknesses varying from 3.1-3.5m, with a general trend of increasing depth with time, within the 19 year observation period (Harris et al., 2009). Also in Switzerland the minimum recorded active layer thickness in the Stockhorn and Schilthorn boreholes was 2.88 and 4.43m respectively during the 5-6 year period that they were measured. The extreme heat of summer 2003 meant that the thaw penetration at Schilthorn was twice the average of the preceding years and, at Stockhorn, it increased by approximately 30%

### **6.3 CURRENT ANALYSIS APPROACHES AT DIFFERENT SCALES (DISTRIBUTION MODELS)**

Landslide maps fall into three groups, inventory maps, density maps and hazard maps. Inventory maps show the location of known landslides, density maps show the spatial abundance of landslides, and hazard maps show the perceived likelihood of a landslide in a given area, obtained by modelling or mapping.

Permafrost distribution is difficult to determine from surface or remote sensing and, therefore, a thorough understanding of permafrost related processes is required for a reliable modelling. Models of permafrost distribution tend to fall into one of two types: regionally calibrated empirical-statistical models and physically based numerical models (Harris et al., 2009). Recently developed models try to include energy exchange in all directions, as opposed to the unidirectional approach, which was taken previously.

Empirical-statistical distributed models directly compare permafrost distribution to topoclimatic factors (altitude, slope and aspect, mean air temperature, solar radiation) which can be measured (Hoelzle and Haeberli, 1995; Hoelzle, 1996; Imhof, 1996).

The Permakart programme (Keller, 1992) uses data gathered from fieldwork and surface analyses to plot the location of permafrost onto a topographical map. First a 3-D mesh is created, plotting x, y and z for a given point, once this mesh has been created the likelihood of permafrost on a given point can be predicted, providing a useful tool for future prediction of landslide events.

Maurer and Hauck (2007) provided a good overview of geophysical techniques used in analysing permafrost distribution: a summary of their work is presented in the following.

A common technique used for 2-D imaging of permafrost is electromagnetic resistance surveying. These surveys work by measuring the speed of electric pulses as they travel through a soil, as the electrical resistivity can vary greatly for typical permafrost material. As the source and receivers do not need to be in contact with the ground, this technique may be used both for ground and airborne surveying, thus making it highly useful in areas which are not easily accessible (Todd and Dallimore, 1998, Hauck et al., 2001 and Bucki et al., 2004).

Geoelectric techniques may also be used to show the electrical resistivity of the ground. This method requires lightweight equipment, which may easily be transported to remote areas, and can deliver two or three dimensional topographic distribution of resistivity with time.

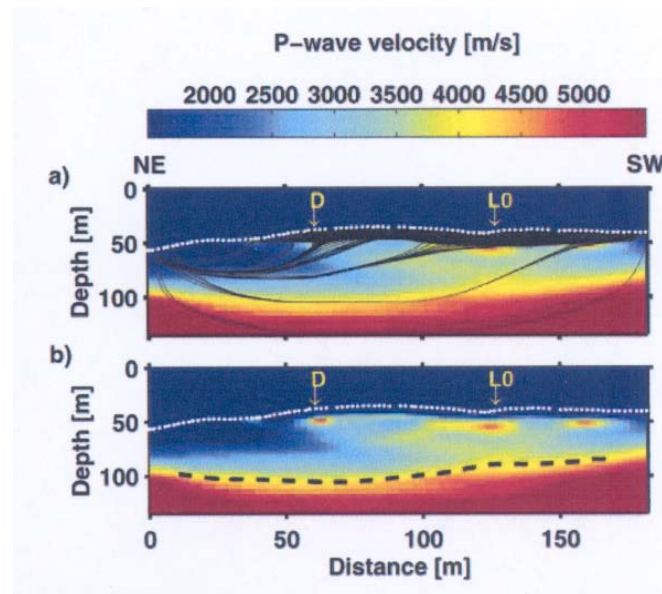


**Figure 6-7** – (a) Final P wave velocity tomogram with associated raypaths from source to receiver points. (b) Final P-wave velocity tomogram. Black dashed line shows interpreted depth to bedrock based on P-wave velocities (Musil et al., 2002).

Seismic techniques may be used. P-waves travel at different speeds which are function of the elastic material properties (Maurer and Hauck, 2007). Musil et al. (2002) presented a case study of a seismic experiment performed at Muragl in Switzerland and some typical P wave velocity profiles through the rock glacier are given in Figure 6-7. In order to interpret the tomography (represented in terms of waves arrival time), it is necessary to know the speeds at which P waves travel through various rock and soil types; Air pockets typically have a speed of 300 m/s, water ~1500 m/s, ice ~350 m/s, unconsolidated glacial sediments have velocities ranging from 500-3000 m/s and boulders have velocities of 4000-5500 m/s. Unfractured gneiss has a velocity of  $\geq 5500$  m/s, with fractured and weathered bedrock having velocities of 10-30% below this (Musil et al., 2002). It should be noted that mixtures of water, ice, air and boulders do not present characteristic speeds.

In the sample tomography given in Figure 6-7, a low-velocity layer can be seen across the top, indicating the presence of loose boulders, air voids and snow in varying proportions. Below this layer, to the right of the image is a low velocity area indicating the presence of a mixture of boulders, fine debris, ice, air voids and water. To the left is a mixture of boulders and fine debris with large air and water filled voids. The basement may be interpreted at the base of the picture, where the velocities show a marked increase.

THM (Thermo-hydro-mechanical) modelling of permafrost gives a valuable insight into the behaviour of frozen soils using the finite element method (Thomas et al., 2009). This method of modelling employs a number of variables including conduction, convection, phase change, movement of water due to suction and ice lenses to give an overall view of the processes at work within a given frozen soil. The main interactions considered are shown in Figure 6-8.

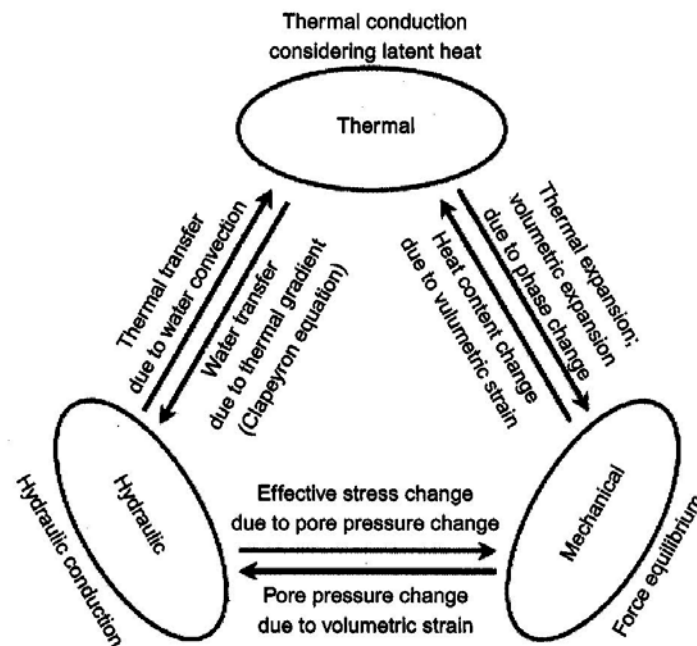


**Figure 6-8** - Thermo-hydro-mechanical interaction mechanisms in freezing soils (Thomas et al., 2009).

With THM modelling, the soil is assumed to be saturated, isotropic and elastic and may be frozen, partially frozen or unfrozen (Thomas et al., 2009). Solid grains, pore water and ice are assumed to be incompressible in a cold climate, and local thermal equilibrium is assumed to have been reached. THM modelling provides a useful tool in predicting the behaviour of soils in a cold climate. There remains a great deal of research to be done in this area to be able to conduct THM modelling effectively on problems relating to permafrost degradation and infiltration of snowmelt (Haeberli et al., 2006).

## 6.4 POTENTIAL CLIMATE CHANGE IMPACTS

Global climate change is estimated to impact sensitive circumpolar and mountainous cryogenic regions to a larger extent than the global average (Vonder Mühl et al., 2008). The rate of these changes are summarized in the 2007 IPCC report which estimates the temperature increase at the top of the Arctic permafrost layer by up to 3°C since the 1980s, and thawing of permafrost base at a rate of up to 0.04 m/yr. These changes are expected to be accentuated in low latitude mountainous cryogenic regions such as found in the European alpine systems. The massive changes to land surface characteristics, activation of various hydrologic and drainage systems, and land destabilization introduce various forms of hazards to human life and infrastructure.

Irrespective of the magnitude and predicted rates of change, critical links between thermohydrological processes and their translation to natural hazards are not fully understood. Lugon et al., (2008) assert that “Scientists have not yet identified all of the processes (e.g. degradation of permafrost due to climate warming); the knowledge about their modes of

*behaviour is insufficient. Also the risks and dangers of natural hazards especially based on the degradation from the climate change, is unknown to the local populations in the Alps.”*



**Figure 6-9** - The rock glacier at Turtmanntal, Canton Valais, CH. Photograph: Sarah Springman.

A recent debris flow that was initiated in the Bérard rock glacier in France (Krysiecki et al., 2008) adds further weight to existing concern about catastrophic slides being triggered due to reduction in strength as the ice phase warms, induced by climate change (e.g. Haeberli, 1992; Zimmermann and Haeberli, 1992; Haeberli et al., 1993; Haeberli et al., 1997; Davies et al., 2001).

Studies have shown that in certain conditions, well-drained rock glaciers may release melt water into the slope causing catastrophic debris flows such as the 1987 event at Val Pola (I) (discussed in section 3.3.1) whereas in other cases, similar changes may induce rapid motion of the entire rock glacier as presumed to occur in Turtmanntal, CH (Figure 6-9). Recent instabilities in Vallée du Durnand (CH) and the Bérard Rock Glacier (F), both in 2006 highlight the growing public concern and urgency for improved understanding and predictability.

Impacts of global climate change on sensitive cryogenic regions are an important area within climate change science. The carbon, locked away within gelisols, is released upon melting and may contribute to a positive feedback system within global warming. These rates of changes are summarized in the IPCC report estimating temperature increase at the top of the Arctic permafrost layer by up to 3°C since the 1980s, and thawing of permafrost base at a rate of up to 0.04 m/yr. These changes, accentuated at other cryogenic regions such as Alpine systems in Switzerland, affect land surface characteristics, drainage systems and introduce various forms of hazards to human life and infrastructure. Rock glaciers and degrading permafrost on steep Alpine slopes may become susceptible to melting of massive ice and initiation of landslides and instabilities due to accelerated motions. The links between thermohydrological processes and natural hazards are not fully understood. In some cases, well-drained rock glaciers may release melt water into the slope causing the 1987 debris flows

at Val Pola (I), whereas in other cases, rapid motion of the entire rock glacier is presumed to occur (Turtmanntal, CH). Recent rock glacier instabilities in 2006 in Vallée du Durnand (CH) and Bérard (F), emphasise the growing public concern and urgency for improved understanding and predictability.

The recent awareness about anthropogenic climate change has raised the issue of how the changing climate will create more natural disasters in the future. It may be reasonably assumed from current climate models and observations from the past decade that with the changing climate the permafrost at lower altitudes will melt, there will be less snowfall (and therefore less snowmelt and shorter seasons) and deglaciation will occur. As the surface temperature increases in permafrost regions, this will lead to a thickening of the active layer and a higher altitude 0°C isotherm. What this will mean, in a practical sense, is that the contribution to the ice in terms of ‘cementing’ potentially unstable ground will not be available, and that the volume within the active layer will increase, leaving the more ground free to slide than before. As ice takes up latent heat and thus increases response time to ground temperature changes, an increase in temperature to the point where permafrost melts will cause the release volumes of debris as intermittent and probably severe landslide events, which have been held back for a period of decades. The increased thickness of the active layer, coupled with the reduced uptake of latent heat and the reduced snowcover will mean that permafrost areas will experience a greater sensitivity to seasonal variations in temperature.

The existence and dynamics of liquid water in frozen soils within permafrost (Boike et al., 1998) strongly affects the hydro-thermal regime within rock glaciers. Hydro-thermal processes within the active layer above alpine permafrost were described by Rist and Phillips (2005) and Rist (2007). They found for thawing periods that hydrological and thermal parameters in the ground, slope stability and meteorological parameters were closely correlated in time. An instantaneous increase in ground temperature was caused by convective heat transfer, while latent heat was released due to phase change of infiltrating meltwater from surficial snow. Downslope displacement also began simultaneously to meltwater infiltration. Results from laboratory tests showed that a slope failure is most likely in summer, when the thawing active layer deepens into finer grained materials and when its water content is at field capacity or even higher due to a heavy rainfall. The situation during snowmelt was found to be less critical, because a large amount of the infiltrating water was freezing in the active layer, which was still cold, and the surficial deposits were stabilised by the ice. The amount of ice formed during this period determined the water content during active layer thawing, which was found to be important for the disposition of slope failure in summer. The three dimensional nature of the active layer was found to be important in degrading zones of rock glaciers and has not yet been investigated in detail and will provide a further challenge to face.

The importance of these relationships lies in the sequence by which water thaws in largest pores first, hence the release of thawed water may not be proportional to temperature rise and large amounts of water may be released first and subsequently create large flow pathways. Consequently, the depth and lateral extent of the active layer may be much larger than predicted by heat conduction alone. The rate and extent of thawing may result in significant transfer of heat and mass to large depths. In addition to transfer of energy, such thermally induced internal flows may encounter low permeability layers and spread laterally, forming weak preferential shear horizons as pore pressure increases reducing effective contact stresses, and hence shear resistance.

---

## 6.5 EXAMPLES

### 6.5.1 Val Pola landslide, Italy

Crosta et al. (2004b) have reported on the landslides at Val Pola in northern Italy in 1987 (a map showing the location is shown in Figure 6-5). A series of hundreds of landslides and severe flooding occurred between 15 and 22nd July 1987, causing loss of life and large scale economic consequences. During this period, the temperature was unusually warm, with the 0° C isotherm having moved to 3500-4000m (the 0° C isotherm is generally at 2500m in the European Alps; Maurer and Hauck, 2007) and an abnormally high rainfall noted (600mm from 15-22/07/87, where the mean annual rainfall is 1200mm). The combination of the heavy rainfall and exceptionally warm temperatures led to frozen soil, interstitial ice and glacier melting, which in turn led to loss of strength, pore pressure build, high runoff, severe flooding and triggered landslides. Landslides were characterised by shallow failures which generally became debris flows as they mobilised.

The largest example of mass movement was concentrated on a prehistoric landslide located on the eastern slope of Mount Zandila (see Figure 6-10). Heavy rainfall on 18-19th July caused flooding, rockfalls and debris flows on the north side of the prehistoric landslide, which in turn formed an alluvial fan, damming up the Adda river valley and causing the creation of a large lake of approximately 1-5m depth and 50,000m<sup>3</sup> volume on the valley floor (see Figure 6-11). On 28th July, a large debris flow (estimated volume 34-43Mm<sup>3</sup>) detached from the prehistoric landslide area and rapidly transformed into a rock avalanche which fell into the Adda river valley, displacing the dammed water in the temporary lake. The leading edge of the debris ran 300m up the opposite valley side, while the avalanche split into two avalanches, with one travelling 1.0 km up the valley, and the other travelling 2.5 km down the valley, destroying all the villages in its path. Upon reaching the lake, the avalanche also sent a mud wave of water 95 m high 2.7 km upstream, damaging Aquilone village and killing 27 people.

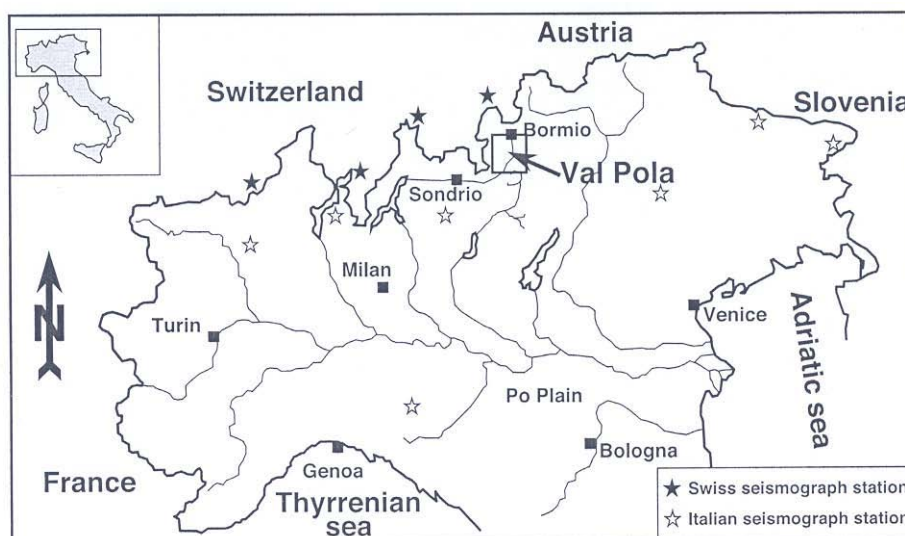


**Figure 6-10** - The location of the Val Pola landslide (Crosta et al., 2004b).  
**Table 6-2** - Known large debris flows during the 20th century at Ritigraben (after Rebetz et al., 1997).

Year	Days
1921/1922	Unknown. 1921 according to Schnydrig (1952), 1922 according to Mani (1994)
1948	4 September
1953	23-24 September
1962	End of June
1977	29-30 August
1987	24-25 August
1991	8-9 August
1993	24 September
1994	24 September

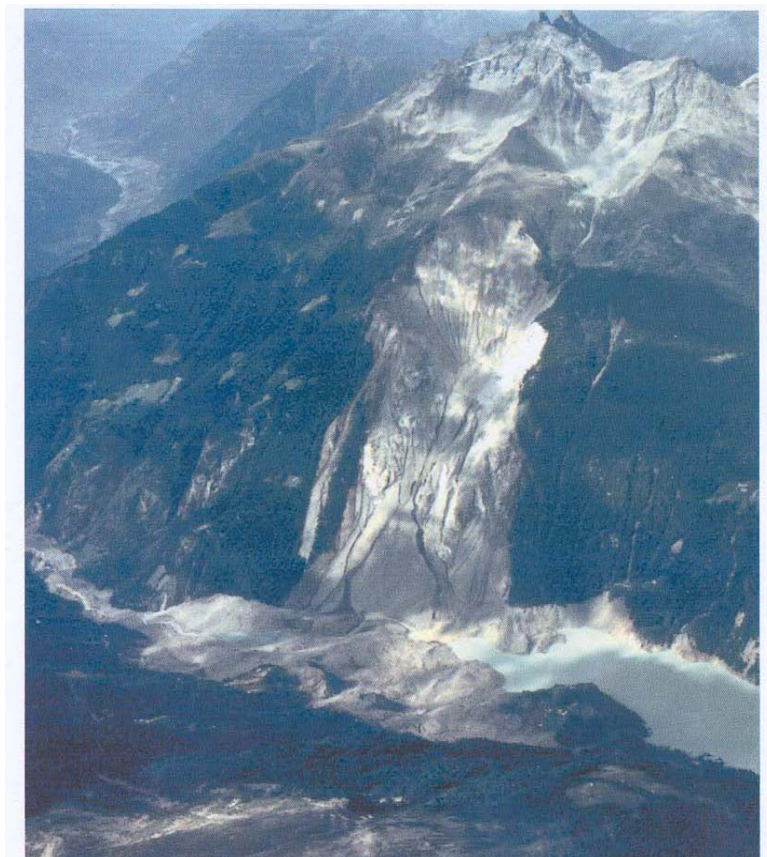


*Figure 6-11 - 28/07/87 Val Pola rock avalanche and temporary lake, looking downstream. North is to the right of the picture (Crosta et al., 2004b).*

### **6.5.2 Ritigraben Torrent, Switzerland**

Numerous debris flows have been noted at Ritigraben in the Pennine Alps, Valais, Ch (Rebetz et al., 1997), with particular interest paid to this area as they directly threaten roads, bridges, a railway line and two villages (Grächen and Sankt Niklaus). The torrent system of the Ritigraben is oriented west/north west, is 3.5 km long and ranges from an altitude of 3100m at the ridge to 1050m at the valley floor. The upper part of the unstable system is in the alpine periglacial zone, with discontinuous frozen ground (King and Akerman, 1993).

Past studies (Pfister and Haechler, 1990; Röthlisberger, 1991 and Mani, 1994, a summary is given in Table 6-2) have provided a record of floods from the Valais/Ritigraben area for the majority of the 20th century. These studies indicate that the Ritigraben has been subject to 9 large debris flows between 1921 (Schnydrig, 1952) or 1922 (Mani, 1994) and now and that these debris flows have become more frequent since the late 1980s (4 major events have occurred between 1987 and 1994).

A large scale debris flow occurred on September 24, 1993 at the Ritigraben torrent, and had a devastating effect on local infrastructure as it cut across two roads, a railway line and destroyed a bridge. The debris carried by the flow created a dam at the outlet of the Ritigraben, causing the water level to rise and consequently flooding of the St. Niklaus filtering plant to occur and 20 hectares of farmland were covered with debris.

All debris flows discussed in the above studies (with the exception of the 1962 event) occurred at the end of summer/beginning of autumn, as this is when the active layer of the permafrost is unfrozen in the periglacial belt. Seven of the nine debris flows were triggered by excessive rainfall events in the Alps, with the remaining two debris flows (1962 and 1994) being triggered by snowmelt. In the 1921/1922, 1953 and 1993 events the flow has been shown to have begun at altitudes of above 2400m (Mani, 1994) and therefore in the Alpine periglacial zone and within the zone of discontinuous permafrost (Haerberli, 1990).

### **6.5.3 Bèrard Rock Glacier (Southern French Alps)**

The Bèrard rock glacier is situated on the Parpallion Range in the Southern Alps and is a good example of the effect of permafrost degradation on the stability of mountains. The area is situated within degrading permafrost, and in the summer of 2006, the sudden collapse of the glacier released 2 Mm<sup>3</sup> of material into the adjacent valley (Krysiecki et al., 2008).

Geomorphological studies have revealed that the collapse was probably related to an underlying rockslide in the schist below (Krysiecki et al., 2008), which may have been activated by storms during summer 2006. Current studies are focusing on any ongoing movements of the rock glacier and indicate that there has been no significant movement of the displaced mass during the first three months of monitoring. The remaining rock glacier was subject to large movements (displacements of more than 5 m in three months). Studies are

still being carried out, but once published, should give an interesting insight into mechanisms affecting rock glaciers in the warming Alps.

#### 6.5.4 1987 Debris Flows in the Swiss Alps

Haeberli et al. (1990) have presented an overview of intense flood and debris flow events in Switzerland in 1987. In the summer of 1987 a significantly above average level of rainfall was experienced, and this combined with snow and ice melt led to the triggering of multiple debris flows in three areas (Figure 6-12). Initial reconnaissance indicated that the periglacial belt had been heavily affected not only by this rainfall, but also by above average temperatures meaning that precipitation was falling as rain in this area.

The three areas were investigated using geophysical methods and the starting zones were found to be in areas where saturation of loose debris on steep slopes was possible immediately below bedrock, snow patches/glaciers and/or permafrost. The erosion had preferably occurred in locations where thaw-destabilisation had allowed the water content of the soil to become non homogenous.



*Figure 6-12 - Three main debris flow affected areas during the summer of 1987 (Haeberli et al., 1990).*

## **7 LANDSLIDE TRIGGERING BY DEGLACIATION (UNIMIB)**

Deglaciation, or the retreat of glacier ice after a glacial period (or pulse of glaciation), involves the onset of different physical processes which are recognised as major landslide triggers in formerly glaciated mountain ranges, including old mountain ranges (e.g. the Caledonian orogen in the Scottish Highlands) and young tectonically active orogens (e.g. the Alps). Debuttressing of slopes steepened by glaciers may result in enhanced rockfall activity, sudden catastrophic slope failures, or slow rock slope deformations, possibly leading to catastrophic failures after long time periods (Ballantyne, 2002).

In general, deglaciation leads to rapid changes in the geomorphic activity of slopes within the context of paraglacial processes, which are defined by Church and Ryder (1972) as “non-glacial processes that are directly conditioned by glaciation”. The paraglacial concept embraces several geomorphic systems, including rock slopes, debris slopes, glacial forelands, as well as alluvial, lacustrine and coastal systems over different spatial and temporal scales (Ballantyne, 2002). The period of time during which a landscape readjustment from glacial to non-glacial conditions occurs is referred to as the “paraglacial period”. According to Church and Ryder (1989) paraglacial processes act with different magnitude and over different periods during and after any periods of glacier retreats, although active and recognisable paraglacial slope instability phenomena are mainly related to Late Pleistocene and later deglaciation periods.

### **7.1 PARAGLACIAL SLOPE MODIFICATION PROCESSES**

Glaciation and deglaciation cycles affect relief production and the distribution of gravitational stresses through valley deepening/enlargement. Moreover, deglaciation causes slope debuttressing and stress release, which condition slope stability through several effects, including modification of stress distribution with respect to a pure gravitational one (Augustinus, 1995), loss of rock mass strength, enhanced weathering and groundwater flow (Crosta, 1996; Ballantyne, 2002; Holm et al., 2004). These processes can interplay with other related to tectonic and locked-in stresses (Savage et al., 1985; Miller and Dunne, 1996), earthquake shaking (possibly itself related to post-glacial rebound; Stewart et al., 2000), structural fabric, tectonic rock uplift, fluvial erosion at slope toe, fatigue and time-effects (Molnar, 2004; Bjerrum, 1973; Pariseau and Voight, 1979; Eberhardt et al., 2004).

#### **7.1.1 Slope steepening**

When ice flow is concentrated in a glacial through or diverted by its regional flow direction (Ballantyne, 2002), glacial erosion tends to both deepen and steepen valley sides. This increases the height and inclination of slopes, resulting in increasing gravitational shear stresses acting in the rock masses (Radbruch-Hall, 1978; Bovis, 1982). These possibly promote slope instability depending on rock mass structure and strength characteristics. Savage et al. (1985) showed that differential gravitational stress acting on valley slopes depends on the relief magnitude, with failure more likely where tensile stress states dominate. Two-dimensional stress distributions have been simulated by several authors for valley-ridge systems of different geometry (e.g. symmetric vs. asymmetric) and assumed material behaviour (e.g. elastic; Savage et al., 1985; Savage and Swolfs, 1986; Pan et al., 1994; elasto

plastic, Kinakin and Stead, 2005), in anisotropic rocks (Pan et al., 1995), and including tectonic stresses (Augustinus, 1995; Miller and Dunne, 1996). All these studies aimed at predicting stress states expected within a given slope, to be compared to rock mass strength characteristics (Hoek and Brown, 1997; Hoek et al., 2002) in order to predict the type and

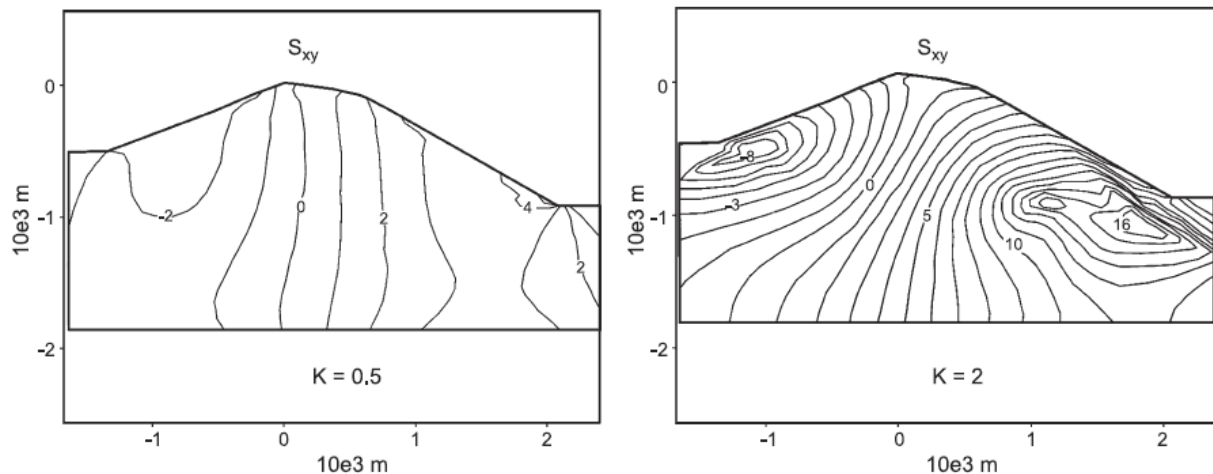


**Figure 7-1** – Shear stress contours for a hogback-shaped ridge under tectonic loading, with values of  $K$  (ratio between horizontal and vertical stresses) of 0.5 and 2 (after Kinakin and Stead, 2005).

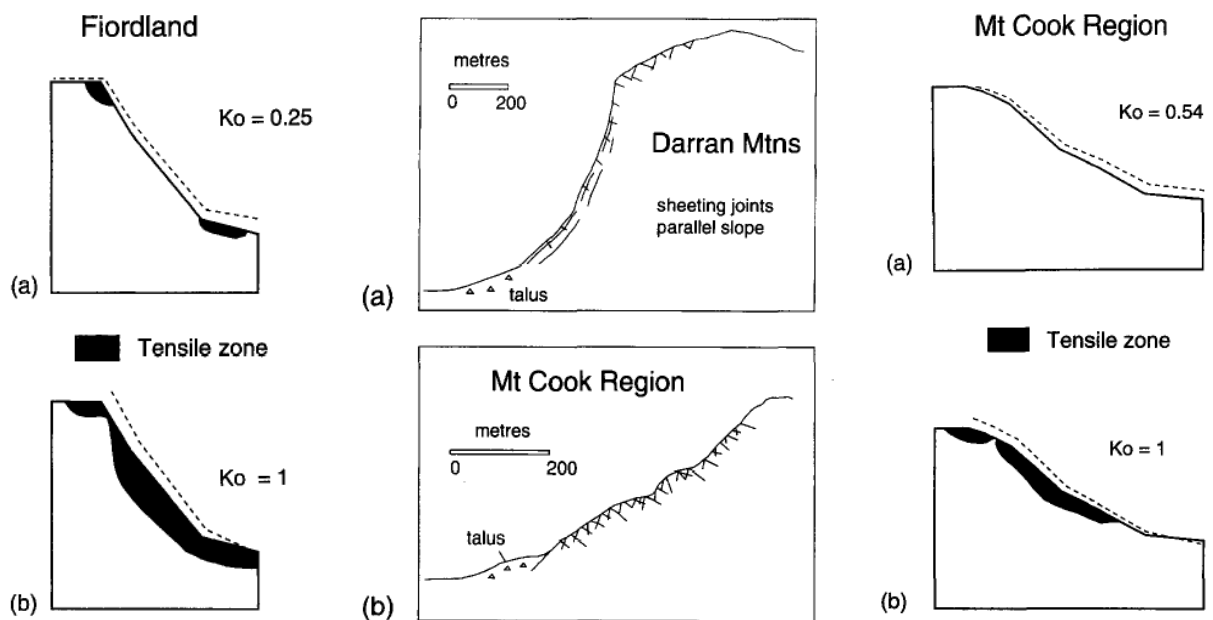


**Figure 7-2** – Displacement profiles of free surface and zones of tensile stress in rock slopes of Fjordland and Mt. Cook regions (New Zealand), computed by Finite Element modelling for: a) gravitational loading only; b) horizontal stress load. Modified after Augustinus, 1995.

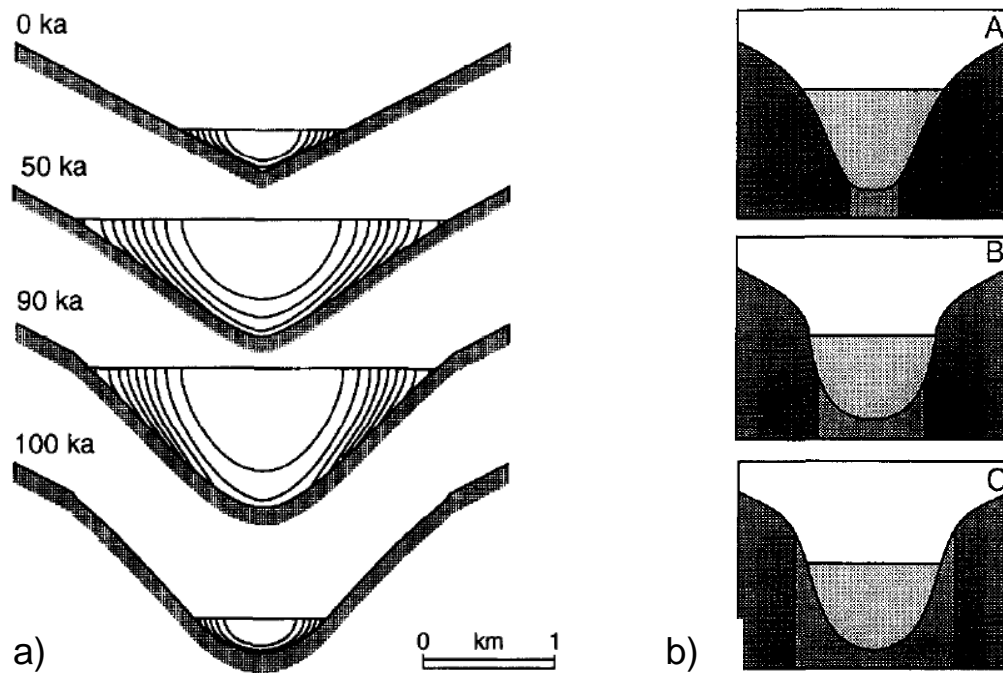


**Figure 7-3** – Controls on the development of glacial valley cross-profile, studied by numerical simulations (modified after Harbor, 1995). a) Cross-section form development over an idealised 100.000 year glacial cycle; b) comparison of glacial valley profiles obtained by considering weak materials forming the 20% (A), 40% (B), and 60% (C) of the initial active channel width.

extent of expected slope instability. Several authors showed that stress distributions in steep slopes with geometry consistent with that of glacial valleys are strongly controlled by in-situ stresses, including active tectonic, locked-in and residual stresses (Wyrwoll, 1977; Augustinus, 1995; Kinakin and Stead, 2005, Fig. 7-1). In particular, for a given slope geometry and rock mass strength, increasing horizontal stress results in deeper zones of tensile stress behind slope faces (Augustinus, 1995; Fig. 7-2).

Stress distributions in glacial valley slopes and their potential effects on slope stability also depend on the evolutionary stage of valley cross-profile development at which deglaciation take place. Harbor (1995) showed that, when a glacier flows into an initially V-shaped valley, erosion dominates to the slope toes, leading to progressively steep valley flanks and the formation of valley shoulders. Therefore, stress redistribution in the valley flank will be different depending of the development stage of the cross-profile (Fig. 7-3a).

The glacial valley cross-profile and width resulting from a cycle of glaciation and deglaciation have also been proved to depend on erosional resistance, which constrains the ratio between resulting valley depth and width, thus affecting the overall cross-profile and consequent stress adjustment upon deglaciation (Harbor, 1995; Fig. 7-3b).

### 7.1.2 Slope debuttressing

The second major way in which glaciation and deglaciation affect rock slope stability is through debuttressing, or “the removal of the support of adjacent glacier ice during periods of downwastage” (Ballantyne, 2002), and consequent stress release. Carlsson and Olsson (1982) showed through in-situ measurement data that, in areas formerly loaded by ice sheets (e.g. Scandinavia), ice loading resulted in stress level higher than those expected by self weight (Fig. 7-4). It has been suggested that also in glacial troughs ice loading induces increased stress levels in the valley floor and walls (Ballantyne, 2002). Part of these additional stresses is stored within rock masses as residual strain energy, and then released when deglaciation

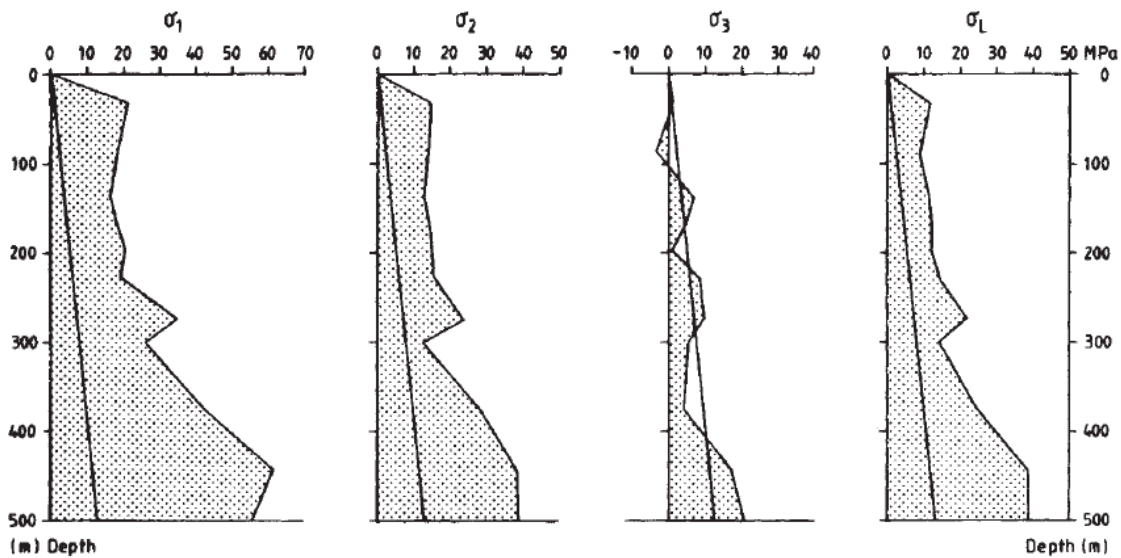


**Figure 7-4** – Comparison of theoretical (self weight) stress distributions and in-situ measured stress in a 500 m deep borehole in Sweden, under a area formerly occupied by a ice sheet (after Carsson and Olsson, 1982).

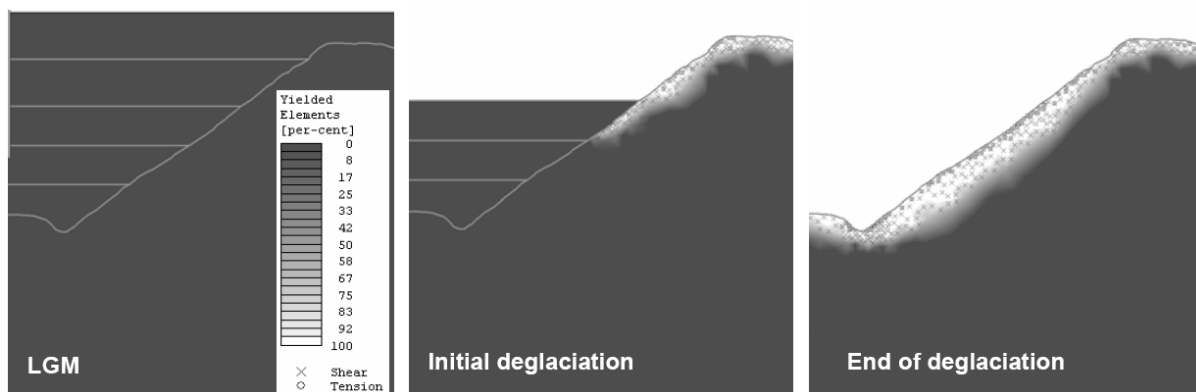


**Figure 7-5** – Multistage Finite Element modelling of a deglaciation sequence, showing the distribution of the resulting tensile and shear damage inside the slope (Agliardi et al., in press).

**Table 7-1** – Paraglacial slope modification processes and related effects on slope stability.

Stage	Processes	Effects on Slope stability
<b>Glaciation</b>	ice loading	increase horizontal stress. Tensile zone
	glacial valley deepening	increase shear stresses (upon unloading)
	slope steepening	
<b>Deglaciation</b>	slope debuttressing	release stress / residual strain energy: rebound
	fracture propagation	increase fracture connectivity / hydraulic conductivity
	rock mass damage	increase rock mass weathering
		reduce rock mass quality / strength
ice melting	increase pore / cleft water pressure	

occurs (Wyrwoll, 1977). High values of residual horizontal stress can result in a major shift of principal stress direction with respect to pure gravitational (self weight) or gravitational and tectonically-induced ones (see previous section), and the development of regions of tensile stress behind the slope faces (Ballantyne, 2002). When deglaciation occurs, such tensile stresses are released and a “rebound” occurs, the magnitude of which is a function of the residual strain energy and the deformation modulus of rock masses.

Slope debuttressing and consequent stress release cause the formation of a zone of tensile damage behind rock faces by the opening and propagation of rock discontinuities. This results in the following effects unfavourable to slope stability:

- a general loss of shear strength along joints, a reduction of interlocking among individual blocks forming rock masses, and decay of the overall rock mass strength. Such kind of damage has been simulated by several authors by numerical modelling, even directly accounting for the removal of glacier ice (Agliardi et al., 2001; Eberhardt et al., 2004; Agliardi et al., in press; Fig. 7-5);
- increased hydraulic conductivity and connectivity of rock discontinuity, resulting in enhanced groundwater discharge and cleft (joint) water pressures, especially when joint outlets are sealed by freezing (Hoek and Bray, 1981);
- enhanced physical (e.g. freeze-thaw) and chemical (e.g. carbonate dissolution) weathering processes, eventually leading to a long term strength reduction of both intact rock material and discontinuity surfaces.

A summary of paraglacial modifications of rock slopes and related effects on slope stability are listed in the following Table 7-1.

## 7.2 PARAGLACIAL LANDSLIDES

### 7.2.1 Rock slope response to paraglacial modifications

Landslide types commonly occurring in the paraglacial context were reviewed by Ballantyne (2002). According to the author, “the nature of paraglacial adjustment of rock slope...reflects the interaction of changing stress conditions associated both with glacial oversteepening and relaxation of individual stresses following unloading and debuttressing on one hand, and rock mass strength controlled by lithology and jointing on the other”. The response of slopes to changes in geometry and stress distributions related to glaciation/deglaciation is thus strongly

constrained by rock mass lithology and structure at different scales. Rock lithology affects the strength, deformability and anisotropy of intact rock (Goodman, 1989; Hoek and Brown, 1980b). On the other hand, since rock masses are physical entities made by intact rock blocks bounded by rock discontinuities, rock mass structure controls its behaviour in different ways. The number of discontinuity sets, their frequency, persistence and strength control the size, shape and degree of interlocking among blocks and, as a consequence, its overall behaviour (“continuum” vs. “discontinuum” medium; Fig. 7-6) in terms of strength, deformability, and hydraulic properties (Hoek et al., 1988):

- when small volumes of rock masses with few sets of spaced discontinuities are considered, overall rock mass strength and deformability are mainly controlled by intact rock properties, and rock slope instabilities will be structurally-controlled (i.e. single discontinuities constrain the location and kinematics of slope failures, e.g. planar, wedge, or toppling failures; Hoek and Bray, 1981; Fig. 7-7a-c). In slopes subjected to deglaciation, the reduced shear strength and increased persistence of rock discontinuities, as well as the modification in subsurface groundwater hydrology, favour the instability of single rock blocks or larger rock mass volume;
- when large volumes of rock masses with several (generally more than three) sets of closely spaced discontinuities are considered, the rock mass tends to behave as a continuum, its equivalent strength and deformability being controlled by the properties of both intact rock and discontinuities (Hoek and Brown, 1988). In this case, some descriptors of rock mass quality (e.g. Rock Mass Rating, Bieniawski, 1989) or rock mass structure (e.g. Geological Strength Index, Hoek et al., 1995) are used to scale intact rock properties and obtain an empirical description of overall rock mass strength. In this case, the kinematics of rock slope failure depends on rock mass strength and on large-scale structural features, allowing for a variety of failure geometries, including circular failure (Fig. 7-7d). Rock mass damage in tensile zones of deglaciated valley slopes tends to reduce the overall rock mass strength and to increase rock mass permeability, at an extent controlled by the properties of intact rock and discontinuities.

Moreover, geological structures including master fractures, faults, folds, etc. constrain the large-scale stability of deglaciated valley flanks, where local relief can attain values exceeding 1000 m or more. In such rock slopes, large-scale structures or anisotropy can lead to the development of either curve/circular or planar failure zones, which can undergo a complete or

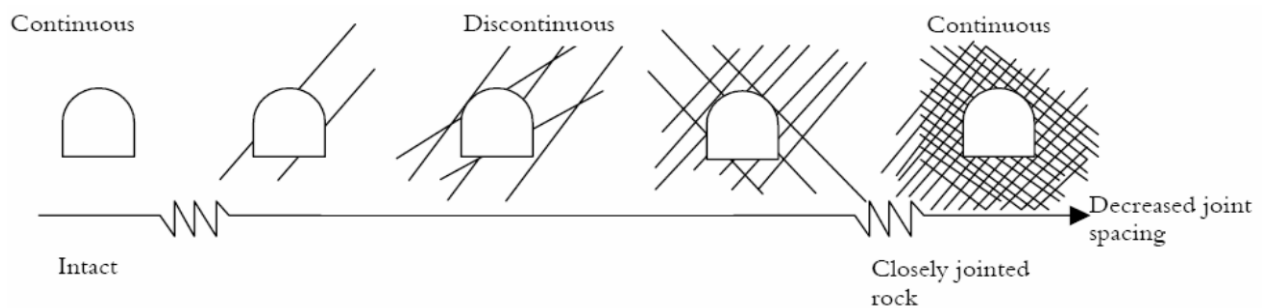


**Figure 7-6** – Continuous versus discontinuous rock mass depending on rock discontinuity number and spacing, for a given spatial scale (e.g. tunnel of constant size). Figure after Edelbro (2003)..

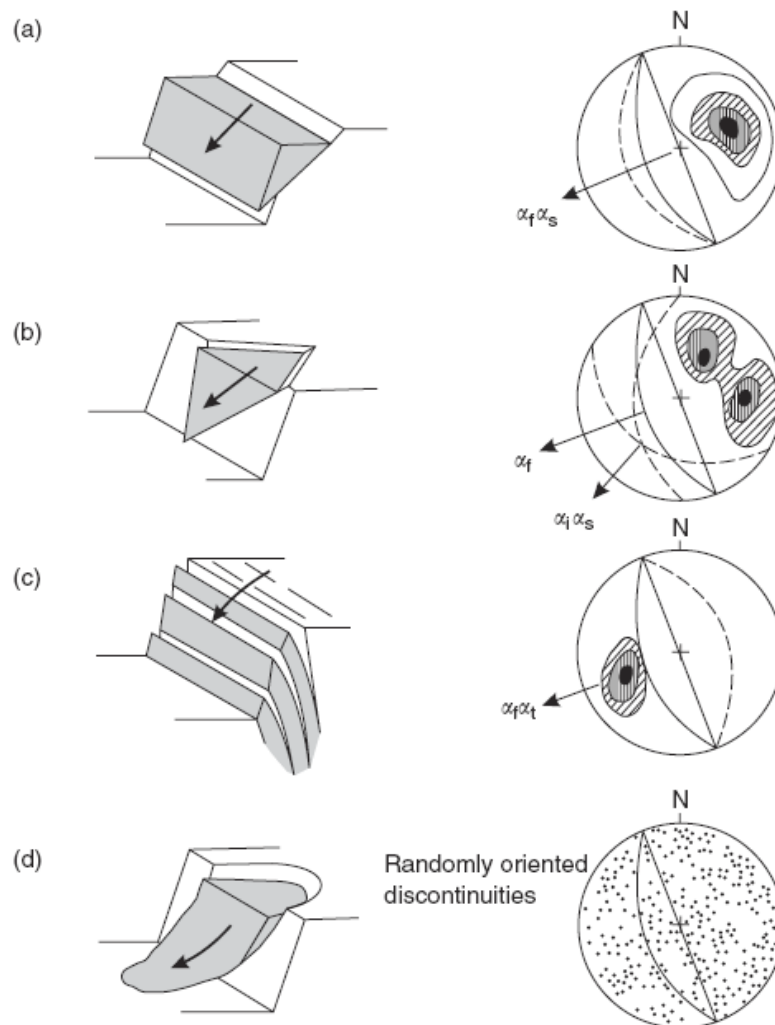


**Figure 7-7** – Main types of block failures in slopes, and structural conditions favourable to their occurrence (after Hoek and Bray, 1981).

partial development. Depending on the slope-scale structural patterns, different failure mechanisms can be observed (Sjöberg, 1999):

- large-scale toppling failures are typical of slopes with persistent discontinuities steeply dipping into the slope, which can lead to rigid-block toppling failures along a gently dipping basal failure surface (Goodman and Bray, 1976) or to flexural toppling failure (either or not associated to shear along a basal failure surface). The latter mechanisms dominates where the tensile strength of rock material is sufficiently low to allow for flexure and shear strength along discontinuities is low;
- underdip toppling and slumping failures (Cruden e Hu, 1994; Kieffer, 1998) can occur in slopes with persistent discontinuities steeply dipping downslope. Here backward rigid or flexural block rotation can be observed, which is associated to different types of slumping (flexural slumping, block flexure slumping, block slumping, kink band slumping; Fig. 7-8) depending on rock strength and discontinuity spacing and strength. When the inclination of discontinuities approaches slope inclination, buckling failures can also occur (Cruden e Hu, 1994).

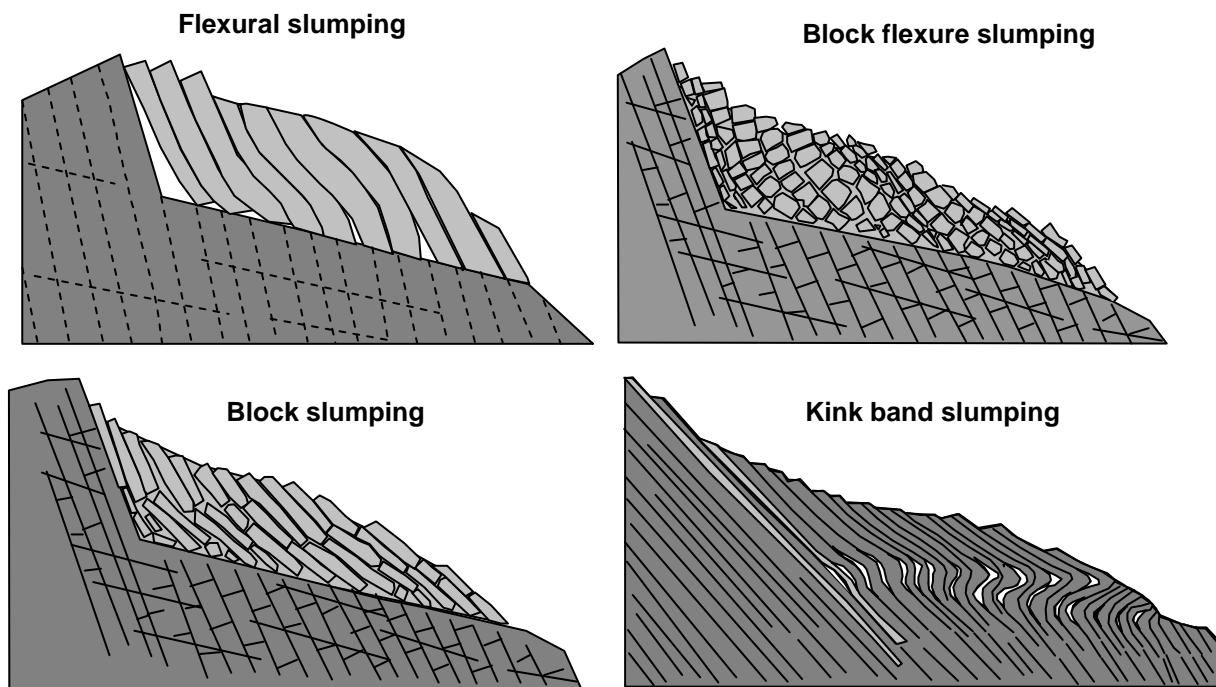


**Figure 7-8** – Mechanisms of large, structurally-controlled slumping failures (after Kieffer, 1998).

The nature, scale and timing of paraglacial rock slope instability depend on the competing interplay between intrinsic rock mass strength and the degree of valley deepening/steepening and debuttressing (Augustinus, 1995; Ballantyne, 2002). The same deglaciated slope can be considered as “oversteepened” or not depending on the strength characteristics of rock masses supporting it. Since “oversteepened” slopes are in critical conditions with respect to equilibrium, they are often prone to fail suddenly. In other cases, sudden or delayed slope failure may occur depending on rock lithology, structure, and the time history of external actions.

In this context, the interaction between paraglacial processes and rock masses results in complex type and pattern (both spatial and temporal) of slope instability. Here we consider the following major categories of rock slope adjustment occurring in a paraglacial context:

- 1) large-scale catastrophic failure of rock slopes;
- 2) large-scale progressive failure of rock slopes;
- 3) deep-seated gravitational slope deformation of rock slopes;
- 4) rockfalls.

### **7.2.2 Large-scale catastrophic rock slope failure**

When the magnitude of deglaciation effects in terms of stress redistribution, stress release and rock damage is large enough, rock slopes can attain critical conditions and fail suddenly. In this case, the onset of such rock-slope failures should be related to the timing of deglaciation. The relationships between deglaciation and massive rock slope instability, including rockslides and rock avalanches, have been usually identified based on three types of studies:

- documentation of observed landslide events;
- geomorphological mapping studies.

- dating studies.

Many catastrophic rockslides have been documented in the literature in areas of recent or ongoing deglaciation. Sever rockslides evolved into catastrophic rock avalanches, possibly running onto glacier surfaces and attaining runouts of tens of kilometres. These observations support the idea that oversteepened slopes can fail soon after glacier retreat (Augustinus, 1995). Ballantyne (2002) recalled a collection of literature examples on this topic, including: the Brenva Glacier rockfall in 1920 (Porter and Orombelli, 1981), the Sioux Glacier rock avalanche in Alaska (Reid, 1969), the rockslides that triggered a surge of Bualtar Glacier in the Karakoram Range (Gardner and Hewitt, 1990). McSaveney (1992) reported the catastrophic failure, in 1992, of a slope flanking the Maud Glacier (New Zealand), exposed by the glacier retreat which amounted to about 250m from its Little Ice Age maximum. As a consequence, a 5-10 Mm<sup>3</sup> rock avalanche occurred (Fig. 7-9). Another large rockslide, occurred in 1972 onto an outlet glacier of the Myrdalsjokull ice cap (Iceland) was interpreted by Sigurdsson and Williams (1991) as the ultimate result of the debuitressing of the valley wall resulting from rapid glacier retreat (Fig. 7-9).

Evans and Clague (1994) reported several examples of catastrophic rock-slope failures associated with retreating glaciers. For example, the authors noted that of 30 large historic rock avalanches exceeding one million cubic meter in the Canadian Cordillera, 16 involved recently deglaciated slopes. They suggested that catastrophic rock slope failure is a characteristic rather than atypical paraglacial response to glacier retreat, at least in alpine environments where glacier ice occupies cirques and troughs flanked by steep rockwalls.

Geomorphic evidence for a paraglacial origin of rock-slope failure is outlined by the spatial coincidence between failure locations and areas where glacial debuitressing was at its maximum (Cossart et al., 2008). Jarman (2006), based on detailed geomorphological mapping resulting in an inventory of 140 large rock slope failures in the Scottish Highlands, related significant clustering of rockslides to recently active glacial breaching of main and secondary watersheds. According to the author, these can be considered as loci of concentrated erosion and stress release, over several cycles of glaciation and deglaciation (Fig. 7-9).

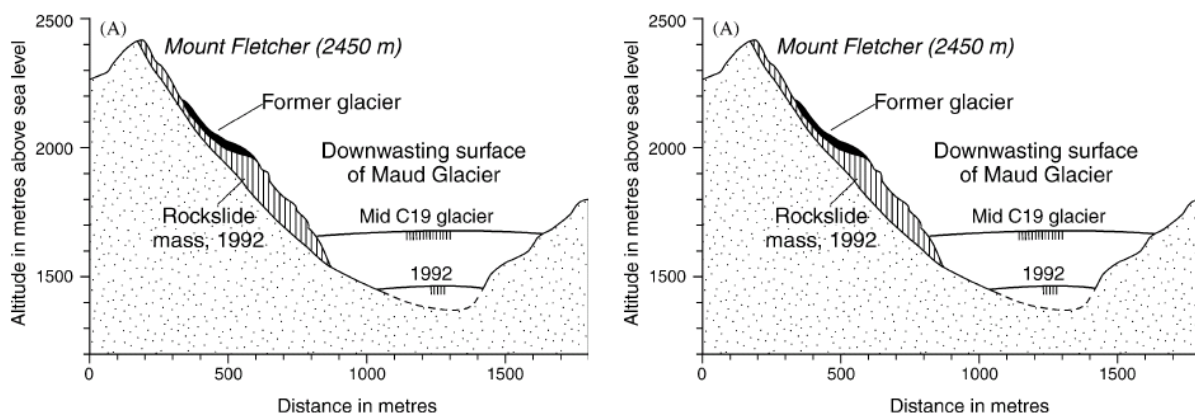


**Figure 7-9** – Documented rock slope failures following recent glacier recession (Ballantyne, 2002). Left: Maud Glacier, New Zealand (after McSaveney, 1992). Right: outlet glacier of the Myrdalsjokull ice cap, Iceland (after Sigurdsson and Williams, 1991).

Despite the large number of reported slope instabilities occurred soon after the retreat of glaciers, the role of deglaciation processes on the deformation and failure of rock slopes remains not obvious. Rock slope instability can also be associated with tectonic stresses, river incision or seismic triggering in tectonically-active mountain ranges (Cossart et al., 2008). In this context, increasingly available advanced absolute dating techniques provided a powerful tool to identify rock-slope response to paraglacial processes. Surface exposure dating using cosmogenic isotopes is particularly useful to establish the age of deglaciation, thus providing the opportunity to assess the time-lag between deglaciation and rock-slope failure. Cossart et al. (2008) used  $^{10}\text{Be}$  cosmic ray exposure ages to demonstrate that rock-slope failures in the upper Durance valley (France) cluster on the lower valley-side slopes within the area occupied by ice at the Last Glacial Maximum, and that their locations coincide with zones of inferred high glacial loading stress. According to the authors, this would be consistent with interpretation of bedrock disruption and large-scale rock-slope failures as paraglacial phenomena associated to deglaciation stress release. Nevertheless, several studies mainly based on radiometric dating of landslides (e.g. Switzerland, Raetzo-Bruelhart, 1997; Italy, Soldati et al., 2004; Agliardi et al., 2009a; Austria, Prager et al., 2008) yielded different clusters of landslide ages, ranging between Lateglacial and Holocene, suggesting that landslides in paraglacial context can be also triggered (or reactivated) after long time after deglaciation, showing a time-dependent evolution and/or undergoing the triggering effects of climate changes occurred during the Holocene (Prager et al., 2008).

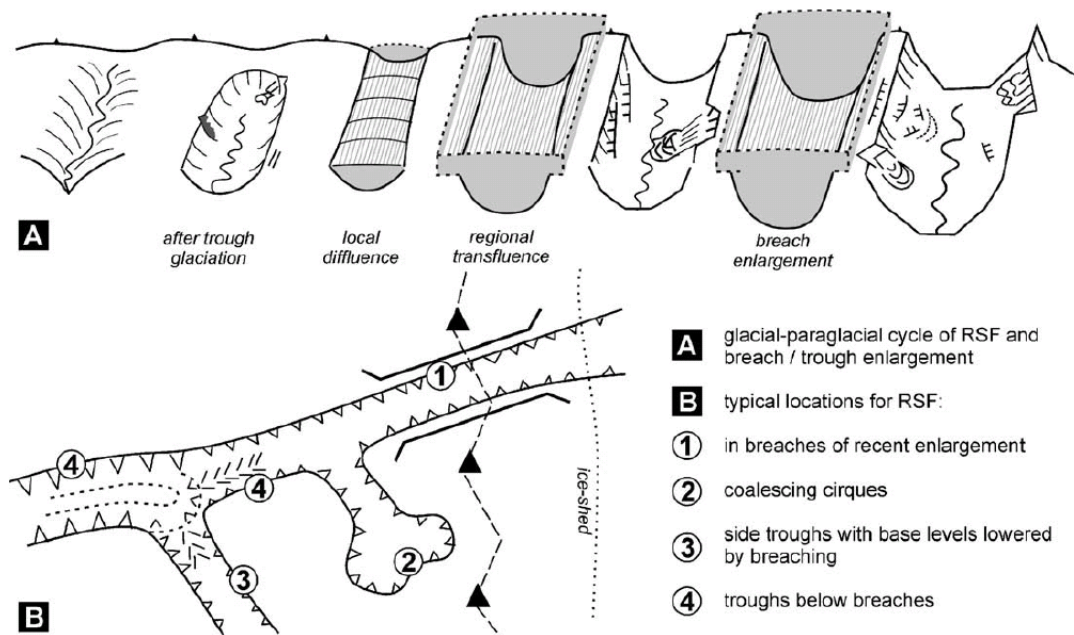


**Figure 7-10** – Relationships between rock slope failure clusters in the Scottish Highlands and the development of glacial breaches over repeated glacial/paraglacial cycles (after Jarman, 2006).

**7.2.2.1 Example: paraglacial rock slope failure in Alaska (Meigs and Sauber, 2000)**

Meigs and Sauber (2000) reported an emblematic example of large rock slope failure almost immediately following valley deglaciation, and suggest that such kind of phenomena could substantially contribute to orogen-scale denudation of mountain ranges. The reported landslide (Fig. 7-11) in the Taan Fjord (Southern Alaska), which was created by the retreat of the Tyndall glacier over the past 50 years. Here glacial retreat between 1983 and 1996 was accompanied by a large-scale landslide failure of the fjord wall, extended over an area 0.4 km<sup>2</sup>, and extending from sea level up to 600 m. Bedrock structure is cross-cut by the head scarp and strikes subparallel to the fjord wall. Because of deglaciation, rockwall length increased rapidly from 700 m in 1983 to 1780 m on deglaciation. Such rapid slope debuttressing led to a net down-dip displacement at the base of the landslide of about 300–400 m in a 13 years period.

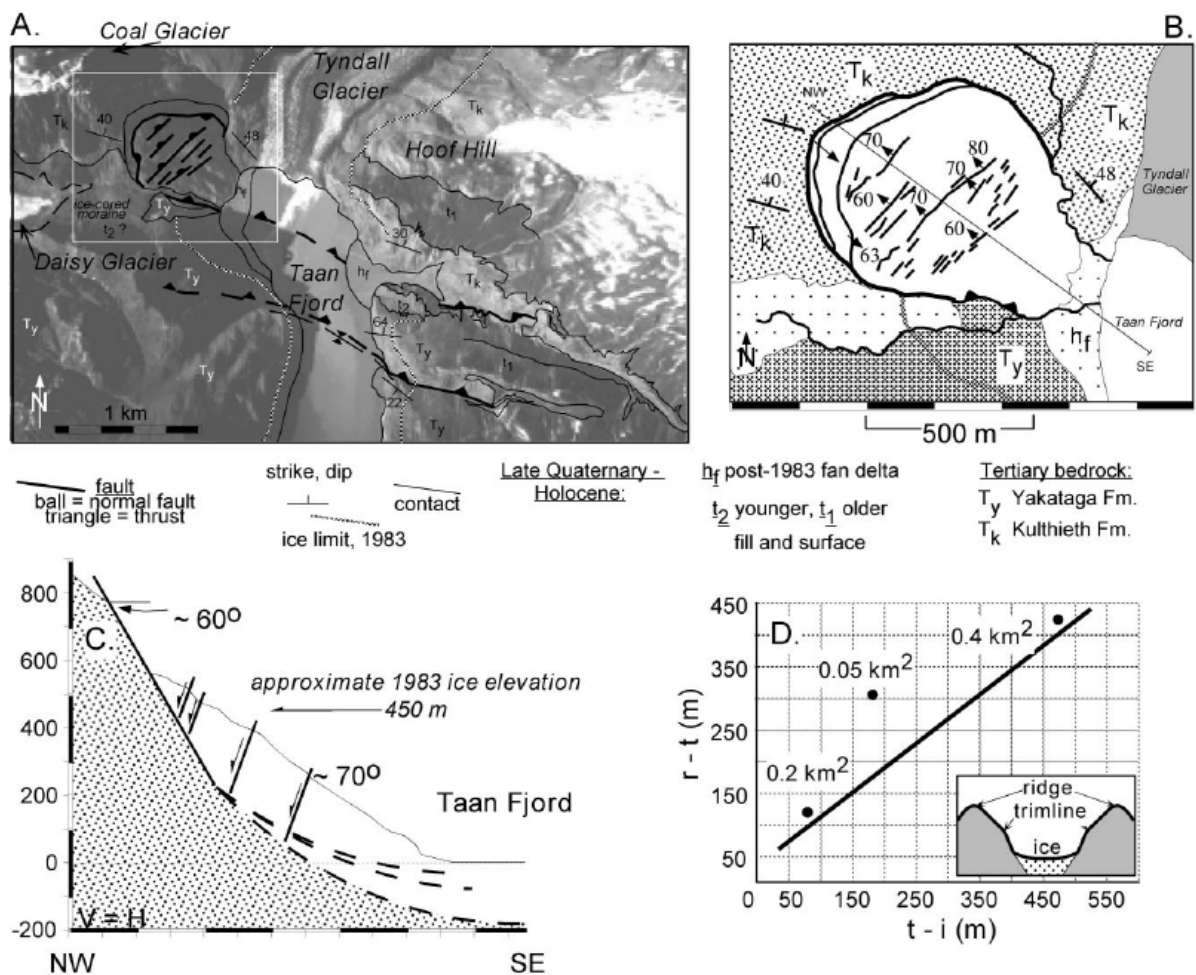


**Figure 7-11** – Large-scale rock slope collapse at the Tyndall Glacier front, Southern Alaska (after Meigs and Sauber, 2000).

### 7.2.3 Progressive rock slope failure

Widespread geomorphological and geochronological evidence of delayed, or time-dependent paraglacial slope failure (Bovis, 1982, 1990, Fig. 7-12; Blair, 1994; Ballantyne, 2002; Prager, 2008) can be strictly related to the concept of progressive failure. This concept was originally introduced to explain discrepancies between the average shear strength values back-calculated along failure surfaces in over consolidated clay slopes and those measured in laboratory testing.

In these slopes, Bjerrum (1967) observed that failure does not occur until a continuous sliding surface has developed. Such sliding surface propagates in a progressive manner until shear strength along it is reduced from peak to residual values (Fig. 7-13), implying a gradual development of the eventual failure surface. For rock slopes, Terzaghi (1972) emphasized that most rock masses contain discontinuous joints characterised by variable persistence (i.e. length and continuity at the scale of the considered rock mass volume). Therefore, the overall rock mass strength to shearing failure depends on both the frictional shear strength of discontinuity surfaces and the cohesion of intact rock bridges between discontinuous joints. These contribute to the strength along the discontinuity (here referred to as “effective cohesion” along the shear surface). Effective cohesion depends on intact rock cohesion, the total area of gaps between discontinuities (i.e. area of the rock bridges, measured along shear

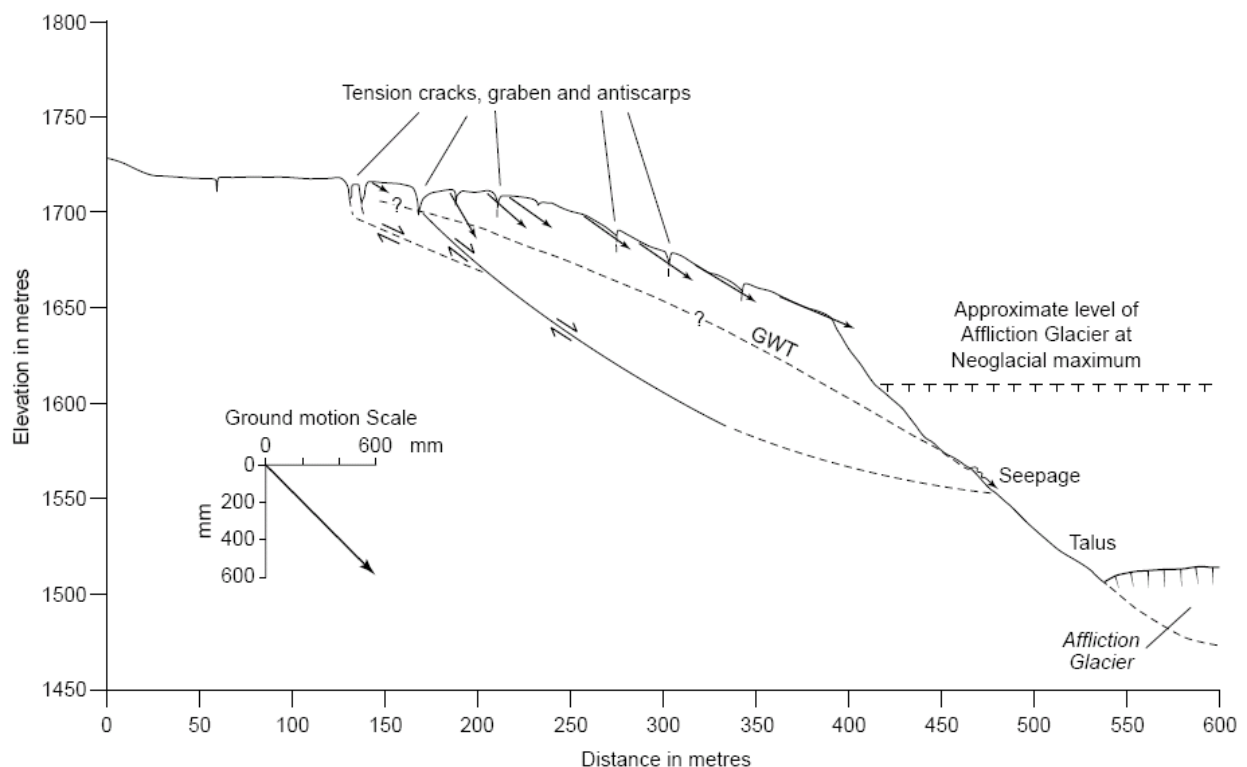


**Figure 7-12** – Rock-slope deformation caused by deglaciation at Affliction Glacier, British Columbia (after Bovis, 1990 in Ballantyne, 2002). Vectors refer to cumulative displacements measured over 4 years (1982-1986).

surfaces), and the total area of discontinuity surfaces. According to this model (Fig. 7-13), progressive failure of rock slopes would require that the shear strength of individual rock bridges is exceeded. Then, the deformation associated to rock bridge failure would redistribute stress ahead of the shear plane, until other rock bridges fail consecutively and the failure surface extends up to a feasible kinematic release (Eberhardt et al., 2004).

In natural rock slopes, a rock mass can be the locus of several potential “failure surfaces”, which can evolve individually or interact according to very complex patterns, depending on the geometry, spacing and persistence of individual discontinuities, and the shear strength of intact rock, discontinuities and overall rock mass.

Terzaghi (1972), Robertson (1970) et other investigators suggested that the persistence of key discontinuity sets in reality is very limited, thus requiring that an interaction between pre-existing discontinuities and fracture propagation through intact rock bridges occurs in order to attain slope failure. Eberhardt et al. (2004) suggested that geometric and kinematic changes experienced by natural slopes upon deglaciation are less rapid than in engineered slopes, therefore the overall progressive failure (i.e. strength degradation) process can last over periods of thousands of years since initial deglaciation. This points to a time-dependent evolution to failure of deglaciated slopes under suitable conditions (i.e. valley deepening, slope steepening/debuttressing, rock mass structure and strength), which is consistent with observations on natural slopes.

Eberhardt et al. (2004) summarized the main factors controlling the mechanisms of brittle progressive failure of rock slopes. According to the authors, if only the processes acting along the developing shear plane are treated, failure should initiate at the toe of the rock slope where the stresses are highest and propagate upwards. On the other hand, field observations suggest that tension cracks often appear at the top of the slope before catastrophic failure occurs. This suggests that failure also occurs with internal deformation and dilation of involved rock masses. In this case, the resulting failure mechanism (Fig.7-14) depends on: 1) the persistence and geometrical arrangement of discontinuity planes potentially driving failure surface development; and 2) the overall strength and deformability of rock mass.

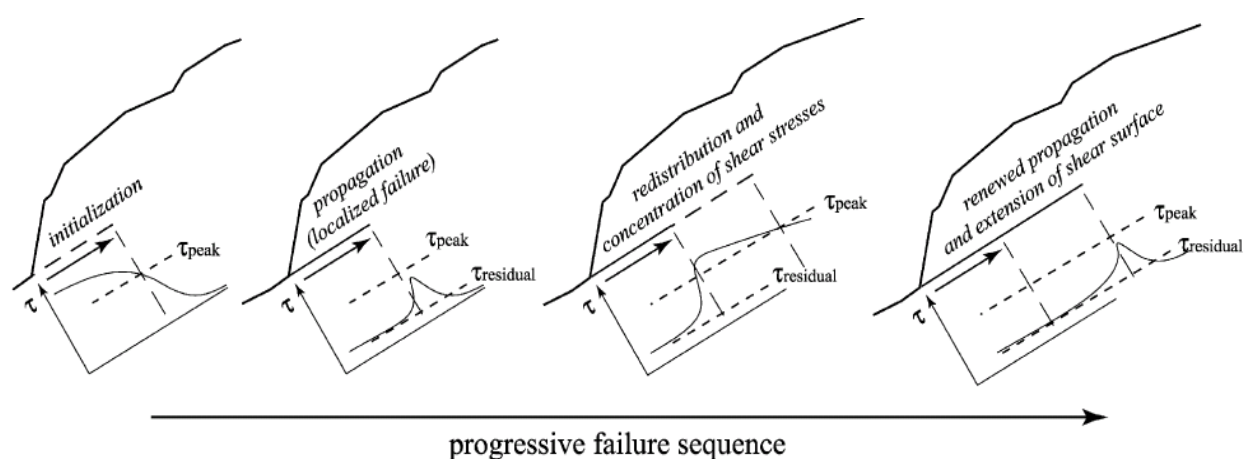


**Figure 7-13** – Shear surface development through progressive failure (after Bjerrum, 1967, adapted by Eberhardt et al., 2004).

Prager et al. (2008), trying to explain the temporal clustering of large landslides in Tyrol between Lateglacial and Holocene, agreed that progressive failure by fracture propagation and stepwise coalescence of pre-existing brittle discontinuities, strongly depending on the existing stress field as well as on the fracture geometry and the joint network, must play a significant role in controlling the time-dependent deformation and failure of deglaciated valley flanks, whereas climate changes (e.g. changes in the long-term rainfall patterns) and seismic activity can be responsible of episodic increased landslide activity (Fig. 7-15).

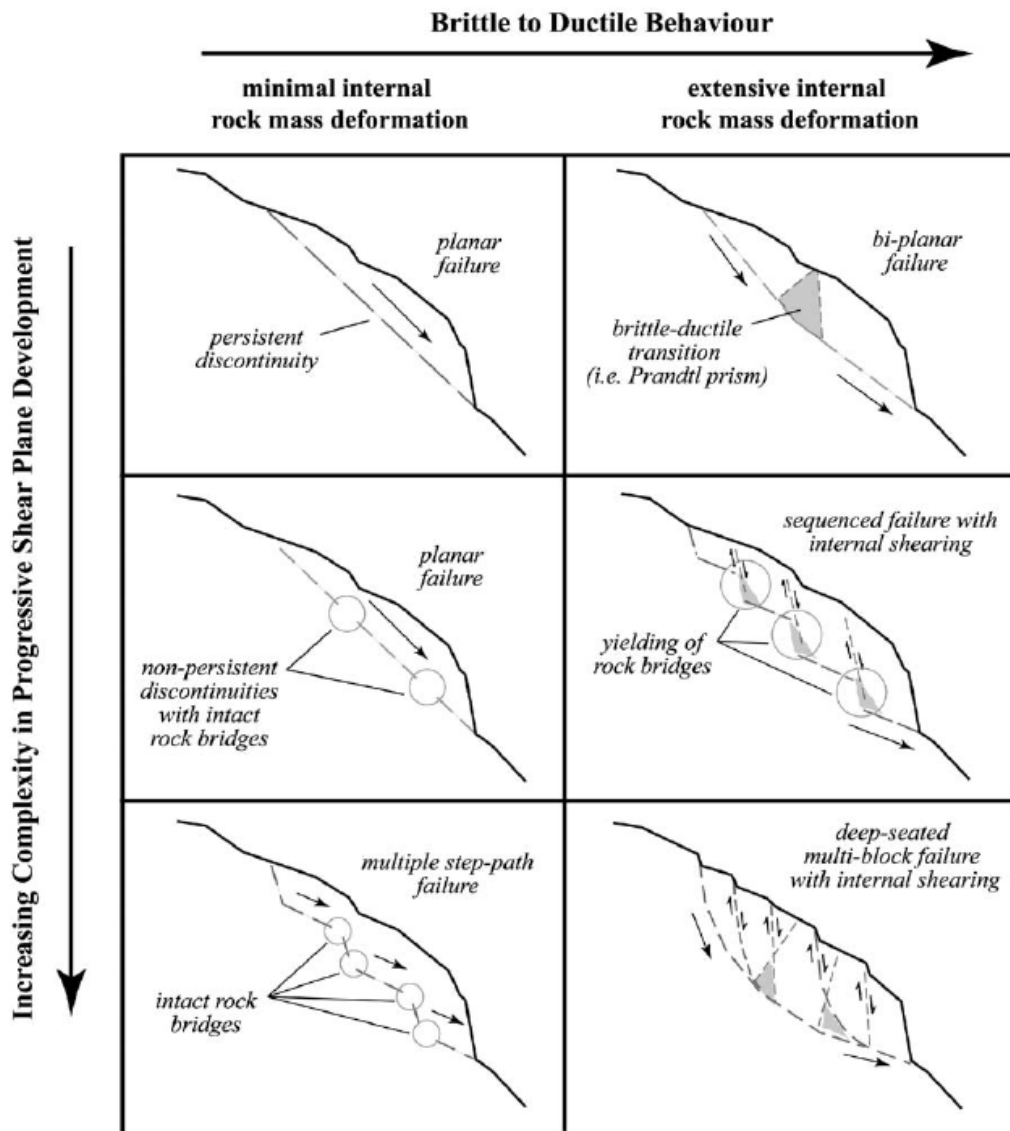


**Figure 7-14** – Rock slope sliding mechanisms resulting from progressive failure (after Eberhardt et al., 2004).

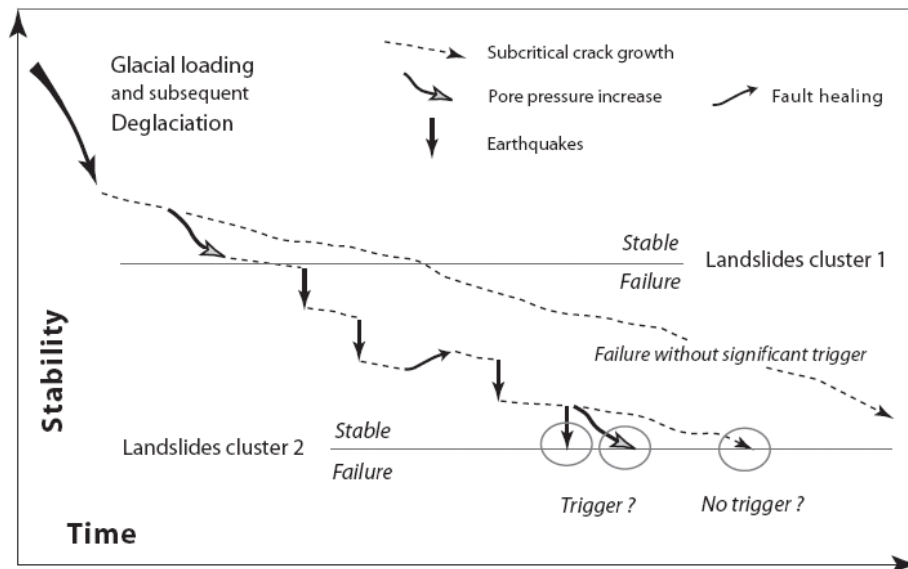


**Figure 7-15** – Conceptual model for rock strength degradation versus time in a post-glacial cycle (after Prager et al., 2008)

### 7.2.3.1 Example: Randa rockslide, Mattertal, Switzerland (Eberhardt et al., 2004)

The 1991 Randa rockslides occurred in the Matter Valley (southwestern Swiss Alps), and involved the failure of 30 Mm<sup>3</sup> of massive crystalline rock (Fig. 7-16). Two distinct rockslide episodes occurred on April 18, 1991 (20 Mm<sup>3</sup>) and May 9, 1991 (10 Mm<sup>3</sup>), respectively. Damage resulting from the two events included the destruction of the main road and rail line along the valley, the damming of the Vispa River and the flooding of the Randa village. Failed rock included massive gneisses alternating with mica-rich paragneiss, with foliation dipping favourably into the slope. Failure probably occurred along extensive joints parallel to the surface, which have very limited persistence in natural outcrops. Steeply-dipping subvertical faults were considered to divide the rock mass into smaller units, which could explain the episodic evolution of the rockslide. No clear indications of a seismic or rainfall triggering were found, although that failure occurred in a period of heavy snowmelt. Eberhardt et al. (2004) suggested that time-dependent mechanisms relating to brittle strength degradation and progressive failure may more likely be the significant contributing factors that brought the slope to failure. The hypothesis was supported by a numerical modelling exercise, accounting for deglaciation and associated stress release, fracture mechanics and rock mass strength degradation.

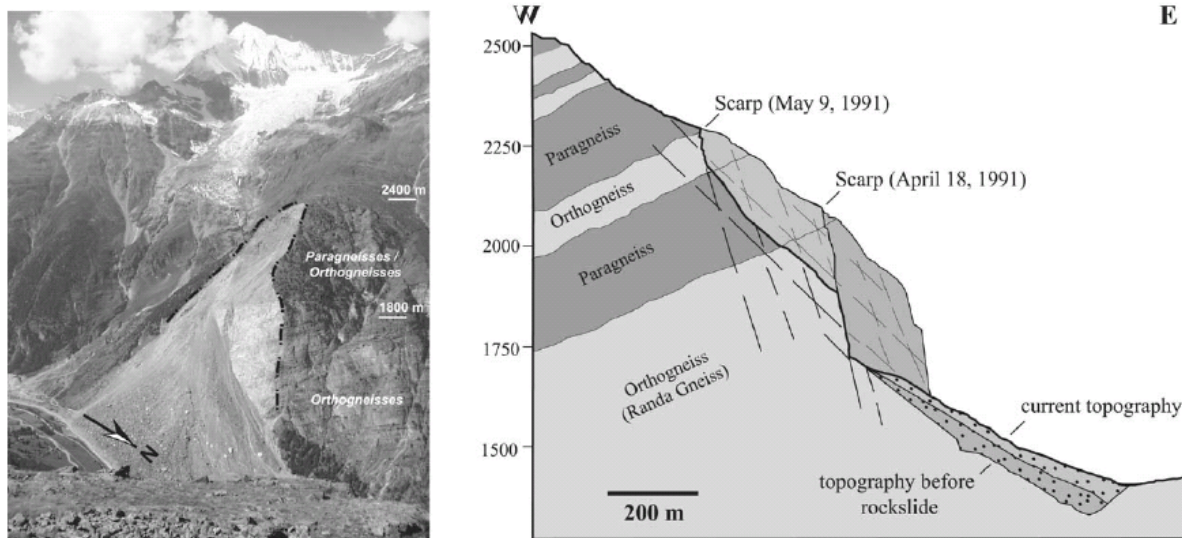


**Figure 7-16** – Oblique aerial view and geological cross section of the slope affected by the 1991 Randa rockslides (after Eberhardt et al., 2004).

#### 7.2.4 Deep-Seated Gravitational Slope Deformations

Deep-Seated Gravitational Slope Deformations (DSGSD) are very large mass movements involving high-relief slopes from their toe up to or beyond the ridge. They can involve nearly all rock types, and are characterised by poorly defined lateral boundaries, large volumes (often exceeding  $0.5 \text{ km}^3$ ) and thickness, and relatively low present-day displacement rates (few to tens mm/yr; Varnes et al., 1990; Ambrosi and Crosta, 2006). Further diagnostic features of DSGSD are the development of persistent linear morpho-structural features (Agliardi et al., 2001; Fig 7-17). Scarps, trenches, grabens, double or multiple ridges are the more frequently described tensional features in the upper slopes, whereas counterscarps (i.e. antislope scarps) are mainly observed in the middle part. Bulging, buckling folds or highly fractured rock masses are compressional features occurring at the slope toe. Large catastrophic slope instabilities (rockslides and rock avalanches) also often occur in DSGSD areas.

In general, DSGSDs appear closely related to specific geological and structural features (bedding, foliations, joints, faults, etc.) and morpho-topographic factors, and frequently occur in tectonically active areas (McCalpin, 1999; Crosta and Zanchi, 2000; Agliardi et al., 2009b). DSGSDs have been shown to occur in areas that underwent glaciation and deglaciation, as well as in unglaciated areas (Crosta and Zanchi, 2000). Nonetheless, most DSGSD in alpine settings occur on valley flanks deglaciated during the Lateglacial or later. Due to complexity and variability of DSGSD evidences and inferred mechanisms, several phenomenological and mechanical descriptions of DSGSD triggering have been proposed in the literature. Authors interpreted features observed in the field as representative of specific mechanisms including: postglacial debuitressing slopes and associated groundwater changes (Agliardi et al., 2001), topographic stresses in high-relief slopes (Radbruch-Hall, 1978; Varnes et al., 1989), effects of tectonic stresses (Miller and Dunne, 1996), earthquake ground shaking (Radbruch-Hall, 1978; McCalpin, 1999), and fluvial erosion of the slope toe (Crosta and Zanchi, 2000). A

pitfall in the analysis of the relationships between deglaciation and DSGSD is the morphological convergence between gravitational morpho-structures and tectonic features (Agliardi et al., 2009b). In fact, widespread evidence of postglacial surface ruptures in the Alps (Forcella et al., 1982; Persaud and Pfiffner, 2004) could be related to recent or active tectonic processes, to the gravitational deformation of large rock slopes, or to a combination of them (McCalpin, 1999), possibly biasing the reconstruction of DSGSD development in changing morpho-climatic settings associated to alpine valley deglaciation.

In order to clarify the role of possible DSGSD triggering processes, some authors (Agliardi et al., 2001; Ambrosi and Crosta, 2006) proposed to adopt a multi-disciplinary analysis approach, integrating information gathered by structural geology, Quaternary geology, geomorphology, geomechanics, and numerical modelling. Agliardi et al. (2009b) analysed more than 100 DSGSDs in the Central Alps (Italy), and showed that the passive controls by major structural features need to be considered to explain the distribution and general features of observed DSGSD as well as for modelling their onset. Numerical models performed by the authors were unable to simulate the observed DSGSD deformation patterns unless these structural elements were introduced, thus confirming the significant structural control on DSGSD development pointed out by several authors (Radbruch-Hall, 1978; Agliardi et al., 2001). Tectonic structures passively control the kinematic degrees of freedom in rock masses and influence rock mass strength, thus constraining DSGSD localisation, geometry, and morpho-structural pattern. Nevertheless, numerical modelling results indicated that slope deglaciation and related processes (e.g. slope unloading, groundwater level fluctuations and water pressure increase because of permafrost conditions, ice melting and fracture unloading) are required to trigger large displacements and related morpho-structural evidence (Fig. 7-18). This agrees with previous findings (Brückl, 2001) and with the available geomorphological and structural constraints.

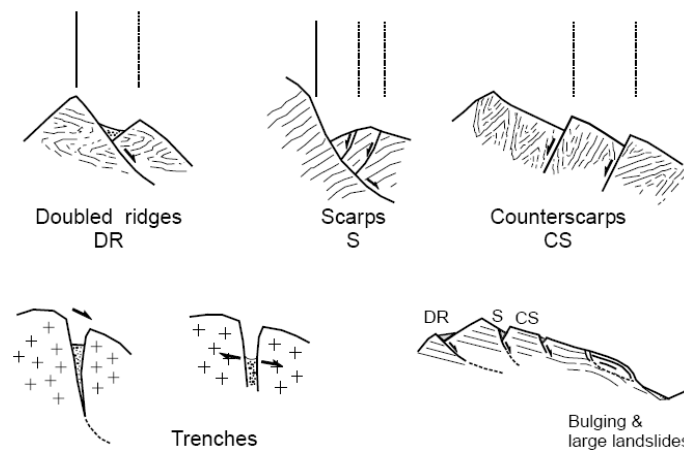


**Figure 7-17** – Morpho-structural features diagnostic of DSGSD (after Agliardi et al., 2001).

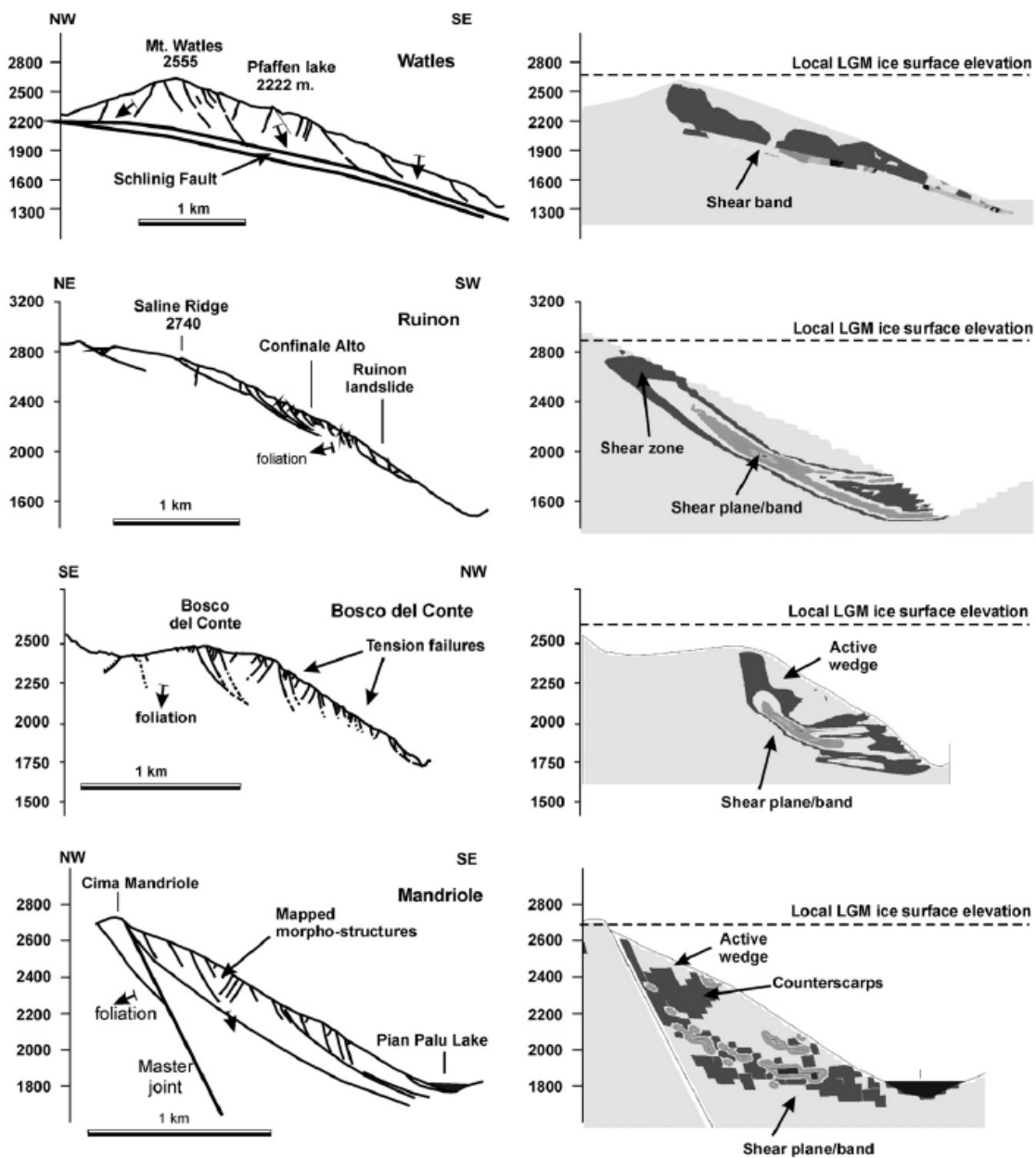


**Figure 7-18** – Results of field morpho-structural studies of selected DSGSD case studies in the Central Alps (Italy), compared to the results of Finite-Difference numerical modelling of slope deglaciation. Model results are represented in terms of computed maximum shear strain increment, which outline the development of basal failure zones (after Agliardi et al., 2009).

In any case, the time-dependent evolution of a DSGSD after its onset can be complex, with long-lasting periods of activity, reactivations and possible partly catastrophic evolution. Agliardi et al. (2009a) reported Lateglacial triggering or evolution of deep-seated gravitational slope deformations in the Central Alps of Italy. This is suggested by cross-cutting relationships between gravitational morpho-structures and glacial deposits, and confirmed by radiocarbon dating of peat deposits sealing major morpho-structures. Radiocarbon dating also demonstrated that sudden activation and largest movements occurred

just after LGM collapse (18–16 ka; Lambeck et al., 2002; Ivy-Ochs et al., 2004). Nevertheless, available monitoring data obtained by SAR satellite interferometry (Colesanti et al., 2004; Ambrosi and Crosta, 2006) suggest that after an initial accelerating stage, slopes movements keep on at slow rates. This is in agreement with the results of Cruden and Hu (1993) and Prager et al. (2008), which suggested that the period of paraglacial slope adjustment could span up to thousand years. Finally, the occurrence of continuing slope movements over long time periods could also suggest a sort of ongoing positive feedback between slope instability, uplift, and valley deepening. In fact, high uplift rates enhance valley deepening, which in turn causes stress concentration at the slope toe, resulting in an increased slope activity and further fracturing.

#### 7.2.4.1 Example: Mt. Watles sackung, Val Venosta, Central Alps, Italy (Agliardi et al., 2009)

A complex system of deep-seated gravitational slope deformations (DSGSD) extends over 20 km along the upper Venosta Valley (Eastern Alps, Italy). In this context, Mt. Watles exhibits the most spectacular morpho-structural features, including double ridges, trenches, and counterscarps characterised by vertical throw exceeding 30 m (Fig. 7-19).

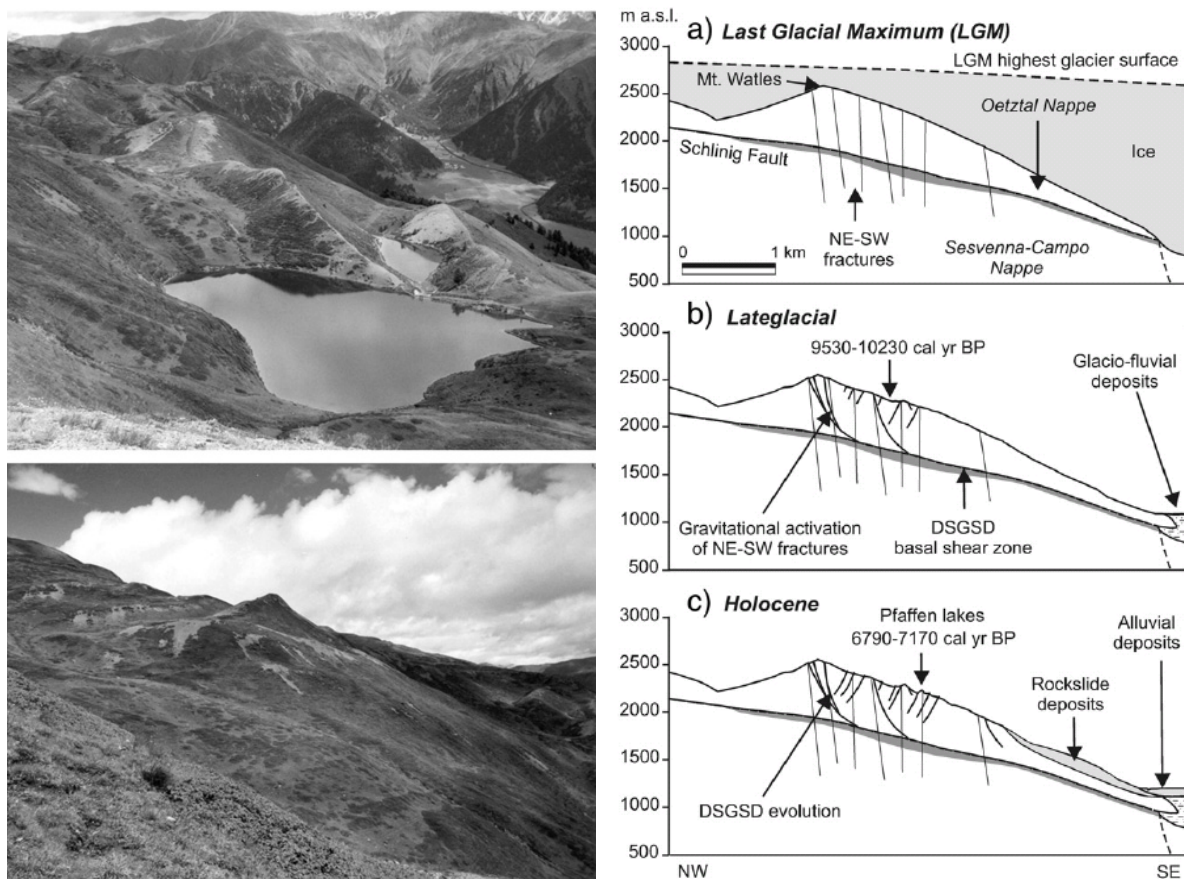


**Figure 7-19** – Left: major DSGSD counterscarps on Mt. Watles. Right: schematic cross-sections showing the inferred evolution of the Mt. Watles slope since the Last Glacial Maximum

The development of this DSGSD was passively constrained by a regional gently dipping fault (i.e. the Schlinig normal fault), and by recent faults marked by shallow earthquakes. Landforms and deposits observed in the area reflect glacial/paraglacial controls on the evolution of the slope. Morpho-structural analysis and related reconstruction revealed that Mt. Watles is affected by a complex, deep-seated, compound slide along a basal shear zone involving the Schlinig fault. Gravitational reactivation of NE-trending fractures formed gravitational scarps, counterscarps, and half-grabens in the upper slope, whereas the lower part of the slope partially collapsed. Although the Schlinig fault and recent fractures are considered important constraints on slope failure, the relationships between morpho-structures and Quaternary landforms and deposits and radiocarbon dating suggested that post-LGM deglaciation was the main DSGSD trigger. Radiocarbon dating of peat deposits within one of the major counterscarps also indicates that slope deformation started during the Lateglacial period and continued during the Holocene in several slope sectors (Fig 7-19).

### 7.2.5 Rockfalls

Rockfalls are among the most common landslide types in mountain areas. Despite usually involving limited volumes, rockfalls are characterised by high energy and mobility, making them a major cause of landslide fatalities (Guzzetti, 2000). Rochet (1987) classified rockfall phenomena into four categories, namely: single block falls (involved volume ranging between  $10^{-2}$  and  $10^2$  m<sup>3</sup>); mass falls ( $10^2$ – $10^5$  m<sup>3</sup>); very large mass falls ( $10^5$ – $10^7$  m<sup>3</sup>) and mass displacement (more than  $10^7$  m<sup>3</sup>). Rockfalls involving volumes up to  $10^5$  m<sup>3</sup> are also known as “fragmental rock falls” (Evans and Hungr, 1993), are characterised by null or negligible interaction among the falling blocks, and are the subject of interest for engineering geologists, due to their hazard and risk potential (Crosta and Agliardi, 2003; Agliardi et al., 2009). Rockfalls can be triggered by earthquakes (Kobayashi et al., 1990), rainfall or freeze-and thaw cycles (Matsuoka and Sakai, 1999) or the progressive weathering of rock material and discontinuities in suitable climatic conditions. They originate from cliffs of different sizes (from few metres to hundreds of metres high) and natures (lithologic, structural, etc.), and involve a wide range of volumes (Rochet, 1987; Evans and Hungr, 1993). The occurrence of rockfalls is constrained by a variety of geomechanical factors, including rock strength (Hoek and Brown, 1988), the geometrical, mechanical and hydraulic conditions of discontinuities (Hoek and Bray, 1981), as well as rock mass weathering (Jaboyedoff et al., 2004) and the local state of static or dynamic stress (Kobayashi et al., 1990).

Since several processes triggers can be responsible for rockfall triggering, it is usually very difficult to ascertain the importance of single triggers in periglacial to non glacial environments. Nevertheless, in the paraglacial environment several authors have recognised an inconsistency between the large volumes of talus accumulations (Fig. 7-20) at the foot of rock cliffs deglaciated since Late Pleistocene and the present-day rates of rockfall accumulations. These have been studied by means of rockfall inventories (Rapp, 1957; Gardner, 1982) or dating techniques as lichenometry (Hieratanta and Liira, 1995; Luckman and Fiske, 1995). For example, Luckman and Fiske (1995, 1997) performed lichenometric measurements of rates of recent scree accumulation in the Canadian Rocky Mountains, and found an average rate of talus accumulation of about ca 0.11m/ka over 300 years. This rate is about one order of magnitude lower than that required to produce the observed talus volume, supporting the idea of an accelerated rockfall activity in the paraglacial phase following

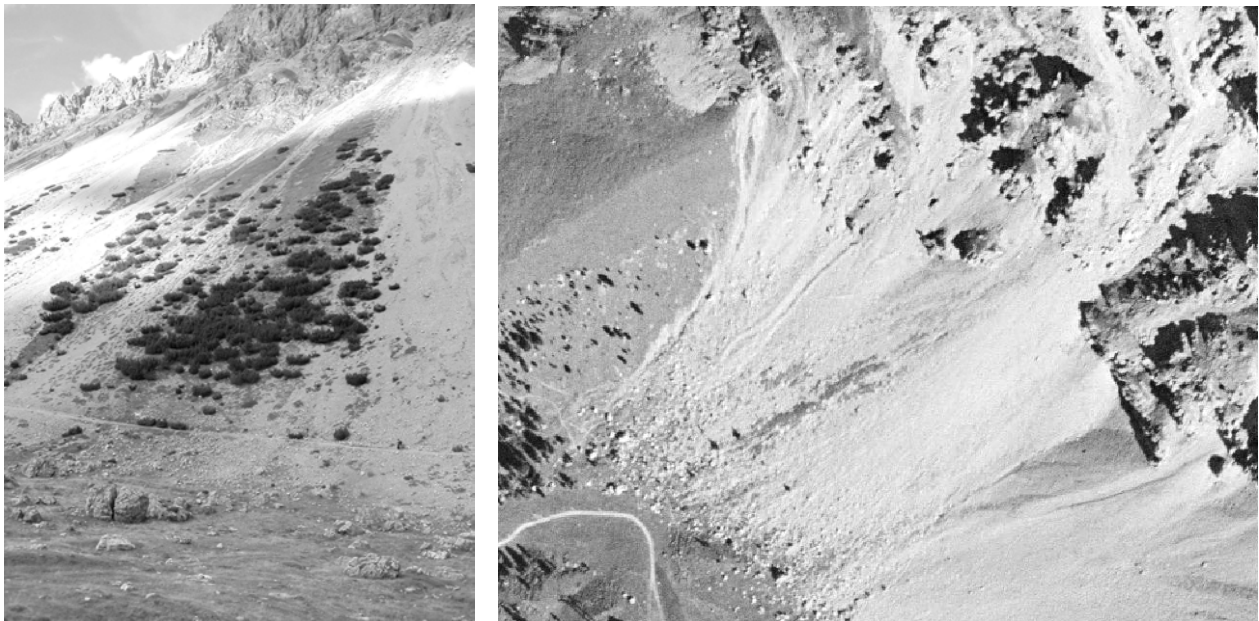


**Figure 7-20** – Rocky cliffs affected by fragmental rockfalls, actively feeding talus slopes. Left: Valle Alpisella (Central Alps, Italy); Right: Val di Fiemme (Eastern Alps, Italy – aerial view).

deglaciation. Although the estimation of past rockfall activity rate is affected by a great amount of uncertainty due to the difficulty of separating paraglacial influence from intrinsic paraglacial wall instability, freeze-thaw effects etc. (Ballantyne, 2002), evidences of enhanced rockfall activity during paraglacial periods are consistent with the general views on paraglacial geomorphology.

#### **7.2.5.1 Example: paraglacial rockfall activity on Isle of Skye, Scotland (Hinchliffe and Ballantyne, 1999)**

According to geomorphological and dating studies conducted by Hinchliffe and Ballantyne (1999) the volume of relict talus on the Trotternish Peninsula (Isle of Skye, Scotland) implies an average of 5.6m of rockwall retreat since deglaciation (occurred at about 17.5 cal ka BP). Nevertheless, about 80% of talus volume accumulated prior to about 11.5 cal ka BP. This means that rockwall retreat during the Lateglacial period averaged 0.75 m/ka, whereas the rate of rockwall retreat during the Holocene averaged only 0.10m/ka. The authors explained the observed talus accumulation pattern as a combination of rapid paraglacial rockwall retreat due to slope debuttressing immediately after deglaciation, with progressive reduction of rockfall activity (model 1 in Fig. 7-21) and enhanced rockfall associated with freeze-thaw activity during periods of stadial (periglacial) climate, with very low rockfall activity during cool temperate climate periods (model 1 in Fig. 7-21).

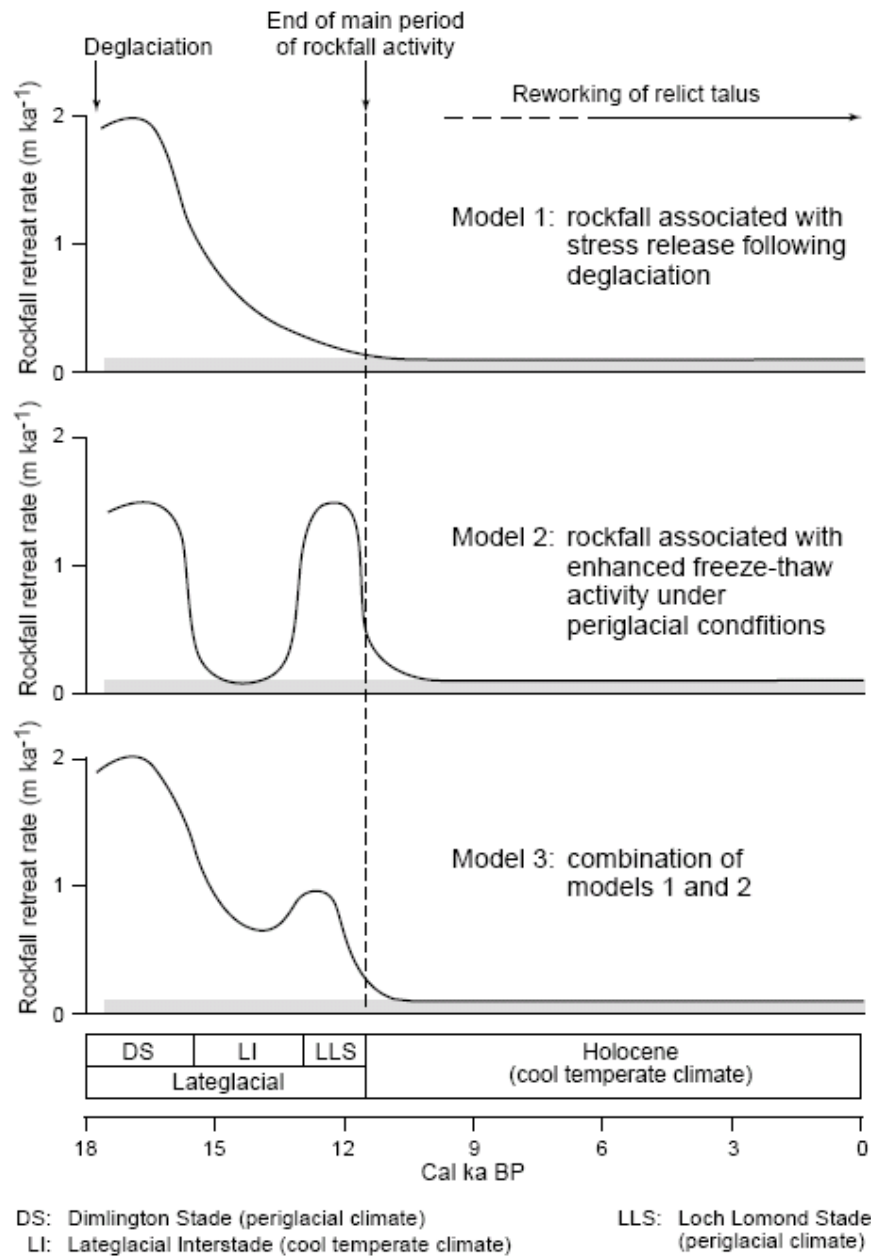


**Figure 7-21**– Models proposed by Hinchliffe and Ballantyne (1999) to explain enhanced paraglacial rockfall activity during Lateglacial on Isle of Skye (Scotland).

---

## **8 LANDSLIDE TRIGGERING BY ROCK/SOIL WEATHERING (UPC)**

### **8.1 GENERAL ASPECTS (UNIMIB)**

Weathering is defined as the modification of physico-chemical properties of minerals, and thus of rocks, by means of atmospheric agents, groundwater and thermal springs (Winkler, 1975). Weathering depends in particular on climatic conditions, water temperature and the type of rock material and associated degree of cracking.

It typically acts to diminish rock consistency, which in turn facilitates rock degradation and eventually fracture (Kasim and Shakoor, 1996; Gupta and Rao, 2000; Massuda, 2001).

Rock weathering is reflected not only by macroscopic modifications, such as the appearance of cracks, microfractures and macroporosity, but also by deposits due to chemical transformations (Norbury et al., 1995; Chigira and Oyama, 1999; Oyama and Chigira, 1999). The weathering of rock material (limestone, tuff, sandstone, crystalline rocks) from dissolution either with or without new mineral formation has been studied by many authors (Farran and Thenoz, 1965; Auger, 1991; Furlan and Girardet, 1991; Chene et al., 1999; Chigira and Oyama, 1999; Gupta and Rao, 2000).

#### **8.1.1 Physical process**

The causes of such weathering can be classified into two major categories, namely internal and external causes:

- External causes characterize the weathering medium, being exhibited regardless of the actual nature of the rock. The physical processes involved are heavily tied to air temperature and humidity variations, which lead to differing degrees of mechanical disintegration of rock material. The presence of chemical processes gets reflected by mineral attack due to aggressive solutions or gases of varying intensities. Rock weathering can be increased by biological factors acting either directly via mechanical action or indirectly via an increase in aggressiveness of the solutions or as a result of deterioration in the organic matter present within the rock material (Winkler, 1975; Fassina, 1995; Gomez-Alarcon et al., 1995);
- Internal causes are related to the intrinsic characteristics of rocks and determine their capability of being altered. Given a certain environment with fixed physico-chemical conditions, rock resistance to weathering agents depends upon specific characteristics such as chemical and mineral composition, structure and texture, porosity and intrinsic permeability (Canton et al., 2001; Inigo and Vicente-Tavera, 2001).

The term aging is often used to describe rock weathering within a medium influenced by human activity and is employed in particular within the scope of underground structures, to describe the range of mineralogical and physical modifications to the rock with respect to time. Such modifications then lead to degradation in either the hydraulic or mechanical properties.

The effect of time on the behaviour of an unlined underground structure comprises various phenomena responsible for the degradation of material properties:

- the degradation of constituent rock minerals by physico-chemical action, and leading to a drop in mechanical characteristics (i.e., the aging effect s.s.);
- differed deformations due to constant loading (i.e. creep);
- variations in hygrometry, saturation and suction conditions affecting the rock mass; these cyclical loadings may induce damage due to hydro-mechanical coupling.

A notable case of weathering is the hydrothermal alteration which affects the properties of volcanic rocks (also discussed in Chapter 9). These geomaterials can undergo extreme changes in physical and mechanical properties that can control slope stability and volcano edifice stability at different scales.

### 8.1.2 Previous studies

The influence of highly weatherable and soluble rocks on slope stability has been only marginally studied in literature, with almost no contributes both on the hydro mechanical and chemio-mechanical aspects.

Guglielmi et al. (2000) and Cappa et al. (2004) present the case study of the La Clapiere landslide in France (Mercantour). The slope is characterised by the presence of two-mica gneisses of the Variscan Argentera-Mercantour massif with steeply dipping foliation transverse to the slope direction. The gneiss tectonically lies upon overturned Triassic sedimentary strata forming a tight syncline with outer sandstone layers and inner gypsum and carnageules (cellular tectonized dolomites) layers. Part of the water springing along the slope are reach in  $\text{SO}_4^{2-}$  and can be partially involved in the weakening of the slope toe. This process is not directly taken into account by Cappa et al. (2004) in their hydro-mechanical modelling but we retain that it could be interesting and important to be considered for the general equilibrium of similar slopes.

Auvray et al. (2004) examine the case of an underground mine where aging involved the pillars left in place during the excavations since different mining periods. They observed a continuous or irregular trend of change of physical mechanical properties (e.g. density, grains density, total porosity, porosity accessible to water, intrinsic permeability to nitrogen, velocity of ultrasonic compression and shear waves, dynamic Young's modulus, dynamic Poisson's ratio, uniaxial compressive strength and static Young's modulus) from the most external to the more internal sectors of each pillar and with time.

The interaction between anhydrite/gypsum and underground excavations has been also investigated by Gysel (2002). He presents three case studies, two from Switzerland and one from Guatemala, showing the relevance of the antecedent natural piezometric level on the evolution of karstic features and weathering in these soluble rocks. More underground problems are connected to karst features (sinkholes, conduits) and dissolution cavities induced by human activities through brine extraction of salts (Johnson, 2005).

It is mandatory, for the study of the weathering and of the stability conditions of a natural or artificial slope as well as of an underground mine or excavation, to couple a chemical model with a mechanical one and eventually with a hydrogeological model.

Raines and Dewers (1997) present a mixed transport/reaction dissolution kinetics model in aqueous solutions for gypsum deposits starting from experimental tests performed in aqueous solutions at 25°C using a mixed flow/rotating disc reactor operating under steady state

conditions. The authors found an increase with velocity of spin under laminar conditions with an asymptotic increase to a constant rate as turbulent conditions develop.

Romanov et al. (2003) apply a similar model for dissolution of fractured soluble and weatherable rocks, to study the evolution of a fracture network below dam sites. In fact, close to dam sites, unnaturally high hydraulic gradients are present to drive the water impounded in the reservoir downstream through fractures below the dam. Under such conditions, the natural process of dissolution is accelerated to such an extent that high leakage rates may arise, endangering the operation of the hydraulic structure.

Furthermore, the natural conditions can be very much complicated by the occurrence of both dissolution and precipitation. While the hydraulic conductivity of fractures is usually orders of magnitude larger than that of the host rock matrix, dissolution and precipitation processes can modify significantly the physical and chemical properties of fractured/unfractured porous media. Qualitative and quantitative description of these coupled processes is fundamental to the analysis of geological formations and to processes of interest in engineering geology. An example in which coupled precipitation and dissolution phenomena occur arises in oil reservoir exploitation. Acid is often injected in an attempt to increase hydraulic conductivity in enhanced oil recovery operations and to reduce the resistance to fluid flow during oil well maintenance procedures. However, some dissolution products can precipitate and ultimately clog the pore space. Singurindy and Berkowitz (2003, 2005) investigated the evolution of hydraulic conductivity in uniform carbonate rock due to competition among flow, dissolution of calcium carbonate and precipitation of gypsum.

From an engineering standpoint, it may be relevant to predict quantitatively which could be the effect on structures of the migration of chemical species through a rock. In order to do that, it is necessary to complete the ordinary mechanical equations governing any geotechnical problem, with the mass balance equations ruling the chemical reactions and the transport of the chemical species. This presents several problematic aspects both at the constitutive and at the numerical level.

The problem of coupling mechanical and chemical equations was tackled first, to the authors' knowledge, by Gens et al. (2002). The mechanical behaviour of unbounded or remoulded soils can be successfully described by constitutive models based on the theory of hardening plasticity or its extensions. For instance, the behaviour of normally consolidated or lightly over-consolidated kaolin, loose or dense silica sand, silt or calcareous sand can be described by strain or work-hardening elastoplastic constitutive models (Nova et al., 2003). Bounding surface plasticity or generalized plasticity were employed for modelling cyclic behaviour.

Natural soils and soft rocks often have a more rigid structure than remoulded soils. Diagenetic bonds are developed between grains. They affect the behaviour of such kind of materials in various ways. Soils acquire tensile strength, and since bonds are often fragile in nature, they also develop a collapsible structure that may give rise to unexpected instabilities. Despite such differences, the mathematical structure of the constitutive models describing bonded geomaterials can be obtained by modifying the original models for unbounded soil only slightly. This fact, originally conjectured by Nova (1992) was exploited by a number of authors to model various kinds of soft rocks (shale, tuff, calcarenite, marl or chalk). Recently Nova et al., (2003) used the same conceptual approach for modelling the effects of weathering on the mechanical behaviour of granite and of calcareous soft rocks.

---

## 8.2 EXAMPLE: DEGRADATION OF A WEALD SILTSTONE

The foundation of a large gravity dam (Castrovido, Burgos, Spain) involved a large excavation, 10 m deep, of the abutments in a hard siltstone from the Weald period. Due to changes introduced in the project, the excavation has remained open and exposed to the atmosphere for a period of three years. During this period the exposed cut slopes have experienced instabilities as shown in Figure 8-1. In addition, shallow landslides developed in the reservoir area due to the removal of the cover of trees and vegetation (Figure 8-2).

A major concern for the subsequent construction of the dam was to establish the intensity and depth of the weathering experienced by the siltstone. The investigation carried out provided a good opportunity to study the weathering profile in the excavated zone by means of field and laboratory tests. In addition the weathered profile in the natural slopes of the valley could also be estimated. In this way, since the time period in which the excavation remained exposed is known, a possibility to estimate the rate of weathering in the field could be determined.

This report provides an account of the work performed. The identification of the weathering effects was approached from different techniques and tests. In the field, boreholes were driven in vertical and horizontal directions (from the excavated slopes for the dam abutments). Core samples were taken for laboratory testing and some geophysical variables (gamma emissions, P and S wave velocities) were recorded. Discontinuities were identified by means of “televviewer” techniques. Seismic profiles were also established following the valley, both in the bottom of the excavated abutments and in the natural ground surface, upstream of the excavation. The comparison of results provides information on the rate of weathering.



*Figure 8-1 - Failure in the excavated abutments. Downstream, right margin. January 2009.*



*Figure 8-2 - Shallow landslide in left margin of Arlanza River, upstream of the dam.*

Laboratory tests aimed at establishing the profile of weathering on the basis of identification tests. Strength data was also obtained by testing undisturbed cores and block samples taken from the upper levels of the weathered profile.

### **8.2.1 Geology**

The site is located in a wide valley excavated by the Arlanza River in Jurassic-Cretacic sediments belonging to the Weald facies. Red siltstone and sandstone layers are interbedded. Transitions from the siltstone to the sandstone levels are often sharp, a consequence of erosive contacts. However, layers are not well defined, especially in the siltstone materials (Figure 8-3).

The Arlanza river flows from South-East to North-West. Layers dip  $10^{\circ}$ - $20^{\circ}$  in the upstream direction. Dip direction follows essentially the river direction (NW to SE).

More precisely, the dam is located in a wide syncline structure dipping about  $15^{\circ}$ - $20^{\circ}$  in the South-West direction. However, sedimentation surfaces may be considered planar at the scale of the slides observed in the area.

Sedimentation planes, including contacts between the two main lithological types mentioned define essentially the structure of the rock mass. A subvertical jointing system (three families of planes) was also identified. They help to weaken the entire rock mass. This report concentrates on the properties of the siltstone materials.



*Figur8-3 - Exposed layer of siltstone and sandstone in the dam abutment excavation.*



*Figure 8-4 - Degradation of Weald siltstone.*

The borehole logs provided additional information on the structure and characteristics of the weald materials. Some relevant features are:

- Muscovite mica was often found. It contributes to create banded structures. Mica is distributed in the mass of the siltstone and it concentrates also in sandstone discontinuities.
- Clayey fillings were often found in sandstone discontinuities.
- In some occasions striated surfaces were found in sandstone siltstone contacts.

A common field observation is the apparently fast degradation of the siltstone and its transformation into a mud-like material (Figure 8-4).

### 8.2.2 Profiles of index properties

Figure 8-5 provides an example of the measured distribution of water content and density (natural, dry and solid density) with depth. Cores were recovered in a vertical boring (SN-1) drilled from the bottom of the excavation (10 m deep). Measured water content and density close to the surface are typical of clayey soils. This soil is classified as a low plasticity clay (CL). Some measured values of liquid limit (decreasing with depth) are also given in the figure.

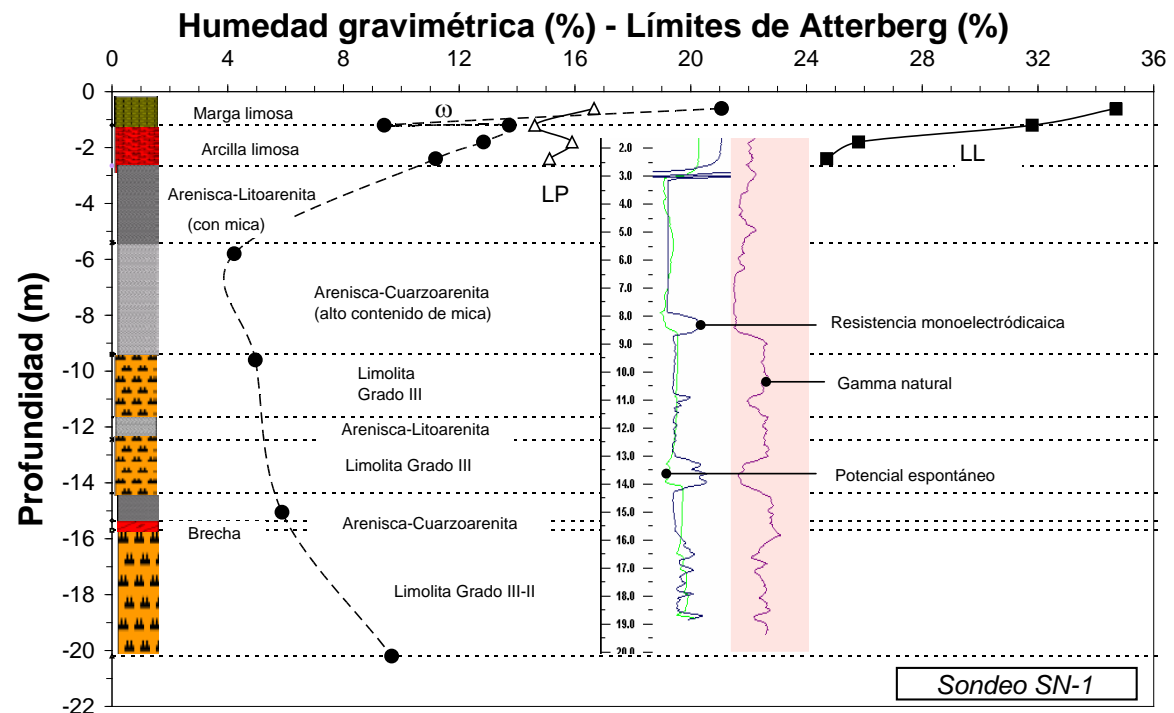
Water content reduces fast with depth. Values of water content at depth ( $w=4-6\%$ ) and natural densities in the range of  $2.45-2.50\text{ Mg/m}^3$  represent undisturbed conditions. The plot (Figure 8-6) shows that the upper 4 m have suffered a strong change in porosity and water content.

A more complete picture is gained if the results for all the vertical borings analyzed are plotted in a common graph. This is shown in Figures 6 and 7. The plot shows a very rapid change of water content with depth. Original conditions are recovered at depths of 4-5 m. This is the depth of the weating “front”. The interesting information is that this weathering phenomenon developed in less than 3 years. (Permeability tests on samples taken in the upper disturbed zone, for a specimen having  $w=10\%$ , provides values of  $3.5\cdot 10^{-8}\text{ m/s}$ . Lower values are to be expected on the unweathered denser siltstone.)

Interestingly, the two valley slopes, despite the uniformity of the site at a large scale, behave in a different manner. It is shown in Figure 8-6 that samples from the left slope experience a slight degradation in terms of water content increase. It was widely accepted by the engineers and geologists working on the dam construction site the the left margin behaved “better” than the right margin. Reasons are not clear but may be related to changes in cementation, intrinsic permeability or structural reasons (a more tectonized area is expected to have higher macro-permeability which facilitate the access of rainwater).

Figure 8-7 provides a similar information, this time in terms of natural density.

There was also an interest in knowing the weathering induced from subvertical exposed surfaces. Therefore, borings were drilled horizontally to the slopes of excavations and tests were performed at short intervals on the cores recovered. Results are collected in Figure 8-8 and 9. No significant water content or density gradients seem to exist in horizontal direction. The different results, when comparing borings, are associated with the degree of internal



(a)

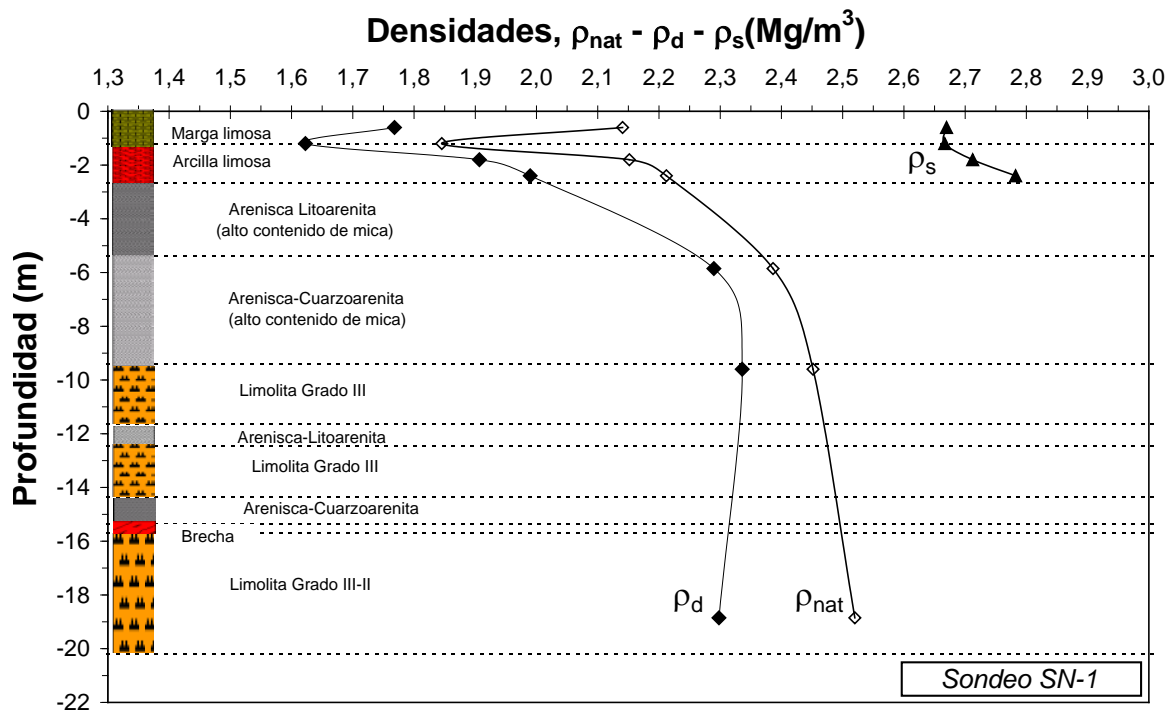
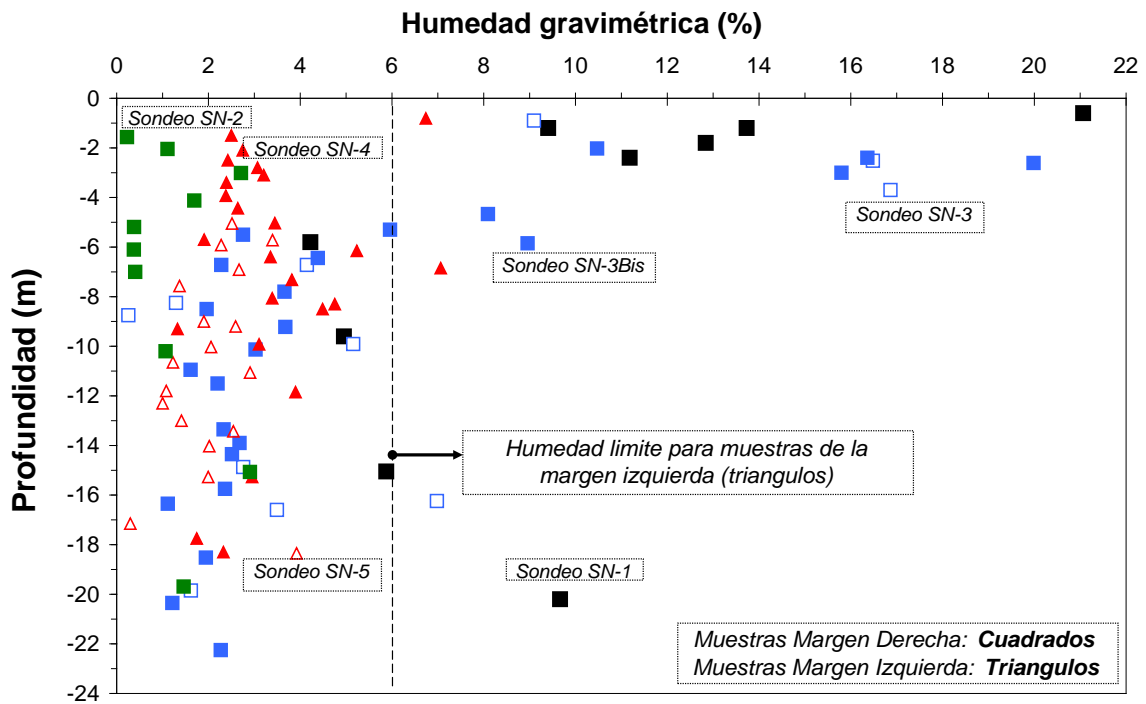
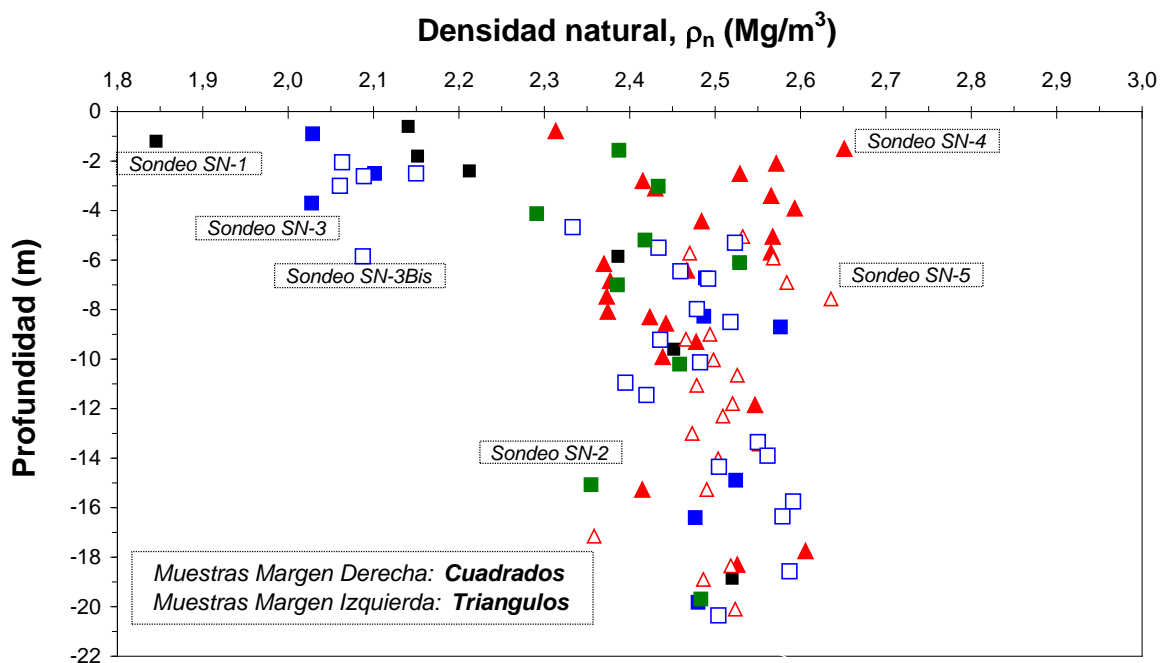


Figure 8-5 - Variation of gravimetric water content and density with depth. Vertical borings form the bottom of the excavation.

fracturing observed during boring operations and also with geophysical observations. It is concluded that weathering progresses in a much slower rate from exposed subvertical slopes compared with vertical direction starting at an essentially horizontal surface.



*Figure 8-6 - Variation of gravimetric water content with depth. Vertical borings form the bottom of the excavation.*



*Figure 8.7 - Variation of natural density with depth. Vertical borings from the bottom of the excavation.*

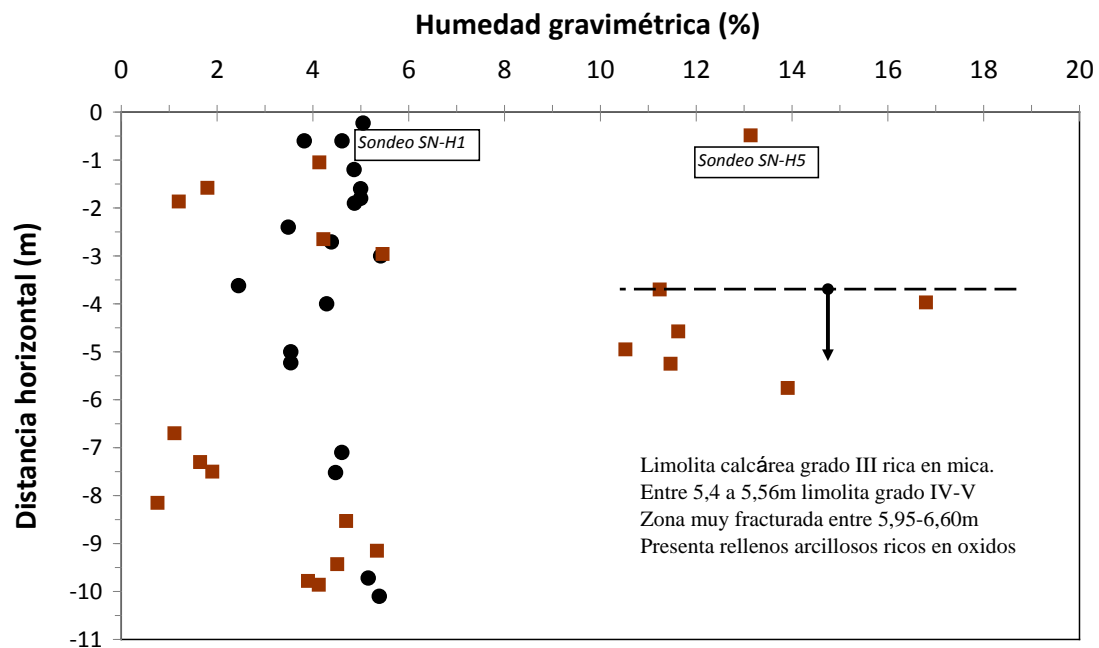


**Figure 8-8** - Variation of gravimetric water content with distance. Horizontal boreholes SN-H1 and SN-H5.

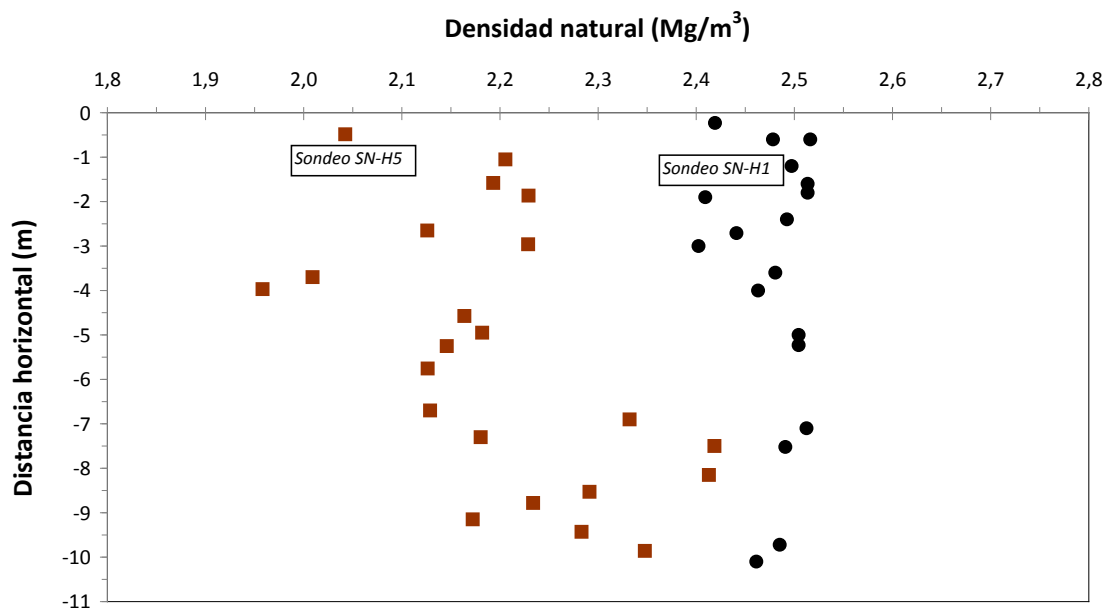


**Figure 8-9** - Variation of natural density with distance. Horizontal boreholes. SN-H1 and SN-H5.

### 8.2.3 Seismic tomography

Refraction seismic profiles were carried out in the position shown in Figure 8-10. The main interest lies in the comparison of the seismic profiles determined from the bottom of the excavation (PS-1 and PS-2 on the right margin and PS-5 and PS-6 on the left margin) and their equivalent profiles, upstream of the excavated trench, on the natural ground surface (PS-

11 and PS-12 on the right margin and PS-13 and PS-14 on the left margin). The results are given in Figure 8-11 to 14. If a p-wave velocity of 250-1000 m/s is accepted as a high degree of “weathering”, the entire site (natural or excavated surfaces after 3 years action of atmosphere) has a 4.5 m depth of surface alteration. The transition around  $v_p = 3000$  m/s is also significant. This threshold is located at a depth of 10-25 m on the right margin, whereas it is shallower (10-12 m) in the left margin. The depth of softer rock increases in the upper levels of the right margin. This is a structural feature, which is also found on the slopes of the valley (no excavation). It is also observed that the depth of the  $v_p = 3000$  m/s contours is always higher on the “natural” slopes (22 m in lower elevations, 35 m in higher elevations; the transition is abrupt and this probably marks the position of the geological fault at mid elevation of the right margin). This is consistent with the laboratory results in part reported previously.

The pattern of seismic profiling suggests the presence of faults parallel to river valley. This feature favours the weathering processes especially at high elevations.

However, a difficulty to interpret weathering based on seismic surveying is the fact that the velocity of p-waves increase with confining stress. “True” degradation and confining stress contribute to define the seismic profiles and it is difficult to separate both effects unless additional direct parameters related with weathering are determined. The water content/density profiles reported before could offer this information. The next section provides additional information on the question of weathering.

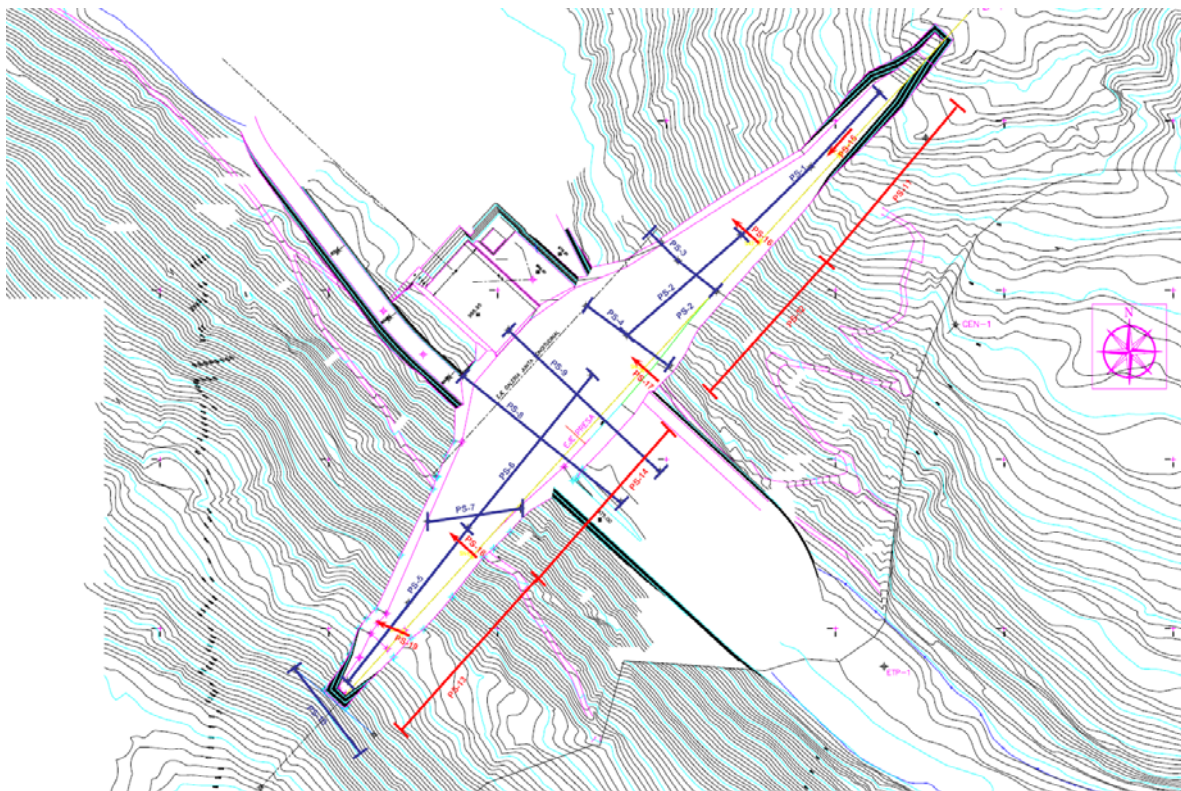


*Figure 8-10 - Position of the seismic profiles.*

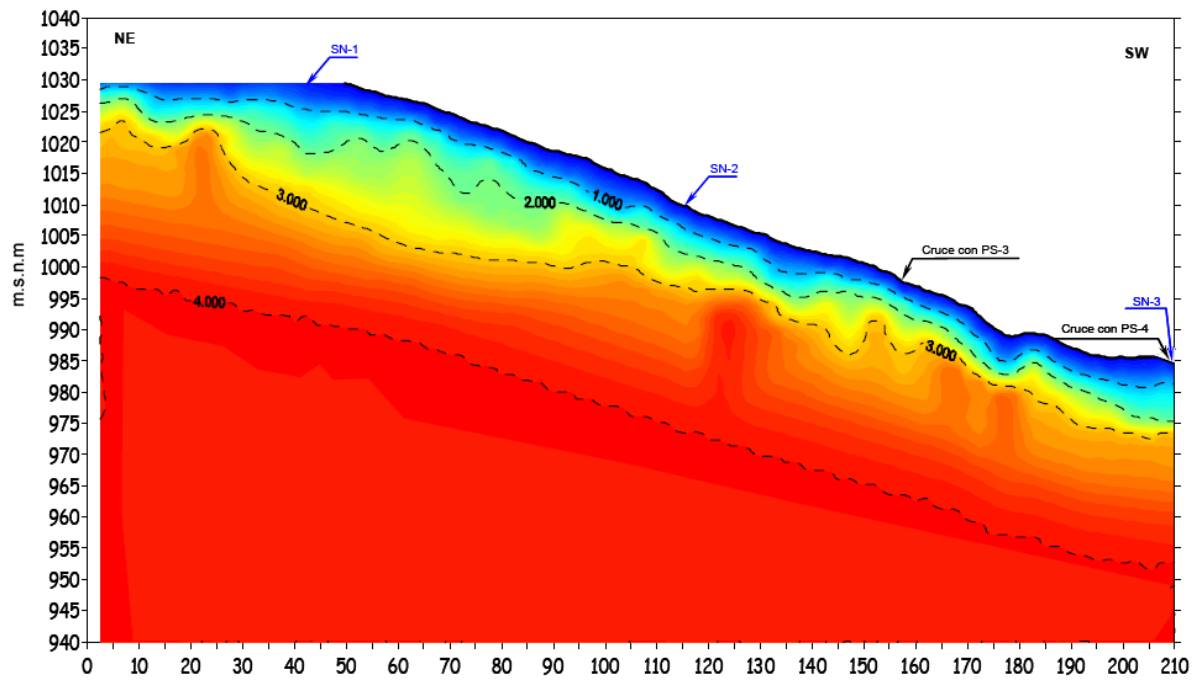


*Figure 8-11 - Intepretation of seismic profiles PS-1, PS-2. Right margin. Dam axis on excavated ground.*

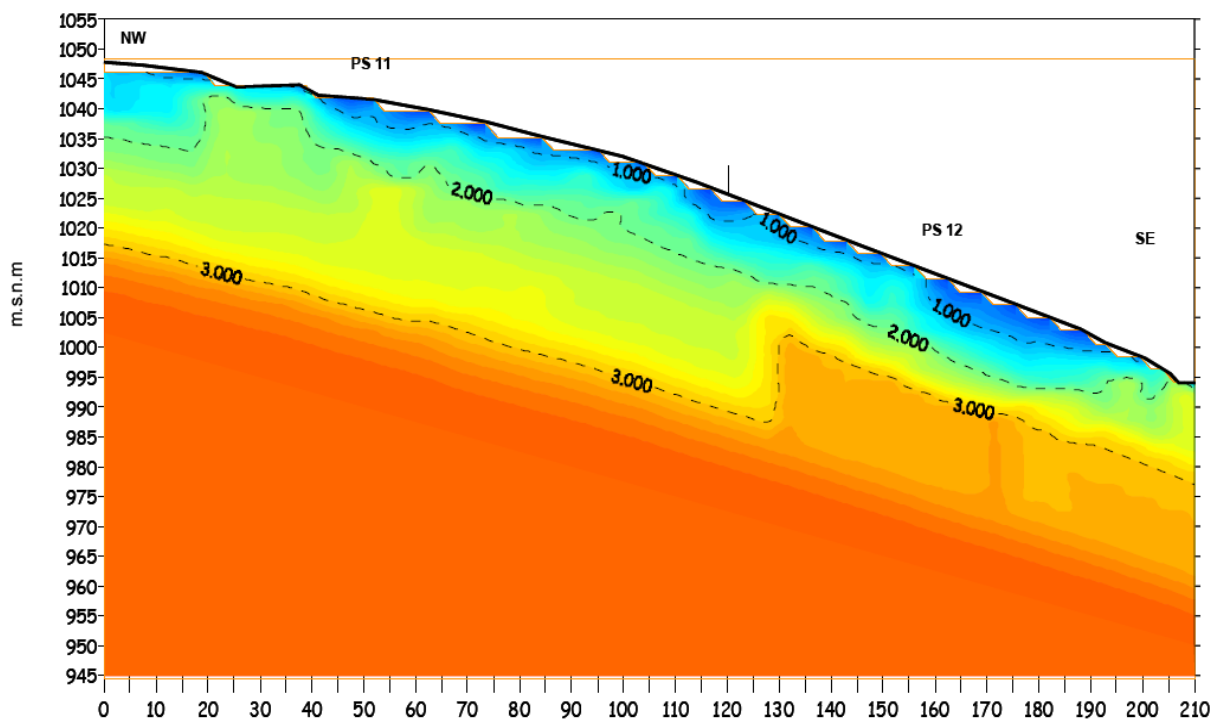


*Figure 8-12 - Intepretation of seismic profiles PS-11, PS-12. Right margin. Upstream of dam excavation on non-excavated ground.*

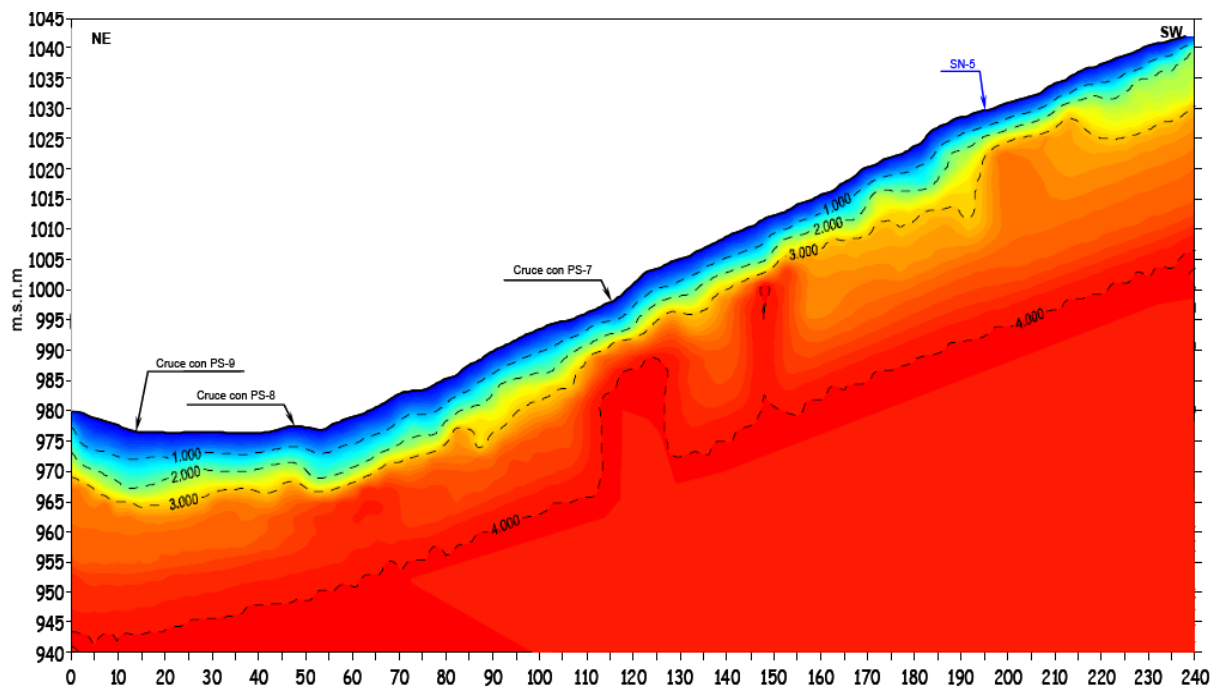


*Figure 8-13 - Intepretation of seismic profiles PS-13, PS-14. Right margin. Dam axis on excavated ground.*

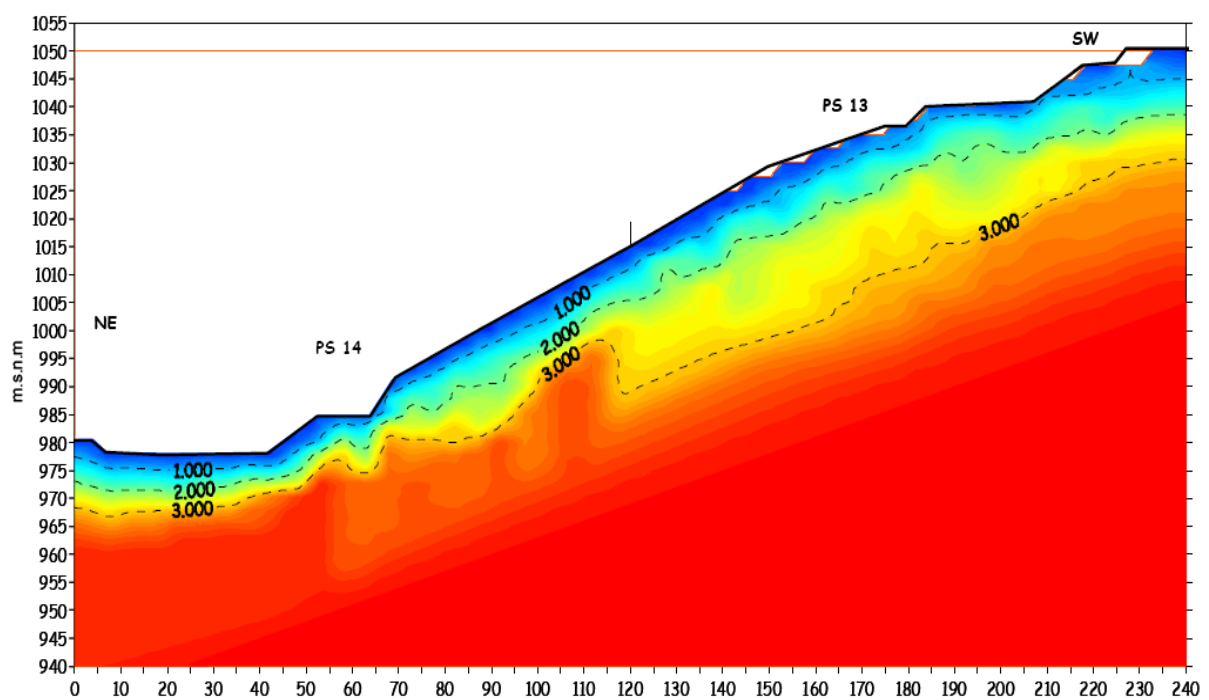


*Figure 8-14 - Intepretation of seismic profiles PS-13, PS-14. Right margin. Upstream of dam excavation on non-excavated ground.*

### 8.2.4 Weathering profiles and strength tests

Unconfined compression test were also determined on cores which experienced some partial drying before being tested (samples were protected by “vinilrel” paper which does not prevent vapour flow). Some results for a vertical boring on the right margin (SN-1) and the left margin (SN-5) are given in Figure 8-15a,b.

The natural siltstone formation was essentially saturated except for the upper most levels. Therefore, the strength values determined tend to overestimate “in situ” values. Figure 8-15 shows gradual increase in strength with depth, which is parallel to the velocity of P-waves determined in the laboratory (Figure 8-16).

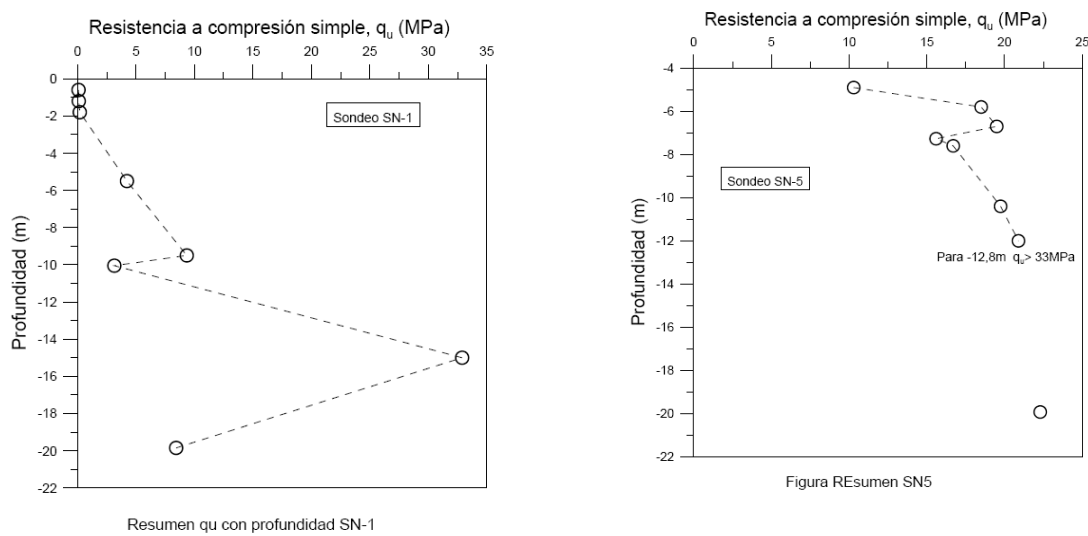


**Figure 8-15** - Variation of unconfined compression strength on two vertical borings (right and left margin, excavated zone).

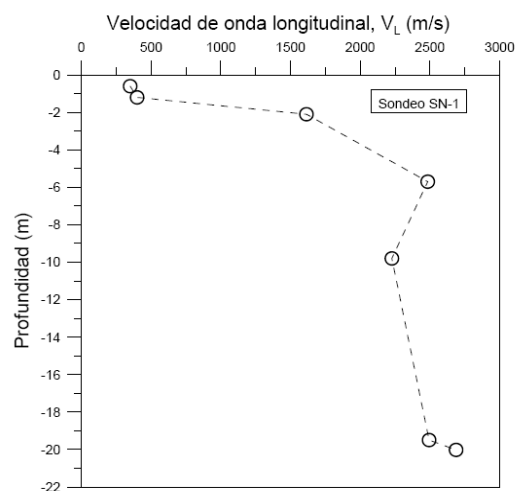


**Figure 8-16** - Variation of  $v_p$  (longitudinal determination in waves) for boring SN-1.

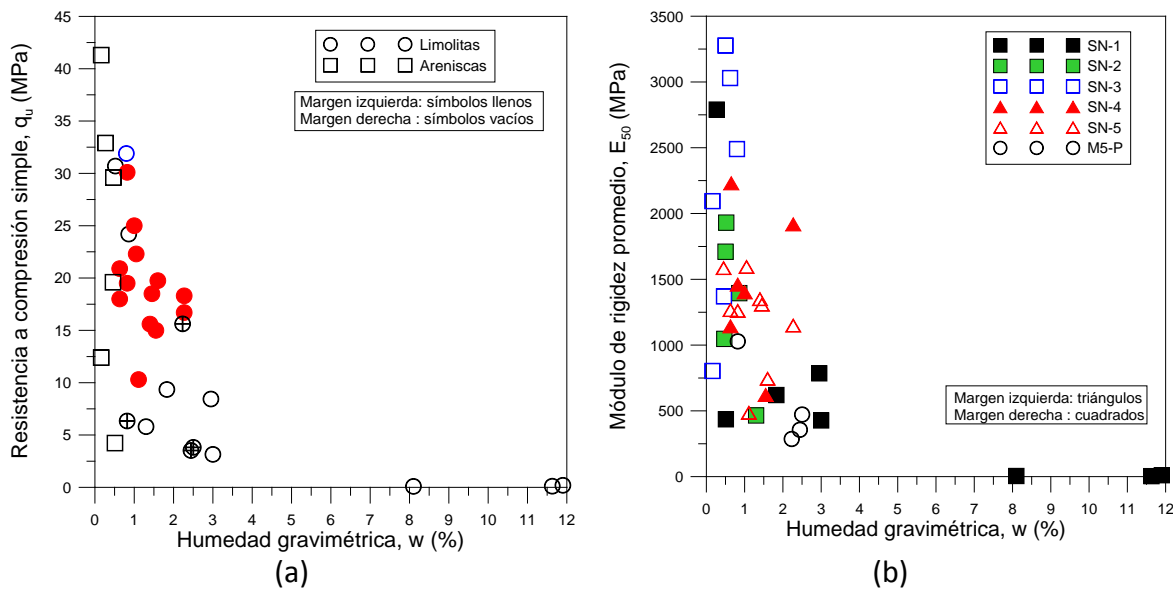


**Figure 8-17** -. Effect of water content on (a) unconfined compression strength; (b) stiffness moduli.

Unconfined compression tests tend to give a high scatter of results in natural formations. However, it is usually meaningful to plot the variation of  $q_u$  (and moduli) with water content. This is shown in Figure 8-17a,b.

The Castrovido weald siltstone behaves in a similar manner to other soft claystones reported in the literature: a small increase in water content in the range of 0.5-3% reduces enormously the measured strength. At water contents in excess of 5% the measured unconfined compression strength or moduli cannot be represented properly in the scale used.

### 8.2.5 Rock matrix properties from laboratory tests

#### 8.2.5.1 Identification, mineralogy, permeability, durability

Clays derived from the Weald siltstone are low plasticity materials. Liquid limit varies between 25 and 34%. The higher liquid limits are found close to the upper levels (Figure 8-18). The fine fraction of weathered materials is around 20%.

X-ray mineralogy determinations were carried out in a few samples. In one of them a series of strong wetting.- drying cycles was previously applied but no changes in mineralogy were noticed. The following results, in qualitative terms, provide a description of the mineralogy of the siltstone.

Mineral	Proportion
Quartz	High
Illite and Muscovite mica	Intermediate
Calcite	Intermediate
Clorite	Weak
Caolinite	weak

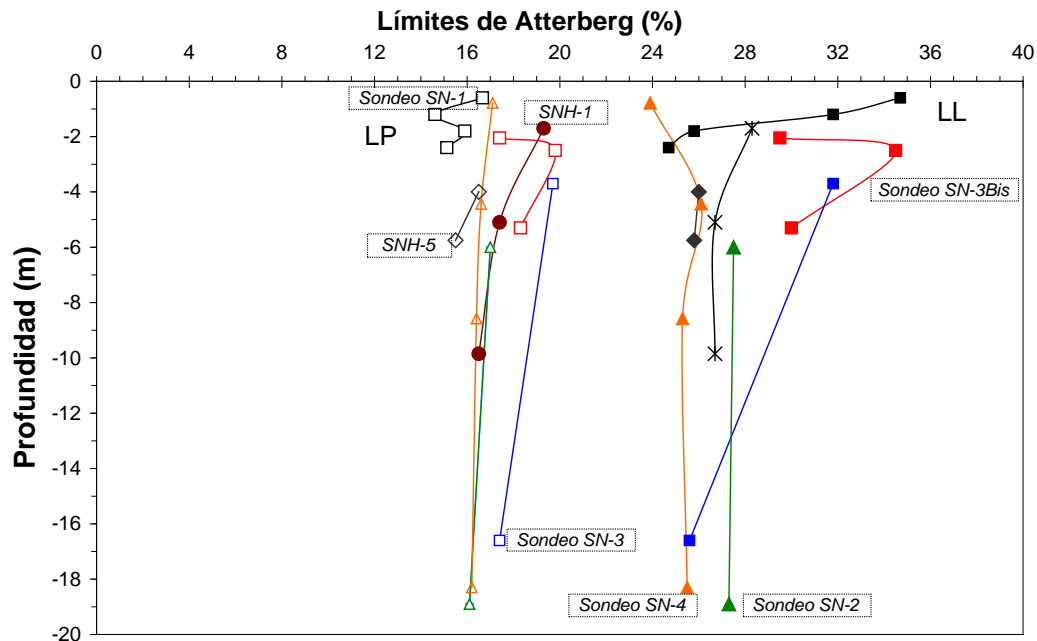


Figure 8-18 - Variation of Plasticity Indices with depth.

In one sample partially weathered ( $w = 10\%$ ) a permeability  $k = 3.6 \cdot 10^{-8}$  m/s was determined in vertical direction.

The durability test (ASTM d 4644-87) provided heterogeneous results in a number of tested samples (Figure 8-19). The test provides a measure of desintegration of the sample when subjected to two normalized cycles of wetting and drying. The interpretation relies on the results for the second cycle applied ( $I_{d2}$ ). The test shows a fast degradation of the siltstone. The best results correspond to siltstone-sandstone transition materials.

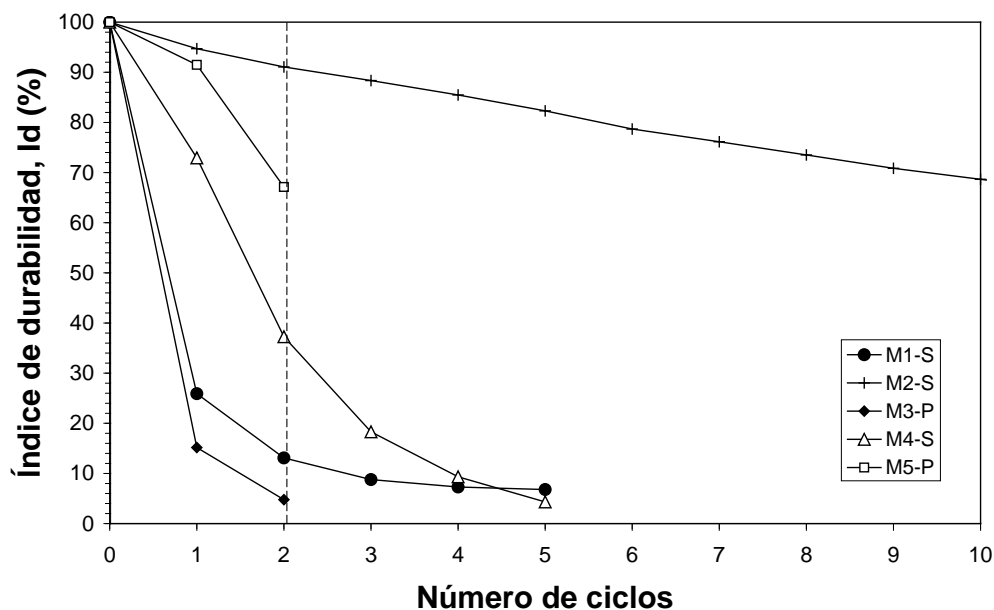


Figure 8-19 - Durability test on siltstone sample.

### 8.2.5.2 Shear strength

Two types of samples were tested: core samples and block samples. In the first case a conventional shear box was used. A large shear box capable of testing up to 30x30 cm samples was used for block specimens.

Results for the first group of tests are given in Figure 8-20. Tests were performed on saturated specimens at low shearing rate to achieve drained conditions. The depth of the core in each case provides an estimation of the degree of weathering experienced. An weathered sample (depth: 1.90 m) resulted in a profound lost of strength ( $c' = 0$ ,  $\phi' = 17^\circ$ ). In a test on a natural discontinuity recovered at a depth of 6 m a low strength ( $c' = 0$ ,  $\phi' = 24^\circ$ ) was also measured. The tested joint was clean and rough.

The shear stress-relative displacement of a few tests on large block samples is given in Figure 8-21. The material exhibits a brittle behaviour an indication of minor alteration. However “surface” blocks could also be tested and the results show a nil cohesive intercept and drained friction angles of 24-29°.

The results of the testing campaign have been collected in Figure 8-22.

Residual friction was also determined on ring shear tests performed on reconstituted material from the block samples recovered. Six tests were performed in samples from the left and right margin. The measured residual friction angles are as follows: 20°, 25°, 15°, 15°, 14° and 14°. They can be classified in two groups: “high” and “low” residual friction. The low values (14-15°) are not very consistent with existing correlations between residual friction and plasticity. However, the significant presence of mica may explain the results. It is then concluded that the other “high residual strength” group corresponds to samples not having mica in their minerals.

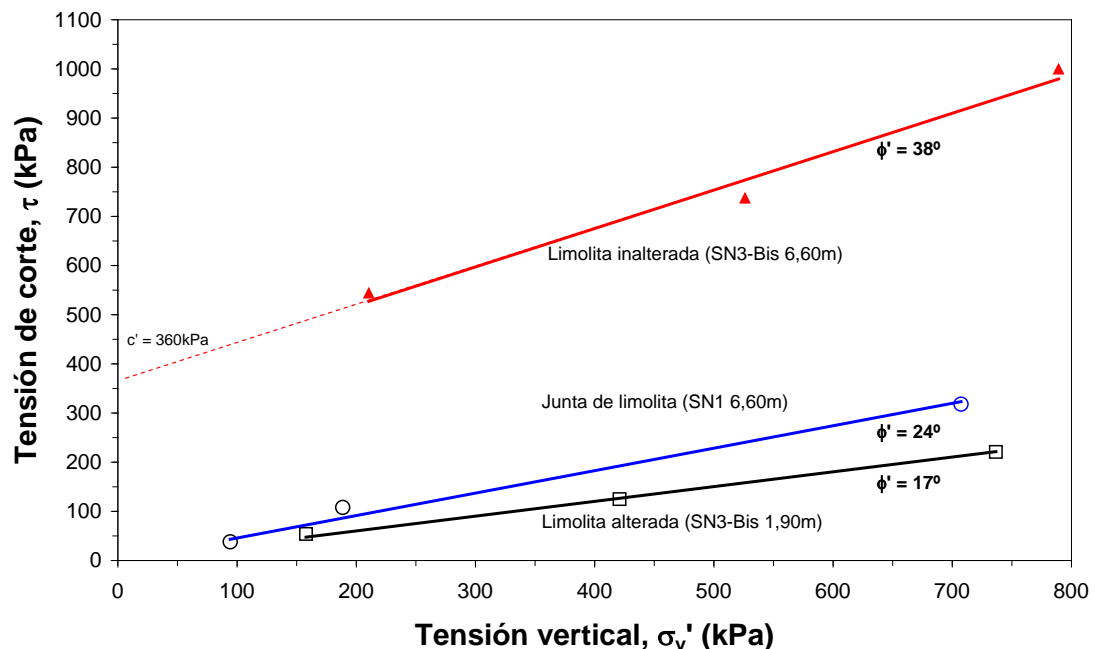


Figura 8-20 - Direct shear tests on core samples.

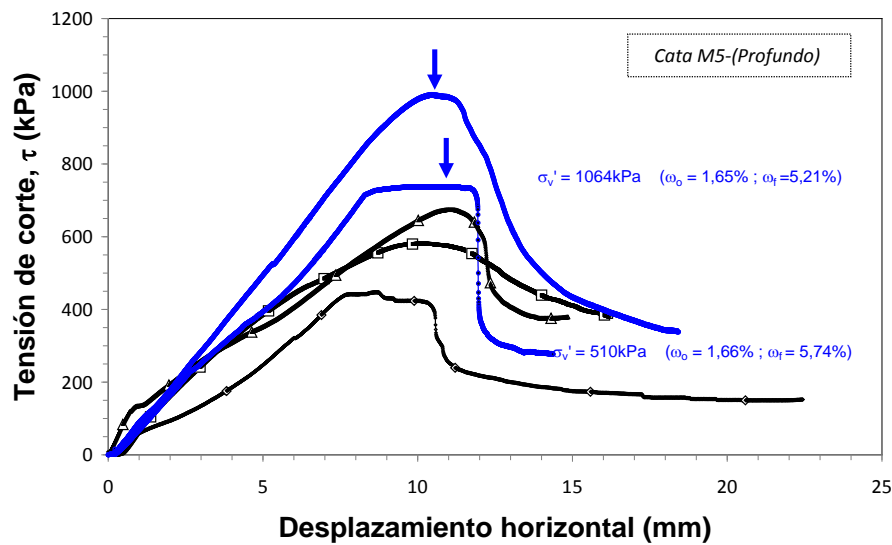


Figure8- 21 - Shear tests on blocks of undisturbed siltstone taken from upper level. Excavated abutments. Depth: 2 m approximately.

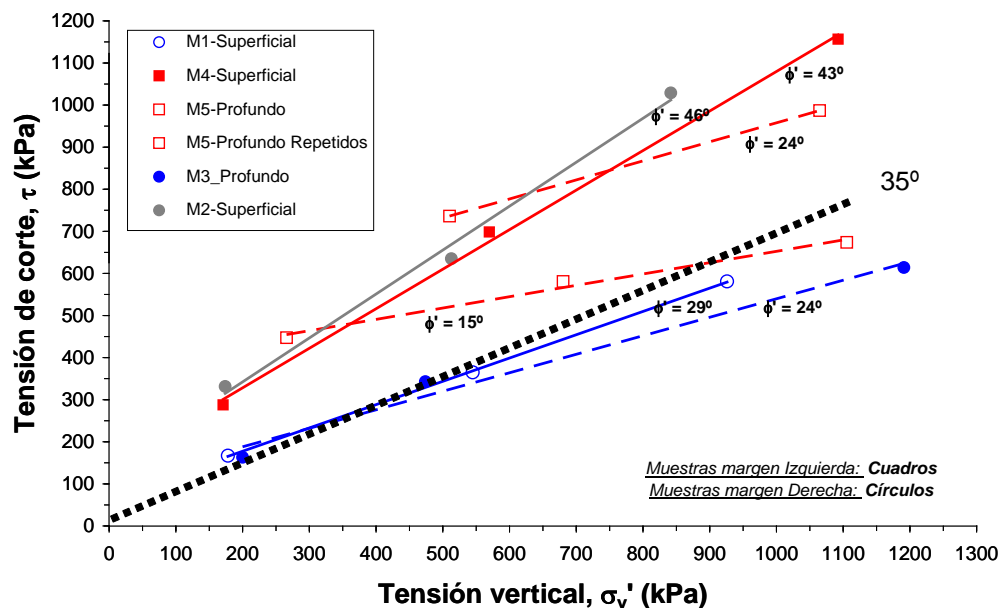
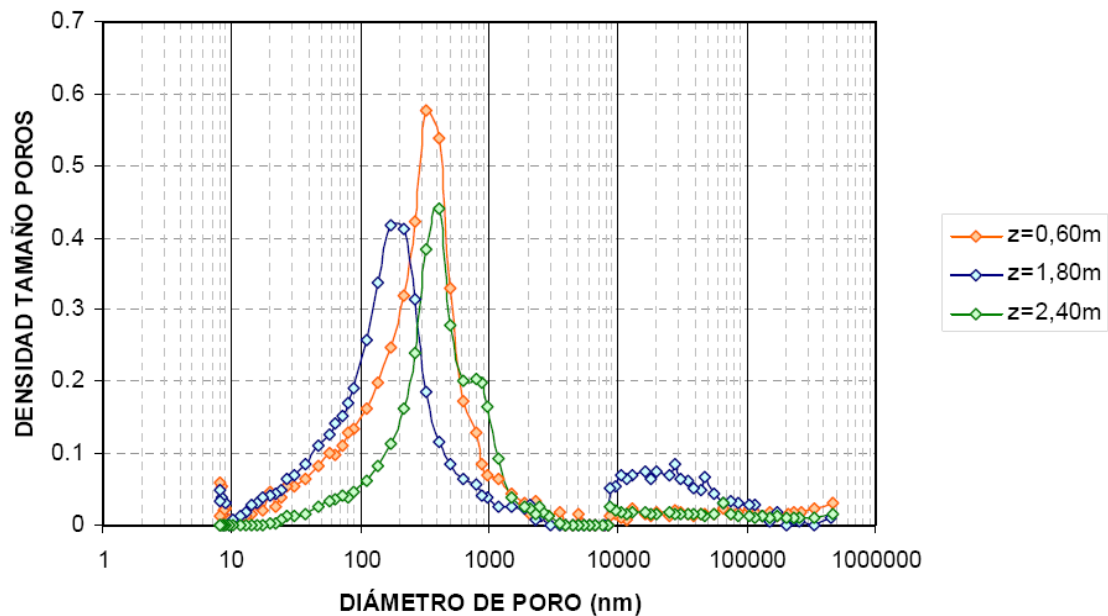


Figure 8-22 - Strength envelopes for tests on large blocks samples.

### 8.2.5.3 Pore size distributions

Pore size distributions were obtained for specimens recovered at increasing depth (on borings SN-1). Results are given in Figure 8-23. There is a trend of decreasing mean pore size with depth (mean pore size of 300 nm for the surface specimen (-1.80 m). The type of pore curves determined corresponds to an overconsolidated soil and not to a rock.

Pore sizes are essentially mono-modal and there is a limited inter-aggregate porosity.



*Figure 8-23 - Pore size distribution of specimens recovered on boring SN-1.*

## 8.2.6 Conclusions

The rock mass is described as a sequence of red siltstone and sandstone layers dipping no more than 20-25°. The red siltstone is a soft rock whose main mineral components are quartz and muscovite mica. Low activity clay minerals are also present. The siltstone degrades fast when unloaded and subjected to atmospheric action and transform into a low plasticity clayey silt.

The alternating siltstone and sandstone layers have a mean spacing of one meter. There are also frequent thin inter-layers (cm size) within the sandstone banks. The siltstone lithology dominates the sequence and thicker siltstone layers are also common.

In addition to layering, three sub-vertical discontinuity families were identified. These joints are filled with clay and they are typically found within the sandstone banks. They contribute to weaken the entire rock mass.

Seismic profiles and the profiles of index properties developed for water content, density and unconfined compression strength allow for the identification of a weathered upper layer in exposed siltstone. The degree of weathering progresses from intact levels at 4 m depth to a maximum weathering at the surface. A significant spatial variation of weathering was also identified and the two valley slopes behaves in a different manner (stronger and deeper degradation on the right margin).

The degradation is directly linked to the increase in water content and the decrease in density. Water content increase is induced by atmospheric action. However, the siltstone maintains probably certain suction during most part of the year in upper layers, close to the surface. Siltstone permeability is low ( $k = 3.6 \cdot 10^{-8}$  m/s) and this is a reason for the difficulty of weathering to advance downwards. On the other hand stress unloading induced by excavations has also an important effect in damaging the weak cementation of the soft rock

and in opening preferential paths for water infiltration. It has been found that the two processes combine into a rapid degradation rate in the field. At the scale of a few months the weathering profile under an open excavation may be similar to the long-term weathering profile under the surface of valley slopes

The presence of Muscovite mica in all the Weald materials is a singular aspect of the case study presented. Mica has a reduced particle to particle friction ( $12^\circ$ ). The planar shape of mica particles leads in a natural way to layering orientations parallel to the maximum dimension of particles (laminae) when mica concentrations are high (as found for instance in some interlayers between sandstone banks). A very low friction is expected in those surfaces. In fact, mica is found in interstratifications in sandstone layers, in siltstone fillings among sandstone layers and scattered within siltstone banks. This presence explain the “anomalous” result of finding very low residual friction angles ( $12^\circ - 14^\circ$ ) measured in remoulded specimens recovered in joint fillings but also in the siltstone matrix. The expected residual friction angle of a low plasticity clayey silt (having a significant proportion of quartz) is no less than  $25^\circ$ .

This mica-related feature and the fast natural weathering explain the observed surface instabilities when vegetation is removed. In addition, when excavated slopes allow a kinematic instability in the dip directions of sedimentation planes, planar slides develop easily even for low dip angles ( $10^\circ - 20^\circ$ ).

## 9 VOLCANIC PROCESSES (*UNIMIB*)

A wide variety of slope failures occur on volcano edifices, ranging from small rockfalls to massive collapses which are directly related to volcanic activity. Although volcanic mass movements initiate as a sliding movement, flow soon dominates, reflecting the two most commonly used terms in a volcanological context, debris avalanche and lahars. This type of movement is favored by the kind of material, often altered, with alternating layers of more or less competent rocks. The rapid transformation into far-traveling lahars is enhanced by the ability of low-strength, clay-rich rocks to retain pore water during collapse (Carrasco-Nunez et al., 1993; Iverson et al., 1997).

### 9.1 TRIGGERING MECHANISMS: DEBRIS AVALANCHES

A wide range of eruptive or non-eruptive phenomena may accompany edifice slope failures, depending on the proximity of the failure plane to magmatic-hydrothermal systems. Most failures develop as rock slides and debris avalanches, characterized by the fast movement of large volumes of rock and debris (to 1-40 km<sup>3</sup>) over great distances (to > 100 km) affecting areas of up to 1500 km<sup>2</sup> (e.g. Siebert, 1984). Debris avalanches are large, extremely rapid and often open-slope landslides, which may have been initiated by the collapse or sliding of a rock mass and might all be classified as flows or complex slides according to the categories of Cruden and Varnes (1996). Debris avalanche deposits at the base of these breached craters or calderas consist primarily of lithic material of the volcanic cone, and often have volumes closely comparable to those of missing sectors of the cones, indicating that the dominant process is not explosive destruction of the cone, but massive slope failure of a portion of the volcanic edifice.

Eruptions associated with volcanic debris avalanches can be divided into two types, those with a magmatic component (Bezymianny-type) and those that are solely phreatic (Bandai-type). Volcanic debris avalanches can also be unrelated to explosive activity, and are in this case purely gravitational (Unzen-type) (Siebert et al., 1987). Structural, morphological, and mechanical factors (Voight and Elsworth, 1997) all contribute to increasing the potential hazard for edifice failure. Magmatic intrusions or phreatic explosions are among the most prominent factors at triggering failure. Nevertheless, lateral failure may pose risk even on magmatically inactive volcanoes, as instability is favored by weakening of the edifice due to hydrothermal alteration of the rock mass or by sub-volcanic basement spreading or more common triggering factors. The same edifice can suffer repeated failures. Different types of volcanic debris avalanches with different mechanical triggers can succeed on the same volcano.

Slope failures themselves can trigger explosive activity by sudden pressure release of hydrothermal-magmatic fluids. These can occur if i) the failure plane truncates magma bodies or associated hydrothermal envelopes in the upper edifice. When the failing block is farther removed, major plinian eruptions can occur without lateral blasts or, in the other hand, eruptions may be restricted to relatively minor scoria ejection or lava effusion; ii) when near surface magma is absent, explosions are strictly phreatic.

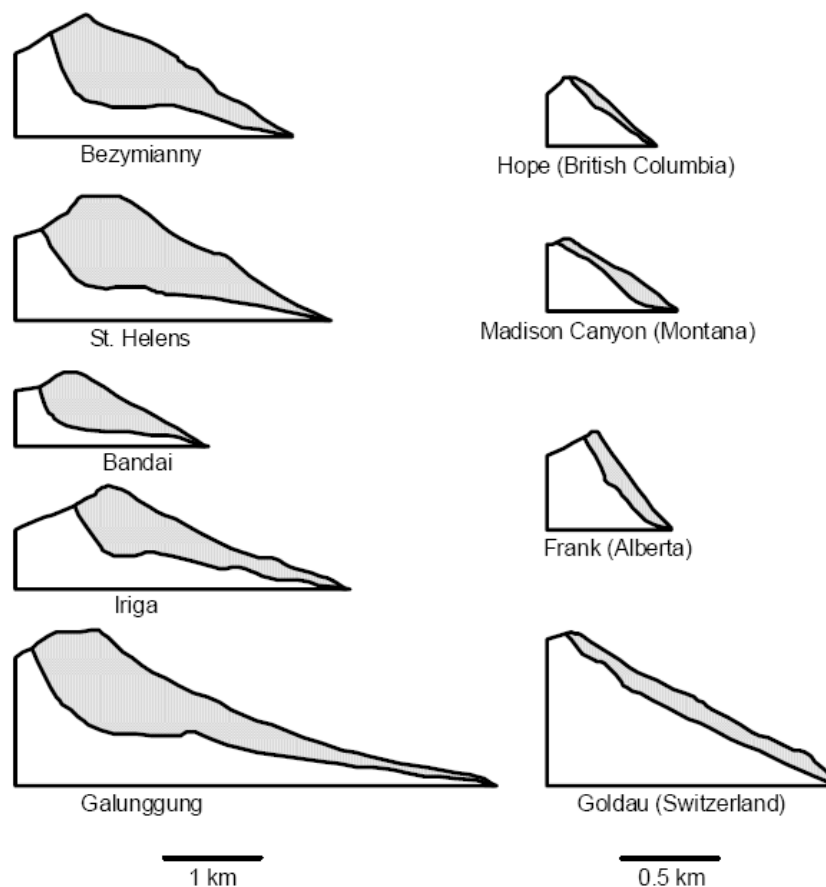


**Figure 9-1** - Cross-sections of volcanic landslides (left column) as compared to non-volcanic landslides (right column, drawn at 2x scale). Shaded portion indicates volume removed by slope failure. Vertical scale equals horizontal scale (Siebert, 1999).

The failure surfaces of volcanic landslides are typically more deeply seated than their non-volcanic counterparts and not as influenced by stratigraphic dip slope (Figure 9-1). Their greater depth may be attributed in part to the presence of large amounts of weakly indurated pyroclastic and altered material (Reid et al. 2000; Siebert 2002).

Deposition of eruption products or magma intrusion causes overloading or oversteepening of slopes (Gorshkov, 1959; Moore and Albee, 1981; Lipman et al., 1981; Voight et al., 1981; Siebert, 1984; Siebert et al., 1987; Murray, 1988; Begét and Kienle, 1992). The typical vertical relief is of several km and upper slopes can exceed 30° (Figure 9-2). Francis and Wells (1988) show that volcano collapses at the Central Andean Cordillera correlate strongly with edifice height (10% of volcanoes <500 m to 75% of volcanoes higher than 2500 m). With this respect, steep-sided andesitic and dacitic stratovolcanoes are the best candidates for slope failures.

Particularly susceptible to failure, as a result of the forceful magmatic intrusion, are steep sided, less voluminous lava-dome complexes which may become oversteepened (Siebert 1996). The presence of cones and domes located eccentrically and/or directly above the magma chamber could have two consequences. Firstly, due to gravitational loading, a

volcanic cone changes the stress field in the vicinity of a shallow magma chamber and could notably influence magma chamber stability (e.g. Pinel and Jaupard 2003) and caldera formation, ie. such as the orientation of caldera faults and type of subsidence of the roof into the magma chamber. This influence of pre-existing topography for caldera fault development was recently studied by analogue experiments (Walter and Troll 2001; Lavallée et al. 2004), highlighting that the topography may influence or even control the style of caldera subsidence. Secondly, if a caldera fault crosses a volcanic edifice, the structural instability that is induced can lead to large-scale landslides.

Edifice weakening is another cause of failure. Stability analyses using limit equilibrium methods indicate that volcano slope composed of material with common strength properties tend to be very stable, even under totally saturated conditions (Hurlimann et al., 1997). This suggests that the presence of a weak layer is required in order to reduce the strength of the volcanic pile as to allow for failures. Volcanic edifice weakening is largely caused by zones of low strength created under the influence of a hydrothermal system. Hydrothermal activity is defined as hot and pressurized fluid circulation maintained by shallow internal or deeper magma sources, rich in corrosive chemicals.

Hydrothermal systems exist at many volcanoes where buried intrusives interact with groundwater producing highly acidic hot fluids. These fluids tend to progressively alter the rocks and increase general pore pressure, weakening the host edifice (Lopez and Williams 1993; Day 1996; Vallance and Scott 1997; Iverson et al. 1997), promoting rock dissolution and clay mineral formation along geologic structures (discontinuities, faults and dykes) and lithologic boundaries (Frank 1983; Carrasco-Nunez et al. 1993; López and Williams 1993; Watters et al. 2000). High-temperature acidic solutions percolating through a volcanic edifice can transform the strongest of volcanic rocks into weak materials (Watters and Delahaut, 1995) by acid-sulphate leaching and replacement of phenocrysts with clay minerals. Studies on stratovolcanoes show that kaolinite, alunite and smectite are the most common hydrothermal alteration mineral groups (Frank, 1995; Rye et al., 2003).

However, not all types of hydrothermal alteration result in lowered rock mass strengths. Silicification for example generally produces a stronger and more elastic rock mass (Watters et al. 2000). While it is difficult to assess the specifics of hydrothermally altered rock masses, a strength decrease is a good first approximation (López and Williams 1993; Watters et al. 2000).

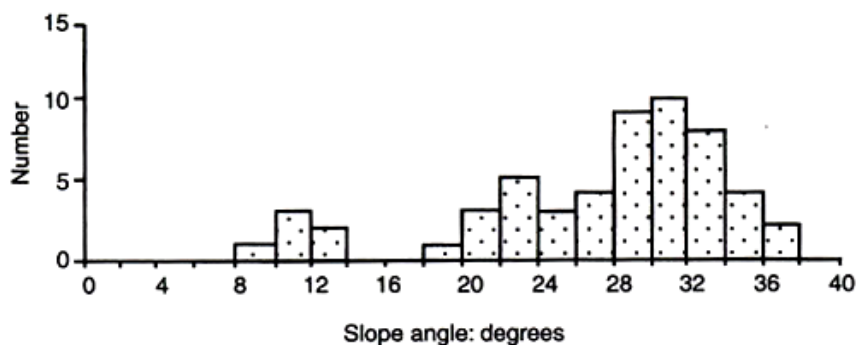


**Figure 9-2** – Slope angle of Quaternary volcanoes that have undergone major slope failure (Siebert, 1999).

Quantifying the decrease in shear strength associated with increasing degrees of argillic hydrothermal alteration is non-trivial, and while there is extensive literature on alteration mineralogy, only a few researchers have studied how such changes affect shear strength (Watters and Delahaut, 1995), and the results are far to definitive (del Potro and Hürlimann, 2008). In case of edifice weakening, the failure can either occur (i) in the zones of alteration, where the flanks, friable and incompetent, are the source area for debris avalanches and rockfalls; (ii) by flank spreading.

Flank collapse can occur also in low-angle volcanoes by gravitational spreading of sub volcanic strata. The concept of gravitational spreading relies mainly on the effects of a volcano's weight on the underlying strata and on the edifice itself. Under the influence of gravity, the volcano deforms, destabilizes, and generates a slump that develops into a large flank collapse. Gravity-driven flank spreading promoted by hydrothermal weakening of the rocks (Lopez and Williams, 1993; Kempter and Rowe, 2000; vanWyk de Vries et al., 2000; Reid et al., 2001) or ductile volcano basement (for example sediments), which deform under the load of the overlying volcanic edifice.

The process was first described by Van Benmelen (1949) and then used by Borgia et al. (1992) to explain the structural formation of Mount Etna. Van Wyk de Vries et al. (1997, 2000, 2001) explored the phenomenon further, demonstrating the relation between collapse, edifice weakening, tectonic faulting, and flank spreading. The thickness of the weak layer can be (i) a small fraction (1%) of the volcano height and act as a slip plane (e.g. in the Hawaiian and other oceanic shield volcanoes, Borgia, 1994), in up to  $\approx 20\%$  and the deformation take place within this layer (e.g. at Mombacho, van Wyk de Vries and Francis, 1997). Summit gräben and basal thrusts are typical spreading structures (Merle and Borgia, 1996), but strike-slip faults are also closely associated with spreading (Borgia and Van Wyk de Vries, 2003).

Structural factors such as alternation of competent lavas with unconsolidated pyroclastic materials (Voight, 2000; Watters et al., 2000), promoted parallel dike swarms and injection of magma (Elsworth and Voight, 1995), pressurization of phreatic waters by magma heat (Reid, 1994), and tectonic movements of faults of volcano basement (Vidal and Merle, 2000) surrounding/underlying active rift zones (van Wyk de Vries and Merle 1996; Day et al. 1999),

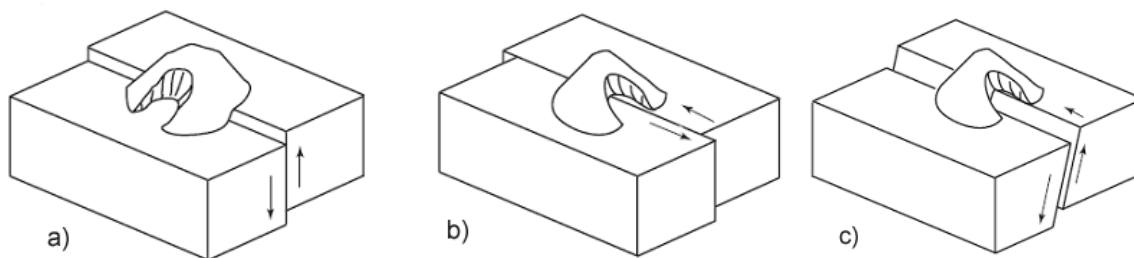


**Figure 9-3** - Influence of structural factors and models for generation of collapse. Modes involving activity of a single normal fault at the basement are (a) a model by Vidal and Merle (2000) of a normal vertical fault; (b) Lagmay et al. (2000) on strike-slip faults; (c) normal faulting of Wooller et al. (2003) at the center of the volcano fault and effects of oblique fault plane (Concha-Dimas et al., 2005).

strike-slip faulting (Lagmay et al. 2000) can lead to failure with or without eruptive activity (Figure 9-3). Intersection of volcanic cones by tectonic faults was investigated experimentally by Vidal and Merle (2000). In their experiments, instability of the volcanic edifice was induced by formation of faults in the volcano's substrate. In some cases, the sliding surface of the collapse scar slopes at a similar angle to the cone surface, suggesting that the avalanche slid along a bedding plane (Naranjo and Francis, 1987; Wyk de Vries and Francis, 1997).

Magma emplacement is possibly the most common triggering factor (Bezymianny-type activity defined by Gorshkov 1959; Glicken et al. 1981; Voight, 1972; Gucwa and Kehle, 1978; Prostka, 1978; Voight et al. 1981, 1983; Siebert et al. 1987; McGuire et al. 1990; Elsworth and Voight, 1995). Many collapses are the consequence of various processes related to magmatic activity: dike emplacement (Nakamura, 1977; Dietrich, 1988; Delaney et al., 1998; Elsworth and Day, 1999; Tibaldi, 2001), volcanic activity (Capra et al., 2002), caldera formation (Marti et al., 1997), the intrusion of viscous magma (Voight et al., 1981; Belousov et al., 1999; Richards and Villeneuve, 2001).

Magmatic activity can be represented by the subvolcanic intrusion of cryptodomes (e.g. St. Helens, Voight et al., 1981; Donnadiu et al., 2001) and dikes (e.g. Stromboli; Tibaldi, 2001), or by blast explosions (e.g. St. Helens; Hoblitt et al., 1981; Druitt, 1992) and pyroclastic flow emplacement (e.g. St. Helens; Lipman et al., 1981; and Cotopaxi; Mothes et al., 1998).

Magma intrusions can have two effects: to increase the driving force by direct magma pressurization or intrusion-related seismic inertial force, and/or to decrease the resisting force by fluid pressure enhancement (Voight and Elsworth 1997). Pore pressures due to poroelastic deformation may be more rapidly transmitted than those due to thermal expansion or degassing (Elsworth and Voight 1992, 1995), but the latter process may be longer lasting and ultimately more effective in provoking volcano collapse (Figure 9-5). Additionally, intrusions can induce mechanical or thermal straining of the rocks, generating excess pore pressures and reducing the sliding resistance on faults within the edifice (Elsworth and Voight 1995) and dilational effect on volcanoes (Voight and Elsworth, 1997). Voight and Elsworth, (1997) suggest that fracturing and weakening promote edifice collapse in a direction perpendicular to that of the intruding dykes (Figure 9-4).

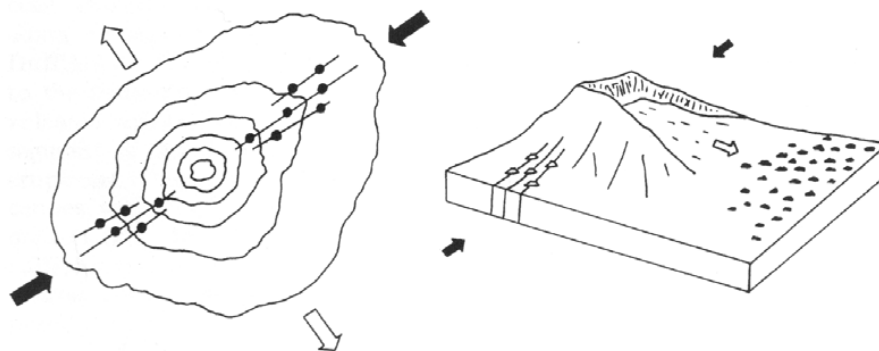


**Figure 9-4** – Schematic illustrating the direction of proposed dilational stresses associated with the intrusion of dykes within the volcano edifice. It is thought that intruding dykes promote collapse in a direction perpendicular to that of intrusion orientation. Black arrows indicate orientation of dyke intrusion. White arrows indicate likely direction of collapse (Adapted from Siebert, 1984).

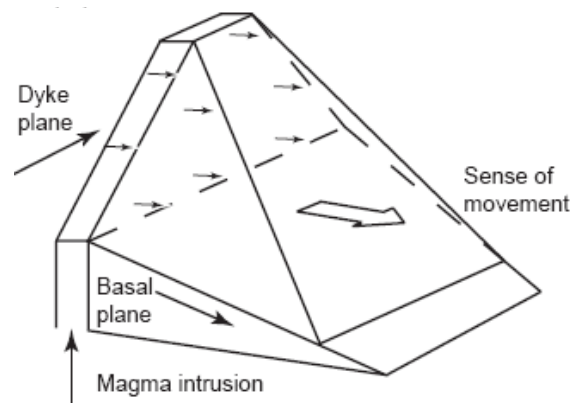


*Figure 9-5 - Wedge mode of failure with magma injection (Elsworth and Voight, 1995).*

Sector collapse can also initiate volcanic activity (Alvarado and Soto, 2002; Acocella et al., 2003), generating a feedback mechanism between gravity failures and magmatic activity (McGuire et al., 1990).

Increase in pore pressure or variations in local water levels (Bray 1977; Elsworth and Voight, 1996; Firth et al. 1996; McGuire 1996, McGuire et al. 1997; Ablay and Hürlimann 2000) is another triggering mechanism of interest. Elevated pore-water pressures affect rock frictional resistance, essentially lowering the strength of rock masses. Magmatic intrusions are a commonly accepted means for creating elevated pore-water pressures in portions of the edifice (Elsworth and Voight 1995; Voight and Elsworth 1997). Alternatively, the resulting increase in permeability of hydrothermally altered rock masses may be responsible for elevated pore-water pressures (Day 1996; Cecchi et al. 2005). Hürlimann et al. (1999) illustrated how pore-water pressures strongly increase during rapid loading in undrained conditions. Earthquakes, a common process in active volcanic areas, can cause fast loading resulting in saturated soil. Heavy rainfall is also known to be a frequent cause of the generation of elevated porewater pressures (Siebert 2002).

Mechanical pressurization has been observed in a series of intrusive events at Krafla, Iceland (Brandsdottir and Einarsson, 1979; Tryggvason, 1980; Stefansson, 1981) or as a result of thermal pressurization during eruptions (Bjornsson et al., 1977). Processes of generating excess fluid pressures are not limited to mid-ocean ridge environments (e.g., island-arc volcanics, Watanabe, 1983), but also to rocks within the core of a volcanic edifice (Sigurdsson, 1982; Elsworth and Voight, 1992).

It is highly likely that the inherent instability of volcanoes is attributable to a combination of events or circumstances rather than any single process. While a final factor may 'trigger' a volcanic landslide, it is never the sole cause (Voight, 1992). It is the superposition of subsequent factors, such as pore water pressure enhancement, that cause this gradually weakened material to fail. The large population of volcanoes meeting slope angle criteria, for example, that have not to this point undergone failure, suggests that a triggering mechanism is required to initiate failure (Siebert 1996).

## 9.2 TRIGGERING MECHANISMS: LAHARS

Cohesive debris flows mobilize directly from flank collapses of saturated, highly altered and clay-rich material (Scott et al., 1995; Crowley and Zimbelman, 1997; Vallance and Scott, 1997).

- Lahars can result from debris avalanches through segregation or acquisition of water, and portions of debris avalanche deposits are gradational with lahars (Glicken, 1991; Siebert 1996) by: (1) transformation of water-saturated parts of mixed facies to lahars during emplacement (Palmer and Neall, 1989); (2) post-depositional remobilization of water-saturated parts of the debris avalanche (3) breakout of debris-avalanche-dammed lakes hours to years after emplacement
- Mechanical scouring of ice and snow by pyroclastic flows is a mechanism for lahars generation in ice capped volcanoes (Pierson and Scott, 1985; Scott, 1988; Dorava and Meyer, 1994; Meyer and Trabant, 1995).
- Lahar generation at glaciated volcanoes also can occur in response to glacier outburst flooding (Walder and Driedger, 1994). Rapid release of water stored beneath or adjacent to a glacier can initiate a flood surge that may entrain large volumes of volcanoclastic sediment and transform to lahars.

Volcanic products themselves can be mobilized by mechanisms which are not directly related to volcanic activity.

## 9.3 APPROACHES

The importance of the collapse failures in volcanic edifices has only been recently recognized. Hence, the information about the exact material properties and the boundary conditions of the model generally lacks.

In the last two decades, many advances have been made in understanding the causes of large volcanic landslides. However a comprehensive analysis and quantification is still in its infancy.

Previous models investigating volcano induced stress have either been numerical (Cyr and Melosh, 1993; van Wyk de Vries and Borgia, 1996) or physical analogue (Merle and Borgia, 1996; van Wyk de Vries and Merle, 1996, van Wyk de Vries and Matela 1998).

### 9.3.1 Numerical modeling

Physically based mechanical models, developed for geotechnical analyses, provide tools for assessing and quantifying slope instability under a wide variety of conditions. A number of different methods have been used to model the stability of volcanic slopes including 2D (Hürlimann et al. 1999; Voight 2000; Moon et al. 2005) and 3D limit equilibrium analysis (Reid et al. 2000).

For homogeneous materials and uniform pore fluid pressures, simple one dimensional force balance analyses predict that steeper slopes are more unstable (Lambe and Whitman, 1969), thus patterns of instability generally tend to mimic topographic slope. However, as above said, the sole gravitational forces are not able to induce failure in volcano slope composed of material with common strength properties, even under totally saturated conditions (Hurlimann

et al., 1997). By numerical analyses, Borgia (1994) recognizes the weight of the edifice onto the substratum and the long-term deformation of the intrusive complexes as the two most prominent elements in driving the volcanic failure.

Numerical models investigated how the load of a volcano may be controlled by magmatic activity. The stability of a volcano slope is evaluated under an increase of internal magmatic pressure (Dietrich, 1988; Russo et al., 1997), excess pore pressures due to intrusion (Voight and Elsworth, 1997; Elsworth and Day, 1999) and during cryptodome emplacement (Donnadieu et al., 2001). Numerical models show that even a magmatically inactive volcano with a significant mass, if resting over a weak substratum, is capable of inducing slope failure (Borgia, 1994; van Wyk de Vries and Matela, 1998). Moreover, numerical models have been applied to reveal the importance of topography on the stability of volcanic edifices (Reid et al., 2000), to simulate the emplacement of landslides resulting from caldera collapse (Hurlimann et al., 2000b), and to simulate the propagation of the debris avalanches from edifice collapse (Sosio and Crosta, in preparation).

### 9.3.2 Analogical modeling

Analogue modeling is widely used to test interpretations of volcanic processes derived from geological data and provide insight into the basic operating mechanisms, such as spreading, magma intrusion and active faulting. Analogue models have also been widely used to simulate sector collapses of volcanoes. Experiments of volcanic spreading were performed to predict the propensity to spread and the rate of spreading in a volcano as a function of its shape and the ratio of brittle to ductile rock in the substrata (Merle and Borgia, 1996), in extensional (van Wyk de Vries and Merle, 1996) and strike-slip (van Wyk de Vries et al., 2003a) settings. The role of a ductile horizon at the base of a hydrothermally altered volcanic pile has also been investigated (Merle and Lenat, 2003).

Attempts have been made to study the collapse of a cone as a consequence of a viscous intrusion, focusing in particular on the possible path of rise of the intrusion and on the deformation induced on the edifice (Donnadieu and Merle, 1998, 2001). Analogue models have been recently used to study the instability of a volcanic cone due to a basal active fault. A vertical fault with a dip-slip movement at the base of a cone may produce distinct types of flank collapse, recognizable even at dormant volcanoes (Vidal and Merle, 2000; Merle et al., 2001). Similarly, the activity of strike-slip (van Wyk de Vries and Merle, 1998; Lagmay et al., 2000) and oblique (Wooller et al., 2003) faults on volcanic cones permits prediction of the location of the associated flank failure. Other recent experiments examine the failures of domes and stratocones after caldera collapse (Belousov et al., 2003).

In the experiments, the major part of the edifice is supposed to be made of a pile of brittle volcanic rocks. In such a material, the deformation is entirely governed by the Navier-Coulomb criterion of brittle failure and is considered to be rate-independent. This brittle part is simulated by a dry sand/plaster mixture (Merle and Borgia 1996; Donnadieu and Merle, 1998; Merle et al., 2001). Ductile part of the edifice is simulated by silicone putty (van Wyk de Vries et al., 2000). As the deformation of a ductile material is time-dependent, the scaling procedure is an attempt to design a consistent model for time and strain rate. The silicone has a Newtonian behavior when pure and a Bingham behavior when mixed with sand.

## 9.4 EXAMPLES

### 9.4.1 Tenerife (Canary Islands)

Tenerife is the largest of the seven Canary Islands and is characterized by a complex volcanic evolution involving several stages of volcanic activity and a variety of constructive and destructive processes (Figure 9-6). The island's volcanic shield was produced by subaerial fissure eruptions lasting from about 8 to 3 Ma and now outcrops in the corners of the island (Fuster et al., 1968; Ancochea et al., 1990). Towards the end of shield growth, volcanic activity migrated to the central part of Tenerife, where the Las Canadas edifice has since developed. The evolution of the Las Canadas edifice has involved several constructive and destructive events, including caldera collapse episodes and lateral and vertical failures (Marti' et al., 1994; Marti' et al., 1997; Ancochea et al., 1999). The current constructive phase corresponds to the formation of the active Teide-Pico Viejo volcanic complex within the Las Canadas caldera.

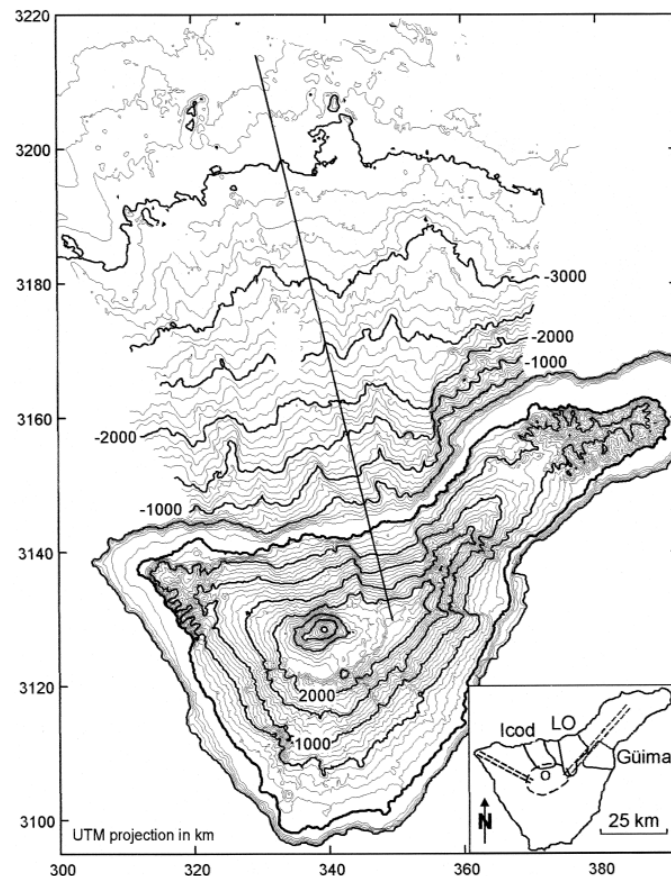


**Figure 9-6** - Topography of Tenerife and bathymetry of the northern offshore slopes (contour interval is 100 m). Bold line indicates the selected profile for the calculations of landslide mobility. Inset map shows the suggested onshore extents of the landslide valleys. Single dashed line represents the Las Canadas Caldera and the Teide volcano (circle). Double

*dashed line indicates the two main structural orientations on the island. LO for the La Orotava valley (Hurlimann et al., 2000b).*

The flanks of the Las Canadas edifices are incised by three large valleys, the Guimar valley on the southeast flank and the La Orotava and Icod valleys on the northern flank, all of which are believed to have been produced by giant landslide events (Bravo, 1962). Recent bathymetric surveys around Tenerife have revealed voluminous, submarine deposits (Teide-Group, 1997; Watts and Masson, 2001) supporting the hypothesis of repeated mass wasting occurring on the edifice flanks.

The causes of large-scale instabilities on Tenerife, however, are not clear. Persistent rift activity along the structural axis of the island, causing gravitational sliding, was proposed by Carracedo (1994). Moreover, the presence of an impermeable, volcanic breccia acting as a 'lubricating level' was assumed as a potential cause (Coello, 1973; Ancochea et al., 1999). Recently, a mechanical relationship between landslides and caldera collapse events was suggested (Martí et al., 1997; Hurlimann et al., 2000a). Hurlimann et al., (2000b) propose the seismicity associated with caldera collapse episodes and also with dike intrusion events as the most probable cause of the large volcanic landslide events at the La Orotava and Icod valleys on the northern flank of Tenerife.

#### 9.4.2 Stromboli (Aeolian Islands)

Stromboli volcano (Figure 9-7) has experienced repeated sector collapses in its NW flank leading to the formation of the Sciara del Fuoco, an horseshoe-shaped depression that extends below sea level down to a depth of 600 m (Rosi, 1980; Pasquarè et al., 1993; Tibaldi, 2001;

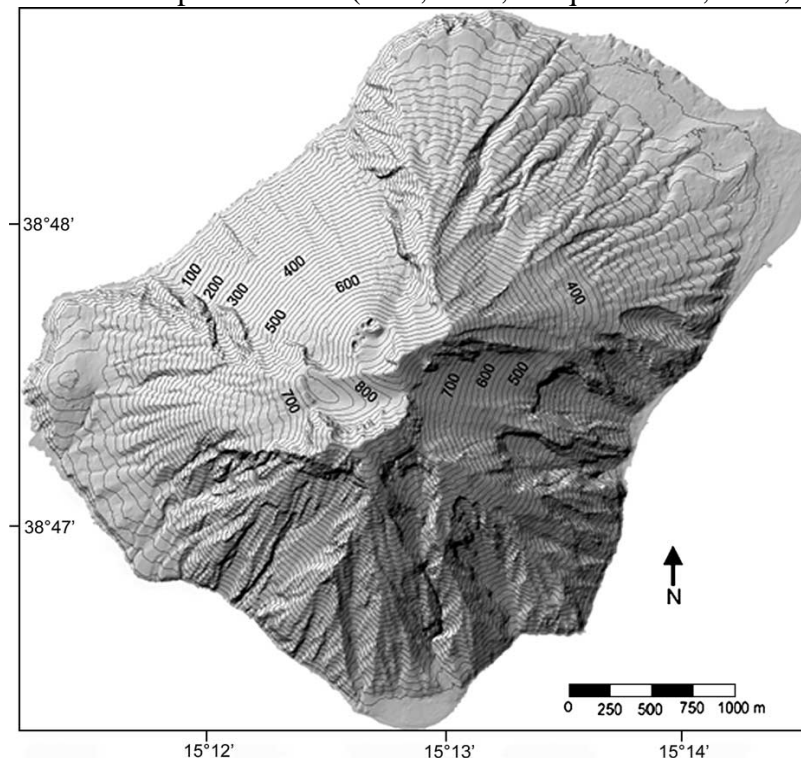


**Figure 9-7** - A shaded relief view of Stromboli Island derived from a 5 m grid DEM (Baldi et al., 2005).

Tibaldi et al., 2003). The lateral collapse scarps are concentric, resulted in the creation of the Sciara del Fuoco horseshoe-shaped depression with the younger sliding planes being less deep and with a smaller surface area. In the initial lateral collapses, sliding surfaces cut the main magma conduit, while in the last collapse event the upper scarp coincided with the conduit location (Apuani et al., 2005). The last collapse event occurred on December 30, 2 days after the onset of the effusion when the eastern part of the Sciara del Fuoco collapsed, producing a tsunami that devastated the NE coast of the island (Tommasi et al., 2003).

Lateral collapses at Stromboli are attributed to various factors such as asymmetric distribution of buttressed flanks (Romagnoli and Tibaldi, 1994), post-glacial sea-level variations, and slope erosion (Tibaldi et al., 1994). The tendency of gliding planes to become shallower have been interpreted by (a) the relative weakness of younger volcanic deposits, from dominant lavas to dominant pyroclastic deposits at upper stratigraphic levels; and (b) by the presence at a high level within the edifice of dyke swarms with preferred horseshoe-shaped orientations resulting in converging magma pressure which drives downslope displacement of the volcano flank (Tibaldi, 2001).

## 10 LANDSLIDE TRIGGERING DUE TO HUMAN ACTIVITY (SGI-MI)

### 10.1 INTRODUCTION

As discussed in Section 2, landslide triggering can always be related to mechanical factors affecting the equilibrium of the slope, namely:

- Increases in driving stresses;
- Decreases in shear strength.

These factors are activated by processes which are, for the greatest part, natural. Human activity can modify the influence on slope stability of natural processes such as rainfall or toe erosion, allowing certain processes to take place on a scale or with an intensity that would not have occurred otherwise, as is the case where deforestation and uncontrolled timbering change both the hydrological balance of slopes and the resistance of soil to erosion.

Human activity can also substitute outright the natural processes with an artificial equivalent, typically accelerated by several orders of magnitude compared to natural timescales, as in the case, for example, of major earthworks or the impoundment of reservoirs.

Human activity can thus precipitate a process that could occur naturally in any case, in which case it affects the frequency but not the pattern of landsliding, or it can cause landslides to occur in places and with mechanisms which would not have occurred naturally. This second case is particularly insidious, because it undermines the principle of many hazard studies based on the implicit assumption that “the past is a guide to the future”.

Typically, lists of human activities capable of causing landslides include:

1. timbering and deforestation for change of land use to agriculture, reducing evapotranspiration, allowing increased infiltration and increased surface erosion through loss of the shallow reinforcement provided by the root system.
2. improper or uncontrolled discharge from sanitation or drainage works and water pipes, typically associated with human settlements and roads, especially in rural areas, which increase water infiltration in the slope, and possibly soil erosion at points of concentrated surface discharge.
3. Infilling and drawdown of reservoirs, altering the hydrogeological regime of large areas.
4. Excavation at the base of or on slopes and/or placement of fill at the top or on slopes, altering the geometry of and the stress distribution in the slope.
5. Quarrying and mining activities, also altering the geometry of and the stress distribution in the slope.
6. Vibration from blasting and heavy construction equipment; besides causing transient stress changes which in extreme cases can trigger landslides by themselves, vibrations can disturb the microstructure of soils, induce fracturing in rock

Experience has shown that formal planning, design and monitoring as applied, for example, to major projects does not always guarantee against these projects causing instability. Furthermore, formal planning, design and monitoring is normally reserved to major works

only; while these works also carry the greatest potential to affect stability, they represent only a small fraction of human activity on or near slopes. In rural areas uncontrolled timbering, improper agricultural practices and housing without access to sanitation and drainage systems can have collectively an equally or even more significant impact on slope stability.

Some examples are discussed in greater detail below of how human activity can be a major contributory or even the sole cause of landslide triggering. The examples below have been selected to illustrate the full range of scale and level of control that may occur in practice, from major projects to small scale works which escape any formal control.

## 10.2 TAILINGS

Failure of tailings dams and of ash pond embankments can pose a significant hazard, both directly in terms of potential loss of life and economic loss and indirectly through the loss of confinement of potential contaminants.

Typically, tailings and wet placed coal ash placed by settling in ponds or “lagoons” are saturated or nearly saturated and characterized by a relatively open microstructure which makes these deposits susceptible to significant sudden loss of strength (collapse – static liquefaction) when overstressed, resulting in flow like failures, especially when failure involves active lagoons.

The nature of the hazard is strictly connected with the techniques traditionally adopted for the wet disposal of ash in ash ponds with limited and uncontrolled underdrainage and, often, construction of the bund over previously deposited ash in the so called “upstream” method of construction often adopted to minimize earthworks (Figure 10-1).

From a geotechnical point of view, the “upstream” method of construction has the following disadvantages (Ghandi, 2005):

- The entire weight of new construction for raising the embankment is supported on deposited ash. Unless ash deposition is carefully done, there can be finer ash particles deposited along the bund and may not have adequate bearing capacity to support the new embankment.

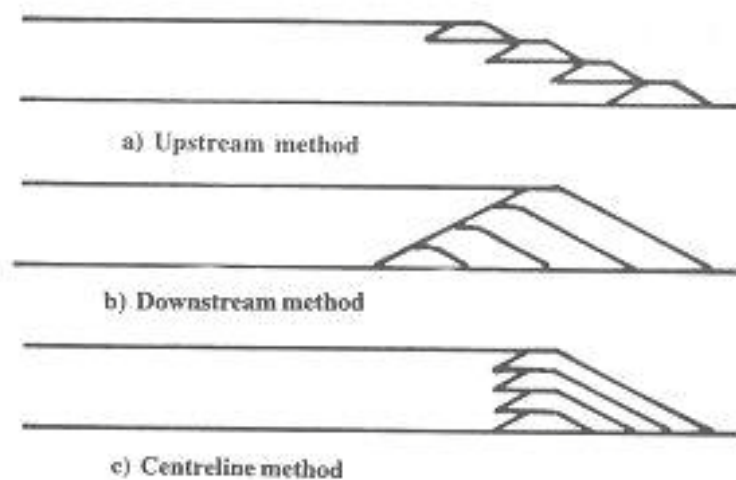


*Figure 10-1 - Conventional methods of progressive construction of pond embankments (after Ghandi, 2005)*

- The drain provided on the upstream face needs to be suitably connected to the drain of the earlier segment. If this is not carried out properly, the drainage can be ineffective resulting in rising of the phreatic line and reducing the stability of slope.
- Since the entire segment of new construction is supported on deposited ash, liquefaction analysis of the deposited ash is very important. If the deposit is not safe against liquefaction, suitable remedial measures need to be adopted before raising dyke.

In traditional tailings pond construction, there is no specific provision for underdrainage or sealing of the base of the pond. Water is decanted in the pond and sluiced over an outlet wall or weir. The discharge and sluicing is operated in such manner as to encourage the coarser material to form a beach near the embankment which is intended to favour drainage in this area and to reduce earth and water pressure on the embankment, but the effectiveness of these arrangements is difficult to control and depends on the exact combination of seepage through the embankment and through the base and outlet layout and levels. Seepage through the embankment is common and can be significant, at least from a geotechnical point of view, and needs to be controlled by internal drainage to prevent piping and internal erosion.

Traditional tailings pond design relies of these seepage patterns to reduce water pressures on the embankments. Where an impervious membrane has been provided in more recent structures to prevent potential pollution of groundwater, provision of the drainage on which traditional designs rely becomes difficult and as result the deposited sediments do not consolidate to the same extent as anticipated in the pond without plastic liner (Ghandi, 2005). The specific characteristics of tailings of mine waste and ash, which typically have a very low plasticity compared to their grain size distribution and are deposited in a very loose state, and the poor control on drainage conditions within the lagooned tailings pose special problems when it comes to evaluating the stability of these structures, which makes limit equilibrium analyses, as typically carried out, not particularly reliable as they do not model the very brittle strain softening behaviour of these materials. As failure occurs in undrained conditions even in relatively coarse tailings, limit equilibrium analyses need to be carried out as undrained strength analyses (USA approach), with appropriate values of undrained strength (Ladd, 1991; Carrier III, 1991; Carrier III, 2003). A more rational approach would be to use advanced numerical analyses with appropriate constitutive models of the type discussed in Example 4 of Section 2, although uncertainties would remain about the actual flow and pore pressure regime within the lagooned tailings.

A worldwide chronology of almost 90 major tailings dam failures from 1960 to date can be found at <http://www.wise-uranium.org/mdaf.html>.

A recent example of the potential consequences of the failure of ash pond embankments occurred at the TVA Kingston Fossil Plant, Harriman, Tennessee (USA) on December 22, 2008, where approximately 4 million m<sup>3</sup> of ash slurry were released. The ash slide covered an area of 160 ha. by up to 2 m; the wave toppled power lines, covered and/or damaged roads, power lines and railways and damaged 12 homes, although no one was seriously injured (Figure 10-2). Other examples are provided and discussed by Blight (2010).

More dramatic were the consequences of the failure of two fluorite tailings ponds which occurred on July, 19, 1985 at Stava, near Trento in northern Italy, when the retaining bund of



**Figure 10-2** - TVA Kingston Plant, Harriman, Tennessee (USA) ash pond the failure of 22 December 2008. Approximately 4.000.000 m<sup>3</sup> of ash escaped. (Photo: Tennessee Valley Authority – Environmental protection Agency).

the upper basin collapsed onto the lower basin, which also failed, killing 268 people. Following the disaster, the NGO "Fondazione Stava 1985" was set up as a memorial to the victims and to promote a culture of prevention. The organization's website <http://www.stava1985.it/> is the main source of the information summarized here, together with the technical description published by Tosatti (2003).

The ponds (Figures 10-3, 10-4 and 10-5) were raised in stages, starting in the early 1960s. In the report of an inspection carried out in 1974 by Mine Bureau of the Autonomous Province of Trento, surprise was expressed that the bunds had not collapsed yet; nevertheless, construction continued, with more waste poured into the ponds.

The ministerial Commission of Inquiry and the experts appointed by the Law Court of Trento ascertained that "the settlement system as a whole constituted a continuous threat looming over the valley. The system collapsed because it was designed, built and managed in such a way as not to provide the security margins that society expects of constructions liable to threaten the existence of entire communities. The upper bank was bound to collapse as a result of the slightest alteration to its precarious balance".

According to the subsequent inquiries, the collapse was caused by the chronic instability of the dams, especially in the upper one, which were below the minimum factor of safety required to avoid collapses. In particular, the causes of instability were found to be as follows:

1. Deposited slime had not settled for the following reasons:
  - a. the marshy nature of the soil on which the dams were built, where it was impossible for the mud to settle;

- b. the bank of the upper basin was not built correctly, and therefore made drainage very difficult;
  - c. the upper basin was built very close to the lower one: as the bank continued to grow, it began to spread to the unsettled slime in the lower basin;
  - d. this made drainage more difficult and stability more precarious.
2. Excessive height and inclination of the dams:
    - a. the bank of the upper basin measured 34 metres in height;
    - b. inclination reached 80 per cent, in other words a 40° angle;
    - c. the tailings dams were built on a slope whose average inclination was approximately 25 per cent.
  3. The decision to enlarge the bank according to the "upstream" method, which was the quickest and most inexpensive, but also the most dangerous;
  4. The drainage pipes were installed incorrectly (on the basin beds and through the banks).

As a result of the breach, approximately 160.000 to 200.000 m<sup>3</sup> of mud flowed downstream at an estimated speed of 90 km/h, killing 268 and destroying 62 buildings and 8 bridges, covering an area of 435.000 square metres (Figures 10-6 and 10-7)

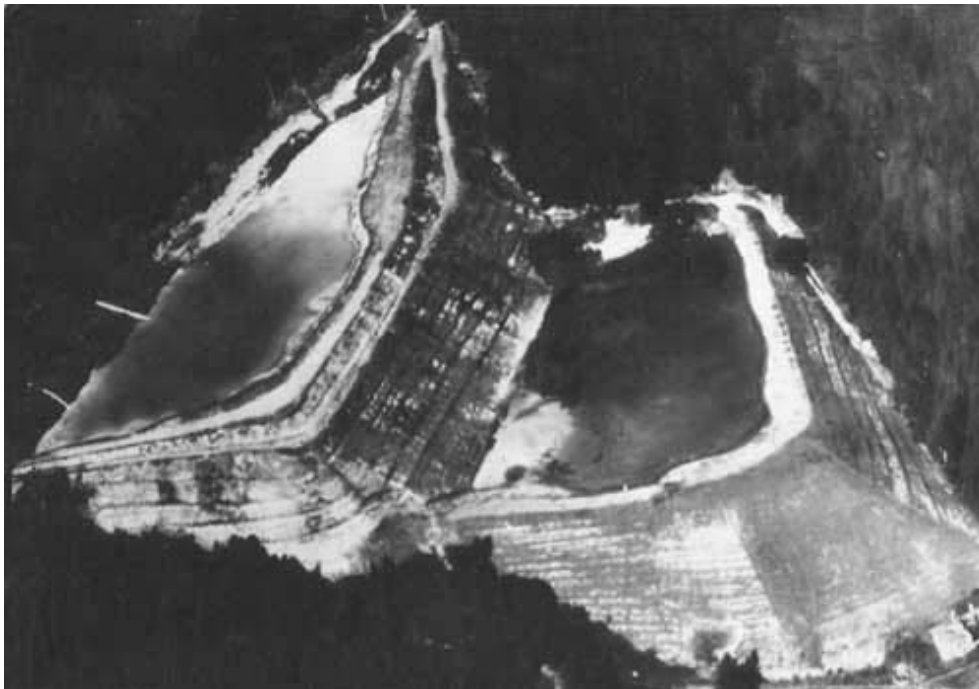


**Figure 10-3** - Aerial view of the Stava ponds before the failure (photo: Fondazione Stava 1985, as published by [www.tailings.info](http://www.tailings.info))



**Figure 10-4** - View of the Stava ponds in the early 1980's (photo: Fondazione Stava 1985, as published by Tosatti, 2007)

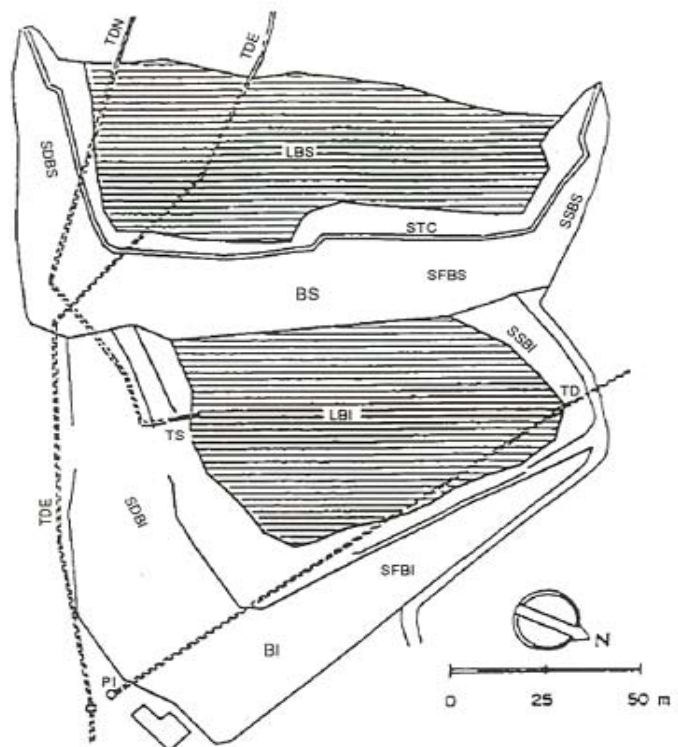


**Figure 10-5** - Plan and drainage system of the Stava ponds (source: Fondazione Stava 1985)



*Figure 10-6 - View of the Stava ponds after the failure (source: Fondazione Stava 1985)*



*Figure 10-7 - Aerial view of the Stava valley after the failure (source: Fondazione Stava 1985)*

### 10.3 IMPOUNDING OF RESERVOIRS

Changes in groundwater pressures are one of the most frequent mechanisms triggering landslides.

Where this occurs as a result of rainfall, snowmelt and other natural processes, the landslide hazard and occurrence are in some form of “dynamic equilibrium” with the hydraulic boundary conditions which can be highly variable in the short term (from the single rainfall event to seasonal variations), but change relatively slowly in the long term.

The impoundment of reservoirs introduces significant abrupt changes to the hydrogeological regime of large areas, which can represent a quantum leap in the baseline long term hydraulic boundary conditions on which natural climatic cycles are superimposed.

Since most major reservoirs are located, necessarily, in hilly or mountainous terrain, their impoundment and the changes that this produces in the hydrogeological regime can affect areas prone to landslides. Considering the potentially devastating effects of landslides impinging on dams and reservoirs, the stability of the slopes of artificial lakes represents a key issue in the planning, design, construction and management of artificial reservoirs.

Whilst actual triggering is often the result of a combination of impoundment and significant climatic events, some landslides have been triggered by impoundment alone.

The process of triggering induced by groundwater changes is described in detail in chapter 3.4 (Current analyses approaches at different scales - changes of groundwater levels). The case of Vajont landslide is given (chapter 3-5-8) as an example of landslide induced by human-induced groundwater changes.

### 10.4 SMALL SCALE EARTHWORKS

In certain conditions, landsliding may be triggered by relatively small earthworks, of the type that normally fall outside the scope of formal investigation, planning and design.

While this can be true in many situations, it can be especially critical at sites where saturated “sensitive” clays and “loose” sands occur which are prone to microstructural collapse processes.

Both in “sensitive” clays and in “loose” sands, classified as material type CA and SA respectively and discussed in detail in chapter 2, shearing beyond a critical stress or strain results in a rapid disruption of the microstructure with strong tendency to contract (reduction in void ratio) which, in undrained conditions results in a rise in pore pressures and a corresponding reduction in shear strength. In other words, when failure is triggered, what was originally a relatively stiff mass changes to a liquid.

A classic example of this triggering mechanism is provided by many landslides which have occurred in “quick clays”, which can be classified as CA type materials with “strength sensitivity” greater than 30 and remoulded undrained shear strengths less than 0.5 kPa.

A graphic example of the behaviour of these clays is shown in Figure 10-8 which shows the difference between “undisturbed” and “disturbed” material at the same moisture content.

“Quick clays” occur worldwide, especially in Scandinavia, Canada and Japan. Irrespective of the specific processes that caused the formation of the microstructure (for details reference can be made for example to Cabrera & Smalley, 1973; Bently & Smalley, 1973; Torrance, 1986), many large retrogressive landslides have formed in “quick clays” due to their fluid behaviour when remoulded.

The main causes of failure in quick clays are localized overloading or undercutting of the slope, leading to a rotational landslide. While the undisturbed shear strength of the material may be sufficient to determine the stability of the original slope, retrogressive landslides are triggered when the remoulded strength of the debris is so low that it does not provide support to stabilize the backscarp.

The original disturbance which triggers the landslide could occur naturally but it can also be due to even relatively small scale human activity, such as even relatively small scale earthworks or vibration, for example by pile driving or blasting, as occurred for example at Namsos, in Norway, on 13 February 2009.

A classic example of a landslide triggered by small scale earthworks is provided by the Rissa landslide, which occurred in 1978 on the shore of lake Botnen in Norway; this landslide, which is particularly famous because a large portion of the slide happened to be recorded on film by two amateur photographers (see the videos published on the web site of the NGI: [http://www.ngi.no/upload/6485/Klipp\\_Rissaskredet\\_web1.wmv](http://www.ngi.no/upload/6485/Klipp_Rissaskredet_web1.wmv) and [web2.wmv](#)), was triggered by an excavation of approximately 800 m<sup>3</sup> for a barn extension and quickly developed to involve approximately 6 million cubic metres of material, retrogressing approximately to 70÷90 m and devastating an area of 0.33 square kilometers, destroying 7 farms and causing one fatality.



*Figure 10-8 - Strength loss of “quick clays” extremely sensitive to remoulding  
(after Mitchell, 1976)*

## 10.5 FARMING

Farming is generally considered as having a low impact on landslides and is often the only activity allowed in landslide prone areas.

Even farming and collateral activities, however, may trigger slope movements, directly or indirectly.

When land is first turned to farming, this often involves extensive deforestation which can lead to soil erosion and landsliding in hilly or mountainous terrain. Quantitative evidence of this process is discussed, for example, by Glade (1998).

Ploughing can cause widespread progressive "creep" of the top soil and/or accelerated soil erosion, depending on whether it is carried out across or along the maximum slope direction.

Farming also requires supporting infrastructures (roads, farmhouses, barns), with their own attendant hazards.

However, probably the main cause of landslide triggering due to farming is related to irrigation and drainage, which can alter the natural groundwater conditions.

This issue may be particularly critical where irrigation is carried out by hydrants served by pressurized pipework, a technique that is increasingly substituting traditional gravity irrigation ditches in many areas of the Alps.

A dramatic and somewhat unfortunate example of this is provided by the fatal rail disaster occurred on 12 April 2010 between Laces and Castelbello near the town of Merano not far from Bolzano in Northern Italy (Figure 10-9), when a two-carriage commuter train was smashed off tracks by a landslide. The landslide was no more than 300 to 400 m<sup>3</sup> in size but had a huge effect. A mass of mud and water knocked down the first carriage of the train into a ditch and nine people died in the accident (Figure 10-10).



*Figure 10-9 - Location of the Laces to Castelbello railway.*



*Figure 10-40 - General view of the 12 April 2010 landslide.*

The railway line runs in a deep cutting alongside the river Adige, in the foothills of the Dolomites; the slope impinging on the railway is supported by a masonry retaining wall approximately 4 m high, having a 2.5 m tall catch fence on its top to restrain debris on account of the terrain in the area being a glacial moraine which could be prone to debris slides. However, the existing catch fall barrier may not have been designed to withstand the specific load of a mudslide which took place.

Investigation works have been carried on site including drilling of four boreholes and installing piezometers to study the soil layering and the specific hydrogeology of the site. Meanwhile, experiments have been carried out on a burst pipe which is part of an irrigation system that serves the adjacent apple orchard located just above the railway-line. These experiments proved that huge quantities of water must have spilled out from the irrigation system.

Press reports (Hansford & Lynch, 2010a, b) reported that investigators focused their attention on the faulty irrigation system which is thought to have triggered the landslip which led to the fatal train crash, whilst natural groundwater seems not to be considered as the main trigger.

## 11 REFERENCES

- Ablay G., Hurlimann M. (2000). Evolution of the north flank of Tenerife by recurrent giant landslides. *J Volcanol. Geotherm. Res.*, **103**, 135-159.
- Acocella V., Behncke B., Neri M., and D'Amico S. (2003). Link between large-scale flank slip and 2002– 2003 eruption at Mt. Etna (Italy). *Geophys. Res. Lett.*, **30(24)**, 2286.
- Adachi K., Tokimatsu K. (1994). Development in sampling of cohesionless soils in Japan. 13<sup>th</sup> ICSMFE, New Delhi, India.
- Adachi T., Oka F., Hirata T., Hashimoto T., Nagaya J., Mimura M., Pradhan T.B.S. (1995). Stress-strain behaviour and yielding characteristics of eastern Osaka clay. *Soils and Foundation*, **35(3)**, 1-13.
- Adachi T., Oka F., Koike M. (1999). Time-dependent behaviour of soft rock and an elasto-viscoplastic constitutive model with strain softening. Proc. 11<sup>th</sup> Asian Regional Conf. on S.M.G.E., Hong et al. editors, Balkema, 117-120.
- Adachi T., Oka F., Koike M. (2005). An elasto-viscoplastic constitutive model with strain-softening for soft sedimentary rocks. *Soils and Foundations*, **45(2)**, 125-133.
- Adachi T., Oka F., Mimura M. (1996). Modelling aspects associated with time dependent behaviour of soils. Geotechnical Special Publication n° 61, on Measuring and Modelling Time Dependent Soil Behavior, sponsored by Geo-Institute of ASCE, in conjunction with ASCE Convention in Washington D.C., Sheahan T.C. and Kallakin V.N. editors.
- Adachi T., Oka F., Zhang F. (1998). An elasto-viscoplastic constitutive model with strain softening. *Soils and Foundations*, **38(2)**, 27-35.
- AGI (1977). Proceedings of International Symposium on the Geotechnics of Structurally Complex Formations. Capri.
- AGI (1979). Some Italian experiences on the mechanical characterization of structurally complex formations. Proc. 4<sup>th</sup> Int. Conf. Rock Mech., Montreux, 1, 827-846.
- AGI (1985). Geotechnical properties and slope stability in structurally complex clay soils. In Geotechnical Engineering in Italy, Ed. AGI, 189-225.
- AGI (1985). Properties of Italian clay soils. In Geotechnical Engineering in Italy, Ed. AGI, 239-249.
- Agliardi F., Crosta G.B., Frattini, P. (2009). Integrating rockfall risk assessment and countermeasure design by 3D modelling techniques. *Natural Hazards and Earth System Science*, **9**, 1059–1073.
- Agliardi F., Crosta G.B., Laini M., Mannucci G., Ballini A., La Rocca L. (in press). Modelling geological and morpho-climatic controls on large alpine rockslides: the Spriana landslide. In: “Frane e dissesto idrogeologico: consuntivo”, 22 marzo 2010, Accademia Nazionale dei Lincei, Roma, 6 pp.
- Agliardi, F., Crosta, G., Zanchi, A. (2001). Structural constraints on deep seated slope deformation kinematics. *Eng. Geol.*, **59**, 83–102.
-

- Agliardi, F., Crosta, G., Zanchi, A., Ravazzi, C. (2009a). Onset and timing of deep-seated gravitational slope deformations in the Eastern Alps, Italy. *Geomorphology*, **103**, 113–129.
- Agliardi, F., Zanchi, A., Crosta, G.B. (2009b). Tectonic vs. gravitational morphostructures in the central Eastern Alps (Italy): Constraints on the recent evolution of the mountain range. *Tectonophysics* **474**, 250–270.
- Airey M., Hulme M. (1995). Validating precipitation simulations by climate models: problems, methods and applications. *Prog. in Phys. Geography*, **19**, 427-448.
- Al Shaikh – Ali M.M.J. (1979). The measurement of  $k_0$  in weathered Keuper Marl by pressuremeter. Proc. 7<sup>th</sup> ECSMFE, Brighton 4, 79-80.
- Alarcon-Guzman A., Leonards G.A., Chameau J.L. (1988). Undrained monotonic and cyclic strength of sands. *J. Geotech. Engineering Division, ASCE*, **114**, GT10, 1089-1109.
- Alberro J. (1979). Stabilité à long terme des excavations dans la ville de Mexico. Proc. Int. Symposium on Soil Mechanics, Oaxaca, 1, 125-143.
- Alonso E.E., Gens A., Josa A. (1990). A constitutive model for partially saturated soils. *Geotechnique*, **40**, 405-430.
- Alonso E.E., Pinyol N. (2009). Slope stability under rapid drawdown conditions. Proceeding of the first IWL conference. 17 pp.
- Al-Tabbaa, A., Wood, M.D. (1989). An experimentally based “bubble” model for clay. Proc. 3<sup>rd</sup> Int. Conf. on Numerical Methods in Geomechanics, 91-99.
- Al-Tabbaa, A., Wood, M.D. (1989). An experimentally based bubble model for clay. Proc. of Numerical Models in Geomechanics. NUMOG III, Pande G. N. and Pietruszczak S. editors, London, Elsevier, 91-98.
- Alvarado G.E., Soto G.J. (2002). Pyroclastic flow generated by crater-wall collapse and outpouring of the lava pool of Arenal Volcano, Costa Rica. *Bull. Volcanol.*, **63**, 557-568.
- Ambrosi, C., Crosta, G.B. (2006). Large sackung along major tectonic features in the Central Italian Alps. *Eng. Geol.*, **83**, 183–200.
- Amiri-Tokaldany E., Darby S.E., Tosswell P. (2003). Bank stability analysis for predicting reach scale land loss and sediment yield. *J. Am. Water Resour. Assoc.*, **39(4)**, 897-909.
- Amorosi, A., Kavvas, M.J. (2000). A plasticity-based constitutive model for natural soils: a hierarchical approach. *Constitutive Modelling of Granular Materials*, D. Kolymbas editor, Springer, 413-438.
- Ancochea E., Fuster J.M., Ibarrola E., Cendrero A., Coello J., Hernan F., Cantagrel J.M., Jamond C., (1990). Volcanic evolution of the island of Tenerife (Canary Islands) in the light of new K-Ar data. *J. Volcanol. Geotherm. Res.*, **44**, 231-249.
- Ancochea E., Huertas M.J., Cantagrel J.M., Coello J., Fuster J.M., Arnau N., Ibarrola E., (1999). Evolution of the Canadas edifice and its implications for the origin of the Canadas Caldera (Tenerife, Canary Islands). *J. Volcanol. Geotherm. Res.*, **88**, 177-199.
- Anderson M. G., Richards K. S. (1987). Modelling slope stability: the complementary of geotechnical and geomorphological approaches. *Slope Stability: Geotechnical Engineering and Geomorphology*, Anderson M.G. and Richards K.S. editors, John Wiley and Sons, 1-9.
-

Anderson M.G., Burt. T.P. (1978). The role of topography in controlling through flow generation. *Earth Surf. Processes and Landforms*, **3**, 331-344.

Anderson M.G., Richards K.S., Kneale P. (1980). The role of stability analysis in the interpretation of the evolution of threshold slopes. *Transactions, Institute of British Geographers*, **5**, 101-112.

Anderson S.A., Sitar N. (1995). Analysis of rainfall-induced debris flows. *J. Geotech. Eng., ASCE*, **121**, 544-552.

Andriola P., Chirico G.B., De Falco M., Di Crescenzo G., Santo A. (2010). Assessing flowslides triggering susceptibility in the pyroclastic deposits of the carbonatic contest: a comparison between physically based models and a statistic-semiquantitative methodology. *Geografia e Dinamica Quaternaria*, **32/2**.

Apuani T., Corazzato C., Cancelli A., Tibaldi A. (2005) Physical and mechanical properties of rock masses at Stromboli: a data set for volcano instability evaluation. *Bull. Eng. Geol. Env.*, **64**, 419-431.

Arenson L. (2003). Unstable Alpine Permafrost: a Potentially Important Natural Hazard – Variations of Geotechnical Behaviour with time and Temperature. PhD thesis, ETH Zürich.

Arenson L., Hoelzle M., Springman S.M. (2002). Borehole deformation measurements and internal structure of some rock glaciers in Switzerland. *Permafrost and Periglacial Processes*, **13(2)**, 117-135.

Argyroudis, S., Kakderi, K., Pitilakis, K. (2006). Technical report on the evaluation of earthquake ground deformations, with applications to representative geological configurations of selected cities. LESSLOSS, (2004-2007). Risk Mitigation for Earthquakes and Landslides, Research Project, European Commission, Sixth Framework Program, Priority 1.1.6.3, Global Change and Ecosystems, Deliverable No 87, Contract Number: GOCE-CT-2003-505448.

Armanini A, Gregoretti C. (2000). Triggering of debris flow by overland flow: a comparison between theoretical and experimental results. In: Wieczorek, Naeser (eds) Proc 2nd Int Conf on Debris flow hazards mitigation, Taipei, August 2000:117-124.

Arulanandan K., Gillogley E., Tully R. (1980). Development of a quantitative method to predict critical shear stress and rate of erosion of natural undisturbed cohesive soils. USACE, Waterways Experiment Station Technical Report GL-80-5, Vicksburg, MS.

Asaoka, A., Nakano, M., Noda, T., Kaneda, K. (2000). Delayed compression/consolidation of natural clay due to degradation of soil structure. *Soils and Foundations*, **40(3)**, 75-85.

ASCE (1968).Task Committee on Erosion of Cohesive Materials Erosion of cohesive sediments. *J. Hydraul. Div., ASCE* **94 (HY4)**, 1017-1047.

Asch F. (1996). *Air humidity effects on transpiration differ among rice varieties subjected to salt stress*. West Africa Rice Development Association. Annual Report 1995. WARDA, Bouaké, Côte d'Ivoire, 97-98.

Atkinson J.H., Bransby P.L. (1978). The mechanics of soils – An introduction to Critical State Soil Mechanics. University Series in Civil Engineering, Mc Graw-Hill.

Atkinson J.H., Richardson D. (1987). The effect of local drainage in shear zones on the undrained shear strength of overconsolidated clay. *Géotechnique*, **37(3)**, 393-403.

---

Atkinson, J.H., Stallebrass, S.E. (1991). A model for recent stress history and non-linearity in the stress-strain behaviour of overconsolidated soil. Proc. 7<sup>th</sup> Int. Conf. on Computer Methods and Advances in Geomechanics, 555-560.

Attewell P.B., Farmer I.W. (1977). Fatigue behaviour of rock. *Int. Journal Rock Mech. Mining Sciences*, **10**, 1-9.

Aubry D., Hujeux J.C., Lassoudiere F., Meimon Y. (1982). A double memory model with multi mechanisms for cyclic soil behaviour. Int. Symp. on Numerical Models in Geomechanics, Zurich.

Auger, F. (1991). Vieillissement par altération atmosphérique des matériaux de construction- Etude comparative in situ et en simulation. In: Colloque International, Détérioration des matériaux de construction, La Rochelle, pp. 115–129.

Augustinus, P.C. (1995). Glacial valley cross-profile development: the influence of in situ rock stress and rock mass strength, with examples from the southern Alps, New Zealand. *Geomorphology*, **14**, 87– 97.

Aulitzky H. (1989). The debris flows of Austria. *Bulletin of the International Association of Engineering Geologists*, **40**, 5-13.

Auvray C., Homand, F., Sorgi, C. (2004). The aging of gypsum in underground mines. *Eng. Geol.*, **74**, 183-196.

Aversa S., Evangelista A., Leroueil S., Picarelli L. (1993). Some aspects of the mechanical behaviour of structured soils and soft rock. Proc. Int. Symp. on Hard Soils – Soft Rocks, Anagnostopoulos A., Schlosser F., Kalteziotis N. and Frank R. editors, Athens, 1, Balkema, 359-366.

Aydan Ö., Nawrocki P. (1998). Rate-dependent deformability and strength characteristics of rocks. Proc. 2<sup>nd</sup> Int. Symp. on The Geotechnics of Hard Soils - Soft Rocks, Evangelista A. and Picarelli L. editors, Naples, **Balkema**, 403-411.

Aydan Ö., Seiki T., Jeong G.C., Tokashiki N. (1994). Mechanical behaviour of rocks, discontinuities and rock masses. Proc. Int. Symp. On Pre-failure Deformation Characteristics of Geomaterials, Sapporo, 2, 1161-1168.

Aydan, Ö., Hamada, M., Itoh, J., Okubo, K. (2009). Damage to Civil Engineering Structures with an Emphasis on Rock Slope Failures and Tunnel Damage Induced by the 2008 Wenchuan Earthquake. *Journal of Disaster Research*, **4(2)**, 153-164.

Aydan, Ö., Ohta, Y. (2006). The characteristics of ground motions in the neighbourhood of earthquake faults and their evaluation. Symposium on the Records and Issues of Recent Great Earthquakes in Japan and Overseas, EEC-JSCE, Tokyo, 114-120.

Azizian A. (2004). Seismic analysis of submarine slopes: Retrogressive and three-dimensional effects. PhD thesis, Faculty of Engineering and Applied Science, Memorial University of Newfoundland, St John's, NL, Canada.

Babaeyan-Koopaei K., Ervine D.A., Carling P.A., Cao, Z. (2002). Velocity and turbulence measurements for two overbank flow events in River Severn. *J. Hydraul. Eng.*, **128(10)**, 891-900.

---

- Bagnold R.A. (1966). An approach to the sediment transport problem from general physics. *U.S. Geol. Surv. Prof. Pap.*, **422-I**, pp. 37.
- Baldi P., Fabris M., Marsella M., Monticelli R. (2005). Monitoring the morphological evolution of the Sciara del Fuoco during the 2002-2003 Stromboli eruption using multi-temporal photogrammetry. *ISPRS Journal of Photogrammetry and Remote Sensing*, **59**, 199-211.
- Ballantyne, C.K. (2002). Paraglacial geomorphology. *Quaternary Science Reviews*, **21**, 1935–2017.
- Bandis S., Lumsden A.C., Barton N.R. (1981). Experimental studies of scale effects on the shear behaviour of rock joints. *Int. Journ. Rock Mech. Mining Sci. Geomech. Abstr.*, **18**, 1-21.
- Banks D.C., Strohm W.E. Jr, De Angulo M., Lutton R.J. (1975). Study of clay shale along the Panama Canal. Report 3: Engineering analysis of slides and strength properties of clay shales along the Gaillard Cut. US Army Engineers Waterways Experiment Station, Vicksburg, Report 5-70-9.
- Barsch D. (1992). Permafrost creep and rockglaciers. *Permafrost and Periglacial Processes*, **3**, 175-188.
- Barsch D. (1996). Rockglaciers, indicators for the present and former geocology in high mountain environments. Springer, New York, 331pp.
- Barton N.R. (1971). Estimation of in situ strength from back analysis of failed rock slopes. Proc. Int. Symp. Rock Fracture, Nancy, France, Paper II-27.
- Barton N.R. (1973). Review of a new shear strength criterion for rock joints. *Eng. Geol.*, **7**, 287-332.
- Barton N.R. (1981). Some size dependent properties of joints and faults. *Geophys. Res. Letters*, **8**, 667-670
- Barton N.R. (1986). Deformation phenomena in jointed rock. *Géotechnique*, **36(2)**, 147-167.
- Barton N.R. (1999). The influence of joint properties in modelling jointed rock masses. Norwegian Technical Institut, Publication n° 204, Oslo.1023-1032.
- Barton N.R., Bandis S. (1980). Some effects of scale on the shear strength of joints. *Int. Journ. Rock Mech. Mining Sci. Geomech. Abstr.*, **17**, 69-73.
- Barton N.R., Choubey V. (1977). The shear strength of rock joints in theory and practice. *Rock Mech.*, **10**, 1-54.
- Bathurst J.C., Graf W.H., Cao H.H. (1987). Bed load discharge equations for steep mountain river. In: Thorne CR, Bathurst JC, Hey R (eds) *Sediment Transport in Gravel-Bed Rivers*. Wiley
- Baudet B., Stallebrass S. (2004). A constitutive model for structured clays. *Géotechnique*, **54(4)**, 269-278.
- Baum R.L., Reid M.E. (2000). Ground water isolation by low-permeability clays in landslide shear zones. In: Bromhead, E.N., Dixon, N., Ibsen, M.-L. (Eds.), *Landslides in Research, Theory and Practice*. Proc. 8th Int. Symp. on Landslides, Cardiff, Wales, vol. 1. Telford, London, 139-144.
-

- Bear J. (1972). *Dynamics of Fluids in Porous Media*, American Elsevier, New York. 579-664.
- Beatty M, Byrne P.M. (1998). An effective stress model for predicting liquefaction behavior of sand. *Geotechnical Earthquake Engineering and Soil Dynamics*, III, P. Dakoulas, M. Yegian, R. Holtz editors, ASCE Geot. Spec. Publ. 75(1), 766-777.
- Been K., Jefferies M.G., Hachey J. (1991). The critical state of sands. *Géotechnique*, **41(3)**, 365-381.
- Been R.R.W. (1967). Waco Dam slide. *Journ of Soil Mech. And Found. Div., ASCE*, **93, SM4**, 35-44.
- Beget J.E., Kienle J., (1992). Cyclic formation of debris avalanches at Mount St. Augustine volcano. *Nature*, **356(6371)**, 701-704.
- Belloni L., Gandolfo M. (1997). La frana di Spriana. *Geologia Tecnica*, 3 Luglio/Settembre 1997. Lombardia. Frane. GT1/92\_b.
- Belousov A., Belousova M., Voight B. (1999). Multiple edifice failures, debris avalanches and associated eruptions in the Holocene history of Shiveluch volcano, Kamchatka, Russia, *Bull. Volcanol.*, **61**, 324-342.
- Belousov A., Walter T., Troll V. (2003). Large-scale failures on domes and stratocones situated on caldera ring faults: Sand-box modelling and natural examples from Kamchatka, Russia, paper presented at IUGG Assembly, Sapporo, Japan.
- Beniston M., Douglas G.F. (1996). Impacts of climate change on mountain regions. In: R.T. Watson, M.C. Zinyowera, R.H. Moss and D.J. Dokken (eds), *Climate Change 1995. Impacts, Adaptations and Mitigation of Climate Change: Scientific-Technical Analysis*, Cambridge Univ. Press, Cambridge, 191-213.
- Beniston M., Stephenson D.B., (2004). Extreme climatic events and their evolution under changing climatic conditions. *Global Planet. Chang*, **44**, 1-9.
- Bently S.P., Smalley I.J. (1978). "Interparticle cementation in Canadian post-glacial clays and problem of high sensitivity". *Sedimentology*, vol. 25, 297-302.
- Bently S.P., Smalley I.J. (1978). Interparticle cementation in Canadian post-glacial clays and problem of high sensitivity. *Sedimentology*, **25**, 297-302.
- Berardi, G., Caroti, L., Giunta, M., Jamiolkowski, M., Lancellotta, R. (1991). Mechanical properties of upper Pisa clay. Proc. 10<sup>th</sup> European Conf. on Soil Mech. and Found. Eng., Florence, Italy, 7, 7-10.
- Berilgen M.M. (2007) Investigation of stability of slopes under drawdown conditions. *Comput Geotech.*, **34**, 81-91. doi:10.1016/j.compgeo.2006.10.004
- Berthling I., Eitzelmüller B., Eiken T., Sollid J.L. (1998). Rock glaciers on Prins Karls Forland, Svalbard. I, Internal structure, flow velocity and morphology. *Permafrost and Periglacial Processes*, **9(2)**, 135-145.
- Berti M., Genevois R., Simoni A., Tecca P.R. (1999). Field observations of a debris flow event in the Dolomites. *Geomorphology*, **29**:265-274.
- Berti M., Simoni A. (2005). Experimental evidences and numerical modelling of debris flow initiated by channel runoff. *Landslides*, **2**, 171-182.
-

- Bieniawski Z.T. (1970). Time-dependent behaviour of fractured rock. *Rock Mech.*, **2**, 123-137.
- Bieniawski Z.T. (1976). Rock mass classification in rock engineering. Proc. of the Symp. on Exploration for Rock Engineering, Bieniawski Z.T. editor, Cape Town, Balkema, 97-107
- Bieniawski, Z.T. (1989). *Engineering rock mass classifications*. John Wiley & Sons, New York, 272 pp.
- Bigot-Cormier, F., Braucher, T, R., Boursès, D., Guglielmi, Y., Dubar, D., Stephan, J.-F. (2005). Chronological constraints on processes leading to large active landslides. *Earth and Planetary Science Letters* **235**, 141– 150.
- Biot M.A. (1941). General theory of three-dimensional consolidation. *Journal of Applied Physics*, **12**, 155-164.
- Biot M.A. (1956). Theory of propagation of elastic waves in a fluid-saturated porous solid. 1. Low frequency range. *Journal of the Acoustical Society of America* **28(2)**, 169-178.
- Bishop A.W. (1954). The use of pore water coefficients in practice. *Geotechnique*, **4(4)**, 148-152.
- Bishop A.W. (1955). The use of the slip circle in the stability analysis of slopes. *Géotechnique*, **5**, 7-17.
- Bishop A.W. (1959). The principle of effective stress. *Tek. Ukeblad*, **106(39)**, 859-863.
- Bishop A.W., Lovenbury H.T. (1969). Creep characteristics of two undisturbed clays. Proc. 7<sup>th</sup> Int. Conf. on S.M.F.E., Mexico City, **1**, 29-37.
- Bishop A.W., Webb D.L., Lewin P.I. (1965). Undisturbed samples of London clay from the Ashford Common shaft: strength-effective stress relationship. *Géotechnique*, **15**, 1-13.
- Bjerrum L. (1967). Progressive failure in slopes of overconsolidated plastic clay and clay shales. *J Soil Mech Foundat Div ASCE*; **93(SM5)**,1–49.
- Bjerrum L. (1967a). Engineering geology of Norwegian normally consolidated marine clays as related to settlements of buildings. *Géotechnique*, **17(2)**, 81-118.
- Bjerrum L. (1967b). Progressive failure in slopes of overconsolidated clays and clay shales. *Journal of Soil Mech. And Found. Div., ASCE*, **93**, 1-49.
- Bjerrum L. (1972). Embankments on soft ground. Proc. of Spec. Conf. on Performance of Earth and Earth-Supported Structures. Lafayette, Indiana, **2**, 1-54.
- Bjerrum L. (1973). Problems of soil mechanics and construction on soft clays. Proc. 8<sup>th</sup> Int. Conf. on Soil Mech. and Found. Eng., Moscow, USSR, SOA report, **3**, 111-159.
- Bjornsson A., Kristjanson L., Johnson H. (1977). Some observations of the Heimaey deep drill hole during the eruption of 1973. *Jokul*, **26**, 52-57.
- Black P.B., Tice A.R. (1988). Comparison of Soil Freezing Curve and Soil Water Curve Data for Windsor Sandy Loam. US Army Cold Regions Research and Engineering Laboratory, CRREL Report 88-16.
- Blair, R.W. (1994). Mountain and valley wall collapse due to rapid deglaciation in Mount Cook National Park, New Zealand. *Mountain Research and Development* **14**, 347–358.
-

Blight G. (2010). *Geotechnical Engineering for Mine Waste Storage Facilities*. CRC Press, Taylor & Francis Group, London, UK.

Blondeau F., Queyroi D. (1976). Rupture de la tranchée expérimentale de la Bosse-Galin (argile molle). *Bulletin de Liaison des Laboratoires des Ponts and Chaussées*, Numéro Spécial III- Stabilité des talus - 2: Déblais et remblais, 59-69.

Bober L., Zabuski L. (1993). Flysch slope classification from viewpoint of the landslide prediction. *Proc. Int. Symp. on the Geotechnics of Hard Soils–Soft Rocks*, Anagnostopoulos A., Schlosser F., Kalteziotis N. and Frank R. editors, Athens, 2, 1065-1072.

Bogaard T.A., Antoine P., Desvarreux P., Giraud A., van Asch T.W.J. (2000) The slope movements within the Mondorès graben (Drôme, France); the interaction between geology, hydrology and typology. *Eng Geol.*, **55**, 297-312

Boike J., Overduin P.P. (1999). Seasonal changes in hydrology, energy balance and chemistry in the active layers of Arctic Tundra soils in Taymyr Peninsula, Russia. *Land-Ocean Systems in the Siberian Arctic, Dynamics and History* (Eds; Kassens, H., Bauch, H.A., Dmitrenko, I., Eicken, H., Hubberten., H.W., Melles, M., Thiede, J. and Timokhov, L.A.) *Lecture notes in Earth Science*, Springer, Berlin, 299-306.

Boike J., Roth K, Overduin P.P. (1998). Thermal and hydrologic dynamics of the active layer at a continuous permafrost site (Taymyr Peninsula, Siberia). *Water Resour. Res.*, **34(3)**, 355-363.

Bonnard C.H., Noverraz F., Parriaux, A. (1987). Origin of Groundwater Likely to Affect a Large Landslide, *Proceedings of the Ninth European Conference on Soil Mechanics and Foundation Engineering*, Balkema, pp. 389–392.

Bonzanigo L. (1999). *Lo slittamento di Campo Vallemaggia*. D.Sc. thesis, Engineering Geology, Swiss Federal Institute of Technology (ETH Zurich), Zurich, Switzerland.

Bonzanigo L., Eberhardt E., Loew S. (2007). Long-term investigation of a deep-seated creeping landslide in crystalline rock. Part I. Geological and hydromechanical factors controlling the Campo Vallemaggia landslide. *Can. Geotech. J.*, **44(10)**, 1157–1180.

Bonzanigo L., Eberhardt E., Loew, S. (2001). Hydromechanical factors controlling the creeping Campo Vallemaggia landslide. *Proceeding: Landslides-Causes, impacts and countermeasures*, Davos, Switzerland, 13–22.

Borga M., Fontana G.D., De Ros D., Marchi L. (1998). Shallow landslide hazard assessment using a physically based model and digital elevation data. *Environ. Geol.*, **35**, 81-88.

Borgatti L., Corsini A., Barbieri M., Sartini G., Truffelli G., Caputo G., Puglisi C. (2006). Large reactivated landslides in weak rock masses: a case study from the Northern Apennines (Italy). *Landslides*, **3**, 115–124.

Borgatti L., Corsini A., Marcato G., Ronchetti F., Zabuski L. (2008). Appraise the structural mitigation of landslide risk via numerical modelling: a case study from the northern Apennines (Italy). *Georisk* **2**, 141–160.

Borgia A, Ferrari L, Pasquarè G (1992). Importance of gravitational spreading in the tectonic and volcanic evolution of Mount Etna. *Nature*, **357**, 231-235.

Borgia A. (1994). Dynamic basis of volcanic spreading. *J. Geophys. Res.*, **99**, 17, 791-17, 804.

---

- Borgia A., van Wyk de Vries B. (2003). The volcano-tectonic evolution of Concepcion, Nicaragua. *Bull. Volcanol.*, **65**, 248-266.
- Botts M.E. (1998). Effects of slacking on the strength of clay shales: A critical state approach. Proc. 2<sup>nd</sup> Int. Symp. on The Geotechnics of Hard Soils-Soft Rocks, Evangelista A. and Picarelli L. editors, Naples, Balkema, 447-458.
- Bourdeau, C., Havenith, H.B. Fleurisson, J.A., Grandjean, A.G. (2004). Numerical Modelling of Seismic Slope Stability. Engineering Geology for Infrastructure Planning in Europe, Springer Berlin / Heidelberg, **104**, 671-684.
- Bovis M.J., Jones P. (1992). Holocene history of earthflow mass movements in south-central British Columbia: the influence of hydroclimatic changes. *Canadian Journal of Earth Sciences*, **29**, 1746-1755.
- Bovis, M.J. (1982). Uphill-facing (antisllope) scarps in the coast mountains, southwest British Columbia. *Geological Society of America Bulletin* **93**, 804–812.
- Bovis, M.J. (1990). Rock-slope deformation at Affliction Creek, southern Coast Mountains, British Columbia. *Canadian Journal of Earth Sciences* **27**, 243–254.
- Brandsdottir B., Einarsson P. (1979). Seismic activity associated with the September 1977 deflation of the Krafla central volcano in north–eastern Iceland. *J. Volcanol. Geotherm. Res.*, **6**, 197-212.
- Bravo T. (1962). El circo de Canadas y sus dependencias. *Bol. R. Soc. Esp. Hist. Nat.*, **40**, 93-108.
- Bray J.R.. (1977). Pleistocene volcanism and glaciation initiation. *Science*, **197**, 251-254.
- Bray, J.D. (2007). Simplified seismic slope displacement procedures. Earthquake geotechnical engineering. K.D. Pitilakis Editor, Springer.
- Bray, J.D., Travasarou, T. (2007). Simplified Procedure for Estimating Earthquake-Induced Deviatoric Slope Displacements. *J. Geotech. Geoenviron. Eng.*, ASCE, **133(4)**, 381-392.
- Breth H. (1967) The dynamics of a landslide produced by filling a reservoir. 9th Int. Cong. on Large Dams, Istanbul, 37-45.
- Bromhead E.N. (1978). Large landslides in London clay at Henre Bay, Kent. *Q. J. Eng. Geol.*, London **11**, 291-304.
- Bromhead E.N., Dixon N. (1984). Pore-water pressure observations in the coastal clay cliffs at the Isle of Sheppey, England. Proc. 4<sup>th</sup> Int. Symp. on Landslides, Toronto **1**, 385-390.
- Bromhead E.N., Ibsen M.L. (2007). “An overview of landslide problems in the British Isle, with reference to geology, geography and conservation”. Chapter 2 of Progress in Landslide Science, Sassa K., Fukuoka H., Wang F., Wang G. editors, Springer, 15-25.
- Brown R.J.E., Johnston G.H., Mackay J.R., Morgenstern N.R., Shilts W.W. (1981). Permafrost distribution and terrain characteristics. Permafrost Engineering Design and Construction, ed. G.H Johnston, New York, Wiley, 31-77.
- Brückl, E. (2001). Cause–effect models of large landslides. *Natural Hazards* **23**, 291–314.
- Brunsdon D., Ibsen M. (1994). The temporal causes of landslides on the south coast of Great Britain. In: Casale, R., Fantechi, R., Flageollet, J.C. (Eds), *Temporal Occurrence and*
-

*Forecasting of Landslides in the European Community*. Final Report. European Commission-Epoch Programme (Ct) 90 0025.1, 339-383.

Bucki A.K., Echelmeyer K.A., MacInnes S. (2004). The thickness and internal structure of Fireweed rock glacier, Alaska, USA as determined by geophysical methods. *J. Glaciol.*, **50(168)**, 67–75.

Buffington J.M., Montgomery D.R. (1997). A systematic analysis of eight decades of incipient motion studies, with special reference to gravel-bedded rivers. *Water Resour. Res.*, **33(8)**, 1993-2029.

Buma J., Dehn M. (1998). A method for predicting the impact of climate change on slope stability. *Environ. Geol.*, **35**, 190-196.

Buma J., Dehn M. (2000). The impact of climate change on a landslide in South East France, simulated using different GCM-scenarios and downscaling methods for local precipitation. *Climate Research*, **15**, 69-81.

Burland J.B., Longworth T.I., Moore J.F.A. (1977). A study of ground movement and progressive failure caused by a deep excavation in Oxford clay. *Géotechnique*, **27(4)**, 557-591.

Burland J.B., Maswoswe J. (1982). In situ measurement of horizontal stress in overconsolidated clay using push-in spade pressure cells. *Géotechnique*, **32**, 285-286.

Burland J.B., Rampello S., Georgiannou V.N., Calabresi G. (1996). A laboratory study of the strength of four stiff clays. *Géotechnique*, **46(3)**, 491-514.

Burland J.B., Rampello S., Georgiannou V.N., Calabresi G. (1996). “A laboratory study of the strength of four stiff clays”. *Géotechnique* 46, n° 3, 491-514.

Burland, J.B. (1990). On the compressibility and shear strength of natural clays. *Géotechnique*, **40(3)**, 329-378.

Cabrera J.G., Smalley I.J. (1973). Quick clays as products of glacial action: a new approach to their nature, geology and distribution and geotechnical properties. *Eng. Geol.*, **7**, 115-133.

Caine N. (1980). The rainfall intensity-duration control of shallow landslides and debris flows. *Geogr. Ann.*, **62a**, 23-27.

Cairo R., Dente G. (2003). A flow slide in a pyroclastic soil fill. *Atti Conf. Int. su “ Fast Slope Movements – Prediction and Prevention for Risk Mitigation ”*. Napoli, Patron Editore Bologna **1**, 93-100

Calabresi G., Rampello S. (1987). Swelling of overconsolidated clays in excavations. Proc. 9<sup>th</sup> European. Conf. on S.M.F.E., Dublin, 1, 11-15.

Calabresi G., Scarpelli G. (1985). Effects of swelling caused by unloading in overconsolidated clays. Proc. 11<sup>th</sup> ICSMFE, San Francisco, 2, 411-414.

Calcaterra D., de Riso R., Di Martire D. (2004). Valutazione della suscettibilità da frana nella Conca di Agnano (Napoli) mediante applicazione di un modello su base fisica (SHALSTAB). *I Workshop Modeci*, Arcavacata di Rende, 30-31 march 2004.

---

- Calcaterra D., Guarino P.M. (1997). Dinamica morfologica e fenomeni franosi recenti nell'area collinare napoletana (settore occidentale). *Geologia Tecnica ed Ambientale*, **2**, 11-17.
- Calcaterra D., Parise M., Palma B., Pelella, L. (2000b). Multiple debris flows in volcanoclastic materials mantling carbonate slopes. Proc. 2<sup>nd</sup> Int. Conf. Debris-Flow Haz. Mitig., Taipei, Taiwan, 16-18/07/00: 99-107.
- Calcaterra D., Santo A. (2004). The January 10, 1997 Pozzano Landslide, Sorrento Peninsula, Italy. *Eng. Geol.*, **75**, 181-200.
- Calcaterra D., Santo A., de Riso R., Budetta P., Di Crescenzo G., Franco I., Galiotta G., Iovinelli R., Napolitano P., Palma B. (1997). Fenomeni franosi connessi all'evento pluviometrico del Gennaio 1997 in Penisola Sorrentina - M.ti Lattari: primo contributo. Atti IX Congresso Nazionale dei Geologi, Roma 17-20 april 1997.
- Calcaterra, D., Parise, M., Palma, B., Pelella, L. (2000). The influence of meteoric events in triggering shallow landslides in pyroclastic deposits of Campania, Italy. In: Thelford, T. (Ed.), *Proc. of the 8th Int. Symp. on Landslides - Landslides in Research, Theory and Practice*, **1**.
- Callerio, A., Faccioli, E., Kaynia, A. (2007a). Landslide risk assessment methods and applications (III) – Application to real active landslides – Phase II. LESSLOSS, (2004-2007). "Risk Mitigation for Earthquakes and Landslides", Research Project, European Commission, Sixth Framework Programme, Priority 1.1.6.3, Global Change and Ecosystems, Contract Number: GOCE-CT-2003-505448. Deliverable No 121.
- Callerio, A., Faccioli, E., Uzielli, M., Kaynia, A. (2007b). Landslides: From Mapping to Loss and Risk Estimation- Risk Analysis of the Corniglio Landslide. LESSLOSS (2004-2007). LessLoss Report No. 2007/01: "Risk Mitigation for Earthquakes and Landslides", Research Project, European Commission, Sixth Framework Programme, Priority 1.1.6.3, Global Change and Ecosystems, Contract Number: GOCE-CT-2003-505448.
- Callisto L., Rampello S. (2004). An interpretation of structural degradation for three natural clays. *Can. Geotech. J.*, **41**, 392-407.
- Campbell R.H. (1975). Soil slips, debris flows, and rainstorms in the Santa Monica Mountains and vicinity, Southern California. *US Geological Survey Professional Paper*, **851**, 1-20.
- Cancelli A., Marabini F., Pellegrini M., Tonnetti G. (1984). "Incidenza delle frane sull'evoluzione della Costa Adriatica da Pesaro a Vasto". *Mem. Soc. Geol. It.*, **27**, 555-568, in italian.
- Cannon S.H., Ellen S.D. (1985). Rainfall conditions for abundant debris avalanches, San Francisco Bay region, California. *California Geology*, **38**, 267-272.
- Canton, Y., Solé-Benet, A., Queralt, I. and Pini, R. (2001). Weathering of a gypsum-calcareous mudstone under semi-arid environment at Tabernas, SE Spain: laboratory and field-based experimental approaches. *Catena*, **44**, 111-132.
- Cappa F., Guglielmi Y., Soukatchoff V.M., Mudry J., Bertrand C., Charvoille A. (2004). Hydromechanical modelling of a large moving rock slope inferred from slope levelling coupled to spring long-term hydrochemical monitoring: example of the La Clapière landslide (Southern Alps, France). *Journal of Hydrology*, **291**, 67-90.
-

- Cappa, F. and Guglielmi, Y., (2004). Hydromechanical modeling of a large moving rock slope inferred from slope levelling coupled to spring long-term hydrochemical monitoring: example of the La Clapiere landslide (Southern Alps, France). *J. Hydrol.*, **291**, 67–90.
- Capra L., Macias J.L., Scott K.M., Abrams M., Garduno Monroy V.H. (2002). Debris avalanches and debris flows transformed from collapses in the Trans-Mexican Volcanic Belt, Mexico—Behavior, and implications for hazard assessment. *J. Volcanol. Geotherm. Res.*, **113**, 81-110.
- Carloni G-C., Mazzanti R. (1964a). “Aspetti geomorfologici della frana del Vajont” Rivista Geografica Italiana, Firenze, Vol. 71, n° 3, September, 201-231 (in Italian with summary in English).
- Carloni G-C., Mazzanti R. (1964b). “Rilevamento geologico della frana del Vajont”. In La frana del Vajont, Annali del Museo Geologico di Bologna, Ser. 2, Vol. 32, Fas. 1, 105-138, including colour maps (scale 1: 5000 and 1: 25000) (in Italian).
- Carracedo, J.C. (1994). The Canary Island: an example of structural control on the growth of large oceanic-island volcanoes. *J. Volcanol. Geotherm. Res.*, **60**, 225-241.
- Carrasco-Nuñez G., Vallance J.W., Rose W.I. (1993). A voluminous avalanche-induced lahar from Citlaltepetl volcano, Mexico: implications for hazard assessment. *J. Volcanol. Geotherm. Res.*, **59**, 35-46.
- Carrier III W.D. (1991). Stability of tailings dams. Proceedings of the 15<sup>th</sup> Conference of Geotechnics of Turin (CGT), Turin (Italy) November 19-22.
- Carrier III W.D. (2003). Stability of tailings dams. Proceedings of the 19<sup>th</sup> Conference of Geotechnics of Turin (CGT), Turin (Italy) November 4-6.
- Carson (1976). Mass-wasting, slope development and climate. *Geomorphology and Climate*, Derbyshire E. editor, John Wiley and Sons, 101-136.
- Casagli N., Rinaldi M., Gargini S., Curini A. (1999). Pore water pressures and streambank stability: Results from a monitoring site on the Sieve River, Italy. *Earth Surf. Process. Landf.*, **24(12)**, 1095-1114.
- Casagrande A. (1936). Characteristics of cohesionless soils affecting the stability of earth fills. *Journal of Boston Society of Civil Engineers*, **33**, 257-276.
- Cascini L. (2008). Applicability of landslide susceptibility and hazard zoning at different scales. *Eng. Geol.*, **102** 164–177.
- Cascini L., Cuomo S., Guida D. (2008). Typical source areas of May 1998 flow-like mass movements in the Campania region, Southern Italy. *Engineering Geology* 96 (2008) 107–125
- Cascini L., Ferlisi S. (2003). Occurrence and consequences flowslide: a case study. *Proc. Of the Int. Conf. On “Fast Slope Movements - Prediction and Prevention for Risk Mitigation”*, Napoli, Patron Editore, **1**, pp. 85-92
- Cascini L., Guida D., Romanzi G., Nocera G., Sorbino G. (2000). A preliminary model for the landslides of May 1998 in Campania Region. *Proc. 2nd Intern. Symp. On Hard Soil Rocks*. Balkema, Rotterdam, pp. 1623-1649.
-

Cascini L., Sorbino G. (2003). The contribution of soil suction measurements to the analysis of 'flowslide triggering. Invited Lecture, Proc. of the Int. Workshop "Flows 2003 - Occurrence and Mechanisms of Flows in Natural Slopes and Earthfill", Sorrento, Patron Ed., pp. 77-86.

Cascini, L., Bonnard, C.h., Corominas, J., Jibson, R., Montero-Olarte, J., (2005). Landslide hazard and risk zoning for urban planning and development. State of the Art Report (SOA7). In: Hungr, O., Fell, R., Couture, R., Eberhardt, E. (Eds.), Proceedings of the International Conference on "Landslide Risk Management", Vancouver (Canada). Taylor and Francis, London, pp. 199–235.

Castro G. (1975). Liquefaction and cyclic mobility of saturated sands. *J. Geotech. Engineering Div., ASCE*, **101**, GT6, 551-569.

Castro G. (1987). On the behaviour of soils during earthquakes – Liquefaction. Soil Dynamics and Liquefaction, Elsevier, 169-204.

Castro G., Poulos S.J. (1977). Factors affecting liquefaction and cyclic mobility. *J. Geotech. Engineering Div., ASCE*, **103**, GT6, 501-516.

Cecchi E., van Wyk de Vries B., Lavest J.M. (2005). Flank spreading and collapse of weak-cored volcanoes. *Bull. Volcanol.*, **67**, 72-91.

Celico P, Aquino S., Esposito L., Piscopo V., (2000). problematiche idrogeologiche connesse con i fenomeni di instabilità delle coltri piroclastiche della dorsale di pizzo D'Alvano. *Quaderni di geologia Applicata* **5(1)**,129-188.

Celico, P. and Guadagno, F. M., 1998: L'instabilità delle coltri piroclastiche delle dorsali carbonatiche in Campania: attuali conoscenze, *Quaderni di Geologia Applicata*, 5–1, 75–133, Bologna.

Chandler R.J. (1969). The effect of weathering on the shear strength properties of Keuper marl. *Géotechnique*, **19(3)**, 321-334.

Chandler R.J. (1972). Lias Clay: weathering processes and their effects on shear strength. *Géotechnique*, **22(3)**, 403-431.

Chandler R.J. (1984). Delayed failure and observed strengths of first-time slides in stiff clay. Proc. 4<sup>th</sup> Int. Conf. on Landslides, Toronto, vol. 2, 9-25.

Chandler R.J. (1984). Recent European experience of landslides in overconsolidated clays and soft rocks. S. O. A. report, Proc. 4<sup>th</sup> Int. Symp. On Landslides, Toronto, **1**, 61-81.

Chandler R.J., Apter J.P. (1988). The effects of weathering on the strength of London clay. *Q. J. Engng. Geol.*, **21**, 59-68.

Chandler R.J., Skempton A.W. (1974). "The design of permanent cutting slopes in stiff fissured clays". *Géotechnique* 24, n° 4, 457-464.

Chandler R.N. Johnson D.L. (1981). The equivalence of quasistatic flow in fluid-saturated porous media and Biot's slow wave in the limit of zero frequency. *Journal of Applied Physics* **52**, 3391-3396.

Chang, Y.C.E. (1981). Long term consolidation beneath the test fills at Väsby, Sweden. Swedish Geotechnical Institute, Report 13, Linköping.

---

- Chêne, G., Bastian, G., Brunjail, C. and Laurent, J.P. (1999). Vieillissement accéléré de bloc de tuffeau en laboratoire sous l'effet de cycles d'imbibition-séchage. *Matériaux et Constructions*, **32**, 525–532.
- Chiessi V., D'Orefice M., Giovagnoli M. C., Graziano R., Vita L. (2003). Colate rapide di fango: un caso di studio nel territorio comunale di S. Felice a cancello (Ce). *Boll. Soc. Geol. It.*, 405-420.
- Chiew Y.M., Parker G. (1994). Incipient sediment motion on non horizontal slopes. *J Hyd. Res.*, **32(5)**, 649-660.
- Chigira, M., Oyama, T. (1999). Mechanism and effect of chemical weathering of sedimentary rocks. *Eng. Geol.*, **55**, 3-14.
- Chirico, G.B., Claps, P., Rossi, F., Villani, P., (2000). Hydrologic conditions leading to debris-flow initiation in the Campanian volcanoclastic soil. Proc. EGS Plinius Conf., Maratea, October 1999, pp. 473–484.
- Chiu C.F., Fu X.J. (2008). Interpreting undrained instability of mixed soils by equivalent intergranular state parameter. *Géotechnique*, **58(9)**, 751-755.
- Chowdhury R., Flentje P. (2002). Uncertainties in rainfall-induced landslide hazard. *Q J Eng Geol Hydrogeol.*, **35**, 61–69.
- Chowdhury R.N., Flentje P. (1998). Hazard Assessment for Rainfall-Triggered Landslides. *Annales Geophysicae*, European Geophysical Society. Abstract only. Supplement IV to Volume 16, page C1176.
- Chowdhury R.N., Flentje P.N. (1998). A landslide database for landslide hazard assessment, In: Sivakumar, M. & Chowdhury, R.N. (eds) Proceedings of the Second International Conference on Environmental Management. February 10–13. Wollongong Australia, 1239, Elsevier London, 1229–1239.
- Christensen O.B., Christensen J.H. (2004). Intensification of extreme European summer precipitation in a warmer climate. *Global Planet. Change*, **44**, 107-117.
- Chu J., Leong W.K. (2002). Effect of fines on instability behaviour of loose sand. *Géotechnique*, **52(10)**, 751-755.
- Chu J., Leroueil S., Leong W.K. (2003). Unstable behaviour of sand and its implication for slope stability. *Can. Geotech. J.*, **40**, 873-885.
- Chu J., Lo R.S.C., Lee I.K. (1993). Instability of granular soils under strain path testing. *Journal of Geotech. Engineering, ASCE*, **119(5)**, 874-892.
- Church, M., Ryder, J.M (1972). Paraglacial sedimentation: a consideration of fluvial processes conditioned by glaciation. *Geological Society of America, Bulletin* **83**, 3059–3071.
- Church, M., Ryder, J.M. (1989). Sedimentology and clast fabric of subaerial debris flow facies in a glacially influenced alluvial fan – a discussion. *Sedimentary Geology* **65**, 195–196
- Civita M & Lucini P. (1968). *Sulla franosità nella zona nord-occidentale della Penisola Sorrentina (Campania)*. Mem. e Note Ist. Geol. App Univ Napoli, 10.
- Civita M., de Riso R., Lucini P. & Nota d'Elogio E. (1975). Studio delle condizioni di stabilità dei terreni della Penisola Sorrentina. *Geol. Appl. e Idr.*, **10**, 129-188.
-

Coe J.A., Ellis W.L., Godt J.W., Savage W.Z., Savage J.E., Michael J.A., Kibler J.D., Powers P.S., Lidke, D.J., Debray S., (2003). Seasonal movement of the Slumgullion landslide determined from Global Positioning System surveys and field instrumentation, July 1998 – March 2002. *Eng. Geol.*, **68**, 67-101.

Coello J. (1973). Las series volcanicas de los subsuelos de Tenerife. *Estudios Geologicos*, **27**, 95-137.

Colesanti, C., Crosta, G.B., Ferretti, A., Ambrosi, C. (2004). Monitoring and assessing the state of activity of slope instabilities by the Permanent Scatterers Technique. In: Evans, S.G., Scarascia-Mugnozza, G., Strom, A., Hermanns, R. (Eds.), *Landslides from Massive Rock Slope Failure. NATO Science Series, IV. Earth and Environmental Sciences*, vol. **49**. Springer, Dordrecht, pp. 175–194.

Collison A., Wade S., Griffiths J., Dehn M. (2000). Modelling the impact of predicted climate change on landslide frequency and magnitude in SE England. *Eng. Geol.*, **55**, 205-218.

Compagnon F., Guglielmi Y., Mudry J., Follacci J.P., Ivaldi, J.P. (1997). Chemical and isotopic natural tracing of seepage waters in an important landslide: example from La Clapière landslide (Alpes-Maritimes, France). *C. R. Acad. Sci. Paris*, **325**, 565–570.

Concha-Dimas A., Cerca M., Rodríguez S.R., Watters R.J. (2005). Geomorphological evidence of the influence of pre-volcanic basement structure on emplacement and deformation of volcanic edifices at the Cofre de Perote-Pico de Orizaba chain and implications for avalanche generation, *Geomorphology*, **72**, 1-4.

Conedera M., Peter L., Marxer P., Forster F., Rickenmann D., Re L. (2003). Consequences of forest fires on the hydrogeological response of mountain catchments: a case study of the Riale Buffaga, Ticino, Switzerland. *Earth Surf. Process. Landf.*, **28**, 117-129.

Cooper M.R., Bromhead e.N., Petley D.J., Grant D.I. (1998). The Selborne cutting stability experiment. *Géotechnique*, **48(1)**, 83-101.

Cordano E., Rigon R. (2008). A perturbative view on the subsurface water pressure response at hillslope scale. *Water Resour. Res.*, **44**, W05407.

Corominas J, Moya J, Ledesma A, Lloret A, Gili JA (2005) Prediction of ground displacements and velocities from groundwater level changes at the Vallcebre landslide (Eastern Pyrenees, Spain). *Landslides* **2**, 83–96.

Corominas J., Moya J. (1999). Reconstructing recent landslide activity in relation to rainfall in the Llobregat River basin, Eastern Pyrenees, Spain. *Geomorphology*, **30**, 79-93.

Corominas J., Moya J., Ledesma A., Lloret A., Gili J.A. (2005). Prediction of ground displacements and velocities from groundwater level changes at the Vallcebre landslide (Eastern Pyrenees, Spain). *Landslides*, **2**, 83–96

Corominas J., Moya J., Ledesma A., Rius J., Gili J.A., Lloret A. (1999). Monitoring of the Vallcebre landslide, Eastern Pyrenees, Spain. In: *Proceedings International Symposium on Slope Stability Engineering*. Matsuyama, Japan, **2**, 1239–1244

Corominas J., Moya J., Lloret A., Gili J.A., Angeli M.G., Pasuto A. (2000). Measurement of landslide displacements using a wire extensometer. *Eng. Geol.*, **55**, 149–166

---

- Corsini A., Borgatti L., Caputo G., De Simone N., Sartini G., Truffelli G. (2006). Investigation and monitoring in support of the structural mitigation of large slow moving landslides: an example from Ca' Lita (Northern Apennines, Reggio Emilia, Italy). *NHESS*, **6**, 55–61.
- Cossart, E., Braucher, E., Fort, M., Bourlès, D.L., Carcaillet, J. (2008). Slope instability in relation to glacial debuitressing in alpine areas (Upper Durance catchment, south-eastern France): Evidence from field data and  $^{10}\text{Be}$  cosmic ray exposure ages. *Geomorphology* **95**, 3–26.
- Cotecchia F., Chandler R.S. (1997). The influence of structure on the pre-failure behaviour of natural clay. *Géotechnique*, **47(3)**, 523-544.
- Cotecchia, F., Chandler, R.J. (2000). A general framework for the mechanical behaviour of clays. *Géotechnique*, **50(4)**, 431-447.
- Cripps J.C., Taylor R.K. (1981). The engineering properties of mudrocks. *Q. J. Eng. Geol., London*, **14**, 325-346.
- Crosato A. (1990). Simulation of Meandering River Processes, Communications on Hydraulic and Geotechnical Engineering. *Technical Rep.*, Civil Engineering Dept., Delft Univ. of Technology, Delft, The Netherlands.
- Crosta G, Di Prisco C (1999). On slope instability induced by seepage erosion. *Can. Geotech. J.*, **36**, 1056–1073.
- Crosta G. (1998). Regionalization of rainfall thresholds: an aid to landslide hazard evaluation. *Environ. Geol.*, **35**, 131–145
- Crosta G.B., Agliardi F. (2003). A methodology for physically based rockfall hazard assessment. *Natural Hazards and Earth System Sciences*, **3**, 407-422.
- Crosta G.B., Dal Negro P. (2003). Observations and modelling of soil slip-Debris flow initiation processes in pyroclastic deposits: the Sarno event. *Natural Hazards And Earth System Sciences*, **3**, 53-69.
- Crosta G.B., Frattini P. (2003). Distributed modelling of shallow landslide triggered by intense rainfall. *NHESS*, **3**, 81-93.
- Crosta GB, Agliardi F (2002) How to obtain alert velocity thresholds for large rockslides. *Phys Chem Earth*, **27**, 1557–1565.
- Crosta GB, Frattini P. (2001). Rainfall thresholds for triggering soil slips and debris flow. In: Proc. Of EGS 2nd Plinius Conference 2000, Mediterranean Storms, Siena, 463–488.
- Crosta, G. (1996). Landslide, spreading, deep-seated gravitational deformation: analysis, examples, problems and proposals. *Geogr. Fis. Dinam. Quat.*, **19**, 2, 297-313.
- Crosta, G., Imposimato, S., Roddeman, D. (2003). Numerical modeling of large landslide stability and runout. *NHESS*, **3(6)**, 523–538.
- Crosta, G., Imposimato, S., Roddeman, D. (2004a). Continuum numerical modeling of flow-like landslides. NATO ARW, Massive Rock Slope Failure: new models for hazard assessment, Celano (Aq), Italy; 16 21 June, 2002. Kluwer Publ. 23 pp.
-

- Crosta, G., Zanchi, A. (2000). Deep seated slope deformations. Huge, extraordinary, enigmatic phenomena. In: Bromhead, E., Dixon, N., Ibsen, M. (Eds.), *Landslides in Research, Theory and Practice*, Proceedings of the 8th International Symposium on Landslides, Cardiff, June 2000. Thomas Telford, London, 351–358.
- Crosta, G.B., Chen, H., Lee, C.F. (2004b). Replay of the 1987 Val Pola Landslide, Italian Alps. *Geomorphology*, 60(1–2), 127-146.
- Crosta, G.B., Imposimato, S., Roddeman, D., Chiesa, S., Moia, F. (2005). Small fast-moving flow-like landslides in volcanic deposits: the 2001 Las Colinas landslide (El Salvador). *Eng. Geol.*, **79**, 185–214.
- Crosta, G.B., Imposimato, S., Roddeman, D.G., Chiesa, S. (2004c). The 2001 Las Colinas landslide, El Salvador: from geology to numerical modeling. Proc. of the IXth International Symp. On Landslides, Rio de Janeiro, Brasil, June 2004.
- Crouch R.S., Wolf J.P. (1994). Unified 3-D critical-state bounding surface plasticity model for soil incorporating continuous plastic loading under cyclic paths. Part I: Constitutive Relations. *Int. J. Num. Anal. Meth. Geom.*, **18(11)**, 735-758.
- Crouch R.S., Wolf J.P., Dafalias Y.F. (1994). Unified critical state bounding surface plasticity model for soil. *J. Eng. Mech.*, **120(11)**, 2251-2270.
- Crowley J.K., Zimbleman D.R. (1997). Mapping hydrothermally altered rocks on Mount Rainier, Washington, with airborne visible/infrared imaging spectrometer (AVIRIS) data. *Geology*, **25(6)**, 559-562.
- Crozier M. (1997). The climate-landslide couple: a Southern Hemisphere perspective. *Palaoklimaforschung. Palaeoclimate Research*, **19**, 333-354.
- Crozier M.J. (1999). Prediction of rainfall-triggered landslides: A test of the antecedent water status model. *Earth Surf. Processes and Landforms*, **24**, 825-833.
- Crozier M.J., Glade T. (1999). Frequency and magnitude of landsliding: fundamental research issues. *Z. Geomorphol. NF Suppl.*, **115**, 141-155.
- Cruden D.M., Varnes D.J. (1996). Landslides Types and Processes. In: Turner A.K. and Schuster R.L. (Eds.) *Landslides: Investigation and Mitigation*. Transportation Research Board Special Report **247**. National Academy Press, Washington, DC, pp. 36–72.
- Cruden, D.M., Hu, X.Q. (1994). Topples on underdip slopes in the Highwood Pass, Alberta, Canada. *Quarterly Journal of Engineering Geology and Hydrogeology*, **27**, 1, 57-68.
- Cruden, D.M., Hu, X.Q. (1993). Exhaustion and steady-state models for predicting landslide hazards in the Canadian Rocky Mountains. *Geomorphology* **8**, 279–285.
- Cubasch U., Waszkewitz G., Hegerl G.C., Perlwitz J. (1995). Regional climate changes as simulated in time slice experiments. MPI Report 153. *Clim. Change*, **31**, 321-304.
- Cubrinowski M., Ishihara K. (1998). Modelling of sand behaviour based on state concept. *Soils and Foundations*, **38(3)**, 115-127.
- Cubrinowski M., Ishihara K. (2000). Flow potential of sandy soils with different grain compositions. *Soils and Foundations*, **40(4)**, 103-119.
-

Cui, P., Chen, X.Q., Zhu, Y.Y., Su, F.H., Wei, F.Q., Han, Y.S., Liu, H.J., Zhuang, J.Q., (2009). The Wenchuan earthquake (May 12, 2008), Sichuan province, China, and resulting geohazards. *Natural Hazards*, 1-18.

Cyr K.E., Melosh H.J. (1993). Tectonic patterns and regional stresses near Venusian Coronae. *Icarus*, **102**, 175-184.

D'Agostino V., Marchi L. (2003). Geomorphological estimation of debris flow volumes in alpine basins. In: Rickenmann D, Chen C (eds) Proc 3rd Int Conf on Debris Flow Hazard Mitigation: Mechanics, Prediction, and Assessment, Davos, 2:1097–1106.

D'Elia B. (1991). Deformation problems in the Italian structurally complex clay soils. Proc. 10<sup>th</sup> Europ. Conf. On S.M.F.E., Florence, 4, 1159-1170.

D'Elia B. (1994). Ricerca sperimentale sul comportamento reologico delle argille sovraconsolidate del Valdarno Superiore - Rapporto Finale. Rapporto Interno, Università di Roma La Sapienza.

D'Elia B., Picarelli L., Leroueil S., Vaunat J. (1998). Geotechnical characterization of slope movements in structurally complex clay soils and stiff jointed clays. *Italian Geotechnical Journal*, **32(3)**, 5-32.

D'Odorico P., Fagherazzi S., Rigon R. (2005). Potential for landsliding: Dependence on topographic characteristic. *J. Geophys. Res.*, **110**, 1-10.

Dafalias Y.F., Herrmann L.R. (1982). Bounding surface formulation of soil plasticity. Soil Mechanics – Transient and Cyclic Loads, Pande G.N. and Zienkiewicz O.C. editors, Wiley, 253-282.

Dafalias Y.F., Manzari M.T. (2004). Simple plasticity sand model accounting for fabric change effects. *Journ. Of Eng. Mech., ASCE*, June, 622-634.

Dafalias Y.F., Popov E.P. (1975). A model of nonlinearly hardening materials for complex loading. *Acta Mechanica*, **21**, 173-192.

Dallan Nardi L., Natdi R. (1975). Structural pattern of the northern Apennines. *Quaderni del CNR*, **90**, 203-250.

Darby S.E., Alabyan A.M., de Wiel M.J.V. (2002). Numerical simulation of bank erosion and channel migration in meandering rivers. *Water Resour. Res.*, **38(9)**, 1163.

Darby S.E., Thorne C.R. (1996). Development and testing of riverbank-stability analysis. *J. Hydraul. Eng.*, **122(8)**, 443-454.

Davies M.C.R., Hamaz O., Harris C. (2001). The effect of rise in mean annual temperature on the stability of rock slopes containing ice-filled discontinuities. *Permafrost and Periglacial Processes*, **12**, 137-144.

Davis R.O., Salt G.A. (1986). Strength of undulating shear surfaces in rock. *Géotechnique*, **36(4)**, 503-509.

Day S.J. (1996). Hydrothermal pore fluid pressure and the stability of porous, permeable volcano. In: McGuire WJ, Jones AP, Neuberg J (eds) Volcano instability on the Earth and other planets. *Geol. Soc. London, Spec. Publ.*, **110**, 77-93.

---

Day S.J., Carracedo J.C., Guillou H., Gravestock P. (1999). Recent structural evolution of the Cumbre Vieja volcano, La Palma, Canary Islands: volcanic rift zone reconfiguration as a precursor to volcano flank instability. *J. Volcanol. Geotherm. Res.*, **94**, 135-167.

De Alba P.A., Seed H.B., Retamal E., Seed R.B. (1988). Analysis of dam failures in 1985 Chilean earthquake. *Journ. of Geotech. Eng. Div., ASCE*, **114**, **GT12**, 1414-1434.

De Falco, M., de Riso, R., Ducci, D., 1997. La piovosità della Penisola Sorrentina e dei M.ti Lattari in relazione all'evento del gennaio 1997, Memorie dell'Istituto di Geologia Applicata Facoltà di Ingegneria – Univ. di Napoli "Federico II", pubbl. 372, Napoli.

De Montety, V., Marc, V., Emblanch, C., Malet, J. P., Bertrand, C., Maquaire, O., and Bogaard, T. A. (2007). Identifying the origin of groundwater and flow processes in complex landslides affecting black marls: insights from a hydrochemical survey. *Earth Surf. Process. Landforms*, **32**, 32–48.

de Riso R. Budetta P, Calcaterra D., De Luca, Del Prete S., Di Crescenzo G, Guarino P., Mele R., Palma G, Santo A. and Sgambati D. (2004). Fenomeni di instabilità dei versanti dei Monti Lattari e dell'Area Flegrea (Campania). *Quaderni di Geologia Applicata*, 11 – 1.

de Riso R., Budetta P. Calcaterra D. and Santo A. (1999). Le colate rapide in terreni piroclastici del territorio campano. Convegno su "Previsione e prevenzione di movimenti franosi rapidi", Trento 17-19 giugno 1999, GEAM.

De Vita P., Celico P. (2006). Distribuzione delle coltri piroclastiche sui versanti carbonatici perivesuviani e suscettibilità a franare. *Giorn. di Geol. Appl.*, **3**, 145-151.

De Vita P., Piscopo V. (2002). Influences of hydrological and hydrogeological conditions on debris flows in peri-vesuvian hillslopes. *NEHSS*, **2**, 27–35.

De Vita, P. (2000). Fenomeni d'instabilità delle coperture piroclastiche dei Monti Lattari, di Sarno e di Salerno (Campania) ed analisi degli eventi pluviometrici determinanti. *Quad. Geol. Appl.* **7(2)**, 213–239.

Dehn M., Burger G., Buma J., Gasparetto P. (2000). Impact of climate change on slope stability using expanded downscaling. *Eng. Geol.*, **55**, 193–204.

Del Gaudio, V., Wasowski, J. (2004). Time probabilistic evaluation of seismically induced landslide hazard in Irpinia (Southern Italy). *Soil Dynamics and Earthquake Engineering*, **24(12)**, 915-928.

del Potro R., Hurlimann M. (2008). Geotechnical classification and characterization of materials for stability analyses of large volcanic slopes. *Eng. Geol.*, **98**, 1-17.

Del Prete M., Gostelow P.T., Pininska J. (1995). The importance of historical observations in the study of climatically controlled mass movement on natural slopes, with examples from Italy, Poland and UK. In: Bell, D.H. (Ed). Proc. 6th Int. Symposium on Landslides. Landslides 3. Balkema, Rotterdam, pp. 1559–1567.

Del Prete M., Guadagno F. M. and Hawkins A. B. (1998). Preliminary report on the landslides of 5 May 1998, Campania, southern Italy. *Bull. Eng. Geol. Env.*, **57**, 113-129.

Delaney P.T., Denlinger R.P., Lisowski M., Miklius A., Okubo P.G., Okamura A.T., Sako M.K. (1998). Volcanic spreading at Kilauea, 1976-1996. *J. Geophys. Res.*, **103**, 18,003-18,023.

---

Delmonaco G., Falconi L., Margottini C., Spizzichino D, Corradini A. (2003). “Il consolidamento della rupe e delle pendici di Civita di Bagnoregio: indagini pregresse e proposte di intervento”. In IUGS-UNESCO Project no. 425 “Landslide Hazard Assessment and Mitigation for Cultural Heritage Sites and Other Locations of High Societal Value”, Sub-project 23: “Linee Guida per la salvaguardia dei beni culturali dai rischi naturali – Guidelines for the safeguard of cultural heritage against natural risk”. Case study no. 7. (<http://www.afs.enea.it/protprev/www/index.htm>) – in italian.

Densmore, A.L., Hovius, N. (2000). Topographic fingerprints of bedrock landslides. *Geology*, **28(4)**, 371–374.

Dhakal A.S. (1995). Disaster of 1993 experienced by Nepal. In Proceedings of the International Sabo Symposium, Tokyo, 115–122.

Dhakal A.S., Sidle R.C. (2004). Pore water pressure assessment in a forest watershed: simulations and distributed field measurements related to forest practices. *Water Resour. Res.*, **40**, W02405.

Di Crescenzo G., Rotella M., Santo A. (2008). Le frane da colata rapida in terreni piroclastici dei contesti in flysch dell’entroterra campano. *Giornale di Geologia Applicata*, 8 (2), 193-215.

Di Crescenzo G., Santo A (1999). Analisi geomorfologica delle frane da scorrimento-colata rapida in depositi piroclastici della Penisola Sorrentina (Campania). *Geografia Fisica e Dinamica Quaternaria*, **22**, 57-72.

Di Crescenzo G., Santo A. (2005). A. Rapid earth flows in the carbonate massifs of the Campania region (Southern Italy): morphological and morphometric data for evaluating triggering susceptibility. *Geomorphology*, **66**, 255-276.

Di Girolamo, P., Ghiara, M.R., Lirer, L., Munno, R., Rolandi, G., Stanzione D. (1984). Vulcanologia e Petrologia dei Campi Flegrei. *Boll. Soc. Geol. It.* **103**, 349-413.

Di Nocera S., Fenelli G.B., Iaccarino G., Pellegrino A., Pescatore T.S., Picarelli L., Urcioli G. (1995). “An Example on the geotechnical implications of geological history”. Proc. of 11<sup>th</sup> E,C,S,M.F.E., Copenhagen, Vol. 8, The Interplay between Geotechnical Engineering and Engineering Geology, Case Histories Demonstrating Interplay, 8.38-8.48.

Di Nocera S., Iaccarino G., Pescatore T.S., Picarelli L., Urcioli G. (1995). An example of the geotechnical implications of geological history. Proc. 11<sup>th</sup> European Conf. on S.M.F.E., Copenhagen, 8, 39-48.

Di Prisco C., Mantiotti R., Nova R. (1995). Theoretical investigation of the undrained stability of shallow submerged slopes. *Géotechnique*, **45(3)**, 479-496.

Di Prisco C., Nova R., Lanier J. (1993). A mixed isotropic kinematic hardening constitutive law for sand. *Modern Approaches to Plasticity*, Kolymbas D. editor, Balkema, 83-124.

Dieterich J.H. (1988). Growth and persistence of Hawaiian volcanic rift zones. *J. Geophys. Res.*, **93**, 4258-4270.

Dilly, Maxx, Cheri R.S., Deichmann U., Lerner-Larn A.L., Arnold M. (2005). Natural Disaster Hotspots, A Global Risk Analysis. Washington, D.C. World Bank.

- Doanh T., Ibraim E., Matiotti R. (1997). Undrained instability of very loose Hostun sand in triaxial compression and extension. Part 1: experimental observations. *J. Cohes.-Fric. Mater.*, **2**, 47-70.
- Dobry R., Vasquez-Herrera A., Mohamad R., Vucetic M. (1985). Liquefaction flow failure of silty sand by torsional cyclic tests. In: Khosla V (ed) Proceedings of a session of ASCE convention in Detroit, Michigan: Advances in the art of testing soils under cyclic conditions. American Society of Civil Engineers, New York, 29-50.
- Donnadieu F., Merle O. (1998). Experiments on the indentation process during cryptodome intrusions: New insights into Mount St. Helens deformation. *Geology*, **26**, 79-82.
- Donnadieu F., Merle O. (2001). Geometrical constraints of the 1980 Mount St. Helens intrusion from analogue models. *Geophys. Res. Lett.*, **28**, 639-642.
- Donnadieu F., Merle O., Besson J.C. (2001). Volcanic edifice stability during cryptodome intrusion. *Bull Volcanol.*, **63**, 61-72.
- Dorava J.M., Meyer D.F. (1994). Hydrologic hazards in the lower Drift River basin associated with the 1989–1990 eruptions of Redoubt Volcano, Alaska. *J. Volcanol. Geotherm. Res.*, **62**, 387-407.
- Dounias G.T., Marinos P.G. (1993). Soil-like and rock-like behaviour of a flysch in slope stability. Proc. Int. Symp. on the Geotechnics of Hard Soils–Soft Rocks, Anagnostopoulos A., Schlosser F., Kalteziotis N. and Frank R. editors, Athens, 2, 1107-1114.
- Druitt T.H. (1992). Emplacement of the 18 May lateral blast deposit ENE of Mount St. Helens, Washington. *Bull. Volcanol.*, **54**, 554-572.
- Duan J.G. (1998). Simulation of Alluvial Channel Migration Processes with a Two-dimensional Numerical Model. *Ph.D thesis*, University of Mississippi, Oxford, Mississippi.
- Duan J.G. (2001). Simulation of streambank erosion processes with a two-dimensional numerical model. *Landscape Erosion and Evolution Modeling*, Chap. 13, R. S. Harmon and W. W. Doe III, eds., Kluwer Academic/Plenum, New York, 389–427.
- Duan J.G. (2005). Analytical approach to calculate the rate of bank erosion. *J. Hydraul. Eng.*, **131(11)**, 980-990.
- Duan, X. Naterer, G.F. (2009). Heat conduction with seasonal freezing in an active layer near a tower foundation. *International Journal of Heat and Mass Transfer*, **52(7-8)**, 2068-2078.
- Duncan J.M., Dunlop P. (1969). Slopes in stiff-fissured clays and shales. *Journ. of Soil Mech. Found. Eng. Division, ASCE*, **96**, 467-492.
- Dunne T., (1978). Field studies of hillslope flow processes. In Hillslope Hydrology, edited by M. J. Kirkby, pp. 227–294, John Wiley, New York.
- Eberhardt, E., Stead, D., Coggan, J.S. (2004). Numerical analysis of initiation and progressive failure in natural rock slopes—the 1991 Randa rockslide. *International Journal of Rock Mechanics & Mining Sciences*, **41** (2004) 69–87
- Edelbro, C. (2003). Rock mass strength: a review. Technical Report, Lulea University of Technology, Sweden, 92 pp. ISSN 1402-1536.
-

- Eden W.J., Fletcher E.B., Mitchell R.J. (1971). South Nation river landslide, 16 May 1971. *Can. Geotech. J.*, **8**, 446-451.
- Eden W.J., Mitchell R.J. (1970). The mechanics of landslides in Leda clays. *Can. Geotech. J.*, **7**, 285-296.
- Eden W.J., Mitchell R.J. (1973). Landslides in marine sensitive clay in Eastern Canada. *Highway Research Board*, **463**, 18-27.
- Einstein H.H., Bruhn R.W., Hirschfield R.C. (1970). Mechanics of jointed rock. Experimental and theoretical studies. Dept. of Civ. Eng. Report, MIT, Cambridge, MA, USA
- Einstein, H.H., Veneziano, D., Baecher, G.B., O'Reilly, K.J. (1983). The effect of discontinuity persistence on rock slope stability. *Int J Rock Mech Min Sci Geomech Abstr*, **20(5)**, 227–36.
- Eisbacher G.H., Clague J.J., (1984). Destructive mass movements in high mountains: hazard and management. *Geological Survey of Canada*, Paper 84-16.
- Elconin R.F., La Chapelle E.R. (1997). Flow and internal structure of a rock glacier. *J. Glaciol.*, **43(144)**, 238-244.
- Elgamal A., Yang Z., Parra E. (2002). Computational modelling of cyclic mobility and post-liquefaction site response. *Soil Dynamics and Earthquake Engineering*, **22**, 259-271.
- Elsworth D., Day S. (1999). Flank collapse triggered by intrusion: The Canarian and Cape Verde Archipelagoes, *J. Volcanol. Geotherm. Res.*, **94**, 323-340.
- Elsworth D., Voight B. (1995). Dike intrusion as a trigger for large earthquakes and the failure of volcano flanks. *J Geophys Res.*, **100**, 6005–6024.
- Elsworth D., Voight, B. (1992). Theory of dike intrusion in a saturated porous solid. *J. Geophys. Res.*, **97**, 9105-9117.
- Elsworth D., Voight, B. (1996). Evaluation of volcano flank instability triggered by dike intrusion. In: McGuire, W.C., Jones, A.P., Neuberg, J. Eds., *Volcano Instability on the Earth and Other Planets. Geol. Soc. London, Spec. Publ.*, **110**, 45–53.
- Esposito L., Magliocca G., Nappi M. (2003). Alcune considerazioni sugli episodi di frana di San felice a Canello (Ce). AIGA – I° Convegno Nazionale 2003.
- Esu F. (1966). Short-term stability of slopes in unweathered jointed clays. *Géotechnique* **16(4)**, 321-328.
- Esu F. (1977). Behaviour of slopes in structurally complex formations. Proc. Int. Symp. on The Geotechnics of Structurally Complex Formations, Capri, 2, 292-304.
- Evans, S.G, Hungr O. (1993). The assessment of rock fall hazard at the base of talus slopes. *Can Geotech J*, **30**, 620–36.
- Evans, S.G., Clague, J.J. (1994). Recent climatic change and catastrophic geomorphic processes in mountain environments. *Geomorphology* **10**, 107–128.
- Farran, J., Thenoz, B. (1965). L'altérabilité des roches, ses facteurs, sa prévision. *Supplément des Annales de l'Institut des Techniques du Bâtiment et des Travaux Publics, France* **215**, 2729–2736.
-

- Fassina, V. (1995). New findings on past treatments carried out on stone and marble monument surfaces. *The Science of the Total Environment* **167**, 185–203.
- Fell R., Hungr O., Leroueil S., Riemer W. (2000). Geotechnical engineering of the stability of natural slopes, and cuts and fills in soil. Proceedings of the Geoengineering Conference, Melbourne, 21–120.
- Fenelli G.B., Picarelli L. (1990). The pore pressure field built up in a rapidly eroded soil mass. *Can. Geotech. J.*, **27**, 397-392.
- Ferguson H.F. (1967). Valley stress release in the Allegheny Plateau. *Eng. Geo.*, **4**, 63-71.
- Ferreira P.M.V., Buca A.V.D. (2006). Problems in identifying the effects of structure and critical state in a soil with transitional behaviour. *Géotechnique*, **56(7)**, 445-454.
- Finlay P.J., Fell R., Meguire P.K. (1997). The relationship between the probability of landslide occurrence and rainfall. *Can. Geotech. J.*, **34**, 811-824.
- Fiorillo F., Guadagno F.M., Aquino S., De Blasio (2001). The december 1999 Cervinara landslides: further debris flows in the pyroclastic deposits of Campania (Southern Italy). *Bull. Eng. Geol. Env.*, **60**, 171-184.
- Fiorillo F., Wilson R.C. (2004). Rainfall induced debris flows in pyroclastic deposits, Campania (southern Italy). *Eng. Geol.*, **75/3-4**, 263-289.
- Firth C., Stewart I., McGuire W.J., Kershaw S., Vita-Finzi C. (1996). Coastal elevation changes in eastern Sicily; implications for volcano instability at Mount Etna. In: McGuire WJ, Jones AP, Neuberg J (eds) Volcano instability on the Earth and other planets. *Geol. Soc. London, Spec. Publ.*, **110**, 153–167.
- FISRWG (1998). Stream Corridor Restoration: Principles, Processes, and Practices. By the Federal Interagency Stream Restoration Working Group (FISRWG)(15 Federal agencies of the US gov't). GPO Item No. 0120-A; SuDocs No. A 57.6/2:EN 3/PT.653. ISBN-0-934213-59-3. [http://www.usda.gov/stream\\_restoration/](http://www.usda.gov/stream_restoration/)
- Flageollet J.C., Maquaire O., Weber D. (1996). Final national report. In: Dikau, R., Schrott, L., Dehn, M., Hennrich, K., Rasemann, S. (Eds.), The Temporal Stability and Activity of Landslides in Europe with respect to Climatic Change (TESLEC). Final Report: Part II. National Reports. European Commission-Environment Programme (Ct) EV5V-CT94- 0454., pp. 27–86. Unpublished.
- Fleming R.W., Spencer G.S., Banks D.C. (1970). Empirical behaviour of clay shale slopes. US Army Eng. Nuclear Cratering Group (NCG), Tech. Rep., 15, 1 and 2.
- Follaci, J.P., (1999). Seize ans de surveillance du glissement de la Clapière (Alpes Maritimes). *Bull. Lab. Ponts Chaussées*, **220**, 35–51.
- Forcella, F., Gallazzi, D., Montrasio, A., Notarpietro, A. (1982). Note illustrative relative all'evoluzione neotettonica dei Fogli 6 – Passo dello Spluga, 7 – Pizzo Bernina, 8 – Bormio, 17 – Chiavenna, 18 – Sondrio, 19 – Tirano. *Contributi alla realizzazione della Carta Neotettonica d'Italia. Progetto Finalizzato Geodinamica*, vol. **513**, 239–288 (in Italian).
- Francis P.W., Wells G.L. (1988). Landsat Thematic Mapper observations of debris avalanche deposits in the Central Andes. *Bull. Volcanol.*, **50**, 258-278.
-

- Frank D. (1983). Origin, distribution, and rapid removal of hydrothermally formed clay at Mount Baker, *U.S. Geol. Surv. Prof. Pap.*, Washington, **1022-B**, pp. 31.
- Frank D., (1995). Surficial extent and conceptual model of hydrothermal system at Mount Rainier. *J. Volcanol. Geotherm. Res.*, **65**, 51-80.
- Frattini P., Crosta G.B. (2007). Hydrological monitoring at the slope scale. In *Landslides: from Mapping to Loss and Risk Estimation*, Crosta G.B., Frattini P. (eds). IUSS Press: Pavia; 1-7.
- Frattini P., Crosta G.B., Fusi N., Dal Negro P. (2004). Shallow landslides in pyroclastic soils: a distributed modeling approach for hazard assessment. *Eng. Geol.*, **73**, 277-295.
- Frattini P., Crosta G.B., Sosio R. (2009). Approaches for defining thresholds and return periods for rainfall-triggered shallow landslides. *Hydrological Processes*, **23(10)**, 1444-1460.
- Fredlund D.G., Morgenstern N.R. (1977). Stress state variables for unsaturated soils. *J. Geotech. Eng. Div., Am. Soc. Civ. Eng.*, **103(5)**, 447-466.
- Fredlund D.G., Rahardjo H. (1987). Soil mechanics principles for highway engineering in arid regions. Transportation Research Board. *Transport Research Record*, **1137**, 1-11.
- Fredlund D.G., Rahardjo H. (1993). Soil mechanics for unsaturated soils. John Wiley and Sons, INC., New York.
- Fredlund D.G., Xing, A. (1994). Equations for the soil-water characteristic curve. *Can. Geotech. J.*, **31(3)**, 521-532.
- Fredlund M.D., Sillers W.S., Fredlund D.G., Wilson G.W. (1996). Design of a knowledge-based system for unsaturated soil properties. Third Canadian Conference on computing on Civil Engineering, pp. 659-677.
- Freeze R.A. (1974). Streamflow generation. *Rev. Geophys.*, **12**, 627-647.
- Frei C., Schär D., Lüthi and H.C. Davies (1998). Heavy precipitation processes in a warmer climate. *Geophys. Res. Lett.*, **25**, 1431-1434.
- Fuhrer J., Beniston M., Fischlin A., Frei Ch., Goyette S., Jasper K., Pfister Ch. (2006). Climate risks and their impact on agriculture and forests in Switzerland. *Clim. Change*, **79**, 79-102.
- Fukuzono T. (1985). A new method for predicting the failure time of a slope. In Proceedings of the 4th International Conference and Field Workshop on Landslides, Tokyo, Tokyo University Press, 145–150.
- Furlan, V. and Girardet, F. (1991). Pollution atmosphérique et durabilité des pierres de construction. In: *Colloque International, Sur la détérioration des matériaux de construction, La Rochelle*, pp. 79–91.
- Fuster J.M., Arana V., Brandle J.L., Navarro M., Alonso U., Aparicio A. (1968). Geologia y Volcanologia de las Islas Canarias - Tenerife. Madrid: Inst "Lucas Mallada", pp. 218.
- Gajo A., Wood M.D. (1999). Seven-Trent sand: a kinematic hardening constitutive model – the q-p formulation. *Géotechnique*, **49(5)**, 595-614.
-

- Gallipoli D., Gens A., Sharma R., Vaunat J. (2003). An elastoplastic model for unsaturated soil incorporating the effects of suction and degree of saturation on mechanical behaviour. *Geotechnique*, **53**, 123-135.
- Gardner, J.S. (1980). Frequency, magnitude and spatial distribution of mountain rockfalls and rockslides in the Highwood Pass area, Alberta, Canada. In: Coates, D.R., Vitek, J.D. (Eds.), *Thresholds in Geomorphology*. Allen and Unwin, London, 267–295.
- Gardner, J.S., Hewitt, K. (1990). A surge of Bualtar Glacier, Karakoram Range, Pakistan: a possible landslide trigger. *Journal of Glaciology* **36**, 159–162.
- Gasparre A., Nishimura S., Coop M.R., Jardine R.J. (2007). The influence of structure on yield behaviour of London clay. *Géotechnique*, **57(1)**, 19-31.
- Gatto L.W. (1995). Soil freeze-thaw effects on bank erodibility and stability. USACE, Cold Regions Research and Engineering Laboratory, Special Report 95-24, Hanover, NH.
- Gens A., Alonso E.E., Sánchez M., Guimarães L., Olivella S. (2002). Modelling approaches used for the EBS: the FEBEX II project. INIST-CNRS. **19954**, 135-144. ISSN 1018-5593.
- Gens A., Vaunat J., Garitte B. (2005). Elastoplastic modeling of hard soils and soft rocks: formulation and application. Proc. 8<sup>th</sup> Int. Conf. On Computational Plasticity, COMPLAS VIII, Onate E. and Owend D.R.J. editors, CIMNE, Barcelona, 47-50.
- Gens, A., Nova, R. (1993). Conceptual bases for a constitutive model for bonded soils and weak rocks. Proc. of Int. Symp. on Geotechnical Engineering of Hard Soils-Soft Rocks, Anagnostopoulos A., Schlosser F., Kalteziotis N. and Frank R. editors, Athens, 1, Balkema, 485-494.
- Geographical Survey Institute, <http://www.gsj.go.jp/English/index.html>
- Geological Survey of Japan, Catalogue of geological maps, Quadrangle series 1/50,000. [http://www.gsj.jp/Map/index\\_e.html](http://www.gsj.jp/Map/index_e.html)
- Georgiannou V.N. Burland J.B., Hight D.W. (1990). The undrained behaviour of clayey sands in triaxial compression and extension. *Géotechnique*, **40(3)**, 431-449.
- Georgiannou V.N., Burland J.B. (2001). A laboratory study of post-rupture strength. *Géotechnique*, **51(8)**, 665-675.
- Georgiannou V.N., Burland J.B. (2006). A laboratory study of slip surface formation in intact natural stiff clay. *Géotechnique*, **56(8)**, 551-559.
- Gerolymos, N. (2009). The Nikawa (1995) and Higashi – Takezawa (2004): Modelling and Numerical Analysis. Proceedings of the 3rd Greek-Japan Workshop: Seismic Design, Observation and Retrofit of Foundations. Santorini.
- Gerolymos, N., Gazetas, G. (2007). Seismic Triggering, Evolution and Deposition of Massive Landslides: The Case of Higashi–Takezawa (2004). Proceedings of the 4th International Conference on Earthquake and Geotechnical Engineering (ICEGE), Thessaloniki, Greece, June 25–28.
- Ghandi S.R. (2005). Design and maintenance of ash pond for fly ash disposal. Proc. Indian Geotechnical Conference-2005, Ahmedabad, India, **1**, 85-90.
-

Giardino J.R., Shroder J.F., Vitek J.D. (1987). Rock glaciers. Allen and Unwin, Boston: 355 pp.

Gili J.A., Corominas J. (1992). Aplicacion de tecnicas fotogrametricas y topograficas en la auscultacion de algunos deslizamientos. III Simposio Nacional sobre Taludes y Laderas Inestables. La Coruna. **3**, 941–952.

Giorgi F., Mearns L. (1991). Approaches to regional climate change simulation: A review. *Review of Geophysics*, **29**, 191–216.

Giudici F., Semenza E. (1960). “Studio geologic del serbatoio del Vajont”. Unpublished Report, Part A, text, 21 pp.; Part B, photographs, 68 with discussions, 42 pp.; 2 maps and sections prepared in 1959 (scale 1: 5000).

Glade T. (1998). Establishing the frequency and magnitude of landslide-triggering rainstorm events in New Zealand. *Environmental Geology*, **35(2-3)**, Springer-Verlag.

Glicken H. (1991). Sedimentary architecture of large volcanic-debris avalanches. In: Fisher RV, Smith GA (eds) Sedimentation in volcanic settings, SEPM Spec Pub **45**, 99-106.

Glicken H., Voight B., Janda R.J. (1981). Rockslide–debris avalanche of May 18, 1980, Mount St. Helens volcano. IAVCEI Symp Arc Volc, Tokyo and Hakone, **QE521.5A12**, 109–110.

Gomez-Alarcon, G., Cilleros, B., Flores, M. Lorenzo, J. (1995). Microbial communities and alteration processes in monuments at Alcala de Henares, Spain. *The Science of the Total Environment* **167**, 231–239.

Goodman R.E. (1997). Block theory and its application. *Géotechnique*, **45(3)**, 383-423.

Goodman, R. E., Bray, J. (1976) Toppling of rock slopes. *ASCE, Proc. Specialty Conf. on Rock Eng. for Foundations and Slopes*, Boulder, CO, 2, 201–34.

Goodman, R.E. (1989). *Rock Mechanics*, 2<sup>nd</sup> edition, John-Wiley, 141 pp..

Gorshkov G.S. (1959). Gigantic eruption of the Volcano Bezymianny. *Bull Volcanol.*, **20**, 77-109.

Goto S., Nishio S., Yoshimi Y. (1994). Dynamic properties of gravels sampled by ground freezing. Ground failures under seismic conditions: Proc. of sessions sponsored by ASCE in conjunction with the ASCE National Convention in Atlanta, Georgia.

Grammatikopoulou A., Zdravkovic L., Potts D.M. (2007). The effect of the yield and plastic potential deviatoric surfaces on the failure height of an embankment. *Géotechnique*, **57(10)**, 795-806.

Gray D.H., Megahan W.P. (1981). Forest vegetation removal and slope stability in the Idaho Batholith. *USDA For. Serv. Res. Paper INT*, **127**, pp. 23.

Green W.H., Ampt G.A. (1911). Studies on soil physics: 1. Flow of air and water through soils. *J. Agric. Sci.*, **4**, 1-24.

Gregoretti C. (2000). The initiation of debris flow at high slopes: experimental results. *J. Hyd. Res.*, **38(2)**, 83-88.

Griffiths D.V. and Lane P.A. (1999). Slope stability analysis by finite elements. *Geotechnique*, **49(3)**, 387–403.

---

Griffiths P.G., Webb R.H., Melis T.S. (1997). Initiation of debris flows in tributaries of the Colorado River in Grand Canyon, Arizona. Chen C (ed) Proceedings First International Conference on Debris Flow Hazards Mitigation: Mechanics, Prediction and Assessment 12–20.

Grøneng G., Christiansen H.H., Nilsen B. and Blikra L.H., (2010). Meteorological effects on seasonal displacements of the Åknes rockslide, western Norway *Landslides*, published online DOI: 10.1007/s10346-010-0224-x

Gruner E.C. (1969). Vigilance over reservoirs. *Water and Water Engineering*, September, 369-373.

Gu W.H., Morgenstern N.T., Robertson P.K. (1993). Progressive failure of the Lower San Fernando Dam. *Journal of Geot. Eng. Div., ASCE*, **119**, 333-348.

Guadagno F.M. (1991). Debris flows in the Campanian volcanoclastic soil. Proc. Int. Conf. on Slope Stability. Thomas Telford, London, pp. 125–130.

Guadagno F.M., Revellino P. (2005). Debris avalanches and debris flows of the Campania Region (Southern Italy). In: Debris-Flow Hazard and Related Phenomena. Matthias Jacob and Oldric Hungr (eds.), Springer and Praxis editorials.

Gucwa P.R., Kehle R.O., (1978). Bearpaw Mountains rockslide, Montana, USA, in *Rockslides and Avalanches, 1: Natural Phenomena*, edited by B. Voight, pp. 393-421, Elsevier Science, New York.

Gudheus G., Wichter L. (1977). Case study of a landslide in jointed and layered red marl. Proc. Int. Symp. on The Geotechnics of Structurally Complex Formations, Capri, 1, 269-280.

Guglielmi Y., Cappa F. and Binet S. (2005). Coupling between hydrogeology and deformation of mountainous rock slopes: insights from La Clapiere area (southern Alps, France). *Geosciences*, **337**, 1154–1163.

Guglielmi, Y., Bertrand, C., Compagnon, F., Follacci, J.P. Mudry, J. (2000). Acquisition of water chemistry in a mobile fissured basement massif: its role in the hydrogeological knowledge of the La Clapière Landslide (Mercantour massif, southern alps, France). *J. Hydrol.*, **229**, 138–148.

Guglielmi, Y., Bertrand, C., Compagnon, F., Follacci, J.P., Mudry, J. (2000). Acquisition of water chemistry in a mobile fissured basement massif: its role in the hydrogeological knowledge of the La Clapiere landslide (Mercantour massif, southern Alps, France). *J. Hydrology*, **229**, 138-148

Guglielmi, Y., Vengeon, J.M., Bertrand, C., Mudry, J., Follacci, J.P., Giraud, A. (2002). Hydrogeochemistry: An investigation tool to evaluate infiltration into large moving rock masses (case study of La Clapière and Séchilienne alpine landslides). *Bulletin of Engineering Geology and the Environment*, **61(4)**, 311-324.

Gupta, A.S., Seshagiri Rao, K., (2000). Weathering effects on the strength and deformational behaviour of crystalline rocks under uniaxial compression state. *Eng. Geol.*, **56**, 257-274.

Guzzetti, F. (2000). Landslide fatalities and the evaluation of landslide risk in Italy. *Engineering Geology* **58**, 89-107.

---

- Gysel, M. (2002) Anhydrite dissolution phenomena: three case histories of anhydrite karst caused by water tunnel operation. *Rock Mech. Rock Eng.*, **35(1)**, 1-21.
- Haberfield C.M. (1998). Panel Report: towards a universal approach to soil and rock engineering: fact or fallacy. Proc. 2<sup>nd</sup> Int. Symp. on The Geotechnics of Hard Soils-Soft Rocks, Evangelista A. and Picarelli L. editors, Naples, Balkema, 1403-1409.
- Haerberli W. (1985). Creep of mountain permafrost; internal structure and flow of alpine rock glaciers. *Mitteilungen der Versuchsanstalt für Wasserbau, Hydrologie und Glaziologie*. ETH, Zürich, Switzerland, 77. 142.
- Haerberli W. (1990). Permafrost. In VAW (ed.), *Schnee, Eis und Wasser der Alpen in einer wärmeren Atmosphäre*, *Mitteilungen der Versuchsanstalt für Wasserbau, Hydrologie und Glaziologie*, ETH Zürich 108, 71-88.
- Haerberli W. (1992). Construction, environmental problems and natural hazards in periglacial mountain belts. *Permafrost and Periglacial Processes*, **3**, 111-124.
- Haerberli W., Hallet B., Arenson L., Elconin R., Humlum O., Käab A., Kaufmann V., Ladanyi B., Matsuoka N., Springman S.M., Vonder Mühll D. (2006). Permafrost Creep and Rock Glacier Dynamics. Final Report of the IPA/ICSI Task Force. *Permafrost and Periglacial Processes*, **17(3)**, 189-214.
- Haerberli W., Hoelzle M., Keller F., Schmid W., Vonder Mühll D., Wagner S. (1993). Monitoring the long-term evolution of mountain permafrost in the Swiss Alps. *Proceedings of the 6th International Conference on Permafrost*, Beijing, 214-219.
- Haerberli W., Rickenmann, M., Zimmermann M. (1990). Investigation of the 1987 debris flows in the Swiss Alps: general concept and geophysical soundings. *Hydrology in Mountainous regions, II – Artificial Reservoirs; Water and Slopes (Proceedings of two Lausanne Symposia, August 1990)*. IAHS Publ. 194.
- Haerberli W., Wegmann M., Vonder Mühll, D.S. (1997). Slope stability problems related to glacier shrinkage and permafrost degradation in the Alps. *Eclogae Geologicae Helveticae*, **90(3)**, 407-414.
- Hansford M., Lynch D. (2010a). Catch fence failure probed in fatal Italian rail disaster. *New Civil Engineer*, 15/04/2010, pag.5.
- Hansford M., Lynch D. (2010b). Catch fence fails to stop landslide topping Italian commuter train. *Ground Engineering*, May 2010, pag.4.
- Hanzawa H. (1980). Undrained strength and stability analysis for a quick sand. *Soils and Foundations*, **20(2)**, 17-29.
- Hanzawa H., Fukaya T., Suzuki K. (1990). Evaluation of engineering properties for an Ariake clay. *Soils and Foundations*, **30(4)**, 11-24.
- Harp E.L., Wells W.G., Sarmiento J.G. (1990). Pore pressure response during failure in soils. *Geol. Soc. Am. Bull.*, **102(4)**, 428-438.
- Harp, E.L., Reid M.E., McKenna J.P., J. Michael A. (2009). Mapping of hazard from rainfall-triggered landslides in developing countries: Examples from Honduras and Micronesia. *Eng. Geol.*, **104**, 295-311.
- Harr R.D. (1977). Water flux in soil and subsoil on a steep forested slope. *J. Hydrol.*, **33**, 37-58.
-

- Harris C., Arenson L.U., Christiansen H.H., Etzelmüller B., Frauenfelder R., Gruber S., Haeberli W., Hauck C., Hölzle M., Humlum O., Isaksen K., Kääh A., Kern-Lütschg M.A., Lehning, M., Matsuoka, N., Murton, J.B., Nötzli, J., Phillips, M., Ross, N., Seppälä, N., Springman S.M., Vonder Mühll, D. (2009). Permafrost and climate in Europe: Monitoring and modelling thermal, geomorphological and geotechnical responses. *Earth Science reviews*, **92(3-4)**, 117-171.
- Harris C., Vonder Mühll D., Isaksen K., Haeberli W., Sollid J.L., King L., Holmlund P., Dramis F., Guglielmin M., and Palacios D. (2003). Warming permafrost in European mountains. *Global Planet. Change*, **39**, 215-225.
- Hassell D., Boorman P., McDonald R., Hill S. (2002). Climate change scenarios for the United Kingdom: the UKCIP02 scientific report. Centre for Climate Change Research, School of Environmental Sciences, University of East Anglia, Norwich.
- Hauck C., Guglielmin M., Isaksen K., Vonder Mühll D. (2001). Applicability of frequency domain and time-domain electromagnetic methods. *Permafrost Periglac. Process*, **12(1)**, 39–52.
- Haverkamp R., Parlange J.Y. (1986). Predicting the water retention curve from particle-size distribution, **1**. Sandy soils without organic matter. *Soil Science*. **142**, 325–339.
- Hegg U. (1984). Case history of a large coastal landslide in Pliocene Clays. Proc. 4<sup>th</sup> Int. Symposium on Landslides, Toronto, 2, 97-102.
- Hencher S.R. (1987). The implications of joints and structures for slope stability. Slope Stability: Geotechnical Engineering and Geomorphology, Anderson M.G. and Richards K.S. editors, John Wiley and Sons, 145-186.
- Hencher S.R. 2010. Preferential flow paths through soil and rock and their association with landslides. *Hydrological Processes*, **24**, 1660–1671.
- Hendron Jr. A.J., Patton F.D. (1985). The Vaiont slide, a geotechnical analysis based on new geologic observations of the failure surface. Technical Report GL-85-5, Department of the Army, U.S. Army Corps of Engineers, Washington D.C., 2 volumes.
- Hendron Jr. A.J., Patton F.D. (1985). The Vaiont slide, a geotechnical analysis based on new geologic observations of the failure surface. Technical Report GL-85-5, Department of the Army, U.S. Army Corps of Engineers, Washington D.C., 2 volumes.
- Henkel D.J. (1960). The shear strength of saturated remoulded clays. Proc. of the ASCE Res. Conf. on Shear Strength of Cohesive Soils, Boulder, Colorado, 533-554.
- Hietaranta, J., Liira, T. (1995). Lichenometry: dating the weathering processes in the Kevojoki river valley, Northern Finland. *Publications-Institute Geographici Universitatis Turkuensis* **147**, 111–121.
- Hight, D.W., Boese, R., Butcher, A.P., Clayton, C.R.I., Smith, P.R. (1992). Disturbance of the Bothkennar clay prior to laboratory testing. *Géotechnique*, **42(2)**, 199-217.
- Hillel D. (1998). Environmental Soil Physics: Fundamentals, Applications, and Environmental Considerations, Elsevier, New York.
- Hinchberger S.D., Qu G. (2009). Viscoplastic constitutive approach for rate-sensitive structured clays. *Can. Geotech. J.*, **46**, 609-626.
-

Hinchliffe, S., Ballantyne, C.K. (1999). Talus accumulation and rockwall retreat, Trotternish, Isle of Skye, Scotland. *Scottish Geographical Journal* **115**, 53–70.

Hoblitt R.P., Miller C.D., Vallance, J.W. (1981). Origin and stratigraphy of the deposit produced by the May 18 directed blast: in Lipman, P.W., and Mullineaux, D.R., eds., The 1980 eruptions of Mount St. Helens, Washington: *U.S. Geol. Surv. Prof. Pap.*, **1250**, 401-420.

Hoek E. (1983). Strength of jointed rock masses. *Géotechnique*, **33(3)**, 187-223.

Hoek E. (1990). Estimating Mohr-Coulomb friction and cohesion values from the Hoek-Brown failure criterion. *Int. Journ. Rock Mech. and Mining Sci. & Geomechanics Abstracts* **12(3)**, 227-229.

Hoek E. (1994). Strength of rock and rock masses. *ISRM News Journal*, **2(2)**, 4-16.

Hoek E., Bray J.W. (1981). *Rock Slope Engineering*. Institution of Mining and Metallurgy, London, 358 pp.

Hoek E., Brown E.T. (1980a). *Underground Excavation in Rock*. Institution of Mining and Metallurgy, 3d edition, London, 527 pp.

Hoek E., Brown E.T. (1980b). Empirical strength criterion for rock masses. *J. of Geot. Eng. Div., ASCE*, **106, GT9**, 1013-1035.

Hoek E., Brown E.T. (1988). The Hoek-Brown failure criterion – a 1988 update. *Proc. 15<sup>th</sup> Canadian Rock Mech. Symp.*, Curran J.C. editor, Dept. Civ. Eng., University of Toronto Toronto, 31-38.

Hoek E., Brown E.T. (1997). Practical estimates of rock mass strength. *Int. Journ. Rock Mech. and Mining Sci. and Geomech. Abstracts* **34(8)**, 1165-1186.

Hoek E., Kaiser P.K., Bawden W.F. (1995). *Support of underground excavations in hard rock*. Balkema, Rotterdam.

Hoek E., Marinos P. (2000). Predicting tunnel squeezing. *Tunnels and Tunnelling International*, Part 1 – November, Part 2 – December.

Hoek E., Marinos P., Benissi M (1998). Applicability of the Geological Strength Index (GSI) classification for very weak and sheared rock masses – The cases of the Athens Scist Formation. *Bull. Eng. Geol. Env.*, **57(2)**, 151-160.

Hoek E., Wood D., Shah S. (1992). A modified Hoek-Brown criterion for jointed rock masses. *Proc. Rock Characterization Symp. Int. Soc. Rock Mech., Eurock '92*, Hudson J.A. editor, British Geot. Soc., London, 209-214.

Hoek, E, Brown, E.T. (1988). The Hoek-Brown failure criterion - a 1988 update. *Proc. 15<sup>th</sup> Canadian Rock Mech. Symp.* (ed. J.H. Curran), pp. 31-38. Toronto: Civil Engineering Dept., University of Toronto.

Hoek, E., Carranza-Torres, C., Corkum, B. (2002). The Hoek–Brown failure criterion — 2002 edition, 5<sup>th</sup> North American Rock Mechanics Symposium and 17<sup>th</sup> Tunneling Association of Canada Conference: NARMS-TAC, Toronto, 267–271.

Hoek, E., Kaiser, P.K. Bawden. W.F. (1995). *Support of underground excavations in hard rock*. Rotterdam: Balkema.

---

- Hoek, E., Diedericks M.S. (2006). Empirical estimation of rock mass modulus. *Int. Journ. of Rock Mechanics and Mining Sciences*, **43**, 203-215.
- Hoelzle M. (1996). Mapping and modelling of mountain permafrost distribution in the Alps. *Geografisk Tidsskrift – Norwegian Journal of Geography*, **50(1)**, 11-15.
- Hoelzle M., Haeberli W. (1995). Simulating the effects of mean annual airtemperature distribution and glacier size: an example from the Upper Engadine, Swiss Alps. *Ann. Glaciol.*, **21**, 399-405.
- Hofmann B.A. (1997). In situ ground freezing to obtain undisturbed samples of loose sand for liquefaction assessment. PhD thesis, University of Alberta, Canada.
- Hofmann H.J. (1966). Deformational structures near Cincinnati, Ohio. *Bull. Geol. Soc. Am.*, **77**, 533-548.
- Holm K, Bovis M, Jakob M. (2004). The landslide response of alpine basins to post-Little Ice Age glacial thinning and retreat in south-western British Columbia. *Geomorphology*, **57(3-4)**, 201-216.
- Hong Y, Hiura H, Shino K, Sassa K, Suemine A, Fukuoka H, Wang G (2005) The influence of intense rainfall on the activity of large-scale crystalline schist landslides in Shikoku Island, Japan. *Landslides* **2**, 97-105. DOI 10.1007/s10346-004-0043-z
- Hooke J.M. (1979). An analysis of the processes of river bank erosion. *J. Hydrol.*, **42**, 39-62.
- Horton R.E. (1940). An approach toward the physical interpretation of infiltration-capacity. *Soil Sci. Soc. Am. Proc.*, **5**, 399-417.
- Houlsby G.T. (1997). The work input to an unsaturated granular material. *Geotechnique*, **47**, 193-196.
- Houpert R. (1974). Le role du temps dans le comportement à la rupture des roches. 3<sup>rd</sup> Int. Congress Rock Mech., Denver, 2A, 325-329.
- Hsü K.J. (1975). Catastrophic debris streams generated by rock falls. *Bull. Geol. Soc. Am.*, **86**, 129-140.
- Hu X.W., Tang H.M., Liu Y.R. (2005). Physical model studies on stability of Zhaoshuling landslide in area of the Three Gorges Reservoir. *Chinese Journal of Rock Mechanics and Engineering*, **24(12)**, 2,089-2,095.
- Hu, X.W. (2008). The proposal for the Open Fund of the State Key Laboratory of the Geohazards Prevention and Geoenvironment Protection. Southwest Jiaotong University, China.
- Humphrey N.F. (1983). Pore pressure in debris flow initiation. M.S. thesis, 169 pp., Univ. of Wash., Seattle.
- Hungr, O., Evans, S., Bovis, M.I., Hutchinson, I.N. (2001). A review of classification of landslides of the flow type. *Environ. Eng. Geosci.*, **7**, 221-238.
- Hurley D.G., Pantelis G. (1985). Unsaturated and saturated flow through a thin porous layer on a hillslope, *Water Resour. Res.*, **21**, 821-824.
-

- Hürlimann M., Garcia-Piera J.O., Ledesma A. (2000b). Causes and mobility of large volcanic landslides: application to Tenerife, Canary Islands. *J. Volcanol. Geotherm. Res.*, **103(1-4)**, 121–134.
- Hürlimann M., Ledesma A., Martí', J. (1997). Analysis of large landslides triggered by volcanic activity. Application to Tenerife (Canary Islands). In: Pawlowsky-Glahn, V. Ed., IAMG CIMNE, Barcelona, pp. 274–279.
- Hürlimann M., Martí', J., Ledesma, A. (2000a). Mechanical relationship between catastrophic volcanic landslides and caldera collapse. *Geophys. Res. Lett.*, **27**, 2393-2396.
- Hürlimann M., Turon E., Martí' J. (1999). Large landslides triggered by caldera collapse events in Tenerife, Canary Islands. *Phys Chem Earth*, **24**, 921-924.
- Hutchinson J.M. (1975). The response of London clay cliffs to differing rates of toe erosion. Building Research Establishment Current Paper 27/75, Watford, U.K.
- Hutchinson J.N. (1967). The free degradation of London clay cliffs. *Proc. Geot. Conf. Oslo*, **1**, 113-118.
- Hutchinson J.N. (1988). Morphology and geotechnical parameters of landslides in relation to geology and hydrogeology. *Proceedings 5<sup>th</sup> Int. Symp. on Landslides*, Lousanne 1, Balkema, 3-35.
- Hutchinson J.N. (1998). Morphological and geotechnical parameters of landslides in relation to geology and hydrogeology. IN: Bonnard C. (Ed.), *Proc. 5th Int. Symp. On Landslides*. Lousanne, vol. 1. Balkema, Rotterdam, pp. 3-36.
- Hutchinson J.N. (2004). Review of flow-like mass movements in granular and fine-grained materials. KeyNote Lecture, atti Int. Workshop on “Occurrence and Mechanisms of Flows in Natural Slopes and Earthfills”, L. Picarelli ed., Sorrento: 3-16. Patron, Bologna
- Hutchinson J.N., Bhandari R.H. (1971). Undrained loading, a fundamental mechanism of mudflows and other mass movements. *Geotechnique*, **21**, 353-358.
- Hutchinson, J.N. (1994). Some aspects of the morphological and geotechnical parameters of landslides, with examples drawn from Italy and elsewhere. *Geologica Romana*, **30**, 1-14.
- Hutchinson, J.N., Del Prete, M. (1985). Landslide at Calitri, southern Apennines, reactivated by the earthquake of 23rd November 1980. *Geol. Appl. Idrogeol.*, **XX(1)**, 9-38.
- Ibsen ML, Casagli N (2004). Rainfall patterns and related landslide incidence in the Porretta-Vergato region, Italy. *Landslides*, **1(2)**, 143–150.
- Ikeda S., Parker G., Sawai K. (1981). Bend theory of river meanders. Part 1: Linear development. *J. Fluid Mech.*, **112**, 363-377.
- Imhof M. (1996). Modelling and verification of the permafrost distribution in the Bernese Alps (Western Switzerland). *Permafrost and Periglacial Processes*, **7(3)**, 267-280.
- Indraratna B., Haque A., Aziz N. (1998). Effect of infill on the shear behaviour of soft joints. *Proc. 2<sup>nd</sup> Int. Symp. on The Geotechnics of Hard Soils-Soft Rocks*, Evangelista A. and Picarelli L. editors, Naples, Balkema, 199-206.
- Inigo, A.C. Vicente-Tavera, S. (2001). Different degrees of stone decay on the inner and outer walls of a cloister. *Building and Environment*, **36**, 911–917.
-

- IPCC. (2007). *Climate Change 2007: Impacts, Adaptation and Vulnerability. Contribution of Working Group II to the Fourth Assessment Report of the Intergovernmental Panel on Climate Change*. Cambridge, UK, Cambridge University Press., pp. 976. <http://www.ipcc.ch/ipccreports/ar4-wg2.htm>
- Isaksen K., Sollid J.L., Holmlund P., Harris C. (2007). Recent warming of mountain permafrost in Svalbard and Scandinavia. *J. Geophys. Res.*, **112**, F02S04.
- Ishihara K. (1993). Liquefaction and flow failure during earthquakes. *Géotechnique*, **43(3)**, 351-415.
- Ishihara K., Tatsuoka F., Yasuda S. (1975). Undrained deformation and liquefaction of sand under cyclic stresses. *Soils and Foundations*, **15(1)**, 29-44.
- Ishihara, K. (1996). *Soil Behaviour in Earthquake Geotechnics*, Clarendon, London, 350 pp.
- Iverson R.M. (2000). Landslide triggering by rain infiltration. *Water Resour. Res.*, **36**, 1897-1910.
- Iverson R.M. (2005). Regulation of landslide motion by dilatancy and pore pressure feedback. *Journal of Geophysical Research*, **110**, F02015.
- Iverson R.M., LaHusen R.G. (1989). Dynamic pore-pressure fluctuations in rapidly shearing granular materials. *Science*, **246(4931)**, 796-799.
- Iverson R.M., Major J.J. (1986). Groundwater seepage vectors and the potential for hillslope failure and debris-flow mobilization. *Water Resour. Res.*, **22(11)**, 1543-1548.
- Iverson R.M., Major J.J. (1987). Rainfall, groundwater flow, and seasonal motion at Minor Creek landslide, northwestern California: Physical interpretation of empirical relations. *Geol. Soc. Am. Bull.*, **99**, 579–594.
- Iverson R.M., Reid M.E., Iverson N.R., LaHusen R.G., Logan M., Mann J.E., Brien D.L. (2000). Acute sensitivity of landslide rates to initial soil porosity. *Science*, **290**, 513-516.
- Iverson R.M., Reid M.E., LaHusen R.G. (1997). Debris-flow mobilization from landslides. *Annu. Rev. Earth Planet. Sci.*, **25**, 85-138.
- Ivy-Ochs, S., Schäfer, J., Kubik, P.W., Synal, H.-A., Schlüchter, C. (2004). Timing of deglaciation on the northern Alpine foreland (Switzerland). *Eclogae Geologicae Helvetiae* **97**, 47–55.
- Jaboyedoff, M., Baillifard, F., Bardou, E., Girod, F. (2004). The effect of weathering on Alpine rock instability. *Quarterly Journal of Engineering Geology and Hydrogeology* **37**, 95–103.
- Jackson R.J. (1966). Slips in relation to rainfall and soil characteristics. *J. Hydrol. (NZ)*, **5**, 45-53.
- Janbu N. (1977). Slopes and excavations in normally and lightly overconsolidated clays. Proc. 9<sup>th</sup> Int. Conf. on S.M.F.E., Tokyo, **2**, 549-566.
- Janbu N., Nestvold J., Grande L. (1995). Winter slides - a new trend in Norway. In: Bell, D.H. Ed., Proc. 6th Int. Symposium on Landslides. Landslides, **3** Balkema, Rotterdam, pp. 1581–1586.
-

Japan Society for Civil Engineers (JSCE) (2007). Earthquake damage in active-folding areas –Creation of a comprehensive data archive and suggestions for its application to remedial measures for civil-infrastructure systems –. Report of JSCE by Special Coordination Funds for Promoting Science and Technology. Japan Science and Technology Agency (in Japanese).

Japan Society of Civil Engineers, JSCE, (2001). The January 13, 2001 Off the Coast of El Salvador Earthquake, Tokyo, Japan, 112pp.

Jardine R.S. (1992). Some observations on the kinematic nature of soil stiffness. *Soils and Foundations*, **32(2)**, 111-124.

Jardine R.S., St John N.D., Hight D.W., Potts D.M. (1991). Some practical applications of a non-linear ground model. Proc. 10<sup>th</sup> ECSMFE, Florence, **1**, 223-228.

Jarman, D. (2006). Large rock slope failures in the Highlands of Scotland: Characterisation, causes and spatial distribution. *Engineering Geology* **83**, 161– 182.

Jefferies M.B. (1993). Nor-sand: a simple critical state model for sand. *Géotechnique*, **43(2)**, 91-103.

Jenkins A, Ashworth PJ, Ferguson RI, Grieve IC, Rowling P, Stott TA. (1988). Slope failures in the Ochil hills, Scotland, November 1984. *Earth Surf. Processes and Landforms*, **13**, 69–76.

Jia GW, Tony L T Zhan, Chen YM, Fredlund DG (2009). Performance of a large-scale slope model subjected to rising and lowering water levels. *Eng Geol.*, **106**, 92–103.

Jiang J., Ehret D., Xiang W., Rohn J., Huang L., Yan S, Bi R. (2010). Numerical simulation of Qiaotou Landslide deformation caused by drawdown of the Three Gorges Reservoir, China. *Environmental Earth Sciences*. published online. 10.1007/s12665-010-0536-0

Jin D.L. Wang G.F. (1988). Tangyanguang landslide in Zhaxi Reservoir, Hunan Province, China, Typical Landslides Occurred in China, Science press, Beijing, 301–307 (in Chinese).

JMA. Japan Meteorological Agency.  
<http://www.seisvol.kishou.go.jp/eq/kyoshin/jishin/index.html>.

Johannesson H. (1985). Computer simulation of migration of meandering rivers. PhD thesis, Dept. of Civil Engineering, Univ. of Minnesota, St. Paul, Minn.

Johnson A.M., Rodine J.R. (1984). Debris flow. In Slope stability. Edited by D. Brunsten and D.B. Prior. John Wiley & Sons, New York, N.Y. pp. 257–361.

Johnson K.A., Sitar N. (1990). Hydrologic conditions leading to debris-flow initiation. *Can. Geotech. J.*, **27**, 789-801.

Johnson, K.S. (2005). Subsidence hazards due to evaporite dissolution in the United States. *Environ. Geol.*, **48**, 395-409.

Johnston, I.W. (1991). Geomechanics and the emergence of soft rock technology. EH Davis Memorial, Australian Geomechanics, 21, 3-26.

Jones F.O., Embody D.R. and Peterson W.L. (1961). Landslides along the Columbia River Valley, Northeastern Washington. U.S. Geological Survey, Professional Paper **367**, pp 98.

---

- Kabbaj, M., Tavenas, F., Leroueil, S. (1988). In situ and laboratory stress-strain relationships. *Géotechnique*, **38(1)**, 83-100.
- Kaliser B.N., R.W. Fleming (1986). The 1983 landslide dam at Thistle, Utah. In: R.L. Schuster, Editor, Proceedings: Landslide Dams; Processes, Risk, and Mitigation, Geotechnical Special Publication, **3**, 59-83.
- Kankare E. (1969). Failures at Kimola floating canal in Southern Finland. Proc. 7<sup>th</sup> Int. Conf. on S.M.F.E., Mexico City, **3**, 609-616.
- Karstunen M., Krenn H., Wheeler S.J., Koskinen M., Zentar R. (2005). Effect of anisotropy and destructuration on the behaviour of Murro test embankment. *International Journal of Geomechanics*, **5(2)**, 87-97.
- Kasim, M., Shakoor, A., (1996). An investigation of the relationship between uniaxial compressive strength and degradation for selected rock types. *Eng. Geol.*, **44**, 213-227.
- Kavvas, M., Amorosi, A. (2000). A constitutive model for structured soils. *Géotechnique*, **50(3)**, 263-273.
- Keefer D.K., Johnson A.M. (1983). Earth flows-Morphology, mobilization and movement. *U.S. Geological Survey Professional Paper* **1264**.
- Keefer D.K., Wilson R.C., Mark R.K., Brabb E.E., Brown WMIII, Ellen S.D., Harp E.L., Wiczorek G.F., Alger C.S., Zatzkin R.S. (1987). Real-time landslide warning during heavy rainfall. *Science*, **238(13)**, 921-925.
- Keefer, D.K. (2000). Statistical analysis of an earthquake-induced landslide distribution – The 1989 Loma Prieta, California event. *Eng. Geol.*, **58**, 231-249.
- Keefer, D.K. (2002). Investigating landslides caused by earthquakes – A historical review. *Surveys in Geophysics*, **23**, 473-510.
- Keefer, D.K., (1984). Landslides caused by earthquakes, *Geol Soc Am Bull.*, **95**, 406- 421.
- Keller F. (1992). Automated Mapping of Mountain Permafrost using the Program PERMAKAR within the Geographical Information System ARC/INFO. *Permafrost and Periglacial Processes*, **3**, 133-138.
- Kempton K.A., Rowe G.L. (2000). Leakage of Active Crater lake brine through the north flank at Rincón de la Vieja volcano, northwest Costa Rica, and implications for crater collapse. In: Varekamp, J.C., Rowe, Jr., G.L. (Eds.), Crater Lakes. *J. Volcanol. Geotherm. Res.*, **97**, 143-159.
- Kenney T.C. (1967). Shear strength of soft clay. Proc. Of Geotechnical Conference, Oslo, **2**, 49-55.
- Kieffer, D.S., 1998. Rock Slumping: A Compound Failure Mode of Jointed Hard Rock Slopes. PhD Thesis, University of California, Berkeley, 166 pp.
- Kim Y.T., Leroueil S. (2001). Modeling the viscoplastic behaviour of clays during consolidation: Application to Berthierville clay in both laboratory and field conditions. *Can. Geotech. J.*, **38**, 484-497.
- Kimoto S., Oka F. (2005). An elasto-viscoplastic model for clay considering destructuration and consolidation analysis of unstable behaviour. *Soils and Foundations*, **45(2)**, 29-42.
-

- Kinakin, D., Stead, D. (2005). Analysis of the distributions of stress in natural ridge forms: implications for the deformation mechanisms of rock slopes and the formation of a sackung. *Geomorphology*, **65**, 85-100.
- King L., Akerman J. (1993). Mountain Permafrost in Europe, in Permafrost, Proceedings of the sixth International Conference, 2, Beijing, 1022-1027.
- K-net. NIED (National Research Institute for Earth Science and Disaster Prevention. <http://www.knet.bosai.go.jp/k-net/>
- Knighton A.D. (1973). Riverbank erosion in relation to streamflow conditions. *River Bollin-Dean, Cheshire. East Midland Geographer*, **6**, 416-426.
- Kobayashi Y., Harp E.L., Kagawa T. (1990). Simulation of rockfalls triggered by earthquakes. *Rock Mechanics and Rock Engineering*, **23**, 1-20.
- Kokusho T., Ishizawa, T. (2005). Energy approach to slope failures and a case study during 2004 Niigata-ken Chuetsu earthquake. Proceedings of Geotechnical Earthquake Engineering Satellite Conference Osaka, Japan, ISSMGE, 255-262.
- Kokusho, T., Ishizawa, T., Hara, T. (2009). Slope failures during the 2004 Niigataken Chuetsu earthquake in Japan, Earthquake geotechnical case histories for performance-based design – Kokusho (ed), 2009 Taylor and Francis Group, London, ISBN 978-0-415-80484-4.
- Konagai, K., Orense, R.P., Johansson, J. (2009). Las Colinas landslide caused by the 2001 El Salvador Earthquake, Earthquake geotechnical case histories for performance-based design – Kokusho (ed), 2009 Taylor and Francis Group, London, ISBN 978-0-415-80484-4.
- Konrad J.M. (1990a). Minimum undrained strength of two sands. *J. Geotech. Engineering Div. ASCE*, **116**, **GT6**, 932-947.
- Konrad J.M. (1990b). Minimum undrained strength versus steady-state strength of sands. *J. Geotech. Engineering Div. ASCE*, **116**, **GT6**, 948-963.
- Kostiakov A.N. (1932). On the dynamics of the coefficient of water-percolation in soils and on the necessity for studying it from a dynamic point of view for purpose of amelioration, *Trans. Int. Congr. Soil Sci.*, 17-21.
- Kotarba A. (1989). On the age of debris flows in the Tatra Mountains. *Studia Geomorphologica Carpatho-Balcanica* **23**, 139-152.
- Kovacevic N., Hight D.W., Potts D.M. (2004). “Temporary slope stability in London clay – back analyses of two case histories”. Proceedings of a three day Conference on Advances in geotechnical engineering: the Skempton Conference, ICE, London U.K., Jardine R.J., Potts D.M. and Higgins K.G. editors, Thomas Telford, vol. 3 (supplement), 1-14.
- Kramer S.L., Seed H.B. (1988). Initiation of soil liquefaction under static loading conditions. *J. Geotech. Eng.* **114**(4), 412–430.
- Kramer, S.L., Stewart, J.P. (2004). Geotechnical Aspects of Seismic Hazards. In: Earthquake Engineering: from Engineering Seismology to Performance-Based Engineering, Y. Bozorgnia, V. Bertero (Eds.), CRC Press, 4, 85 pp.
- Krysiecki J.M., Bodin X., Schoeneich P. (2008). Collapse of the Bérard Rock Glacier (Southern French Alps). Extended Abstracts, 9th International Conference on Permafrost, University of Alaska Fairbanks, USA, 29.6.-3.7.2008, 153-154.
-

- Ktenidou, O.-J. (2010). Theoretical and instrumental study of site and topographic effects on strong ground motion in Aegion. Ph.D. thesis, Aristotle University Thessaloniki, Greece.
- Ladanyi B., Archambault G. (1970). Simulation of shear behaviour of a jointed rock mass. 11<sup>th</sup> Symp. on Rock Mechanics, published by AIME, New York, 105-125.
- Ladanyi B., Archambault G. (1972). Evaluation de la résistance au cisaillement d'un massif rocheux fragmenté. 24<sup>th</sup> Int. Geological Congress, Montréal, 249-260.
- Ladd, C.C. (1991). Stability evaluation during staged construction. *Journal of Geotechnical Engineering ASCE*, **117(4)**, 540-615.
- Ladd, C.C. (1991). Stability evaluation during staged construction. *Journal of Geotechnical Engineering* 117, n° 4, ASCE, 540-615.
- Ladd, C.C. (1991). Stability evaluation during staged construction. *Journal of Geotechnical Engineering* 117, n° 4, ASCE, 540-615.
- Lade P.V. (1992). Static instability and liquefaction of loose fine sandy slopes. *Journ. of Geotech. Engineering, ASCE*, **118(1)**, 51-71.
- Lade P.V. (1993). Initiation of static instability in the submarine Nerlerk berm. *Can. Geotech. J.*, **30**, 895-904.
- Lade P.V. (1999). Instability of granular materials Physics and Mechanics of Soil Liquefaction, Lade P.V. and Yamamuro J.A. editors, Balkema, 3-16.
- Lade P.V., Kim M.K. (1988). Single hardening constitutive model for frictional materials. III: Comparisons with experimental data. *Comp. Comput. Geotech.*, **6**, 31-47.
- Lade P.V., Pradel D. (1990). Instability and plastic flow of soil. I: Experimental observations. *Journal of Engineering Mechanics, ASCE*, **116(11)**, 2532-2550.
- Lade P.V., Yamamuro J.A. (1997). Effects of non-plastic fines on static liquefaction of sands. *Can. Geotech. J.*, **34**, 905-917.
- Lade P.V., Yamamuro J.A., Liggio Jr C.D. (2009). Effects of fines content on void ratio, compressibility and static liquefaction of silty sand. *Geomechanics and Engineering*, **1(1)**, 1-15.
- Laflamme J.F., Leroueil S. (1999). Analyse des pressions interstitielles mesurées aux sites d'excavation de Saint-Hilaire et de Rivière-Vachon, Quebec. Report GCT-99-10 prepared for the Ministère des Transports du Quebec, Université Laval.
- Lafleur J., Silvestri V., Asselin R., Soulié M. (1888b). Behaviour of a test excavation in soft Champlain Sea clay. *Can. Geotech. J.*, **25**, 705-715.
- Lafleur J., Soulié M., Silvestri V. (1988a). Pression interstitielles autour d'une fouille expérimentale dans l'argile molle. Proc. 5<sup>th</sup> Int. Symp. on Landslides, Lausanne, **1**, 707-712.
- Lagmay A.M.F., van Wyk de Vries B., Kerle N., Pyle D.M. (2000). Volcano instability induced by strike-slip faulting. *Bull Volcanol.*, **62**, 331-346.
- Lama R.D. (1972). Mechanical behaviour of jointed rock mass. Report K-126, Institute of Soil Mechanics and Rock Mechanics, University of Karlsruhe, Karlsruhe
- Lambe T.W., Whitman R.V. (1968). Soil Mechanics. John Wiley and Sons.
-

- Lambe T.W., Whitman R.V. (1969). *Soil Mechanics*, John Wiley and Sons, New York.
- Lambeck, K., Yokoyama, Y., Purcell, T. (2002). Into and out of the Last Glacial Maximum: sea-level change during Oxygen Isotope Stages 3 and 2. *Quaternary Science Reviews* **21**, 343–360.
- Lane K.S., (1967). Stability of reservoir slopes. In: Charles Fairhurst, Editor, Failure and breakage of rock, Proceedings of the 8th Symposium on Rock Mechanics, September 15–17, 1966, University of Minnesota, Minneapolis, Minnesota, pp. 321–336.
- Lane P.A. and Griffiths D.V. (2000). Assessment of stability of slopes under drawdown conditions. *J. Geotechnical and Geoenvironmental Engineering, ASCE*, **126**(5), 443–450.
- Langendoen E.J. Simon A. (2008). Modeling the Evolution of Incised Streams: II. Streambank Erosion. *J. Hydraul. Eng.*, **134**(7), 905-915.
- Larsen E.W. (1995). Mechanics and modeling of river meander migration. PhD thesis, Univ. of California at Berkeley, Berkeley, Calif.
- Larsson R. (1977). Basic behaviour of Scandinavian soft clays. Report 4, Swedish Geotechnical Institute, Linköping.
- Larsson, R., Bengtsson, P.E., Eriksson, L. (1997). Prediction of settlements of embankments on soft, fine-grained soils – Calculation of settlements and their course with time. Swedish Geotechnical Institute, Linköping.
- Lavallée Y., Stix J., Kennedy B., Richer M., Longpr M.A. (2004). Caldera subsidence in areas of variable topographic relief: results from analogue modeling. *J. Volcanol Geotherm Res.*, **129**, 219-236.
- Lawler D.M. (1986). River bank erosion and the influence of frost: a statistical examination. *Transactions of the Institute of British Geographers New Series*, **11**, 227-242.
- Lawler D.M. (1993). Needle ice processes and sediment mobilization on river banks: the River Ilston, West Glamorgan, UK. *J. Hydrol.*, **150**, 81-114.
- Lazzari A. (1954). Aspetti geologici dei fenomeni verificatesi nel Salernitano in conseguenza del nubifragio del 25-26 ottobre 1954. *Boll. Soc. Nat.*, **63**, 131-142.
- Leach B.A., Medland J.W., Sutherland H.B. (1976). The ultimate bearing capacity of bored piles in weathered Keuper Marl. Proc. 6<sup>th</sup> ECSMFE, Wien, **1**(2), 507-514.
- Lefebvre G., La Rochelle P. (1974). The analysis of two slope failures in cemented Champlain clays. *Can. Geotech. J.*, **11**, 89-108.
- Leong W.K., Chu J., The C.I. (2000). Liquefaction and instability of a granular fill material. *Geotechnical Testing Journal*, **23**(2), 178-192.
- Leroueil S. (1998). Contribution to the Round Table: Peculiar aspects of structured soils. Proc. 2<sup>nd</sup> Int. Symp. on the Geotechnics of Hard Soils – Soft Rocks, Evangelista A. & Picarelli L. editors, Naples, Balkema, 1669-1678.
- Leroueil S. (2001). Natural slopes and cuts: movement and failure mechanism. *Géotechnique*, **51**(3), 197-243.
-

- Leroueil S., Marques M.E.S. (1996). State of the art on the importance of strain rate and temperature effects in geotechnical engineering. Geotechnical Special Publication n° 61, on Measuring and Modeling Time Dependent Soil Behaviour, sponsored by Geo-Institute of ASCE, in conjunction with ASCE Convention in Washington D.C., Sheahan T.C. and Kallakin V.N. editors.
- Leroueil S., Vaughan P.R. (1990). The general and congruent effects of structure in natural soils and weak rocks. *Géotechnique*, **40(3)**, 467-488.
- Leroueil S., Vaunat J., Picarelli L., Locat J., Faure R., Lee H. (1996). A geotechnical characterization of slope movements. Proc. of 7<sup>th</sup> Int. Symp. on Landslides, Senneset K. editor, Trondheim 1, Balkema, 53-74.
- Leroueil, S., Kabbaj, M., Tavenas, F. (1988). Study of the validity of a  $\sigma'_v$ ,  $e_v$ ,  $\dot{e}_v$  model in situ conditions. *Soils and Foundations*, **28(3)**, 13-25.
- Leroueil, S., Kabbaj, M., Tavenas, F., Bouchard, R. (1985). Stress-strain-strain rate relation for the compressibility of sensitive natural clays. *Géotechnique*, **35(2)**, 159-180.
- Lessloss (2007). Landslides: from mapping to loss and risk estimation. Lessloss Report 2007/01, Crosta G.B. and Frattini P. editors, IUSS Press, Pavia, Italy.
- Li T.C. (1978). Relation between earthquakes and landslides and prediction on earthquake induced landslides. (in Chinese). In: Chengdu Institute of Geography (ed) Earthquakes and landslides, 1–22.
- Li X.S., Dafalias Y.F. (2000). Dilatancy for cohesionless soils. *Géotechnique*, **50(4)**, 449-460.
- Li X.S., Dafalias Y.F., Wang Z.L. (1999). State dependent dilatancy in critical state constitutive modelling of sand. *Can. Geotech. J.*, **36**, 599-611.
- Li X.S., Wang Y. (1998). Linear representation of steady-state line for sand. *Journal of Geotech. and Geoenv. Engineering, ASCE*, **124(12)**, 1215-1217.
- Li, X.S. (2002). A sand model with state-dependent dilatancy. *Géotechnique*, **52(3)**, 173-186.
- Liao Q.L., Li X., Dong Y.H., (2005). Occurrence, geology and geomorphy characteristics and origin of Qianjiangping landslide in Three Gorges Reservoir area and study on ancient landslide criterion. *Chinese Journal of Rock Mechanics and Engineering*, **24(17)** 3146–3153.
- Lim T.T., Rahardjo H., Chang M.F., Fredlund D.G. (1996). Effect of rainfall on matric suctions in a residual soil slope. *Can. Geotech. J.*, **33**, 618-628.
- Lipman P.W., Moore J.C., Swanson D.A. (1981). Bulging of the north flank before the May 18 eruption: Geodetic data, *U.S. Geol. Surv. Prof. Pap.*, **1250**, 143-156.
- Lirer L., Munno R., Petrosino P., Vinci A. (1993). Tephrostratigraphy of the A.D. 79 Pyroclastic deposits in perivolcanic areas of Mt. Vesuvio (Italy). *J. Volcanol. Geotherm. Res.*, **58**, 133-149.
- Liu, M.D., Carter, J.P. (2002). A structured CAM CLAY model. Research Report R814, The University of Sydney, Department of Civil Engineering, Australia.
- Lo K.Y., Lee C.F. (1974). An evaluation of the stability of natural slope in plastic Champlain clays. *Can. Geotech. J.*, **11**, 165-181.
-

- Lo Presti C.F., Pallara O., Froio F., Rinolfi A., Jamiolkowski M. (2006). Stress-strain-strength behaviour of undisturbed and reconstituted gravelly soil samples. *Italian Geotechnical Journal*, **1**, 9-27.
- Londe P. (1988). Discussion on the determination of the shear stress failure in rock masses. *Journ. of Geotech. Eng. Div. ASCE*, **114(3)**, 374-376.
- Lopez D.L., Williams S.T. (1993). Catastrophic volcanic collapse: relation to hydrothermal processes. *Science*, **260**, 1794-1796.
- Lotti, C., Associati-Enel. Hydro (2001). Investigacion Geotecnical Integral, Informe Final, Sintesis Geologicay Modelos Numericos, Anexo: 2.2.1.1 – El Salvador, Technical Report, financed by BID, property of Ministerio de Medio Ambiente y Recursos Naturales, 37pp.
- Lowe III J., Karafiath L. (1960). Effect of anisotropic consolidation on the undrained shear strength of compacted clays. Proc. of the ASCE Res. Conf. on Shear Strength of Cohesive Soils, Boulder, Colorado, 837-858.
- Lu N., Godt J. (2008). Infinite slope stability under steady unsaturated seepage conditions, *Water Resour. Res.*, **44(60-77)**, W11404.
- Lu N., Likos W.J (2006). Suction stress characteristic curve for unsaturated soil. *Journal of Geotechnical and Geoenvironmental Engineering*; **132(2)**, 131-142.
- Luckman, B.H., Fiske, C.J. (1995). Estimating long-term rockfall accretion rates by lichenometry. In: Slaymaker, O. (Ed.), *Steepland Geomorphology*. Wiley, New York, 233-255.
- Lugon R., Delaloye R., Perruchoud E. (2008). Aléas naturels en zone de pergélisol et détection des risques, Alpes valaisannes, Suisse. I.I.A. France-Suisse, 52. [http://www.institut-montagne.org/IMG/pdf/Volet1\\_RLugon.pdf](http://www.institut-montagne.org/IMG/pdf/Volet1_RLugon.pdf)
- Lumb P. (1962). Effect of rain storms on slope stability. Proceedings of the Symposium on Hong Kong Soils, Hong Kong: 73-87.
- Luo X.Q., Liu D.F., Wu J., Cheng S.G. (2005). Model test study on landslide under rainfall and reservoir water fluctuation. *Chinese Journal of Rock Mechanics and Engineering*, **24(14)**, 2,476-2,483.
- Luo, H.Y., Zhou ,W., Huang, S.L. (2004). Earthquake-induced landslide stability analysis of The Las Colinas landslide in El Salvador. *Int. J. Rock Mech. Mining Sci*, **41**, 617-622.
- Lupini J.F., Skinner A. E., Vaughan P.R. (1981). “The drained residual strength of cohesive soils”. *Géotechnique* 31, n° 2, 181-213.
- Lynch D. (2010), “Merano train crash probe focuses on cause of landslide”, *New Civil Engineer International Edition* 06/2010, pp.4-5
- Macfarlane DF. 2009. Observations and predictions of the behaviour of large, slow-moving landslides in schist, Clyde Dam reservoir, New Zealand. *Eng. Geol.*, **109**, 5-15.
- Madritsch, H., Millen, B.M.J. (2007). Hydrogeologic evidence for a continuous basal shear zone within a deep-seated gravitational slope deformation (Eastern Alps, Tyrol, Austria). *Landslides*, **4**, 149-162. doi 10.1007/s10346- 006-0072-x
-

- Makdisi, F. Seed, H. (1978). Simplified procedure for estimating dam and embankment earthquake induced deformations. *J. Geotech. Eng.*, **104(7)**, 849–867.
- Malet J.-P., Van Asch Th.W.J., Van Beek R. and Maquaire O., (2005). Forecasting the behaviour of complex landslides with a spatially distributed hydrological model, NHESS.
- Manfredini M., Bertini T., Cugusi F., Grisolia M., Rossi Doria M. (1985). Geological outline of Italy: bearing of the geological features on the geotechnical characterization on the example of some typical formations. *Geotechnical Engineering in Italy – An overview, Associazione Geotecnica Italiana*, 159-184.
- Mani P. (1994). Ritigraben (Mattertal), Grundlagen-Zusammenstellung und erste Interpretation, Geo7 Bericht fuer sad Baudepartement des Kantons Wallis, 9407.01.
- Manzari, M.T., Dafalias, Y.F. (1997). A critical state two-surface plasticity model for sands. *Géotechnique*, **47(2)**, 255-272.
- Marchand G. (1982). Quelques considérations sur le comportement avant rupture des pentes argileuses naturelles. MSc thesis, Université Laval, Quebec.
- Marcuson III W.F., Hynes M.E., Franklin A.G. (1990). Evaluation and use of residual strength in seismic safety analysis of embankments. *Earthquake Spectra*, **6(3)**, 529-572.
- Marinos P., Hoek E. (2000a). GSI – A geologically friendly tool for rock mass strength estimation. Proc. GeoEng2000 Conference, Melbourne.
- Marinos P., Hoek E. (2000b). From the geological to rock mass model: Driving the Egnatia Highway through difficult geological conditions, Northern Greece. Proc. 10<sup>th</sup> Int. Conf. Of Italian National Council of Geologists, Rome.
- Marinos P., Hoek E. (2001). Estimating the geotechnical properties of heterogeneous rock masses such as flysch. *Bull. Eng. Geol. Env., IAEG*, **60**, 85-92.
- Marsland A. (1971). The shear strength of fissured clays. *Stress-Strain Behaviour of Soils, Roscoe Memorial Symposium, Henley-on-Thames, Foulis*, 59-68.
- Marsland A. (1974). Comparison of the results from static penetration tests and large in-situ tests in London clay. Proc. of the European Symposium on Penetration Testing, Stockholm.
- Marsland A. (1977). In-situ measurement of the large scale properties of Keuper marl. Proc. Int. Symp. on The Geotechnics of Structurally Complex Formations, Capri, 1, 335-344.
- Marsland A., Butler M.F. (1967). Strength measurement of stiff fissured Barton clay from Fawley, Hampshire. Proc. Of the Geotechn. Conf., Oslo, 1, 139-145.
- Marsland A., Randolph M.F. (1977). Comparison of the results from pressuremeter tests and large in situ plate tests in London clay. Building Research Establishment, current paper 78/10, 26 pp.
- Marti' J., Hurlimann M., Ablay G.J., Gudmundsson A. (1997). Vertical and lateral collapses on Tenerife (Canary Islands) and other volcanic ocean islands. *Geology*, **25**, 879-882.
- Marti' J., Mitjavila J., Arana V. (1994). Stratigraphy, structure and geochronology of the Las Canadas caldera (Tenerife, Canary Island). *Geolog. Mag.*, **131(6)**, 715-727.
- Martin D.A., Moody J.A. (2001). Comparison of soil infiltration rates in burned and unburned mountainous watersheds. *Hydrol. Process.*, **15**, 2893-2903.
-

- Martin H.E., Whalley W.B. (1987). Rock glaciers: I rock glacier morphology: classification and distribution. *Progress in Physical Geography*, **11**, 261-282.
- Martino, S., Mugnozza, G.S. (2005). The role of the seismic trigger in the Calitri landslide (Italy): historical reconstruction and dynamic analysis. *Soil Dynamics and Earthquake Engineering*, **25(12)**, 933-950.
- Martins F.B., Bressani L.A., Coop M.R., Bica V.D. (2002). Some aspects of the compressibility behaviour of a clayey sand. *Can. Geotech. J.*, **38**, 1177-1186.
- Martins-Campina, B., Huneau, F., Fabre, R., (2008). The Eaux-Bonnes landslide (Western Pyrenees, France): overview of possible triggering factors with emphasis on the role of groundwater. *Environ. Geol.*, **55**, 397-404.
- Massuda, K. (2000). Effects of water on rock strength in a brittle regime. *Jour. Structural Geol.*, **23**, 1653-1657.
- Mathewson C.C., Keaton J.R., Santi P.M. (1990). Role of bedrock ground water in the initiation of debris flow and sustained post-flow stream discharge. *Bulletin of the Association of Engineering Geologists*, **27**, 73-83.
- Matsuoka N., Sakai H. (1999). Rockfall activity from an alpine cliff during thawing periods. *Geomorphology*, **28**, 309-328.
- Matyas E.L., Radhakrishna H.S. (1968). Volume change characteristics of partially saturated soils. *Geotechnique*, **18**, 432-448.
- Maurer H., Hauck C. (2007). Instruments and Methods Geophysical imaging of alpine rock glaciers. *J. Glaciol.*, **53(180)**, 110-120
- McCalpin, J.P. (1999). Criteria for determining the seismic significance of sackungen and other scarp-like landforms in mountainous regions. *Techniques for Identifying Faults and Determining their Origins*. U.S. Nuclear Regulatory Commission, Washington, pp. 2.55–2.59.
- McGuire W.J. (1996). Volcano instability: a review of contemporary themes. In: McGuire WJ, Jones AP, Neuberg J (eds) *Volcano instability on the Earth and other planets*. London, Geological Society Special Publication **110**, 1-23.
- McGuire W.J., Pullen A.D., Saunders S.J. (1990). Recent dyke-induced large-scale block movement at Mount Etna and potential slope failure. *Nature*, **343**, 357-359.
- McGuire W.J., Stewart L.S., Saunders S.J. (1997). Intra-volcanic rifting at Mount Etna in the context of regional tectonics. *Acta Vulcanol.*, **9**, 147-156.
- Merle O., Borgia A. (1996). Scaled experiments of volcanic spreading. *J. Geophys. Res.*, **101**, 13,805-13,817.
- Merle O., Lenat J.F. (2003). Hybrid collapse mechanism at Piton de la Fournaise volcano, Reunion Island, Indian Ocean. *J. Geophys. Res.*, **108(B3)**, 2166.
- Merle O., Vidal N., van Wyk de Vries B. (2001). Experiments on vertical basement fault reactivation below volcanoes. *J. Geophys. Res.*, **106**, 2153-2162.
- Mesri G., Shahien, M. (2003). Residual shear strength mobilized in first-time slope failures. *Journal of Geoth. And Geoenv. Eng., ASCE*, **129(1)**, 12-31.
-

- Mesri, G., Shahien, M., Hedi, J.E. (1997). Geotechnical characteristics and compression of Pisa clay. Proc. 14<sup>th</sup> Int. Conf. on Soil Mech. and Found. Eng., Hamburg, Germany, 1, 373-376.
- Meyer D.F., Trabant D.C. (1995). Lahars from the 1992 eruptions of Crater Peak, Mount Spurr Volcano, Alaska. In: T.E.C. Keith, Editor, The 1992 Eruptions of Crater Peak Vent, Mount Spurr Volcano, Alaska. *U. S. Geol. Surv. Bull.*, **2139**, 183-198.
- Miller, D. J., Sias, J. (1998). Deciphering large landslides: linking hydrological groundwater and stability models through GIS. *Hydrological Processes*, **12**, 923–941.
- Miller, D.J., Dunne, T. (1996). Topographic perturbations of regional stresses and consequent bedrock fracturing. *J. Geophys. Res.*, **101**, B11, 25523-25536.
- Mitchell J.K. (1976). Fundamentals of soil behavior. John Wiley and Sons, New York.
- Mohamed R., Dobry R. (1986). Undrained monotonic and cyclic triaxial strength of sand. *Journ. of Geotech. Eng. Div., ASCE*, **112**, GT10, 941-958.
- Molnar, P. (2004). Interactions among topographically induced elastic stress, static fatigue, and valley incision. *J. Geophys. Res.*, **109**, F02010, doi: 10.1029/2003/JF000097.
- Mondada G., (1977). Commerci e commercianti di Campo Vallemaggia nel settecento. Edizioni del canto netto, Lugano, 242 pp.
- Montgomery D., Dietrich W.E. (1989). Channel initiation, drainage density and slope. *Water Resour. Res.*, **25**(8), 1907-1918.
- Montgomery D.R., Dietrich W.E. (1994). A physically based model for the topographic control on shallow landsliding. *Water Resour. Res.*, **30**(4), 1153-1171.
- Montgomery D.R., Dietrich W.E., Torres R., Anderson S.P., Heffner J.T., Loague K. (1997). Hydrologic response of a steep, unchanneled valley to natural and applied rainfall. *Water Resour. Res.*, **33**, 91-109.
- Moon V., Bradshaw J., Smith R., de Lange W. (2005). Geotechnical characterization of stratocone crater wall sequences, White Island Volcano, New Zealand. *Eng. Geol.*, **81**, 146-178.
- Moore J.G., Albee W.C. (1981). Topographic and structural changes, March–July 1980-photogrammetric data. In: Lipman, P.W., Mullineaux, D.R. (Eds.), The 1980 Eruptions of Mount St. Helens, 1250. U.S. Geol. Surv. Prof. Pap., Washington.
- Morgenstern N.R. (1992). Managing risk in geotechnical engineering. Proc. of 10<sup>th</sup> Pan-American Conf. on S.M.F.E., Guardalajara 4, 102-106
- Morgenstern N.R. (2000-2001). Terzaghi and liquefaction flow slides. Reports on Geotechnical Engineering, Soil Mechanics and Rock Engineering, Jubilee Volume in celebration of 75<sup>th</sup> Anniversary of K. Terzaghi's Erdbaumechanik – 60<sup>th</sup> Birthday of O. Univ. Prof. Dr. Heinz Brandl, vol. 5, Vienna.
- Morgenstern N.R., (1963). Stability charts for earth slopes during rapid drawdown, *Geotechnique*, **13**(2), 121–131.
-

- Morgenstern N.R., Sangrey D.A. (1978). Methods of stability analysis. in Schuster, R.L. and Krizek, R.E.J., Eds., Landslides, Analysis and Control. Transportation Research Board Special Report 176, Washington, D.C., p. 155-171.
- Mosely M.P. (1979). Streamflow generation in a forested watershed, New Zealand, *Water Resour. Res.*, **15**(4), 795–806.
- Mosely M.P. (1982). Subsurface flow velocities through selected forest soils, South Island, New Zealand. *J. Hydrol.*, **55**, 65-92.
- Moser, M., Hohensinn, F., (1983). Geotechnical aspects of soil slips in Alpine regions. *Eng. Geol.*, **22**(A), 23– 27.
- Mosselman E. (1991). Modelling of river morphology with non-orthogonal horizontal curvilinear coordinates. Commun. Hydraul. Geotech. Eng. 91-1, Delft Univ. of Technol., Netherlands.
- Mosselman E. (1992). Mathematical modelling of morphological processes in rivers with erodible cohesive banks, Commun. Hydraul. Geotech. Eng. 92-3, Delft Univ. of Technol., Netherlands.
- Mosselman E. (1998). Morphological modelling of rivers with erodible banks. *Hydrol. Process.*, **12**, 1357-1370.
- Mothes P., Hall M. Janda R. (1998). The enormous Chillos Valley Lahar: an ash-flow-generated debris flow from Cotopaxi Volcano, Ecuador. *Bull. Volcanol.*, **59**, 233-244.
- Mroz Z., Norris V.A., Zienkiewicz O.C. (1978). An anisotropic hardening model for soils and its application to cyclic loading. *Int. J. Num. Anal. Meth. Geom.*, **2**, 203-221.
- Müller L., (1964). The rock slide in the Vajont Valley, *Rock Mechanics and Engineering Geology*, **4**, 148–212.
- Muntohar A.S., Liao H.J. (2009). Analysis of rainfall induced infinite slope failure during typhoon using a hydrological – geotechnical model. *Environmental Geology*, **56**(1), 1145-1159.
- Murray J.B. (1988). The influence of loading by lavas on the siting of volcanic eruption vents on Mt. Etna. *J. Volcanol. Geotherm. Res.*, **35**, 121-139.
- Musil M., Maurer H., Green A.G., Horstmeyer H., Nitsche F.O., Vonder Mühl D., Springman S.M. (2002). *Geophysics*, **67**(6), 1701-1710.
- Musso A., Olivares L. (2004). Flowslides in pyroclastic soils – transitino from “static liquefaction” to “fluidification”. In L. Picarelli (ed.), Occurrence and Mechanism of Flows in Natural Slopes and Earthfills, Proceed. Int. Workshop, Sorrento, 14-16 May, 117-127, Patron Ed. Bologna.
- Nagaraj T.S., Miura N. (2001). *Soft Clay Behaviour: Analysis and Assessment*. Balkema.
- Nagata N., Hosoda T., Muramoto Y. (2000). Numerical analysis of river channel processes with bank erosion. *J. Hydraul. Eng.*, **126**(4), 243-252.
- Nakamura K. (1977). Volcanoes as possible indicators of tectonic stress orientation - Principle and proposal. *J. Volcanol. Geotherm. Res.*, **2**, 1-16.
-

- Nakamura K. (1990). On reservoir landslide. *Bulletin of Soil and Water Conservation*, **10(1)**, 53–64 (In Chinese).
- Naoki S., Kunitomo N., Tetsuo O. (2004). Centrifuge tests on seepage behaviour in embankment dams during rapid drawdown. *Bulletin of Aichi Institute of Technology*, **B39**, 85–90 (In Japanese).
- Naranjo J.A., Francis P. (1987). High velocity debris avalanche at Lastarria Volcano in the North Chilean Andes. *Bull. Volcanol.*, **49**, 509-514.
- Nash D. (1987). A comparative review of limit equilibrium methods of stability analysis. *Slope Stability: Geotechnical Engineering and Geomorphology*, edited by M.G.Anderson and K.S. Richards, Yohn Wiley and Sons, 11-75.
- Nawrocki P.A., Mroz Z. (1998). A viscoplastic degradation model for rocks. *Int. Journal Rock Mech. Min. Sci.*, **35(7)**, Technical Note, Elsevier Science Ltd., 991-1000.
- Nelson F.E., Shiklomanov N.I., Mueller G.R. (1999). Variability of active-layer thickness at multiple spatial scales, north-central Alaska, USA. *Arctic and Alpine Research*, **31**, 158-165.
- Neuzil C.E. (1993). Low fluid pressure within the Pierre Shale: a transient response to erosion. *Water Resour. Res.*, **29(7)**, 2007-2020.
- Newland P.L. and Allely B.H. (1957). Volume changes in drained triaxial tests on granular materials. *Géotechnique*, **7**, 17-34.
- Newmark, N.M. (1965). Effects of earthquakes on dams and embankments. *Geotechnique*, **15(2)**, 139-159.
- Ni Q., Tan T.S., Dasari G.R., Hight D.W. (2004). Contribution of fines to the compressive strength of mixed soils. *Géotechnique*, **54(9)**, 561-569.
- Nicholson N.R., Hough V.N.D. (1967). Jointing in the Appalachian Plateau of Pennsylvania. *Bull. Geol. Soc. Am.*, **78**, 609-629.
- Nichols T.C. (1980). Rebound, its nature and effect on engineering works. *Q. J. Eng. Geol., London*, **13**, 133-152.
- Nocilla A., Coop M.R. (2008). The behaviour of sub-soils from the Po river embankments: an example of transitional behaviour in natural soils. *Italian Geotechnical Journal*, **1**, 49-58.
- Nocilla A., Coop M.R., Colleselli F. (2006). The mechanics of an Italian silt: an example of transitional behaviour. *Géotechnique*, **56(4)**, 261-271.
- Norbury, D., Hencher, S., Cripps, J., Lumsden, A. (1995). The description and classification of weathered rocks for engineering purposes. Geol. Soc. Engineering Group, Working Party Rep., *Quart. J. Eng. Geology*, **28**, 207-242.
- Nostro C., Cocco M., Belardinelli M.E. (1997). Static changes in extensional regimes: an application to southern Apennines (Italy). *Bull. Seism. Soc. Am.*, **1**, 234-248.
- Nova, R. (1992). Mathematical modelling of natural and engineered geomaterials, *Europ. J. Mech. A Solids*, **11(special issue)**, 135-154.
- Nova, R., Castellanza, R., Tamagnini, C. (2003). A constitutive model for bonded geomaterials subject to mechanical and/or chemical degradation. *Int. J. Num. Anal. Meth. Geomech.*, **27(9)**, 705-732.
-

Núria M. Pinyol, Eduardo E. Alonso, and Sebastià Olivella (2008). Rapid drawdown in slopes and embankments *Water Resour. Res.*, **44**. W00D03, doi:10.1029/2007WR006525.

O'Loughlin E.M. (1986). Prediction of surface saturated zones in natural catchments by topographic analysis. *Water Resour. Res.*, **22**, 794-804.

Ochiai H., Okada Y., Furuya G., Okura Y., Matsui T., Sammori T., Terajima T., Sassa K. (2004). A fluidized landslide on a natural slope by artificial rainfall. *Landslides*, **1(3)**, 211-219.

Odgaard A.J. (1989a). River meander model. I: Development. *J. Hydraul. Eng.*, **115(11)**, 1433–1450.

Odgaard A.J. (1989b). River meander model. II: Applications. *J. Hydraul. Eng.*, **115(11)**, 1451–1464.

Ohta T, Tsukamoto Y, Noguchi H. (1981). An analysis of pipeflow and landslide. In Proceedings of Annual Meeting of the Japan Society of Erosion Control Engineering, 92–93 (in Japanese).

Okimura T., Kawatani T. (1987). Mapping of the potential surface failure sites on granite mountain slopes, in Proceedings of the First International Conference on Geomorphology, Part 1, edited by V. Gardiner, pp. 131–138, Int. Assoc. Geomorphol., Manchester, England.

Okura Y., Kitahara H., Ochiai H., Sammori T., Kawanami A. (2002). Landslide fluidization process by flume experiments. *Eng. Geol.*, **66(1-2)**, 65-78.

Olivares L., Picarelli L. (2001a). Susceptibility of loose pyroclastic soils to static liquefaction: some preliminary data. Proc. Int. Conf. Landslides – Causes, Impacts and Countermeasures, Davos.

O'Loughlin C.L., Pearce A.J. (1976). Influence of Cenozoic geology on mass movement and sediment yield response to forest removal, North Westland, New Zealand. *Bulletin of the International Association of Engineering Geologists*, **14**, 41-46.

Olsen N.R.B. (2003). Three-dimensional CFD modeling of self-forming meandering channel. *J. Hydraul. Eng.*, **129(5)**, 366-372.

Onda Y. (1994). Seepage erosion and its implication to the formation of amphitheater valley head: a case study at Obara, Japan. *Earth Surf. Processes and Landforms*, **19**, 627–640.

Onorati G., Pagliara P. (1999). L'evento idrometeorologico del settembre 1996-gennaio 1997 in Campania. *Atti Accademia Nazionale dei Lincei* 154, 97– 102.

Orense, R.P., Vargas-Monge W., Cepeda R. (2002). Geotechnical aspects of the January 13, 2001 El Salvador Earthquake. *Soils and Foundations*, **42(4)**, 57–68.

Orlandini S., Lamberti A. (2000). Effect of wind on precipitation intercepted by steep mountain slopes. *J Hydrol. Eng. Am. Soc. Civ. Eng.*, **5**, 346-354.

Osman A.M., Thorne C.R. (1988). Riverbank stability analysis. I: Theory. *J. Hydraul. Eng.*, **114(2)**, 134-150.

Oyagi N., Terashima H., Moriwaki H. (1977). Report on the Fukuchi-Nukeyama Landslide disaster in Ichinomiya Town, Hyogo Prefecture and debris-flow disaster in Syodo Island, Kagawa Prefecture, due to Typhoon No. 17, 1977. Natural Disaster Research Report No. 13,

National Research Center for Disaster Prevention (NRCDP), Tsukuba, Japan, 68 pp. (in Japanese).

Oyama, T., Chigira, M. (1999). Chemical weathering rate and the change of mechanical properties of sedimentary rocks. *Eng. Geol.*, **55**, 15-27.

Pack R.T., Tarboton D.G., Goodwin C.N. (1998). The Sinmap Approach to Terrain Stability Mapping. Proc. 8th Congress of the International Association of Engineering Geology, Vancouver, British Columbia.

Palmer B.A., Neall V.E. (1989). The Murimotu Formation: 9500 year old deposits of a debris avalanche and associated lahars, Mount Ruapehu, North Island, New Zealand. *J. Geol. Geophys. (NZ)*, **32**, 477-486.

Pan, E., Amadei, B., Savage, W. (1994). Gravitational stresses in long symmetric ridges and valleys in anisotropic rock. *Int. Jour. of Rock Mechanics and Mining Sciences & Geomechanics Abstracts*, **31 (4)**, 293–312.

Pan, E., Amadei, B., Savage, W.Z. (1995). Gravitational and tectonic stresses in anisotropic rock with irregular topography. *International Journal of Rock Mechanics and Mining Science & Geomechanics Abstracts*, **32**, 3, 201-214.

Panday S., Huyakorn P.S. (2004). A fully coupled physically-based spatially-distributed model for evaluating surface/subsurface flow. *Adv. Water Resour.*, **27**, 361-382.

Pareschi M.T., Santacroce R., Sulpizio R., Zanchetta G. (2002). Volcanoclastic debris flows in the Clanio Valley (Campania, Italy): insight for the assessment of hazard potential. *Geomorphology*, **43**, 219-231.

Parise, M., Polemio, M., Wasowski, J. (1997). Rainfall and landslides in the upper valleys of Sele and Ofanto Rivers, Italy. Proc. Int. Symp. Engineering Geology and the Environment (Athens) 1, 955–960.

Pariseau, W.G., and Voight, B. (1979). Rock slides and avalanches: basic principles, and perspectives in the realm of civil and mining operations. In *Rock slides & avalanches*. Edited by B. Voight. *Developments in Geotechnical Engineering*, **14b**, Elsevier, Amsterdam, 1–92.

Parker G. (1976). On the cause and characteristic scales of meandering and braiding in rivers. *J. Fluid Mech.*, **76**, 457-480.

Parry R.H.G. (1972). Some properties of heavily overconsolidated Oxford clay at site near Bedford. *Géotechnique*, **22(3)**, 485-507.

Parry, R.H.G. (1960). Triaxial compression and extension tests on remoulded saturated clay. *Géotechnique* 10, n°10, 166-180.

Pasquarè G., Francalanci L., Garduno V.H., Tibaldi A. (1993). Structure and geological evolution of the Stromboli volcano, Aeolian Islands, Italy. *Acta Vulcanol.*, **3**, 79-89.

Pastor M., Fernandez Merodo J.A., Herreros M.I., Gonzales E., Mira P., B. Haddad, Quecedo M. (2005b). The role of pore pressures on fast landslides triggering and propagation: a mathematical modelling approach. Proc. 11<sup>th</sup> Int. Conf. of IACMAG, 4, G. Barla and M. Barla editors, Turin, 671-682.

---

- Pastor M., Quecedo M., Fernandez Merodo J.A., Herreros M.I., Gonzales E., Mira P. (2002). Modelling tailings dams and mine waste dumps failures. *Géotechnique*, **52(8)**, 579-591.
- Pastor M., Quecedo M., Herreros M.I., Gonzales E., Haddad B., Fernandez Merodo J.A., Mira P. (2005a). Modelling of fast landslides and waves induced by them in reservoirs and other water bodies. *Rivista Italiana di Geotecnica*, **2**, 46-62.
- Pastor M., Zienkiewicz O.C., Chan H.C. (1990). Generalized plasticity and the modelling of soil behaviour. *Int. J. Num. Anal. Meth. Geom.*, **14**, 151-190.
- Patacca, E., Sartori, R., Scandone, P. (1990). Tyrrhian basin and appenninic arc: kinematic relations since late Miocene. *Mem Soc Geol It.*, **45**, 425-51.
- Patton F.D. (1966). Multiple modes of shear failure in rock. 1<sup>st</sup> Int. Congress of Rock Mechanics, Lisbon, 1, 509-513.
- Pauls, G.J., Karlsauer, E., Christiansen, E.A., Wigder, R.A. (1999). A transient analysis of slope stability following drawdown after flooding of highly plastic clay. *Can. Geotech. J.*, **36**, 1151-1171.
- Peng, W.F., Wang, C.L., Chen S.T., Lee, S.T., (2009). Incorporating the effects of topographic amplification and sliding areas in the modeling of earthquake-induced landslide hazards, using the cumulative displacement method. *Computers and Geosciences*, **35(5)**, 946-966.
- Persaud, M., Pfiffner, O.A. (2004). Active deformation in the eastern Swiss Alps: postglacial faults, seismicity and surface uplift. *Tectonophysics* **385**, 59-84.
- Pestana J.M., Whittle A.J. (1995). Compression model for cohesionless soils. *Géotechnique*, **45(4)**, 611-631.
- Pestana J.M., Whittle A.J. (1998). Time effects in the compression of sands. *Géotechnique*, **48(5)**, 695-701.
- Peterson R. (1958). Rebound in Bearpaw Shale in Western Canada. *Bull. Geol. Soc. Am.*, **69**, 1113-1123.
- Pfister C., Hächler S. (1990). Hochwasserkatastrophen im schweizerischen Alpenraun seit dem 14 Jahrhundert, Bericht Nationales Forschungsprogramm. Analyse der Hochwasser 1987'
- Philip J.R. (1957). The theory of infiltration. *Soil Science*, **83**, 345-357.
- Picarelli L. (1991). Resistenza e meccanismi di rottura in terreni naturali. Convegno dei ricercatori sul tema: Deformazioni in prossimità della rottura e resistenza dei terreni naturali e delle rocce. Ravello 2, II.7- II.61.
- Picarelli L. (2001). Transition from slide to earthflow, and the reverse. Proc. TC-11 Conference on Transition from slide to flow, Trabzon.
- Picarelli L. (2007). "Considerations about the mechanics of slow active landslides in clay". Chapter 3 of Progress in Landslide Science, Sassa K., Fukuoka H., Wang F., Wang G. editors, Springer, 27-45.
- Picarelli L. (2009). "Conoscere per prevedere (dall'equilibrio limite alla meccanica dei pendii)". Rivista Italiana di Geotecnica, AGI, Anno XLIII, n° 4, 12-68, Ottava conferenza annuale "Arrigo Croce" dell'Associazione Geotecnica Italiana, in italian.
-

- Picarelli L., Olivares L. (1998). Ingredients for modelling the mechanical behaviour of intensely fissured clay shales. Proc. 2<sup>nd</sup> Int. Symp. on The Geotechnics of Hard Soils-Soft Rocks, Evangelista A. and Picarelli L. editors, Naples, Balkema, 1669-1678.
- Picarelli L., Olivares L., Avorio B. (2008). Zoning for flowslide and debris flows in pyroclastic soils of Campania Region based on “infinite slope” analysis. *Eng. Geol.*, **112**, 132-141.
- Picarelli L., Urcioli G. (1993). “Effetti dell’erosione in argilliti di alta plasticità”. Rivista Italiana di Geotecnica, AGI, Anno XXVII, n° 1, 29-47, in Italian.
- Picarelli, L., Evangelista, A., Rolandi, G., Paone, A., Nicotera, M.V., Olivares, L., Scotto di Santolo, A., Lampitiello, S., Rolandi, M. (2006). Mechanical properties of pyroclastic soils in Campania Region. Proceed. Int. Symp. Characterisation and Engineering Properties of Natural Soils. Taylor and Francis, London, pp. 2331–2384. 4.
- Picarelli, L., Olivares, L., 2001. Innesco e formazione di colate di fango in terreni sciolti di origine piroclastica. Forum su Fenomeni di colata rapida di fango, maggio 1998: 26-38. Napoli.
- Pierce M., Brandshaug T., Ward M. (2001). Slope stability assessment in the Main Cresson Mine. In Slope Stability in Surface Mining, Hustrulid W.A., Mc Carter M.J. and Van Zyl D.J.A. editors, Littleton: Society for Mining, Metallurgy and Exploration Inc., 239-250.
- Pierson T.C. (1980). Piezometric response to rainstorms on forested hillslope rainage depressions. *J. Hydrol. (NZ)*, **19(1)**, 1-10.
- Pierson T.C. Scott K.M. (1985). Downstream dilution of a lahar: transition from debris flow to hyperconcentrated streamflow. *Water Resour. Res.*, **21**, 1511-1524.
- Pierson TC. (1983). Soil pipes and slope stability. *Quarterly J. Eng. Geol.*, **16**, 1–11.
- Pinel V., Jaupart C. (2003). Magma chamber behavior beneath a volcanic edifice. *J. Geophys. Res.*, **108(B2)**, 2072.
- Pinyol N.M., Alonso E.E., Olivella S. (2008). Rapid drawdown in slopes and embankments. *Water Resour. Res.*, **44**, W00D03. doi:10.1029/2007WR006525
- Pitilakis, K.D. (2004). Site effects. Recent Advances in Earthquake Geotechnical Engineering and Microzonation (A. Ansal, ed.), Kluwer Publications Chapter 5.
- Pitilakis, K.D. (2010). Geotechnical Earthquake Engineering, (in Greek), (under publication).
- Pitman T.D., Robertson P.K., Segal D.C. (1994). Influence of fines on the collapse of loose sands. *Can. Geotech. J.*, **31**, 728-739.
- Porcino D., Marcianò V. (2010). Evaluating liquefaction resistance of calcareous sand using the cone penetration test Proc. 5<sup>th</sup> Int. Conf. on Recent Advances in Geotechnical Earthquake Engineering and Soil Dynamics and Symposium in Honor of Professor I.M. Idriss, San Diego, California. Paper **4.15a**.
- Porter, S.C., Orombelli, G. (1981). Alpine rockfall hazards. *American Scientist* **69**, 67–75.
- Potts D.M., Kovacevic N., Vaughan P.R. (1997). Delayed collapse of cut slopes in stiff clays. *Géotechnique*, **47(5)**, 953-982.
-

- Prager, C., Zangerl, C., Patzelt, G., Brandner, R. (2008). Age distribution of fossil landslides in the Tyrol (Austria) and its surrounding areas. *Nat. Hazards Earth Syst. Sci.*, **8**, 377–407, 2008
- Prevost J.H. (1978). Plasticity theory for soil stress-strain behaviour. *J. Eng. Mech., ASCE*, **104(5)**, 1177-1194.
- Prevost J.H. (1985). A simple plasticity theory for frictional cohesionless soils. *Soil Dynamics and Earthquake Engineering*, **4(1)**, 9-17.
- Prevost J.H. (1993). Nonlinear dynamic response analysis of soil and soil-structure interacting system. *Soil Dynamics and Geotechnical Earthquake Engineering*, P. Seco and Pinto editor, Balkema.
- Prostka H.J., (1978). Heart Mountain fault and Absaroka volcanism, in *Rockslides and Avalanches, Natural Phenomena*, edited by B. Voight, **1**, 423-437, Elsevier Science, New York.
- Radbruch-Hall D. (1978). Gravitational creep of rock masses on slopes. In: Voight B. (ed.), *Rockslides and Avalanches; Natural Phenomena*. Elsevier, Amsterdam, 607-657.
- Raetzo-Bruelhart, H. (1997). Massenbewegungen im Gurnigelflysch und Einfluss der Klimaänderung, Arb.-Ber. NFP, 31, 256 pp., ETH Zurich.
- Rahardjo H., Lim T.T., Chang M.F., Fredlund D.G. (1995). Shear Strength Characteristics of a Residual Soil in Singapore. *Can. Geotech. J.*, **32**, 60-77.
- Rahardjo, H, X.W. Li, D.G. Toll E.C. Leong (2001). The effect of antecedent rainfall on slope stability. *Geotech. and Geological Engrg.*, **19**, 371-399.
- Rahman M.M., Lo S.R. (2008). The prediction of equivalent granular steady state line of loose sand with fines. *Geomechanics and Geoengineering: An International Journal*, **3(3)**, 179-190.
- Raines, M.A., Dewers, T.A. (1997). Mixed transport/reaction control of gypsum dissolution kinetics in aqueous solution and initiation of gypsum karst. *Chem. Geol.*, **140**, 29-48.
- Rampello S. (1989). Effetti del rigonfiamento sul comportamento meccanico di argille fortemente sovraconsolidate. PhD Thesis, University of Rome.
- Rampello S. (1991). Some remarks on the mechanical behaviour of stiff clays: the example of Todi clay. Proc. Of the Workshop on Experimental Characterization and Modelling of Soils and Soft Rocks, Naples, 131-186.
- Rampello, S., Callisto, L., Viggiani, G.M.B. (1996). The Leaning Tower of Pisa – Soil parameters for the numerical modelling of the Tower resulting from the most recent investigations. Research Contract on Modellazione numerica del sottosuolo della Torre di Pisa between the University of Rome La Sapienza and the Consorzio Progetto Torre di Pisa.
- Rankka K. (1994). In situ stress conditions across clay slopes: a study comprising seven test sites. PhD Thesis, Chalmers University of Technology, Gothenburg, Sweden.
- Rapp, A. (1957). Studien .uber Schutthalden in Lappland und auf Spitzbergen. *Zeitschrift f.ur Geomorphologie* **1**, 179–200.
-

- Rebetez M., Lugon R., Baeriswyl P. (1997). Climatic change and Debris flows in high mountain regions: The case study of the Ritigraben torrent (Swiss Alps). *Clim. Change*, **36**, 371-389.
- Rebetez M.R. Lugon P.A. Baeriswyl (1997). Climatic change and debris flows in high mountain regions: the case study of the Ritigraben Torrent (Swiss Alps). *Clim. Change*, **36**, 371-389.
- Reid M.E. (1994). A pore-pressure diffusion model for estimating landslide-inducing rainfall. *The Journal of Geology*, **102**, 709-717.
- Reid M.E. (1994). Transient thermal pressurization in hydrothermal systems: A cause of large-scale edifice collapse at volcanoes? (abstract), Geol. Soc. Am. Abstr. Programs, 26, A376.
- Reid M.E., LaHusen R.G., Iverson R.M. (1997). Debris-flow initiation experiments using diverse hydrologic triggers, In: Chen C (ed) (1997) First International Conference on Debris-Flow Hazards Mitigation: Mechanics, Prediction, and Assessment: ASCE, pp 1-11.
- Reid M.E., Nielson H.P., Dreiss S.J. (1988). Hydrologic factors triggering a shallow hillslope failure. *Bull. Assoc. Eng. Geol.*, **25**, 349-361.
- Reid M.E., Sisson T.W., Brien D.L. (2001). Volcano collapse promoted by hydrothermal alteration and edifice shape, Mount Rainier, Washington. *Geology*, **29**, 779-782.
- Reid ME, Christian SB, Brien DL (2000). Gravitational stability of three-dimensional stratovolcano edifices. *J Geophys Res.*, **105**, 6043–6056.
- Reid, J.R. (1969). Effects of a debris slide on ‘Sioux Glacier’, southcentral Alaska. *Journal of Glaciology* **8**, 353–367.
- Revellino P., Hungr O., Guadagno F. M., Evans S. G. (2004). Velocità and runout simulation of destructive debris flows and debris avalanches in pyroclastic deposits, Campania Region, Italy. *Environmental Geology*, **45**, 295-311.
- Richard KS, Reddy KR (2007) Critical appraisal of piping phenomena in earth dams. *Bull Eng Geol Environ.*, **66(4)**, 381–402.
- Richards J.P., Villeneuve M. (2001). The Lullailaco volcano, northwest Argentina: Construction by Pleistocene volcanism and destruction by sector collapse. *J. Volcanol. Geotherm. Res.*, **105**, 77-105.
- Richards K.S., Lorriman N.R. (1987). Basal erosion and mass movement. Slope Stability: Geotechnical Engineering and Geomorphology, Anderson M.G. and Richards K.S. editors, John Wiley and Sons, 331-357.
- Richards L.A. (1931). Capillary conduction of liquids through porous mediums. *Physics*, **1**, 318-333.
- Richart R.E., Hall J.R., Woods R.D. (1970). Vibrations of soils and foundations. Englewood Cliffs, NH, Prentice-Hall.
- Riemer M.F., Seed R.B. (1997). Factors affecting apparent positions of steady state line. *Journal of Geot. and Geoenv. Eng., ASCE*, **123(3)**, 281-288.
-

- Rinaldi M., Casagli N. (1999). Stability of streambanks formed in partially saturated soils and effects of negative pore water pressure: The Sieve River (Italy). *Geomorphology*, **26(4)**, 253-277.
- Rinaldi M., Casagli N., Dapporto S., Gargini A. (2004). Monitoring and modelling of pore water pressure changes and riverbank stability during flow events. *Earth Surf. Processes and Landforms*, **29(2)**, 237–254.
- Ringheim A.S. (1964). Experiences with the Bearpaw shale at the South Saskatchewan River Dam. Proc. 8<sup>th</sup> Int. Conf. on Large Dams, Edinburgh, 1, 529-549.
- Rist A. (2007). Hydrothermal Processes within the Active Layer above Alpine Permafrost in Steep Scree Slopes and their Influence on Slope Stability. Faculty of Science. Zurich, University of Zurich, 168.
- Rist A., Phillips M. (2005). First results of investigations on hydrothermal processes within active layer above alpine permafrost in steep terrain. *Norwegian J. of Geography*, **59**, 177-183.
- Robertson, A.M. (1970). The interpretation of geological factors for use in slope theory. In: *Planning Open Pit Mines*, Proceedings, Johannesburg, 1970. p. 55–71.
- Rocchi G., Vaciago G., Fontana M. Da Prat M. (in preparation). Understanding sampling disturbance and behaviour of structured clays through constitutive modelling.
- Rocchi, G., Fontana, M., Da Prat, M. (2003). Modelling of natural soft clay destruction processes using viscoplasticity theory. *Géotechnique*, **53(8)**, 729-745.
- Rocchi, G., Vaciago, G., Fontana, M., Plebani, F. (2006). Enhanced prediction of settlement in structured clays with examples from Osaka Bay. *Geomechanics and Geoengineering: An International Journal* 1(3), Taylor and Francis, 217-237.
- Rocchi, G., Vaciago, G., Fontana, M., Plebani, F. (2007). Further insight into the behaviour of Pleistocene Osaka clays at KIA Phase 1 island. *Geomechanics and Geoengineering: An International Journal* 2(3), Taylor and Francis, 159-173.
- Rocchi, G.F., Albert, L.F., Vacca, O., Totani, G. (1991). Instrumented loading tests to failure on a very long, steel, driven, cast in situ multiton pile. Proc. 4<sup>th</sup> Int. Conf. on Piling and Deep Foundations, Stresa, Italy, Balkema, 307-317.
- Rochet, L. (1987)- Application des modèles numériques de propagation à l'étude des éboulements rocheux. *Bull Liaison Pont Chaussée*; **150/151**, 84–95 [in French].
- Rodríguez, C.E., Bommer, J.J., Chandler, R.J. (1999). Earthquake-induced landslides: 1980-1997. *Soil Dynamics and Earthquake Engineering*, **18**, 325-246.
- Rogers N.W., Selby M.J. (1980). Mechanisms of shallow translational landsliding during summer rainstorms: North Island, New Zealand. *Geograf. Ann.*, **62A**, 11-21.
- Rolandi, G., Bertolino, F., Cozzolino, G., Esposito, N. Sannino, D. (2000). Sull'origine delle coltri piroclastiche presenti sul versante occidentale del Pizzo d'Alvano (Sarno – Campania). *Quaderni di Geologia Applicata*, 7 – I.
- Romagnoli C., Tibaldi A. (1994). Volcanic collapse in different tectonic settings: an example from the Aeolian Arc, Italy. Proc Int. Conference on Volcano Instability on the Earth and Other Planets. The Geological Society of London.
-

- Romanov, D., Gabrovsek, F., Dreybrodt, W. (2003). Dam sites in soluble rocks: a model of increasing leakage by dissolutional widening of fractures beneath a dam. *Eng. Geol.*, **70**, 13-35.
- Romanovsky V.E., Osterkamp T.E. (2000). Effects of unfrozen water on heat and mass transport processes in the active layer and permafrost. *Permafrost and Periglacial Processes*, **11(3)**, 219-239.
- Ronchetti F., Borgatti L., Cervi F., Corsini, A. (2010). Hydro-mechanical features of landslide reactivation in weak clayey rock masses. *Bulletin of Engineering Geology and the Environment*, **69(2)**, 267-274. DOI: 10.1007/s10064-009-0249-3
- Roscoe K.H., Schofield A.N., Wroth C.P. (1958) On the yielding of soils. *Géotechnique*, **8(1)**, 22-53.
- Rosi M, Sbrana A. (1987). The Campanian Ignimbrite. In: Rosi M, Sbrana A. (Eds) Phlegrean Fields. Quad, Ric. Sci CNR (114), 13-14.
- Rosi M. (1980). The island of Stromboli. *Rend Soc Ital Mineral Petrol.*, **36**, 345-368.
- Rosi, M., Principe C., Vecci R. (1993). The 1631 eruption of Vesuvius reconstructed from the review of chronicles and study of deposits. *J. Volcanol. Geotherm. Res.* **58**, 151-182.
- Rossi D., Semenza E. (1965). “Carte geologiche del versante settentrionale del Monte Toc e zone limitrofe, prima e dopo il fenomeno di scivolamento del 9 Ottobre 1963”. Istituto di Geologia dell’Università di Ferrara, Scale 1: 5000, 2 maps (in Italian).
- Rossi F., Chirico G.B. & Ricciardi F. (1998). Guida alle soglie pluviometriche d’allarme. Dep. Of the Civil Protection – G.N.D.C.I. – University of Salerno (Italy)
- Rossi F., Villani P., Tropeano R., Mastrandrea G., & Longobardi A., 2005. Final Report of the research Line on hydraulic risk. C.E.R.I.U.S.: Centre of excellence on “Forecasting and prevention of hydrogeological risk over large areas”, University of Salerno, Italy.
- Röthlisberger G. (1991). Chronik der Unwetterschäden in der Schweiz. Berichte der Eidgenössischen Forschungsanstalt für Wald, Schnee und Landschaft., 330, 122.
- Rouainia, M., Wood, M.D. (2000). A kinematic hardening constitutive model for natural clays with loss of structure. *Géotechnique*, **50(2)**, 152-164.
- Russel D.J., Parker A. (1969). Geotechnical, mineralogical and chemical inter-relationships in weathering profiles in an overconsolidated clay. *Q. J. Eng. Geol., London*, **12**, 107-116.
- Russo G., Giberti G., Sartoris G. (1997). Numerical modeling of surface deformation and mechanical stability of Vesuvius volcano, Italy. *J. Geophys. Res.*, **102**, 24,785-24,800.
- Rye R.O., Breit G.N. Zimbelman D.R. (2003). Preliminary mineralogic and stable isotope studies of altered summit and flank rocks and Osceola Mudflow deposits on Mount Rainier, Washington. U.S., *Geological Survey Open-File Report 03-464*, pp. 26.
- Samuels S. G. (1975). Some properties of the Gault clay from the Ely-Ouse Essex water tunnel. *Building Research Establishment, current paper 3/75*, 19 pp.
- Sanderson F., Bakkehøi S., Hestenes E., Lied K. (1996). The influence of meteorological factors on the initiation of debris flows, rockfalls, rockslides and rockmass stability, in:

Landslides Proceedings 7th International Symposium on Landslides, edited by: Senneset, K., A.A. Balkema, 1.

Santalòia F., Cotecchia V., Monterisi L. (2004). Geological evolution and landslide mechanisms along the central Adriatic coastal slopes. *Advances in Geotechnical Engineering, the Skempton Conference*, **2**, 943-954.

Sasitharan S., Robertson P.K., Segó D.C., Morgenstern N.R. (1993). Collapse behaviour of sand. *Can. Geotech. J.*, **30**, 569-577.

Sassa K. (1985). The mechanism of debris flows. Proceedings, XI Internat. Conference on Soil Mechanics and Foundation Engineering, San Francisco, **1**, 1173-1176.

Sassa K. (2000). Mechanisms of flows in granular soils. Int. Conf. Geotechnical and Geological Engineering GEOENG2000, Melbourne: 1671-1702.

Sassa, K. (2005). Landslide disasters triggered by the 2004 Mid-Niigata Prefecture earthquake in Japan. *Landslides*, **2**, 135-142.

Savage, W.Z., Swolfs, H.S., Powers, P.S. (1986). Gravitational stresses in long symmetric ridges 668 and valleys. *Int. Jour. of Rock Mechanics and Mining Sciences & Geomechanics Abstracts*, **22**, 53, 291-302.

Schanz T., Vermeer P.A., Bonnier P.G. (1999). “The hardening soil model : formulation and verification”. Beyond 2000 in Computational Geotechnics – 10 years of Plaxis, Balkema, Rotterdam

Schmidt J., Dikau R. (2004). Modeling historical climate variability and slope stability, *Geomorphology*, **60**, 433-447.

Schnydrig A.L. (1952). Grächen, Walliser Bergdorf an der Mischabel’, Paul Haupt, Bern, 104.

Schofield A. N., Wroth C. P. (1968). Critical state soil mechanics. Mc Graw-Hill.

Schuster R. L. (1979) Reservoir-induced landslides. *Bull Eng Geol Environ.*, **20(1)**, 8-15, DOI: 10.1007/BF02591233

Scott K.M. (1988). Origins, behaviour, and sedimentology of lahars and lahar-runout flows in the Toutle–Cowlitz River system. *U. S. Geol. Surv. Prof. Pap.*, **1447-A8**, pp. 74.

Scott K.M., Vallance J.W., Pringle P.T. (1995). Sedimentology, behavior, and hazards of debris flows at Mount Rainier, Washington. *U. S. Geol. Surv. Prof. Pap.*, **1547**, pp. 56.

Segó D.C., Hofman B.A., Robertson P.K., Wride C.E. (1998). Undisturbed sampling of loose sand using in-situ ground freezing. Physics and Mechanics of Soil Liquefaction, Proc. Int. Workshop, Baltimore, Lade and Yamamuro editors, Balkema.

Segó D.C., Roberson P.K., Sasitharan S., Kilpatrick B.L., Pillai V.S. (1994). Ground freezing and sampling of foundation soils at Duncan Dam. *Can. Geotech. J.*, **31**, pp.

Selby M.J. (1985). Earth's Changing Surface. Clarendon Press, Oxford, pp. 607.

Selby M.J. (1987). Rock slopes. Slope Stability: Geotechnical Engineering and Geomorphology, Anderson M.G. and Richards K.S. editors, John Wiley and Sons, 475-504.

---

Selli R., Trevisan L. (1964). Caratteri e interpretazione delle Frana del Vajont. In *La Frana del Vajont*, Annali del Museo Geologico di Bologna, Ser. 2, **32**, Fas. 1, 8-104 (in Italian).

Semenza E. (1965). Sintesi degli studi geologici sulla frana del Vajont dal 1959 al 1964. *Memorie del Museo Tridentino di Scienze Naturali*. A. XXIX-XXX 1966-67, Trento, **16(1)**, 1-52.

Serdengecti S., Boozer G. (1961). The effects of strain rate and temperature on the behaviour of rocks subjected to triaxial compression. 4<sup>th</sup> U.S. Rock Mechanics Symposium, Penn. State Univ., 83-97.

Shibuya S., Mitachi T., Tanaka H., Kawaguchi T., Lee I. (1999). Measurement and application of quasi-elastic properties in geotechnical site characterization. Proc. 11<sup>th</sup> Asian Regional Conference on S.M.F.E., Theme Lecture for Plenary Discussion Session 1, 1-72.

Shields I.A. (1936). Application of similarity principles and turbulence research to bed-load movement. In: Ott, W.P., van Uchelen, J.C. (Eds.), (Translators), Hydrodynamics Laboratory Publication, **167**. California Institute of Technology, Pasadena.

Shrestha HK, Yatabe R, Bhandary NP (2008). Groundwater flow modeling for effective implementation of landslide stability enhancement measures. *Landslides*, **5**, 281–290.

Sidle R.C. (1984). Shallow groundwater fluctuations in unstable hillslopes coastal Alaska. *Zeitschrift für Gletscherkunde und Glazialgeologie*, **20**, 79–95.

Sidle R.C. (1986). Groundwater accretion in unstable hillslopes of coastal Alaska. In *Conjunctive Water Use*, Goreluck SM (ed.). IAHS Publication no. 156. IAHS Press: Wallingford; 335–343.

Sidle R.C., Swanston D.N. (1982). Analysis of a small debris slide in coastal Alaska. *Can. Geotech. J.*, **19**, 167-174.

Sidle R.C., Tsuboyama Y., Noguchi S., Hosoda I., Fujieda M., Shimizu T. (2000). Stormflow generation in steep forested headwater: a linked hydrogeomorphic paradigm. *Hydrol. Process.*, **14**, 369–385.

Sidle RC. (1994). Hydrological process related to landslide initiation. In *Proceeding of the SABO Workshop on Experimental Research on Landslide Mechanism*; 19–27.

Siebert L. (1996). Hazards of large volcanic debris avalanches and associated eruptive phenomena, in *Monitoring and Mitigation of Volcano Hazards*, edited by R. Scarpa and R. I. Tilling, 541-572, Springer- Verlag, New York.

Siebert L. (2002). Landslides resulting from structural failure of volcanoes. In: Evans, S.G., DeGraff, J.V. (Eds.), *Catastrophic Landslides: Effects, Occurrence, and Mechanisms*: Boulder, Colorado. *Geological Society of America Reviews in Engineering Geology*, **XV**, 209-235.

Siebert L., Glicken H., Ui T. (1987). Volcanic hazards from Bezymiannyand Bandai-type eruptions. *Bull Volcanol.*, **49**, 435-459.

Siebert, L. (1984). Large volcanic debris avalanches: characteristics of source areas, deposits, and associated eruptions. *J. Volcanol. Geotherm. Res.*, **22**, 163-197.

---

Sigaran-Loria, C. (2003). Numerical assessment of the influence of earthquakes on irregular morphologies: analysis of Colombia, 1999 and El Salvador, 2001 earthquakes, MSc Thesis, International Institute for Geo-Information Science and Earth Observation, Technical University of Delft, The Netherlands, 141pp.

Sigurdsson O., (1982). Analysis of pressure pulses resulting from volcanic activity in the vicinity of a well, M.S. thesis, 72 pp., Univ. of Okla., Norman.

Sigurdsson, O., Williams, R.S. (1991). Rockslides on the terminus of ‘Jokuls!argilsjokull’, southern Iceland. *Geografiska Annaler* **73A**, 129–140.

Simon A., Curini A., Darby S.E., Langendoen E.J. (2000). Bank and near-bank processes in an incised channel. *Geomorphology*, **35(3-4)**, 193-217.

Simoni A., Berti M., Generali M., Elmi C., Ghirotti M. (2004). Preliminary result from pore pressure monitoring on an unstable clay slope. *Eng. Geol.*, **73**, 117-128.

Singurindy O, Berkowitz B. (2003). Evolution of hydraulic conductivity by precipitation and dissolution in carbonate rock. *Water Resour. Res.*, **39(1)**, 1016.

Singurindy, O., Berkowitz, B. (2005). The role of fractures on coupled dissolution and precipitation patterns in carbonate rocks. *Advances in Water Resources*, **28**, 507-521.

Siöberg J., Sharp J.C., Malorey D.J. (2001). Slope stability at Aznalcóllar. In Slope Stability in Surface Mining, Hustrulid W.A., Mc Carter M.J. and Van Zyl D.J.A. editors, Littleton: Society for Mining, Metallurgy and Exploration Inc., 183-202.

Sirangelo B., Braca G. (2004). Identification of hazard conditions for mudflow occurrence by hydrological model Application of FLAIR model to Sarno warning system. *Eng. Geol.*, **73**, 267–276.

Sjöberg J. (1997). Estimating rock mass strength using the Hoek-Brown failure criterion and rock mass classification – A review and application to the Aznalcóllar open pit. Lulea University of Technology, Internal Report BM-1997:02, Division of Rock Mechanics,

Sjoberg, J. (1999). Analysis of large-scale rock slopes. Doctoral Thesis 1999:01. Division of rock mechanics, Lulea University of Technology, Sweden.

Skempton A. W., La Rochelle P. (1965). The Bradwell slip, a short term failure in London clay. *Géotechnique*, **15**, 221-242.

Skempton A.W. (1961). Horizontal stresses in overconsolidated London clay. Proc. 5<sup>th</sup> ICSMFE, Paris 1, 351-357.

Skempton A.W. (1970). “The consolidation of clays by gravitational compaction”. Q. J. Geol. Soc., London, 125, 373-412.

Skempton A.W. (1977). “Slope stability of cuttings in brown London clay”. Proc. 9<sup>th</sup> Int. Conf. on S.M.F.E., Tokyo, 3, 261-270.

Skempton A.W. (1977). Slope stability of cuttings in brown London clay. Proc. 9<sup>th</sup> Int. Conf. on S.M.F.E., Tokyo, 3, 261-270.

Skempton A.W. (1985). Residual strength of clays in landslides, folded strata and the laboratory. *Géotechnique*, **35(1)**, 3-18.

---

Skempton A.W. (1995). “Embankments and cuttings on the early railways”. *Construction History*, vol. 11, 33-49.

Skempton A.W., Hutchinson J.N. (1969). Stability of natural slopes and embankment foundations. *Proc. of 7<sup>th</sup> Int. Conf. on S.M.F.E., Mexico City, S.O.A. Volume*, 291-340.

Sladen J.A., D’Hollander R.D., Krahn J. (1985). The liquefaction of sands, a collapse surface approach. *Can. Geotech. J.*, **22**, 564-578.

Soldati M., Corsini A., Pasuto A. (2004) Landslides and climate change in the Italian Dolomites since the late glacial. *Geomorphic Impacts of Rapid Environmental Change*, **55(2)**, 141-161.

Soldati, M., Corsini, A., Pasuto, A. (2004). Landslides and climate change in the Italian Dolomites since the Late Glacial, *Catena*, **55**, 141–161, 2004.

Sorbino G., Sica C., Cascini L., Cuomo S. (2006) – Un’applicazione dei modelli di innsco su area vasta sede di frane rapide in terreni piroclastici. Incontro Annuale dei Giovani Ricercatori di Geotecnica 2006 – IARG 2006. Pisa, 26-28 Giugno 2006.

Sorensen K.K., Baudet B.A., Simpson B. (2007). Influence of structure on the time-dependent behaviour of a stiff sedimentary clay. *Géotechnique*, **57(1)**, 113-124.

Sosio R., Crosta G. B. (in preparation). Debris avalanche propagation from collapse of volcanic edifices.

Sovinc I. (1977). Cliff hotel foundation in alternating flysch rock formation. *Proc. Int. Symp. on The Geotechnics of Structurally Complex Formations, Capri*, 1, 449-458.

Spears D.A., Taylor R.K. (1972). Influence of weathering on the composition and engineering properties of in situ Coal Measures rocks. *Int. J. Rock Mech. Mining Sci.*, **9**, 729-756.

Stallebrass, S.E., Taylor R.N. (1997). The development and evaluation of a constitutive model for the prediction of ground movements in overconsolidated clay. *Géotechnique*, **47(2)**, 235-253.

Stewart, I.S, Sauber, J., Rose, J. (2000). Glacio-seismotectonics: ice sheet, crustal deformation and seismicity. *Quaternary Science Reviews*, **19**, 1367–1389.

Swanston D.N. (1967). Geology and slope failure in the Maybeso Valley, Prince of Wales Island, Alaska. Ph.D. Dissertation. Michigan State University, East Lansing, MI.

Tacher L, Bonnard C, Laloui L, Parriaux A (2005). Modelling the behaviour of a large landslide with respect to hydrogeological and geomechanical parameter heterogeneity. *Landslides*, **2**, 3–14.

Takahashi T. (1978). Mechanical characteristics of debris flow. *J. Hydraul. Div., ASCE*, **104**, 1153-1169.

Takahashi T. (1980). Debris flow on prismatic open channel. *J. Hydraul. Div., ASCE*, **106**, 381-396.

Takahashi T. (1981). Debris flow. *Ann. Rev. Fluid Mech.*, **13**, 57-77.

Takahashi T. (1991). Debris Flow. IAHR Monograph Balkema, Rotterdam

- Takahashi T. (2000). Initiation and flow of various types of debris flow. In: Wieczoreck GF (ed) Proceedings Second International Conference on Debris Flow Hazards Mitigation: Mechanics, Prediction and Assessment, Taipei: 15–25
- Tanaka, H., Sharma, P., Tsuchida, T., Tanaka, M. (1996). Comparative study on sample quality using several types of samplers. *Soils and Foundations*, **36(2)**, 57-68.
- Tatsuoka F., Santucci De Magistris F., Hayano K., Momoya Y., Koseki J. (2000). Some new aspects of time effects on the stress-strain behaviour of stiff geomaterials. Proc. 2<sup>nd</sup> Int. Symposium on The Geotechnics of Hard Soils-Soft Rocks, Evangelista A. and Picarelli L. editors, Naples, Balkema, 1285-1372.
- Tatsuoka F., Uchimura T., Hayano K., Di Benedetto H., Koseki J., Siddique M.S.A. (1999). Time-dependent deformation characteristics of stiff geomaterials in engineering practice. Proc. 2<sup>nd</sup> Int. Symposium on Pre-failure Deformation Characteristics of Geomaterials, Jamolkowski M., Lancellotta R. and LoPresti D. editors, Turin, 2, 1161-1250.
- Tavenas F., Chagnon J. Y., La Rochelle P. (1971). The Saint-Jean-Vianney landslide: Observations and eyewitnesses accounts. *Can. Geotech. J.*, **8**, 463-478.
- Tavenas F., Leroueil S. (1981). Creep and failure of slopes in clays. *Can. Geotech. J.*, **18**, 106-120.
- Tavenas F., Leroueil S., La Rochelle P., Roy M. (1978). Creep behaviour of an undisturbed lightly overconsolidated clay. *Can. Geotech. J.*, **15**, 402-423.
- Tavenas, F., Jean, P., Leblond, P., Leroueil, S. (1983). The permeability of natural soft clays. Part II: Permeability characteristics. *Canadian Geotechnical Journal* 20, 645-660.
- Taylor R.K., Cripps J.C. (1987). Weathering effects: slopes in mudrocks and overconsolidated clays. Slope Stability: Geotechnical Engineering and Geomorphology, Anderson M.G. and Richards K.S. editors, John Wiley and Sons, 405-445.
- Taylor, D.W. (1948). Fundamentals of Soil Mechanics. Wiley, New York.
- Tedd P. Charles J. A. (1981). In situ measurements of horizontal stress in overconsolidated clay using push-in spade shaped pressure cell. *Géotechnique*, **31**, 554-558.
- Teide-Group, (1997). Tenerife. Instituto Lucas Mallada, CSIC, Madrid, 218 pp.
- Terlien M.T.J. (1996). Modelling spatial and temporal variations in rainfall-triggered landslides. ITC publication 32. ITC, Enschede, The Netherlands
- Terzaghi K. (1936). The shearing resistance of saturated soils. Proc., 1st Int. Conf. on Soil Mechanics, Vol. 1, Cambridge, Mass., 54–56.
- Terzaghi K. (1943). Theoretical soil mechanics, Wiley, New York.
- Terzaghi K. (1961). Discussion of A.W. Skempton's paper on Horizontal stresses in overconsolidated London clay. Proc. 5<sup>th</sup> Int. Conf. on S.M.F.E., Paris, 3, 144-145.
- Terzaghi, K. (1962). Stability of steep slopes on hard unweathered rock. *Geotechnique*, **12**, 251–70.
- Thevanayagam S. (1998). Effect of fines and confining stress on steady state strength of silty sands. *J. Geotech. and Geoenv. Engineering, ASCE*, **124(6)**, 479-491.
-

- Thevanayagam S. (1999). Effect of fines and confining stress on steady state strength of silty sands. Closure, *J. Geotech. and Geoenv. Engineering, ASCE*, **125(11)**, 1024-1027.
- Thevanayagam S. (2002). Liquefaction potential and undrained fragility of silty sands. Proc. 12<sup>th</sup> Int. Conf. on Earthquake Engineering, R. Park editor, Auckland, New Zealand, Paper 2383, New Zealand Society of Earthquake Engineers.
- Thevanayagam S., Liang J. (2001). Shear wave velocity relations for silty and gravely soils. Proc. 4<sup>th</sup> Int. Conf. on Recent Advances in Geotech. Earthquake Eng. And Soil Dynamics and Symposium in Honor of Professor w.D. Liam Finn, San Diego, California, 1-6.
- Thevanayagam S., Martin G.R. (2002). Liquefaction on silty soils – screening and remediation issues. *Soil Dynamics and Earthquake Engineering* **22**, 1035-1042.
- Thevanayagam S., Ravishankar K., Mohan s. (1996). Steady state strength, relative density and fines content relationships for sands. *Transp. Res. Record*, **1547**, 61-67.
- Thevanayagam S., Shenthan T., Mohan S., Liang J. (2002). Undrained fragility of clean sands, silty sands and sandy silts. *J. Geotech. and Geoenv. Eng. Div., ASCE*, **128(10)**, 849-859.
- Thomas H.R., Cleall P., Li Y.C., Harris C., Kern-Leutschg M. (2009). Modelling of cryogenic processes in permafrost and seasonally frozen soils. *Géotechnique*, **59(3)**, 173-184.
- Thomson P.R., Wong R.C.K. (2008). Specimen nonuniformities in water-pluviated and moist-tamped sands under undrained triaxial compression and extension. *Can. Geotech. J.*, **45**, 939-956.
- Thorne C.R. (1982). Processes and mechanisms of river bank erosion. *Gravel-bed rivers*, R. D. Hey, J. C. Bathurst, and C. R. Thorne, eds., Wiley, New York, 227–271.
- Thorne C.R. (1990). Effects of vegetation on river-bank erosion and stability. In: Thornes, J.B. (Ed.), *Vegetation and Erosion*. Wiley and Sons, Chichester, U.K., pp. 203– 233.
- Tibaldi A. (2001). Multiple sector collapses at Stromboli volcano, Italy: How they work. *Bull. Volcanol.*, **63**, 112-125.
- Tibaldi A., Corazzato C., Apuani T., Cancelli A. (2003). Deformation at Stromboli volcano (Italy) revealed by rock mechanics and structural geology. *Tectonophysics*, **361**, 187-204.
- Tibaldi A., Pasquarè G., Francalanci L., Garduno V.H. (1994). Collapse type and recurrence at Stromboli volcano, associated volcanic activity, and sea level changes. *Atti Conv Lincei*, **112**, 143–151.
- Tien Y.M., Lee D.H., Juang C.H. (1990). Strain, pore pressure and fatigue characteristics of sandstone under various load conditions. *Int. J. Rock Mech. Mining Sci*, **27(4)**, 283-289.
- Ting J.M., Martin R.T., Ladd C.C. (1983). Mechanisms of strength for frozen sand. *J. of Geot. Eng. Div., ASCE*, **109**, 1286-1302.
- Todd B.J., S.R. Dallimore. (1998). Electromagnetical and geological transect across permafrost terrain, Mackenzie River delta, Canada. *Geophysics*, **63(6)**, 1914–1924.
- Tognacca C., Bezzola G.R., Minor H.E. (2000). Threshold criterion for debris-flow initiation due to channel bed failure. In: Wiczoreck GF (ed) *Proceedings Second International Conference on Debris Flow Hazards Mitigation: Mechanics, Prediction and Assessment*, Taipei: 89-97.
-

Tommasi P., Chiocci F.L., Marsella M., Coltelli M., Pompilio M. (2003). Preliminary analysis of the December 2002 instability phenomena at Stromboli volcano. Proceedings of International Workshop on Occurrence and Mechanisms of Flows in Natural Slopes and Earthfills (Sorrento, Italy), 297–306.

Torrance Y.K. (1987). Quick clays. Slope Stability: Geotechnical Engineering and Geomorphology, Anderson M.G. and Richards K.S. editors, John Wiley and Sons, 447-473.

Torres R., Dietrich W.E., Anderson S.P., Loague K., (1998). Unsaturated zone processes and the hydrologic response of a steep unchannelled catchment. *Water Resour. Res.*, **34(8)**, 1865-1879.

Tosatti G. (2003). Rassegna dei contributi scientifici sul disastro della Val di Stava (Provincia di Trento) 19 Luglio 1985/A review of scientific contributions on the Stava valley disaster (Eastern Italian Alp), 19th July 1985. Special volume of GNDCI-CNR, Pitagora Editrice, Bologna, 480 pp. (comprehensive compilation of 24 papers on the causes of the Stava tailings dam failure, most of which first appear in various scientific journals; all papers are in original language, Italian, English, Japanese, German).

Trenberth K.E. (1997). Short-term climate variations: Recent accomplishments and issues for future progress. *Bull. Amer. Met. Soc.*, **78**, 1081-1096.

Tsukamoto Y., Ohta T. (1988). Runoff process on a steep forested slope. *J. Hydrol.*, **102**, 165-178.

Tsukamoto, Y., Ishihara, K. (2005). Residual strength of soils involved in earthquake-induced landslides, Proceedings of Geotechnical Earthquake Engineering Satellite Conference, Osaka, Japan, 10 September 2005, Performance Based Design in Earthquake Geotechnical Engineering: Concepts and Research, ISSMGE, 117-123.

Ucar R. (1986). Determination of shear failure envelope in rock masses. *Journ of Geotech. Eng. Div., ASCE*, **112(3)**, 303-315.

Uchida T, Kosugi K, Mizuyama T. (2001). Effects of pipeflow on hydrological process and its relation to landslide: a review of pipeflow studies in forested headwater catchments. *Hydrol. Process.*, 15, 2151–2174.

USGS. U. S. Geological Survey. <http://www.usgs.gov/>

Vaid Y.P., Chern J.C. (1985). Cyclic and monotonic undrained response of saturated sands. In: Khosla V (ed) Proceedings of a session of ASCE Convention in Detroit, Michigan: Advances in the art of testing soils under cyclic conditions. American Society of Civil Engineers, New York, pp 120-147.

Vaid Y.P., Ghung E.K.F., Kuerbis R.H. (1990). Stress path and steady state. *Can. Geotech. J.*, **27**, 1-7.

Vallance J.W., Scott K.M. (1997). The Osceola mud-flow from Mount Rainier: Sedimentology and hazard implications of a huge clayrich debris-flow. *Geol Soc Am Bull.*, **109**, 143-163.

Van Asch T.W.J., Bogaard T.A. (1998). A study on the displacement of a landslide near Salins-les-Bains, eastern France. Proceedings 8th International Congress IAEG, Vancouver. 1641–1646.

---

- Van Asch T.W.J., Buma, J. (1997). Modelling groundwater fluctuations and the frequency of movement of a landslide in the Terres Noires region of Barcelonnette, France. *Earth Surf. Processes and Landforms*, **22**, 131-141.
- Van Asch T.W.J., Sukmantalya I.N. (1993). The modelling of soil slip erosion in the Upper Komerin area South Sumatra province, Indonesia. *Geogr Fis Din Quarternaria*, **16**, 81-87.
- van Asch Th.W.J., Malet J.P. Bogaard T.A. (2009). The effect of groundwater fluctuations on the velocity pattern of slow-moving landslides. *NHESS*, **3**, 739-749.
- Van Beek H. (2002). Assessment of the Influence of Changes in Land Use and Climate on Landslide Activity in a Mediterranean Environment. PhD thesis, Utrecht University.
- Van Benmelen (1949). The geology of Indonesia. vol. IA. General geology of Indonesia and adjacent archipelagos, 732 pp, vol. IB (portfolio), 60 pp.
- van Genuchten M. Th. (1980). A closed-form equation for predicting the hydraulic conductivity of unsaturated soils. *Soil. Sci. Soc. Am. J.* **44**, 892-898.
- van Wyk de Vries B., Borgia A. (1996). The role of basement in volcano deformation. In: McGuire WJ, Jones AP, Neuberg J (eds) *Volcano instability on the Earth and other planets*. London, Geological Society Special Publication, 110, 95-110.
- van Wyk de Vries B., Francis P.W. (1997). Catastrophic collapse at statovolcanoes induced by gradual volcano spreading. *Nature*, **387**, 387-390.
- van Wyk de Vries B., Kerle N., Petley D. (2000). Sector collapse forming at Casita volcano, Nicaragua. *Geology*, **28**, 167-170.
- van Wyk de Vries B., Merle O. (1996). The effect of volcanic constructs on rift fault patterns. *Geology*, **24**, 643-646.
- van Wyk de Vries B., Self S., Francis P.W., Keszthelyi L. (2001). A gravitational spreading origin for the Socompa debris avalanche. *J. Volcanol. Geotherm. Res.*, **105**, 225-247.
- van Wyk de Vries, B., Matela, R. (1998). Styles of volcano-induced deformation: numerical models of substratum flexure, spreading and extrusion. *J. Volcanol. Geotherm. Res.*, **81**, 1-18.
- van Wyk de Vries, B., O. Merle (1998). Extension induced by volcanic loading in regional strike-slip zones. *Geology*, **26**, 983-986.
- van Wyk de Vries, B., Self S., Francis, P.W. (1997). Did Socompa collapse or did it fall? *J. Conf. Abstr.* **2(1)**, 78.
- van Wyk de Vries, B., Wooller L., Cecchi E., Murray J. (2003). The importance of strike-slip faulting in spreading volcanoes. Abstract presented at EGS-AGU-EUG Meeting, Nice, France, 6–11 April 2003.
- Varnes, D.J. (1978). Slope movement types and processes. In: R.L. Schuster and R.J. Krizek, Editors, *Landslide Analysis and Control Special Report 176*, Transportation Research Board, N.R.C., National Academy of Sciences, Washington, DC, 2, 11–33.
- Varnes, D.J., Radbruch-Hall, D., Savage, W.Z. (1989). Topographic and structural conditions in areas of gravitational spreading of ridges in the Western United States. *U.S. Geological Survey Professional Paper*, p. 1496. 28 pp.
-

- Varnes, D.J., Radbruch-Hall, D., Varnes, K.L., Smith, W.K., Savage, W.Z. (1990). Measurement of ridge-spreading movements (sackungen) at Bald Eagle Mountain, Lake County, Colorado, 1975–1989. *U.S. Geological Survey Open-File Report*, **90–543**. 13 pp.
- Vaughan P.R. (1994). Assumption, prediction and reality in geotechnical engineering. *Géotechnique*, **44(4)**, 571-609.
- Vaughan P.R., Kovacevic N., Potts D.M. (2004). “Then and now: some comments on the design and analysis of slopes and embankments” Proceedings of a three day Conference on Advances in geotechnical engineering: the Skempton conference, ICE, London U.K., Jardine R.J., Potts D.M. and Higgins K.G. editors, Thomas Telford, vol. 3 (supplement), 15-64.
- Vaughan P.R., Walbancke H.J. (1973). “Pore pressure changes and delayed failure of cutting slopes on over-consolidated clay”. *Géotechnique* 23, n° 3, 531-539.
- Vaunat J., Lerouil S., Faure R. (1994). Slope movements: a geotechnical prospective. Proceeding of 7<sup>th</sup> Conf. Int. Ass. Engineering Geol., Lisbon, 1637-1646.
- Vaunat J., Lerouil S., Tavenas F. (1992). Hazard and risk analysis of slope instability. Proc. 1<sup>st</sup> Con. Symp. on Geotechnique and Natural Hazards, Vancouver, 397-404.
- Vengeon, J.M., 1998. De´formation et rupture des versants en terrain me´tamorphique anisotrope. PhD Thesis. University Joseph Fourier-Grenoble 1, 186 p.
- Verdugo R., Ishihara K. (1996). The steady state of sandy soils. *Soils and Foundations*, **36(2)**, 81-91.
- Versace, P., Sirangelo, B., Iritano, G. (2000). Soglie pluviometriche d’inesco dei movimenti franosi. *L’Acqua* 3, 113–130.
- Vidal N., Merle O. (2000). Reactivation of basement faults beneath volcanoes: a new model of flank collapse. *J. Volcanol. Geotherm. Res.*, **99**, 9-26.
- Viggiani G., Atkinson J.H. (1995) “Stiffness of fine-grained soil at very small strains” *Géotechnique* 45, n° 2, 249-265.
- Viggiani G., Finno R. J., Harris W. U. (1994). Experimental observations of strain localisation in plane strain compression of stiff clay. Proc. 3<sup>rd</sup> Int. Workshop on Localisation and Bifurcation Theory for Soils and Rocks, Balkema, 189-198.
- Viggiani G., Rampello S., Georgiannou V.N. (1993). Experimental analysis of localisation phenomena in triaxial tests on stiff clays. Proc. Int. Symp. on Geotechnical Engineering of Hard Soils – Soft Rocks, Athens, Anagnostopoulos A., Schlosser F., Kalteziotis N., Frank R. editors, Balkema, 849-856.
- Voight B. (1972). Fluid-wedge hypothesis and the Heart Mountain and Reef Creek décollements, northwestern Wyoming, USA, *Geol. Soc. Am. Abstr. Programs*, 4, 698.
- Voight B. (1988). A method for prediction of volcanic eruption. *Nature*, **332**, 125–130.
- Voight B. (1989). A relation to describe rate-dependent material failure. *Science*, **243**, 200–203.
- Voight B. (2000). Structural stability of andesite volcanoes and lava domes. *Philos. Trans. R. Soc. Lond., A*, 1663–1703.
-

- Voight B., Elsworth D. (1997). Failure of volcano slopes. *Geotechnique*, **47**, 1-31.
- Voight B., Glicken H., Janda R.J., Douglass P.M. (1981). Catastrophic rockslide avalanche of May 18. In: Lipman PW, Mullineaux DR (eds) The 1980 eruptions of Mount St. Helens, *U. S. Geol. Surv. Prof. Pap.*, **1250**, 347-377.
- Voight B., Janda R.J., Glicken H., Douglass P.M. (1983). Nature and mechanics of the Mount St Helens rockslide avalanche of 18 May 1980. *Geotechnique*, **33**, 243-273.
- Vonder Mühl D., Noetzli J. Roer I. (2008). PERMOS: A comprehensive monitoring network of mountain permafrost in the Swiss Alps. Ninth international conference on Permafrost, Fairbanks, AK.
- Walder J.S., Driedger, C.L. (1994). Geomorphic Change Caused by Outburst Floods and Debris Flows at Mount Rainier, Washington, with Emphasis on Tahoma Creek Valley. USGS WRI-93-4093.
- Walker H.J., Arnborg L. (1966). Permafrost and ice-wedge effect on river bank erosion. Proceedings of the International Conference on Permafrost Washington, D.C., 164-171.
- Walker, S.R., Santi, P.M. (2004). Influence of the Blue Mesa Reservoir on the Red Creek Landslide, Colorado. *Environmental and Engineering Geoscience*, **10**, 13–26.
- Walter T.R., Troll V.R. (2001). Formation of caldera periphery faults: an experimental study. *Bull. Volcanol.*, **63**, 191-203.
- Wan R.G., Guo R.G. (1998). A simple constitutive model for granular soils: modified stress-dilatancy approach. *Comput. Geotech.*, **22(2)**, 109-133.
- Wang C.H., Thomas H.R. (2000). Rainfall induced instability of partially saturated soil slopes. A parametric study of some factors. In: Bromhead E.N., Dixon N. and Ibsen M.-L., Eds., *Landslides in Research, Theory and Practice: Proc. 8th Int. Symp. on Landslides*, Cardiff, UK – Thomas Telford, London, 1545-1550.
- Wang F, Zhang Y, Huo Z, Peng X, Araiba K, Wang G (2008). Movement of the Shuping landslide in the first four years after the initial impoundment of the Three Gorges Dam Reservoir, China. *Landslides*, **5**, 321–329
- Wang FW, Zhang YM, Huo ZT, Matsumoto T, Huang BL (2004). The July 14, 2003 Qianjiangping Landslide, Three Gorges Reservoir, China. *Landslides*, **1(2)**, 157–162.
- Wang Z.L., Dafalias Y.F., Li X.S., Makdisi F.I. (2002). State pressure index for modeling sand behavior. *J. of Geot. And Geoenv. Eng., ASCE*, **128(6)**, 511-519.
- Watanabe H. (1983). Changes in water level and their implications to the 1977–1978 activity of Usu volcano. In: Shimozuru D., Yokoyama, J. Eds., *Arc Volcanism: Physics and Tectonics*. Terra Scientific, Tokyo, 81-93.
- Watters R. J., Delahaut W.D. (1995). Effect of argillic alteration on rock mass stability. In: *Clay and Shale Slope Instability*, Rev. Eng. Geol., edited by W. C. Haneburg and S. A. Anderson, Geol. Soc. of Am., Boulder, Colo., **10**, 139–150.
- Watters R.J., Zimelman D.R., Bowman S.D., Crowley J.K. (2000). Rock mass strength assessment and significance to edifice stability, Mount Rainier and Mount Hood, Cascade Range Volcanoes. *Pure and Applied Geophysics*, **157**, 957-976.
-

- Watts A.B., Masson D.G. (1995). A giant landslide on the north flank of Tenerife, Canary Islands. *J. Geophys. Res.*, **100(B12)**, 24 487-24 498.
- Wen, B., Wang, S., Wang, E., Zhang, J. (2004). Characteristics of rapid giant landslides in China, *Landslides*, **1(4)**, 247-261.
- Whalley W.B. (1983). The magnitude and frequency of large rockslides in Iceland in the postglacial. *Geografiska Annaler*, **65A(1-2)**, 99–110.
- Whalley W.B., Palmer C., Hamilton S., Gordon J. (1994). Ice exposures in rock glaciers. *J. Glaciol.*, **40(135)**, 427-429.
- Wieczorek G, Glade T. (2005). Climatic factors influencing occurrence of debris flows. In Debris-flow hazards and related phenomena, Jakob M, Hungr O (eds). Praxis and Springer: Berlin, Heidelberg, New York, 2005. 325–362.
- Wieczorek G.F. (1987). Effect of rainfall intensity and duration on debris flows in central Santa Cruz Mountains, California, Geological Society of America. *Reviews in Engineering Geology*, **7**, 93-104.
- Wigley T.M.L., Jones P.D., Briffa K.R., Smith G. (1990). Obtaining sub-grid scale information from coarse-resolution general circulation model output. *J. Geophys. Res.*, **95**, 1943-1953.
- Williams P.J. (1967). Unfrozen water in frozen soils: pore size – freezing temperature – pressure relationship. *Norwegian Geotechnical Institute*, **72**, 37- 48.
- Wilson R.C., Wieczorek G.F. (1995). Rainfall thresholds for the initiation of debris flows at La Honda, California. *Environ. Eng. Geosc.*, **1**, 11-27.
- Wilson, R.C., (1989). Rainstorms, pore pressures, and debris flows: a theoretical framework. In: Sadler, P.M., Norton, D.M. (Eds.), *Landslides in the Semiarid Environment*, Publication of the Inland Geological Society, Riverside, CA, **2**, 101–117.
- Windle D., Wroth C.P. (1977). The in situ measurements of the properties of stiff clays. Proc. 9<sup>th</sup> ICSMFE, Tokyo, 1, 347-352.
- Winkler, E.M. (1975). *Applied mineralogy, Stone: properties, durability in men's environment*. Springer, 230 pp.
- Wolman M.G. (1959). Factors influencing erosion of a cohesive river bank. *American Journal of Science*, **257**, 204–216.
- Wood M.D. (1990). *Soil behaviour and critical state soil mechanics*. Cambridge University Press, Cambridge.
- Wood M.D., Belkheir K., Liu D.F. (1994). Strain softening and state parameters for sand modeling. *Géotechnique*, **44(2)**, 335-339.
- Woods R., Rowe L. (1996). The Changing Spatial Variability of Subsurface Flow Across a Hillside. *J. Hydrol. (NZ)*, **35(1)**, 51-86.
- Wooller L., van Wyk de Vries B., Murray J.B., Rymer H. (2003). Volcano instability and collapse from basement faulting. Abstract presented at the EGS-AGU-EUG Meeting, Nice, France, 6–11 April 2003.
-

Wu W., Sidle R.C. (1995). A distributed slope stability model for steep forested basins, *Water Resour. Res.*, **31**, 2097–2110.

Wu Y (2003) Mechanism analysis of hazards caused by the interaction between groundwater and geo-environment. *Environ. Geol.*, **44(7)**, 811–819.

Wyrwoll, K-H. (1977). Causes of rock-slope failure in a cold area: Labrador-Ungava. *Geological Society of America Reviews in Engineering Geology*, **3**, 59–67.

Xu K.M., Zhang M., Eitzen Z.A., Ghan S.J., Klein S.A., Wu X., Xie S., Mranson M., Del Genio A.D., Iacobellis S.F., Khairoutdinov M., Lin W., Löhmann Ü., Randall D.A., Somerville R.C.J., Sud Y.C., Walker G.K., Wolf A., Yio J.J., Zhang J. (2005). Modeling springtime shallow frontal clouds with cloud-resolving and single-column models. *J. Geophys. Res.*, **110**, D15S04. doi:10.1029/2004JD005153.

Xu, Q., Fan, X.M., Huang, R.Q., Westen, C.V. (2009). Landslide dams triggered by the Wenchuan Earthquake, Sichuan Province, south west China. *Bull. Eng. Geol. Env.*, **68(3)**, 373-386.

Yamamuro J.A., Lade P.V. (1997). Static liquefaction of very loose sands. *Can. Geotech. J.*, **34**, 917-928.

Yamamuro J.A., Lade P.V. (1998). Steady-state concept and static liquefaction of silty sands. *Journ. of Geot. And Geoenv. Engineering*, **124(9)**, 868-877.

Yang Z., Elgamal A., Parra E. (2003). Computational model for cyclic mobility and associated shear deformation. *Journ. of Geot. And Geoenv. Engineering*, **129(12)**, 1119-1127.

Yin, Y., Wang, F., Sun, P., (2009). Landslide hazards triggered by the 2008 Wenchuan earthquake, Sichuan, China. *Landslides*, **6(2)**, 139-152.

Yoshimi Y. (2000). A frozen sample of sand that did not melt. Geotech. Year 2000, Developments in Geotechnical Engineering, Bangkok, Thailand.

Yoshimi Y., Tokimatsu K., Ohara J. (1994). In situ liquefaction resistance of clean sands over a wide density range. *Géotechnique*, **44(3)**.

Yoshimine M., Ishihara K. (1998). Flow potential of sand during liquefaction. *Soils and Foundations*, **38(3)**, 189-198.

Yoshimine M., Ishihara K., Vargas W. (1998). Effects of principal stress direction and intermediate principal stress on undrained behaviour of sand. *Soils and Foundations*, **38(3)**, 179-188.

Yoshimine M., Robertson P.K., Wride C.E. (1999). Undrained shear strength of clean sands to trigger flow liquefaction. *Can. Geotech. J.*, **36**, 891-906.

Yoshinaka R., Osada M. (1995). The comparison between dynamic and static strength of soft sedimentary rocks. In Rock Foundation, Yoshinaka R. and Kikuchi K. editors, Balkema, 109-114.

Youd T.L., Idriss I.M., Andrus R.D., Castro G., Christian J.T., Dobry R., Finn L.W.D., Harder L.F. Jr., Hynes M.H., Ishihara K., Koester J.P., Liao S.S.C., Marcuson W.F. III, Martin G.R., Mitchell J.K., Moriwaki Y., Power M.S., Robertson P.K., Seed R.B., Stokoe K.H. II (2001). Liquefaction resistance of soils: summary report from the 1996 NCEER and

1998 NCEER/NSF workshops on evaluation of liquefaction resistance of soils. *Journ. of Geot. And Geoenv. Engineering*, **127(10)**, 817-833.

Zêzere J.L., Ferreira A.B., Rodrigues M.L. (1999). The role of conditioning and triggering factors in the occurrence of landslides: a case study in the area north of Lisbon (Portugal). *Geomorphology*, **30**, 133-146.

Zhang F., Yashima A., Nakai T., Ye G.L., Aung H. (2005). An elasto-viscoplastic model for soft sedimentary rock based on TIJ concept and subloading yield surface. *Soils and Foundations*, **45(1)**, 65-73.

Zhang T., Barry R.G., Knowles K., Ling F., Armstrong R.L. (2003). Distribution of seasonally and perennally frozen ground in the Northern Hemisphere. In Permafrost. Phillips, Springman, and Arenson, eds. Swets and Zeitlinger.

Zhang Y.M., Liu G.R., Chang H., Huang B.L., Pan W. (2004). Tectonic analysis on the Qianjiangping landslide in Three Gorges Reservoir area and a revelation. *Journal of Yangtze River* (submitted, in Chinese).

Zimmermann M., Haeberli W. (1992). Climatic change and debris flow activity in high-mountain areas - A case study in the Swiss Alps. *Catena Supplement*, **22**, 59-72.

Zimmermann U., Münnich K.O., Roether W. (1966). Tracers determine movement of soil moisture and evapotranspiration. *Science*, **152**, 346-347.

Zlatovic S., Ishihara K. (1995). On the influence of non-plastic fines on residual strength. Proc. IS-TOKYO'95, 1<sup>st</sup> Int. Conf. On Earthquake Geotech. Engineering, Ishihara editor, Balkema, 239-244.

Zlatovic S., Ishihara K. (1997). Normalized behaviour of very loose non-plastic soils: effects of fabric. *Soils and Foundations*, **37(4)**, 47-56.